

Coal Structure

Martin L. Gorbaty, EDITOR

*Exxon Research and Engineering
Company*

K. Ouchi, EDITOR

Hokkaido University

Based on a symposium sponsored by
the Division of Fuel Chemistry
at the ACS/CSJ Chemical Congress,
Honolulu, Hawaii,
April 3–4, 1979.

ADVANCES IN CHEMISTRY SERIES

192

AMERICAN CHEMICAL SOCIETY

WASHINGTON, D. C.

1981



Library of Congress CIP Data

Coal structure.

(Advances in chemistry series; 192 ISSN 0065-2393)

Includes bibliographies and index.

1. Coal—Congresses.

I. Gorbaty, Martin L., 1942— . II. Ouchi, Kjöi, 1926— . III. American Chemical Society. Division of Fuel Chemistry. IV. ACS/CSJ Chemical Congress, Honolulu, 1979. V. Series.

QD1.A355 no. 192 [TP325] 540s [662.6'22]
ISBN 0-8412-0524-8 ADCSAJ 192 1-376 80-24104
1981

Copyright © 1981

American Chemical Society

All Rights Reserved. The appearance of the code at the bottom of the first page of each article in this volume indicates the copyright owner's consent that reprographic copies of the article may be made for personal or internal use or for the personal or internal use of specific clients. This consent is given on the condition, however, that the copier pay the stated per copy fee through the Copyright Clearance Center, Inc. for copying beyond that permitted by Sections 107 or 108 of the U.S. Copyright Law. This consent does not extend to copying or transmission by any means—graphic or electronic—for any other purpose, such as for general distribution, for advertising or promotional purposes, for creating new collective work, for resale, or for information storage and retrieval systems.

The citation of trade names and/or names of manufacturers in this publication is not to be construed as an endorsement or as approval by ACS of the commercial products or services referenced herein; nor should the mere reference herein to any drawing, specification, chemical process, or other data be regarded as a license or as a conveyance of any right or permission, to the holder, reader, or any other person or corporation, to manufacture, reproduce, use, or sell any patented invention or copyrighted work that may in any way be related thereto.

PRINTED IN THE UNITED STATES

**American Chemical
Society Library
1155 16th St. N. W.
Washington, D. C. 20036**

Advances in Chemistry Series

M. Joan Comstock, *Series Editor*

Advisory Board

David L. Allara

Kenneth B. Bischoff

Donald D. Dollberg

Robert E. Feeney

Jack Halpern

Brian M. Harney

W. Jeffrey Howe

James D. Idol, Jr.

James P. Lodge

Marvin Margoshes

Leon Petrakis

Theodore Provder

F. Sherwood Rowland

Dennis Schuetzle

Davis L. Temple, Jr.

Gunter Zweig

FOREWORD

ADVANCES IN CHEMISTRY SERIES was founded in 1949 by the American Chemical Society as an outlet for symposia and collections of data in special areas of topical interest that could not be accommodated in the Society's journals. It provides a medium for symposia that would otherwise be fragmented, their papers distributed among several journals or not published at all. Papers are reviewed critically according to ACS editorial standards and receive the careful attention and processing characteristic of ACS publications. Volumes in the **ADVANCES IN CHEMISTRY SERIES** maintain the integrity of the symposia on which they are based; however, verbatim reproductions of previously published papers are not accepted. Papers may include reports of research as well as reviews since symposia may embrace both types of presentation.

PREFACE

The need to produce additional liquid and gaseous fuels from coal is apparent. Today sophisticated and elegant engineering work is aimed at developing better coal conversion processes. However, these processes are based on chemistry that is at least 50 years old. Key limitations of this chemistry include poor selectivity and thermal efficiency, and high hydrogen consumption. New and more efficient processes will arise from breakthroughs in the chemistry of coal utilization, and these breakthroughs will have to come from a better understanding of coal structures.

Coal may be viewed as an organic rock. As such, it has an organic, an inorganic, and a physical structure. It is by nature a heterogeneous substance that varies from millimeter to millimeter in the same seam; coals of different rank formed from different species of plant matter during different geological periods in swamps hundreds or thousands of miles apart vary just as much. While it may not be possible to determine a coal structure absolutely, it is possible to determine key structural features of coals that affect their reactivity and ultimately their utility.

The coal science of today can be compared with the biochemistry of 50 or 75 years ago in the sense that the new tools required to answer key questions in that field were just then becoming available. Today major advances in magnetic resonance and other spectroscopic techniques make the hope of determining how carbon is arranged in coal a near reality.

This volume describes the current state-of-the-art understanding of the organic, inorganic, and physical structure of the substance called coal. After an introductory overview, which sets the field in perspective, the advances in applying new spectroscopic techniques to gain a better understanding of coal structure are described. Following this, current work on the organic, physical, and inorganic structures of coal is presented.

Many of the chapters in this volume originally were presented at a symposium sponsored by the Division of Fuel Chemistry of the American Chemical Society during the ADS/CSJ Chemical Congress in April 1979. Several have been revised and others added. We wish to thank the contributing authors for their efforts.

It is our belief that this volume can serve as a source of information and a base from which further science and technology advances will be made.

MARTIN L. GORBATY
Exxon Research and Engineering Company
P.O. Box 45
Linden, New Jersey 07036

K. OUCHI
Faculty of Engineering
Hokkaido University
Sapporo Japan 060

August 22, 1979

Coal Structure and Coal Science: Overview and Recommendations

RICHARD C. NEAVEL

Exxon Research and Engineering Company, P.O. Box 4255, Baytown, TX

A new procedure for classifying coals is needed. This procedure must recognize both coal type (proportions of various macerals and minerals) and rank (stage of metamorphic development). An integrated program must be instigated to study a large number of vitrinite-rich samples covering a broad range of ranks. Fundamental properties, including molecular structures, must be related to responses of the samples in conversion processes. Properties and responses of liptinite and inertinite, and interactions of inorganics, subsequently must be integrated with the data from vitrinites. Multivariate statistical treatment of the data will be required. Until such a unified classification system is devised, we shall continue to be limited to applying empirical tests to predict process responses, a procedure hardly deserving to be called a science.

Coal is a sedimentary rock accumulated as peat, composed principally of macerals and subordinately of minerals, and containing water and gases in submicroscopic pores. Macerals (mas' er-als) are organic substances derived from plant tissues, cell contents, and exudates that were variably subjected to decay, incorporated into sedimentary strata, and then altered physically and chemically by natural (geological) processes.

Coal is not a uniform mixture of carbon, hydrogen, oxygen, sulfur, and minor proportions of other elements; nor is it, as is often implied, simply a uniform, polyaromatic, polymeric substance. Rather, it is an aggregate of microscopically distinguishable, physically distinctive, and chemically different macerals and minerals.

Coal is analogous to a fruitcake, formed initially as a mixture of diverse ingredients, then baked to a product that is visibly heterogeneous. The heterogeneous nature of coal is evident in Figure 1, a

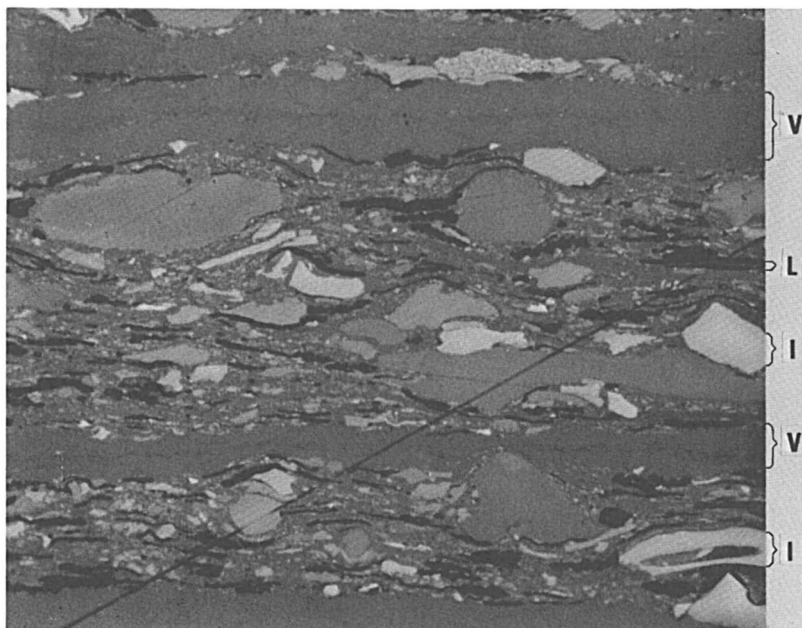


Figure 1. Photomicrograph of a polished surface of a bituminous coal. Representatives of the three major classes of maceral materials are identified: (V), vitrinite; (L), liptinite; (I), inertinite.

photomicrograph of a polished surface of a piece of typical coal. The different macerals reflect different proportions of incident light and are therefore distinguished as discrete areas exhibiting different shades of gray. It should be evident that any attempt to characterize the chemical structure of this coal without recognizing the organization of the elements and molecules into discrete substances would be like trying to describe the essence of a fruitcake by grinding it up and analyzing its elemental composition.

The heterogeneity of coal, exemplified by Figure 1, is inherited from the diversity of source materials that accumulated in a peat swamp. Coals may be compared, contrasted, and classified on the basis of variations in the proportions of these microscopically identifiable components. Such a classification is referred to as a classification according to type. Coals may also be classified according to how severely geological alteration processes, referred to collectively as metamorphism, have affected their properties; this is classification according to rank. These two classification methods are independent and orthogonal; therefore, within certain limits, any type of coal can be found at any rank.

Classification according to type involves the relative proportions of both the inorganic substances and the different organic substances. Because only the organic material is altered by metamorphic processes, rank

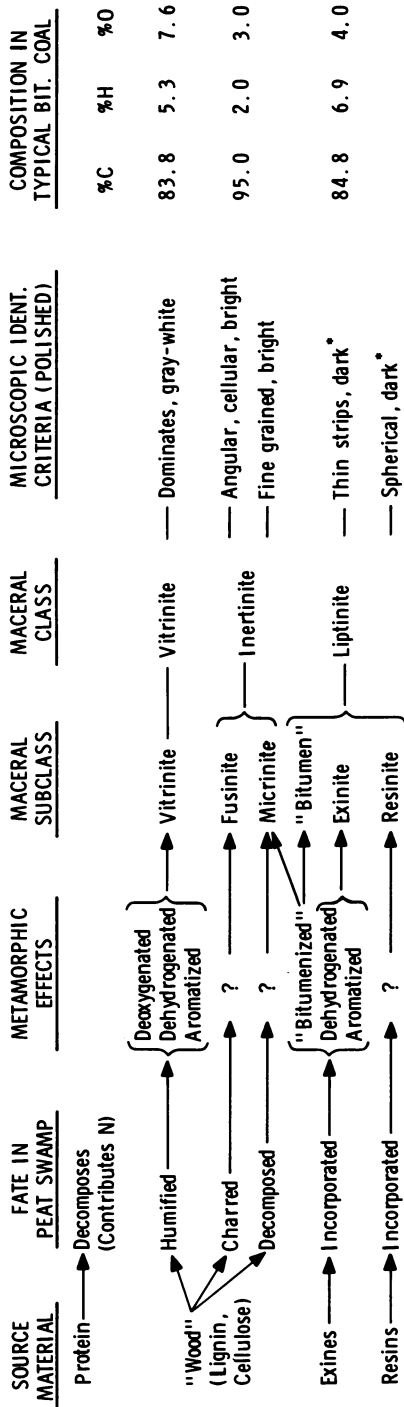
classification is independent of inorganic content. Inorganic material is significant in commercial uses of coal, and its presence must be accounted for in scientific studies. The present discussion, however, concentrates on the properties of the organic substances, because only the organic macerals make coal the valuable material that it is.

In Figure 1 selected areas are identified as vitrinite, liptinite, and inertinite. These terms refer to the three major classes of macerals recognizable in all ranks of coal except those of the highest ranks. A few of the more significant features of these major classes of macerals and of their more important subclasses are summarized in Figure 2. It can be seen from Figure 2 that the differentiation of coals according to type — viz., according to the content of materials assignable to each of the maceral classes — is really a differentiation according to the ingredients that initially accumulated as peat to form that coal. Although the rank scale according to ASTM has been arbitrarily divided and specific segments have been identified by a name (e.g., lignitic, bituminous, anthracitic coals), there are no such well-organized classes of coal types.

In this sense, there is essentially a continuous series of coals of different types, defined by microscopic quantification of their maceral (and mineral) contents. Particles of crushed coal when cemented together as a solid block with a catalytically solidified resin or plastic, can be polished and examined microscopically. Individual particles derived from different layers of a coal seam may differ significantly in maceral and mineral contents. Recognition of this feature has led to the concept of the microlithotype, wherein each particle can be classified according to its maceral content. In this procedure arbitrary classes of particles are recognized according to specific maceral proportions, as shown in Table I. The scientist or technologist should recognize that particles of the different microlithotypes are likely to perform quite dissimilarly when analyzed or processed; therefore, coals must be sampled carefully to prevent the selection of nonrepresentative particles.

Each of the materials recognized as belonging to a specific maceral class (according to the criteria shown in Figure 2) has physical and chemical properties that depend upon its composition in the peat swamp and the effects of subsequent metamorphic alteration. Thus, for instance, in all coals there is material derived from the structural tissues (“wood”) of plants. These woody substances (lignin, cellulose) are the dominant components of plants, and hence their derivatives dominate in typical coals. In the peat swamp some of the woody tissues may have been pyrolyzed by fire, forming a carbon-rich char recognized as fusinite in the coal. In some coal layers fusinite may be the dominant maceral, and such layers would be referred to as fusinite-rich types of coal.

Much more commonly, though, the woody tissues accumulated below a water covering, where imperfectly understood, largely microbiological processes converted them to humic substances of somewhat variable



• In Low-Vol Bituminous and Anthracites, Liptinite Indistinguishable from Vitrinite

Figure 2. Principal features of the major classes of macerals

Table I. Classification of Microlithotypes (1)

	<i>Microlithotype</i>	<i>Maceral</i>	<i>Volume Percent</i>
<i>Monomaceralic</i>	Vitrite	Vitrinite (V)	>95%
	Liptite	Liptinite (L)	>95%
	Inertite	Inertinite (I)	>95%
<i>Bimaceralic</i>	Clarite	V + L	>95%
	Vitrinertite	V + I	95%
	Durite	I + L	95%
<i>Trimaceralic</i>	Duroclarite	V + I + L	V > (I + L)
	Clarodurite	V + I + L	I > (L + V)
	Vitrinertoliptite	V + I + L	L > (I + V)
	Carbominerite	V, L, I, and mineral matter (MM)	20% < MM < 60%

composition. These highly functionalized, aromatic, humic substances subsequently were altered by metamorphic processes (heat, pressure) into substances classifiable as one of the vitrinitic macerals. Therefore, the physical and chemical properties of the vitrinitic materials in a specific coal were conditioned largely by the magnitude of temperature and pressure to which they were subjected after burial. One could say that the properties of the macerals in a given coal reflect the rank of the coal; or, more correctly, one should say that the rank of the coal reflects the properties of macerals as conditioned by the severity of the metamorphic processes to which the coal was subjected.

One of the properties of macerals that changes progressively with metamorphic severity is the microscopically measurable reflectance of polished surfaces. When a sensitive photomultiplier cell mounted on a microscope is used, it is possible to measure objectively the absolute percentage of incident light reflected from very small areas (about 5 μm diameter) of polished coal surfaces. In Figure 3 is shown a series of reflectance distributions, each representing a sampling of the material in a coal of the rank indicated. These distributions are arbitrarily constructed to show what would happen to a given peat if it were to be subjected to increasingly more severe metamorphism. Recognize, of course, that these are slices through a continuum and that no jump from rank to rank is implied. Properties such as carbon content, oxygen content, degree of aromaticity, and many others could be substituted for the reflectance scale and a similar sort of picture would emerge. In Table II some typical values are shown for selected properties of vitrinite macerals in different rank coals. In Table III a number of the properties of nonvitrinite macerals are compared to those of vitrinite from coal of the same rank.

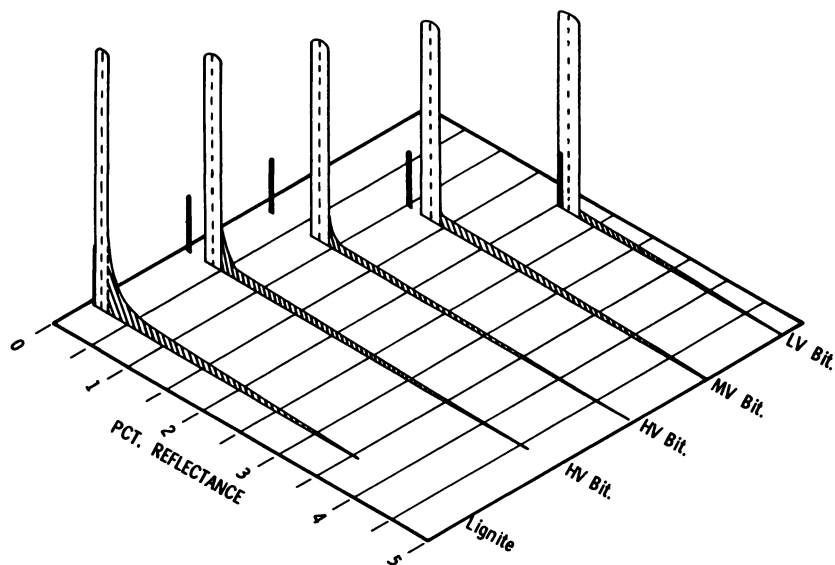


Figure 3. Reflectance distribution of macerals in typical coals with the same maceral contents but of different ranks ((■) liptinite; (□) vitrinite; (▨) inertinite)

Table II. Selected Properties of Vitrinites in Coals of Different Ranks

	Lignite	Subbitu- minous	Bitu- minous	Anthracite
Moisture capacity, wt % ^a	40	25	10	< 5
Carbon, wt % DMMF ^b	69	74.6	83	94
Hydrogen, wt % DMMF	5.0	5.1	5.5	3.0
Oxygen, wt % DMMF	24	18.5	10	2.5
Volatile matter, wt % DMMF	53	48	38	6
Aromatic C/total C	0.7	0.78	0.84	1.0
Density (He, g/cm ³)	1.43	1.39	1.30	1.5
Grindability (hardgrove)	48	51	61	40
Btullb, DMMF	11,600	12,700	14,700	15,200

^aThe values shown are typical for the ranks indicated and are not limiting.

^bDMMF = dry, mineral-matter-free basis.

Table III. Properties of Macerals Compared to Vitrinite in Same Coal (Subbituminous and High-Volatile Bituminous Only); Magnitude of Property Greater Than (>), Less Than (<), or Equal to (=) That of Associated Vitrinite

	<i>Fusinite</i>	<i>Micrinite</i>	<i>Exinite</i>
<i>Optical Properties</i>			
Reflectance	> >	>	<
Fluorescence			>
<i>Chemical Structure</i>			
Molecular weight			>
H/C ratio	< <	<	>
H aliphatic/H total; —CH ₂ ; hydroaromaticity			>
Fraction Aromatic C	>	>	<
Oxygen _{OH} /oxygen total	<		<
Unpaired spins by ESR	>		<
<i>Reactivity</i>			
Methane sorption	>		
Decomposition temperature			<
Oxidizability	<	<	<
Reduction with Li in Ethyl- enediamine	<	=	<

Typical U.S. coals are relatively vitrinite-rich. Therefore analyses of whole coals, when appropriately corrected for inorganic content, reflect, to a first approximation, the composition and properties of the included vitrinite. For this reason the parameters employed to classify coals according to rank reflect the rank (stage of metaphoric development) of the vitrinite. Calorific values or fixed carbon yields are calculated to a so-called mineral-matter-free basis for use in the ASTM classification of coals according to rank (2). It is essentially impossible to obtain inorganic-free samples; therefore, if organic matter is to be represented accurately in comparative studies of any of the organic properties of coal, analytical data must be converted to an inorganic-free basis. Commonly, a dry, ash-free (DAF, not MAF, which, unfortunately, is often used as an abbreviation for moisture-and-ash-free) basis is employed. It is preferable, however, to convert to a dry, mineral-matter-free (DMMF) basis, as discussed by Given and co-workers (3, 4, 5). In fact, the most meaningful assessment of coal rank or of the properties of coals of different ranks should be done with samples of concentrated vitrinite or on samples where the vitrinite comprises more than about 80% of the organic fraction. Because reflectance is closely correlative with many rank-sensitive properties and its determination can be made on vitrinite alone, it has become a widely accepted parameter to designate the rank of a coal (*see*

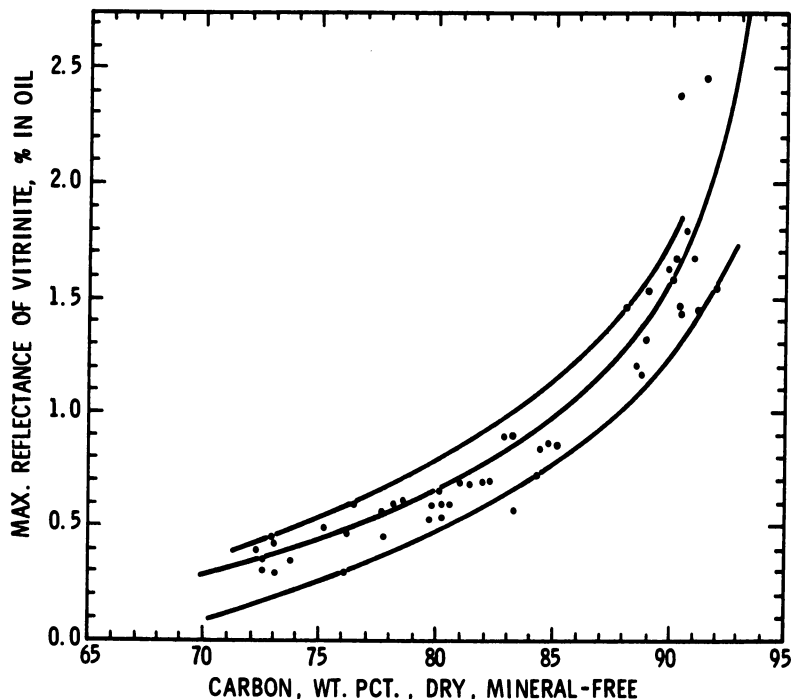


Figure 4. Correlation of reflectance of vitrinite and carbon content of coals (6)

Figure 4). Unfortunately, even when a reflectance value is available, it may not be reported in scientific publications. I strongly recommend that petrographic analyses and vitrinite reflectance be reported for samples on which structural studies are conducted.

Although many properties of vitrinites appear to change in a more or less parallel fashion as a result of metamorphism, there is considerable scatter in their correlation. Figure 5 is offered as evidence of this contention. The data plotted in Figure 5 are from coals containing more than 80% vitrinite on a DMMF basis (6). It is obvious that the progression from high to low H/C and O/C values reflects the influence of more severe metamorphic alteration; in other words, coals toward the lower-H/C-and-O/C end of the band are higher in rank. However, the fact that the data do form a band, rather than a linear progression, implies that there is not a simple scale that defines the rank progression. As Given and his co-workers have so eloquently shown, the geological-geographical disposition of U.S. coals appears to exert some, as yet undefined, influence on the intercorrelations of coal properties (7).

Clearly, neither geology nor geography is a property of coal and hence neither one can be measured. Different source materials, de-

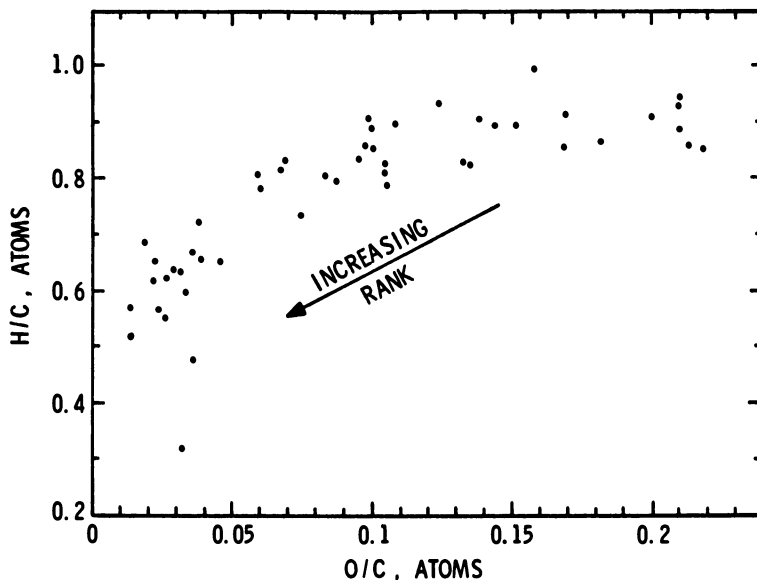


Figure 5. Correlation of atomic H/C and O/C for coals of different ranks (6)

positional conditions (including especially sulfur availability), and time-temperature-pressure conditions during metamorphism interacted to provide a multitude of potential paths that different coals (or even vitrinites in different coals) followed to their present condition. In other words, the concept of a single rank progression is more fallacy than fact.

As unifying, underlying concepts, type and rank certainly can be employed to envision why coals have the properties that they do. However, it is time for a reevaluation of coal classification concepts. How can we measure rank when we analyze coals of different types and when there is no simple rank progression even when vitrinite or vitrinite-rich coals are compared? And how can we assess type when maceral identification criteria are highly subjective, except for reflectance measurements that routinely are not even applied to the liptinite and highly variable inertinite macerals? And, finally, how can coals be classified scientifically when empirical and derived properties like calorific value and fixed carbon yield are employed as classifying parameters?

A scientific classification should be based first on the fundamental properties of the vitrinite in coals. This means, at the very least, that element concentrations and molecular structure configurations must be assessed. The structural properties of most importance to classification and process responses appear to be the following:

1. The nature of hydrogen bonding and physical entanglement that cohere molecular moieties

2. The nature of cyclical structures (e.g., ring condensation index, aromaticity, heteroatoms)
3. Amount and distribution of hydroaromatic hydrogen
4. Scissle bridging structures (e.g., ethers, sulfides, polymethylenes)
5. Functional group characteristics (especially oxygen- and sulfur-containing)
6. Organic–inorganic interactions

For the development of a scientific classification, these determinations need to be made on many vitrinite-rich coal samples spanning a wide range of rank. Because coals are sensitive to oxidation and moisture changes during handling, these samples must be carefully collected, prepared, and preserved.

It is fairly evident that because of the complex interactions of depositionally influenced and metamorphically influenced properties, the fundamental chemical–structural properties will need to be related to each other in a complex statistical fashion. A multivariate correlation matrix such as that pioneered by Waddell (8) appears to be an absolute requirement. However, characterization parameters far more sophisticated than those employed by Waddell are required. One can hope that, as correlations between parameters become evident, certain key properties will be discovered that will allow coal scientists and technologists to identify and classify vitrinites uniquely. Measurement of reflectance or other optical properties, if carried out properly, possibly on somewhat modified samples, might prove valuable in this respect. It then would not be necessary for every laboratory to have supersophisticated analytical equipment at its disposal in order to classify a coal properly. By properly identifying and classifying the vitrinite in a coal, one then could estimate accurately the many other vitrinite properties available in the multivariate correlation matrix.

Of course, elucidation of vitrinite properties and establishment of unique vitrinite class identifiers would not solve all the problems of coal classification. Once vitrinites could be properly identified and classified, it would be necessary to characterize and to identify uniquely the members of the other maceral classes. It is probable that liptinite properties change in some fashion correlative with the changes wrought by metamorphism on vitrinite. Therefore, classification of vitrinite would automatically classify liptinite. Whether inertinite changes with rank is uncertain; but it is certain that far better differentiation of fusinites needs to be employed, for it is evident that fusinite reflectance values span wide ranges in a given coal. Further work also needs to be done to characterize the inorganic materials in coals, especially developing simple tests for quantification of inorganic species.

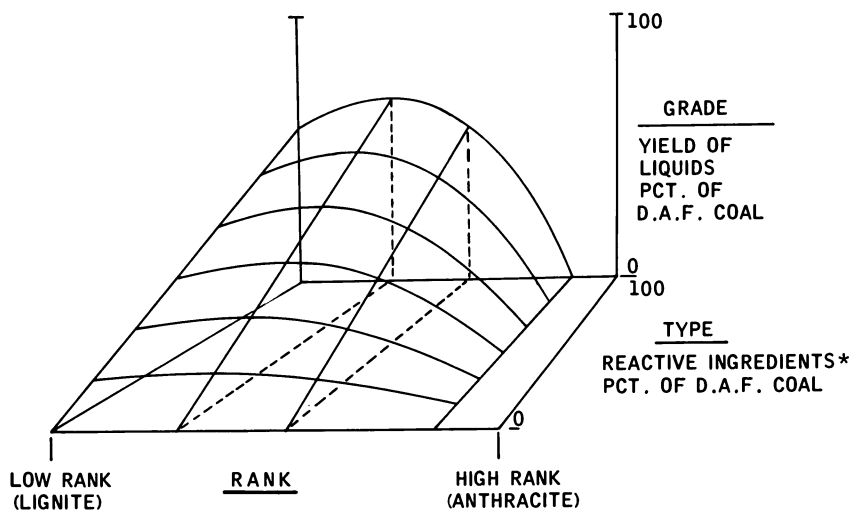


Figure 6. Highly schematized depiction of the orthogonal influences of coal rank and coal type on coal grade (economic value) as reflected simply by the yield of liquids in a coal conversion (liquefaction) process (**) reactive ingredients are vitrinite and exinite; in higher rank coals, vitrinite and exinite give low yields)

A multivariate vitrinite classification, supplemented by information about the inorganic matter and the proportions and properties of associated macerals, would be of little value if it could not be used to predict the response of a given coal in a processing system and thereby provide an estimate of the value of that coal. The orthogonal effects of rank and type on coal grade (economic value) are shown schematically in Figure 6. As shown in Figure 7, significant strides have been made in relating coal rank and type to coke strength, an important economic parameter (9). In reality, however, the relationships between coal properties and process responses are far more complex than shown in Figures 6 and 7. In the areas of liquefaction, gasification, pyrolysis, and coking, there is still much to be learned, and relatively large research programs are still required. These programs should concentrate initially upon a broad suite of vitrinite-rich coals covering a wide range of ranks. Here also, multivariate statistical correlations will be required.

Integrated programs designed to develop correlation matrices such as shown in simplified form in Figure 8 are badly needed to optimize the use of our nation's coals. Optimum uses must be found for available coals, and optimum coals must be found for available processes. The essence of such programs would be to discover the key properties needed to identify coals uniquely so that process responses could be predicted.

Only through the conduct of such integrated programs is coal science going to move out of the era of the 1950s where it is now mired. For

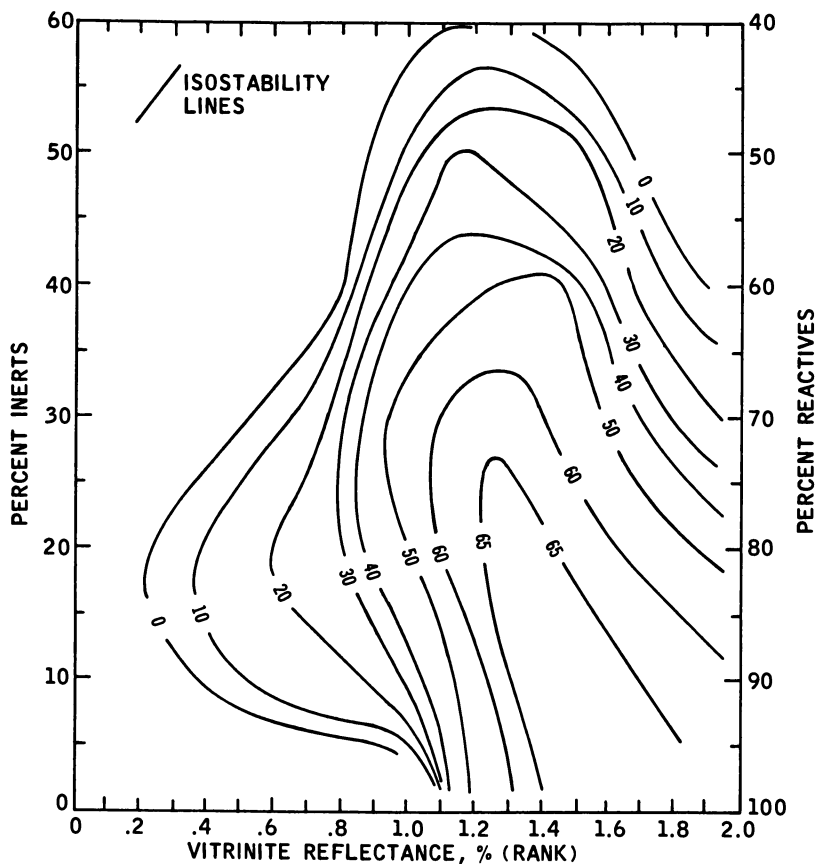


Figure 7. Influence of rank (as measured by vitrinite reflectance) and type (as measured by percentage of reactive macerals) on metallurgical coke strength. Contour lines of equal coke strength (tumbler stability) were calculated by the author according to the procedures pioneered in the U.S. by Schapiro and Gray (9).

whether the individual investigator feels comfortable with the idea or not, all coal science investigations should lead to the ability to predict (and improve) coal value. The scattered probes of coal structural properties on a bewildering range of poorly selected, poorly collected, poorly prepared, poorly preserved, and poorly characterized coal samples will lead us only into further confusion. Progress in coal science can be made only when scientific and technological investigations on coal result in a comprehensive integration and synthesis of data and information. The essence of science is "the reduction of the bewildering diversity of unique events to manageable uniformity within one of a number of symbol systems" (10). Present investigations of coal structure seldom conform to that definition today and therefore hardly deserve to be described as coal science.

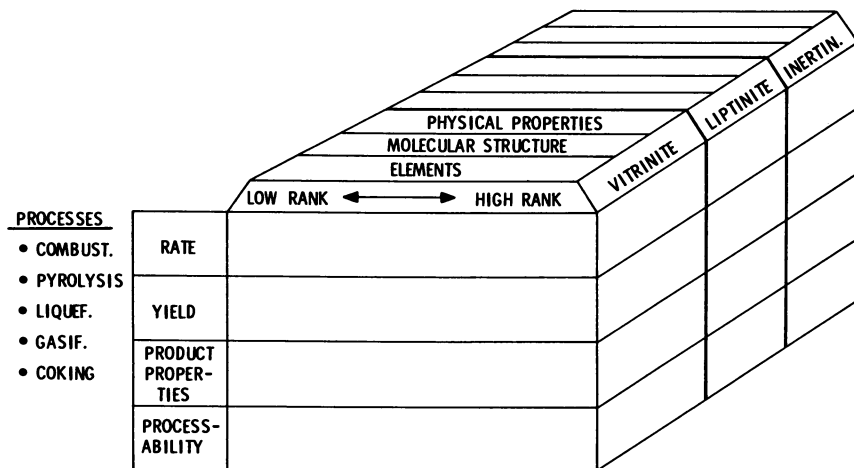


Figure 8. Schematic of the major elements of a matrix relating fundamental coal properties and the responses of coals to various processes. Real life matrices would have many dimensions.

Literature Cited

1. Stach, E. In "Textbook of Coal Petrology"; Stach, E., Ed.; Grebrüder Borntraeger: Berlin, 1978; p. 110.
2. "Annual Book of ASTM Standards," Designation D388; A.S.T.M., Philadelphia, 1979.
3. Given, P. H.; Yarzab, R. F. Coal Research Section, Penn. State Univ., 1975, Tech. Rpt. No. FE 0390-1.
4. Given, P. H. "The Use of DAF and DMMF Ultimate Analyses of Coals," *Fuel* 1976, 55(3), 256.
5. Given, P. H.; Spackman, W. "Reporting of Analyses of Low-Rank Coals on the Dry, Mineral-Matter-Free Basis," *Fuel* 1978, 57(4), 219.
6. Spackman, W. Coal Research Section, Penn. State Univ., 1976, Tech. Rpt. No. FE 0390-2.
7. Abdel-Baset, M. B.; Yarzab, R. F.; Given, P. H. "Dependence of Coal Liquefaction Behavior on Coal Characteristics. 3. Statistical Correlations of Conversion in Coal-Tetralin Interactions," *Fuel* 1978, 57(2), 89-94.
8. Waddell, C; Davis, A.; Spackman, W.; Griffiths, J. C. Coal Research Section, Penn. State Univ., 1978, Tech. Rpt. FE-2030-9.
9. Schapiro, N.; Gray, R. J.; Eusner, G. R. *Blast Furn., Coke Oven Raw Mater. Proc.* 1961, 20, 81-112.
10. Huxley, Aldous, "Education at the Non-Verbal Level," *Daedalus*: 1962.

RECEIVED July 19, 1979.

An Estimation of Average Polynuclear Aromatic Ring Size in an Iowa Vitrain and a Virginia Vitrain

B. C. GERSTEIN, L. M. RYAN, and P. DUBOIS MURPHY

Ames Laboratory, U.S. Department of Energy, and Department of Chemistry, Iowa State University, Ames, IA 50011

High-resolution techniques for NMR in solids have been used to obtain spectra of ^{13}C and ^1H in an Iowa and a Virginia vitrain. The carbon spectrum separated into two well-defined peaks from which an aromatic and an aliphatic portion were estimated. A superposition of Lorentzian lines was used to represent the aliphatic and aromatic proton signals, which were not well separated under high-resolution techniques. The fractions of aromatic carbon and hydrogen thus obtained were used to estimate an average polynuclear aromatic ring size in the coals studied.

A knowledge of the average polynuclear aromatic ring size in coals would be useful not only as an indicator of the appropriate chemistry one might use for conversion to fuels but also as an indicator of possible physiological effects of contact with coals and coal products. In principle, NMR offers the capability of a direct determination of average ring size via an identification of the fractions of aromatic ^{13}C and ^1H in solid coals. Three factors prevent the use of conventional NMR for this purpose. The first is the effect of homonuclear and heteronuclear dipolar interactions, which lead to line widths of hundreds of ppm for both ^1H and ^{13}C in solid coals (1, 2). The second is the fact that even in the absence of dipolar broadening, chemical shift anisotropies of ^1H can be as large as 34 ppm (3)—e.g., for the single species ^1H in $\text{H}_2\text{O}(\text{s})$ —so that a randomly oriented solid sample containing many protons in different chemical environments would exhibit an NMR spectrum in which individual protons could not be identified easily. A similar statement applies to NMR spectra of ^{13}C in solids. The third factor, peculiar to coals, is the possibility of an enormous number of chemically shifted species of a given

nucleus, leading to NMR spectra in which individual lines are still severely overlapping even in the absence of broadening due to dipolar interactions and chemical shift anisotropies.

In the present work cross-polarization to enhance sensitivity (4) combined with strong heteronuclear decoupling (5) and magic angle spinning (6) to remove heteronuclear dipolar broadening and chemical shift anisotropy broadening are used to estimate the fraction of aliphatic and aromatic carbon in Pocahontas No. 4 vitrain and Star vitrain. Combined rotation and multiple-pulse (NMR) spectroscopy (CRAMPS) (7, 8) is used similarly to narrow NMR spectra of ^1H in these coals. The ratios of aromatic ^1H to aromatic ^{13}C thus inferred are used in an attempt to guess an average polynuclear aromatic ring size in the samples investigated.

Experimental

The NMR spectrometer used for determinations of spectra of both ^1H and ^{13}C has previously been described (1), as have the probes used for magic angle spinning (9, 10). The Virginia coal Pocahontas No. 4 was supplied by H. L. Retcofsky of the Pittsburgh Energy Research Center of the U.S. Department of Energy. A vitrain portion of the Iowa coal Star was supplied by D. L. Biggs of the Iowa State University Department of Earth Sciences and the Ames Laboratory of the U.S. Department of Energy. The coals were analyzed for major constituents and free radical content as previously reported (1). Results of these analyses are given in Table I.

Results

The high-resolution solid state ^{13}C spectra of Pocahontas No. 4 and Star vitrains are shown in Figure 1. The values indicated for f_{ar} are an average of three determinations, the error limits indicating one standard deviation. Figure 2 is the high-resolution spectrum of ^1H in 2,6-dimethylbenzoic acid. This spectrum shows the resolution available for protons in the present experiments in the absence of the extreme chemical shift dispersion observed in the coals. The high-resolution solid state spectra of ^1H in both coals are shown in Figure 3.

Also indicated in Figures 2 and 3 are the Lorentzian lines used to approximate the chemical fractions of protons making up the experimental spectra (crosses) and the sum of these lines (indicated by the smooth curve through the experimental points). In Figure 2 the integrated areas of the three Lorentzians are 8.5%, 27.5%, and 64.0% of the total spectral area, in substantial agreement with the 1:3:6 ratio expected. It is less obvious that the coal spectra in Figure 3 should be fit also to Lorentzian line shapes, since they are actually comprised of a distribution of proton resonances. The two lines used in this case are meant to approximate the aromatic and aliphatic regions, which are assumed, with one caveat (vide

Table I. Elemental Analyses, Wt% (MAF), Free Radical Concentration, and Fractions of Aromatic Hydrogen and Carbon

Sample	% C	% H	% N	% S	$[e]$ (spins g^{-1}) $\times 10^{-19a}$	$f_{C,ar}$	$f_{H,ar}$
Pocahontas No. 4 vitrain	90.3(2)	4.43(4)	1.28	0.85	4	0.86	0.73
Star vitrain	77.0(1)	5.46(4)	1.17(14)	5.02	1.6	0.71	0.23

^aDetermination made on unheated sample.

infra), to account for all the hydrogen in the coals. Other work in this laboratory (11), on a cannel coal in which 75% or more of the protons are in aliphatic groups, suggests that the Lorentzian line shape is appropriate, at least for the aliphatic region. As a further test of the applicability of Lorentzian line shapes, we have recorded solid state ¹H NMR spectra for mixtures of polynuclear aromatics and compounds with a variety of aliphatic functional groups to model the chemical dispersity of the coals. Specifically, mixtures were composed of (1) polyethylene, (2)

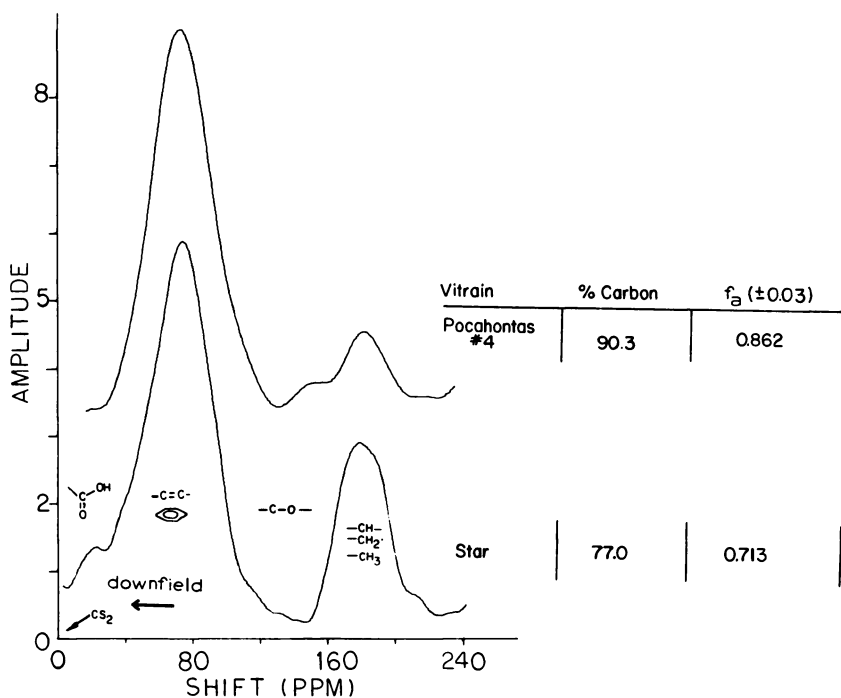


Figure 1. High-resolution NMR spectra of ¹³C in Pocahontas No. 4 vitrain and Star vitrain. Combined cross-polarization, strong heteronuclear decoupling, and magic angle spinning. (speed: 2.4–2.6 kHz; fields: 9.8 and 39.2 gauss; samples: 0.25 g; scans: 20,000; T_{cp} = 1.5 msec).

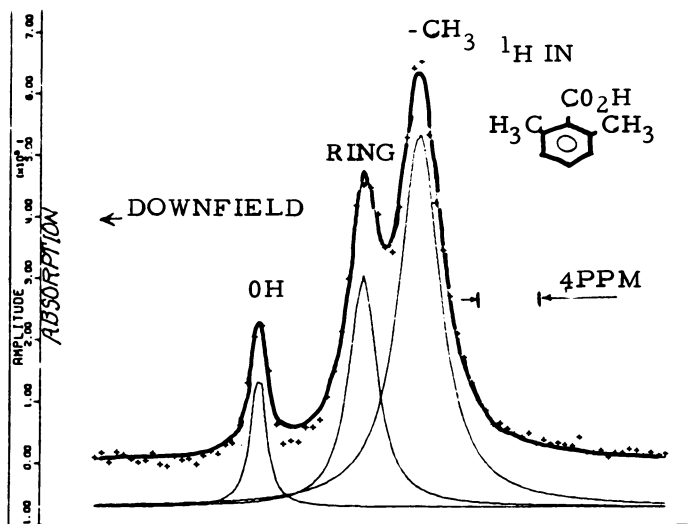


Figure 2. High-resolution NMR of protons in 2,6-dimethylbenzoic acid. Combined rotation and multiple-pulse spectroscopy.

polystyrene, (3) 2,6-dimethylbenzoic acid, (4) naphthalene, (5) anthracene, (6) chrysene, and (7) perylene. Figure 4 shows the results for a mixture in which 22% of the hydrogen is aromatic, 73% is aliphatic, and 5% is in acid OH groups. The Lorentzian fit implies 26, 70, and 4%, respectively. Fitted values for other mixtures were also within 5% of the measured fractions. Finally, fits to Gaussian line shapes were also attempted for each coal-and-model mixture, with the result that the experimental spectra could not be reproduced. Our experience thus indicates that these spectra are best fit by superpositions of Lorentzian lines, although there is certainly no a priori reason to expect that this would be the case.

Fractions of aromatic to total carbon and hydrogen estimated from the integrated spectral areas associated with these species are given in Table I for Pocahontas No. 4 and Star vitrains, along with elemental analyses of the two coals. Since hydroxyl protons would be expected to occur in the same chemical shift region as aromatic species, $f_{H,ar}$ values have been corrected by subtracting the OH proton fractions in the coals (0.03 for Pocahontas No. 4 and 0.08 for Star), as determined by Fourier transform infrared spectroscopy (12). Using the values in Table I, we then can estimate the mole ratios of aromatic hydrogen to aromatic carbon (H_{ar}/C_{ar}): Pocahontas No. 4, 0.50; Star, 0.28. At first thought these numbers seem a bit surprising, since, in general, larger polynuclear aromatic ring clusters imply smaller values of H_{ar}/C_{ar} , Pocahontas No. 4, having the higher carbon content, is an older coal, and one would expect a larger ring

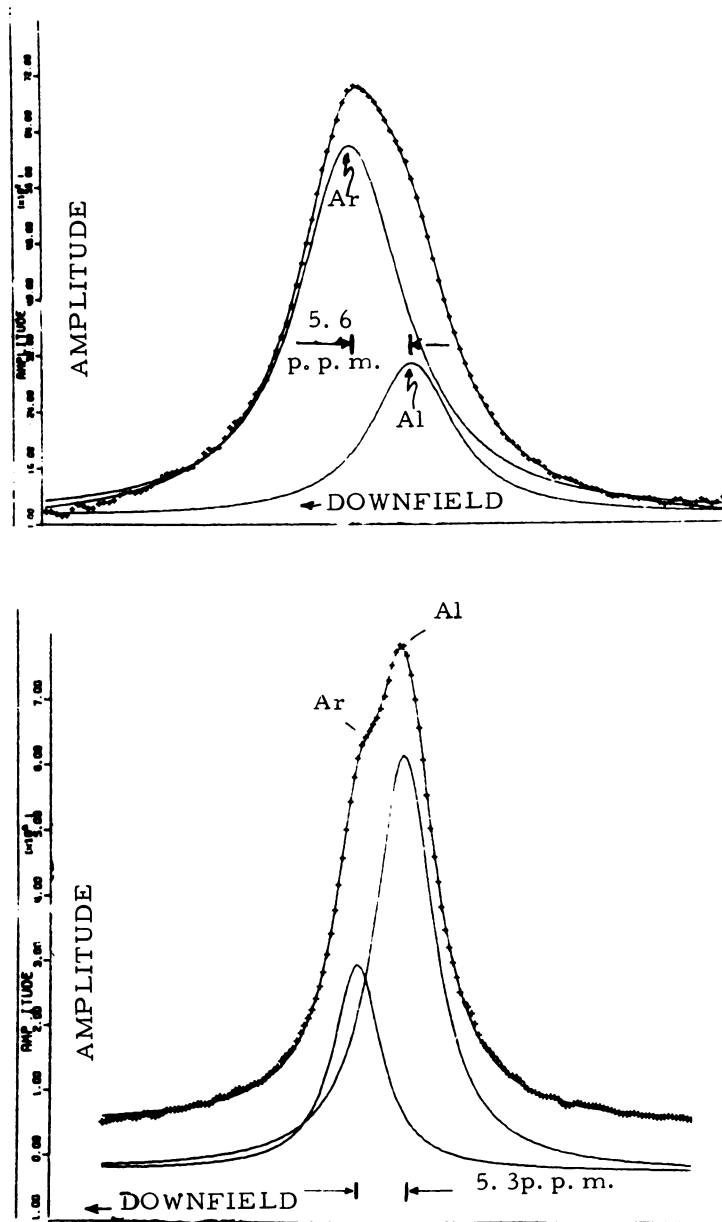


Figure 3. High-resolution NMR spectra of protons in Pocahontas No. 4 vitrain (top) and Star vitrain (bottom). Combined rotation and multiple-pulse spectroscopy. (top) ^1H in Pocahontas No. 4 vitrain CRAMPS at $t_c = 36 \mu\text{sec}$; $f_{\text{rot}} = 2.5 \text{ kHz}$; $f_{\text{ar}} = 0.73$ corrected for hydroxyl. (bottom) ^1H in Star vitrain CRAMPS at $t_c = 36 \mu\text{sec}$; $f_{\text{rot}} = 2.5 \text{ kHz}$; $f_{\text{ar}} = 0.23$ corrected for hydroxyl.

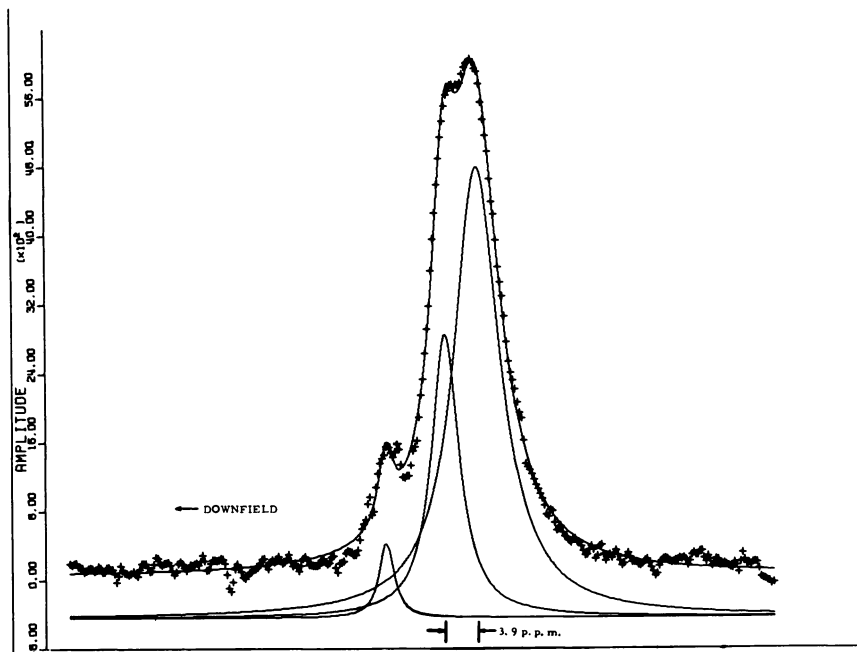
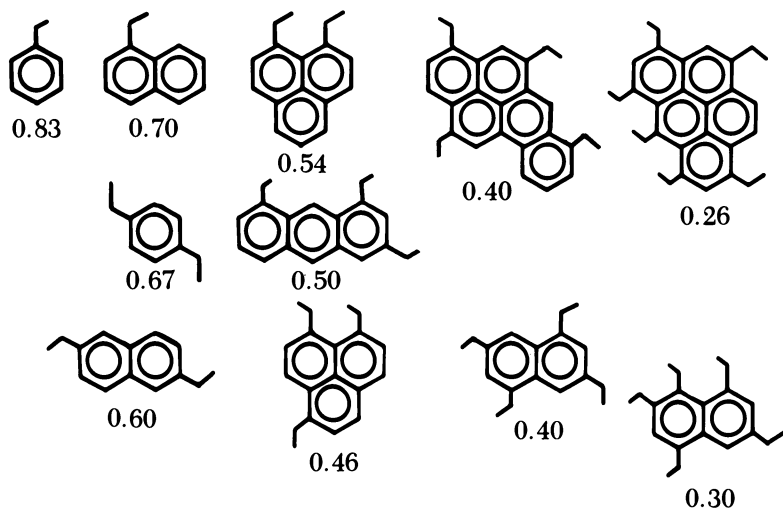


Figure 4. High-resolution ^1H NMR spectrum of model mixture (^1H in model mixture; $f_{ar} = 0.22$)

size to correspond to the more graphitized material. A bit of reflection, as illustrated by the entries in Table II, might help to remove the ambiguity.

The point to be made from Table II is that the average aromatic ring size inferred from the aromatic hydrogen-to-carbon ratios depends a good deal upon the number of side chains, or functional groups (indicated by the symbol \int in Table II), connected to the ring in question. We see that a value of 0.50 for this ratio is not inconsistent with an average ring size of 3, with two or three connections per polyaromatic ring. On the other hand, a value of 0.28 is not inconsistent with an average ring size of 2, with five connections per polyaromatic ring (but it is also not in disagreement with an average ring size of 4 to 6, as indicated in the fifth column of Table II). Our present prejudice is that the average polyaromatic hydrocarbon ring size in the older coal should be greater than that in the younger. With what we feel are reasonable values for connectivities, we thus infer that the average polyaromatic hydrocarbon ring size in Pocahontas No. 4 is no greater than 3, and that in Star is no greater than 2, the values thus inferred being dependent upon the assumption that, on the average, the younger coal has more aliphatic

Table II. Average Aromatic Ring Size as a Function of H_{ar}/C_{ar} and Connectivity

chains attached to the rings. Inferences from ^{13}C spectra yield similar values (13).

One source of error in the inferences above is the fraction of aromatic carbon, since it is known that not all carbons are polarized in cross-polarization experiments (14). A second more obvious source of error is the accuracy of resolving the high-resolution solid state spectra of protons in these coals. The former error would tend to increase the ring size on the average, since it is possible that the carbons not seen in cross-polarization experiments are in the neighborhood of stable free radicals, characterized by relatively large polyaromatic hydrocarbon rings. Alternatively, nonpolarized carbons may also be in diamond line structures, and the resulting error in detection would decrease the average ring size. Relaxation times of protons under the spin-locking conditions of the cross-polarization experiments (15) may be sufficiently short to obviate effective cross-polarization. Spin counting of protons with and without strong homonuclear decoupling indicates that at least 95% of the protons in the present samples are being detected under the high-resolution solid state techniques used in the present work.

Acknowledgment

This work was supported by the U.S. Department of Energy, contract No. W-7405-Eng-82, Division of Basic Energy Sciences, budget code No. AK-01-02-033.

Literature Cited

1. Gerstein, B. C.; Chow, C.; Pembleton, R. G.; Wilson, R. C. *J. Phys. Chem.* 1977, 81, 565.
2. Retcofsky, H. L.; Friedel, R. A. *J. Phys. Chem.* 1973, 77, 68.
3. Ryan, L. M.; Wilson, R. C.; Gerstein, B. C. *Chem. Phys. Lett.* 1977, 52, 341.
4. Hartman, S. R.; Hahn, E. L. *Phys. Rev.* 1962, 128, 2042.
5. Pines, A.; Gibby, M. G.; Waugh, J. S. *J. Chem. Phys.* 1973, 59, 569.
6. Andrew, E. R. In "Progress in Nuclear Magnetic Resonance Spectroscopy"; Emsley, J., Feeney, J., Sutcliffe, L. H., Eds.; Pergamon: New York, 1971; Vol. 8, Part 1.
7. Gerstein, B. C.; Pembleton, R. G.; Wilson, R. C.; Ryan, L. M. *J. Chem. Phys.* 1977, 66, 361.
8. Ryan, L. M.; Taylor, R. E.; Paff, A. J.; Gerstein, B. C. *J. Chem. Phys.* 1980, 72, 508.
9. Pembleton, R. G.; Ryan, L. M.; Gerstein, B. C. *Rev. Sci. Instrum.* 1977, 48, 1286.
10. Murphy, P. D.; Gerstein, B. C. Report IS-4388, Iowa State Univ., Ames, IA, 1978.
11. Unpublished results.
12. Solomon, P., private communication.
13. Retcofsky, H. L.; VanderHart, D. L. *Fuel* 1978, 57, 421.
14. VanderHart, D. L.; Retcofsky, H. L. *Fuel* 1976, 55, 202.
15. Gerstein, B. C. "Fingerprinting Solid Coals Using Pulse and Multiple Pulse Nuclear Magnetic Resonance", In "Analytical Methods for Coal and Coal Products"; Karr, C., Jr., Ed.; Academic: New York, 1980; Vol. 3, Chap. 52.

RECEIVED July 19, 1979.

Magnetic Resonance Study of Labeled Guest Molecules in Coal

B. G. SILBERNAGEL, L. B. EBERT, R. H. SCHLOSBERG, and R. B. LONG

Corporate Research Laboratories, Exxon Research and Engineering Company, Linden, NJ 07036

NMR and ESR techniques were used to study the motion of guest molecules imbibed in Illinois No. 6 and Wyodak coals. Molecules labeled with deuterium and fluorine were employed in the NMR studies and a nitroxide spin label (TEMPOL) in the ESR studies, to distinguish the guest molecules from the host coal matrix. Combined wide-line and transient techniques probed rates of molecular motion spanning more than six orders of magnitude. Narrow ^{19}F wide-line NMR spectra at 300K indicate guest motion at times shorter than 3×10^{-5} sec. Broadened ESR spin label spectra and ^{19}F spin lattice relaxation times suggest a time scale longer than about 10^{-8} sec. The ^2D wide-line NMR studies reveal constrained motions for a fraction of the C_6D_6 and $\text{C}_5\text{D}_5\text{N}$ molecules in the coal.

Magnetic resonance techniques are being applied increasingly to the study of coal and coal products. Electron spin resonance (ESR) has been used to examine stable carbon radicals in coal solids (1). High-resolution nuclear magnetic resonance (NMR) is employed extensively to examine liquid coal products (2). Recently developed multiple-pulse and magic angle spinning techniques provide opportunities for quasi-high-resolution NMR studies of coal solids (3, 4). These studies have provided a clearer picture of the distribution of different carbon types and chemical functionalities and the effects of selected treatments on the chemical forms in the coal. The present report addresses a very different, and complementary, question: NMR and ESR studies of molecules in the coal. These guests are labeled by deuteration or fluorination or by the use of nitroxide electron paramagnetic resonance (EPR) spin labels, so that they can be distinguished from the coal structure itself. By examining the type and rate of motion of the included molecules, one can probe

the pore distribution, microstructure, and accessible chemical functionalities of the coal matrix. Although NMR studies of naturally occurring water molecules in coal have appeared (5, 6), we believe that this is the first example of the study of labeled species included in the coal matrix. In this brief survey we present examples of the application of three different magnetic resonance techniques—wide-line NMR, ESR, and transient NMR—to the study of these labeled guests.

Experimental

Significant numbers of small molecules can be imbibed by dry coals. In the discussion that follows, coals dried at 110°C for 4 hr were exposed to a variety of molecular vapors at ambient temperatures in closed systems. In a typical experiment containers of coal and the imbibing molecules were placed in a nitrogen-flushed desiccator. The coal sample was weighed at regular intervals to determine the extent of molecular uptake. The rate and amount of molecular uptake depend on the size and functionality of the molecules. Dramatic differences in behavior are shown in Figure 1, where the uptake (in millimoles/gram coal) is shown as a function of time for benzene and pyridine. Benzene uptake is essentially complete after 5 days of exposure to the vapor. By contrast, significant amounts of pyridine are still being imbibed after 3 months of exposure. The magnetic resonance measurements described here were begun to provide a microscopic understanding for these very different behaviors.

Samples of dried Illinois No. 6 and Wyodak coals were exposed to several deuterated or fluorinated molecular types. Exposure times for the deuterated samples were on the order of several months, while time scales of several weeks were employed for fluorinated samples. In light of the pyridine results shown in

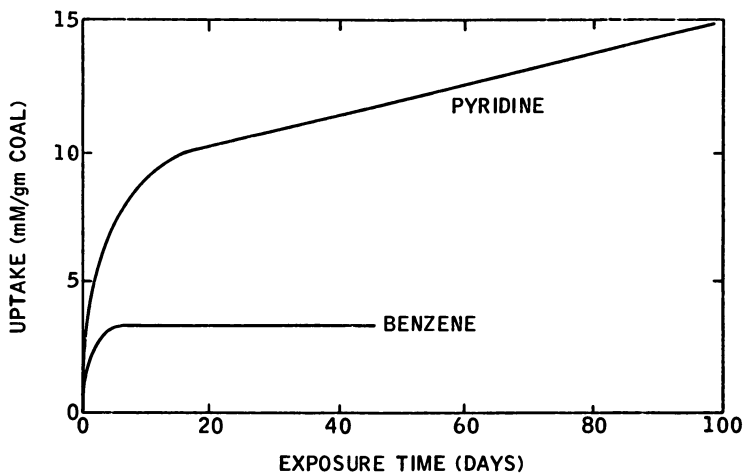


Figure 1. Molecular uptake as a function of time for benzene and pyridine in Illinois No. 6 coal

**Table I. Molecular Uptake During the Swelling Process:
Deuterated Guests**

<i>Coal Type</i>	<i>Guest Molecule</i>	<i>mmol Imbibed Per g of Coal</i>	<i>Volume Uptake cm³/g of Coal</i>
Wyodak	D ₂ O	8.49	0.153
	C ₅ D ₅ N	8.93	0.720
	C ₆ D ₆	1.26	0.112
Illinois	D ₂ O	5.79	0.104
	C ₅ D ₅ N	6.21	0.500
	C ₆ D ₆	2.08	0.184

**Table II. Molecular Uptake During the Swelling Process
Fluorinated Guests**

<i>Coal Type</i>	<i>Guest Molecule</i>	<i>mmol Imbibed Per g of Coal</i>	<i>Volume Uptake cm³/g of Coal</i>
Illinois No. 6	2-Fluorophenol	4.88	0.428
	4-Fluorophenol	1.88	0.165
	2-Fluoropyridine	6.09	0.490
	C ₆ F ₆	0.47	0.042
	Hexafluoro- propane diamine	0.29	0.017

Figure 1, exposures of these durations may not ensure the uptake of an equilibrium amount of the guest. Uptake data for the deuterated and fluorinated samples employed in the NMR studies are shown in Tables I and II, respectively. Uptake is reported on both a molar (millimoles/gram) and volume (cubic centimeters/gram) basis because such numbers furnish complementary information about the system. The magnitudes of uptake for the deuterated molecules are very similar to those of their protonated analogues.

Relative amounts of molecules imbibed are found to be roughly similar for deuterated guests in Wyodak and Illinois No. 6 coals, although the relative capacity of Wyodak coal for D₂O and C₅D₅N is greater than that of Illinois No. 6, and Wyodak's C₆D₆ capacity is less. Comparable amounts of 2-fluoropyridine and C₅D₅N are imbibed in Illinois No. 6, while C₆F₆ uptake is considerably less than for C₆D₆. Roughly comparable amounts of the acidic 2-fluorophenol and basic 2-fluoropyridine can be accommodated in the coal structure. The striking difference between amounts of 2-fluorophenol and 4-fluorophenol is attributed to the lower vapor pressure of the latter liquid at ambient temperatures, leading to very different uptake rates. Larger molecules and weaker bases are less readily included, as indicated for hexafluoropropane diamine.

Wide-line ²D and ¹⁹F NMR spectra were obtained at frequencies of 13 MHz and 35 MHz, respectively, using a Varian WL-112 spectrometer. The ESR data were accumulated on a Varian Century Series (E-12) spectrometer operating at 9.5 GHz. A Bruker SXP spectrometer operating from 10 to 80 MHz was used for ¹⁹F spin lattice relaxation time measurements. Measurements reported here were at 300K.

Molecular Motion and Magnetic Resonance

The motion of imbibed molecules reflects their environment. Non-equivalent sites may well be expected in the coal: even the distribution in pore size can have an effect. The goal of the present magnetic resonance observations is to provide some measure of the rate and types of allowable molecular motion. These data will be correlated with the size and chemistry of the molecules to provide a picture of the coal matrix. Magnetic resonance has been employed in the studies of analogous materials such as clays (7), surfaces (8), and biological membranes (9). Further, labeling enables us to focus directly on the guest species, since the levels of ^2D and ^{19}F in the coal structure are vanishingly small.

For the present discussion we confine our attention to two motion-related effects on the resonance properties. The first of these is the phenomenon of narrowing of wide-line NMR and ESR spectra, shown schematically in Figure 2. At low temperatures, when the molecules are immobile, the nuclear or electronic spins will experience strong, static interactions with their environment. For ^{19}F nuclei or the paramagnetic spin labels, these interactions are predominantly dipolar interactions with other spins in their vicinity. For ^2D nuclei the most important interaction is between the electric quadrupole moment of the deuterium nucleus and the inhomogeneous electric field in its vicinity caused by the carbon-deuterium bond. At sufficiently high temperatures rapid isotropic molecular motion can average these interactions to zero. If the molecular motion is partially confined, this averaging process may be incomplete. At intermediate temperatures the width of the resonance line varies from the static to the averaged values.

While the relationship between molecular dynamics and averaging can be analyzed in considerable detail (10), for the purposes of the present discussion we will employ a simple picture (11) that illustrates the basic principles. Averaging will occur when the rate of motion becomes comparable to the strength of the interaction. If, for example, the width of a ^{19}F NMR line were $\Delta H = 1$ G, narrowing would be expected for guest motions at rates of approximately $\gamma\Delta H = 2\pi \times 4.0 \times 10^3 \text{ c/G} \times 1 \text{ G} = 30 \text{ kHz}$. Since the three labels we have used have significantly different interaction strengths, we can use them to study narrowing on different time scales. For ^{19}F NMR, averaging will occur for hopping times shorter than about 3×10^{-5} sec. The stronger ^2D quadrupolar interactions will not be narrowed until hopping times shorter than about 10^{-6} sec are achieved. Because of their larger dipole moment, the electronic spin labels require times shorter than about 10^{-8} sec to accomplish averaging.

Transient NMR observations are a complementary probe of the system. In these measurements excess energy is given to the nuclear spin system by applying a radio frequency field, and the rate of loss of this

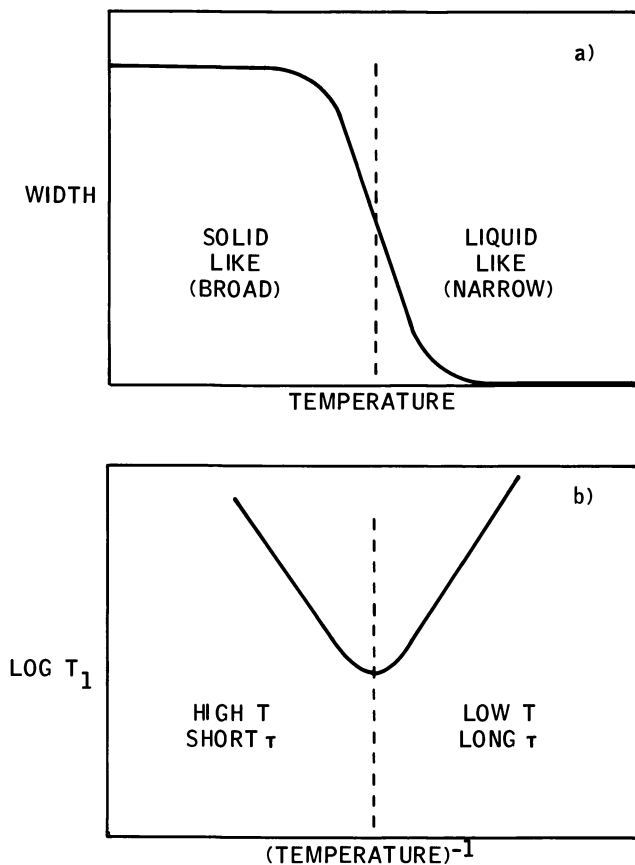


Figure 2. Variations of NMR linewidths (a) and spin lattice relaxation times (b) associated with molecular motion.

energy from the nuclei to the environment, called the spin lattice relaxation time (T_1), is determined. A principal cause for this energy transfer is the coupling between an individual nucleus and magnetic field fluctuations that arise from the motion of other nuclei in its vicinity. The underlying theory of this relaxation process is well understood (12), and here we merely observe that for a fluctuation to be effective in the energy transfer process it must be at a frequency comparable to the resonance frequency of the nucleus (ω_0). Thus as shown in Figure 2(b), relaxation will be most rapid, and T_1 shortest, for a rate of motion comparable to ω_0 . For either faster or slower motions the relaxation time increases.

Magnetic Resonance Observations

In the ^{19}F wide-line NMR observations we find a single narrow component to the spectrum at room temperature. The residual line

width (about 100 mG at 35 MHz) is instrumental, being associated with magnetic field nonhomogeneities. An example of the spectrum is shown in Figure 3(a) for Illinois No. 6 coal containing 2-fluoropyridine. In this figure a large modulation field was employed (H_{mod} about 1 G) in an attempt to find a broader component, but none was observed. Line width estimates for 2-fluoropyridine can be made by using standard second-moment calculations (13), and they indicate a width of 1–2 G if the molecules were stationary. The present data would place an upper limit of 10% for the number of molecules that might appear in that form. These data collectively suggest that almost all the 2-fluoropyridine molecules must be moving on a time scale faster than 10^{-4} sec. Similar results were obtained with other fluorinated guests.

By contrast, the ^2D wide-line NMR studies show evidence for both narrowed and unnarrowed components to the spectrum for both C_6D_6 and $\text{C}_5\text{D}_5\text{N}$. A typical example, shown in Figure 3(b) for C_6D_6 included

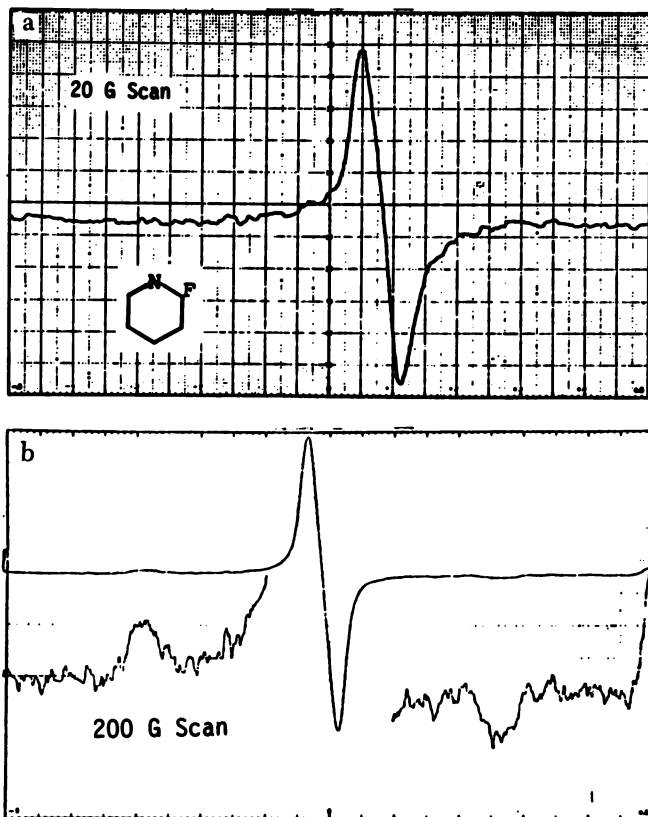


Figure 3. Wide-line NMR spectra from Illinois No. 6 coal: (a) ^{19}F in 2-fluoropyridine; (b) ^2D in perdeuterobenzene

in Illinois No. 6 coal, shows the derivative of the NMR absorption displayed at two levels of gain. A very conspicuous central component comes from molecules moving rapidly and isotropically: the ^2D nuclear quadrupole interaction is averaged to zero. Such rapid motion would be expected for the liquidlike molecules included in coal pores. The satellites reflect the typical NMR absorption expected for the unnarrowed ^2D NMR line in a powder sample (14). It is extremely difficult to accurately integrate this broad signal and determine the relative number of molecules in the narrowed and unnarrowed conditions. However, estimates suggest that the relative amounts of both types are comparable.

The width of this broader absorption indicates that some types of residual motion are still in evidence. The effective quadrupole coupling constant $(e^2 qQ/h)_{\text{eff}}$ can be related to the splitting between the satellites, ΔH_Q , by (14)

$$(e^2 qQ/h)_{\text{eff}} = 2\gamma_D \Delta H_Q / 3\pi \quad (1)$$

where γ_D is the gyromagnetic factor of the deuteron. The effective quadrupole coupling constants for $\text{C}_5\text{D}_5\text{N}$ and C_6D_6 in Illinois No. 6 and Wyodak coals are shown in Table III. Also included for comparison are measurements of these molecules in solid $\text{C}_5\text{D}_5\text{N}$ and C_6D_6 measured at liquid helium temperatures (15). The most striking observation is that the effective coupling constants for the C_6D_6 cases are less than half the molecular solid values. This phenomenon is readily explained by assuming that the C_6D_6 molecules are spinning in the plane of the molecule at a sufficiently rapid rate to partially average the quadrupole interaction, which would be expected to lead to a reduction of its magnitude by exactly a factor of 2 (16). The remaining difference between the observed values of the coupling constants and the values found for the low-temperature molecular solids is associated with molecular vibrations.

An additional probe of the system is the spin label that we have examined by using ESR. The experimental sequence employed is shown in Figure 4. It is well known that coals contain significant amounts of kinetically stable carbon radicals, which yield an ESR spectrum of the type shown in Figure 4(a). In this particular sample of Wyodak coal, weighing about 200 mg, 3.6×10^{18} spins were observed. Immediately after, a hexane solution containing the spin label TEMPOL (2,2,6,6-

Table III. Effective ^2D Quadrupole Coupling Constants (kHz)

	$\text{C}_5\text{D}_5\text{N}$	C_6D_6
Illinois	171.7	82.0
Wyodak	170.4	82.5
Molecular solid (Barnes)	178.0	180.7

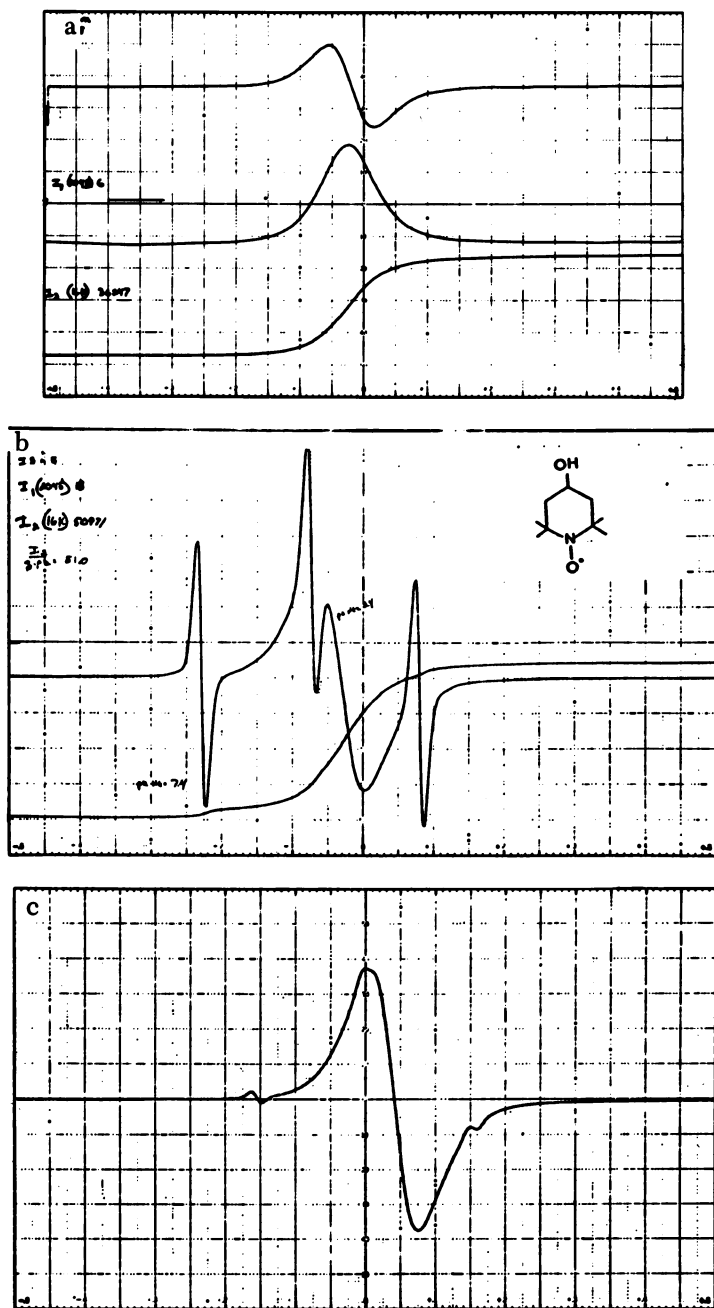


Figure 4. TEMPOL ESR spin label studies in Wyodak coal: (a) coal radicals prior to spin label addition; (b) ESR spectrum immediately after TEMPOL addition, showing carbon radical in coal and the narrow triplet spin label spectrum (the chemical form of the TEMPOL is indicated in the inset); (c) the narrow TEMPOL spectrum broadens with time.

tetramethyl-4-piperidinol-1-oxyl) is added to such a coal sample, a superposition of the carbon radical ESR signal and the triplet ESR spectrum characteristic of the TEMPOL is observed [Figure 4(b)]. This highly articulated triplet spectrum diminishes on a time scale of several hours, producing the resulting spectrum shown in Figure 4(c). However, the total spin density is not diminished during this time, which implies that the TEMPOL spin label is not being destroyed. The observed change in the TEMPOL signal is associated with a broadening of its resonance line. This change occurs when the rate of motion of these labels falls below the value needed for motional narrowing (about $10^8/\text{sec}$) upon inclusion of the molecule in the coal structure.

To study the dynamics of this inclusion process, we measured the variation of the derivative height of the TEMPOL spectrum as a function of time after the spin label addition, and the results are shown in Figure 5. A very rapid reduction of the derivative intensity occurs in the first few minutes after TEMPOL addition, but after that time a much slower rate of change is observed. This behavior may be explained by assuming that some of the TEMPOL molecules are rapidly adsorbed on the surface of the coal and that subsequent loss of TEMPOL from the liquid phase is associated with diffusion of the molecules into the coal matrix. In the case of a simple process one anticipates that diffusion into the coal should exhibit a $t^{1/2}$ time dependence. To test this model, we plotted the product of the derivative intensity and $t^{1/2}$ as a function of time in Figure 6. To a good approximation, a diffusive motion appears to hold after the first 30 min.

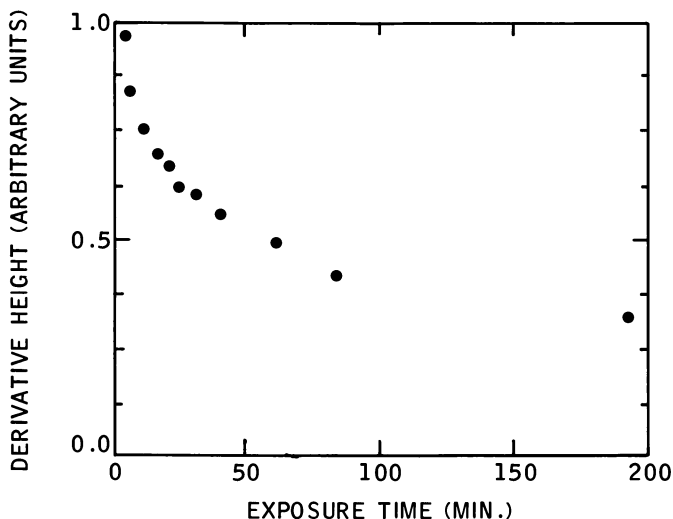


Figure 5. Decay of spin label intensity with time (Illinois No. 6 + TEMPOL (in C_6H_6))

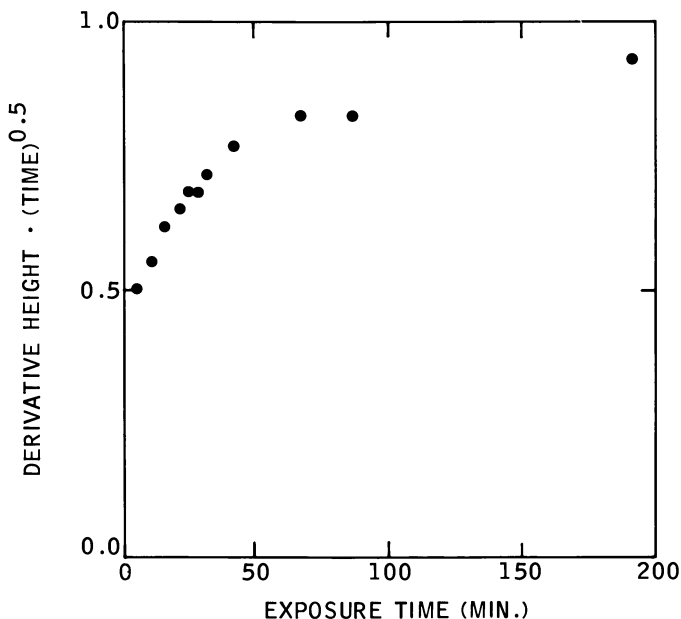


Figure 6. An asymptotic dependence of spin label intensity proportional to $t^{1/2}$ suggests diffusion of the label into the coal.

An example of the use of transient NMR is shown in Figure 7, where spin lattice relaxation measurements for 2-fluorophenol molecules in the neat liquids [Figure 7(a)] and in coal [Figure 7(b)] are shown for comparison. The ^{19}F nucleus is an excellent nuclear label to use for these transient studies because the resonance line is narrow and easy to manipulate with radio frequency pulses. The two plots in Figure 7 show the loss of the excess energy given to the nuclei by the radio frequency field as a function of time. For the case of a single source of energy transfer, the energy loss should be exponential (i.e., linear on these semilogarithmic plots) and the slope should be proportional to the spin lattice relaxation time T_1 .

In neat 2-fluorophenol liquid a linear decay is, in fact, observed, with $T_1 = 1.64$ sec. By contrast, 2-fluorophenol in coal exhibits a nonexponential decay, suggesting that not all the molecules in the coal are equivalent. The time scale for the decay is more than two orders of magnitude faster in the coal than in neat liquid. The rate of relaxation is found to be independent of the frequency for resonance, demonstrating that molecular motion (and not paramagnetic impurities, for example) is responsible for this rapid decay. The dramatic change in T_1 seen in coal is explained by a slowing down of molecular motion. As shown in Figure 2(b), for the very rapid motions encountered in liquids (on about a 10^{-10} -

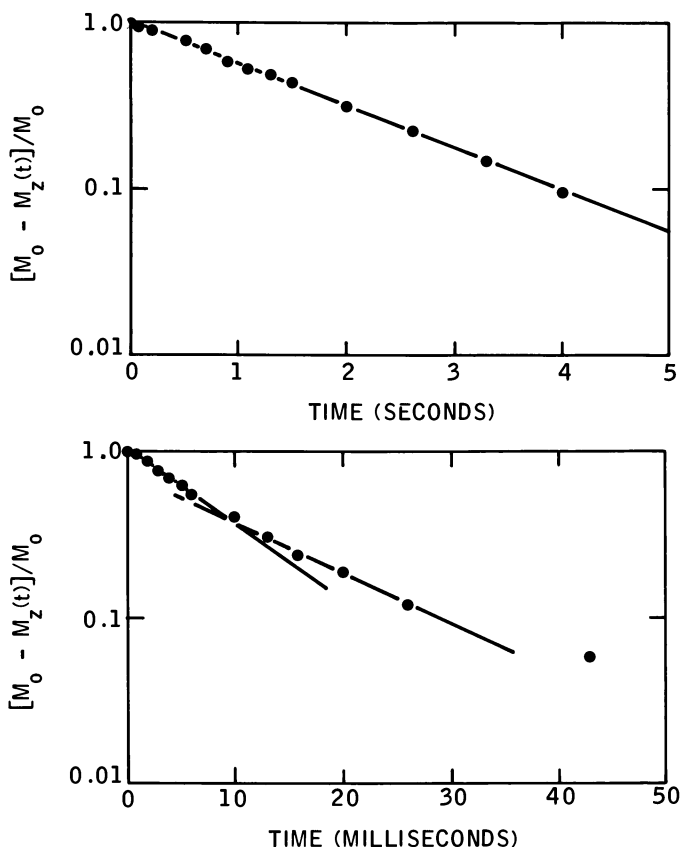


Figure 7. ^{19}F relaxation measurements for 2-fluorophenol: (a) a single long relaxation process is observed in the neat liquid ($T_1 = 1.64$ sec); (b) a much shorter, multiple-component process is seen for these molecules in Illinois No. 6 coal.

sec time scale), T_1 will be long; but a slowing down of motion will bring the characteristic time formation closer to the resonance frequency and reduce T_1 . In the present case the reduction observed, roughly two orders of magnitude, suggests that these times have dropped from about 10^{-10} sec to 10^{-8} sec.

Conclusion

The present paper is intended as a brief summary of the various magnetic resonance tools that can be employed to study molecular motion in coal. Rather than discussing the magnetic resonance theory at length, we have been content to outline the major considerations and indicate the references that provide more details. In the present section we will

summarize our findings about each of the labels and experimental techniques applied and then review the information they provide about the coals themselves.

It is clear that each of the label types discussed here has its own unique virtue. For example, ^{19}F nuclei are ideal probes for use in transient NMR studies. The ^{19}F nuclei are relatively easy to see and the resonance lines are narrow (about 1 G), making them easy to manipulate with radio frequency pulses. By contrast, ^2D nuclei are more difficult to observe, but the ^2D quadrupolar interactions are very sensitive to both the presence and type of molecular motion. While spin labels are chemically complex and sufficiently large that steric effects may retard their motion into coal, their large electron spin is easy to detect at concentrations a thousand times less than those used for NMR studies. Thus these various labels are not competing, but rather complementary, probes of the coal structure. As shown in Figure 8, their concerted use enables us to probe molecular motions varying in rate by more than six orders of magnitude.

These probes have told us a great deal about such molecules in coal. The ^{19}F NMR and ESR experiments bracket the time scales for motion for the molecules we have examined as lying between 10^{-4} sec and 10^{-8} sec. Further, the T_1 measurements of fluorinated molecules in coal reveal several nonequivalent relaxation times. This nonequivalence in motion appears related to nonequivalent positions for these molecules in the coal structure. The fact that C_6D_6 molecules can spin in their plane but not tumble suggests that they are sterically confined, perhaps between planar elements of the coal structure. The fact that C_6D_6 mole-

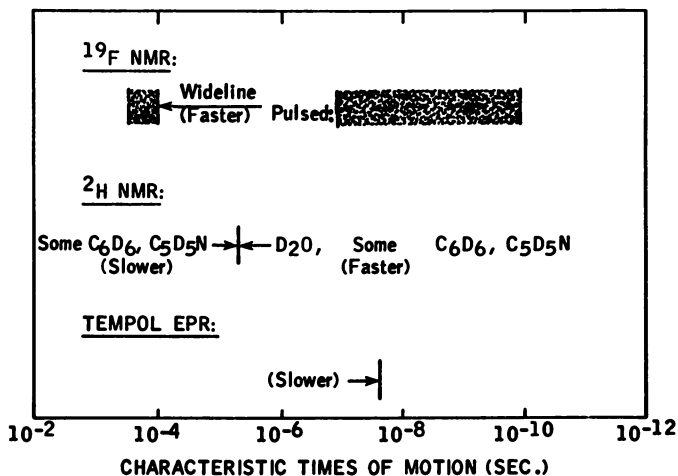


Figure 8. These label techniques cover a wide range of characteristic times of motion.

cules can spin while C_5D_5N molecules cannot suggests that the nitrogen lone pair is interacting with chemical functionalities in the coal matrix. Finally, the TEMPOL studies suggest that surface adsorption and diffusion in the coal structure can be analyzed.

There is clearly much work to be done in refining the chemical and observational techniques outlined here, but we believe that this approach can provide valuable information about the coal structure.

Literature Cited

1. Retkofsky, H. L.; Hough, M. R.; Clarkson, R. B. Chapter 4 in this book.
2. Alemany, L. B.; Handy, C. I.; Stock, L. M. Chapter 14 in this book.
3. Gerstein, B. G.; Murphy, P. D.; Ryan, L. M. Chapter 2 in this book.
4. Bartuska, V. J.; Maciel, G. E.; Schaefer, J.; Stejskal, E. O. *Fuel* 1977, 56, 354.
5. Ladner, W. R.; Stacey, A. E. *Brit. J. Appl. Phys.* 1962, 13, 139.
6. Alekseev, A. D.; Krivitskaya, R. M.; Pestryakov, B. V.; Serebova, N. N. *Khim. Tver. Topl.* 1977, 11, 94.
7. Cruz, M. I.; Letellier, M.; Fripiat, J. J. *J. Chem. Phys.* 1978, 69, 2018.
8. Diehl, P. In "NMR: Basic Principles and Progress"; Springer: Berlin, 1973; p. 1.
9. McConnell, H. M. In "Spin Labeling: Theory and Applications"; Berliner, L. J., Ed.; Academic: New York, 1976; p. 335.
10. Abragam, A. "Principles of Nuclear Magnetism"; Oxford Univ. Press, 1961; chap. 10, p. 525.
11. Bloembergen, N.; Purcell, E. M.; Pound, R. V. *Phys. Rev.* 1948, 73, 679.
12. Kubo, R.; Tomita, K. *J. Phys. Soc. Jpn.* 1954, 9, 316.
13. Van Vleck, J. H. *Phys. Rev.* 1948, 74, 1168.
14. Cohen, M. H.; Reif, F. *Solid State Phys.* 1957, 5, 321.
15. Barnes, R. G. "In Advances in Nuclear Quadrupole Resonance"; Smith, J. A. S., Ed.; Heydon and Sons: London, 1974; p. 235.
16. Silbernagel, B. G.; Gamble, F. R. *J. Chem. Phys.* 1976, 65, 1915.

RECEIVED July 19, 1979.

Nature of the Free Radicals in Coals, Pyrolyzed Coals, Solvent-Refined Coal, and Coal Liquefaction Products

H. L. RETCOFSKY and M. R. HOUGH—U. S. Department of Energy, Pittsburgh Energy Technology Center, P.O. Box 10940, Pittsburgh, PA 15236

M. M. MAGUIRE—Department of Chemistry, Waynesburg College, Waynesburg, PA 15370

R. B. CLARKSON—Varian Associates, Instrument Division, 611 Hansen Way, Palo Alto, CA 94303

Electron spin resonance (ESR) and electron nuclear double resonance (ENDOR) spectrometries were applied to elucidate the nature of the free radicals in coals, heat-treated coals, and selected coal conversion products. It was found that particular attention must be paid to sample preparation to ensure reliability of the spectral data. For example, failure to prevent electrical contact between particles of heat-treated coals may lead to grossly inaccurate g values, and ENDOR hyperfine lines have been found to disappear in unevacuated coal samples. ESR g values and ENDOR couplings for coals provided considerable information with regard to the aromatic and heteroatomic nature of the radicals. Experiments were conducted to show that the ESR and ENDOR resonances both originated from the organic matter rather than from the inorganic matter in coal. Changes in the quantity and nature of the free radicals during coal liquefaction in the Pittsburgh Energy Research Center's 400-lb coal/day process development unit were determined by applying the ESR and ENDOR techniques to samples of the process coal, preasphaltenes, asphaltenes, and coal-derived oils.

Characterization of the stable radicals present in coals, pyrolyzed coals, and liquefaction and other coal conversion products is a necessary first step toward elucidating the role of radicals in coal liquefaction. Electron

spin resonance (ESR) spectrometry has proved to be a powerful instrumental tool to probe the nature of these radicals (1, 2, 3). Recently, it was shown that coals and coal-derived materials are also amenable to study by electron nuclear double resonance (ENDOR) spectrometry (4, 5). The ENDOR technique is becoming increasingly popular in free radical studies because frequently the resulting spectra are much more highly resolved than corresponding ESR spectra of the same materials (6). During the present investigation, ESR and, to a lesser extent, ENDOR spectrometries were applied to (a) a series of vitrains from selected coals; (b) a high-volatile bituminous coal heat-treated to various temperatures; (c) five samples of solvent-refined coal (SRC); and (d) several coal-derived materials produced by liquefaction of selected coals in the Pittsburgh Energy Technology Center's 400-lb coal/day process development unit.

Experimental

Samples. Most of the vitrains studied were of high petrographic purity, although several are described more appropriately as vitrain-rich samples. Sixty-three vitrains, including samples from Antarctica, Austria, Canada, Germany, Japan, Pakistan, Peru, the United States, and Yugoslavia were investigated. Petrographic characterization and other properties of many of these samples were published previously (7).

Ireland Mine hvAb coal was used in the coal pyrolysis studies. The method of heat treatment was essentially that reported by Petrakis and Grandy (8). Ireland Mine coal was also the feed coal used to obtain most of the coal liquefaction products. The coal-derived liquids investigated were centrifuged liquid products (CLP) and their subfractions from selected runs in the Pittsburgh Energy Technology Center's 400-lb coal/day coal liquefaction process development unit (PDU) (9).

The solvent-refined coal samples examined were from the Wilsonville SRC plant and were provided generously by Larry Taylor of the Virginia Polytechnic Institute and State University.

Spectral Measurements. For the ESR measurements, solid samples were ground to particle sizes between 44 and 74 μm , diluted as needed with silicon dioxide or potassium bromide, degassed at 10^{-4} Pa and sealed in quartz sample tubes. Spectra were obtained using either a Varian Associates Model V-4500 or an E-112 spectrometer equipped with a dual cavity. (Reference to brand names is to facilitate understanding and does not imply endorsement by the U.S. Department of Energy.) The resonant frequency of the cavity (~ 9.5 MHz) was determined with an EIP Model 3500 microwave counter. A glass capillary containing a buffered aqueous solution of peroxyaminedisulfonate was used to calibrate both the magnetic field at the sample and the field scanning rate. Spin concentrations were determined by comparing spectral intensities with that of a dilute mixture of diphenylpicrylhydrazyl in silicon dioxide.

A Varian Associates Model E 1700 spectrometer operating at a nominal frequency of 9.26 GHz was used in the ENDOR studies. The rf pulse frequency was 34.7 Hz and the magnetic field was modulated at a frequency of 1000 Hz. ENDOR measurements were made on both unevacuated samples and samples evacuated to 10^{-4} Pa.

Results and Discussion

Coals. GENERAL FEATURES OF ESR AND ENDOR SPECTRA OF COALS. ESR spectra of coal vitrains usually consist of a single, more or less symmetrical resonance near $g=2$ (Figure 1). Spectral fine structure resulting from electron coupling with neighboring magnetic nuclei has never been observed (10). ESR spectra of raw coals and impure vitrains frequently show a narrow peak in addition to the usual vitrain resonance. An example is shown in the upper portion of Figure 2. The narrow signal, attributed to the presence of fusain (a lithotype commonly found in U.S. coals), broadens and merges with the broader vitrain signal when air is admitted to the sample (11). The narrow signal is not seen in the ESR spectra of soluble material extracted from the coal because of the insolubility of fusain (bottom of Figure 2).

Spectral line widths, as measured from peak-to-peak on the derivative of the ESR absorption curve, may vary from a few tenths of a gauss to nearly one hundred gauss depending on the rank of the coal (1, 2, 3, 8, 10, 11). For coals having carbon contents between 55 and 90%, peak-to-peak line widths range from ~ 5.2 to ~ 8.6 . A gradual increase in line width with increasing carbon content is observed first; this trend is

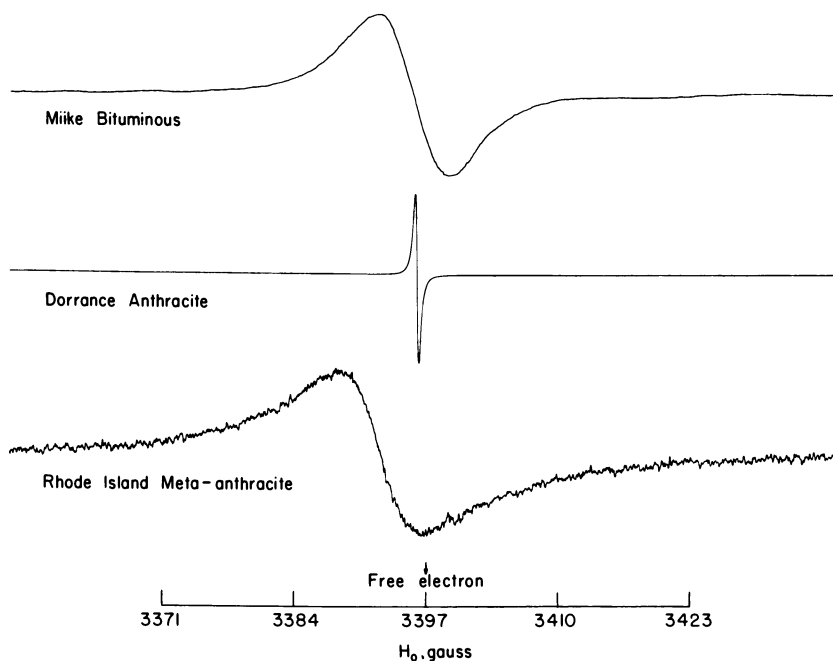


Figure 1. The 9.5-GHz ESR spectra of selected coals

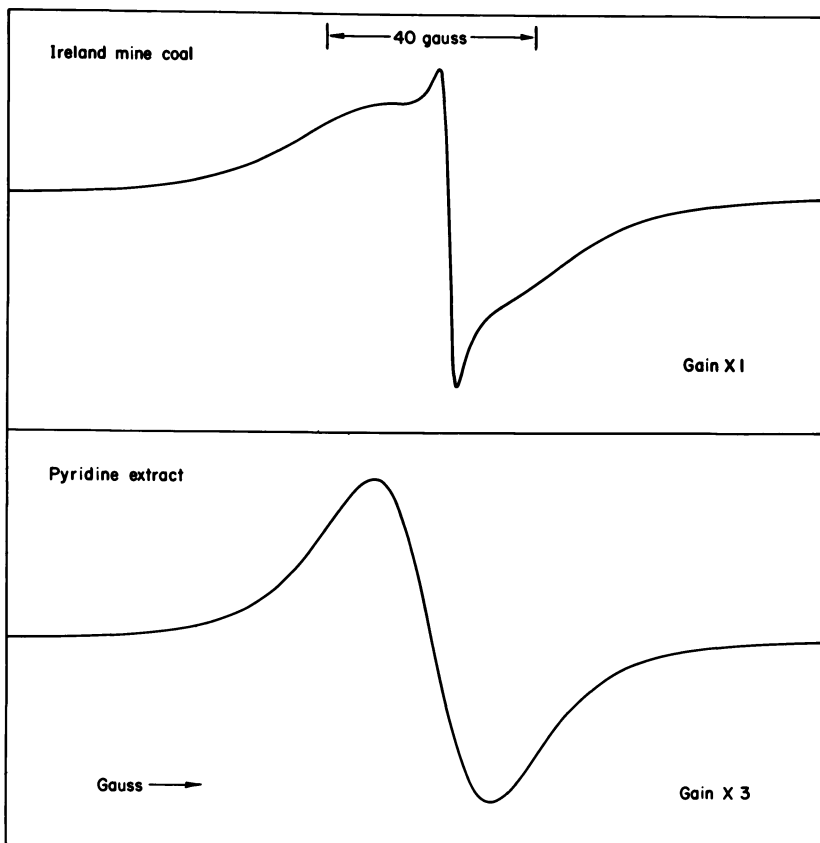


Figure 2. The 9.5-GHz spectra of West Virginia (Ireland Mine) hvAb coal and its pyridine extract

reversed at a carbon content of $\sim 80\%$. The rate of decrease becomes very rapid for coals having carbon contents between 90 and 95%; line widths of only a few tenths of a gauss have been measured for several such coals. Coals of the very highest rank, i.e., meta-anthracites, with carbon contents generally in excess of 95%, often exhibit very broad ESR resonances. This general trend in spectral line width (and in other spectral parameters) which is observed for coals also is exhibited by heat-treated coals and low-temperature organic chars in plots of ESR data as a function of pyrolysis temperature (12).

The g value (spectroscopic splitting factor), a very important ESR spectral parameter that is sensitive to the molecular environment of an unpaired electron, unfortunately was treated only casually in early coal studies. The utility of the parameter in coal research is becoming more apparent as more precise values become available. A plot of the ESR g

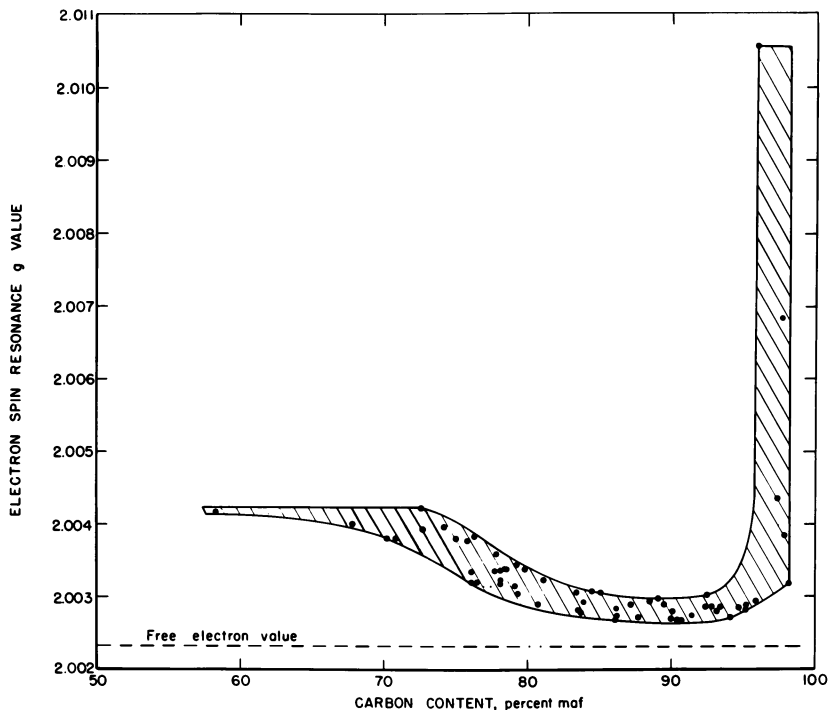


Figure 3. ESR g values of vitrains from selected coals

values of coals as a function of carbon content is reproduced in Figure 3. Certain anthracitic coals have been reported to exhibit anisotropic g values (10, 13).

The integrated intensities of ESR signals can be used to estimate the number of unpaired electrons in materials. For coals, the concentrations of unpaired electrons rise nearly exponentially with increasing coal rank up to approximately 94% C, after which the spin concentrations decrease rapidly. The variation of spin concentration with coal rank has been observed by a number of researchers (11–15).

In contrast to the lack of resolution in ESR spectra of coals, ENDOR spectra are rich in detail. For example, five well-resolved hyperfine lines above and three below the free proton frequency (14.1 MHz) are clearly evident in the ENDOR spectrum of vitrain-rich Pittsburgh coal shown in Figure 4. This observation was quite surprising in light of recently published spectra that showed only a single matrix ENDOR resonance near the free proton frequency (4). During experiments designed to deduce the reasons for this apparent discrepancy of results, a reversible effect of air (oxygen?) on the ENDOR spectrum was discovered, i.e., the hyperfine lines were observed for evacuated samples

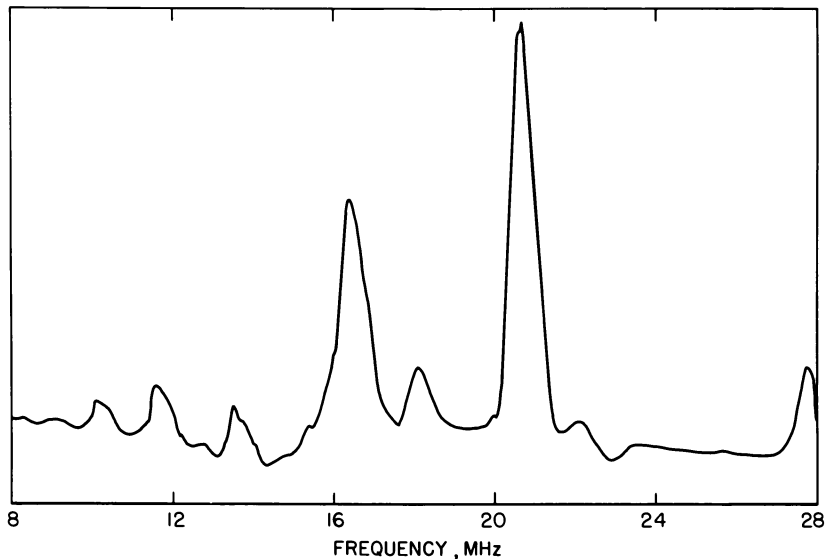


Figure 4. ENDOR spectrum of vitrain-rich Pittsburgh coal

but disappeared upon admission of air. Presumably, the presence of paramagnetic oxygen results in a decrease of the electron relaxation times, leading to broadening of spectral lines beyond the point of detection. Similar, albeit less pronounced, effects have been observed in ESR spectra of high-rank coals (1) and certain petrographic constituents of coals (13).

ORIGIN OF THE ESR SIGNALS. *Organic Materials or Mineral Matter?* The basic question, "Are the origins of the ESR signals in coal organic or inorganic?" has never received a completely satisfactory answer. In an attempt to resolve this matter, ESR spectra of a coal and its low-temperature ash were obtained under precisely identical spectrometer conditions. The results, shown in Figure 5, indicate that the $g=2$ signal observed in the spectrum of the coal does not appear in that of the ash. The ash, of course, should be free of the organic matrix of the original coal. This suggests strongly, but does not prove conclusively, that the spectrum of the coal results from organic species. It can be argued that mineral matter could still be responsible for the resonance and that it simply has been altered during the process of low-temperature ashing.

To pursue this issue, the coal and ash samples were examined under higher modulation and increased gain to enhance the signal-to-noise in the ESR spectra; the results are shown in Figure 6. Of special interest are the broad resonance at low field (left side of figure), the four sharp

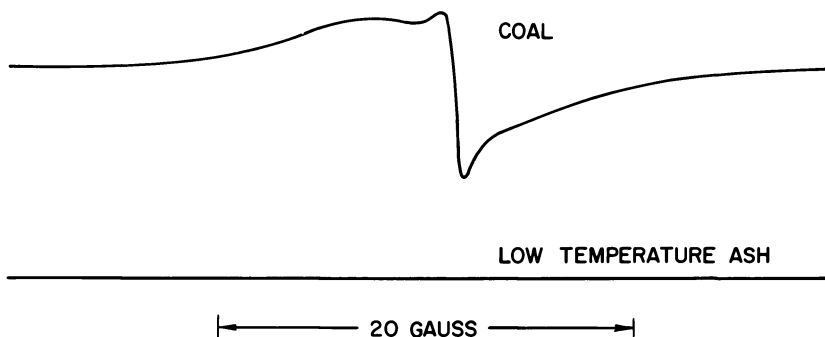


Figure 5. The 9.5-GHz ESR spectra of Kentucky, Homestead Mine, hvAb coal and its low-temperature ash

resonances flanking the $g=2$ resonance of the coal (center of figure), and the two sharp resonances in the spectrum of the low-temperature ash corresponding to two of the four lines observed in the coal spectrum. The low-field line appears near $g=4$ and is assigned tentatively to the presence of high-spin iron(III) in both the coal and the ash. Wooten et al. observed a similar $g=4$ resonance in the ESR spectrum of a frozen solution of solvent-refined coal in tetrahydrofuran (16).

The sharper lines near $g=2$ are thought to be components of the Mn(II) six-line electron-nuclear spin-spin multiplet. Manganese, having a spin quantum number of $5/2$, would give rise to a six-line pattern. Both the spacing of the lines (hyperfine coupling) and the g value estimated from the coal and ash spectra agree with published values (17). Mn(II) also has been identified in hydrogenated coal product fractions (18).

The above results, considered collectively, are strong evidence that the ESR signals in coals originate from organic matter. To summarize; (1) the $g=2$ coal resonance does not appear in the spectrum of low-temperature ash from the coal and (2) at least for Fe(III) and Mn(II), the ESR resonances of the mineral matter are of very low intensity in the coal spectrum and do not appear to be altered during the ashing procedure. The fact that the principal resonance appears at $g=2$ also supports the organic hypothesis.

The ENDOR signals, on the other hand, are almost assuredly organic in nature. As pointed out by Schlick et al. (4), "The very observation of a proton matrix ENDOR line shows interaction of the electron with nearby protons." That these protons are associated with organic structures is a logical extension since the hyperfine lines observed are characteristic of ENDOR spectra of organic free radicals. The sharpness of the ENDOR lines was completely unexpected and indicates that either the radical sites are isotropic or there is motional narrowing of an anisotropic site.

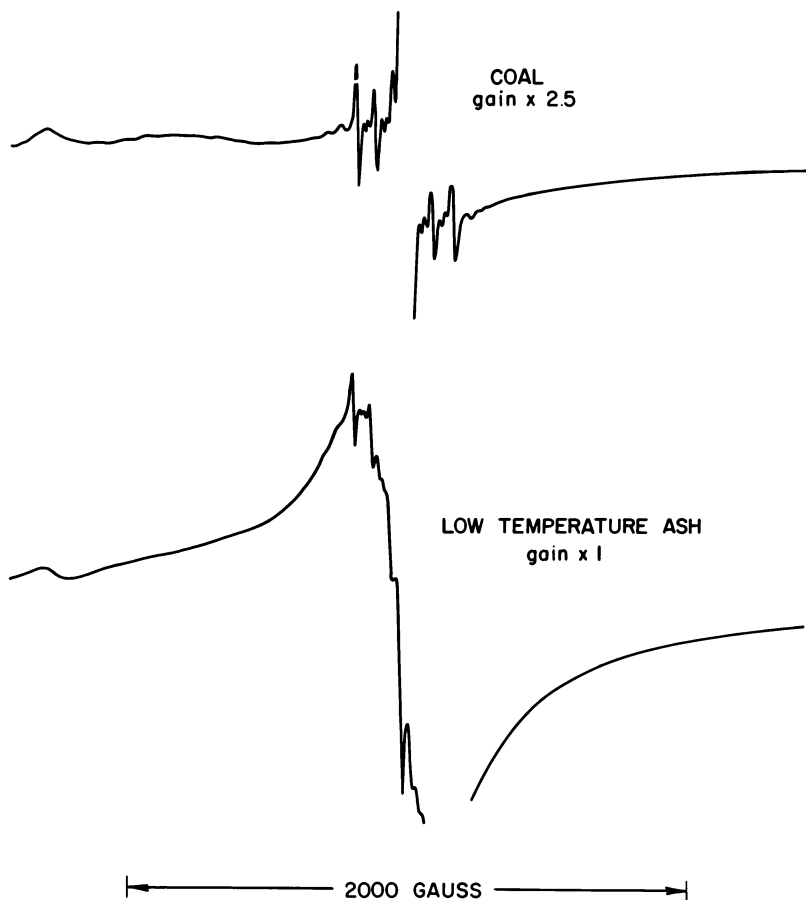


Figure 6. The 9.5-GHz ESR spectra of Kentucky, Homestead Mine, hvAb coal and its low-temperature ash (spectra obtained at higher gain than Figure 5)

Free radicals or charge transfer? Although the ESR spectra of coals and coal derivatives generally are attributed to free radicals, the possibility of charge-transfer interactions, particularly in the cases of coal (19) and coal- (13, 20) and petroleum-derived asphaltenes (21, 22), has been considered. ESR studies have shown that, while charge-transfer interactions may be important in petroleum asphaltenes (21, 22), their role as binding forces in coal-derived asphaltenes is a relatively minor one if existent at all (13). The evidence for these conclusions is based on variable-temperature ESR studies and ESR intensity additivity studies.

Free radicals generally exhibit ESR intensities that obey the Curie law ($I=CT^{-1}$). Although ESR intensities of coals have been reported to increase with decreasing temperature as required by Curie's law (12, 23),

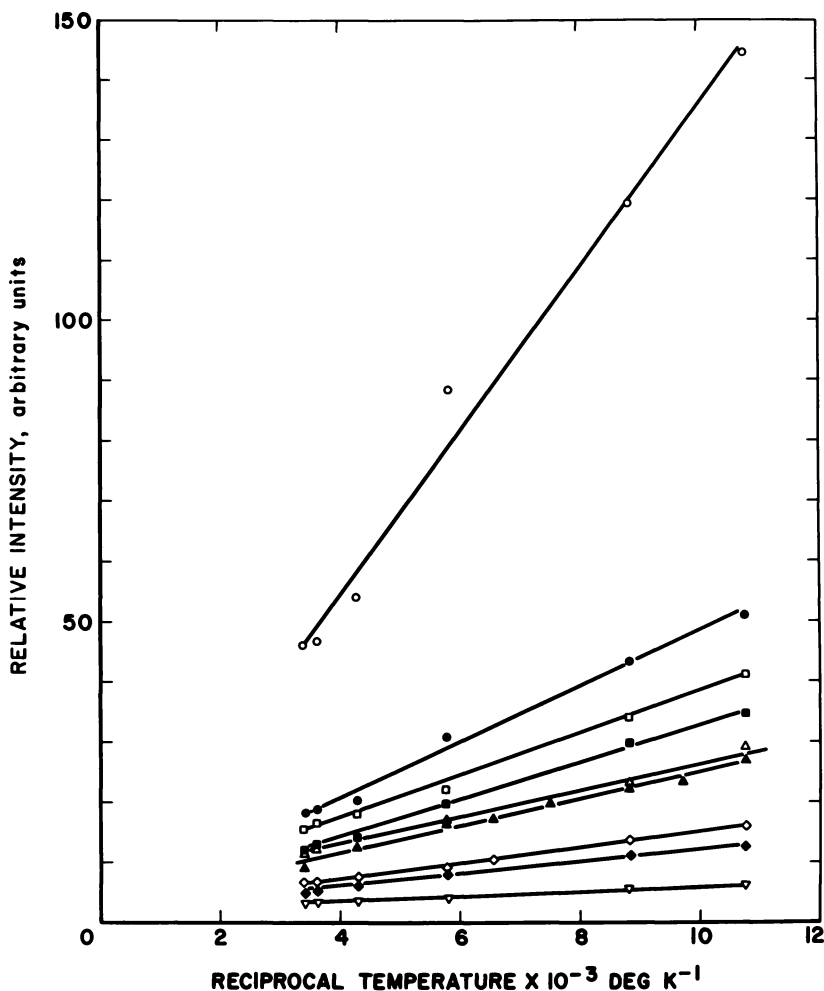


Figure 7. Variable temperature ESR data for selected coals: (∇) peat, 61.2% C; (\blacklozenge) lignite, 71.2% C; (\diamond) Adaville vitrain, 76.3% C; (Δ) Homestead Kentucky coal, 77.6% C; (o) Dorrance coal, 92.7% C; (\blacktriangle) Ireland Mine Coal, 78.5% C; (\blacksquare) Pittsburgh vitrain, 82.6% C; (\square) Lower Banner No. 2 vitrain, 86.1% C; (\bullet) Pocohontas No. 3 vitrain, 90.0% C

no systematic studies have been published. During the present investigation, temperature dependencies of ESR intensities were determined for vitrains from nine coals. The results, presented graphically in Figure 7, show that each coal investigated exhibits Curie law-type behavior (at least down to liquid nitrogen temperature) in support of the free radical hypothesis. It is emphasized that the evidence must be regarded as supportive and not conclusive, as Curie law behavior is also observed for species other than free radicals, e.g., dilute transition metal ions.

NATURE OF THE FREE RADICALS. *Aromatic?* Once the free radical hypothesis is accepted, the nature of the radicals remains to be deduced. Early workers postulated that the relationship between ESR intensities and coal rank results from the formation of radicals through chemical reactions or degradations and subsequent stabilization of the radicals by resonance in the aromatic portion of the organic structure of coal. Resonance stabilization would be greatest for coals containing the larger condensed polynuclear aromatic structures. Thus, the exponential change in the ESR intensities of coals with increasing rank (up to coals having carbon contents <94%) is in agreement with behavior expected on the basis of commonly accepted views on coal metamorphism, that is, both the carbon aromaticity and the average size of the aromatic lamellae of coals increase with increasing rank. This explanation remains a very tenable one and no convincing arguments to the contrary have been presented.

The magnitude of the electron-nuclear hyperfine constants for coals as determined by ENDOR spectrometry (*see* Table I) is also strong evidence for the existence of aromatic free radicals in the samples. The hyperfine couplings are all quite small, i.e., less than 10 G, as would be expected for radicals in which the unpaired electrons are largely delocalized as, for example, over aromatic rings. Kevan and Kispert (24) explicitly stated "In aromatic radicals proton coupling constants are always less than 10 G. . .". The statement is supported by a wealth of experimental data (6, 25-28). Hyperfine couplings between unpaired electrons and ring protons in hydrocarbon free radicals seldom exceed 5-6 G. The three vitrains examined each have well-resolved hyperfine lines (Table I) that no doubt result from such structures.

The lack of large hyperfine couplings (18-27 G) in the ENDOR spectra of coals is interesting from another point of view. It precludes the existence of radicals having their unpaired spins strongly localized on

Table I. Electron-Nuclear Hyperfine Constants for Vitrains from Selected Coals as Determined by ENDOR Spectrometry

A (G)		
<i>Adaville</i> (SubA-76.3% C)	<i>Pittsburgh</i> (hvAb-82.6% C)	<i>Pocahontas No. 4</i> (lvb-90.4% C)
0.4	0.4	0.4
1.6	1.6	1.6
1.9	—	—
3.0	2.9	3.0
4.6	4.6	4.7
—	5.9	5.7
6.9	—	—
9.7	9.8	—

specific carbon atoms as in alkyl radicals. It is of further interest that hyperfine couplings in the range 14.5–16.4 G, such as those reported for the α carbons in benzylic radicals (28), are also absent in the ENDOR spectra of the coals investigated in this study.

Heteroatomic? Coals, especially low-rank coals that are rich in oxygen, might be expected to contain heteroatomic free radicals. Yen and Sprang (29) showed that the g values of coals as well as those of other bituminous materials showed a systematic trend with their heteroatom content. In particular, they plotted the ESR g values as a function of $\sum \xi_n X_n$ where X refers to the atom fractions of oxygen, nitrogen, and sulfur in the coals and ξ values are spin-orbit coupling constants of the respective atoms, i.e., $\xi_O \sim 152 \text{ cm}^{-1}$, $\xi_N \sim 70 \text{ cm}^{-1}$, and $\xi_S \sim 382 \text{ cm}^{-1}$. This treatment of the data is based on the well-accepted view that deviations of the g values of organic free radicals from that of the free electron ($g = 2.002319$) are greatest for those radicals in which the unpaired electrons are localized or partially localized on atoms having strong spin-orbit interactions.

The relationships between the g values of coals and coal rank (13) and between g values and carbon contents (Figure 3) are reasonably well understood. The high g values observed for peats and lignites can be interpreted in terms of the presence of aromatic radicals, with some partial localization of the unpaired electrons on heteroatoms, particularly, but not exclusively, oxygen. As coalification progresses the g values decrease, suggesting that the radicals become more hydrocarbon-like. The g values of many of the vitrains from bituminous and young anthracitic coals compare favorably with those exhibited by aromatic hydrocarbon radicals. During the final stages of coalification the g values become quite large, as one would expect if continued condensation of the aromatic rings into graphite structures occurs. The observation of a small, but reproducible, anisotropy in the g value of certain anthracites (with respect to the bedding plane of the coal) (13) suggests that some ordering of the polynuclear condensed aromatic rings is occurring.

Evidence supporting the heteroatom hypothesis is depicted in the plots of Figure 8. The near-linear plot observed for g values vs. oxygen contents of the coals suggests that the unpaired electrons in low-rank coals interact with oxygen atoms in the sample. Statistical treatment of the data revealed that the g values of only two of the coals fall outside the area bounded by the dashed lines drawn plus or minus twice the standard error of estimate from the linear regression line. These two coals are somewhat unique in that they contain an unusually high content of organic sulfur (30, 31). In the second plot of Figure 8, the abscissa has been changed to reflect the sum of the oxygen and sulfur contents of the coals (each element being weighted according to its spin-orbit coupling constant). This latter plot exhibits a much smaller ($\sim 10\%$) standard error of estimate suggesting that the unpaired electrons interact with sulfur as well as with oxygen. Attempts to extend the statistical treat-

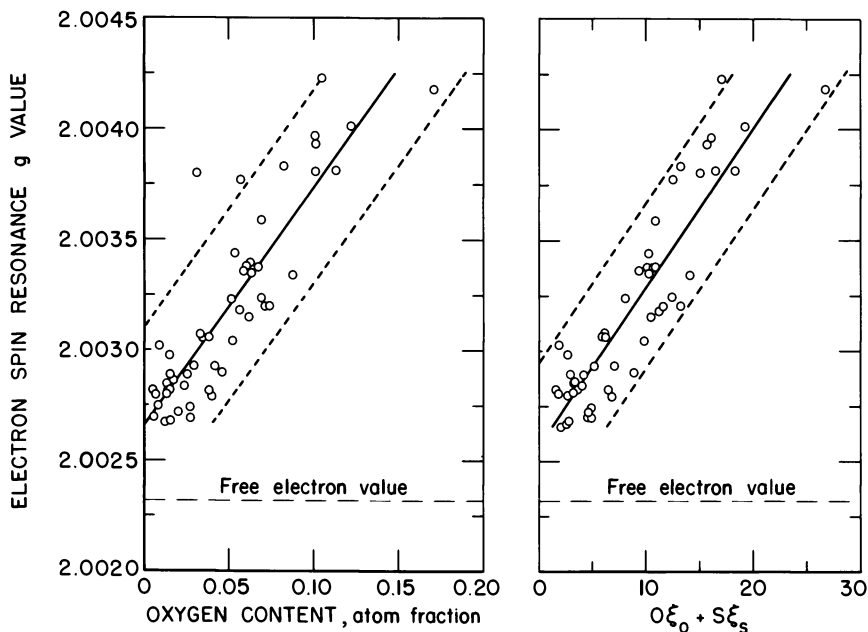
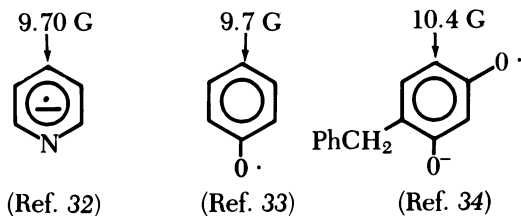


Figure 8. Functional dependencies of the ESR g values of vitrains from selected coals

ment to nitrogen in the samples were inconclusive. Thus, oxygen and sulfur atoms appear to play important roles in the structure of the naturally occurring free radicals in low- and medium-rank coals. The ENDOR results provide additional evidence supporting this view.

As stated earlier, the hyperfine coupling constants for coals (Table I) are within the range commonly attributed to aromatic free radicals. The largest of these couplings (9.8 G) and its variation with coal rank (at least for the three coals examined) favor the heteroatom concept, i.e., the radicals become more hydrocarbon-like as coalification progresses. As discussed previously, the <5–6 G hyperfine lines undoubtedly result from ring couplings not influenced by heteroatoms. Couplings of 9–10 G, as observed for the subbituminous and hvAb coal, are not unusual for heteroaromatic free radicals or for aromatic radicals with heteroatom substituents. A few examples are shown:



The fact that the 9.8 G coupling is observed for the subbituminous and high-volatile bituminous coals, which have high heteroatom contents (18.5 wt % and 11.4 wt %, respectively (35)), and not for the low-volatile bituminous coal, which contains only 3.6% (35), suggests that its assignment to a heteroatomic radical is not unreasonable.

Pyrolyzed Coals. A fundamental understanding of coal pyrolysis may assist in elucidating the mechanism of coal liquefaction since the primary step in each process is thought to involve thermal decomposition of coal to produce free radicals. Several investigators have applied ESR techniques to heat-treated coals (1, 2, 3, 8, 15). However, recent reports (36, 37) cast doubts on the validity of some of the published data. In particular, it was found that failure to grind and dilute samples of heat-treated coals with an electrically nonconducting medium can result in grossly inaccurate g values. For example, two groups of investigators (8, 15) have reported g values less than that of the free electron for certain coals heat-treated at commonly used liquefaction temperatures. The low g values are quite reproducible but unfortunately reflect an apparent rather than a true g value because of electrical contact between the semiconducting heat-treated coal particles.

ESR g values for West Virginia (Ireland Mine) hvAb coal heat-treated at four different temperatures are shown graphically in Figure 9. The points connected by the dashed lines represent the results of measurements made on neat samples after heat treatment. The general shape of this curve has been established for other coals (8, 15). The point for the sample heat-treated at 450°C falls considerably below the free electron value; similar results for other coals have been attributed to the formation of sigma radicals during heat treatment (8). Three experiments were conducted to show that this observed g value was an apparent and not a true value.

Singer (38) pointed out that ESR characteristics of materials that have electrical resistivities less than 10 ohm-cm can be dominated by their electric rather than their magnetic properties. If the dimensions of particles in such samples are of the order of, or greater than, the microwave skin depth, decreases in ESR signal intensities, changes in line shape, and shifts in signal position (apparent g value) may occur. The most practical solution to the skin depth problem is to obtain particles of a size less than a skin depth and disperse them with an insulating material. In this manner, all parts of the volume of the conductive specimen are exposed to the microwave fields, and the resulting ESR signal is identical to that which would occur if the spins were contained in an insulator.

Since the resistivity of coals decreases sharply with increasing pyrolysis temperature (39), conductivity effects on ESR measurements should be anticipated. To investigate this possibility, the sample was ground under nitrogen to pass 200 mesh and diluted with electronic grade silicon

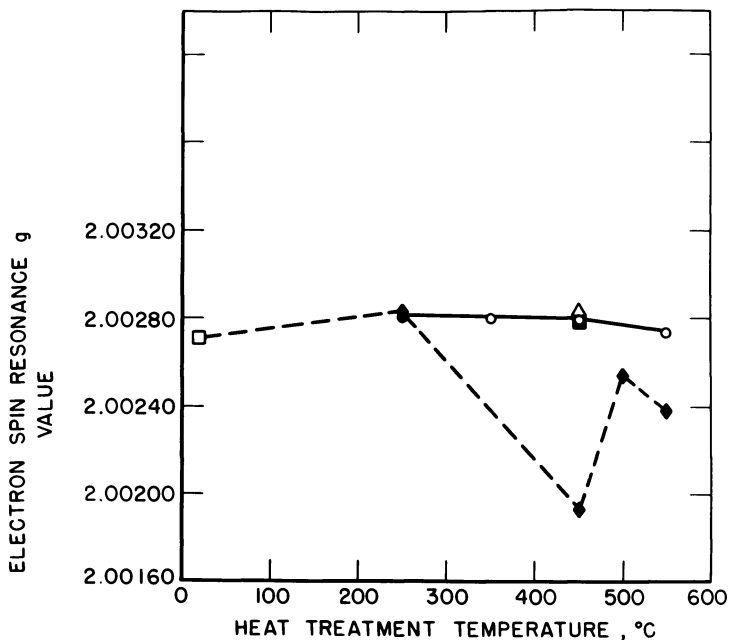


Figure 9. ESR g values for heat-treated Ireland Mine hvAb coal: (◆) measurement made on neat samples after heat treatment; (■) measurement made on sample of 1% heat-treated coal in KBr; (Δ) measurement made on sample of 1% heat-treated coal in SiO₂; (○) measurement made on sample of coal heat treated in the presence of KBr; (□) sample not heat treated

dioxide to prevent electrical contact between the coal particles. The result, designated by the open triangle in Figure 9, indicates that the actual g value for the sample is 2.0028, which is higher than that of the free electron. To ensure that this variation of g value with sample dilution was not attributable to interaction with the silicon dioxide, several measurements were made using a second diluent, potassium bromide. The g value was found to be independent of the diluent used (Figure 9, point represented by the darkened square). As a third check, a sample of unheated coal was diluted with potassium bromide prior to heat treatment. ESR measurement made on the mixture after heat treatment at 450°C gave a g value (Figure 9, open circle) quite comparable to those for the samples that were diluted after heat treatment. Thus, there is little doubt that the low g values sometimes reported for heat-treated coals reflect the physical properties of the samples and not the chemical nature of the radicals involved.

To establish the true relationship between ESR g values and coal heat treatment, samples of Ireland Mine coal diluted with potassium bromide were heat-treated at different temperatures. The results, represented by the open circles in Figure 9, show that the g value is

essentially independent of heat-treatment temperature, at least up to 550°C, and suggest that the sigma radical hypothesis requires re-examination.

Solvent-Refined Coal. The solvent-refined coal (SRC 1) process (40) produces a low-sulfur, low-ash solid fuel from coal. Through the courtesy of L. Taylor, samples of SRC produced from five different feed coals were made available to us for ESR studies. Each of the five samples gave a strong ESR resonance near $g=2$; g values and spectral line widths are summarized in Table II. The g value and line width data, viewed collectively, suggest the presence of organic free radicals, with only minor interaction (except possibly for the Monterey sample) between the unpaired electrons and heteroatoms in the samples.

Coal Liquefaction Products. The materials discussed in this section were obtained from the U.S. Department of Energy's 400-1b coal/day PDU located at the Pittsburgh Energy Technology Center. The PDU was designed to convert a high-sulfur, high-ash bituminous coal into a low-sulfur, low-ash boiler feed. The process uses a unique reactor system to accomplish a mild hydrogenation of the feed coal. Basically, a feed paste consisting of 35% coal and 65% vehicle oil (recycled product oil) is passed in a rapid, turbulent flow of hydrogen through a preheater and then through a fixed-bed catalytic reactor. The catalyst used is a commercial $\text{CoO-MoO}_3\text{-SiO}_2\text{-Al}_2\text{O}_3$ catalyst in the form of 1/8 in. \times 1/8 in. cylindrical pellets, although sometimes the PDU is operated with the catalytic reactor packed with glass beads rather than catalyst. The product, formerly referred to as SYNTHOIL, is initially separated from gaseous and low-boiling liquid components in liquid receivers. The primary liquid products are separated from solid materials (primarily mineral matter) by centrifugation, yielding the centrifuged liquid product (CLP). More detailed descriptions of the process are given elsewhere (41, 42).

COAL-DERIVED ASPHALTENES. Asphaltene, operationally defined as the fraction of a coal liquefaction product that is soluble in benzene and insoluble in pentane (or hexane), are considered by many to be key intermediates in the conversion of coal to oil-like products (43, 44). Recently it was reported that coal-derived asphaltene consist of

Table II. ESR g Values and Spectral Line Widths for Selected Samples of Solvent-Refined Coal

<i>Process Coal</i>	<i>g Value</i>	<i>Line width (G)</i>
Amax	2.0027 ₂	6.1
West Kentucky	2.0027 ₇	6.3
Pittsburgh	2.0029 ₂	7.0
Illinois No. 6	2.0029 ₈	7.5
Monterey	2.0030 ₇	8.5

hydrogen-bonded complexes that can be separated into their acidic and basic components (45). As pointed out previously, the hypothesis that charge-transfer interactions rather than hydrogen bonding are the predominant building forces between the acid and base components (20) is not supported by ESR measurements (13).

An important point that cannot be overly emphasized is that coal-derived asphaltenes and petroleum asphaltenes are considerably different materials. Other than the fact that they are derived using essentially the same solvent fractionation scheme, the two have little in common. For example, asphaltenes from the liquefaction of coal are known to be much more highly aromatic (46) than asphaltenes from petroleum (47, 48). During the present investigation, it was determined that the ESR behavior of the two types of materials is also quite different.

The temperature dependencies of ESR intensities for the known free radical diphenylpicrylhydrazyl (DPPH), a coal-derived asphaltene separated from the CLP obtained from a coal liquefaction run in the Pittsburgh Energy Technology Center's 400-lb coal/day PDU, the acid and base subfractions from the coal-derived asphaltene, and asphaltenes separated from Baxterville crude oil are shown in Figure 10. DPPH and the coal-derived materials each exhibit Curie law-like behavior, although the temperature dependencies of the coal-derived materials suggest that a Weiss constant may be involved. In contrast, the petroleum asphaltene displays a rather complex temperature behavior. Previous work has shown that the plot for the petroleum asphaltene can be resolved into two components, one representing the contribution of doublet states, the other the contribution from singlet-triplet states (22). Thus, ESR measurement also indicates little similarity between the coal- and petroleum-derived materials.

ESR g values and spectral line widths for selected coal-derived asphaltenes and their acid and base subfractions are given in Table III and, as might be expected, are quite similar to those given in Table II for SRC samples. In previous work it was shown that the number of unpaired electrons (at room temperature) in the basic subfraction exceeded that in the acid/neutral fraction by a factor of nearly 20. The concentrating of radicals in the basic fraction most probably results from resonance stabilization of the radicals by aromatic and heteroaromatic rings. The higher ESR g value of the base fraction and its higher nitrogen content (45) and carbon aromaticity (49), coupled with the fact that it contains most of the nitrogen base structures, provide strong support for this view.

In an attempt to further elucidate the nature of the free radicals, ENDOR spectra of the asphaltenes were obtained. Unfortunately, these spectra revealed no hyperfine lines and consisted only of a matrix peak as was found for solvent-refined coal (4).

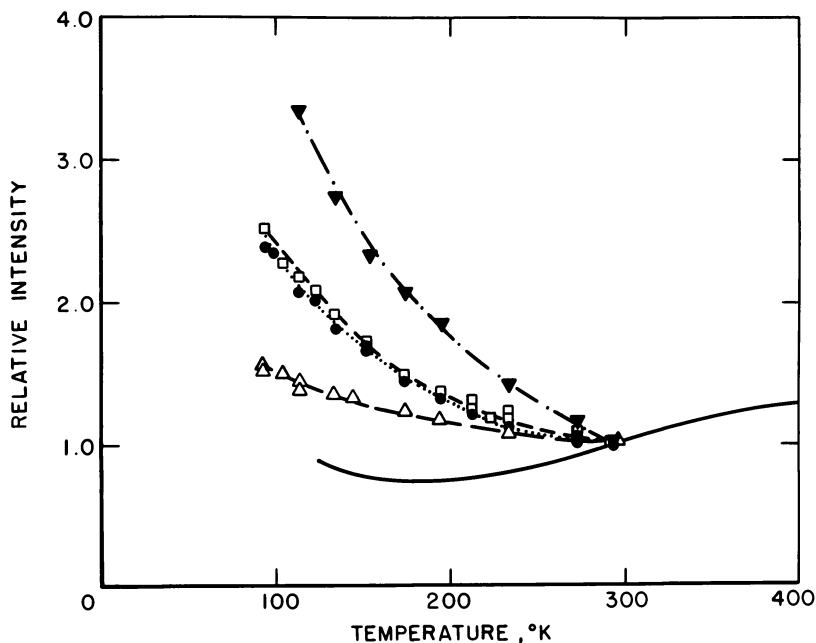


Figure 10. Variable temperature ESR data for coal- and petroleum-derived asphaltenes: (●) SYNTHOIL asphaltenes; (Δ) SYNTHOIL asphaltene acids; (□) SYNTHOIL asphaltene bases; (▼) DPPH; (—) Baxterville, petroleum asphaltene (22)

COAL-DERIVED OILS. Coal-derived oil from the solvent fractionation of CLP from the 400-lb coal/day PDU described previously exhibits a slightly higher g value, a broader spectral line, and a significantly lower spin concentration than the process coal from which it was derived (36). Only a limited number of oils have been examined by ESR; additional work is needed before the results can be generalized.

Table III. ESR g Values and Spectral Line Widths for Selected Asphaltenes and Acid/Base Subfractions

Material	g value	Line width (G)
West Virginia Feed Coal		
Asphaltenes	2.0030 ₂	6.8
Acid/Neutrals	2.0029 ₄	6.6
Bases	2.0030 ₉	6.4
Homestead Kentucky Feed Coal		
Asphaltenes	2.0028 ₆	7.5
Acid/Neutrals	2.0028 ₇	8.2
Bases	2.0030 ₂	6.3

ENDOR results on the oil (Figure 11), although preliminary, are quite interesting in terms of their temperature dependence. Two hyperfine lines flank the free proton frequency at 0°C; no matrix line is observed since the sample is fluid. As the temperature is reduced from 0° to -40°C, a matrix peak appears and slowly grows in intensity, while the two hyperfine lines ($A = 1.3$ G) gradually lose intensity and shift toward and finally coalesce with the matrix peak. This suggests a transition from a freely rotating radical(s) to a more rigid one. The widths of the ENDOR transitions indicate that these observed molecular dynamics are on the order of 10^{-6} sec.

CHANGES IN THE QUANTITY AND NATURE OF FREE RADICALS DURING COAL LIQUEFACTION. Although the actual reaction mechanisms involved in the liquefaction of coal via any process remain elusive, proposed mechanisms frequently invoked the formation of preasphaltenes and asphaltenes as intermediate steps. For this reason, ESR measurements were made for the series,



The sequence depicted is not meant to exclude reversible and/or parallel reactions. The results of the ESR measurements are shown in Figure 12. Spectral line widths increase in the order coal, preasphaltenes, asphaltenes, oil, which crudely parallels the hydrogen contents of the materials. ESR characteristics of the process coal and the preasphaltenes, particularly the number of free spins, are surprisingly similar, suggesting that radicals formed by thermolysis are quickly capped. Grandy and Petrakis (50), in a recent ESR study of SRC, concluded that many of the thermally produced radicals are stabilized by hydrogen during the liquefaction process. The free radicals in the asphaltene fraction of the product from the PDU at PETC are characterized by a higher g value and a reduced number of spins in comparison with the process coal and preasphaltenes. The asphaltene radicals undoubtedly contain structures in which the unpaired electrons interact with heteroatoms associated with aromatic units. The oil fraction has the lowest concentration of free radicals, the largest ESR spectral line width, and a g value intermediate between those of the process coal and the asphaltene fraction. Goldberg et al. (18) recently have reported an ESR investigation of the products from the hydrogenation of Loveridge Mine coal (81.8% C). For experiments carried out under hydrogen, using tetralin as a hydrogen transfer agent, they found that the asphaltene fraction exhibited a higher g value, a larger spectral line width, and a lower spin concentration than the starting coal, as was found in the present study of the liquefaction of Ireland Mine coal. Analogous data for materials from liquefaction processes now under serious consideration by the U.S. Department of Energy for extensive scale-up now are being obtained and will be reported in the near future.

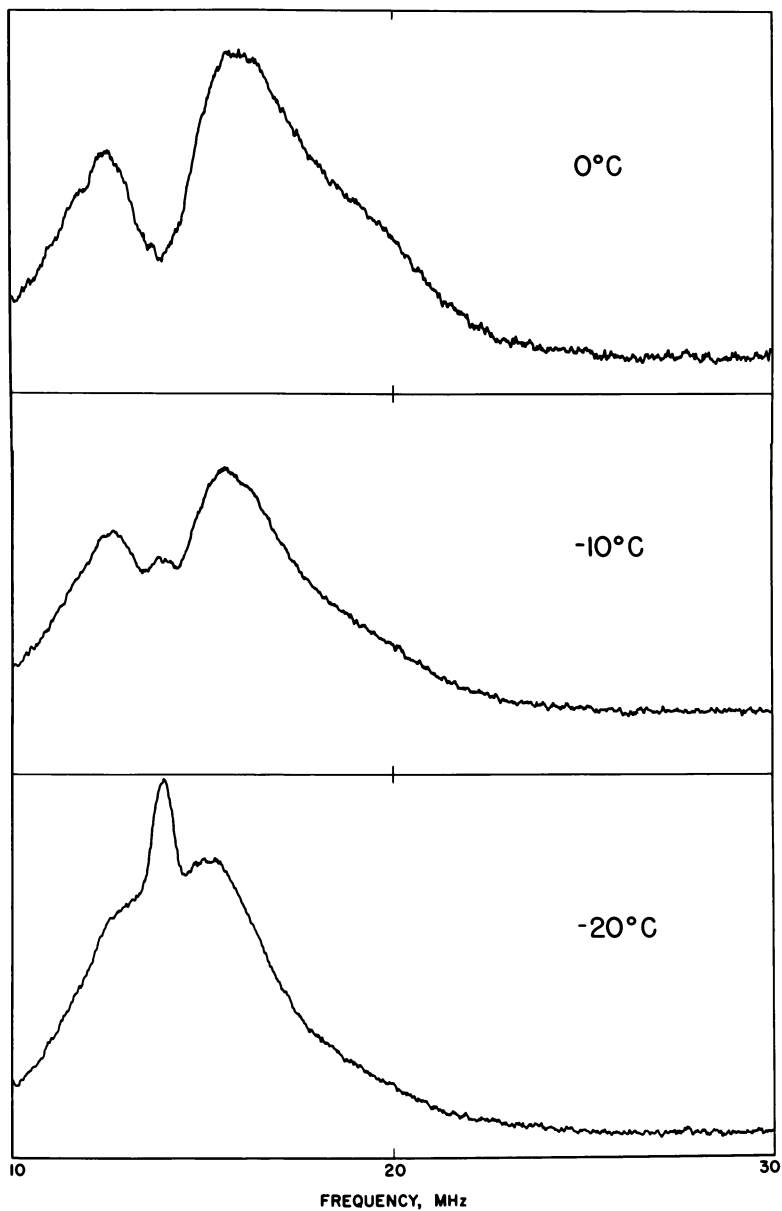


Figure 11. Variable temperature ENDOR spectra of oil produced from West Virginia coal in the Pittsburgh Energy Technology Center's 400-lb coal/day PDU

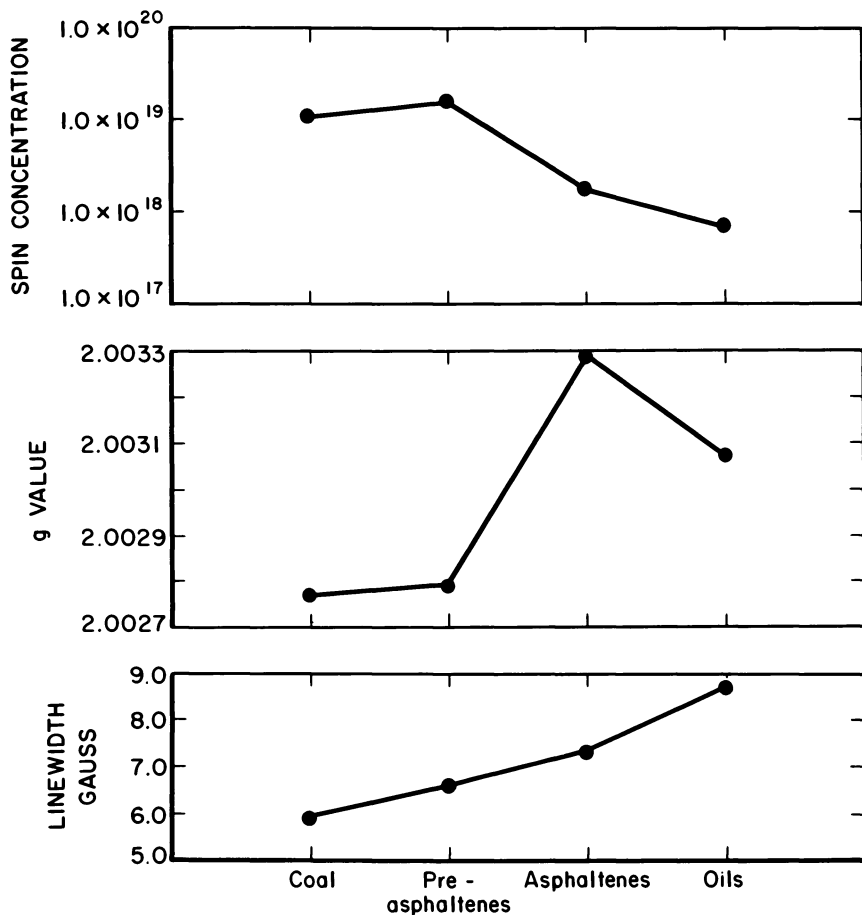


Figure 12. The 9.5 GHz ESR spectral parameters for West Virginia Ireland Mine coal and subfractions of its liquefaction products

Summary and Prognosis

The material presented herein was meant to provide an indication of the utility of ESR and ENDOR spectrometries as probes to characterize the free radicals in coals and coal-derived materials. The results suggest that, in addition to their use in characterization studies, the techniques may have potential in helping to elucidate the mechanism of coal liquefaction. They further suggest that coals may be heat-treated directly in the cavity of an ESR spectrometer with the assurance that reliable data will be obtained provided simple precautionary measures are taken to avoid unwanted effects. Similar in situ ESR measurement of coals under liquefaction conditions remains a possibility, although considerable

ground work is needed. Preliminary results on the temperature variation of the ENDOR transitions in coal-derived oils indicate that molecular dynamics, perhaps as they relate to product viscosity, may be investigated to supplement spin-labeling and other techniques (51).

Acknowledgments

The authors wish to thank M. L. Gorbaty for his invitation and encouragement to prepare this chapter. The authors are indebted to Ira Goldberg for transmitting his experimental results prior to publication and to Larry Taylor for his gift of the SRC samples investigated.

Literature Cited

1. Tschamler, H.; De Ruiter, E. "Chemistry of Coal Utilization"; Lowry, H. H., Ed.; Wiley: New York, 1963; Suppl. Vol., p. 78.
2. Ladner, W. R.; Wheatley, R. *Brit. Coal Util. Res. Assoc. Mon. Bull.* **1965**, *29*, 202.
3. Van Krevelen, D. W. "Coal"; Elsevier: Amsterdam, 1961; p. 393.
4. Schlick, S.; Narayana, P. A.; Kevan, L. *J. Am. Chem. Soc.* **1978**, *100*, 3322.
5. Retcofsky, H. L.; Hough, M. R. "Electron Spin Resonance Studies of Coals and Coal Liquefaction," *Pittsburgh Conf. Anal. Chem. Appl. Spectrosc.*, *29th, Cleveland, 1978*.
6. Kevan, L.; Kispert, L. D. "Electron Spin Double Resonance Spectroscopy"; Wiley: New York, 1976; p. 2.
7. Parks, B. C.; O'Donnell, H. J. *U. S. Bur. Mines Bull.* **1956**, 550.
8. Petrakis, L.; Grandy, D. W. *Anal. Chem.* **1978**, *50*, 303.
9. Yavorsky, P. M.; Akhtar, S.; Lacey, J. J.; Weintraub, M.; Reznik, A. A. *Chem. Eng. Prog.* **1975**, *71*, 79.
10. Retcofsky, H. L.; Thompson, G. P.; Raymond, R.; Friedel, R. A. *Fuel* **1975**, *54*, 126.
11. Retcofsky, H. L.; Stark, J. M.; Friedel, R. A. *Anal. Chem.* **1969**, *40*, 1699.
12. Austen, D. E. G.; Ingram, D. J. E.; Tapley, J. G. *Trans. Faraday Soc.* **1958**, *54*, 400.
13. Retcofsky, H. L.; Thompson, G. P.; Hough, M.; Friedel, R. A. In "Organic Chemistry of Coal," *ACS Symp. Ser.* **1978**, *71*, 142.
14. Smidt, J.; Van Krevelen, D. W. *Fuel*, **1959**, *38*, 355.
15. Toyoda, S.; Honda, H. *Carbon* **1966**, *3*, 527.
16. Wooten, D. L.; Dorn, H. C.; Taylor, L. T.; Coleman, W. C. *Fuel*, **1976**, *55*, 224.
17. Alger, R. S. "Electron Paramagnetic Resonance: Techniques and Applications"; Interscience: New York, 1968; p. 35.
18. Goldberg, I. B.; Crowe, H. R.; Ratto, J. J.; Skowronski, R. P.; Heredy, L. A. *Fuel* **1980**, *59*, 133.
19. Elofson, R. M.; Schulz, K. F.; *Am. Chem. Soc. Fuel Chem. Div., Prepr.* (Chicago, September, 1967), *11*, 513.
20. Schwager, I.; Yen, T. F.; *Am. Chem. Soc. Fuel Chem. Div., Prepr.* (San Francisco, Aug.-Sept., 1976) *21*, 199.
21. Yen, T. F. *Fuel* **1973**, *52*, 93.
22. Yen, T. F.; Young, D. K. *Carbon* **1973**, *11*, 33.
23. Van Gerven, J.; Van Itterbeck, A.; De Wolf, E., *J. Phys. Radium* **1956**, *17*, 140.
24. Kevan, L.; Kispert, L. D. "Electron Spin Double Resonance Spectroscopy"; Wiley: New York, 1976; p. 98.

25. Bielski, B. H. J.; Gebicki, J. M. "Atlas of Electron Spin Resonance Spectra"; Academic: New York, 1967.
26. Wertz, J. E.; Bolton, J. R. "Electron Spin Resonance: Elementary Theory and Practical Applications"; McGraw-Hill: New York, 1972.
27. Ayscough, P. B. "Electron Spin Resonance in Chemistry"; Methuen: London, 1967.
28. Livingston, R.; Zeldes, H.; Conradi, M. S., *J. Am. Chem. Soc.* **1979**, *101*, 4312.
29. Yen, T. F.; Sprang, S. R. *Geochim. Cosmochim. Acta* **1977**, *41*, 1007.
30. Elofson, R. M.; Schulz, K. F. *Am. Chem. Soc. Fuel Chem. Div., Prepr.*, (Chicago, Sept., 1967) *11*, 513.
31. Kreulen, D. J. W. *Fuel* **1952**, *31*, 462.
32. Talcott, C. L. Myers, R. J. *Mol. Phys.* **1967**, *12*, 549.
33. Ayscough, P. B. "Electron Spin Resonance in Chemistry"; Methuen: London, 1967.
34. Stone, T. J.; Waters, W. A. *J. Chem. Soc.* **1964**, 4302.
35. Retcofsky, H. L.; Friedel, R. A. "Spectrometry of Fuels"; Friedel, R. A., Ed.; Plenum: New York, 1970; p. 39.
36. Retcofsky, H. L.; Hough, M. R.; Clarkson, R. B. *Am. Chem. Soc. Fuel Chem. Div., Prepr.* (Honolulu, April, 1979) *24*(1), 83.
37. Retcofsky, H. L.; Hough, M. R.; Maguire, M. M.; Clarkson, R. B. "Some Cautionary Notes on Magnetic Resonance Measurements in Coal Research" in *Appl. Spectrosc.*, in press.
38. Singer L. S. *Proc. Conf. Carbon, 5th*; Pergamon : New York, 1963; p. 37.
39. Ouchi, L., *Fuel* **1967**, *46*, 71.
40. Klass, D. L. *Chem. Technol.* **1975**, *5*, 499.
41. Yavorsky, P. M.; Akhtar, S.; Lacey, J. J.; Weintraub, M.; Reznik, A. A. *Chem. Eng. Prog.* **1975**, *71*, 79.
42. Akhtar, S.; Mazzocco, N. J.; Weintraub, M.; Yavorsky, P. M.; *Energy Commun.* **1975**, *1*, 21.
43. Weller, S.; Pelipetz, M. G.; Friedman, S. *Ind. Eng. Chem.* **1951**, *43*, 1572.
44. *Ibid.*, 1575.
45. Sternberg, H. W.; Raymond, R.; Schweighardt, F. K. *Science* **1975**, *188*, 49.
46. Retcofsky, H. L.; Schweighardt, F. K.; Hough, M. *Anal. Chem.* **1977**, *49*, 585.
47. Yen, T. F.; Erdman, J. G.; Pollack, S. S. *Anal. Chem.* **1961**, *33*, 1587.
48. Koots, J. A.; Speight, J. G. *Fuel* **1975**, *54*, 179.
49. Staff, Spectrometry Branch, Chemical and Instrumental Analysis Division, U.S. DOE PERC/RI-77/14, 1977; p. 23.
50. Grandy, D. W.; Petrakis, L. *Anal. Chem.* **1979**, *58*, 239.
51. Ebert, L. B.; Long, R. B.; Schlosberg, R. H.; Silbernagel, B. G. *Am. Chem. Soc., Div. Fuel Chem. Prepr.* (Honolulu, April, 1979) *24*(1); p. 104.

RECEIVED August 17, 1979.

Temperature Dependence of ^1H NMR Absorption in Coal and Pitch

KUNIO MIYAZAWA, TETSURO YOKONO, TADATOSHI CHIBA,
and YUZO SANADA

Coal Research Institute, Faculty of Engineering, Hokkaido University,
Sapporo 060, Japan

EIJI YAMADA and SHIGEZO SHIMOKAWA

NMR Laboratory, Faculty of Engineering, Hokkaido University,
Sapporo, 060, Japan

The temperature dependence of the ^1H NMR absorption in coals and pitches has been obtained by using a pulsed Fourier transform NMR spectrometer with a high-temperature probe. With increasing temperature the value of the line width at half height ($\Delta H_{1/2}$) of a brown coal decreases and then increases rapidly. On the other hand, tar pitches and the γ component of a coal indicate that the value of $\Delta H_{1/2}$ remains small from 400 to 700K. An excellent relation was found between the temperature dependence of $\Delta H_{1/2}$ of samples and the optical texture of the mesophase transformed from them. Well-resolved spectra of ethylene tar pitch corresponding to aromatic and aliphatic protons were observed at high temperatures, and hydrogen aromaticity was estimated from the resolved spectra.

Many kinds of reactions—such as pyrolysis, depolymerization, polycondensation, and so on—coexist in a complicated way in coals and pitches over the temperature range from 600 to 800 K. In order that the processes of coal liquefaction and coal carbonization be understood, it is important to clarify the characteristics of reaction behavior for coals and pitches over this temperature range.

The characteristics of magnetic resonance signals of nuclei in organic solids are sensitive to molecular mobility. Nuclear magnetic resonance methods therefore have potential for the study of changes in the molecular mobility or viscosity of coal during heating. It is sometimes possible to observe from proton magnetic resonance (^1H NMR) signals a division of the structure into two or more parts distinguished by their

molecular mobilities. In previous papers (1, 2) the temperature dependence of ^1H NMR absorption signals of a vitrain [84.9% C, dry ash-free (daf)] and a pyridine extraction residue was measured between 90 and 423 K (i.e., below the plastic and thermal decomposition regions). Below 300 K the ^1H NMR absorption was a single broad band, and at higher temperatures a second narrower band was gradually resolved. A transition in the width of the narrow band occurred near 333 K and was associated with a glass transition in a component of the material. Calculation of the activation energy has been attempted by using a correlation frequency obtained from the broadband ^1H NMR method. The values of activation energy are higher than those for synthetic high polymers, and this fact suggests a motion hindered by strong molecular forces in coal. The degree of crystallinity derived from the ^1H NMR intensity ratio, i.e., the relative amounts of mobile and rigid protons, is consistent with the results of X-ray diffraction measurements.

It is well known that pitch, solvent-refined coal (SRC), and coking coal produce various kinds of mesophase at the early stages of carbonization (3, 4, 5). The mechanisms of many chemical reactions and physical transformations relating to mesophase formation are studied by quenching techniques. Such research techniques as polarized-light microscopy can be extremely fruitful. On the other hand, observation of phenomena at reaction temperatures may yield more easily interpretable or more relevant results.

This study has been undertaken in an effort to acquire information on these phenomena by using a pulsed Fourier transform (FT) NMR spectrometer with a high-temperature probe. No report has appeared on direct measurement of the changes of hydrogen aromaticity (f_{Ha}) for coal and pitch in the early stages of carbonization. The resolved ^1H NMR spectra corresponding to aromatic and aliphatic protons have been successfully obtained by using a shim system attached to the magnet of an NMR spectrometer over the temperature range from about 400 to 700 K.

Experimental

Sample. Characteristics of all samples studied so far are shown in Table I. In the table the values of carbon aromaticity (f_a) were estimated from proton spin-spin relaxation time at 173 K (6).

Procedures. The experiments were carried out by using a Bruker Sxp 4-100 pulsed FT NMR spectrometer with a high-temperature probe and an improved JEOL 3H electromagnet (0.88 T) with a 60-mm gap operating at 36.4 MHz for ^1H NMR. In order to improve the resolution of a spectrum at higher temperatures, we built (7) and used an NMR system including a current shim in this study. Outlines of the high-temperature probe and flowing gas system are illustrated in Figure 1. Heat treatment of the specimen was carried out directly in the high-temperature probe under nitrogen gas flow, and ^1H NMR spectra were

Table I.

Sample	Weight % (daf)					f_a^a
	C	H	N	S	O	
Taiheiyo coal	77.0	6.0	1.4	0.1	15.5	0.70
Hongei coal	93.1	3.2	1.0	2.7	—	0.70
Miike coal	83.5	6.2	1.2	1.8	7.3	—
Yubarishinko coal	86.6	5.9	2.0	0.3	5.2	0.79
β -Component of Yubarishinko coal	82.2	5.7	2.2	—	—	0.78
γ -Component of Yubarishinko coal	87.8	7.0	1.5	—	—	0.80
Kureha pitch	95.2	4.2	0.1	0.2	0.3	0.86
Ethylene tar pitch	94.3	5.5	0	0.1	0.1	0.76
Coal tar pitch	92.1	4.8	1.3	0.3	1.5	0.83

^a Values obtained from proton spin-spin relaxation time at 173K (6).

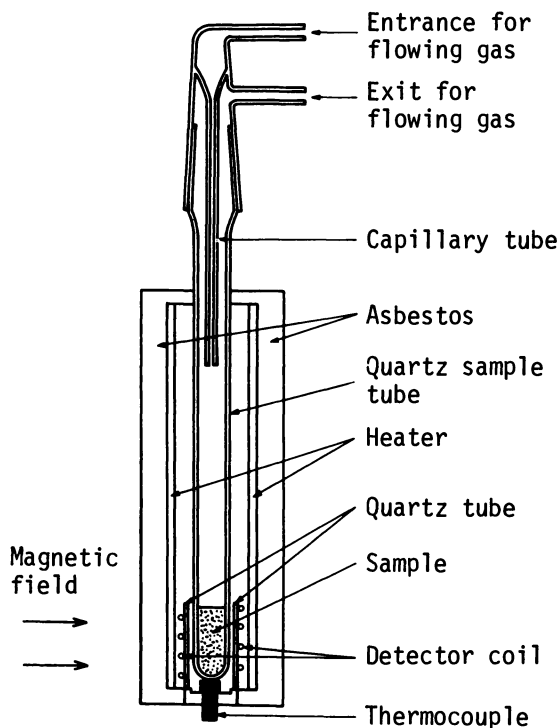


Figure 1. Outlines of the high temperature probe and flowing gas system

obtained simultaneously. The heating rates employed were in the range from 1 to 10 K/min. The carbonization process at low temperature has been studied by the method of polarized-light microscopy (8).

Results and Discussion

Temperature Dependence of Molecular and/or Segmental Motion. Representative ^1H NMR spectra are shown in Figure 2. Apparently there is no structure in the lines. Increasing the temperature produces changes in the spectra. In order to discuss the broadening behavior quantitatively, we utilized the values of the line widths at half height ($\Delta H_{1/2}$). The temperature dependence of $\Delta H_{1/2}$ is shown in Figure 3. It is obvious that there are three different groups with respect to temperature dependence of $\Delta H_{1/2}$. The value of $\Delta H_{1/2}$ of the first group, to which Taiheiyo coal belongs, decreases and then increases rapidly with increasing temperature. The behavior of $\Delta H_{1/2}$ of the second group, Yubarishinko coal and the β component of Yubarishinko coal, resembles that of the first group, but the curve of $\Delta H_{1/2}$ is shifted to higher temperatures. The third group, which includes the γ component of Yubarishinko coal, coal tar pitch, and ethylene tar pitch, indicates that the values of $\Delta H_{1/2}$ remain small over a wide temperature range. This result suggests that the molecules and/or segments in them are mobile throughout the temperature range.

The optically anisotropic textures of mesophase from the samples heat-treated at the early stages of carbonization are classified into five types corresponding to isotropic, fine mosaic, coarse mosaic, fibrous, and domain.

There is a close relation between the proton spin lattice relaxation time (T_1) observed with pulsed NMR at room temperature (8, 9) and the microstructure of mesophase (8) transformed from the parent matrix of coal. That is, the longer the relaxation time is, the more sufficient the growth of mesophase from the matrix occurs, and shown in Table II. The parent materials, which give the fibrous-domain texture at the early stages of carbonization, have the longest relaxation time found so far, as described in the table.

There is also an excellent relation between the microstructure of mesophase and the temperature dependence of $\Delta H_{1/2}$. For Taiheiyo coal (no anisotropic texture was observed over the temperature range from 400 to 600 K), the temperature at which the value of $\Delta H_{1/2}$ shows its minimum ($\Delta H_{1/2, \text{min}}$) is lower than that for materials that exhibit a fine mosaic mesophase. The values of $\Delta H_{1/2}$ for materials that exhibit a coarse mosaic or fibrous mesophase stay small over a wide temperature range (see Table II and Figure 3).

Regarding the concentration of free radicals and the ESR line width, these values remain almost constant up to about 700 K for coals of

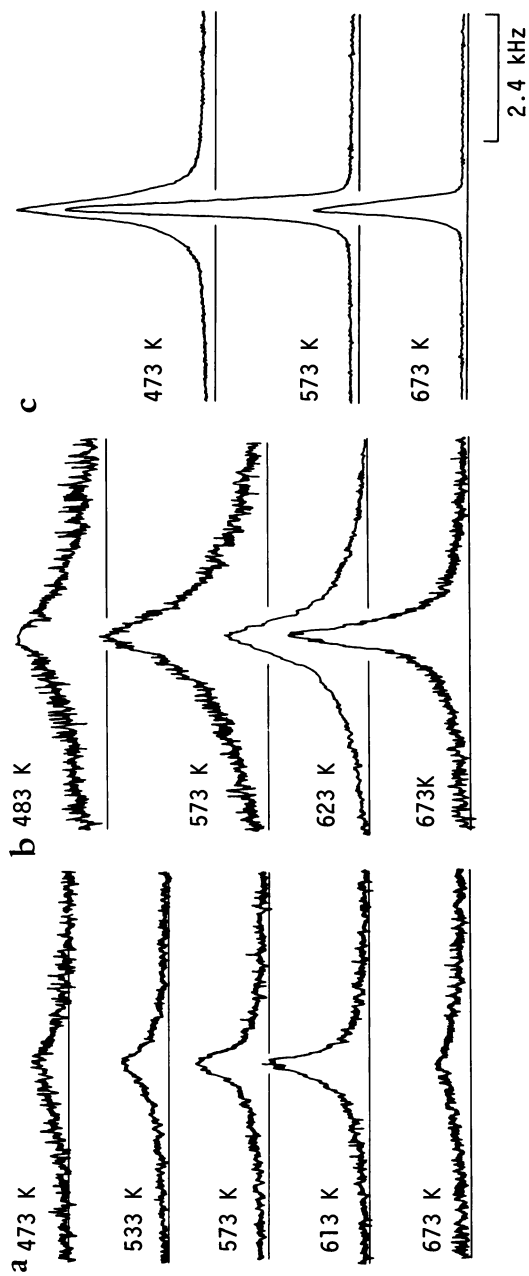


Figure 2. ^1H NMR spectra of (a) Taiheiyo coal; (b) Yubarishinko coal; and (c) γ component of Yubarishinko coal at high temperatures during heating at $5\text{ K}\cdot\text{min}^{-1}$.

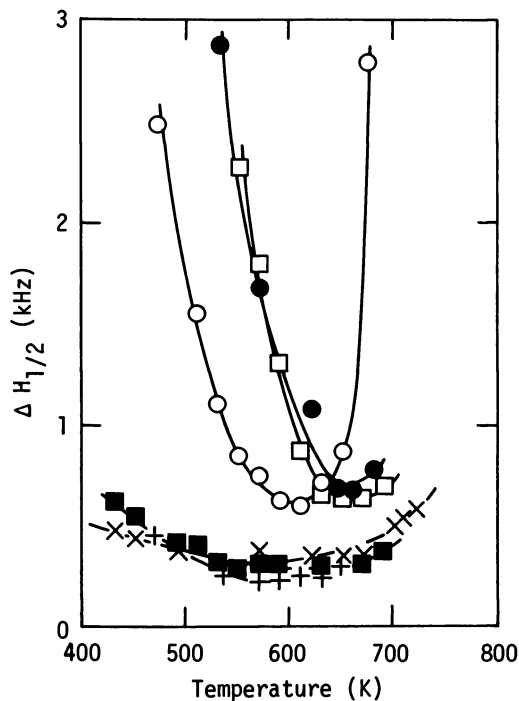


Figure 3. Temperature dependence of the line width at half-height ($\Delta H_{1/2}$) during heating at $5 \text{ K} \cdot \text{min}^{-1}$ (O) Taiheiyo coal; (●) Yubarishinko coal; (□) β component of Yubarishinko coal; (■) γ component of Yubarishinko coal; (+) coal tar pitch; and (×) ethylene tar pitch

Table II.

Sample	T_1 (msec) ^a	Optical Texture in Carbonized Sample
Taiheiyo coal	18	isotropic
Hongei coal	58	isotropic
Miike coal	421	fine mosaic
Yubarishinko coal	488	fine mosaic
β -Component of Yubarishinko coal	531	fine mosaic
γ -Component of Yubarishinko coal	719	coarse mosaic
Kureha pitch	952	fibrous/domain
Ethylene tar pitch	1103	fibrous/domain
Coal tar pitch	1560	fibrous/domain

^a Proton spin-lattice relaxation time (8, 9).

different rank (10). The contribution of free radicals to the NMR line width is thus not as important as that of the proton dipole-dipole interaction.

At higher temperatures we estimate the value of T_1 according to the following equation:

$$\tau = T_1 \ln 2 \quad (1)$$

where τ is the time at the amplitude of the free induction decay (FID) following the 90° pulse being equal to zero. The pulse sequence used was $180^\circ\text{-}\tau\text{-}90^\circ$ in this experiment.

Figure 4 shows the relation between the T_1 of ethylene tar pitch and the inverse of temperature. The T_1 of ethylene tar pitch has the value of 400 msec at room temperature. It decreases with increasing temperature, and reaches its minimum value at about 420 K. As is shown in the figure, it has its maximum value of 190 msec at about 600 K, and the value decreases rapidly with increasing temperature.

Resolved ^1H NMR Spectra and Hydrogen Aromaticity. Typical spectra for ethylene tar pitch are shown in Figure 5. On heating up to about 357 K, a broad resonance with no resolved structure becomes observable. At about 396 K the ^1H NMR spectrum shows two discrete lines, 200 Hz apart, which correspond to aromatic and aliphatic protons.

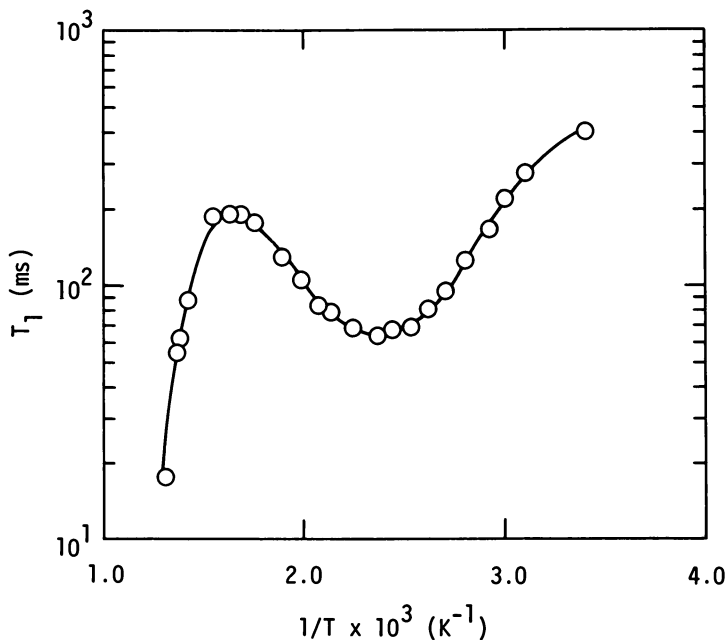


Figure 4. Temperature dependence of proton spin-lattice relaxation time (T_1) of ethylene tar pitch during heating at $2 \text{ K}\cdot\text{min}^{-1}$

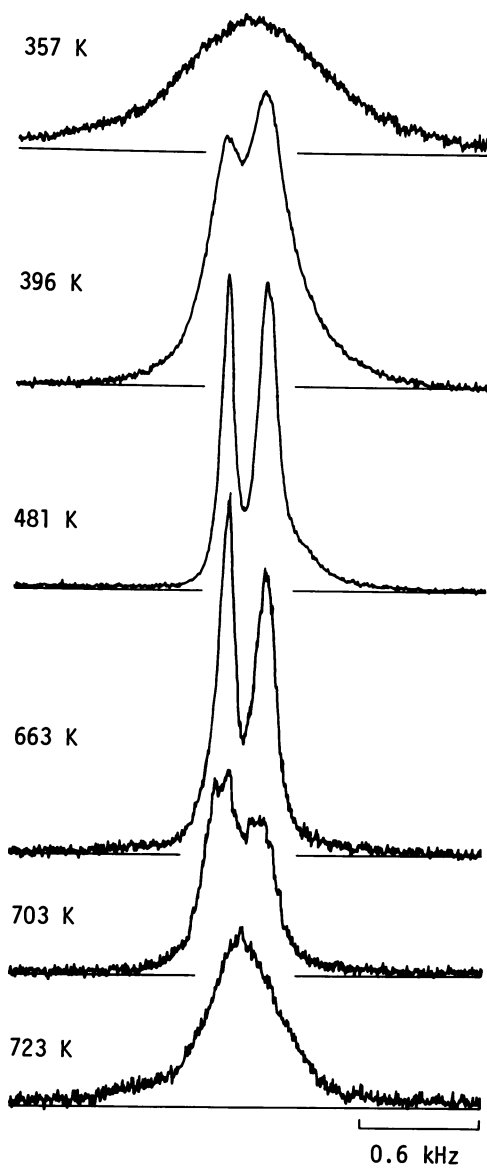


Figure 5. ^1H NMR spectra of ethylene tar pitch at high temperatures during heating at $1\text{ K}\cdot\text{min}^{-1}$

Assignment of the two peaks was made by comparing them with the peaks of pure compounds, acenaphthylene and ethylbenzene, which have values of 0.75 and 0.50 hydrogen aromaticity (f_{Ha}), respectively. At about 481 K the ¹H NMR spectrum becomes narrow, clearly owing to the anisotropic motion of the molecules in ethylene tar pitch. The molecules also exhibit random motion like an isotropic solution, and the value of the dipolar tensor over all orientations is almost zero near this temperature. However, fine structure due to protons attached to α , β , and γ carbons with reference to aromatic rings was not observable at higher temperatures because of the superposition of protons having different chemical shifts and an inability to spin the sample tube. The peak height of aliphatic protons is higher than that of aromatic ones up to 481 K. The values of f_{Ha} were estimated from the intensities of the split spectra. Two lines merge and broaden at about 723 K. Heating of the specimen to higher temperatures accelerates the degree of broadening of the spectrum. Therefore, it is difficult to observe the spectrum in the range of a usual high-resolution NMR sweep width.

From the temperature dependence of f_{Ha} it is clearly seen that the value of f_{Ha} increases drastically at about 600 K, from 0.4 to 0.6 with increasing temperature. Variation of the f_{Ha} with temperature may be accompanied by the process of aromatization and/or the elimination of aliphatic chains from the aromatic ring system.

Kinetic Analysis of Hydrogen Aromaticity Changes. Kinetic analysis has been attempted for the temperature-dependent hydrogen aromaticity (f_{Ha}) obtained from the ¹H NMR measurements described above.

When a sample is heated, hydrogen aromaticity increases owing to the decrease of hydrogen in the species other than aromatics. If this change can be expressed as a first-order irreversible reaction, the rate of change in a batch system is written as

$$-\frac{d(1-f_{\text{Ha}})}{dt} = \frac{df_{\text{Ha}}}{dt} = k(1-f_{\text{Ha}}) \quad (2)$$

where k is the rate constant and is given by the Arrhenius equation:

$$k = A \cdot \exp\left(-\frac{\Delta E}{RT}\right) \quad (3)$$

For a constant-rate heating operation, Equation 2 is nonlinear and hence must be solved numerically. However, if a heating operation can be approximately expressed as

$$\frac{1}{T_0} - \frac{1}{T} = \left(\frac{1}{q_H} \right) (t - t_0) \quad (4)$$

where T_0 and T are temperatures at t_0 and t , respectively; t_0 and t are arbitrary times during the reaction; q_H is an experimental constant; then the equation can be integrated analytically and can be written as

$$\ln \left(\frac{1 - f_{Ha0}}{1 - f_{Ha}} \right) = (A) \left(\frac{Rq_H}{\Delta E} \right) \exp \left(- \frac{\Delta E}{RT_0} \right) \left\{ \exp \left[\frac{\Delta E}{Rq_H} (t - t_0) \right] - 1 \right\} \quad (5)$$

where $f_{Ha,0}$ denotes the hydrogen aromaticity at t_0 . Furthermore, differentiating Equation 5 and taking logarithms, we obtain the following equation:

$$\ln \left[(1 - f_{Ha}) \left(\frac{df_{Ha}}{dt} \right) \right] = \left(\ln A - \frac{\Delta E}{RT_0} \right) + \frac{\Delta E}{Rq_H} (t - t_0) \quad (6)$$

Figure 6 shows the relation between f_{Ha} of ethylene tar pitch and the elevating temperature with the range of 1 K/min. It is clear that f_{Ha} increases drastically after the temperature exceeds about 593 K. Hence T_0 and t_0 in Equation 4 can be taken as 593 K and 300 min, respectively. Based on Equation 6, observed values of $\ln [(1 - f_{Ha})(df_{Ha}/dt)]$ for ethylene tar pitch were plotted against $(t - t_0)$. A typical example of the results is shown in Figure 7, with $q_H 4.17 \times 10^5 \text{ K} \cdot \text{min}$, which corresponds to the heating rate of about 1 K/min. As expected, a

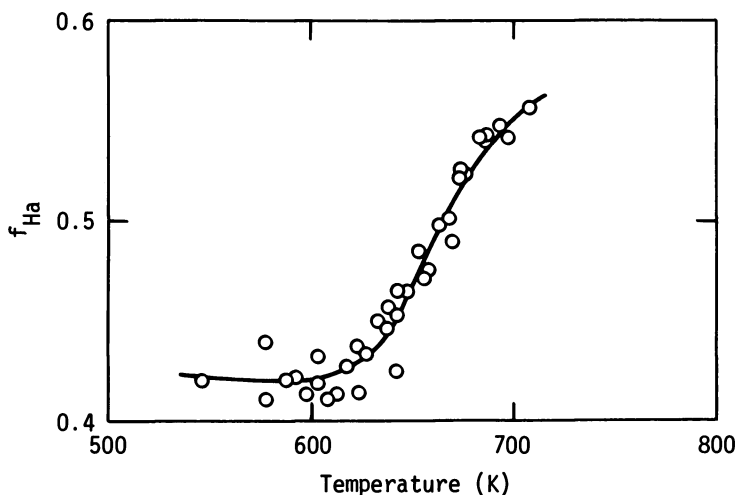


Figure 6. Temperature dependence of hydrogen aromaticity (f_{Ha}) for ethylene tar pitch (heating rate is $1 \text{ K} \cdot \text{min}^{-1}$)

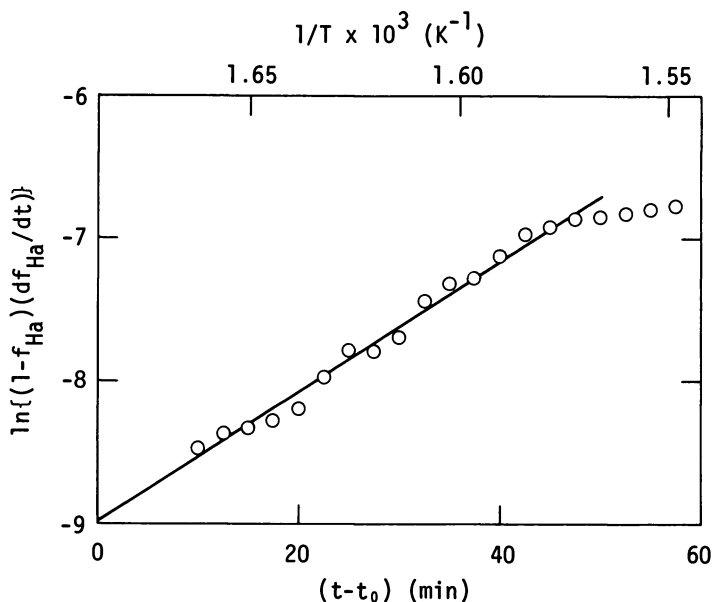


Figure 7. Plot of $\ln [(1-f_{\text{Ha}})(df_{\text{Ha}}/dt)]$ vs. $(t-t_0)$ for ethylene tar pitch (heating rate is $1 \text{ K}\cdot\text{min}^{-1}$)

straight line can be drawn in the figure, and the values for ΔE and A obtained from the line are 38 kcal/mol and $9.1 \times 10^9 \text{ min}^{-1}$, respectively. In the case of $q_{\text{H}} = 2.15 \times 10^5 \text{ K/min}$, which corresponds to the heating rate of about 2 K/min , the values for ΔE and A are 38 kcal/mol and $1.9 \times 10^{10} \text{ min}^{-1}$, respectively.

From the results of kinetic analysis it seems probable that a model of the rearrangement of C-C bonding together with vaporization of low molecular substances is applicable for the change of f_{Ha} values. Previously H. Honda and Y. Sanada (11) used an isothermal method of kinetic analysis to study the changes of stacking height of aromatic lamellae, interlamellar spacing, weight loss, density, and quinoline insolubles of coal tar pitch and naphtha tar pitch at temperatures from 663 to 703 K . The results from nonisothermal methods coincide with those of isothermal methods.

^1H NMR Line Shape at Higher Temperature and Simulation by Means of Computer. As mentioned above, the lines of split spectra merge and broaden at about 720 K . Heating of the specimen at higher temperatures accelerates the degree of broadening of the specimen. Figure 8(a) illustrates a ^1H NMR spectrum from Kureha pitch at 723 K (for 15 min) obtained with a wider sweep width (25 kHz), and Figure 8(b) shows a comparison of the experimentally observed spectrum with a computer-simulated spectrum. The spectrum (a) contains considerable

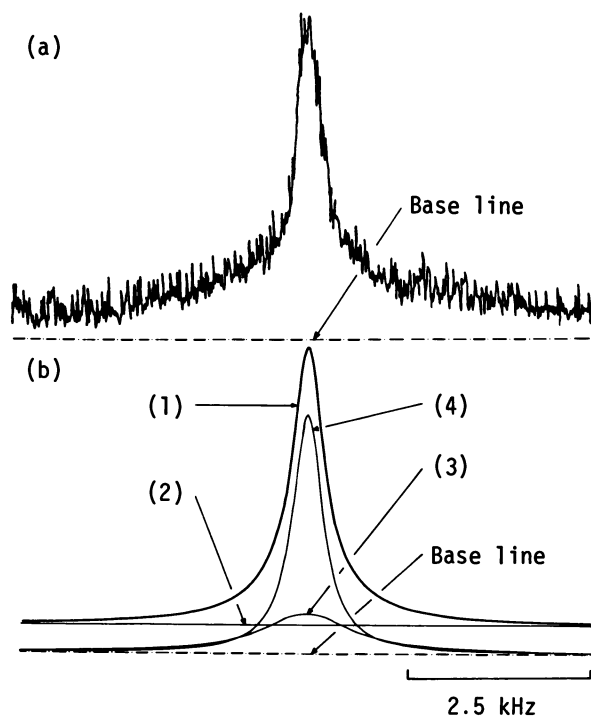


Figure 8. A ^1H NMR spectrum (a) from Kureha pitch at 723 K (for 15 min) and (b) a comparison of the experimentally observed spectrum with a computer-simulated spectrum: (1) total simulated curve; (2) Gaussian component with $T_2 = 7 \mu\text{sec}$; (3) Lorentzian component with $T_2 = 210 \mu\text{sec}$; and (4) Lorentzian component with $T_2 = 636 \mu\text{sec}$. Heating rate is $10 \text{ K} \cdot \text{min}^{-1}$.

intensity in the wings of the line, and the ratio of the width at one-eighth height to that at one-half height, indicated by the symbol $R(8/2)$, is 6.4. The ratio for a pure Lorentzian line is 2.64 and for a pure Gaussian line is 1.73 (12). Thus this line shape is designated as super Lorentzian (13). In the case of ethylene tar pitch a similar spectrum was observed, as is shown in Figure 9.

After the measurement of the ^1H NMR spectra of Kureha pitch at 723 K and ethylene tar pitch at 743 K, the samples were immediately quenched to room temperature and observed by polarized-light microscopy. It was confirmed that the bulk mesophase was produced.

When a magnetic field is applied, the direction of alignment of the C axes of mesophase spherules is perpendicular to that of the magnetic field, because of the interaction of the magnetic anisotropy of polycondensed aromatic molecules with the magnetic field applied (14). On the heating of pitches beyond 720 K in a magnetic field, a dipolar tensor is

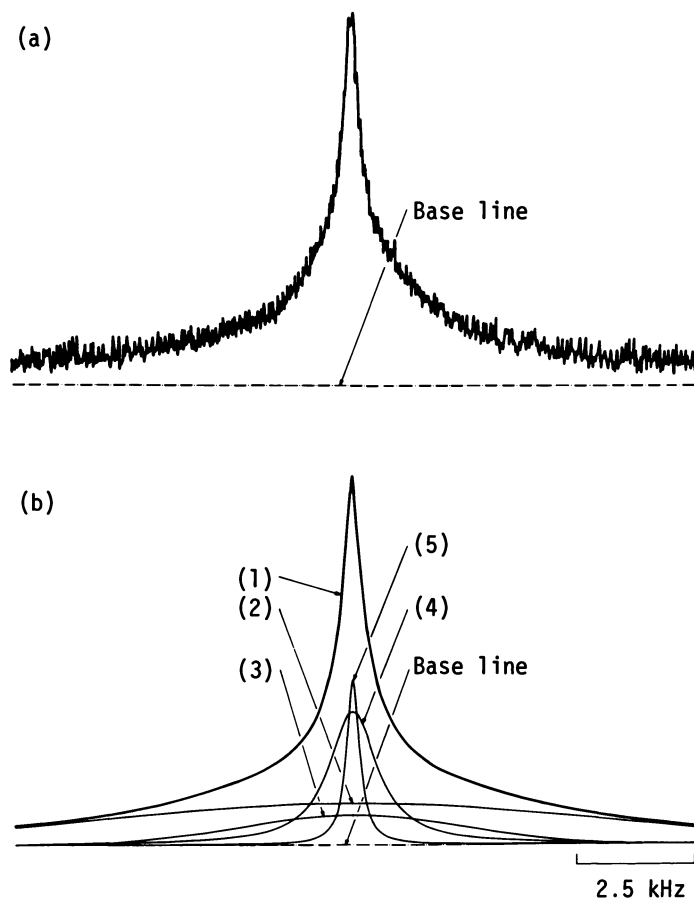


Figure 9. A ^1H NMR spectrum (a) from ethylene tar pitch at 743 K during heating at $1\text{ K} \cdot \text{min}^{-1}$ and (b) a comparison of the experimentally observed spectrum with a computer-simulated spectrum: (1) total simulated curve; (2) Gaussian component with $T_2 = 30\ \mu\text{sec}$; (3) Gaussian component with $T_2 = 70\ \mu\text{sec}$; (4) Lorentzian component with $T_2 = 260\ \mu\text{sec}$; and (5) Lorentzian component with $T_2 = 970\ \mu\text{sec}$.

only partially averaged, owing to anisotropic molecular motion. The resulting line broadens but is not as broad as that of the ^1H NMR line in the solid. The structure of the mesophase produced in an NMR magnetic field is more rigid than that of an isotropic liquid.

Generally the sweep width of broad-line NMR is about 10^5 to 10^6 Hz, while that of high-resolution NMR is about 10^3 Hz at 36.4 MHz for a proton. But the ^1H NMR spectra of the mesophase for Kureha pitch (Figure 8) and ethylene tar pitch (Figure 9) were swept over 2.5×10^6 Hz. Thus the sweep width of the ^1H NMR spectrum for the carbonaceous mesophase is intermediate between those of broad-line ^1H NMR

and high-resolution ^1H NMR. The line widths of the spectra of the mesophase correspond to those of conventional nematic and smectic liquid crystals obtained by J. J. Fink et al. (15).

In some liquid crystal systems, broad, partially resolved spectra with some structure attributed to proton dipole-dipole interaction have been observed (16, 17, 18). On the other hand, such spectra were not observed in this study, so that the ordering parameters of the samples employed would be expected to be very small. This result is compatible with that of the ESR study reported by Y. Yamada et al. (19).

By means of computer simulation we found that the ^1H NMR lines for the mesophase include several components. The results with computer simulation are summarized in Table III. From the viewpoint of general NMR behavior (20), Kureha pitch and ethylene tar pitch at the early stages of carbonization contain about 85% and 68% rigid structures, respectively.

Recently L. J. Lynch and D. S. Webster (21) observed the ^1H NMR of bituminous coal specimens at regular intervals of temperature during heating up to 800 K. The ^1H NMR signal recorded was the free induction decay following a 90° pulse, and useful insight into the molecular basis of thermally induced changes in coal was obtained. The measured ^1H NMR free induction decay deviated greatly from the simple Gaussian or exponential functions that could be expected for homogeneous materials. The relative intensity of the first decaying component of the free induction decay (I_R) was taken as an estimate of the percentage of the total hydrogen of the coal contained in a rigid molecular structure. Initially at room temperature about 90% of the protons are rigid, and this percentage begins to fall above about 470 K, reaches a minimum of less than 20% at 682 K, and on further heating increases to greater than 50% near 770 K; this value is maintained on cooling back to room temperature. The result of this experiment can be compared with the variation of the bulk viscosity as measured by the Gieseler plastometer method during heating. The Gieseler region of bulk fluidity generally coincides with the region of minimum rigid structure as determined by the ^1H NMR experiments. This ^1H NMR result is consistent with a depolymerization of the initially rigid coal structure followed at higher temperatures and/or time by recondensation of a significant portion of the material. The nonrigid portion of the coal after heating is similar to the standard volatile matter yield. It should be noted, however, that there is an uncertain systematic bias error in these measurements consistent with the method of deconvolution of the ^1H NMR signals.

Conclusion

We may conclude from the results above that the materials that give fibrous-domain mesophase on heating show a narrowing of the ^1H NMR

Table III.

Sample	Heating Rate ($K \cdot min^{-1}$)	Heat-Treatment Temperature (K)	Residence Time (min)	Component	Spin-Spin Relaxation Time T_2 (μsec)	Fraction
Kureha pitch	10	723	15	Gaussian	7	0.85
				Lorentzian	210	0.05
				Lorentzian	636	0.10
Ethylene tar pitch	1	743	0	Gaussian	30	0.52
				Gaussian	70	0.16
				Lorentzian	260	0.24
				Lorentzian	970	0.08

with increasing temperature, which corresponds to so-called softening and plastic stages. Moreover, the degree of motional narrowing of the ^1H NMR spectra reflects the degree of fluidity at the plastic stage. The temperature dependence of the hydrogen aromaticity can be monitored directly by high-temperature ^1H NMR in appropriate temperature regions.

Chemical reactions such as pyrolysis, depolymerization, and condensation could be clarified. Moreover, application of the technique seems to be promising in the mechanism of coal liquefaction as well as in that of mesophase formation.

Literature Cited

1. Sanada, Y.; Honda, H.; Nishioka, A. *J. Appl. Polym. Sci.* **1962**, *6*, 94.
2. Sanada, Y.; Honda, H. *Fuel* **1962**, *41*, 437.
3. Brooks, J. D.; Taylor, G. H. *Carbon* **1965**, *3*, 185.
4. Dubois, J.; Agache, C.; White, J. L. *Metallography* **1970**, *3*, 337.
5. Marsh, H. *Fuel* **1973**, *52*, 205.
6. Yokono, T.; Miyazawa, K.; Sanada, Y. *Fuel* **1978**, *57*, 555.
7. Shimokawa, S.; Yamada, E. *Am. Chem. Soc., Div. Polym. Chem. Prepr.* **1979**, *20*(1), 683.
8. Miyazawa, K.; Yokono, T.; Sanada, Y.; Marsh, H. *Fuel* **1979**, *58*, 691.
9. Yokono, T.; Sanada, Y. *Fuel* **1978**, *57*, 334.
10. Smidt, J.; van Krevelen, D. W. *Fuel* **1959**, *38*, 355.
11. Honda, H.; Kimura, H.; Sanada, Y.; Sugawara, S.; Furuta, T. *Carbon* **1970**, *8*, 181.
12. Poole, C. P., Jr.; Farach, H. "The Theory of Magnetic Resonance"; Wiley: New York, 1972.
13. Lawson, K. D.; Flautt, T. J. *J. Phys. Chem.* **1968**, *72*, 2066.
14. Singer, L. S.; Lewis, R. T. *Biennial Conference on Carbon, 11th, Gatlinburg, 1973*, preprint, CG-27.
15. Fink, J. J.; Moses, H. A.; Cohen, P. S. *J. Chem. Phys.* **1972**, *56*, 6198.
16. Saupe, A.; Englert, G. *Phys. Rev. Lett.* **1963**, *11*, 462.
17. Easwaran, K. R. K. *J. Magn. Reson.* **1973**, *9*, 190.
18. Rowell, J. C.; Phillips, W. D.; Melby, L. R.; Panar, M. *J. Chem. Phys.* **1965**, *43*, 3443.
19. Yamada, Y.; Ouchi, K.; Sanada, Y.; Sohma, J. *Fuel* **1978**, *57*, 79.
20. Abragam, A. "The Principles of Nuclear Magnetism"; Clarendon: Oxford, 1961.
21. Lynch, L. J.; Webster, D. S. *Fuel* **1979**, *58*, 235.

RECEIVED July 19, 1979.

Application of ^{13}C , ^2H , ^1H NMR and GPC to the Study of Structural Evolution of Subbituminous Coal in Tetralin at 427°C

JAMES A. FRANZ, DONALD M. CAMAIONI, and W. E. SKIENS

Pacific Northwest Laboratory, Battelle Memorial Institute,
Richland, WA 99352

The products from the treatment of subbituminous coal at 427°C in tetralin or 1,1-d₂-tetralin for times varying from 2.5 to 120 min were examined by ^{13}C , ^2H , and ^1H Fourier transform nuclear magnetic resonance (FTNMR), gel permeation chromatography (GPC), and elemental and hydroxyl group analysis. NMR and elemental analysis revealed that the flash hydroliquefaction products contained about 10% of aromatic ether carbon and phenolic carbon in roughly equal amounts, but no aliphatic ether, carboxyl, or quinone carbon. The combined asphaltenes and preasphaltenes from a 10-min reaction exhibited 68% carbon, 30% hydrogen, and 30% deuterium aromaticity, with aromaticity slowly increasing at longer reaction times. GPC analysis revealed that approximately 10% of the products were greater than 1500 mol wt, with number-average molecular weights reduced from 840 to 500 over a 2-hr reaction. Deuterium NMR revealed that the majority of deuterium transferred to coal appeared at benzylic carbons.

An understanding of the chemical transformations that occur during the conversion of coal to preasphaltenes, asphaltenes, and oils is essential if optimum conversion of coals to useful fuels and chemicals is to be achieved. Although many papers dealing with the conversion of coal in hydrogen-donor media have appeared (for leading references see Refs. 1 and 2; for a review see Ref. 3), only in recent years have advances in spectroscopy (^{13}C and multinuclear Fourier transform nuclear magnetic resonance (FTNMR) of solutions, magic angle/cross polarization ^{13}C NMR of solids (4) and analytical techniques (high-performance liquid chromatography)

graphy, gel permeation chromatography (GPC), capillary gas chromatography, etc.) made possible sophisticated structural characterization of coal conversion products. Relatively little effort has been made to apply these recent developments to the characterization of the evolution of coal structure in a kinetic fashion under conditions of flash hydroliquefaction in donor media. The very short temperature rise times, short reaction times, and high yields from flash hydroliquefaction provide products thought to be similar in structure to the parent coals. In this chapter we describe short (2.5–10 min) as well as long (35–120 min) reactions. The longer reaction times provide a guide to the rates of aromatization and other changes by which the structural distributions of the short reaction time products may be interpreted. Since the soluble products are much more amenable to structural characterization, and since the products are related directly to industrial processes currently being developed, the method of flash hydroliquefaction offers great potential in understanding the structure of parent coals and the evolution of coals to form preasphaltenes and asphaltenes.

In this work the products from the thermal dissolution of subbituminous Kaiparowitz coal at 427°C in tetralin are examined by spectroscopic (^{13}C , ^1H , ^2H NMR), molecular weight (GPC and vapor pressure osmometry (VPO)), and elemental and hydroxyl group analysis. Some of the data presented here are a refinement and extension of data presented in part in earlier work (5). The use of 1,1-dideuterotetralin (5) in conjunction with ^2H NMR to monitor the time dependence of introduction of deuterium into aliphatic and aromatic structures is presented along with the structural distributions of deuterium transferred.

Experimental

Reactions of Coal and Tetralin or 1,1-Dideuterotetralin. The procedure for these reactions is similar to that of Neavel (2) and Curran (1). A 0.6 cm \times 6.3 cm stainless steel tube equipped with threaded caps was charged with 0.75 g of tetralin or 1,1- d_2 -tetralin and 0.25 g of coal or a 0.95 cm \times 6.3 cm tube was charged with 1 g of coal and 2 g of tetralin. One or more tubes attached to a compressed-air vibrator were plunged into a molten lead bath maintained at a temperature that would compensate for the heat uptake by the reaction vessel, and were stabilized as rapidly as possible at 427°C. The sample tubes were withdrawn from the bath at various times from 2.5 min to 2 hr and quenched in water; the contents were washed out with 50 mL of tetrahydrofuran (THF) and filtered through a 0.45- μm Millipore filter. The insoluble material was dried and weighed. The THF-soluble portions were analyzed directly by GPC in THF on a series of 30-cm $\mu\text{Styragel}$ columns consisting of one 1000- \AA , two 550- \AA , and one 100- \AA column, and by gas chromatography (GC) to determine tetralin, naphthalene, and other products. GPC columns were calibrated with polystyrene and polyethyleneglycol standards above 1500 and with a wide variety of polynuclear aromatics, steroids, and phenols below 1500. A plot of log molecular weight vs. retention volume is linear above 500 mol wt, but gently deviates from linearity below 500. Significant deviation from predicted retention behavior becomes apparent only for standards below 150 mol wt. The pentane-soluble fractions were

Table I. Elemental and Hydroxyl Group Analyses of Kaiparowitz Coal (5)

	Reaction time (min)	Weight (%)						
		C	H	N	S	O (diff) ^a	Ash	OH ^b
Kaiparowitz coal		71.0	5.2	1.1	0.3	17.1	8.6	
THF-insoluble residue	10	67.0	4.7	1.7	0.3	15.2 ^a	11.1	
	35	67.3	4.0	1.6	0.31	10.1 ^a	16.7	
	60	62.4	3.4	1.5	0.31	9.7 ^a	22.7	
	120	70.9	3.1	1.4	0.2	6.1 ^a	18.3	
THF-soluble, pentane-insoluble fraction	10	75.4	6.2	1.3	0.3	14.0	1.2	5.1
	35	76.2	6.3	1.4	0.2	13.9	1.0	4.2
	60	77.8	6.1	1.5	0.3	13.5	0.6	3.9
	120	79.5	6.0	1.7	0.1	13.3	0.8	2.2

^a Oxygen analyses by difference in the presence of large ash residues are subject to large errors, and in general O (diff) values are subject to the sum of errors from all of the contributing analyses.

^b Hydroxyl accuracy is $\pm 1.5\%$ for model compounds.

concentrated to an oil, heated at 150°C and 10^{-1} torr to remove tetralin and naphthalene, and then examined by GPC and NMR.

¹H FTNMR of Preparative GPC Fractions. The THF-soluble portions of products of 10-, 35-, 60-, and 120-min reactions were chromatographed on the GPC columns described previously using THF freshly distilled from lithium aluminum hydride and carefully stored under positive argon pressure to avoid the formation of peroxide decomposition products. The fractions eluting between 19,000 to 170 mol wt and from 170 to 60 mol wt were collected and immediately concentrated to a residue. The lower molecular weight fraction consists of tetralin-derived products (see Figure 3). The 19,000–170 fractions (ca. 1 mg) were examined by FTNMR in pyridine-*d*₅ in 1.7-mm capillary NMR tubes with a total sample volume of 35 μ L. The lower solvent/solute ratio in the 1.7-mm tubes allows a satisfactory correction of the aromatic integral for contributions of protonated pyridine (see Figure 10).

¹³C, ²H, and ¹H NMR and Elemental and Hydroxyl Group Analysis of THF-Soluble, Pentane-Insoluble Fractions. The total THF-soluble product mixtures were concentrated to about 2 mL, precipitated by addition of pentane, and filtered off and washed with about 300 mL of pentane. The THF-soluble, pentane-insoluble fractions were examined by ¹³C, ²H (when 1,1-*d*₂-tetralin was used), ¹H NMR in THF-*d*₆, pyridine-*d*₅, or THF for ²H NMR and examined by elemental analysis (Table I), vapor pressure osmometry, and hydroxyl group analysis (acetylation in pyridine).

¹³C NMR SPECTRA. ¹³C spectra were obtained with a Varian Associates FT-80 spectrometer at 20,000 MHz under several conditions. Samples from 10-, 35-, 60-, and 120-min reaction times were examined in THF-*d*₆ in the presence of 0.1M tris-(acetylacetonate)-chromium(III) (Cr(acac)₃) using 90° pulses and 1.4-sec recycle times with gated proton decoupling for Nuclear Overhauser enhancement (NOE) suppression (6). These parameters gave quantitative results for all carbons of 2,2-dihydroxy diphenylmethane as well as pyrene, whose innermost carbons (10b and 10c) exhibit *T*₁ values of greater than 200 sec (7). Ladner has reported a 14.0-sec delay and a 0.3-sec acquisition time with 0.04M Cr(acac)₃ (8) using a 35°

pulse, gated decoupling. With higher concentrations of $\text{Cr}(\text{acac})_3$, faster recycle times are possible without sacrificing intensities of carbons with very long T_1 's. The fraction of aromatic carbon (f_a) was 68%, for the 10-min, 35-min, and 120-min THF-soluble pentane insoluble products. It was found by examining the coal products by ^{13}C NMR in pyridine- d_5 that no detectable aliphatic ethers at 50–80 ppm exist in any of the THF-soluble, pentane-insoluble fractions. Hence, it was possible to correct for the contribution of the integral of the 3-carbon of THF- d_8 to the total aliphatic integral for ^{13}C NMR spectra of THF- d_8 solutions by comparison with the integrals of spectra of neat THF- d_8 run under identical conditions.

^2H NMR SPECTRA. Proton-decoupled ^2H NMR spectra were determined at 12.211 MHz in THF with an external D_2O lock for reactions in which 1,1- d_2 -tetralin was used. For examination of deuterium scrambling during the reaction, tetralin and naphthalene were recovered from the concentrated pentane-soluble fraction by heating (150°C) under vacuum (10^{-1} torr). The resulting mixture of tetralin and naphthalene and other low-boiling components was chromatographed by preparative reverse-phase chromatography using a Waters Associates Prep LC/System 500 instrument equipped with one C_{18} reverse-phase preparative cartridge using 40% THF in water as the eluent. Pure recovered samples of naphthalene and tetralin were examined by ^2H NMR.

^1H NMR SPECTRA. ^1H NMR spectra of THF-soluble, pentane-insoluble products were determined at 79.54 MHz in pyridine- d_5 of 5% solutions. Integrals were corrected for contributions of protonated pyridine to the aromatic region.

Results and Discussion

Yields of Preasphaltenes and Asphaltenes. Subbituminous coal is converted very rapidly to soluble products in tetralin at 427°C. Figure 1 shows the yields of THF-soluble but pentane-insoluble, benzene-soluble and pentane-soluble products vs. reaction time. These fractions correspond respectively to a mixture of preasphaltenes and asphaltenes, asphaltenes and oils. Of the 78% ultimate yield of THF-soluble products based on the dry coal containing 8.6% ash, 55–60% are formed within 5 to 10 min of reaction time. By 35 min of reaction time, conversion of coal to soluble products is essentially complete. In contrast to the extremely rapid process of conversion of the parent coal to preasphaltenes, the further degradation of preasphaltenes occurs only very gradually, the yield of asphaltenes increasing from 10 to only 25% over a 1-hr reaction time.

Uptake of Hydrogen and Product Formation. Figures 2 and 7 show that while the absolute amount of hydrogen consumed per mole of carbon in the coal is greatest up to 10 min, the yield of coal rendered soluble per increment of hydrogen transferred within 10 min is more than double that between 10 to 20 and 20 to 30 min. Greater yields of products with less hydrogen uptake must indicate that (1) fewer hydrogen abstracting radicals or ions are formed per weight of coal rendered soluble during the early stages of reaction, or (2) radicals or ions formed initially abstract hydrogen from hydrogen sources in the coal, or (3) a significant degree of

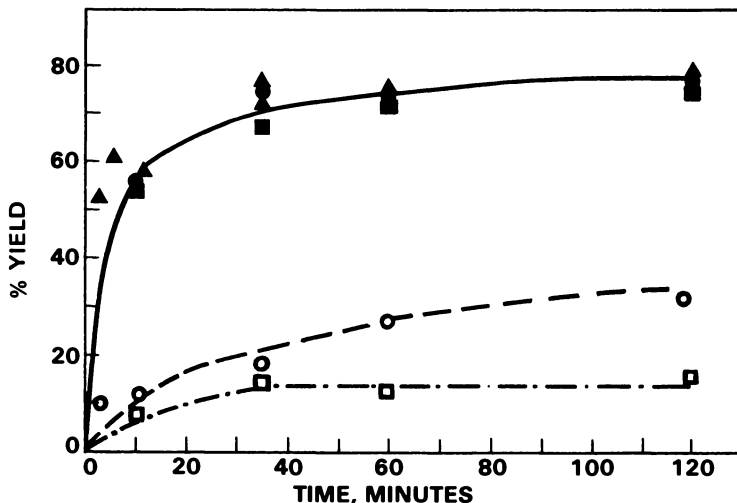


Figure 1. Conversion yields of coal based on the dry coal, without correction for mineral matter.

(▲) THF-soluble, pentane-insoluble yields at 15°C/sec heat-up rate; (●) yields of THF-soluble, pentane-insoluble products at 1°C/sec heat-up rate; (■) yields of carbon converted to THF-soluble, pentane-insoluble product as a percent of the total carbon in the coal; (○) yields of pentane-insoluble, benzene-soluble products; (□) yields of pentane-soluble products after removal of tetralin and naphthalene and other components boiling below 150°C at 10^{-1} torr.

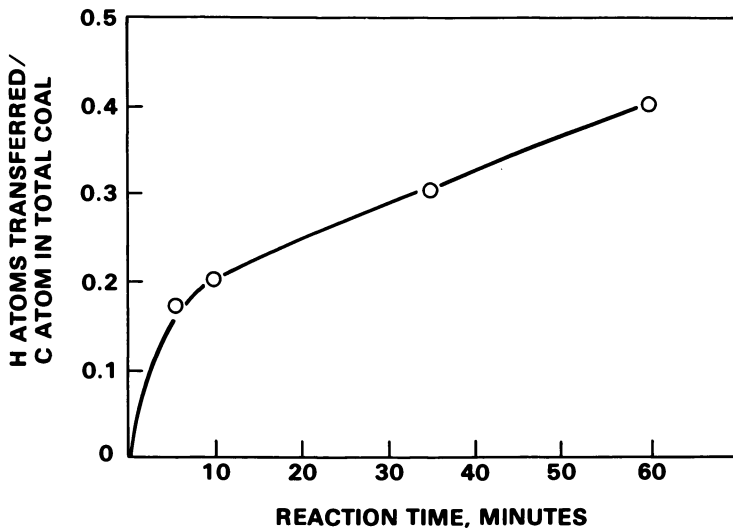


Figure 2. Total hydrogen uptake during the reaction divided by the total weight of carbon in the coal. Hydrogen uptake was determined by quantitative GC analysis of naphthalene formation. Gas formation was neglected.

solubilization occurs via physical disruption or disentanglement of the coal structure. Probably all of these processes contribute to initial solubilization of the coal. With regard to the second pathway leading to increased incremental yields based on hydrogen, we note that significant amounts of potential hydrogen donors exist in the coal itself (*see* the NMR discussion that follows). Initial abstraction reactions need not involve the donor solvent. In fact, Collins et al. have found the vitrinite of Illinois No. 6 coal to be superior to tetralin for the reduction of benzophenone (9). Neavel (2) has invoked autogeneous hydrogen transfer to account for some of the observed product formation.

The third source of enhanced incremental yields simply may be attributable to physical reorganization of the coal structure which liberates trapped molecules. Physical entrapment of components in the coal structure, including water, has been noted by Cronauer et al. (10). In our work we observed that a direct pentane Soxhlet extraction of the coal gave 0.1% by weight of straight-chain aliphatic hydrocarbons and terpenoids, but the yield of these products jumps to nearly 6% after only 2.5 min of reaction time at 427°C. Since the straight-chain aliphatics are not likely to be created in this yield in this time frame, this is evidence for processes that lead to physical accessibility of the coal structure. Swelling, mechanical fracturing, and disentanglement may be invoked to explain this behavior.

Evolution of Molecular Weight. GPC and VPO reveal that preasphaltenes and asphaltenes exhibit a substantial fraction (10%) of material between 5,300 and 19,000 mol wt that is rapidly converted to material with molecular weight less than 1500 between 10- and 35-min reaction times. Since the cleavage of only a few bonds will achieve a drastic reduction in average molecular weight, it can be surmised that a relatively small amount of bond breaking would result in significant solubilization. VPO of THF-soluble, pentane-insoluble fractions from 10-, 35-, 60-, and 120-min reactions of tetralin and coal gives number-average molecular weights (\overline{M}_n) of 840, 490, 360, and 480, respectively. Figure 3 shows gel permeation chromatograms of the fraction of crude reaction mixtures (10-, 35-, 60-, and 120- min) which were THF-soluble and of the pentane-soluble fractions after removal of tetralin and naphthalene under vacuum. After 10 min, 10% of the total products above 160 mol wt possess apparent molecular weights above 1550, with detectable material up to 19,000 mol wt (Figure 4). The fraction above 1550 decreases gradually as lower molecular weight fractions build in. The GPC behavior of the THF-soluble, pentane-insoluble fractions (Figure 5) exhibits weight average molecular weights (\overline{M}_w) that gradually decrease from 740 at 10 min to 370 at 120 min. Both VPC and GPC values show that the most rapid changes in apparent \overline{M}_w or \overline{M}_n occur between 10 and 35 min, with only very slow additional reduction in \overline{M}_w or \overline{M}_n beyond 35 min

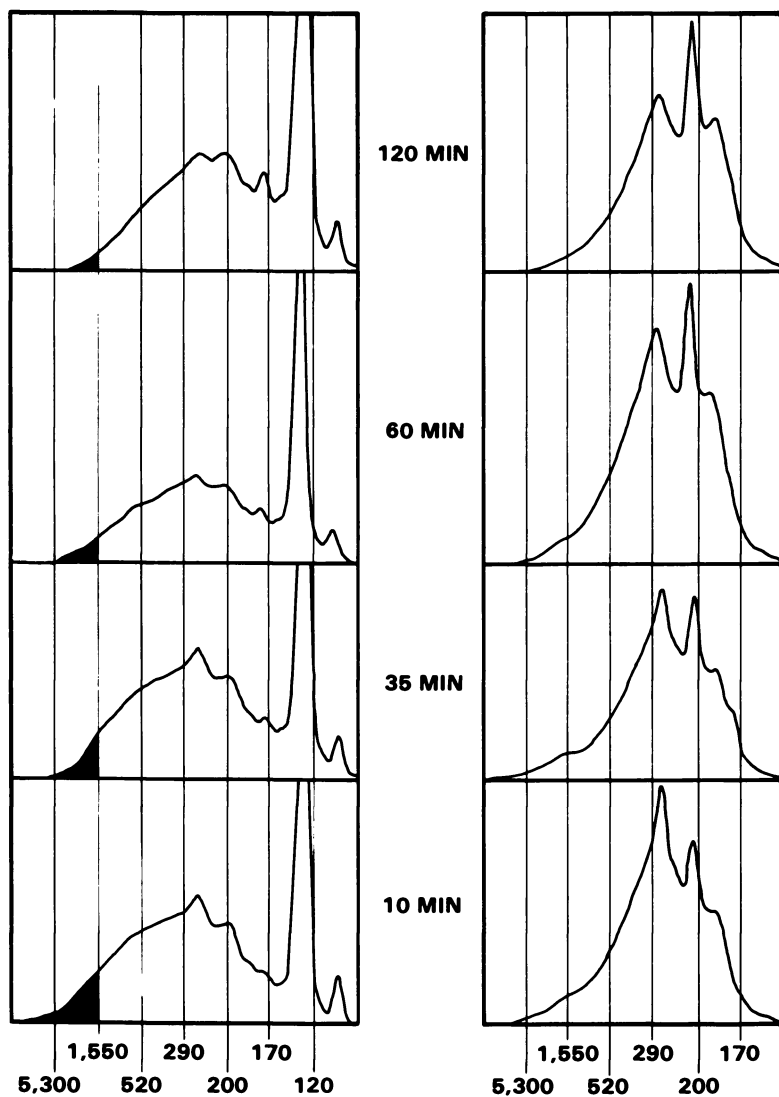


Figure 3. Gel permeation chromatograms of the THF-soluble fraction of the reactions of subbituminous coal in tetralin (left column) and the pentane-soluble fraction after removal of tetralin and naphthalene (right column). The 254-nm UV traces were determined on a series of one 1000-Å, two 500-Å, and two 100-Å μ Styragel columns.

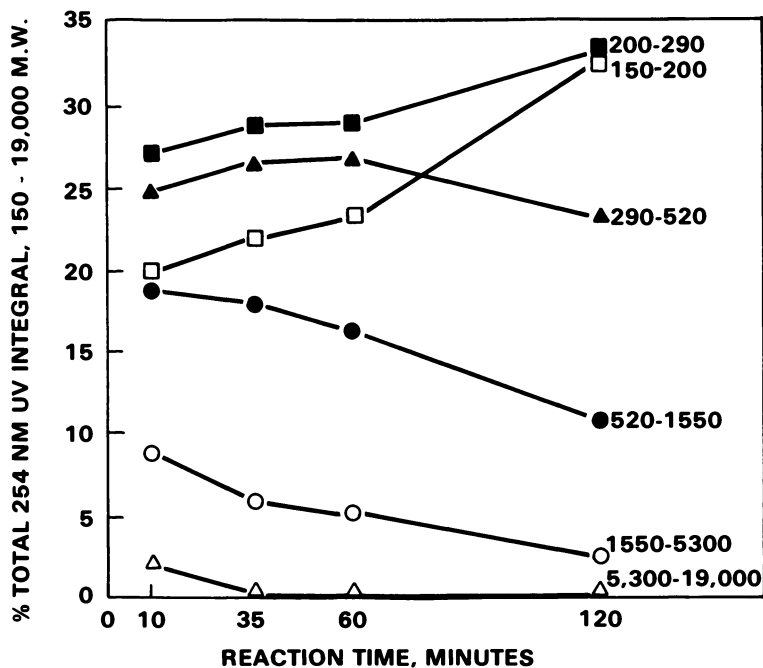


Figure 4. The behavior of molecular size fractions vs. time. The integrals were determined by cutting and weighing the GPC traces of Figure 1, (left column) in the six fractions shown and setting the sum of each 150–19,000 mol wt to 100%.

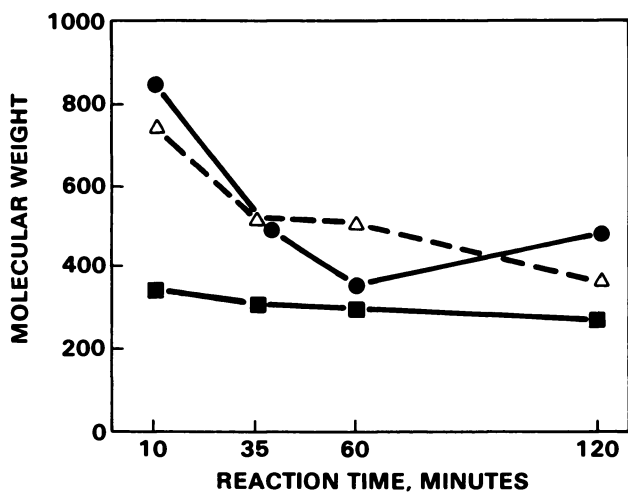


Figure 5. The \bar{M}_n by GPC in THF (□) and by VPO in pyridine (●) and the \bar{M}_n by GPC in THF (△) of THF-soluble, pentane-insoluble products vs. reaction time

of reaction time. The absolute values of the GPC and VPO results are subject to considerable uncertainty because of possible agglomeration or colloid formation, or, with GPC, the tendency toward absorption chromatographic behavior as well as size exclusion for low molecular weight (<350) compounds. In addition, molecular sizes may vary for different molecules possessing the same molecular weight. Finally, some irreversible sorption of coal products may occur on μ Styragel. However, these uncertainties should not invalidate the qualitative trends suggested by the data.

^{13}C NMR Characterization of THF-Soluble, Pentane-Insoluble Products. Figure 6 shows the ^{13}C NMR spectrum of THF-soluble, pentane-insoluble products from a 2-hr reaction. Figure 7 shows the aromatic regions of ^{13}C NMR spectra of 10-, 35-, and 120-min reactions. The aromatic regions of these spectra clearly show the presence of aromatic carbon bonded to oxygen between 150 and 160 ppm (aryl ethers and phenols) (11, 12, 13). For a detailed breakdown of ^{13}C chemical shift assignments in coal-derived products see Ref. 8. In the region between 130 and 145 ppm, alkyl- and aryl-substituted aromatic carbon is detected in significant quantities. The region between 120 and 130 ppm corresponds to protonated aromatic carbon. In the region between 113 and 120 ppm lie protonated aromatic carbons that are ortho to oxygen-substituted carbons. Between 97 and 113 ppm are carbons adjacent to two oxygen-substituted aromatic carbons or situated both ortho and para to oxygen-substituted aromatic carbons (14). Olefins also appear in this region (110–145 ppm), but are known to be absent because of their very short lifetimes under these reaction conditions. As the reaction progresses, the region of protonated aromatic carbon between 125 and 129 ppm grows relative to oxygenated and alkylated aromatic carbon. The results are consistent with the aromatization of initially formed products with time or the liberation of highly aromatic structure from the residue at longer reaction times. We cannot rule out some incorporation of tetralin or naphthalene moieties into the products at long reaction times.

OXYGEN FUNCTIONAL GROUPS. The percent of the total carbon that is oxygen-substituted changes from 11% at 10 min to 9% at 35 min and from 7% at 60 min to 6.8% at 120 min. These values are quantitative and are more reliable than oxygen values by difference from elemental analysis. Hydroxyl group analysis revealed a decline from 5.1% to 4.2% to 3.9% to 2.2% at 10-, 35-, 60-, and 120-min reaction times. These results indicate that about half of the oxygen is in the form of diaryl ethers and half is in the form of aromatic phenols at 10 min of reaction time and very slowly decreases to about 30% by 120 min of reaction time. These results support a very slow loss of aromatic phenolic oxygen and the conversion of phenols to diaryl ethers. Since the accuracy in hydroxyl

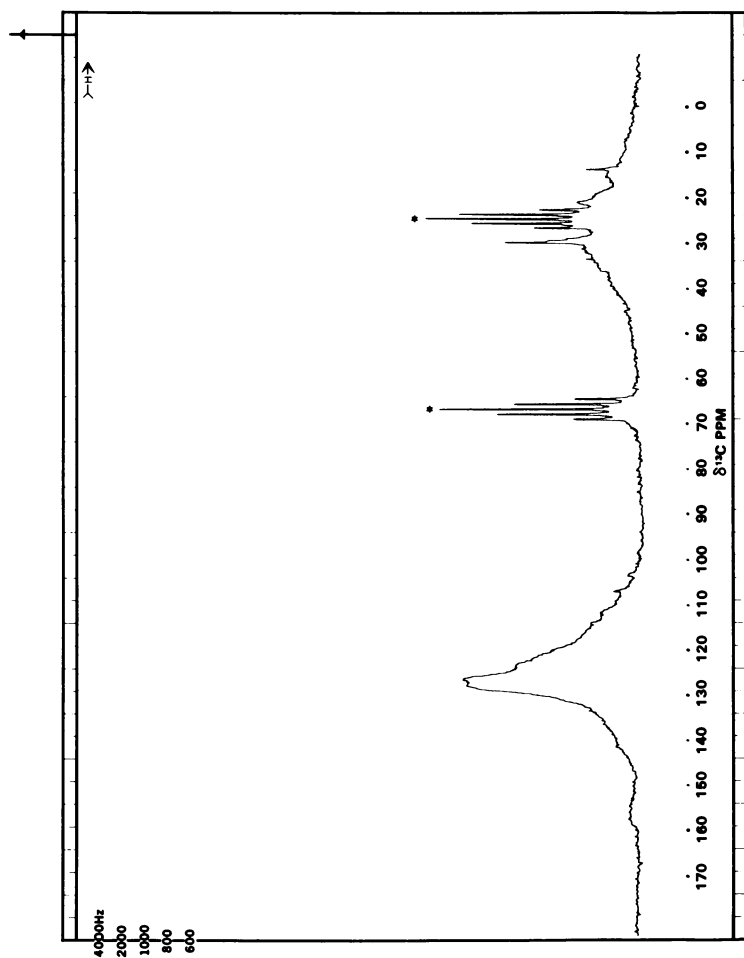


Figure 6. Proton-decoupled ^{13}C NMR spectrum at 20,000 MHz in THF-d_8 of the THF-soluble, pentane-insoluble products of a 2-hr reaction of subbituminous coal in tetralin

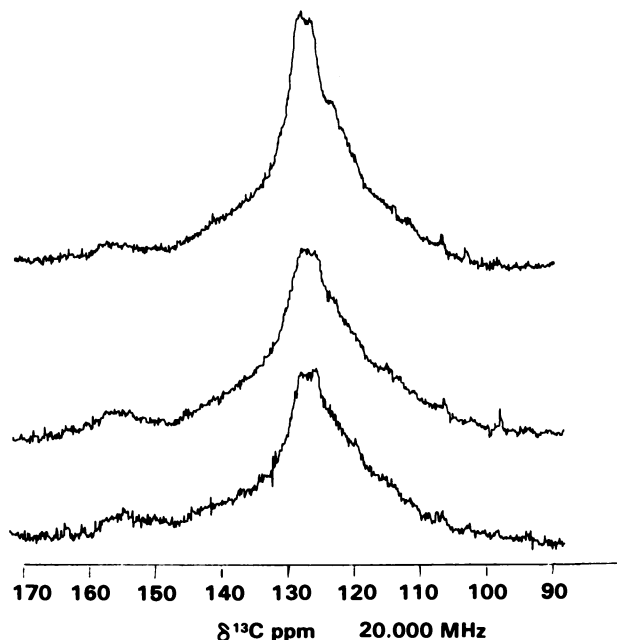


Figure 7. Aromatic regions of proton-decoupled ^{13}C NMR spectra of THF-soluble, pentane-insoluble reaction products of 10- (bottom), 35- (middle), and 120-min (top) reactions in THF- d_6 .

group analysis is about $\pm 1.5\%$, and since similar or larger errors may accrue in the other oxygen analyses, the results must be interpreted with care.

The aliphatic structural distribution from the ^{13}C spectra allows several observations to be made. Approximately 4% of the total carbon in the THF-soluble, pentane-insoluble products of a 10-min reaction occur at benzylic carbons of hydroaromatic rings or at straight-chain paraffinic carbon (28–31 ppm). Approximately 11% of the total carbon occurs between 32 and 45 ppm. This region includes ring-joining methylene groups, methine CH, CH_2 adjacent to methine CH, and CH in naphthenic rings (8). These structures, which are almost certainly in the parent coal, would provide hydrogen for abstraction by thermal radicals leading to autogeneous hydrogen transfer during the early stages of reaction, assuming their presence in the parent coal. The remaining aliphatic carbon (17%) is distributed between naphthenic methylenes (24–28 ppm), methylene in terminal alkyls of greater than C_4 (22–24 ppm), and a variety of methyl groups.

^{13}C NMR and GPC Characterization of the Pentane-Soluble Products. Figure 8 shows the proton-decoupled ^{13}C NMR spectrum of the pentane-soluble products of a 35-min reaction after removal of tetralin

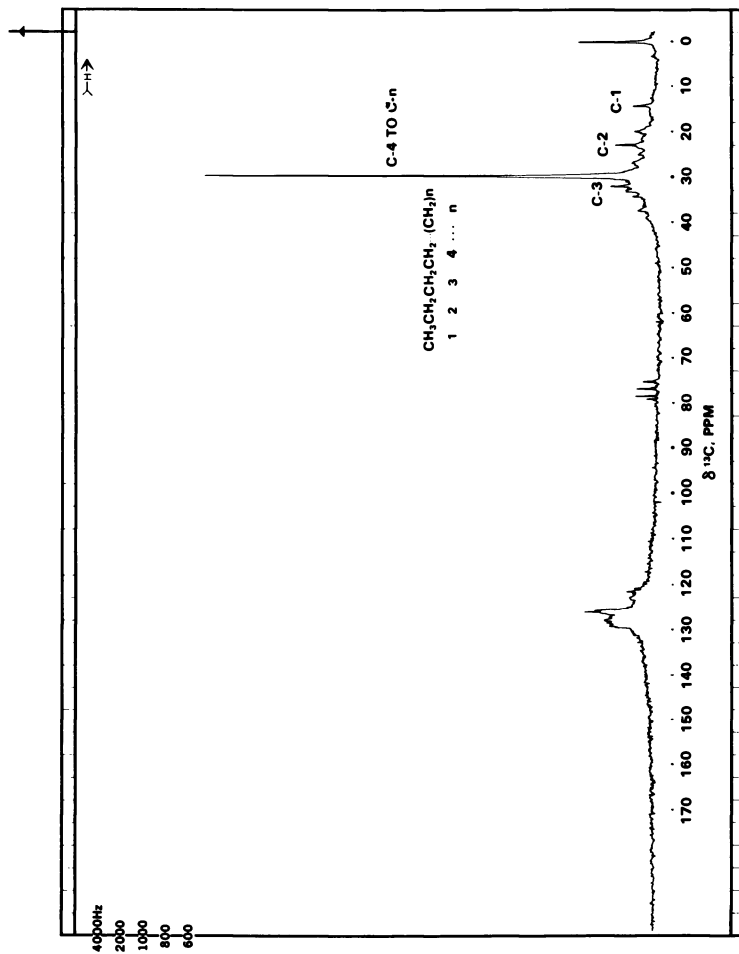


Figure 8. Proton-decoupled ^{13}C NMR spectrum of pentane-soluble products after removal of tetralin and naphthalene

and naphthalene at 150°C and 10⁻¹ torr. The spectrum is dominated by straight-chain aliphatic hydrocarbons shown by GC to include paraffins *n*-C₁₄ to *n*-C₄₀. The carbons that are four carbons or further from the end of linear paraffins appear at 29.7 ppm (11, 12). The remaining material is a large variety of terpenoid and other aliphatic structures possessing aromatic character, but negligible oxygenated structures. As indicated by GPC (Figure 3, right column) the pentane solubles include a substantial fraction of material above 500 mol wt, which undergoes very slow conversion to lower molecular weights. The bulk of the aromatic carbon appears from 125 to 130 ppm in the region of protonated carbon. The aromatic portions of pentane solubles thus appear significantly less substituted than the THF-soluble, pentane-insoluble products, from the relative absence of detectable structure from 160 to 130 ppm.

¹H NMR Characterization of the THF-Soluble, Pentane-Insoluble Fraction, the Pentane-Soluble Fractions, and Preparative GPC Fractions. Proton NMR spectra of 10-, 35-, 60-, and 120-min THF-soluble, pentane-insoluble fractions (Figure 9) reveal a steady growth of aromatic hydrogen and a steady growth in the percent of aliphatic hydrogen on carbons adjacent to one (α) or more (α²) aromatic rings, and a steady decrease of hydrogen two or more carbons removed from aromatic rings. Figure 10 shows the growth in aromatic structure expressed as the aliphatic/aromatic ratio. To determine the contribution of pentane solubles to the aliphatic/aromatic ratio of the coal products, preparative GPC was carried out on the total crude reaction mixtures (Figure 3, left column) between 170 and 19,000 mol wt. As expected, the inclusion of the pentane solubles increases the aliphatic content. However, the gradual aromatization of the overall product mixture is still apparent.

²H NMR of THF-Soluble, Pentane-Insoluble Fractions and Exchange Pathways. The THF-soluble, pentane-insoluble fractions from the reaction of the subbituminous coal in 1,1-*d*₂-tetralin were examined by ²H {¹H} NMR for various reaction times. The spectrum of a 35-min reaction (Figure 11) revealed 30% deuterium aromaticity. The fraction of deuterium aromaticity remained nearly constant over a 2-hr reaction time. Although the aromaticity is close to the hydrogen aromaticity, the distribution of aliphatic deuterium differs greatly from the hydrogen distribution (Table II). More than twice the percent of deuterium occurs at alkyl carbons adjacent to one aromatic ring and more than three times the percentage of deuterium occurs at carbons adjacent to two aryl rings. By contrast, deuterium occurs at 1–1.9 (cyclohexyl and linear paraffins, etc.) to only half the extent to which hydrogen appears in this region. These results clearly indicate that deuterium transfer occurs predominantly to benzylic and diaryl methyl-type structures during the hydrogen transfer reaction. This is consistent with the view that thermal scission of structure leading to resonance-stabilized radicals (e.g., benzylic) is the principal

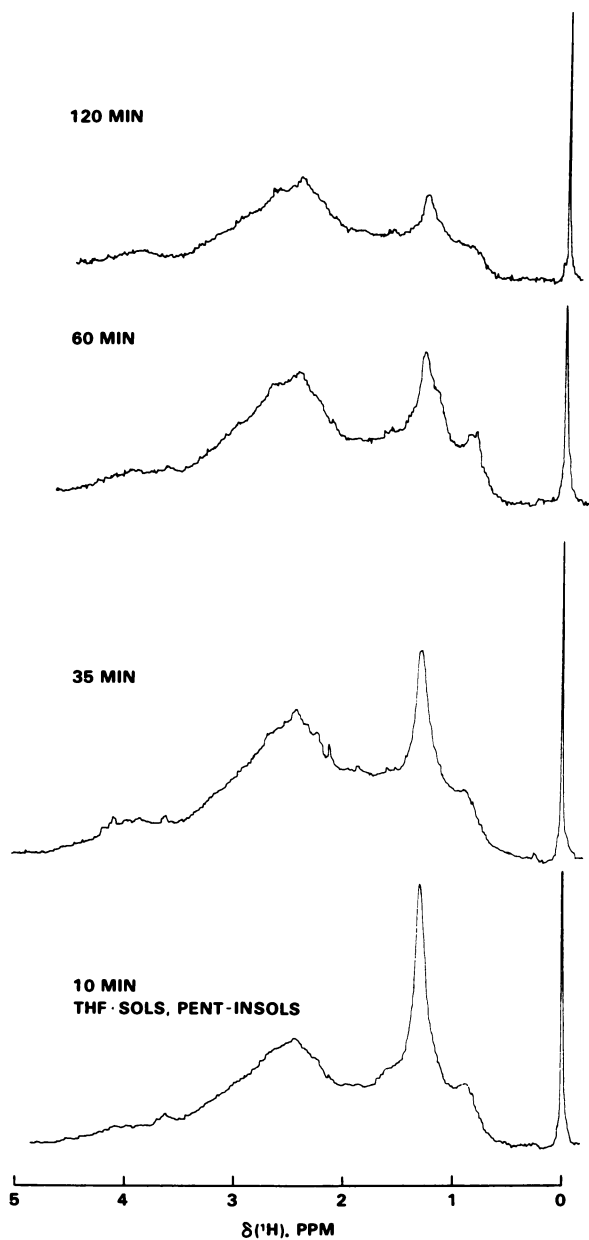


Figure 9. Aliphatic regions of ^1H NMR spectra (79.54 MHz) of THF-soluble, pentane-insoluble products for 10-, 35-, 60-, and 120-min reaction times

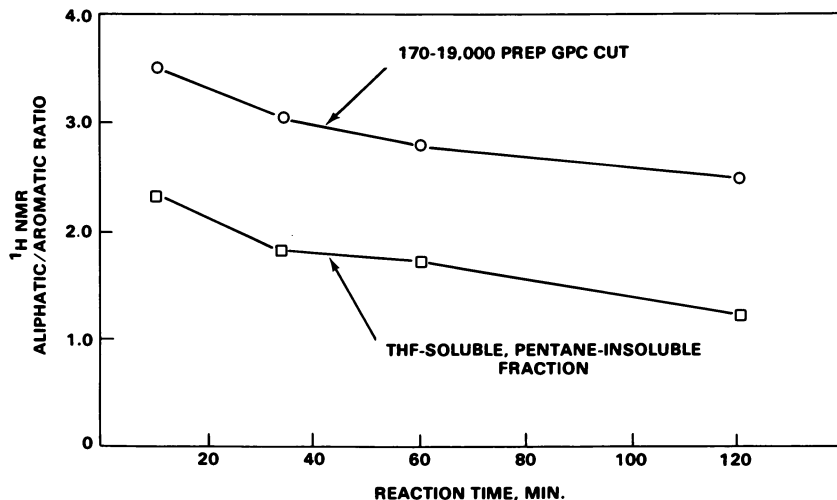


Figure 10. ^1H aliphatic/aromatic ratios of preparative GPC fractions of the THF-soluble fractions between 150 and 19,000 mol wt, and the THF-soluble, pentane-insoluble fractions vs. reaction time

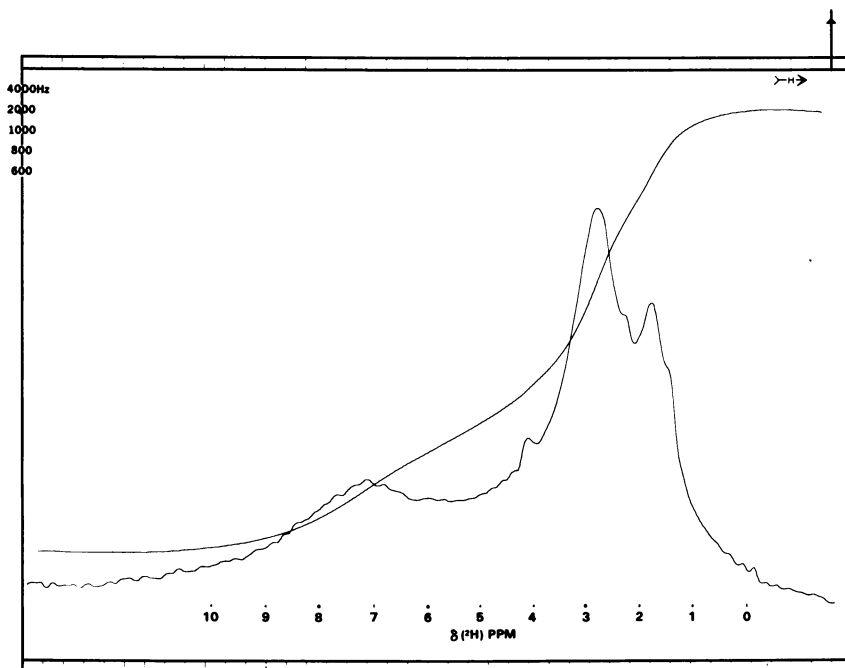


Figure 11. Proton-decoupled ^2H NMR spectrum (12.211 MHz) of the THF-soluble, pentane-insoluble fraction of products from the 35-min reaction of 1,1- d_2 -tetralin and subbituminous coal

Table II. Distributions of Aliphatic Hydrogen with Time from ^1H and ^2H [^1H] Spectra of THF-Soluble, Pentane-Insoluble Products (5)

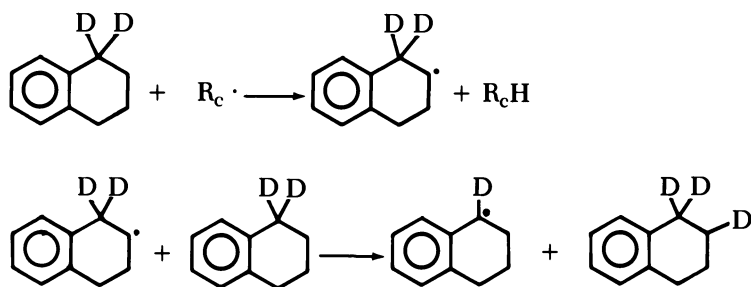
	Reaction Time (min)	Chemical Shift Range δ (ppm)			
		$\delta 0-1.0$	$\delta 1.0-1.9$	$\delta 1.9-3.2$	$\delta 3.2-4.0$
^1H NMR Data (pyridine- d_5)	2.5	18%	55%	24%	3%
	10	13%	48%	34%	5%
	35	10%	38%	44%	7%
	60	9%	45%	39%	8%
$^2\text{H}\{^1\text{H}\}$ NMR Data (THF)	5	6%	24%	47%	24%
	10	4%	26%	46%	23%
	35	5%	23%	48%	23%

mode of reaction leading from coal to preasphaltenes. The incorporation of deuterium preferentially at α -alkyl positions also has been observed by Heredy and co-workers, and is consistent with these results (14). The results of Schweighart discussed in Ref. 16 also indicate a selectivity for deuteration at benzylic and aryl sites.

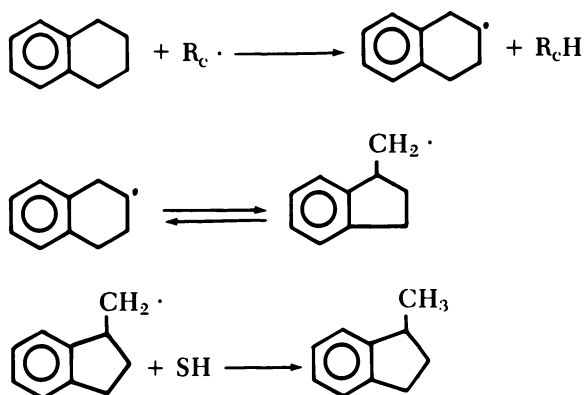
The distribution of deuterium in the THF-soluble, pentane-insoluble fractions remains surprisingly constant, in contrast to the dramatic changes in hydrogen distribution and aromaticity that occur during the same reaction time (Table II). The constant distribution of deuterium may reflect the selective extraction of specific structural types rendered more soluble in pentane or that very similar structures become deuterated during the reaction and remain unchanged upon further reaction.

Interpretation of deuterium is complicated by scrambling pathways during the reaction. To determine the degree of scrambling in aromatic compounds, reactions of phenol with 1,1- d_2 -tetralin in the presence of coal were carried out, as well as a series of experiments in which unreacted 1,1- d_2 -tetralin and naphthalene were recovered from reactions with coal at different times. For a discussion of the results with phenol see Ref. 5. Recovery of tetralin after 10 min revealed only 3% deuterium in the aromatic ring and 3% at the aliphatic 2-position. Recovery of unreacted 1,1- d_2 -tetralin from a 1 hr reaction with the subbituminous coal revealed 5% of the deuterium to be in aromatic positions, 83% in the 1-position, and 12% in the 2-position. These results show that while scrambling does occur, it is insignificant at 10 min and has occurred to only a partial extent at 1 hr of reaction time. Thus, the qualitative conclusions drawn from the distribution of deuterium in the THF-soluble fractions are probably valid, especially at 10- and 35-min reaction times, although some scrambling to the benzylic positions cannot be ruled out. The exchange of deuterium from the 1- to the 2-position of tetralin,

however, does indicate that coal-derived radicals ($R_c\cdot$) of intermediate selectivity, such as methyl or *tert*-butoxy (16), abstract hydrogen from the 2-position as well as from the 1-position:



The scrambling of 12% deuterium to the 2-position is consistent with a relative reactivity of hydrogen at the 1-position to hydrogen at the 2-position of (very roughly) 3:1 toward hydrogen abstraction. Further evidence for the formation of 2-tetralyl radical comes from the observation of 1-methylindan from the thermal rearrangement of tetralin. Work in our laboratory has shown that 1-methylindan results from the 1,2-phenyl migration of 2-tetralyl radical and does not occur via 1-tetralyl (17).



Conclusions

THF-soluble, pentane-insoluble products from the thermal dissolution of Kaiparowitz coal in tetralin comprise most of the soluble products. These materials are highly aromatic with a carbon aromaticity of about 70%. The aromatic portions are on the average highly substituted, possessing roughly one oxygen, 2.2 aryl or alkyl substituents, and 2.6 hydro-

gens for every six aromatic carbons. The THF-soluble materials undergo continuous aromatization throughout the reaction, and undergo a relatively rapid initial drop in average molecular weights, followed by a slow further reduction in molecular weight beyond 35 min. It has been demonstrated that hydrogen transfer occurs preferentially to α^2 -alkyl sites, consistent with the early formation of resonance-stabilized aryl-alkyl radicals that abstract hydrogen from tetralin or from other donors available in the coal matrix. Finally, the degree of aromaticity found for the short (10-min) reaction time is probably slightly less than or approaching the aromaticity expected for the parent subbituminous coal. More work at the shorter reaction times (2–5 min) is needed to establish this relationship, as well as carbon aromaticities from magic angle/cross polarization ^{13}C NMR studies.

Acknowledgment

This work was supported by the U.S. Department of Energy, Office of Basic Energy Sciences, Division of Chemical Sciences, under Contract EY-76-C-06-1830 with Battelle Memorial Institute, Pacific Northwest Laboratory.

Literature Cited

1. Curran, G. P.; Struck, R. T.; Gorin, E. *Ind. Eng. Chem., Process Des. Dev.* **1967**, *6*, 166.
2. Neavel, R. C. *Fuel* **1976**, *55*, 237.
3. Kang, D.; Anderson, L. L.; Wisler, W. H. "Elucidation of Coal Structural Components By Short Residence Time Extractive Liquefaction", Technical Report, Department of Energy under contract number E (49-18)-2006, Univ. of Utah, Department of Mining and Fuels Engineering, Salt Lake City, Utah, Aug. 1979.
4. Bartuska, V. J.; Maciel, G. E.; Schaefer, J.; Stejskal, E. O. *Fuel* **1977**, *56*, 354.
5. Franz, J. A. *Fuel* **1979**, *58*, 405.
6. Natusch, D. F. S. *J. Am. Chem. Soc.* **1971**, *93*, 2566 and La Mar, G. N., *J. Am. Chem. Soc.* **1971**, *93*, 1040.
7. Alger, T. D.; Pugmire, R. J.; Grant, D. M. *Fuel Div. Am. Chem. Soc., Prepr.* (Honolulu, April, 1979) *24*, pp. 334–337.
8. Snape, C. E.; Ladner, W. R.; Bartle, K. D. *Anal. Chem.* **1979**, *51*, 2189.
9. Benjamin, B. M.; Raaen, V. F.; Maupin, P. H.; Brown, L. L.; Collins, C. J. *Fuel* **1976**, *55*, 269.
10. Ruberto, R. G.; Cronauer, D. C.; Jewell, D. M.; Seshadri, K. S. *Fuel* **1977**, *56*, 17, 26.
11. Levy, G. C.; Nelson, G. L. "Carbon-13 Nuclear Magnetic Resonance for Organic Chemists"; Wiley-Interscience: New York, 1972.
12. Stothers, J. B. "Carbon-13 NMR Spectroscopy"; Academic: New York, 1972.
13. Johnson, L. F.; Jankowski, W. C. "A Collection of Signed, Coded, and Indexed Spectra"; Wiley-Interscience: New York, 1972.
14. Skowronski, R. P.; Ratto, J. J.; Heredy, L. A. "Deuterium Tracer Method for Investigating the Chemistry of Coal Liquefaction", Quarterly Technical

- Progress Report, U.S. Department of Energy Document FE-2781-3, Energy Systems Group, Rockwell International, Canoga Park, CA, July 1978.
15. Retcofsky, H. L.; Link, T. In "Analytical Methods for Coal and Coal Products"; Karr, C., Jr., Ed.; Academic: New York, 1978; Vol. 2, pp. 162-206.
 16. Ingold, K. U. In "Free Radicals"; Kochi, J. K., Ed.; Wiley-Interscience: New York, 1973; pp. 38-112.
 17. Franz, J. A.; Camaioni, D. M. *J. Org. Chem.* **1980**, *45*, 5247-5255.

RECEIVED July 19, 1979.

Relation Between Coal Structure and Thermal Decomposition Products

P. R. SOLOMON¹

United Technologies Research Center, East Hartford, CT 06108

A relation between coal organic structure and the products of thermal decomposition was developed by measuring and modeling vacuum devolatilization of 12 bituminous coals and a lignite. The distribution of devolatilization products is related to the concentration of aromatic and aliphatic carbons and hydrogens, and oxygen functional groups. Structure information on the coals, tars, and chars was provided by IR spectra obtained with a Fourier transform infrared spectrometer (FTIR). Quantitative determinations of aromatic and aliphatic hydrogens and hydroxyl oxygens can be made from the IR spectra, and concentrations of aromatic and aliphatic carbons and ether oxygens may be inferred. These quantities may be used to predict the time-dependent evolution of thermal decomposition products by using kinetic constants that depend on the functional group but are independent of coal rank.

In a recent study the thermal decomposition of 13 coals was examined in over 600 vacuum devolatilization experiments (1). The results for all 13 coals were successfully simulated in a model that assumes that large molecular fragments (monomers) are released from the coal polymer, with only minor alteration, to form tar, while simultaneous cracking of the chemical structure forms the light molecules of the gas (2, 3). The evolution of each species is characterized by rate constants that do not vary with coal rank. The differences between coals are due to differences in the mix of sources in the coal for the evolved species. The sources were tentatively related to the functional group concentrations in the coal.

¹Current address: Advanced Fuel Research, Inc., 87 Church Street, East Hartford, CT 06108.

This paper reports a study to verify the relationship between functional group distribution and thermal decomposition behavior. A Fourier transform infrared spectrometer (FTIR) has been employed to obtain quantitative infrared spectra of the coals, chars, and tars produced in the devolatilization experiments. The spectra have been deconvoluted by using a computerized spectral synthesis routine to obtain functional group distributions, which are compared to the model parameters.

Model

The thermal decomposition model is illustrated in Figure 1. The coal is represented as an area with X and Y dimensions. The Y dimension is divided into fractions according to the chemical composition of the coal. Y_i° represents the initial fraction of a particular component (carboxyl, aromatic hydrogen, etc.) and $\sum Y_i^\circ = 1$. The evolution of each component into the gas (carboxyl into CO_2 , aromatic hydrogen into H_2 , etc.) is represented by the first-order diminishing of the Y_i dimension, $Y_i = Y_i^\circ \exp(-k_i t)$. The relationship between the functional groups and the thermal decomposition products is discussed by Solomon and Colket (2). More complicated reaction steps have been observed at high temperature (4). The X dimension is divided into a potential tar-forming fraction X° and a non-tar-forming fraction $1 - X^\circ$, with the evolution of the tar being represented by the first-order diminishing of the X dimension, $X = X^\circ \exp(-k_x t)$. k_i and k_x are rate constants given in Table I.

The amount of a component in each of the pyrolysis products is given by the following equations:

$$W(i)_{\text{char}} = (1 - X^\circ + X)Y_i$$

$$W(i)_{\text{tar}} = (X^\circ Y_i^\circ - X Y_i) k_x / (k_i + k_x)$$

$$W(i)_{\text{gas}} = (1 - X^\circ) (Y_i^\circ - Y_i) + W(i)_{\text{tar}} k_i / k_x$$

Table I. Kinetic Constants for Lignite and Bituminous Coals

Functional Group	Kinetic Rates
Carboxyl	$k_1 = 6 \exp(-4,000/T) \text{ sec}^{-1}$
Hydroxyl	$k_2 = 15 \exp(-4,950/T)$
Ether loose	$k_3 = 7,000 \exp(-10,300/T)$
Ether tight	$k_4 = 890 \exp(-12,000/T)$
Aliphatic	$k_5 = 4,200 \exp(-9,000/T)$
Aromatic H	$k_6 = 3,600 \exp(-12,700/T)$
Nonvolatile C	$k_7 = 0$
Tar	$k_x = 750 \exp(-8,000/T)$

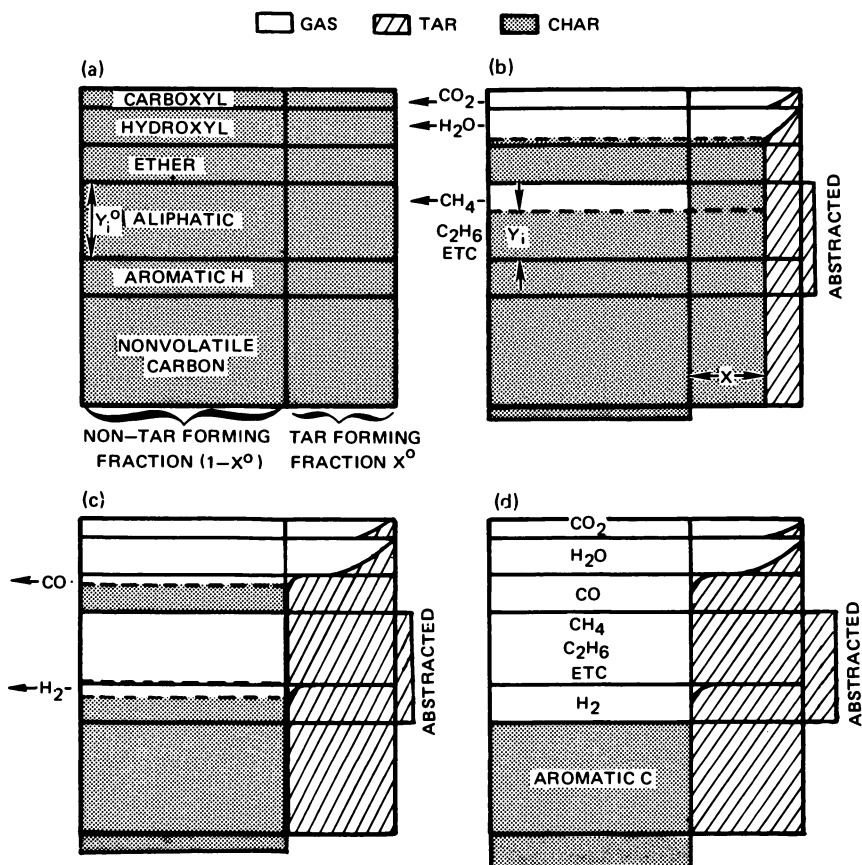


Figure 1. Progress of thermal decomposition according to model: (a) functional group composition of coal; (b) initial state of decomposition; (c) later stage of decomposition; (d) completion of decomposition

According to this model the tar contains a mix of functional groups similar to that in the parent coal. This concept is based on the strong similarity between vacuum devolatilized tar and the parent coal observed in chemical composition (1, 2, 3), infrared spectra (1, 3, 5, 6), and NMR spectra (1, 3). The similarity of the IR spectra is illustrated in Figure 2 for four coals. The resemblance is strong for the three bituminous coals but not for the lignite. The resemblance of the tar and parent coal suggests that the tar consists of monomers released from the coal polymer. The major difference observed in the IR spectra between tar and parent coal is the higher quantity of aliphatic CH_2 and CH_3 , presumably resulting because the monomers abstract hydrogen to stabilize the free radical sites produced when the monomer was freed. Similar arguments

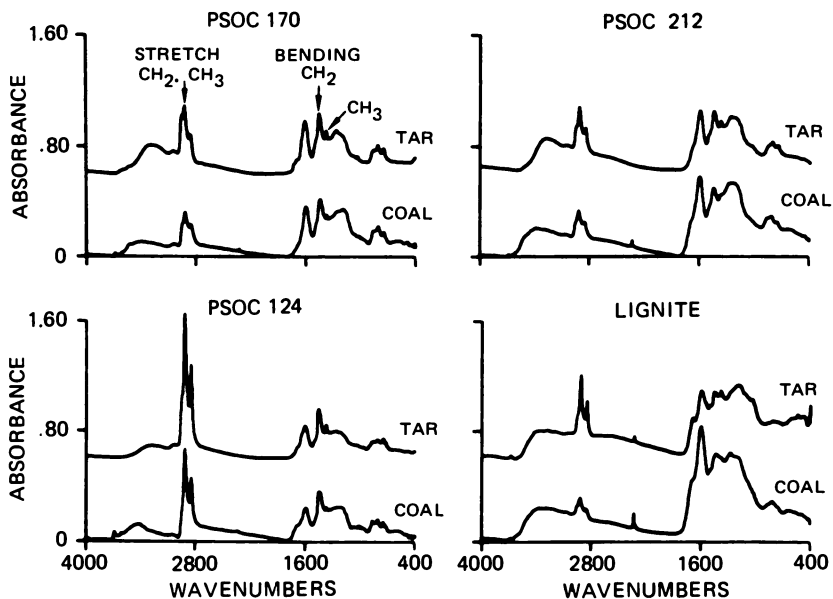


Figure 2. IR spectra of coals and tars. The absorbance is normalized to a sample size of 1 mg/cm^2 in the KBr disk.

were given for pyrolysis of model compounds by Wolfs, van Krevelen, and Waterman (7).

Figure 1(b) illustrates the initial stage of thermal decomposition during which the volatile components H_2O and CO_2 evolve from the hydroxyl and carboxyl groups, respectively, along with aliphatics and tar. At a later stage [Figure 1(c)] CO and H_2 are evolved from the ether and aromatic H. Some CO is also released at low temperatures, so two kinetic rates are listed for ether.

To simulate the abstraction of H by the tar, the aliphatic fraction in the tar is assumed to be retained together with some additional aliphatic material, which may be added directly or may contribute its hydrogen. When hydrogen from the aliphatic material is contributed, its associated carbons remain with the nonvolatile carbon fraction, which eventually forms the char [Figure 1(d)]. The nonvolatile carbon fraction is the aromatic carbon fraction minus the fraction of carbons released as CO from ether tight.

Infrared Spectra

Infrared spectra of coals, tars, and chars were obtained on a Nicolet FTIR. KBr pellets of coals and chars were prepared by mixing 1 mg of a

dry, finely ground (20 min in a Wig-L-Bug) sample with 300 mg of KBr. Pellets 13 mm in diameter were pressed in an evacuated die under 20,000 lb of pressure for 1 min and dried at 110°C overnight to remove water. Since the heating process destroyed similarly prepared tar pellets, the water correction was obtained by subtracting the spectrum of a blank disk prepared under the same conditions. The H₂O-corrected spectra matched those from samples prepared by allowing the tar produced in thermal decomposition to fall directly onto a water-free blank KBr disk. Spectra are obtained by using 4-wave number resolution, 100 scans of the sample, and 100 scans of the background. A globar source and cooled mercury-cadmium-telluride detector are used.

The FTIR obtains spectra in digital form, and corrections for particle scattering, mineral content, and water may be easily made. A typical correction sequence is illustrated in Figure 3. The lower curve in Figure 3(a) is the uncorrected spectrum of a dried coal. It has a slope, owing to particle scattering, and peaks from the mineral components near 3600, 1000, and 450 cm⁻¹. The middle spectrum in Figure 3(a) has had the mineral peaks removed, which is done by subtracting appropriate amounts of the reference spectra shown in Figure 3(b) to produce a smooth spectrum in the region of the mineral peaks. The sum of the reference spectra subtracted from the coal is shown as the top spectrum in Figure 3(b). Similar procedures for mineral analysis using FTIR have recently been reported (8). The top spectrum in Figure 3(a) represents the coal on a mineral-matter-free basis. It has had a straight-line scattering correction and has been scaled to give the absorbance for 1 mg/cm² of dry, mineral-matter-free (DMMF) coal.

Much previous work has been done to identify the functional groups responsible for the observed peaks. Extensive references may be found in Lowry (9) and van Krevelen (10). To get a quantitative measure of the functional group concentrations, we used a curve analysis program (CAP), available in the Nicolet library, to synthesize the IR spectra. The synthesis is accomplished by adding 26 absorption peaks with Gaussian shapes and variable position, width, and height, as shown in Figure 4. The peaks are separated according to the identified functional group. All the coals, chars, and tars that were studied could be synthesized by varying only the magnitudes of a set of Gaussians whose widths and positions were held constant. These samples could be analyzed, therefore, in terms of a fixed mix of functional groups.

The set of peaks M, N, and Q simulates the absorption assumed to result from hydrogen-bonded OH. To verify this assumption, we obtained spectra, at elevated temperatures, of a tar sample coated on a KBr pellet. Figure 5 shows a spectrum taken near room temperature, one at 250°C, and their difference. As expected for hydrogen bonding, the absorption for bonded OH groups (3400–2400 cm⁻¹) decreased, while that

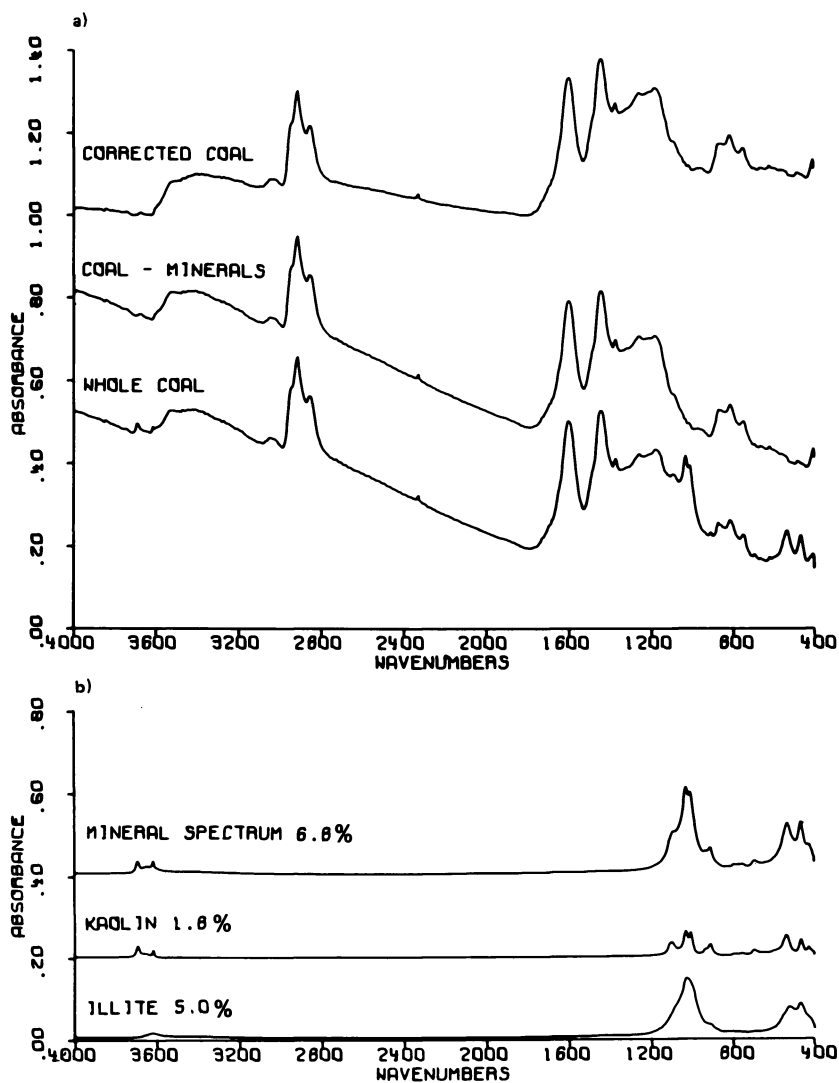


Figure 3. Correction of coal spectrum for scattering and minerals: (a) correction of coal spectrum; (b) determination of mineral spectrum by addition of reference spectra. The absorbance is normalized to a sample size of 1 mg/cm^2 in the KBr disk.

for free OH (3500 cm^{-1}) increased. The change in the high-temperature spectrum was not permanent; the room temperature spectrum returned after cooling.

Peak O at 1600 cm^{-1} has been included with the hydroxyl group. The identity of this peak has caused much speculation in the literature (9, 10). Fujii et al. (11) showed that the intensity of the

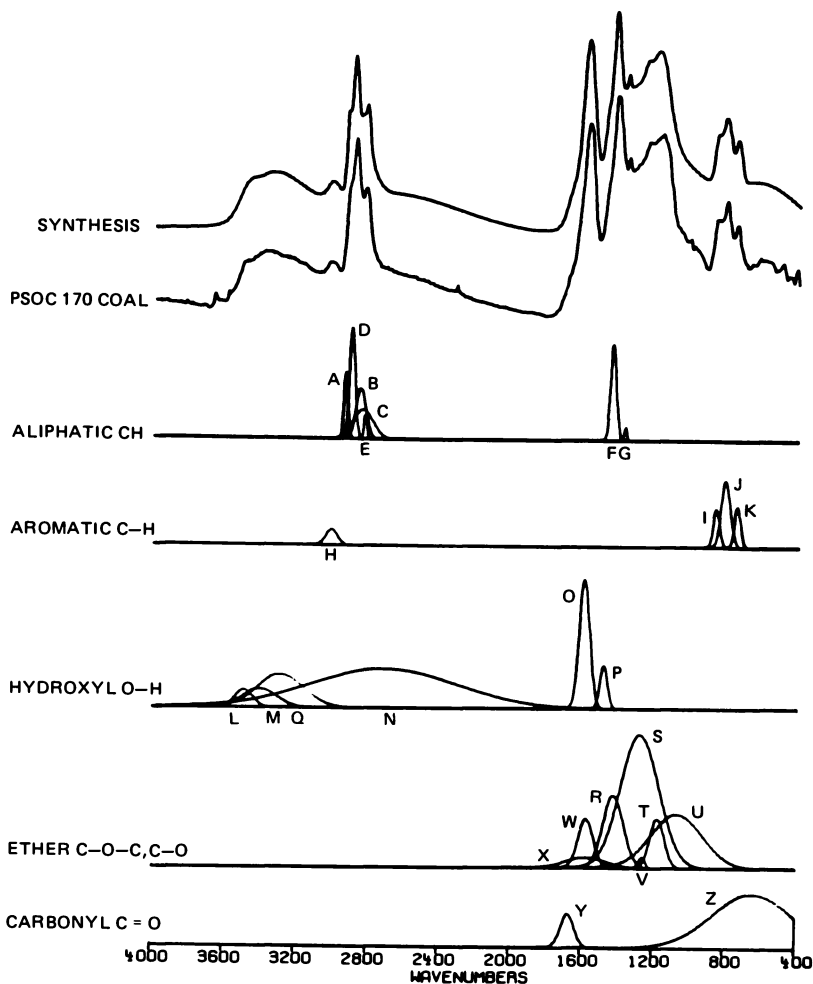


Figure 4. Synthesis of IR spectrum

1600-cm^{-1} peak varied linearly with oxygen content in the coal. The present study narrows the correlation still further. Figure 6 shows a linear relation between the intensity of the O peak at 1600 cm^{-1} and the hydroxyl content measure by peaks L, M, N, and Q. The correlation includes chars that have a high oxygen content in ether groups but low O peaks, so that the correlation with total oxygen would no longer hold. It also includes samples that have a large aliphatic content and a small value of O and samples with a small aliphatic content and a large value of O, so that enhanced aromatic ring resonance due to aliphatic substitutions is unlikely. It therefore has been concluded that the sharp line at 1600 cm^{-1} is caused mainly by enhanced aromatic ring resonance due to OH substitutions.

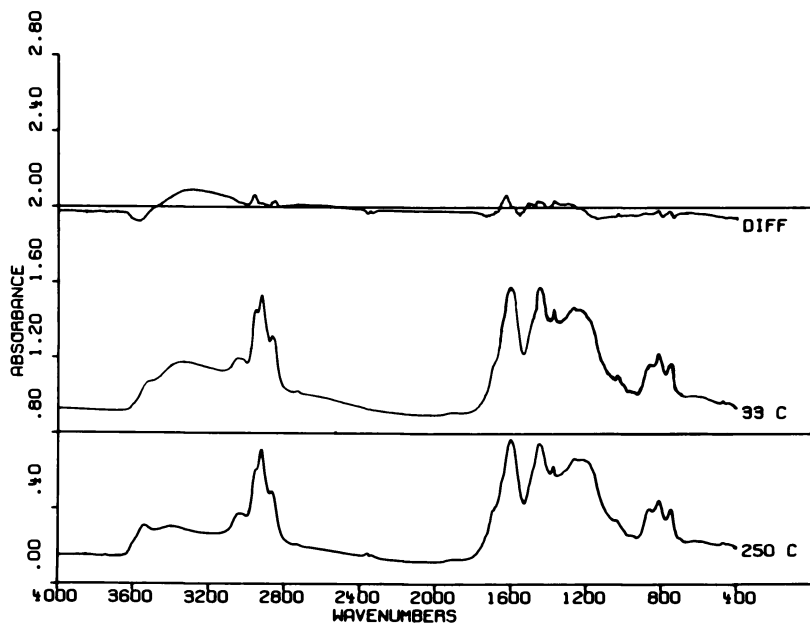


Figure 5. Variation of hydrogen bonding with temperature

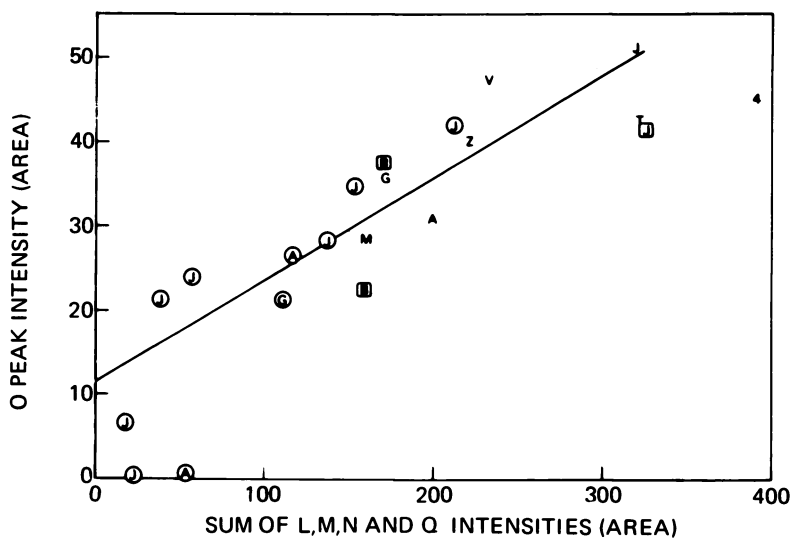


Figure 6. Correlation of 1600-cm^{-1} absorption with OH absorption intensity. Letters designate coals (see Table II); (O) chars; (□) tars.

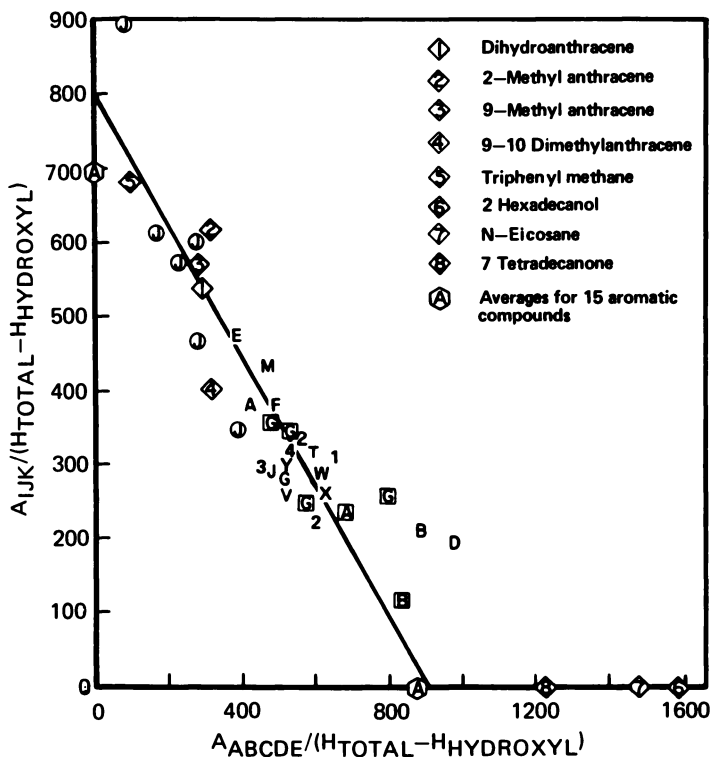


Figure 7. Calibration of aromatic and aliphatic absorption peaks. Letters and numbers designate coals (see Table II); (O) chars; (□) tars. (Several coals not included in Table II were supplied by Bernard Gerstein of Iowa State University.)

The calibration of the aliphatic peaks near 2900 cm^{-1} (lines A–E) and the aromatic peaks near 800 cm^{-1} (lines I–K) is shown in Figure 7. The objective is to determine the values of the constants a and b [in (milligrams/square centimeter)/absorbance units centimeters $^{-1}$], which relate peak areas (in absorbance units centimeters $^{-1}$) to the corresponding hydrogen concentration (in milligrams/square centimeter); i.e.,

$$H_{\text{ali}} = aA_{\text{ABCDE}} \text{ and } H_{\text{ar}} = bA_{\text{IJK}}$$

where A_{ABCDE} is the area under the aliphatic peaks A–E, A_{IJK} is the area under the aromatic peaks I–K, and H_{ali} and H_{ar} are the aliphatic (or alicyclic) and aromatic hydrogen concentrations in the KBr pellet, respectively. The equation for total hydrogen concentration, $H_{\text{total}} = H_{\text{ali}} + H_{\text{ar}} + H_{\text{hydroxy}}$, may be combined with the equations above to yield

$$a \left[\frac{A_{ABCDE}}{H_{\text{total}} - H_{\text{hydroxyl}}} \right] = 1 - b \left[\frac{A_{IJK}}{H_{\text{total}} - H_{\text{hydroxyl}}} \right]$$

where H_{hydroxyl} is the hydrogen content in hydroxyl groups obtained from

$$H_{\text{hydroxyl}} = cA_{LMNQ}$$

where c has been determined by using the relation between hydroxyl content and the specific extinction coefficient at 3450 cm^{-1} derived by Ōsawa and Shih (12).

The same analysis has been applied to several model compounds. If a and b are constant for all products, then plotting one term in the square brackets against the other should yield a straight line with intercepts $1/a$ and $1/b$. The results indicate a and b to be constant for most coal products as well as many model compounds containing aromatic rings. Exceptions are long aliphatic chains (model compounds 6, 7, and 8), coals B and D, and a low-temperature tar G. The latter three products have an aliphatic stretch spectrum that resembles the long-chain aliphatics, for which a different calibration should be used. The presence of long-chain aliphatics was also observed in a recent study of coal and coal-derived liquids, using ^{13}C NMR (13).

Table II. Hydrogen Distribution in Coals (DMMF)

Coal	Plotting Symbol	C	H	O	From IR			
					$H_{\text{ar}}\%$	$H_{\text{ali}}\%$	$H_{\text{hydr}}\%$	$H_{\text{ar}}/H_{\text{ali}}$
PSOC 268	M	86.2	5.24	6.13	2.2	2.8	0.28	0.79
PSOC 124	B	84.8	7.17	6.35	1.6	6.0	0.42	0.27
PSOC 170	G	81.8	5.37	9.12	1.8	3.2	0.31	0.56
PSOC 103	A	82.9	5.11	10.04	2.0	2.4	0.36	0.83
Bu Mi 40660	Z	79.9	5.32	11.74	2.0	3.1	0.42	0.65
PSOC 330	V	80.4	5.09	12.21	1.9	2.8	0.42	0.68
PSOC 212	J	76.2	4.81	16.81	1.5	2.5	0.58	0.60
PSOC 308	T	74.0	5.11	18.14	1.7	3.0	0.58	0.57
Montana lignite	4	65.2	3.60	29.44	1.1	1.7	0.71	0.65

The hydrogen distribution computed using the determined values of $a = 1/900$ and $b = 1/800$ are shown in Table II. In the present investigation it was felt that the determination of peak areas rather than peak intensities would be the more accurate method for determining quantitative functional group concentration. For comparison to other infrared investigations, useful relations are

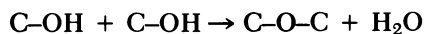
$$H_{\text{ali}} = 11.5 \times D_{\text{ali}}A/M\% \quad \text{and} \quad H_{\text{ar}} = 19.2 \times D_{\text{ar}}A/M\%$$

where A is the area of the pellet in square centimeters, M is the sample weight in milligrams, D_{ali} is the optical density of the peak at 2920 cm^{-1} , and D_{ar} is the average optical density of the I, J, and K peaks near 800 cm^{-1} .

The aromatic hydrogen values are in agreement with those determined by van Krevelen (10) and by Mazumdar et al. (14) from pyrolysis measurements but are larger (by about a factor of 2) than those determined by Brown (15) using IR techniques. Brown measured the ratio of extinction coefficients at 3030 cm^{-1} (line H) and 2920 cm^{-1} (line D) and used an assumed value of 2 (this value has been open to question) for the ratio of absorption strength for aliphatic and aromatic C—H bonds. The ratio of extinction coefficients determined in the present study are in reasonable agreement with those determined by Brown; thus the absorption strength ratio must be approximately 4 to produce the measured values of $H_{\text{ar}}/H_{\text{ali}}$.

Thermal Decomposition

The progress of thermal decomposition is illustrated by the series of spectra for chars in Figure 8. The chars were produced by devolatilizing coal PSOC 212 for 80 sec at the indicated temperature. The results are similar to those observed by Brown (16) and Oelert (17). The rapid disappearance of the aliphatic and hydroxyl peaks is apparent. The aromatic peaks remain to high temperature, and the ether peaks are observed to increase in intensity, possibly from the creation of new ether linkages by



For high-temperature chars whose carbon content exceeds 92%, a broad absorption begins to dominate the spectrum. This effect is similar to that observed in high-rank coals (above 92% C), which has been attributed to electronic absorption (9, 10).

Figure 9 compares the disappearances of the aliphatic groups in a char (*solid triangles*) with the evolution of tar and heavy aliphatics predicted from the model (*lines*) and experimentally determined (*squares* and *circles*). The agreement is consistent with the assumptions of the model.

Figure 10 shows the quantitative determination of the hydrogen functional group distribution for the chars in Figure 8. Figure 11 shows the measured hydrogen content and model prediction. The agreement is good. Comparison of Figures 10 and 11 shows how the low-temperature loss of aliphatic material and tar and the retention of aromatic hydrogen produced the observed shape for the curve of total hydrogen content vs. temperature. The distribution of other products of thermal decomposition for the same coal is shown in Figures 12 and 13.

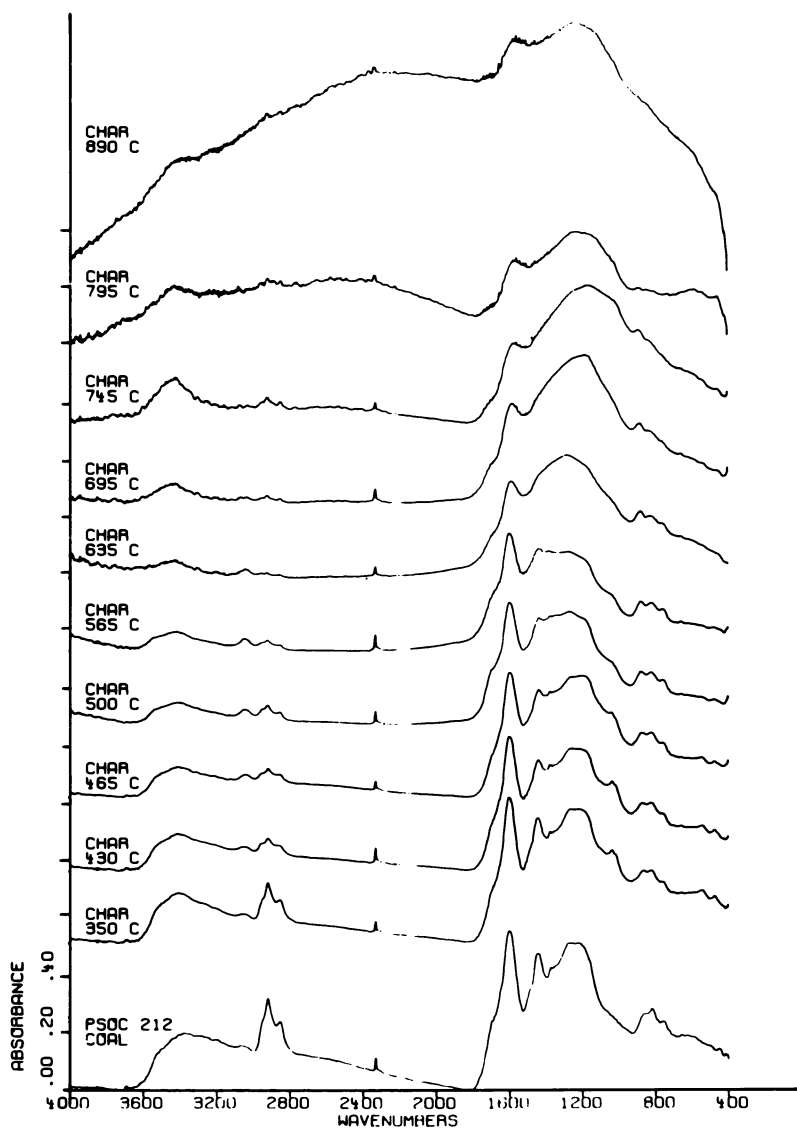


Figure 8. Spectra of chars of PSOC 212 coal; chars from 80-sec vacuum pyrolysis at the indicated temperature

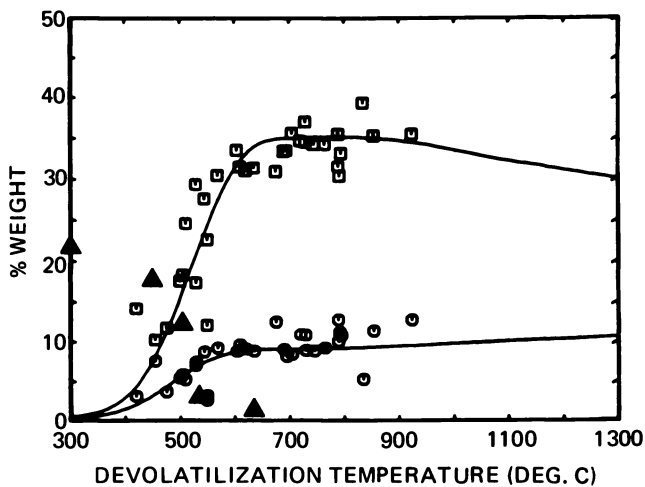


Figure 9. Comparison of tar and heavy aliphatic evolution with diminishing char aliphatic content; products from 20-sec vacuum pyrolysis run of PSOC 170 coal (□) tar released; (○) hydrocarbons released; (▲) aliphatic C-H in char

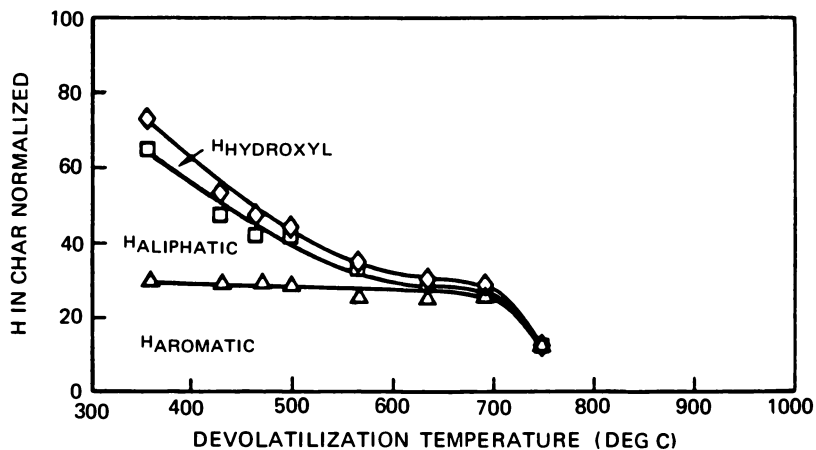


Figure 10. Hydrogen distribution in char from infrared analysis. The hydrogen in the char is normalized by the amount of hydrogen in the starting coal sample. Chars from 80-sec vacuum pyrolysis of PSOC 212 coal.

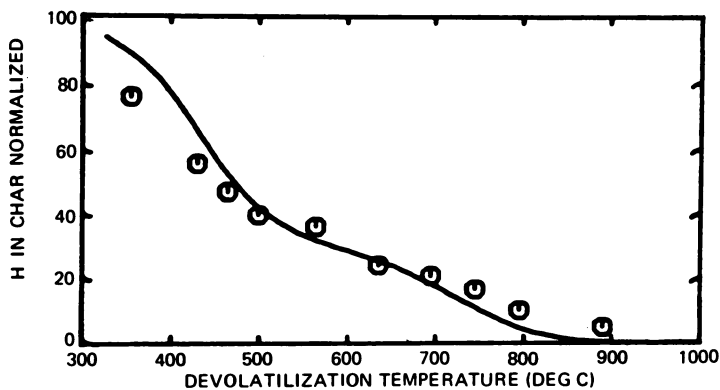


Figure 11. Hydrogen in char; experiment and theory. The hydrogen in the char is normalized by the amount of hydrogen in the starting coal sample. Chars from 80-sec vacuum pyrolysis of PSOC 212 coal.

The thermal decomposition model was developed by using parameters derived from the decomposition experiments (1, 2, 3). The observed relationship between the products and the functional group compositions determined from IR measurements indicates that several of these model parameters may be obtained directly from the IR spectra. A comparison of parameters determined from the thermal decomposition experiments with those determined from the IR measurements is made in Figure 14. Figure 14(a) shows the results for aliphatic CH. For the IR determination it has been assumed that the aliphatics have the stoichiometry $\text{CH}_{1.8}$ (18). Figure 14(b) shows the results for aromatic carbon. For the IR determinations $C_{\text{ar}} = C_{\text{total}} - C_{\text{ali}}$. For the model the arom-

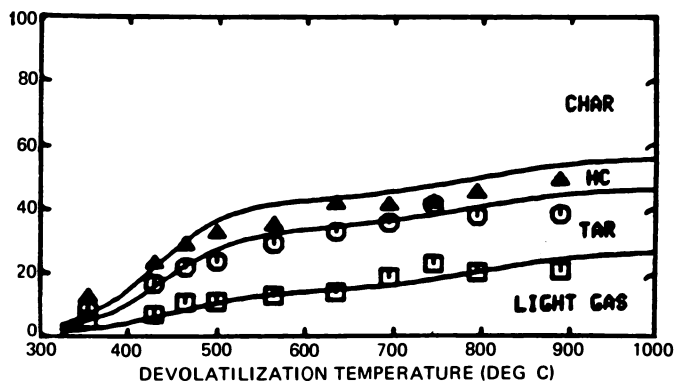


Figure 12. Products of thermal decomposition, experiment and theory. Products from 80-sec vacuum pyrolysis of PSOC 212.

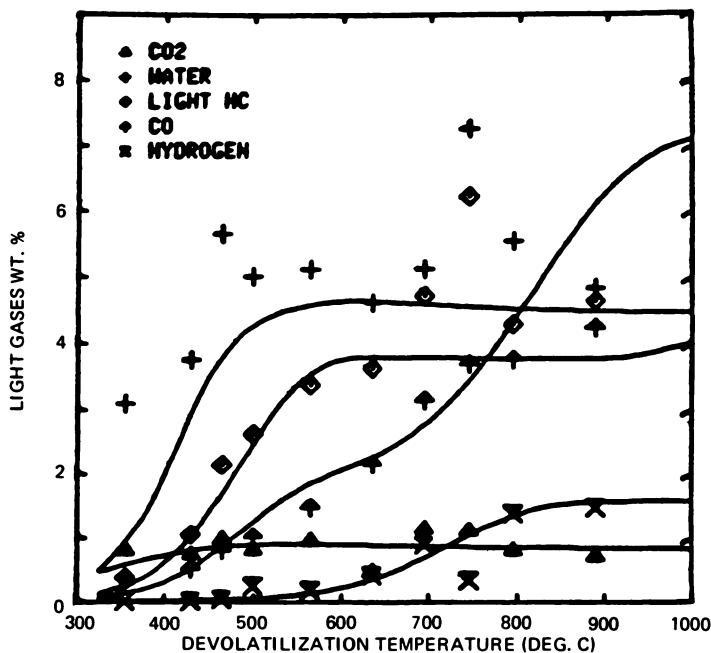


Figure 13. Products of thermal decomposition, experiment and theory; light gases. Products from 80-sec vacuum pyrolysis of PSOC 212.

atic carbon is the nonvolatile carbon plus the carbon associated with ether tight, $C = C_{NVC} + 12/28$ (ether tight). The agreements between functional group concentrations determined from FTIR measurements and the model parameters are good.

Comparisons were previously made for oxygen groups (2).

Conclusions

The results of the present investigation have yielded the following conclusions:

1. FTIR provides a convenient tool for obtaining quantitative infrared spectra of coals, chars, and tars on a dry, mineral-matter-free basis.
2. The spectra of all the coals, chars, and tars studied could be deconvoluted by varying the magnitudes of a set of 26 Gaussians whose widths and positions were held constant. This method provides a good way for determining magnitudes of individual peaks.

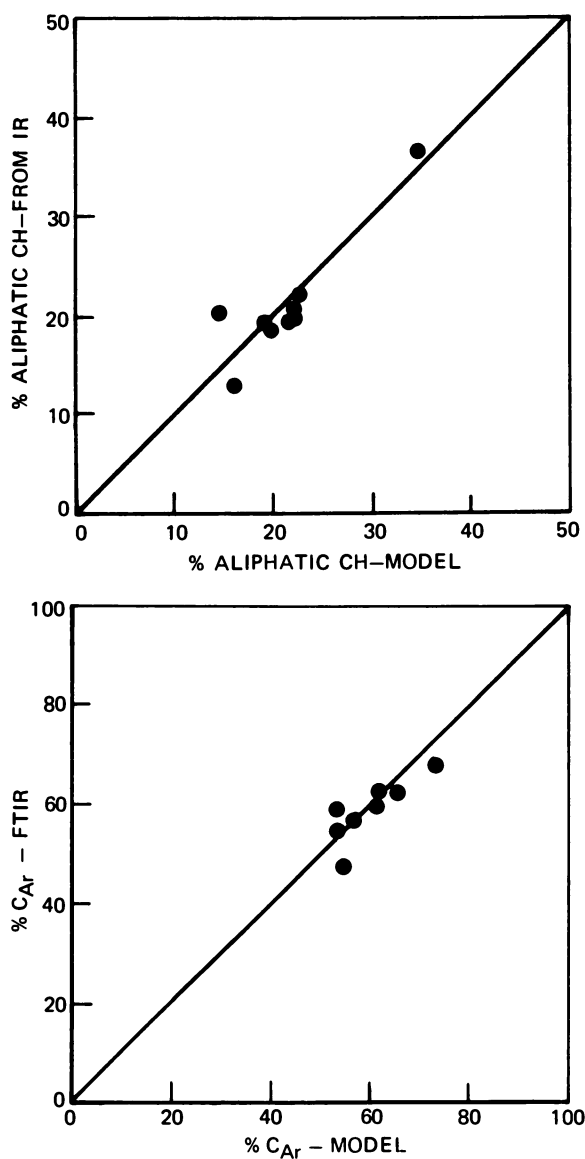


Figure 14. Comparison of model parameters with IR intensities

3. Correlation of the magnitudes of the 1600-cm^{-1} peak with the hydroxyl content of a variety of coals, tars, and chars indicates that hydroxyl, probably in the form of phenols, contributes strongly to this peak.
4. A regression analysis applied to a series of coals, chars, and tars with widely differing ratios of aliphatic-to-aromatic hydrogen has been used to calibrate the aliphatic and aromatic C-H absorption intensities.
5. The values of aromatic hydrogen for coals derived from the infrared analysis are in reasonable agreement with those of van Krevelen (10) and Mazumdar (14) but are roughly a factor of 2 larger than those derived by Brown (15).
6. Infrared spectra of a series of coals and tars demonstrate the very close similarity of tars to their parent coals, providing further evidence that the tar consists of hydrogen-stabilized monomers derived from decomposition of the coal polymer.
7. The variation of functional group concentrations in the products of thermal decomposition is in good agreement with the predictions of a detailed thermal decomposition model (1, 2, 3).
8. Most of the coal parameters used in the thermal decomposition model may be obtained directly from an infrared, ultimate, and proximate analysis of the coal, allowing prediction of thermal decomposition behavior from a general set of kinetic constants applicable to lignite and bituminous coals.
9. While the model is successful in simulating the results for vacuum pyrolysis, care must be taken in extending the results to other thermal decomposition processes where the reactions may be more complicated.

Acknowledgments

The author wishes to acknowledge the able technical assistance of David Santos and Gerald Wagner and helpful discussions with Med Colket and Daniel Seery. The thermal decomposition studies upon which this work was based were supported in part by grant No. AER75-17247 from the National Science Foundation. Additional work has been performed under contract No. ET-78-C-01-3167 with the U.S. Department of Energy.

Literature Cited

1. Solomon, P. R. "The Evolution of Pollutants During the Rapid Devolatilization of Coal," Report NSF/RA-770422, NTIS No. PB278496/AS.
2. Solomon, P. R.; Colket, M. B. "Seventeenth Symposium (International) on Combustion"; The Combustion Institute: 1979; p. 131.

3. Solomon, P. R.; Colket, M. B. *Fuel*, 1978, 57, 751.
4. Solomon, P. R. *Am. Chem. Soc. Div. Fuel Chem. Prepr.* 1979, 24(3), 154.
5. Orning, A. A.; Greifer, B. *Fuel* 1956, 35, 381.
6. Brown, J. K.; Dryden, I. G. C.; Dunevein, D. H.; Joy, W. K.; Pankhurst, K. S. *J. Inst. Fuels* 1958, 31, 259.
7. Wolfs, P. M. J.; van Krevelen, D. W.; Waterman, H. I. *Fuel* 1960, 39, 25.
8. Painter, P. C.; Coleman, M. M.; Jenkins, R. G.; Walker, P. L., Jr. *Fuel* 1978, 57, 124.
9. Lowry, H. H. "Chemistry of Coal Utilization" (Supplementary Volume), Wiley: New York, 1963.
10. van Krevelen, D. W.; Schuyer, J. "Coal Science," Elsevier: Amsterdam, 1957.
11. Fujii, S.; Ōsawa, Y.; Sugimura, H. *Fuel* 1970, 49, 68.
12. Ōsawa, W.; Shih, J. W. *Fuel* 1971, 50, 53.
13. Pugmire, R. J.; Grant, D. M.; Zilm, K. W.; Anderson, L. L.; Oblad, A. G.; Wood, R. E. *Fuel* 1977, 56, 295.
14. Mazumdar, B. K.; Chakrabartty, S. K.; Lahiri, A. *Fuel* 1962, 41, 129.
15. Brown, J. K. *J. Chem. Soc.* 1955, 744.
16. Brown, J. K. *J. Chem. Soc.* 1955, 752.
17. Oelert, H. H. *Fuel* 1968, 47, 433.
18. Dryden, I. G. C. *Fuel* 1962, 41, 55.

RECEIVED July 19, 1979.

Carboxylic Acids and Coal Structure

A. L. CHAFFEE, G. J. PERRY¹, and R. B. JOHNS

Department of Organic Chemistry, University of Melbourne, Parkville 3052, Australia

A. M. GEORGE

Herman Research Laboratory, State Electricity Commission of Victoria, Howard Street, Richmond 3121, Australia

The monofatty acids (C₁₄-C₃₂) from five lithotypes of Victorian brown coal and from a Sydney Basin black coal were analyzed by gas-liquid chromatography. The different profiles observed for the various lithotypes have been interpreted in terms of differences in depositional environment, while differences in rank appear to be responsible for the large differences between the brown and black coal samples. The presence of several classes of acids in these coals is reported, but of these the presence of monounsaturated and diunsaturated acids is particularly important in view of their assumed geochemical instability.

Fatty acids are widely distributed in nature and have been studied extensively in petroleum (1, 2) and sediments (1, 3, 4, 5), as well as in living organisms (6, 7, 8). Fatty acids are major components in most living organisms, and since they are geochemically quite stable (9), they are important components in most depositional environments. The presence of fatty acids in coals has been recorded (10, 11, 12), but there appears to be little published information available on their distribution, particularly in brown coals, except in montan wax deposits (13, 14). In contrast, the distribution of *n*-alkanes in coals has been widely studied, and the maxima of the distributions have been shown to range from C₂₉

¹ Current address: Herman Research Laboratory, State Electricity Commission of Victoria, Howard Street, Richmond, Vic. 3121, Australia.

and C_{31} in lower-rank coals to as low as C_{16} in higher-rank coals (10, 15). Many authors have proposed a genetic relationship between fatty acids and *n*-alkanes in petroleum and sediments (2, 16, 17).

Fatty acids have been used as biological markers (18), particularly in recent sediments, to suggest input from particular source organisms (5, 19, 20). For example, long-chain acids ($>C_{22}$) are thought to be derived largely from higher plant sources alone, while the shorter-chain acids are considered more universal in their origin (4, 21, 22, 23). Branched-chain acids belonging to the iso- and anteiso- series are often thought to represent a bacterial input to sediments (1, 21, 24). Recently several other structural types of fatty acids have been proposed as bacterial markers (19).

This study reports the monocarboxylic fatty acid content of a series of brown coal lithotypes from the Latrobe Valley, Victoria, Australia. We have looked both at the solvent-extractable, or free, fatty acids (which include those extractable as esters or intact lipids) and at those that are released upon hydrolysis (saponification) of the residue after solvent extraction. The latter are presumably bound chemically to the coal matrix (kerogen) and are therefore designated as bound acids. The total acids are taken as the sum of the free and bound acids.

Lithotypes (25, 26) can be described as the various macroscopically recognizable bands or strata occurring within a coal seam. These bands are not always distinguishable in fresh, moist coal, but as the coal is air-dried, a distinct banding becomes apparent. The five basic lithotypes are described in Table I. Although lithotypes are named in terms of color, this is a generalization, and the classification of lithotype is carried out with regard to color and texture. The degree of gelification, weathering patterns, and physical properties serve as supplementary characteristics.

It should be pointed out that the lithotype classification for brown coal does not conform to that for black coal. To date, the International Committee for Coal Petrology (ICCP) has not finalized a brown coal lithotype classification; however, it is generally agreed that a lithotype classification should be based on macroscopic characteristics that can be determined in open cut faces. This principle has been followed in classifying the Latrobe Valley coals according to a system developed and used by the State Electricity Commission of Victoria (SECV) (25).

During the long period required for the accumulation of sufficient plant debris to form a thick coal seam [estimated as 100,000 years per 100 m (26)], the environment of deposition will show significant changes at any given locality. Variations in the prevailing botanical community, in the depth and nature of the swamp water, and in the conditions of decay and decomposition of plant material result in the formation of coals with different characteristics, i.e., lithotypes. A thick coal seam, therefore, will have a stratified or layered structure, where each layer can be

Table I. Lithotype Classification: Typical Characteristics of Air-Dried Coal

<i>Lithotype</i>	<i>Color</i>	<i>Texture^a</i>	<i>Gelification</i>	<i>Physical Properties^b</i>
Dark	Dark brown to black brown	High wood content. Often small fragments	Gelification, partic. of woody material, common	Strong, hard, heavy (high sp gr)
Medium dark	Dark brown to medium brown	High to medium wood content. Often large pieces	Some gelification but not extensive	Strength variable, hardness and sp gr above average
Medium light	Medium brown to light brown	High to low wood content. Often well preserved	Gelification uncommon. Confined mainly to wood	Intermediate physical properties
Light	Light brown	Medium to low wood content	Gelification rare	Generally soft and relatively light (low sp gr)
Pale	Pale brown to yellow brown	Wood present but uncommon	Gelification very rare	Soft, crumbles readily, very low sp gr

^a Wood content includes all tissue clearly distinguishable from the groundmass.

^b sp gr = specific gravity.

classified as a basic coal type (*see* Table I). As the input of plants, organisms, and inorganic materials and the prevailing biochemical processes change from one depositional environment to another, one might expect that a change in the input of various fatty acids (and the levels thereof) would occur. Hence one might expect to observe different fatty acid levels and/or distributions in the various lithotypes.

Samples of each lithotype were taken from a single core within a small depth range (approximately 8 m) in which all five lithotypes occurred. This small depth range was desirable to minimize the effect of diagenetic change that might be expected to alter the fatty acid distribution and/or levels as one proceeds down the core. Studies of possible diagenetic changes of fatty acids with depth, taking samples from coal belonging to one lithotype, are presently underway in our laboratories.

The changes in fatty acid distributions and levels with lithotype might well be different from the changes observed with varying coal rank. In order to compare coals of significantly different rank, we also examined the monocarboxylic acids from a highly volatile bituminous coal.

Experimental

Samples. Brown coal lithotype samples were taken from a bore core from the Flynn field in the Loy Yang region of the Latrobe Valley, Victoria, Australia. The brown coal deposits in this area are believed to be Miocene to Eocene in age. All five lithotype samples were taken at depths between 93 and 100.5 m below the surface in a 120-m core and were provided by the SECV. The black coal sample was from the Upper Hunter region (Permian) of New South Wales (Sydney Basin), Australia, and had a carbon content of 81.3%, dry, ash-free basis (DAF). This sample was provided by the Australian Coal Industry Research Laboratories Ltd. (ACIRL). The characteristics of these samples are set out in Table II.

All samples were ground (ball and mill) and freeze-dried at -40° prior to extraction. They were stored under vacuum (over P_2O_5) to prevent uptake of moisture. This was particularly important for brown coals, which are very hygroscopic.

Extraction of Free and Bound Acids. The freeze-dried coal samples (10.0 g) were Soxhlet-extracted in a preextracted thimble with chloroform-methanol (2:1, v/v, two periods of 100 hr each) and then with toluene-methanol (3:1, v/v, one period of 100 hr). Finally, the solid residues were sonicated in chloroform-methanol (2:1, v/v, three periods of 1 hr each), and the weight of the total solvent-extractable material was determined. This lengthy procedure was necessary to ensure complete extraction of soluble organic material. The extract produced by the last sonication accounted for less than 3% of the total solvent extract. A portion of the total solvent extract was saponified in methanol-water (4:1, v/v, 150 mL) with potassium hydroxide (2 g) by heating at reflux for 4 hr. Distilled water (200 mL) was added to the mixture, and the neutral material was extracted with dichloromethane-*n*-heptane (1:5, v/v, 4×100 mL) after ensuring that the aqueous layer was alkaline ($pH > 12$). The aqueous layer was acidified ($pH < 2$), and the acidic material was extracted with chloroform (4×100 mL), dried (anhydrous $MgSO_4$), evaporated under vacuum, and weighed. Emul-

Table II. Coal Properties

Lithotype	Depth (m)	Moisture (%)	Color Index ^a	Ash (% DB) ^b	Minerals & Inorganics (% DB) ^b	Proximate and Ultimate (%DMIF) ^c					
						Volatile	C	H	N	S _o ^d	O (diff) ^e
Pale	96.5-97.0	60.0	146.0	1.2	0.928	51.7	69.0	4.9	0.55	0.57	24.98
Light	98.0-98.5	58.8	136.0	1.2	1.046	51.7	68.7	5.0	0.57	0.41	25.32
Med. light	100.0-100.5	52.7	117.4	1.1	1.016	49.0	68.8	4.6	0.57	0.32	25.71
Med. dark	93.0-93.5	61.9	91.9	1.5	1.598	48.6	68.1	4.7	0.49	0.28	26.43
Dark	95.0-95.5	66.0	50.2	1.3	1.261	45.6	69.6	4.6	0.64	0.45	24.71

^a Calculated from colorimeter measurements. Color index of 100.0 approximates an average Latrobe Valley coal.

^b DB = dry basis.

^c DMIF = dry, mineral-inorganic-free.

^d S_o = sulfur (organic).

^e Oxygen calculated by difference.

sions that sometimes formed at this stage were dispersed by the addition of sodium chloride or by centrifugation. In this manner the free acids were obtained.

Humic acid material was observed to precipitate out on acidification of the aqueous layer and remained at the interface between the two phases.

The bound acids were obtained after saponification of a portion of the solvent-extracted residue in methanol-water (5:1, v/v, 200 mL) with potassium hydroxide (5 g). This experiment was performed in an atmosphere of nitrogen for two periods of 5 days each, after which time saponification was complete. The solid residue was separated by filtration, and the neutral and acidic materials were extracted from the filtrate as described for the free acids.

Analyses of Fatty Acids. Acids were methylated prior to gas-liquid chromatography (GLC) analysis with 14% boron trifluoride in methanol according to the procedure of Metcalfe and Schmitz (27). The acidic methyl esters (AMEs) were extracted into chloroform, evaporated to dryness, and weighed.

The monocarboxylic esters were separated from other acid esters by thin-layer chromatography (TLC) on silica GF₂₅₄ (Merck) by development in *n*-heptane-diethyl ether-methanol (80:20:2, v/v/v). TLC plates were visualized under ultraviolet light after spraying with 2,7-dichlorofluorescein, and the mono carboxylic ester band ($R_f = 0.52$) was removed and extracted with chloroform.

Monocarboxylic esters were further separated by argentation TLC [silica GF₂₅₄ impregnated with 5% (w/v) silver nitrate] into saturated esters ($R_f = 0.51$), monounsaturated esters ($R_f = 0.42$), diunsaturated esters ($R_f = 0.29$), and polyunsaturated esters ($R_f < 0.29$) by development in *n*-heptane-diethyl ether-methanol (90:10:1, v/v/v) (19).

Quantitative determination of AMEs was achieved by high-resolution GLC analyses on a glass, support-coated, open, tubular (SCOT) SE-30 column (57 m × 0.5 mm i.d., S.G.E., Australia) in a Perkin-Elmer 910 gas chromatograph equipped with a flame ionization detector. Individual compounds were identified on the basis of GLC retention times, coinjection with authentic standards (Analabs), and their performance on argentation TLC.

Maceral Analyses. Maceral analyses were carried out under the microscope in reflected and fluorescent (blue-light excitation) light at magnifications of ×250 and ×500. A point-count method counting 500 points was used. This gives an accuracy of ± 2-3% for each maceral.

Results and Discussion

Maceral Analyses. The changes in the basic nature of coal between lithotypes are perhaps best demonstrated by micropetrographic methods (25, 26, 28). Brown coal is composed of the maceral groups huminite, liptinite, and inertinite, which can be differentiated under the microscope by their structure, texture, reflectance, color, and form. The huminite group can be divided further into three subgroups, viz., humodetrinite, humotelinite, and humocollinite. A brief definition of these groups and subgroups is provided in Table III.

Results of the maceral analyses for the five samples of different lithotypes are presented in Table IV. One observes a general decrease in the concentrations of humodetrinite and liptinite and an increase in

Table III. Definitions for Maceral Groups

	<i>Description</i>
Humodetrinite	This is the finely granular to amorphous groundmass of the coal. The fragments making up this material are generally less than 10 μm in size. Normal coal in the Latrobe Valley usually contains 50% or more humodetrinite.
Humotelinite	This material is composed of recognizable plant tissue in varying stages of decomposition, gelification, and coalification. The group includes wood, roots, leaves, bark, etc.
Humocollinite	Humocollinite consists mainly of amorphous humic gels, but it also includes structureless cell excretions formed by living plants.
Liptinite	This group is made up of substances that fluoresce under blue light. They tend to be resistant to chemical alteration and decay and have a high volatile matter and hydrogen content. Typical macerals are derived from spores, pollen, cuticle, and resin.
Inertinite	As the name implies, these substances tend to be inert chemically, and they are the last macerals to show alteration during carbonization. They are generally dense and hard or brittle and show a very high reflectance in incident light. Fusinite, which is similar in nature to wood charcoal, is representative of this group.

humotelinite as one proceeds from the pale to the dark lithotype. The dark lithotype, however, shows an anomalously low value for humocollinite, which is accompanied by a relatively high concentration of densinite (gelified groundmass of coal sample). From other studies (25, 26, 28) maceral concentrations are observed to vary in a regular fashion with lithotype. These varying concentrations, then, appear to be associated with differences in plant communities and environmental conditions at the time of deposition.

Solvent Extraction. A significant portion of brown coal is solvent-extractable. Figure 1 shows that for the lithotypes examined in this study, between 9.5% and 15% of the coal was solvent-extractable. Indeed, more than 20% of brown coal has been shown to be extractable for particular samples (29). The amount of material solvent-extractable from black coals is substantially less (5.6%) and, from our work on coals ranging from 81% to 89% C [DAF] (29), was observed to decrease with increasing rank. Leythaeuser and Welte (30) observed that their ex-

Table IV. Maceral Analyses

	<i>Lithotype</i>				
	<i>Pale</i>	<i>Light</i>	<i>Medium Light</i>	<i>Medium Dark</i>	<i>Dark</i>
<i>Maceral Groups</i>					
1. Humodetrinite	73.4	76.4	76.0	43.2	58.6
2. Humotelinite	5.8	4.0	12.2	35.8	37.8
3. Humocollinite	6.4	6.2	8.0	16.8	1.0
4. Liptinite	13.6	12.4	3.4	4.2	1.8
5. Inertinite	0.6	0.6	0.4	—	0.8
6. Minerals	0.2	0.4	—	—	—
<i>Macerals</i>					
1. Attrinite	73.2	76.4	75.8	42.6	47.0
Densinite	0.2	—	0.2	0.6	11.6
2. Textinite	—	—	0.6	0.4	1.0
Textu-ulminite	4.4	3.6	11.2	22.8	27.4
Eu-ulminite	1.4	0.4	0.4	12.6	9.4
3. Telogelinite	—	—	—	—	—
Detrogelinite	—	—	—	—	—
Eugelinite	—	—	—	—	—
Porigelinite	—	1.4	1.0	4.4	—
Phlobaphinite	5.4	2.6	6.2	8.8	0.2
Pseudophlobaphinite	1.0	2.2	0.8	3.6	0.8
4. Sporinite	2.4	1.6	0.8	0.6	0.2
Cutinite	—	—	—	—	0.4
Resinite	0.2	0.6	0.8	0.4	—
Suberinite	1.0	0.6	0.4	1.4	—
Liptodetrinite	10.0	9.6	1.4	1.8	1.2
5. Schlerotinite	0.6	0.6	0.2	—	0.2
Fusinite	—	—	—	—	0.2
Semifusinite	—	—	0.2	—	0.4
Inertodetrinite	—	—	—	—	—
6. Clay	—	0.4	—	—	—
Quartz	0.2	—	—	—	—
Pyrite	—	—	—	—	—

traction yield reached a maximum for a coal with 30% volatile matter. Unfortunately, they do not report the rank of their coal samples on the basis of %C [DAF], so it is difficult to relate our results to theirs.

Fatty Acid Analyses. The amounts of AMEs (free, bound, and total) obtained from each lithotype and from the black coal are plotted in Figure 2. The general decrease in the total AMEs observable as one proceeds from the pale to the dark lithotype corresponds with a general decrease in the concentration of liptinite in these lithotypes. This decrease is not surprising, since many of the liptinite macerals (sporinite, cutinite, resinite, etc.) might be expected to be lipid-rich macerals. It is also notable that, apart from the pale lithotype, the levels of free AMEs are higher than those of the bound AMEs. The total AMEs represent between 3.0% (dark) and 7.2% (pale) of the whole, freeze-dried coal. For the black coal this figure is 2.3%.

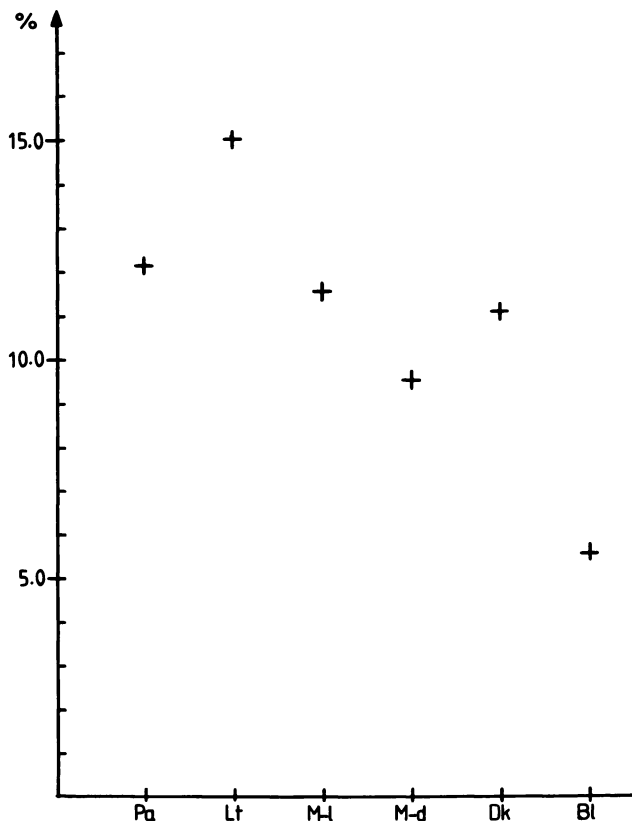


Figure 1. Percentage of coal solvent-extractable vs. lithotype

The total monocarboxylic esters (mono-AMEs) obtainable from each lithotype are plotted in Figure 3. One readily notes that, while the points seem to be distributed somewhat randomly, the levels of free mono-AMEs are substantially higher than the levels of bound mono-AMEs for every sample. The levels of total mono-AMEs for the light and dark lithotypes appear to be substantially higher than those of the other lithotypes.

Figure 3 shows that the levels of monofatty acids in brown coals are in the vicinity of 1000 ppm (some more, some less). Even the black coal sample exhibits a level of 670 ppm. (This figure is somewhat misleading, since high-molecular-weight, unidentified compounds, presumably triterpenoid or steroid acids, account for a substantial proportion, ca. 30%, of this value.) These levels are substantially higher than those generally observed in recent and ancient sediments. Volkman et al. (31) have reported a monofatty acid level of 93 ppm from a surface scraping of a recent marine sediment at Corner Inlet, Victoria, Australia. Recently other reports have indicated levels of 150 ppm (32) (from Port Franklin,

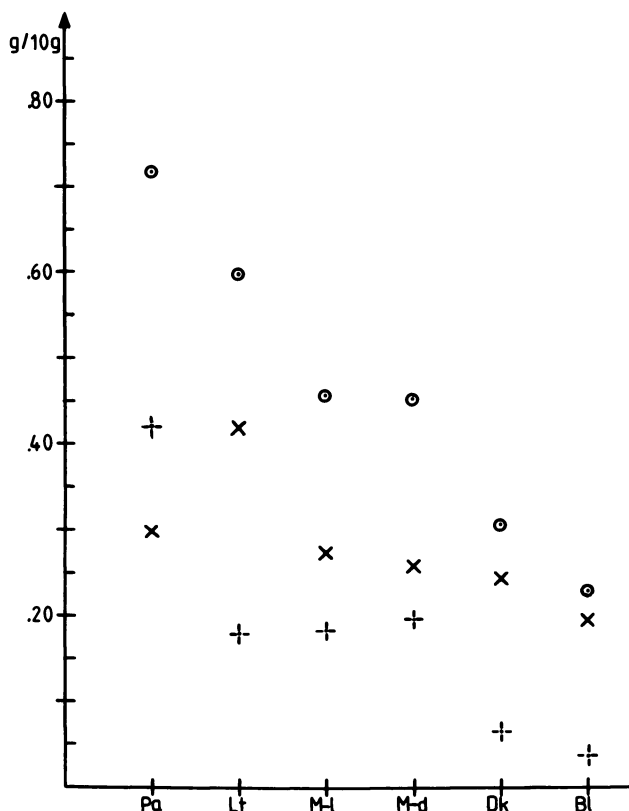


Figure 2. AMEs vs. lithotype ((\odot) total AMEs; (X) free AMEs; (+) bound AMEs)

Victoria) and 50 ppm (33) (from a mangrove swamp at the Low Isles, North Queensland, Australia) for monofatty acids in recent marine sediments at depths in the vicinity of 20 cm. Douglas et al. (4) observed higher levels in the Eocene Green River shale (650 ppm) and the Carboniferous Scottish Torbanite (110 ppm). Considering the relatively high levels of organic carbon in our samples, in contrast to recent marine sediments, the observed high levels of fatty acids are perhaps not unexpected.

The distributions of the *n*-alkanoic acids obtained for all samples are shown in Figures 4(a)–4(f) and Figure 5. For the brown coal samples the changes in the distributions of total fatty acids with lithotypes are obvious in Figure 5. These analyses are quantitatively diverse, yet all samples exhibit similar bimodal distributions. The major maximum is observed at C_{26} or C_{28} , with a secondary, but often very much less intense, maximum at C_{16} . The high levels of high-molecular-weight acids in all samples indicate that the input of lipids of higher plants is very important

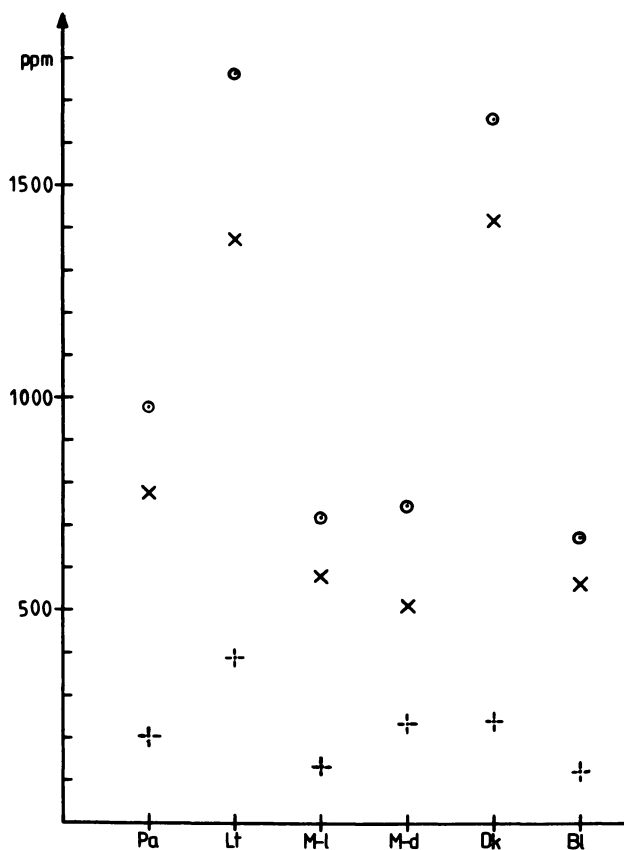


Figure 3. Monofatty acid concentrations vs. lithotype (○) total; (X) free; (+) bound)

for every lithotype, yet the quantitative and qualitative differences in fatty acid distributions would tend to support the thesis that different lithotypes are derived from different depositional environments.

One also notes that the levels and distributions of the free and bound acids are substantially different in the case of each lithotype sample. It is very interesting to note that for each sample the low-molecular-weight fatty acids ($C \leq 23$) are present in similar concentrations in both the free and bound fractions. However, a massive difference in the concentrations of the high-molecular-weight acids ($C \geq 24$) is observed. It is largely this difference in the concentrations of the high-molecular-weight acids that accounts for the difference in the total levels of the free and bound mono-AMEs reported in Figure 3.

The ratio of high to low molecular weight fatty acids has been calculated as a measure of the abovementioned difference in high-molecular-weight fatty acid concentrations. Table V shows that absolute values

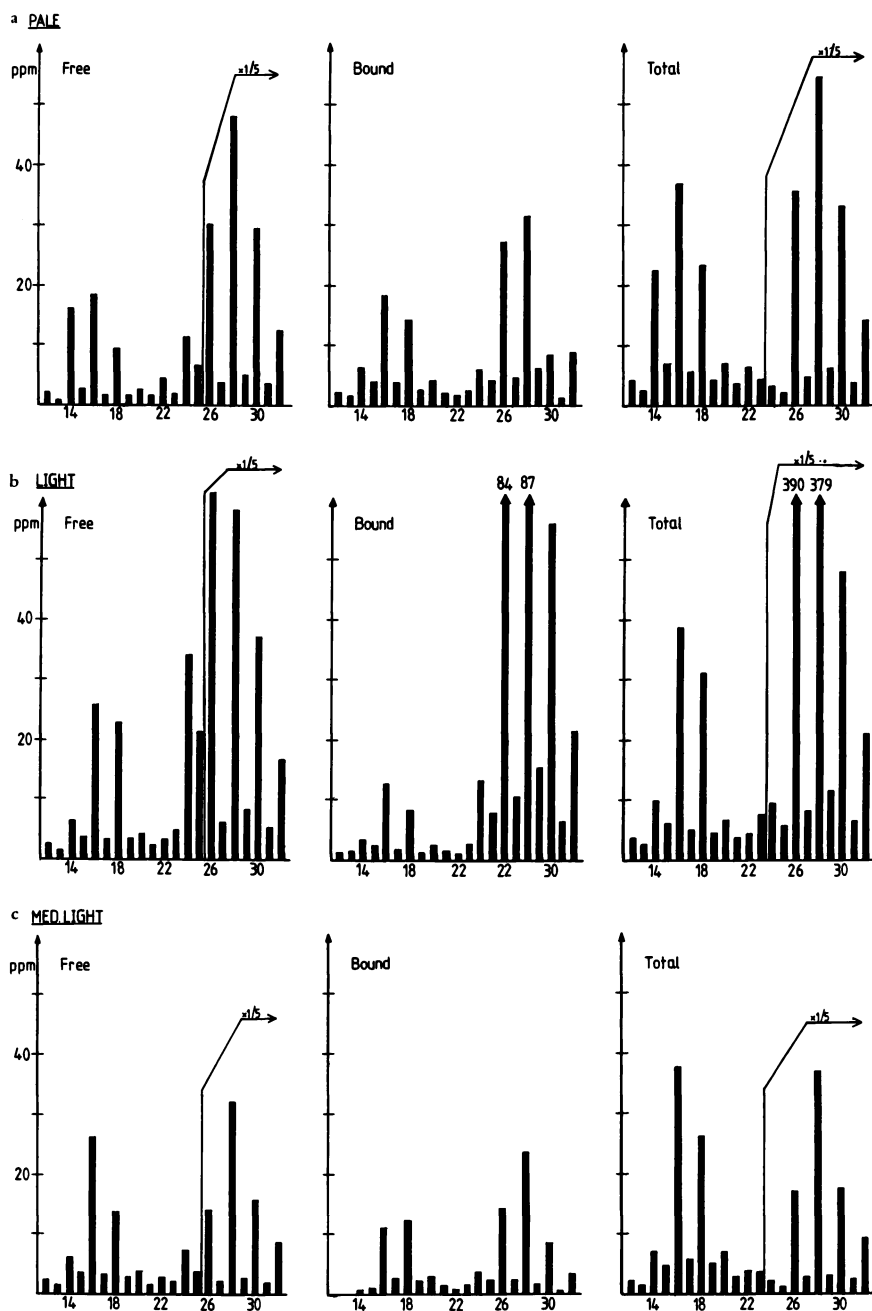


Figure 4. Monofatty acid distributions: (a) pale lithotype; (b) light lithotype; (c) medium light lithotype

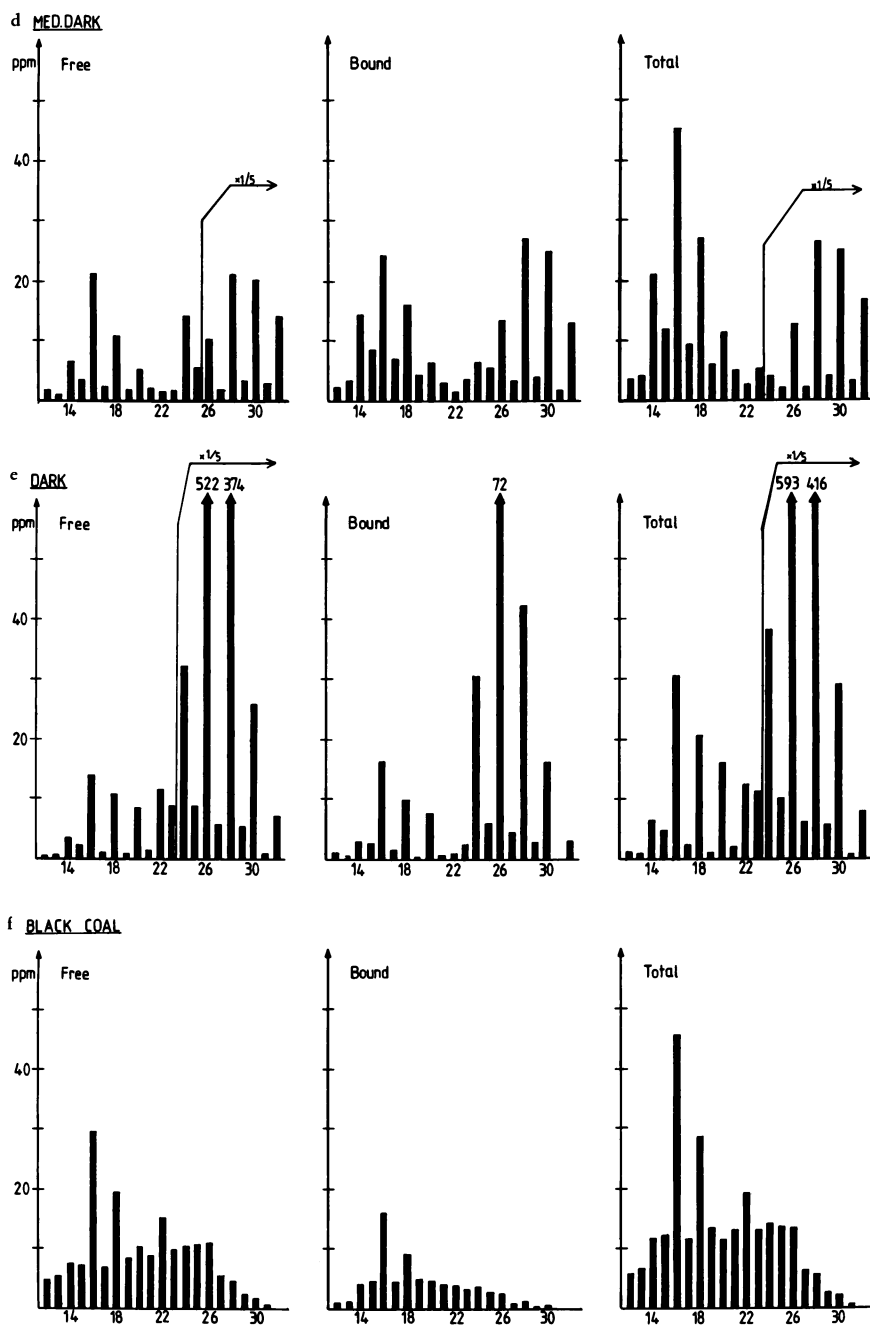


Figure 4. Monofatty acid distributions (continued): (d) medium dark lithotype; (e) dark lithotype; (f) black coal

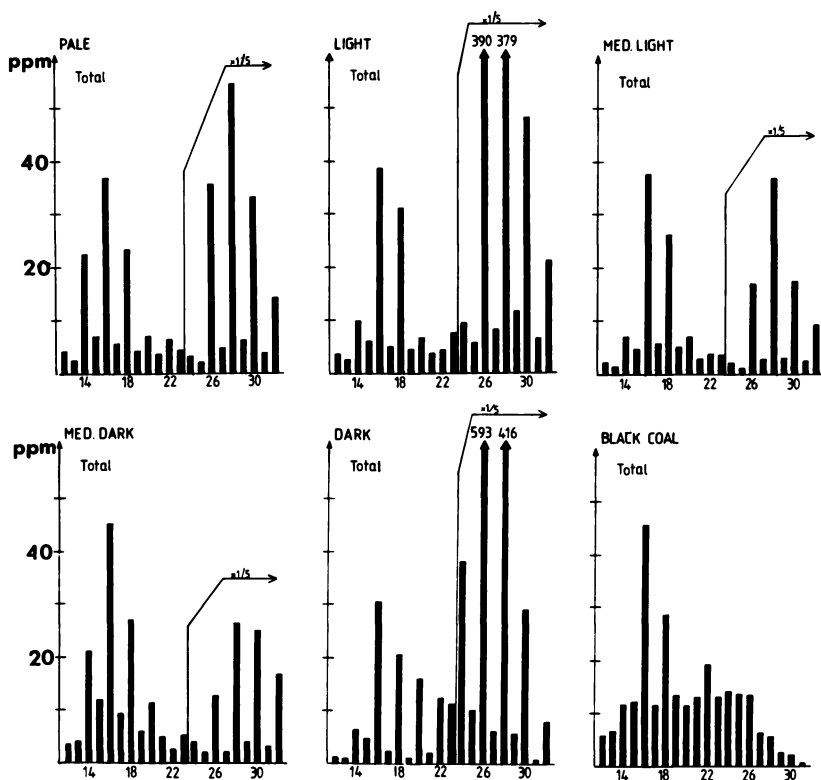


Figure 5. Total monofatty acid distributions of coal samples

Table V. Ratio of High-to Low-Molecular-Weight Monofatty Acids^a

Sample	Free	Bound	Total
Pale	11.2	1.8	6.5
Light	12.6	8.1	11.2
Medium light	5.9	1.7	4.4
Medium dark	6.9	1.1	3.4
Dark	20.6	3.9	13.6
Black	0.4	0.2	0.3

^aRatio measured is $\Sigma(C_{24} \text{ to } C_{32} \text{ fatty acids})/\Sigma(C_{14} \text{ to } C_{23} \text{ fatty acids})$.

of the calculated ratio vary markedly from lithotype to lithotype. The table does emphasize, however, the relative importance of the high-molecular-weight components in the free fatty acid fractions, since for every sample the ratio for free acids is substantially higher than the ratio for bound acids. The full meaning of this result is not clear, but it does indicate that a good deal of the lipid material from higher plant sources has not been incorporated into the kerogen or matrix of the coal during the 30–40 million years it has been deposited.

In the bound fractions the levels of high-molecular-weight fatty acids are still generally greater than those of the low-molecular-weight acids. The exception to this generalization is the medium dark lithotype, which shows almost equal levels of C_{16} , C_{28} and C_{30} *n*-fatty acids.

Other fatty acid distributions that are similarly high in levels of high-molecular-weight acids and low in levels of low-molecular-weight acids have been reported in ancient sediments such as the Green River shale (34) (Lower Cretaceous). Kvenvolden (34) noted that the distributions of both fatty acids and hydrocarbons from two samples (from different locations) of the same shale were substantially different. He suggested that these differences were not necessarily caused by differences in diagenetic parameters (pressure, temperature, and time) but could have been caused by differences in the original distributions of acids and paraffins. Such differences in the original distributions of fatty acids and paraffins may well have been caused by different prevailing environments.

In contrast to brown coals the distribution of *n*-alkanoic acids in the black coal sample, Figure 4(f), can be seen to maximize at C_{16} with a very weak secondary maximum at C_{24} . The levels shown for the C_{22} acid in the free and total graphs are probably too high because of the presence of another unresolved peak in the gas chromatogram of the free acid sample. The distributions of the free and bound acids are similar, though the level of free fatty acids is somewhat higher. There is an obvious decrease in the average molecular weight of the fatty acid distribution relative to that of the brown coal. Black coals, being of higher rank than brown coals, are generally assumed to have undergone further diagenetic change (35). Decreases in the distribution maxima of both fatty acids and hydrocarbons with an increase in geochemical time or diagenetic change are well documented (1, 15, 36). The change in the distribution maximum is underlined by the observed low value of the ratio of high-to low-molecular-weight fatty acids (Table V).

The differences in fatty acid distributions brought about by varying lithotype are rather more subtle than the differences brought about by varying the rank, since variation of rank brings about a change in the position of the maximum of the distribution.

The carbon preference index (CPI) (1) for fatty acids in the coal samples examined has been calculated (see Table VI). The CPI is a

Table VI. Carbon Preference Index (CPI)^a for Monofatty Acids

Sample	Free	Bound	Total
Pale	8.5	4.1	7.2
Light	7.1	5.8	6.7
Medium light	8.0	5.1	7.2
Medium dark	6.6	3.2	5.1
Dark	10.9	10.0	10.7
Black	1.8	1.8	1.8

$${}^a\text{CPI} = \frac{1}{2} \left[\frac{\sum(\text{concn of even } n\text{-fatty acids } C_{16} \text{ to } C_{30})}{\sum(\text{concn of odd } n\text{-fatty acids } C_{15} \text{ to } C_{29})} + \frac{\sum(\text{concn of even } n\text{-fatty acids } C_{16} \text{ to } C_{30})}{\sum(\text{concn of odd } n\text{-fatty acids } C_{17} \text{ to } C_{31})} \right]$$

measure of the predominance of even over odd carbon chain fatty acids. In general, as the age of a sediment increases, the predominance of even acids decreases because of diagenetic alteration of the fatty acid distribution. The CPI value of 1.8 for the black coal is much lower than the values observed for the brown coal samples (5.1–10.7), and this result is a further indication of the large differences in the fatty acid distributions of coals of significantly different rank.

The CPI values for the brown coal samples are observed to vary quite markedly. However, two features are noticeable: (1) The free acids exhibit higher CPI values than do the bound acids. This result appears to be caused by the much higher abundance of the even-carbon-number, higher-molecular-weight acids (C_{24} , C_{26} , C_{28} , C_{30}) in the free acid fractions of each sample. (2) The CPI values for the total samples appear to be lower than those observed in living plants (37, 38) but similar to those found in some recent sediments (22, 23, 39) and soils (38). They are certainly higher than those observed in some ancient sediments (34). One might conclude that this brown coal is a sediment in the early or middle stages of its diagenesis.

Acids other than *n*-fatty acids have been shown to be important components in the mono-AME fraction, though they are generally present in much smaller concentration than in the straight-chain acids. The branched-chain acids *iso*-14:0 (14:0 refers to the *n*-fatty acid with 14 C atoms and 0 double bonds; *iso*-14:0 indicates the *iso* isomer of 14:0), *iso*-15:0, *ant*-15:0, *iso*-17:0, and *ant*-17:0 were observed to be present in most samples. As previously mentioned, branched-chain acids are often taken to be representative of a bacterial input to sediments (1, 21, 24). Since bacteria are known to be active in assisting plant diagenesis, which leads to coalification (40), one would expect to find evidence of their presence.

Unsaturated acids were also present in all lithotypes and in the black coal sample. The acids 16:1 ω 7 and 18:1 (two isomers present, mainly

ω9) were particularly prevalent, but there is evidence that suggests that higher homologues are also present in lesser concentrations. The presence of these acids in sedimentary deposits of these ages might be thought unusual, as unsaturated acids generally are assumed to be relatively susceptible toward bacterial and other hydrogenative attack in the early stages of sedimentation. Nevertheless, monounsaturated acids have been reported in Green River shale (1) and in fossil fruits of *Nyssa fissilis* (41) and in fossil walnut stones (42).

Even more surprising is the presence of the diunsaturated acid 18:2 in all coal samples studied. The presence of diunsaturated acids is indeed highly unusual because of their inherent instability under geological conditions. Itihara et al. (42) have reported the presence of 18:2 in a fossil walnut stone of estimated age one million years (Pleistocene), but this appears to be the first report of a diunsaturated acid in a sediment or coal from the Eocene epoch or the Permian period.

Acid groups such as triterpenoid acids, dicarboxylic acids, and hydroxy acids also are present in brown coal. Although this paper is restricted to the monofatty acid levels and distributions in brown coal lithotypes, these other acid types also have been observed to vary in level and distribution with lithotype and may, in fact, prove to be useful as indicators of the depositional environments.

Summary and Conclusions

1. The large differences in the distributions of *n*-fatty acids between the black and brown coal samples examined have been attributed to the significantly different rank of these coals.
2. Changes in the *n*-fatty acid distributions due to varying lithotype are substantial but somewhat subtle. The high concentration of high-molecular-weight fatty acids in all samples points to the overall importance of the input of higher plants, but changes in the actual levels and distributions may be a reflection of different environments and/or conditions of decomposition at the time of deposition.
Some particular classes of fatty acids may prove to be valuable markers for the input from specific sources or organisms.
3. These chemical data support the concept of lithotype variation and demonstrate heterogeneity within a thick coal seam.
4. The presence of unsaturated acids in these coals has been reported.

Acknowledgments

The authors thank the State Electricity Commission of Victoria for provision of the brown coal samples and the analytical data on them, the Australian Coal Industries Research Laboratories Ltd. for provision of the black coal sample, and the National Coal Research Advisory Council for financial assistance. We also thank J. K. Emmett for helpful discussions.

Literature Cited

1. Siefert, W. K. "Carboxylic Acids in Petroleum and Sediments", *Fortsch. Chem. Org. Naturst.* 1975, 32, 1-49.
2. Cooper, J. E.; Bray, E. E. "A Postulated Role of Fatty Acids in Petroleum Formation", *Geochim. Cosmochim. Acta* 1963, 27, 1113-1127.
3. Kvenvolden, K. A. "Normal Fatty Acids in Sediments", *J. Am. Oil Chem. Soc.* 1967, 44, 628-636.
4. Douglas, A. G.; Douraghi-Zadeh K.; Eglinton, G.; Maxwell, J. R.; Ramsay, J. N. In "Advances in Organic Geochemistry"; Hobson, G. D.; Speers, G. C. Eds.; Pergamon: Oxford, 1970; pp. 315-344.
5. Brooks, P. W.; Eglinton, G.; Gaskell, S. J.; McHugh, D. J.; Maxwell, D. R.; Philp, R. P. "Lipids of Recent Sediments", *Chem. Geol.* 1976, 18, 21-38.
6. Morris, R. J.; Culkin, F. "Marine Lipids: Analytical Techniques and Fatty Acid Ester Analyses", *Oceanogr. Mar. Biol. Ann. Rev.* 1976, 14, 391-433.
7. Shorland, F. B. In "Chemical Plant Taxonomy"; Swain, T., Ed.; Academic: New York, 1963; p. 254.
8. Johns, R. B.; Perry, G. J. "Lipids in the Marine Bacterium *flexibacter polymorphus*", *Arch. Microbiol.* 1977, 114, 267-271.
9. White, C. M.; Shultz, J. L.; Sharkey, A. G., Jr. "Biological Markers in Coal and Coal Liquefaction Products", *Nature (London)* 1977, 268 (5621), 620-622.
10. Brooks, J. D.; Smith, J. W. "The Diagenesis of Plant Lipids During the Formation of Coal, Petroleum and Natural Gas—I", *Geochim. Cosmochim. Acta* 1967, 31, 2389-2397.
11. Emmett, J. K., M.Sc. thesis, University of Melbourne, Parkville, Victoria, Australia, 1977.
12. Pederson, K. R.; Lam, J. "Precambrian Organic Compounds from the Ketilidian of South West Greenland", *Medd. Groenl.* 1970, 185 (7), 1-42.
13. Wollrab, V.; Striebl, M.; Sorm, F. "Composition of Brown Coal—VI", *Collect. Czech. Chem. Commun.* 1963, 28, 1904-1913.
14. Hewett, D. R.; Kipping, P. J.; Jeffery, P. G. "Separation, Identification and Determination of the Fatty Acids of Montan Wax", *Nature (London)* 1961, 192, 65.
15. Allan, J.; Douglas, A. G. "Variation in the Content and Distribution of *n*-Alkanes in a Series of Carboniferous Vitrinites and Sporinites of Bituminous Rank", *Geochim. Cosmochim. Acta* 1977, 41, 1223-1230.
16. Kvenvolden, K. A.; Weiser, D. "A Mathematical Model of a Geochemical Process", *Geochim. Cosmochim. Acta* 1967, 31, 1281-1309.
17. Waples, D. W. "Catalytic Formation of Hydrocarbons from Fatty Acids", *Nature (London) Phys. Sci.* 1972, 237, 63-64.
18. Johns, R. B.; Belsky, T.; McCarthy, E. D.; Burlingame, A. L.; Haug, P.; Schnoes, H. K.; Richter, W.; Calvin, M. "The Organic Geochemistry of Ancient Sediments—II", *Geochim. Cosmochim. Acta* 1966, 30, 1191-1222.

19. Perry, G. J.; Volkman, J. K.; Johns, R. B.; Bavor, H. J., Jr. "Fatty Acids of Bacterial Origin in Contemporary Marine Sediments", *Geochim. Cosmochim. Acta* 1979, 43, 1715-1725.
20. Brooks, P. W.; Eglinton, G.; Gaskell, S. J.; McHugh, D. J.; Maxwell, J. R.; Philp, R. P. "Lipids of Recent Sediments, Part 2", *Chem. Geol.* 1977, 20, 189-204.
21. Cranwell, P. A. "Monocarboxylic Acids in Lake Sediments: Indicators Derived from Terrestrial and Aquatic Biota of Paleoenvironmental Trophic Levels", *Chem. Geol.* 1974, 14, 1-14.
22. Matsuda, Hiromi. "Early Diagenesis of Fatty Acids in Lacustrine Sediments—III", *Geochim. Cosmochim. Acta* 1978, 42, 1027-1034.
23. Gaskell, S. J.; Morris, R. J.; Eglinton, G.; Calvert, S. E. "The Geochemistry of a Recent Marine Sediment off Northwest Africa", *Deep Sea Res.* 1975, 22, 777-789.
24. Johns, R. B.; Perry, G. J.; Jackson, K. S. "Contribution of Bacterial Lipids to Recent Marine Sediments", *Estuarine Coastal Mar. Sci.* 1977, 5, 521-529.
25. George, A. M. Victoria, State Electricity Commission, Exploration and Geological Division, Aug. 1975, Petrographical Report No. 17.
26. Allardice, D. J.; George, A. M.; King, T. N. W.; Kiss, L. T. Victoria, State Electricity Commission, Brown Coal Research Division, Dec. 1978, Report No. 357.
27. Metcalfe, L. D.; Schmitz, A. A. "Rapid Preparation of Fatty Acid Esters for Gas Chromatographic Analysis", *Anal. Chem.* 1961, 33, 363-364.
28. Allardice, D. J.; George, A. M.; Häusser, D.; Neubert, K. H.; Smith, G. C. Victoria, State Electricity Commission, Brown Coal Research Division, Sept. 1977, Report No. 342.
29. Chaffee, A. L.; Perry, G. J.; Johns, R. B., unpublished data.
30. Leythaeuser, D.; Welte, D. H. In "Advances in Organic Geochemistry"; Schenk, P. A.; Havenaar, I., Eds.; Pergamon: Oxford, 1969; pp. 429-442.
31. Volkman, J. K.; Johns, R. B.; Gillan, F. T.; Perry, G. J.; Bavor, H. J., Jr., *Geochim. Cosmochim. Acta* 1980, 44, 1133-1143.
32. Volkman, J. K., Ph.D. Thesis, University of Melbourne, Parkville, Victoria, Australia, 1977.
33. Thomas, P. A.; Johns, R. B. unpublished data.
34. Kvenvolden, K. A. "Molecular Distributions of Normal Fatty Acids and Paraffins in Some Lower Cretaceous Sediments", *Nature (London)* 1966, 209 (5023), 573-577.
35. "Stach's Textbook of Coal Petrology", Stach, E.; Mackowsky, M.-Th.; Teichmüller, M.; Taylor G. H.; Chandra, D.; Teichmüller, R., Eds.; Gebrüder Borntraeger: Berlin, 1975.
36. Maxwell, J. R.; Pillinger, C. T.; Eglinton, G. "Organic Geochemistry", *Q. Rev., Chem. Soc.* 1971, 25, 571-628.
37. Lytle, T. F.; Lytle, J. S.; Caruso, A. "Hydrocarbons and Fatty Acids of Ferns", *Phytochemistry* 1976, 15, 965-970.
38. Matsuda, Hiromi; Koyama, T. "Early Diagenesis of Fatty Acids in Lacustrine Sediments—II", *Geochim. Cosmochim. Acta.* 1977, 41, 1825-1834.
39. Brown, F. S.; Baedeker, M. J.; Nissenbaum, A.; Kaplan, I. R. "Early Diagenesis in a Reducing Fjord, Saanich Inlet, British Columbia—III", *Geochim. Cosmochim. Acta* 1972, 36, 1185-1203.
40. Given, P. H. In "Advances in Organic Geochemistry"; Gaertner, H. R. U., Wehner, J., Eds.; Pergamon: Oxford, 1972; pp. 69-92.
41. Hohn, M. E.; Meinschein, W. G. "Fatty Acids in Fossil Fruits", *Geochim. Cosmochim. Acta* 1977, 41, 189-193.
42. Ithihara, Yuuko; Inoue, M.; Nirei, H. "Lipids in Fossil Walnut Stones", *J. Geosciences Osaka City Univ.* 1974, 18, 1-6.

RECEIVED July 19, 1979.

Structural Characterization of Coal: Lignin-Like Polymers in Coals

RYOICHI HAYATSU, RANDALL E. WINANS, ROBERT L. McBETH,
ROBERT G. SCOTT, LEON P. MOORE, and MARTIN H. STUDIER

Chemistry Division, Argonne National Laboratory, Argonne, IL 60439

Alkaline cupric oxidation of coals produced phenolic acids (p-hydroxy- and 3,4-hydroxy-benzoic acids, 4-hydroxy-1,2- and 4-hydroxy-1,3-benzenedicarboxylic acids), which are known as characteristic lignin oxidation products. The results indicate that lignin-like polymers are incorporated into macromolecules of coals and still are identifiable in lower rank coals.

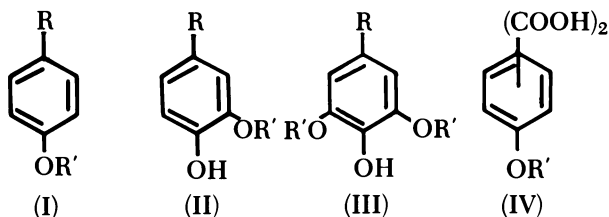
Although lignins are major constituents of vascular plants from which coals are derived, their roles in the coalification process and resulting coal structures have not been defined. On the basis of chemical and biological degradations, lignins are considered to be polymers of propyl-phenyl compounds, coniferyl alcohol and related alcohols (1, 2, 3, 4). Because of their great abundance, high resistance to biological degradation, and characteristic occurrence in land plants, isolation of coal degradation products related to these lignin compounds should shed some light on the roles, if any, played by lignins during coalification and in the final structure of coals. To date such studies have had only limited success.

Although lignin, fulvic acids, and humic acids have been degraded successfully with alkaline solutions under mild conditions ($\leq 200^{\circ}\text{C}$) to produce lignin-related phenols (5, 6, 7), this method has not proved to be useful for coals (8, 9, 10). Our results are similar. The alkaline degradation of model compounds representing structural units in lignin also has been investigated (11).

Reductive degradations of soil and coal-derived humic acids with sodium amalgam have been reported to produce a variety of phenolic compounds (12, 13, 14); however, this procedure has been questioned by

other laboratories (15, 16) because of its low yields and its severity (resulting chemical structures may have little relation to the starting material). These discrepant results have not been resolved (17).

Many oxidative degradations also have been carried out to break coal down into simpler species (10, 18–21); however, isolation and identification of phenols such as *p*-hydroxybenzene (I), vanillic (II), and syringic (III) derivatives, which are considered as characteristic lignin oxidation products (1, 4, 17, 22, 23), have not yet been confirmed definitely.



4-Hydroxybenzenedicarboxylic acid derivatives (IV) also are considered to be typical lignin degradation products (17, 24).

In general, commonly used oxidants destroy phenolic rings or give complex products (25, 26). Some of the oxidants such as nitrobenzene produce reaction byproducts that may interfere with the analysis of the oxidation products (23, 27, 28). To obtain lignin oxidation products from coals, we resorted to the alkaline cupric oxide oxidation method which has been applied successfully to analysis of lignins in plants (23), fulvic and humic acids (24, 27), and land-derived marine sediments (23).

Experimental

Seven coals were used in this study (Table I). To remove trapped organic materials (21, 29), all coal samples were extracted with benzene-methanol (3:1 refluxing for 48 hr) and 2.5% aqueous NaOH (20–35°C for 16 hr) before oxidation.

Each coal sample (5 g) was oxidized with alkaline cupric oxide (CuO) (51.9 g of $\text{CuSO}_4 \cdot 5\text{H}_2\text{O}$, 37.3 g of NaOH, and 185 mL of water) in a rocking stainless steel autoclave at 200°C for 8–10 hr by the method of Green et al. (30). The air in the autoclave was displaced by nitrogen. In general, lignin, plant materials, fulvic acids, humic acids, and marine sediments are oxidized at 170°C for 3–4 hr. However, this condition has not been found to be strong enough to oxidize coals, in particular high-rank coals.

The reaction mixture was removed and centrifuged, and the liquid phase was decanted and filtered. The alkaline-insoluble residue was washed with warm water and methanol; the alkaline solution and washings then were combined and acidified with HCl to pH 2. After concentration of the acidic solution under reduced pressure, the slushy residue was extracted repeatedly with a mixture of benzene-ether (1:3) and chloroform (organic acid fraction). The residue was extracted further with methanol (humic acid-like material A). Materials soluble

Table I. Elemental Analysis of Samples^a (maf %)

No.	Sample	C	H	N	S	O	H/C
						(by diff)	
1	Lignite (Sheridan Wyoming)	66.4	4.8	1.5	1.1	26.2	0.87
2	Bituminous (IL. No. 2)	73.9	5.2	1.4	2.4	17.1	0.84
3	Bituminous (IL. No. 6)	77.7	5.4	1.4	4.1	11.4	0.83
4	Bituminous (Ohio PSOC No. 297)	80.5	5.6	1.6	1.9	10.4	0.83
5	Bituminous (Pitt. No. 8)	82.0	5.5	1.4	2.7	8.4	0.81
6	Bituminous (Penn. PSOC No. 258)	86.5	4.8	1.3	2.6	4.8	0.67
7	Anthracite (Penn. PSOC No. 85)	91.0	3.8	0.7	1.2	3.3	0.50

^aAll samples were pretreated to remove solvent-extractable trapped organic materials and were dried at 110°–120°C for 16–18 hr under vacuum before oxidation.

in alkali only also were isolated from all samples (humic acid-like material B). To recover nonoxidized coal, the alkaline-insoluble residue was treated repeatedly with concentrated HCl, and finally washed with water.

Solid-probe mass spectrometric analysis (31) showed that the benzene–ether extracts consist mainly of organic acids. Therefore, these extracts were derivatized with dimethylsulfate-*d*₆ to yield methyl-*d*₃-labeled derivatives. The derivatives were analyzed by GCMS and high resolution MS using techniques that have been described previously (31). Authentic samples of phenolic acids derivatized with dimethylsulfate-*d*₆ or diazomethane were also analyzed by GCMS for reference. The distribution of the organic acids as methyl esters was determined by measuring areas of GC flame ionization detector peaks with a correction for the effective carbon number for each compound.

The methanol extracts and fractions soluble in alkali only were found by gel permeation chromatography (GPC) and solid-probe MS to consist essentially of humic acid-like materials.

Results of the Oxidation of Model Compounds and Polymers

To obtain detailed information on the CuO–NaOH oxidation at elevated temperatures (170°–200°C for 3–8 hr), control experiments with a number of compounds and polymers containing a variety of functional groups were carried out. As shown in Table II, the copper oxide was found to be a selective oxidant. The results can be generalized as follows: (1) the treatment results in hydrolytic oxidation of ether linkages in the aliphatic side chain of aromatics; (2) oxidation is not effective for cleavage of C–C bonds such as aryl methyl and methylene chains; (3) effective oxidation of aliphatic chains containing oxygen or sulfur functional groups such as –OH, –C=O, =COOH, –S–, –S–S–; (4) there is no hydroxylation of aromatic rings; (5) no ring destruction of polynuclear aromatics occurs; (6) no oxidation of mono- and dihydric phenols occurs.

Although trihydroxybenzenes and their derivatives have been isolated from the oxidation products of lignins, humic acids, and land-derived marine sediments (5, 17, 23, 24, 27), it was found that 2,6-dimethoxy-

Table II. CuO-NaOH Oxidation of Model Compound at 200°C for 8 Hr

<i>Compound</i>	<i>Type of Reaction</i>	<i>Major Products^a</i>	<i>Yield (mol %)</i>
4-Methylbenzyl alcohol	$-\text{CH}_2\text{OH} \rightarrow -\text{COOH}$	4-Methylbenzoic acid	93
3-Phenylpropan-1-ol	$-(\text{CH}_2)_2-\text{CH}_2\text{OH} \rightarrow -\text{COOH}$	Benzoic acid	68 ^b
Benzylmethylcarbinol	$-\text{CH}_2-\text{CH}(\text{OH})-\text{CH}_3 \rightarrow \text{COOH}$	Benzoic acid	70
β -Naphthyl methylcarbinol	$-\text{CH}_2\text{OH} \rightarrow -\text{COOH}$	2-Naphthoic acid	77
Benzaldehyde	$-\text{CHO} \rightarrow -\text{COOH}$	Benzoic acid	95
4-Methoxybenzaldehyde	$-\text{CHO} \rightarrow -\text{COOH}$	4-Hydroxybenzoic acid	89 ^c
2,6-Dimethoxyphenol	$-\text{OCH}_3 \rightarrow -\text{OH}$	1,2,6-Trihydroxybenzene	2.0 ^d
Syringaldehyde	$-\text{CHO} \rightarrow -\text{COOH}$	3,4,5-Trihydroxybenzoic acid	4.5 ^d
Dibenzoylmethane	$-\text{CO}-\text{CH}_2 \rightarrow -\text{COOH}$	Benzoic acid	76
1,4-Naphthoquinone	$-\text{CO}-\text{C} \rightarrow -\text{COOH}$	Phthalic acid	91
Flavone	$-\text{CO}-\text{C}=\text{C} \rightarrow \text{COOH}$	Benzoic acid	37
Phenylacetic acid	$-\text{CH}_2-\text{CO} \rightarrow -\text{COOH}$	Salicylic acid	41
Diphenyl ether	$-\text{O} \rightarrow -\text{OH}$	Benzoic acid	68
		Phenol	67

Dibenzyl ether	$-\text{CH}_2-\text{O}-\text{CH}_2-$	$\rightarrow -\text{COOH}$	Benzoic acid	81
4,4-Dihydroxydibenzyl ether	$-\text{CH}_2-\text{O}-\text{CH}_2-$	$\rightarrow -\text{COOH}$	<i>p</i> -Hydroxybenzoic acid	79
Dibenzyl sulfide	$-\text{C}-\text{S}-\text{C}-$	$\rightarrow -\text{COOH}$	Benzoic acid	64 ^e
Dibenzyl disulfide	$-\text{C}-\text{S}-\text{S}-\text{C}-$	$\rightarrow -\text{COOH}$	Benzoic acid	72 ^e
Diphenyl methane	$=\text{C}-\text{C}-$	$\rightarrow -\text{COOH}$	Benzoic acid	11
2,4-Dimethoxytoluene	$-\text{C}-\text{C}-$	$\rightarrow -\text{COOH}$	2,4-Dihydroxybenzoic acid	5 ^{f,g}
3,4-Dimethoxytoluene	$-\text{C}-\text{C}-$	$\rightarrow -\text{COOH}$	3,4-Dihydroxybenzoic acid	7 ^f
Poly-(4-methoxystyrene)	$-\text{C}-\text{C}-$	$\rightarrow \text{COOH}$	4-Hydroxybenzoic acid	6 ^h
Poly-(2-vinylnaphthalene)	$-\text{C}-\text{C}-$	$\rightarrow -\text{COOH}$	2-Naphthoic acid	4 ^h
1-Methylnaphthalene	$-\text{C}-\text{C}-$	$\rightarrow -\text{COOH}$	1-Naphthoic acid	3
β -Naphthol	$=\text{C}-\text{OH}$		Naphthoquinone	≤ 3
1-Methylphenanthrene	$-\text{C}-\text{C}-$	$\rightarrow -\text{COOH}$	Phenanthrene-1-carboxylic acid	≤ 2 ^g

^a All products were derivatized with dimethylsulfate-*d*₆ or diazomethane, and analyzed by GCMS.

^b Phenylacetic acid and hydrocinnamic acid were also obtained as minor products.

^c 45% of the product was found to be demethylated.

^d The product consisted mainly of polymerized material and of extensively degraded product. Milder oxidation (170°C for 4 hr) also gave similar results.

^e As a minor product, dibenzoyldisulfide was tentatively identified from both samples.

^f Nonoxidized compounds were obtained amply under the conditions of 170°–200°C for 4–8 hr.; they are (1) starting material (recovery 40–45 wt %), (2) monomethoxy compound (32–37 wt %), (3) dihydroxy compound (16–20 wt %).

^g The oxidation was also carried out in the presence of lignite coal. The coal mineral did not make any hydroxylation, ring destruction, or other side reactions.

^h Yield is shown as wt %.

phenol and syringaldehyde are quite susceptible to the CuO-oxidation. The oxidation products were found to consist mainly of unidentified degradation products and polymerized materials by solid-probe MS and GCMS analyses (*see* Table II). According to the suggested mechanism of CuO oxidation for lignin (5, 17), the reaction is initiated by extraction of an electron to give a phenoxy group radical. A second electron is then rapidly transferred to another CuO molecule, preventing coupling even when using a large excess of CuO at high temperature. Indeed, we have not isolated any oxidative coupling products from the oxidation of mono- and dihydric phenols and their derivatives. Perhaps our conditions (170°–200°C for 4–8 hr) were somewhat drastic for trihydric phenol derivatives.

Many CuO–NaOH oxidation studies for lignin and humic acids show that copper oxide does not affect cleavage of phenyl methyl ether. However, we have found that about 50% of methoxy groups are cleaved under various conditions (*see* Table V).

In general, alkaline copper oxide is a relatively weak oxidant for lignin degradation (*cf.* silver and mercuric oxides, *see* Ref. 17), therefore, aromatic aldehydes and/or ketones are isolated as major oxidation products of lignin. However, we have found that aromatic acids were major products from the control experiments under the conditions used in this study. Indeed, as shown in Table III, aromatic acids were major products from the oxidation of coals where more rigorous conditions of oxidation are required.

Results and Discussion

A summary of the oxidation products is shown in Table III. To determine the carbon balance and estimate the amount of CO₂ formed, carbon distributions of the oxidation products and nonoxidized residue from Samples 1 and 4 are given as examples in Table IV. Gas chromatograms of the derivatives obtained from Samples 1–6 are shown in Figure 1(a–f) with numbered peaks identified in Table V.

As shown in our previous communication (32), most informative was the identification of large amounts of *p*-hydroxy- and 3,4-dihydroxybenzoic acids in the oxidation products of low-rank coals (these coals are listed as Samples 1 and 2 in this chapter). These are regarded as lignin oxidation products. In this study we have found that, while no *o*- and *m*-hydroxybenzoic acids were found in the oxidation products of Samples 1 and 2, all three isomers were identified in small amounts in other rank bituminous coals (Samples 3, 5, 6). From Sample 3, 3,4-dihydroxybenzoic acid also was isolated in small amounts, however, this compound was not detected in the oxidation product of other bituminous coals (Samples 4, 5, and 6).

Table III. Summary of CuO-NaOH Oxidation Products

Wt % ^b	Sample No. ^a						
	1	2	3	4	5	6	7
Organic acid (benzene-ether extract)	35.3	19.6	17.1	7.0	14.7	1.3	—
Humic acid-like Material A (methanol extract)	54.3	61.0	46.2	9.3	39.5	69.5	—
Humic acid-like Material B (only aqueous alkali soluble)	≤1.0	≤1.5	16.1	51.0	20.2	2.0	7.5
Nonoxidized coal ^c	11.0	21.0	22.2	30.4	26.5	32.0	95.0
<i>Wt % of identified acids^d</i>							
Phenolic	66.6	54.1	14.6	41.0	8.3	5.8	—
Benzene carboxylic	26.0	36.2	69.4	50.2	62.7	76.7	—
Naphthalene carboxylic	2.0	3.3	6.2	5.5	22.9	10.6	—
Heterocyclic ^e	—	1.6	3.5	2.0	2.0	3.2	—
Aliphatic dibasic	2.6	1.0	1.4	—	≤1.0	≤1.0	—
Others	2.8	3.8	4.9	1.3	3.5	3.0	—
Ratio of phenol/ benzene acid	2.56	1.49	0.21	0.82	0.13	0.07	—

^a See Table I for information.^b Wt % was obtained from coal sample on a dry, ash-free basis.^c Small amount of insoluble copper salts are present.^d Wt % was obtained from each benzene-ether extract. Determination was made from the gas chromatograms of their methyl esters.^e Thiophene- and pyridine carboxylic acids for Samples 2-6, and pyridine tricarboxylic acids for Sample 1.

Table IV. Distribution of Carbon (%) in the Oxidation Products of Coals^a

Sample No.	%C of the Oxidation Products		%C in Nonoxidized coal	%C Lost
	Organic Acid	Humic acid-Material A		
1	27.8	44.5	0.9	11.0
4	4.5	6.6	38.2	30.3

^a Calculation was made from equation of: $\%C = \frac{\text{Carbon (g) in oxidation product (or in nonoxidized coal)} (\text{g}) / 100}{\text{Carbon (g) in coal sample (daf)}}$.

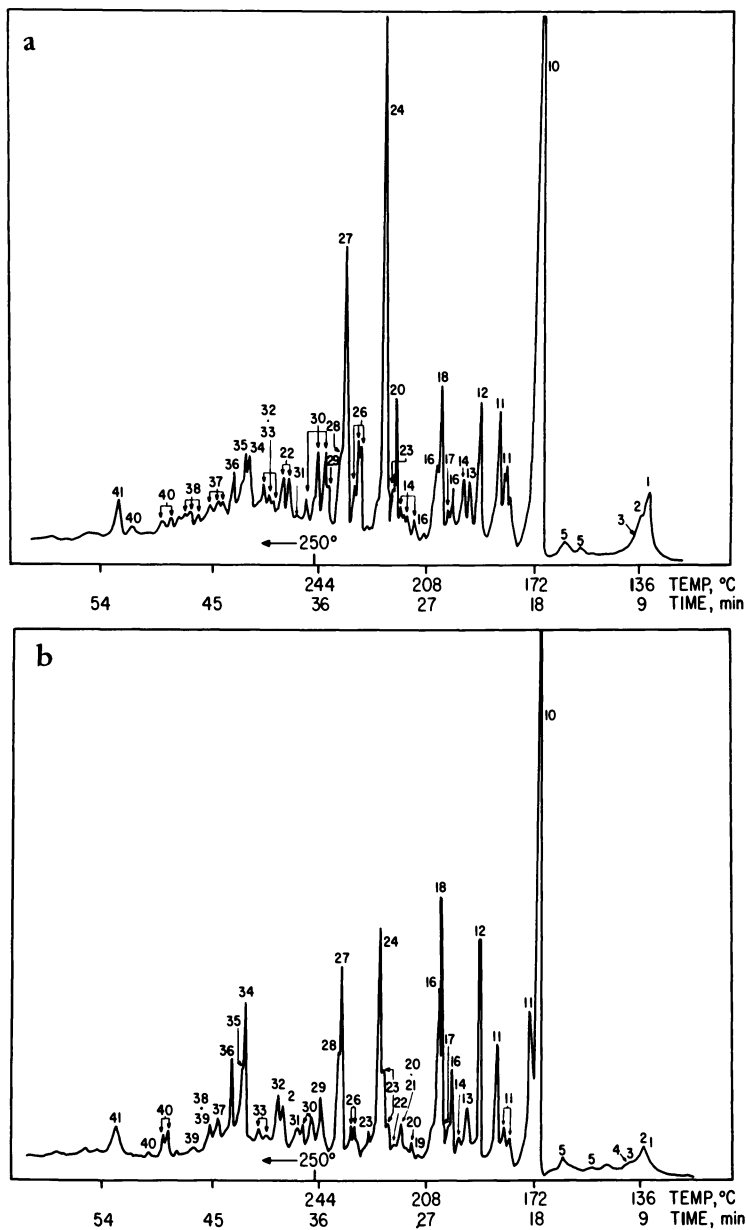
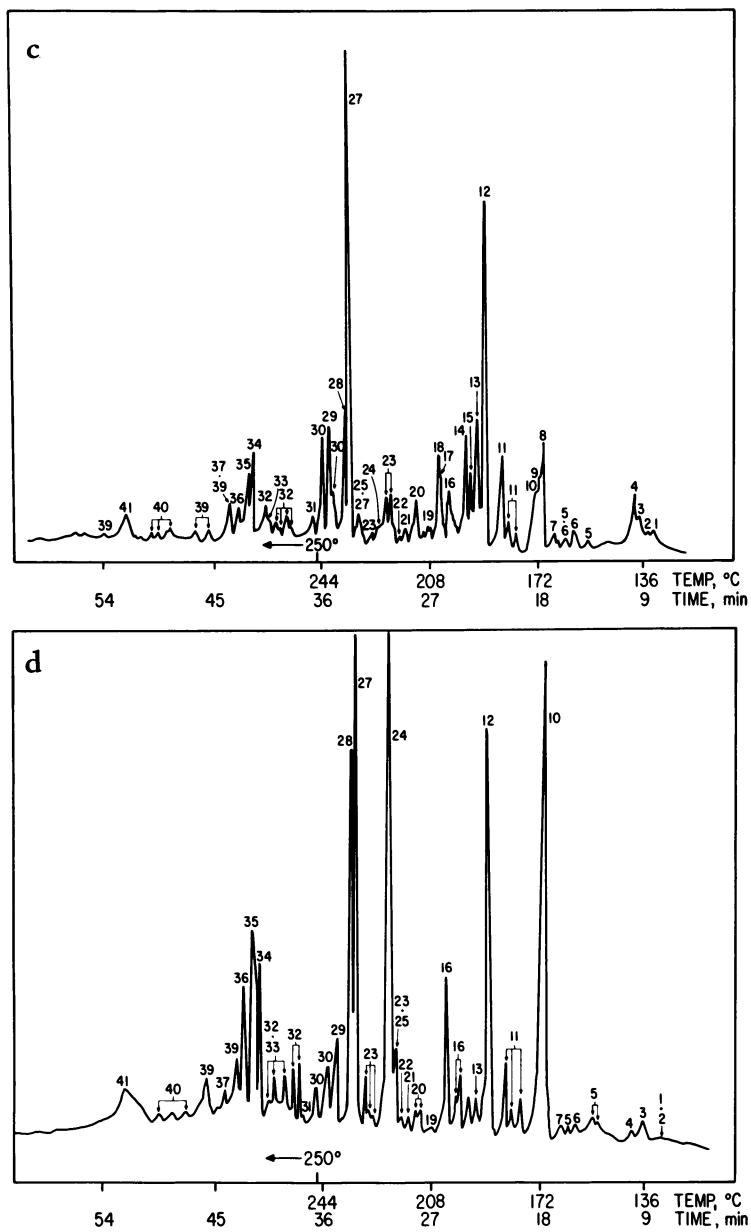


Figure 1(a). Gas chromatogram of methyl esters of the organic acid fraction from Sample 1; (b, c, d, e, and f) from Samples 2, 3, 4, 5, and 6, respectively.

The analysis was carried out on a Perkin-Elmer 3920B gas chromatograph interfaced to a modified Bendix model 12 time-of-flight mass spectrometer with a variable split between a flame ionization detector and the source of the mass spectrometer. The separation was made on a 15.2 m \times 0.51 mm SCOT column coated with OV 17 and temperature programmed from 100°–250°C at 4°C min⁻¹.

*Figure 1. Continued*

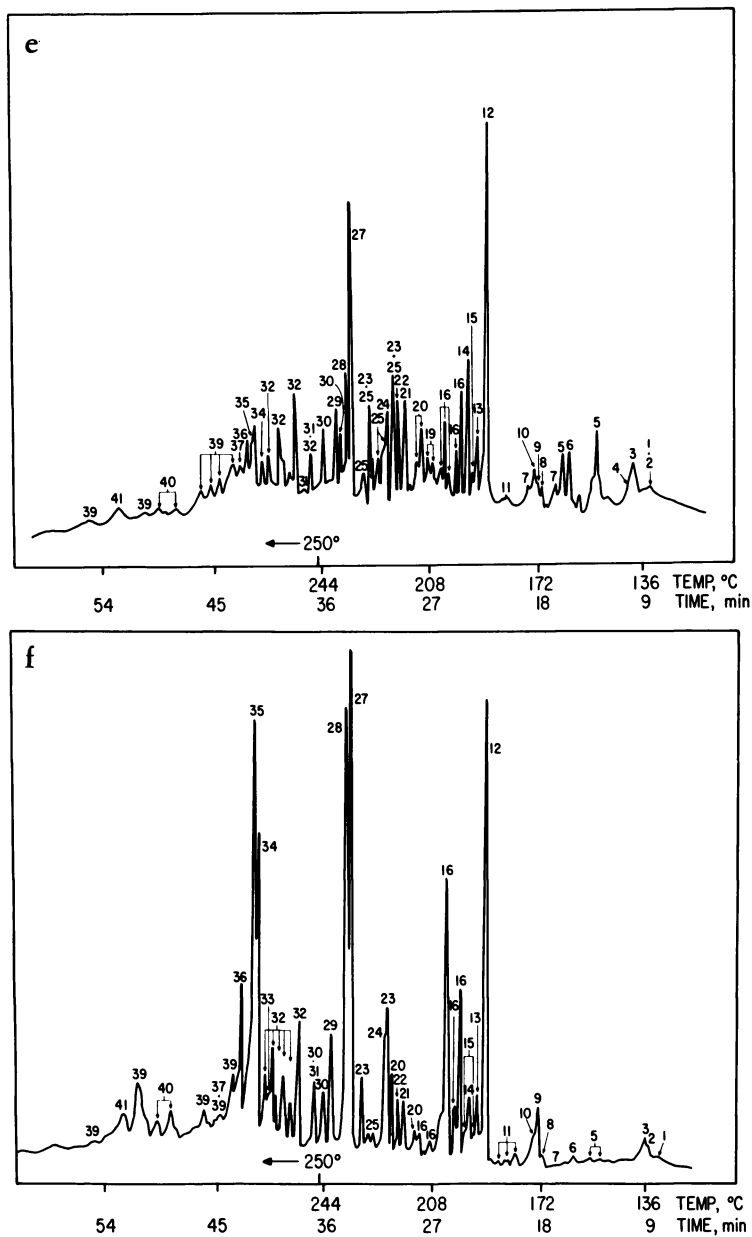


Figure 1. Continued

Table V. Organic Acids Identified as Their Methyl- d_3 Esters By GCMS and High-Resolution MS

GC Peak

1	Succinic acid
2	Methyl succinic acid
3	Benzoic acid
4	Thiophenemonocarboxylic acid
5	Methylbenzoic acid
6	Methylthiophenemonocarboxylic acid
7	Dimethylbenzoic acid
8	<i>m</i> -Hydroxybenzoic acid
9	<i>o</i> -Hydroxybenzoic acid
10	<i>p</i> -Hydroxybenzoic acid
11	Hydroxytoluic acid
12	1,2-Benzenedicarboxylic acid
13	1,4-Benzenedicarboxylic acid
14	1,3-Benzenedicarboxylic acid
15	Thiophenedicarboxylic acid
16	Methylbenzenedicarboxylic acid
17	Dihydroxybenzoic acid
18	3,4-Dihydroxybenzoic acid
19	Pyridinedicarboxylic acid
20	Dimethylbenzenedicarboxylic acid
21	1-Naphthoic acid
22	2-Naphthoic acid
23	Hydroxybenzenedicarboxylic acid ^a
24	4-Hydroxy-1,2-benzenedicarboxylic acid + 4-hydroxy-1,3-benzenedicarboxylic acid ^a
25	Methylnaphthoic acid
26	Methylhydroxybenzenedicarboxylic acid
27	1,2,4-Benzenetricarboxylic acid
28	1,2,3-Benzenetricarboxylic acid
29	1,3,5-Benzenetricarboxylic acid
30	Methylbenzenetricarboxylic acid
31	Pyridinetricarboxylic acid
32	Naphthalenedicarboxylic acid
33	Hydroxybenzenetricarboxylic acid
34	1,2,4,5-Benzenetetracarboxylic acid
35	1,2,3,4-Benzenetetracarboxylic acid
36	1,2,3,5-Benzenetetracarboxylic acid
37	Methylbenzenetetracarboxylic acid
38	Dihydroxybiphenyldicarboxylic acid ^b
39	Methylnaphthalenedicarboxylic acid
40	Hydroxynaphthalenedicarboxylic acid
41	Benzenepentacarboxylic acid

^a The GC peaks were checked by taking consecutive MS scans; mass spectra showed the ortho effect for Peak 23. For Peak 24, two components were detected by MS; 4-hydroxy-1,2-benzenedicarboxylic acid (as $-OCD_3-CO OCD_3$ derivative) showed no ortho effect, but the other component did.

^b Identification is tentative.

Two of the six possible isomers of hydroxybenzenedicarboxylic acids (4-OH-1,2-di-COOH and 4-OH-1,3-di-COOH) were identified in large amounts in the oxidation products of Samples 1, 2, and 4. These dicarboxylic acids also are considered to be typical lignin degradation products (17, 24). Individual identification of other isomers has not been completed positively at present because of lack of authentic standards or published GC data.

It is interesting that a bituminous coal (Sample 4) gave organic acids qualitatively similar to those of lignite coal (*see* Figure 1d). Major identified compounds were *p*-hydroxybenzoic acid and two isomers of hydroxybenzenedicarboxylic acid, benzene di- and tricarboxylic acids. No ortho or meta isomer of hydroxybenzoic acid was detected. We have found that solvent-extractable hydrocarbons obtained from this raw coal consist mainly of *n*-alkanes (C₁₁ to C₃₁). This is quite different from other results which showed that aromatic hydrocarbons were the major solvent-extractable material of several bituminous and anthracite coals (21). Indeed, petrographic analysis shows that this coal has a high content of sporinite (14.3 wt %) and a low content of vitrinite (30.2 wt %) (33).

As shown in Figure 2, lower-rank coals gave higher yields of organic acids as the oxidation products. Apparently this shows that lower-rank coals contain more ether linkages and some activated aliphatic chains (*see* Table II) in their structures, which can be cleaved by the CuO-NaOH. Low-volatile bituminous coal (Sample 6) produced very small amounts of organic acid (1.2 wt %). Anthracite coal (Sample 7) did not yield any organic acids. It seems certain that most of the organic oxygen in these high-rank coals is incorporated into heterocyclics.

Some acids not found in oxidation products of lignins, land plants, and marine sediments were found in the oxidation products of coals. Among these were phenolic di- and tricarboxylic acids and hydroxynaphthalenecarboxylic acids. From some soil fulvic and humic acids, phenolic polycarboxylic acids have been found in the oxidation products together with considerable amounts of fatty acids. Therefore, phenolic esters of fatty acids are considered to be present in these soil acids (6, 27). However, little or no fatty acids were observed in the coal oxidation products.

Trihydroxybenzoic acids or its methoxy derivatives (syringic group) which are obtained from the oxidation of lignins, fulvic and humic acids, and marine sediments were not found in any of our oxidation products. As already discussed, the authentic syringaldehyde and 2,6-dimethoxyphenol were degraded largely by the oxidation (Table II). This may account for the fact that we did not observe them; however, the syringic groups also might have been degraded during coalification.

All phenolic acids and hydroxynaphthalenecarboxylic acids identified were found as OCD₃-derivatives. The mass spectra showed the complete

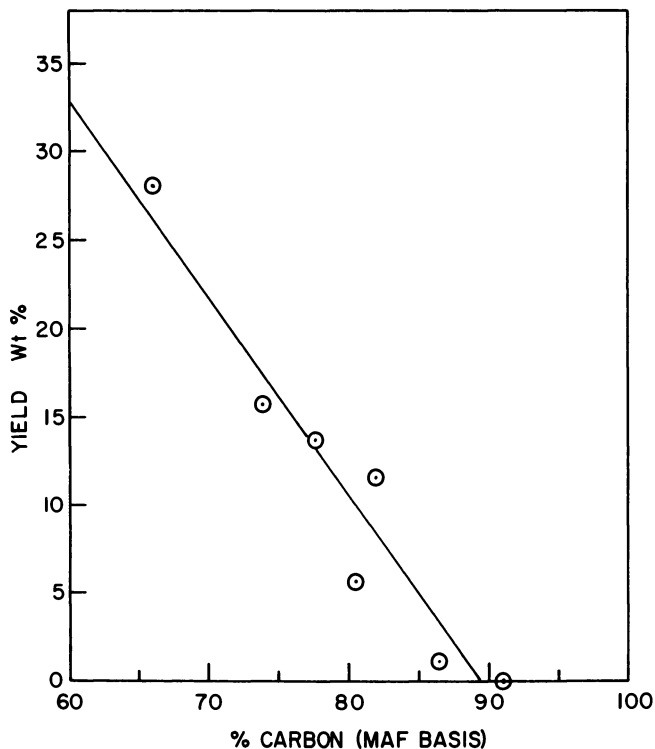
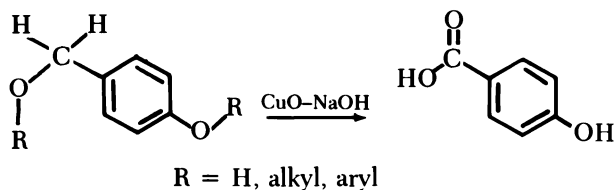


Figure 2. Yields of organic acids obtained from the CuO oxidation of coals (Samples 1-6) plotted against the % C in the coal.

absence of OCH_3 -groups. It has been confirmed that no isotope exchange of the H in OCH_3 with D occurred under our procedures. Although partial demethylation reactions during the oxidation cannot be excluded on the basis of the control experiment (see Table II), it is probable that the phenolic acids found were derived mainly from the fission of ether-linked aromatic systems as shown in the following example rather than from aryl methoxy units.



Indeed, it is known that very few or no methoxy groups are present in bituminous coals (34). In the lignite coal (Sample 1) aryl methoxy groups

are not present in significant amounts. Recently, we have confirmed these facts from mild KMnO_4 oxidation of d_3 -methylated Samples 1, 2, and 4 (unpublished results).

Nonhydroxybenzene-, naphthalene-, pyridine-, and thiophenecarboxylic acids identified (see Table V and Figure 1) may be derived from the cleavage of (1) benzyl-ether, -sulfide, -disulfide and other oxygen- and sulfur-function containing aliphatic linkages between aromatic rings one or both of which are not hydroxylated or (2) aliphatic and alicyclic methylene chains between aromatic systems. However, the second case is less probable because of the nature of the CuO-NaOH oxidation. Humic acid-like materials abundantly isolated from the oxidation products might be derived from nonlignin or extensively transformed lignin polymers that are not susceptible to the oxidation.

The oxidation of methyl groups of aromatic compounds by CuO-NaOH has been found to be ineffective. Therefore, relatively large amounts of methyl-substituted phenolic and benzene carboxylic acids were isolated from the coal oxidation.

We failed to isolate phenylpropane moieties that are related to coniferyl and other alcohols from the oxidation products of coals. In general, it seems to be difficult to isolate phenylpropane compounds as the CuO oxidation products from plant and humic materials, sediments, and coals. Hedges and Parker have reported (23) that *p*-coumaric and ferulic acids were isolated only from the CuO-NaOH oxidation of nonwoody tissues of angiosperms, but not from angiosperm woods and pine woods. These two cinnamic acids (phenylpropane moiety) are thought to be bonded to lignin polymers by ester linkages that are hydrolyzed readily, but not oxidized. It is not plausible that such ester linkages are present in coal.

Conclusions

1. Although one cannot rule out the possibility that plant phenols (3, 22, 35) could be one of the important precursors for coal formation, the present work shows that lignin-like polymers have been incorporated into the macromolecules of coals, and are still identifiable in lower-rank coals. Evidence for this is the identification of *p*-hydroxy- and 3,4-dihydroxybenzoic acids, and hydroxybenzenedicarboxylic acids which are known lignin oxidation products.

2. As coalification progresses, cross-linking increases and the lignin-derived polymers become more aromatic. Phenolic polycarboxylic acids and hydroxynaphthalene dicarboxylic acids which were identified are not found in the CuO-NaOH oxidation products of lignins and plant materials.

3. It is obvious that extensive transformation of lignin-like polymers occurred perhaps through reactions (17, 22, 36) such as demethylation, demethoxylation, isomerization, dehydrogenation, oxidation, cleavage of

ring structures, recondensation, etc. during coalification from lignite to bituminous and anthracite coals. It may be possible that clay minerals which are major inorganic constituents of coals have acted as solid acid catalysts (37, 38) for these reactions. This is shown by the fact that:

- a. Lower-rank coals gave higher yields of the CuO–NaOH oxidation products.
- b. A higher phenolic acid/benzenecarboxylic acid ratio is shown for the lower-rank coals.
- c. Very little or no dihydroxy benzoic acid was identified in the oxidation products of higher-rank coals (Samples 3–6)
- d. More naphthalene- and heterocarboxylic acids are found in the oxidation products of higher-rank coals. Finally, major parts of lignin-like polymers are transformed into nonlignin-type polymers at a later stage of coalification. Indeed, the later coalification product, anthracite coal (Sample 7), did not yield any phenolic acid by the oxidation.

4. In a previous paper (21) we characterized aromatic acids trapped in lignite coal, and have found that these acids are quite similar qualitatively to those obtained from the present oxidation of the same pretreated coal. This indicated that the trapped acids were derived mainly from the hydrolytic degradation of lignin-like polymers. We also have observed that no trapped organic acid is isolated from the anthracite coal that no longer contains lignin-like polymers.

Acknowledgment

We thank N. Berkowitz, P. H. Given, K. A. Kvenvolden, J. W. Larsen, and F. R. Mayo for helpful comments and suggestions. This work was supported by the Division of Basic Energy Sciences of the U.S. Department of Energy.

Literature Cited

1. Freudenberg, K.; Neish, A. C. "Constitution and Biosynthesis of Lignin"; Springer Verlag: New York, 1968.
2. Bolker, H. I.; Brenner, H. S. *Science* **1970**, *170*, 173.
3. Coffey, S., Ed. "Rodd's Chemistry of Carbon Compounds"; Elsevier: New York, 1976; Vol. 3, Chap. 16, Part D.
4. Adler, E. *Wood Sci. Technol.* **1977**, *11*, 169.
5. Sarkanen, K. V.; Ludwig, C. H., Eds. "Lignins"; Wiley Interscience: New York, 1971; pp. 345, 433.
6. Neyroud, J. A.; Schnitzer, M. *Can. J. Chem.* **1974**, *52*, 4123.
7. Schnitzer, M.; Neyroud, J. A. *Fuel* **1975**, *54*, 17.
8. Pew, J. C.; Withrow, J. R. *Fuel* **1931**, *10*, 44.
9. Sharma, J. N.; Wilson, M. J. G. *Fuel* **1961**, *40*, 331.
10. Ouchi, K. *J. Fuel Soc. Jpn.* **1977**, *56*, 779.
11. Gierer, J.; Noren, I. *Acta Chim. Scand.* **1962**, *16*, 1713.

12. Burges, N. A.; Hurst, M. H.; Walkden, G. *Geochim. Cosmochim. Acta* **1964**, *28*, 1547.
13. Martin, J. P.; Haider, K.; Saiz-Jimenez, C. *Soil Sci. Soc. Am. Proc.* **1974**, *38*, 760.
14. Bimer, J.; Given, P. H.; Raj, S. In "Organic Chemistry of Coal", *ACS Symp. Ser.* **1978**, *71*, 86.
15. Stevenson, F. J.; Mendez, J. *Soil Sci.* **1967**, *103*, 383.
16. Schnitzer, M.; De Serra, M. I. O.; Ivanson, K. *Soil Sci. Soc. Am. Proc.* **1973**, *37*, 229.
17. Greenland, D. J.; Hayes, M. H. B., Eds. "The Chemistry of Soil Science"; John Wiley: New York, 1978; Chap. 3.
18. Van Krevelen, D. W. "Coal"; Elsevier: New York, 1961; Chap. 12.
19. Bearse, A. E.; Cox, J. L.; Hillman, M. "Production of Chemicals by Oxidation of Coal"; Battelle Energy Program Report, Battelle Memorial Institute, Columbus, OH, 1975.
20. Hayatsu, R.; Winans, R. E.; Scott, R. G.; Moore, L. P.; Studier, M. H. In "Organic Chemistry of Coal," *ACS Symp. Ser.* **1978**, *71*, 108.
21. Hayatsu, R.; Winans, R. E.; Scott, R. G.; Moore, L. P.; Studier, M. H. *Fuel* **1978**, *57*, 541.
22. Murchison, D.; Westoll, T.S., Eds. "Coal and Coal-Bearing Strata"; Oliver & Boyd: London, 1968; Chap. 10.
23. Hedges, J. I.; Parker, P. L. *Geochim. Cosmochim. Acta* **1976**, *40*, 1019.
24. Griffith, S. M.; Schnitzer, M. *Soil Sci.* **1976**, *122*, 191.
25. Coffey, S., Ed. "Rodd's Chemistry of Carbon Compounds"; Elsevier: New York; Vol. 3, Chap. 4, Part A.
26. Musgrave, O. C. *Chem. Rev.* **1969**, *69*, 499.
27. Neyroud, J. A.; Schnitzer, M. *Soil Sci. Soc. Am. Proc.* **1974**, *38*, 907.
28. Bugur, K.; Gaines, A. F.; Gulec, A.; Guyer, S.; Yurum, Y.; Olcay, A. *Fuel* **1973**, *52*, 115.
29. Hayatsu, R.; Winans, R. E.; Scott, R. G.; Moore, L. P.; Studier, M. H. *Nature (London)* **1978**, *275*, 116.
30. Green, G.; Steelink, C. *J. Org. Chem.* **1962**, *27*, 170.
31. Karr, C., Jr., Ed. "Analytical Methods for Coal and Coal Products"; Academic: New York, 1978; Vol. 2, Chap. 21.
32. Hayatsu, R.; Winans, R. E.; McBeth, R. L.; Scott, R. G.; Moore, L. P.; Studier, M. H. *Nature (London)* **1979**, *278*, 41.
33. Spackman, W.; Davis, A.; Walker, P. L.; Lovell, H. L.; Stefanko, R.; Essenhig, R. H.; Vastola, F. J.; Given, P. H. "Evaluation of Development of Special Purpose Coals", Final Report FE-0390-2, ERDA, Oak Ridge, TN, Sept. 1976.
34. Lowry, H. H. Ed. "Chemistry and Utilization of Coal"; John Wiley: New York, 1963, Suppl. Vol., Chap. 6.
35. Timell, T. E., Ed. "Wood Chemicals—A Future Challenge." In *Proc. Cellul. Conf.*, *8th*, 1975, John Wiley: New York, 1975; p. 363.
36. Swain, F. M. "Non-Marine Organic Geochemistry"; Cambridge Univ. Press: Cambridge, 1970.
37. Tanabe, K. "Solid Acids and Bases"; Academic: New York, 1970.
38. Theng, R. K. G. "The Chemistry of Clay-Organic Reactions"; John Wiley: New York, 1974.

RECEIVED July 19, 1979.

Short-Time Reaction Products of Coal Liquefaction and Their Relevance to the Structure of Coal

MALVINA FARCASIU

Mobil Research and Development Corporation, Central Research Division,
P.O. Box 1025, Princeton, NJ 08540

The structure of chemical classes of soluble coal products produced at short contact times (1–5 min), at temperatures of 400°–425°C, and in the presence of an H-donor solvent relates to the elements of structure in the initial coal. Under these conditions only a few of the chemical bonds present in the coal molecule are actually broken. The fragments (elements of structure) that, linked by weaker bonds, constitute the larger coal molecule differ in molecular weight, functionality, and relative abundance, but the structures of their carbon skeletons are similar for a given coal. The carbon skeleton of a coal, and especially the aliphatic part, is used to distinguish among coals, even those of the same rank. The methodology employed in this work could be used for any coal.

A better understanding of the chemical structure of coal will help in the improvement of the known procedures for coal liquefaction and the evolution of new technology for the transformation of coal into more petroleumlike products.

Coal is a rock containing both organic and inorganic parts, and each part differs from one coal to another. This paper will be concerned only with the structure of the organic part. More specifically, we will discuss the basic elements of structure that are internally bound by stronger chemical bonds and that are interconnected in the larger coal molecule by relatively weaker bonds. The main questions we will try to answer are these:

1. In any process that will selectively break some of the bonds in a large coal molecule to produce smaller soluble mole-

- cules, are these fragments of the initial structure essentially identical with each other, or are they different (chemical functionality, carbon skeleton, molecular weight)?
2. Can the chemical characterization of the solubilized coal be used to determine the initial coal structure?
 3. How could coal structure be better visualized: by models of a coal molecule or by models of elements of structure? What chemical characteristics can be used to differentiate among coals, and which of these characteristics has more influence on coal liquefaction?

The most useful data for structural characterization were obtained in the present work by the use of short-time (1–5 min) thermal treatment with an H-donor solvent under hydrogen pressure at 425°C as the method to solubilize coal (1, 2). We will discuss how the chemical structure of the products of this reaction can be used to determine characteristic elements of the structure of coals. Other and more limited information can be obtained from the study of solid coal itself and can be used to complement the data gathered with the solubilized coal.

Results and Discussions

Data Obtained from the Study of Solid Coal. The quantitative ratio of the atoms in the organic part of coal gives the first information about its chemical structure. For example, for two coals whose liquefaction behavior has been extensively studied, the elemental composition for 100 atoms is as shown below.

<i>Coal</i>	<i>Elemental Composition for 100 Atoms</i>
Illinois No. 6 (Monterey)	$C_{49}H_{43}O_{6.4}S_{0.8}N_{0.8}$
Wyodak	$C_{48.3}H_{42.6}O_{8.6}S_{0.07}N_{0.5}$

These simple data reveal the following:

1. The main nonhydrocarbon functions in coal are oxygen functions.
2. Sulfur and nitrogen are minor constituents of coal molecules.
3. In coals the majority of the chemical bonds must be carbon–carbon bonds. For example, in Monterey coal the carbon will form 196 bonds/100 atoms/molecule ($49 C \times 4$). Even if all the other atoms are bonded exclusively to car-

bons (an extremely unlikely hypothesis), the stoichiometry still requires there to be 136 carbon-carbon bonds. The way these carbon atoms are bonded is obviously important for understanding of coal structure.

The heteroatoms are present in coal in the following major chemical functions (3): *oxygen*: phenols, ethers, heteroaromatic ethers, carboxylic acids, quinones; and *nitrogen*: pyrrole and pyridine derivatives. These chemical functions can be present in smaller or larger amounts, but, qualitatively, all coals contain the same kind of chemical functions.

The carbon skeleton is perhaps the most controversial aspect of the research on coal structure. Three major questions are of interest in this field: What is the percentage of aromatic carbons? How condensed are the aromatic ring structures? What is the carbon skeleton of the aliphatic portion of coal?

The percentage of aromatic carbon can be determined now by solid state ^{13}C NMR. Extensive work in this area is reported in the literature (2, 4, 5). The other two questions cannot be answered definitively by solid state studies alone. One should mention the work of Friedel and Queiser (6) in which information on the degree of aromatic ring condensation was obtained by UV-visible spectroscopy on coal itself. They concluded that the degree of aromatic ring condensation is quite low in bituminous coals.

Data Obtained from Solubilized Coal. We have found that the careful use of the structural information provided by short-contact-time coal thermal liquefaction products can give relevant information on coal structure.

The obvious danger of structural studies involving coal solubilization followed by the investigation of the reaction products is the possibility of transformation of the primary products by further reaction. However, our results (1, 2) indicate that at short contact times the principal reactions involve only thermal cleavage of the weaker bonds, and therefore the intrinsic elements of the coal structure are preserved without modification.

At times of 1-5 min and temperatures of 400°-425°C, only a few bonds actually are broken (2). At temperatures above 450°C under the same conditions, an increase in the aromatic content usually is observed. In the range of temperatures of 400°-425°C, however, the aromatic content, as defined by ^{13}C NMR, is slightly smaller than it is in the initial coal.

The elemental composition for the initial coal [for Monterey coal (2)] and its short-contact-time liquefaction products (defined as pyridine soluble) are shown in Table II.

Table II.

<i>Illinois No. 6 (Monterey)</i>	<i>Composition for 100 Atoms</i>	<i>H/C Atomic Ratio</i>
Coal	$C_{49}H_{43}O_{6.4}S_{0.8}N_{0.8}$	0.88
Short-contact-time liquefaction products ^a (91% conversion, (7) 64% pyridine-soluble products)	$C_{50}H_{44}O_{4.5}S_{0.6}N_{0.8}$	0.88

^a Conversion is defined as the sum of the products that distill below 400°C and the pyridine-soluble fraction of the 400+°C material. Thus in the example given, 91 - 64 = 27% represents water and volatile products, a minor 400°C fraction, and manipulation losses. The balance of 9% is ash and insoluble material.

From the table we see that no change in the H/C ratio took place in this time. Work at Mobil (1, 2), Exxon (7, 8), and Oak Ridge National Laboratory (9) indicate that none of the following reactions takes place under the liquefaction conditions described above: hydrogenation of aromatic polycyclic hydrocarbons; significant aromatization of the hydroaromatic structures; or destruction or formation of polycyclic saturated structures.

A corollary of this statement is the following: If these polyaromatic or polycyclic saturated structures are present in the carbon skeleton of coal, they should be identified in the short-contact-time liquefaction products. The possibility of some isomerization reactions in the carbon skeleton cannot be excluded totally, but the most important fact is that no dramatic aromatization of hydroaromatic rings or saturation of aromatic rings takes place under these conditions. Many of the chemical functions also are stable under these conditions, especially the O, S, and N heterocyclic aromatic structures. Water formation by phenol dehydroxylation is minimal. In coal liquefaction under our conditions, even at long reaction times (up to 90 min) in the absence of an added catalyst, the -OH bonded to a monoaromatic ring is stable. Under the same conditions, dehydroxylation of polyaromatic phenols does occur (10).

The data above show that the structure of short-contact-time products of coal liquefaction is indicative of the main characteristics of the carbon skeleton in coal itself, the distribution and abundance of the majority of heteroatomic functions, and the statistical distribution of the weak bonds in the parent coal.

The fractionation and chemical characterization of these short-time coal liquids were conducted by a method that has been reported (11). According to this method the coal liquids are fractionated by chemical classes and each fraction is then characterized by a variety of physical and

chemical methods. The results were used to answer the questions we addressed in the introduction to this paper and are discussed in the paragraphs that follow.

Distribution of the Elements of Structure in Coal. A typical distribution of chemical classes in a short- and a long-contact-time thermal-solubilized coal is given in Table III. The data in the table, together with those published previously (1, 2), reveal that coal liquefaction is not a depolymerization with the formation of identical monomeric units but a breakdown into fragments of different molecular weight, carbon structure, and functionality. It is also worth noting that in bituminous coal, such as West Kentucky No. 9 and Illinois No 6 (Monterey and Burning Star), the less functional fractions SESC 3, 4, and 5 (defined in Table III) have average molecular weights of 400–600, while the more functional fractions SESC 7 and 8 have molecular weights of 800–1000 (1, 2). In the case of a subbituminous coal (Wyodak) the average molecular weights of all the fractions were about 600; this weight indicates a more uniform distribution of the weak bonds in the initial coal. The aromatic content (^1H NMR, ^{13}C NMR data) of the fraction SESC 3–9 is similar for a given coal liquid (2). Relating these data to the initial coal structure indicates that the elements of structure in a coal have similar carbon skeletons but an uneven distribution of chemical functionalities.

Short-Contact-Time Coal Liquefaction Products and the Initial Structure of Coal. Our own data and those from the literature indicate that no major changes take place in the different elements of coal structure under short-contact-time reaction conditions and at relatively low temperature. It is obvious, however, that fragmentation occurs by

Table III. Distribution of Chemical Classes in the Solubilized Products from Wyodak Coal (2) (Percent Composition)

SESC Frac- tion Number	Chemical Classes	Short-Contact- Time SRC	Long-Contact- Time SRC
1	Saturated hydrocarbons	0.5	0.5
2	Aromatic hydrocarbons	4.0	~20.0
3	Heteroaromatic compounds	6.6	20.8
4	Monophenols	7.0	20.0
5	Basic nitrogen compounds	17.5	10.7
6	Highly functional compounds	6.3	4.4
7	Polyphenols	11.0	4.7
8	Polyphenols	26.3	16.3
9	Polyphenols	20.0	3.0

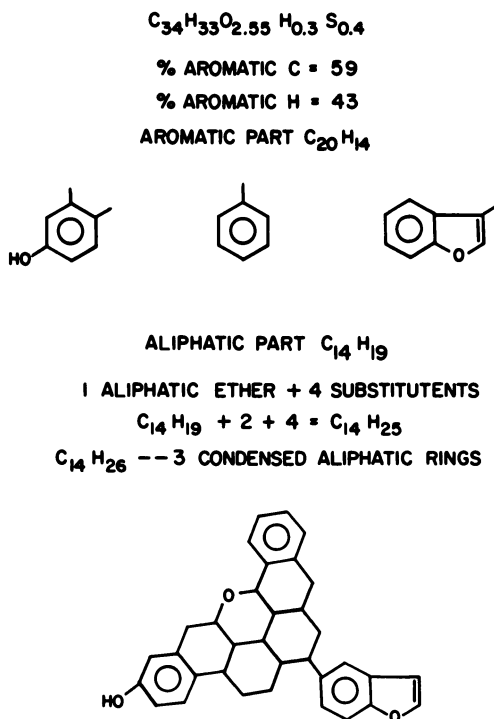


Figure 1. Fraction SESC 4 Monterey coal, short-contact-time SRC

breaking some weak bonds between the structural elements. While the stabilization of the molecular fragments thus formed will involve some transformations (H elimination, H addition, etc.), these transformations will not change the overall structure of the molecules. On the other hand, longer reaction times or higher temperatures or both result in more extensive structural differences between the resulting liquid products and the starting material (coal), as discussed elsewhere (2, 10).

Representations of Coal Structure. Several authors (12, 13) have attempted to write representative formulas for different coals, or at least for petrographic fractions of them. These representative formulas can be very helpful for chemists who are used to writing and thinking in terms of structural formulas. However, in view of the nature and properties of coal, the structural information that can be obtained about the coal itself is limited, at best. Therefore, we prefer to describe the structural

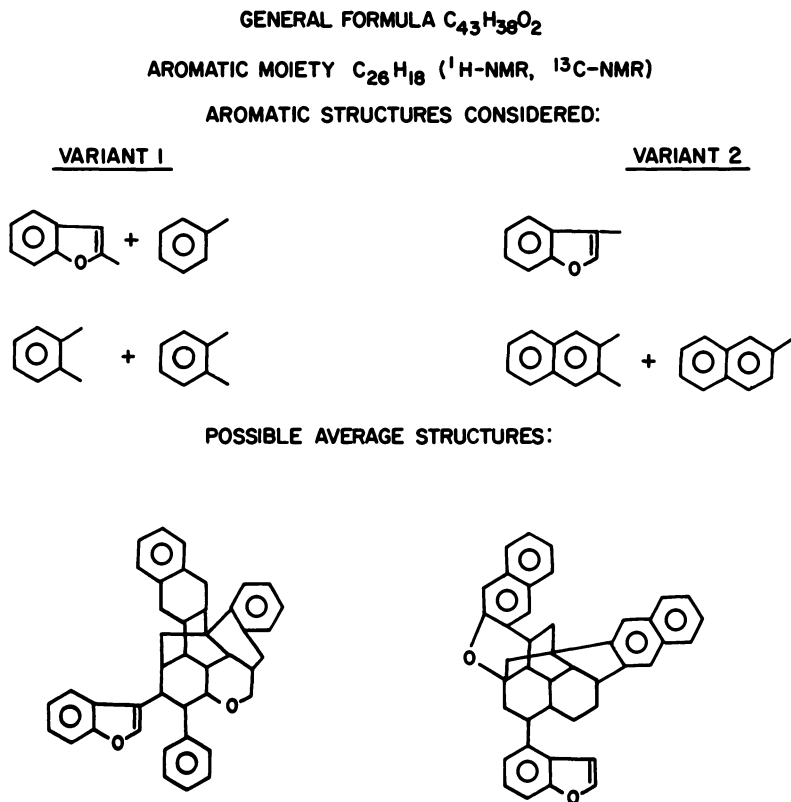
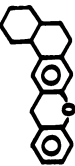
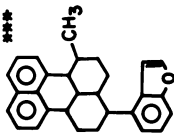
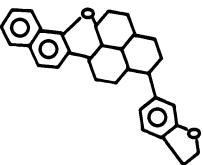
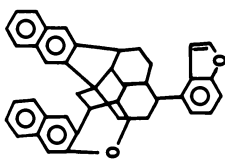


Figure 2. Possible average structures for Wyodak SESC-3 short-contact-time SRC

formulas of coal fragments as represented by the short-time liquefaction products and then try to ascertain the nature of the weaker bonds connecting these fragments in the original coal. Examples of such elements of coal structure are shown in Figures 1 and 2. The procedure used to arrive at such average molecular structures is discussed in Whitehurst et al. (1, 2).

The structure of these fragments (elements of structure) can be studied conveniently after their fractionation in chemical classes such as was referred to earlier [SESC method (11)]. The fractions characterized by the same degree of functionalization and nature of functional groups (same SESC fraction number) obtained from two different coals can differ from each other in their relative abundance and/or in their carbon skel-

COAL COMPOSITION	KENTUCKY	HIAWATHA	MONTEREY	WYODAK
NO. POLYCONDENSED SATURATED RINGS/100C	$C_{100}^H 82^M 1.7^O 9.4$	$C_{100}^H 64^M 2^O 9.5$	$C_{100}^H 88^M 1.6^O 13.2^S 1.74$	$C_{100}^H 86^M 18$
COAL	4		6	10
SESC-3	2		4	5
SCT*				
STRUCTURE				
g H CONSUMED/100g COAL DURING LIQUEFACTION (NORMALIZED TO 100% CONVERSION)	SCT 0.43	***	0.63	0.89
	LCT** 0.96		2.03	2.80

*SCT = SHORT CONTACT TIME <2 MIN.

**LCT = LONG CONTACT TIME >30 MIN.

***CA. 30 MIN. CONTACT TIME

Figure 3. Comparison of structures and hydrogen consumption for four coals (11)

eton. We found that the main difference is in the carbon skeleton, especially the degree of condensation of the aliphatic rings, as shown in Figure 3.

Our data suggest that the structure of the aliphatic part in a coal could be very important for its processing. An increased number of aliphatic rings would mean a larger hydrogen consumption in the fragmentation process, as shown in Figure 3. The larger hydrogen consumption results because more than one bond must be broken to form smaller molecules from such a structure. Also, the hydroaromatic structures would need higher hydrogen pressure during any processing to compensate for their thermodynamically favored tendency toward aromatization and gas formation.

Conclusions

The structure of chemical classes of soluble coal products produced at short contact times (1–5 min) and at temperatures of 400°–425°C relates to the elements of structure in the initial coal. The fragments (elements of structure) that, linked by weaker bonds, constitute the larger coal molecule differ in molecular weight, functionality, and relative abundance, but the structures of their carbon skeletons are similar for a given coal. The carbon skeleton of a coal, and especially the aliphatic part, can be used to distinguish among coals, even those of the same rank. The methodology employed in this work could be used for any coal.

Acknowledgments

The work presented here was conducted under a program jointly sponsored by the Electrical Power Research Institute (EPRI) and Mobil Research and Development Corp. Co-workers in this project are: J. J. Dickert, T. O. Mitchell, and D. D. Whitehurst. Technical assistance was provided by B. O. Heady and G. Odoerfer.

Literature Cited

1. Whitehurst, D. D.; Farcasiu, M.; Mitchell, T. O. Feb. 1976, EPRI Report AF-252.
2. Whitehurst, D. D.; Farcasiu, M.; Mitchell, T. O.; Dickert, J. J., Jr. July 1977, EPRI Report AF-252.
3. Francis, W. "Coal"; Edward Arnold: London, 1961.
4. Miknis, F. P.; Maciel, G. E.; Bartuska, V. J. *Am. Chem. Soc. Div. Fuel Chem. Prepr.* 1979, 24, 327.
5. Alger, T. D.; Pugmire, R. J.; Hamill, W. D.; Grant, D. M. *Am. Chem. Soc. Div. Fuel Chem. Prepr.* 1979, 24, 334.
6. Friedel, R. A.; Queiser, J. A. *Fuel* 1959, 38, 369.
7. Aczel, T.; Gorbaty, M. L.; Moa, P. S.; Schlosberg, R. H. *Fuel* 1975, 54, 295.
8. Aczel, T.; Gorbaty, M. L.; Moa, P. S.; Schlosberg, R. H. *Preprints of the 1976 Coal Chemistry Workshop*, 1976, 165.

9. Benjamin B. M.; Raaen, V. F.; Maupin, R. H.; Brown, L. L.; Collins, C. J. *Fuel* 1978, 57, 269.
10. Whitehurst, D. D.; Farcasiu, M.; Mitchell, T. O.; Dickert, J. J., Jr. EPRI Report, to be published.
11. Farcasiu, M. *Fuel* 1977, 56, 9.
12. Given, P. J. *Fuel* 1960, 39, 147.
13. Wiser, W., presented at the American Chemical Society National Meeting, Miami, FL, September, 1978.

RECEIVED August 6, 1978.

Characterization of Hydrolytically Solubilized Coal

RANDALL E. WINANS, RYOICHI HAYATSU, ROBERT L. McBETH,
ROBERT G. SCOTT, LEON P. MOORE, and MARTIN H. STUDIER

Chemistry Division, Argonne National Laboratory, Argonne, IL 60439

Treating a bituminous coal with potassium hydroxide in glycols at 250°C yields a largely soluble product that results from the reduction of polycyclic aromatics and the cleavage of aryl ether linkages. The reduction in aromaticity was demonstrated in two ways. First, the fraction of aromatic carbons (f_a) of the soluble product, which was determined by ^{13}C NMR, was compared with the f_a of the whole coal determined by fluorination. Secondly, the aromatic acids produced in a selective oxidation of both the product and coal were compared, and evidence for ether cleavage was obtained from the oxidation results. The effects of rank and different protic solvents on the reaction were examined.

Since many of the techniques used for structural or functional group analysis of organic species require either an appreciable solubility or volatility, the virtual insolubility of coals in all solvents constitutes a major problem in their study. In a search for relatively mild methods for solubilizing coal, we have found that a hydrolytic solubilization technique that consists of treating a bituminous coal with potassium hydroxide in ethylene glycol at 250°C is quite effective. This study has several objectives relating to hydrolytic solubilization, coal structure, and conversion processes. First, the role of linkages susceptible to hydrolytic cleavage in the solubilization process must be assessed. Secondly, the role of the solvent must be defined in its effect on the action of the potassium hydroxide (KOH), covalent bonding of solvent or its degradation products to the coal, and as a source of hydrogen. Also, the hydrolytic product should be compared to products obtained from other conversion processes such as solvent-refined coal (SRC). Finally, this study

will demonstrate the utility of a broad analytical approach including the use of selective oxidants to characterize coals and nonvolatile coal products.

The use of alkali in protic solvents to solubilize coal is not new. In an early study Pew and Withrow found that the yield of 2-ethoxy-ethanol extract at 135°C for a bituminous coal increased from 9.4 to 31.3% with the addition of KOH (1). Recently, two different groups have reported studies of hydrolytic reactions on coals. Ross and Blessing have looked at both potassium isopropoxide in isopropanol (2) and KOH in methanol (3) systems at a 400°C reaction temperature. The use of such a high reaction temperature precludes any direct comparison between their results and the data presented in this study. It has been shown that thermal intramolecular reactions in coal begin occurring at temperatures greater than 250°–300°C (4). Therefore, at 400°C it would be difficult to separate the hydrolytic reaction from these internal coal reactions. Recently, Ouchi and co-workers (5–29) reported in detail the reactions of coals with ethanolic NaOH at temperatures ranging from 260° to 450°C. Although their results are similar to those presented in this chapter, the interpretation is different with regard to two main points. First, in these reactions reduction of aromatic rings apparently is involved as indicated by an increase in the H/C ratio and a decrease in the fraction of aromatic carbons (f_a). There are at least three possible pathways for this to occur including: (1) hydrogenation via H₂ formed by alkaline decomposition of the solvent, the route noted in Ref. 5; (2) hydride or hydrogen transfer from the solvent; or (3) attachment of the solvent to the coal. Evidence will be presented showing that true reduction is occurring, which supports pathway 2. Secondly, we have found that this reduction occurs even at the lower temperatures used in this study. This contradicts results recently reported for the NaOH/EtOH reaction at 260°C (9), where it is claimed that saturation of the aromatic rings and other structural changes are minimal.

We decided to use glycol as a solvent for several reasons. First, the results of Pew and Withrow (1) indicate that the properties of glycol and KOH are such that more drastic conditions could be expected to result in improved extract yields. In addition, it is possible to obtain higher reaction temperature with glycols without using an autoclave, and cleavage of C–C bonds has occurred as a side reaction in Wolff–Kishner reductions (10). Finally, alkaline hydrolysis at high temperatures (\cong 200°C) will cleave ethers (11, 12) and carbonyls (12).

In the analysis of the glycol-solubilized coal we applied all the techniques used in our studies on coals, SRC and SRL products (4). The effect of the reaction on the aromatic units was shown by comparing selective oxidation products from the coal and its hydrolytic product. These results were compared with the aromaticity of the product deter-

mined by ^{13}C NMR. The molecular size distribution was determined using gel permeation chromatography (GPC). Also, we compared the products from glycols to those from water and alcohol alkaline hydrolysis.

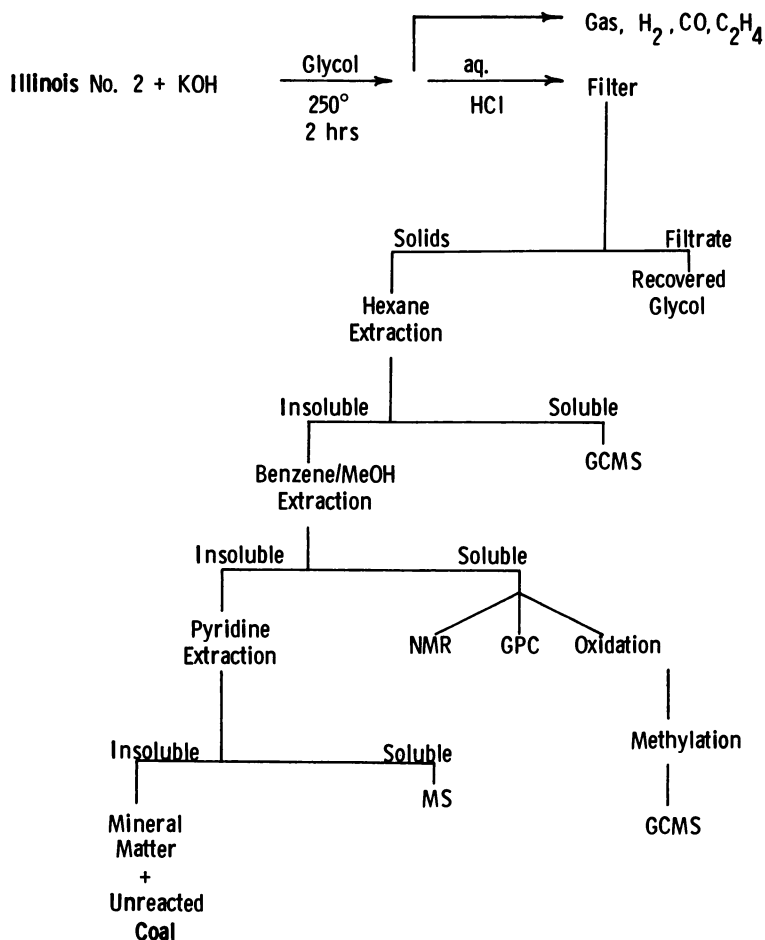
Experimental

The elemental analyses for the coals and coal products used in these experiments are given in Table I. In a typical reaction, 10 g of coal, 10–13 g of KOH, and 100 mL of solvent were heated in a stirred or rocking autoclave at 250°C for 2 hr. The gases produced in these reactions were separated on a 1 m \times 3.2 mm Porapak Q column using a mass spectrometer or microwave plasma analyzer for detection and identification. The reaction products were worked up by the method outlined in Scheme 1. The homogeneous, alkaline, reaction mixture was transferred into water, acidified with concentrated HCl, filtered, washed with water, and dried in vacuo at 80–100°C. A portion of the product was extracted successively under reflux with hexane, benzene–methanol (1/1), and pyridine. The results of these extractions are listed in Table II for the various coals studied using ethylene glycol as a solvent. In Table III the extract yields are given for the reaction of KOH with the Illinois No. 2 bituminous coal as a function of the reaction solvent.

The hexane-insoluble product from Reaction 6 (Table III) and the original coal were derivatized with d_6 -dimethylsulfate and oxidized with aqueous $\text{Na}_2\text{Cr}_2\text{O}_7$ buffered with NaH_2PO_4 at 250°C for 38–48 hr (4). The yields of 68% for the coal and 63% for the product were calculated from the ratio of the weight of the acids to the initial weight of the coal or product. The resulting aromatic acids were derivatized with diazomethane and analyzed by gas chromatography mass spectrometry (GCMS). The esters were separated on an OV-17 support-coated open tubular column (15 m \times 0.5 mm i.d.) temperature programmed from 100–250°C at 4°/min. Using a variable split the gas chromatograph is connected to a flame ionization detector (FID) and a modified time-of-flight mass spectrometer (13). The identifications of the esters were confirmed from retention times and mass spectra of authentic compounds, from published data, and from high-resolution mass spectrometric analysis of the mixture. Distribution of the esters was obtained from the FID output using the effective carbon number for each ester.

Table I. Elemental Analysis on a % MAF Basis

Coal	% C	% H	% N	% S (total)	% O (by difference)
Wyoming lignite	66.4	4.8	1.5	1.1	26.2
Illinois No. 2 bituminous	73.9	5.2	1.4	2.4	17.1
Illinois No. 6 bituminous	77.7	5.4	1.4	4.1	11.4
Pittsburgh No. 8 bituminous	82.7	5.5	1.3	2.8	7.7
Low volatile bituminous (PSOC258)	86.5	4.8	1.3	2.6	4.8
SRC (Pittsburgh No. 8)	87.2	5.5	1.8	1.2	4.3
SRL (N. Dakota lignite)	89.3	5.8	1.1	0.9	2.9



Scheme 1.

Table II. Solubilities of Coals after Treatment with KOH in Ethylene Glycol at 250°C^a

Reaction No.	Coal	Yield ^b	Hexane	Bz/MeOH (1/1)	Pyridine	In-soluble
1	Wyoming lignite	114	—	47.2	13.2	39.2
2	Illinois No. 2	90	1.3	48.9	42.2	7.4
3	Illinois No. 6	102	0.1	25.8	48.6	25.6
4	Pittsburgh No. 8	95	0.3	8.9	32.3	58.6
5	LV bituminous (PSOC258)	100	0.2	0.5	3.2	96.1

^a Extract yields normalized to 100%.

^b Weight of product/weight of coal (maf basis).

Table III. Solubilities of Illinois No. 2 Bituminous Coal after Treatment with KOH in Various Solvents at 250°C^a

Reaction No.	Solvent	Yield ^b	Bz/			
			Hexane	MeOH (1/1)	Pyridine	In-Soluble
6	Triethylene glycol (TEG)	123	11.9	46.8	37.3	4.1
2	Ethylene glycol	90	1.3	48.9	42.2	7.4
7	Toluene/TEG	124	0.6	46.6	35.1	17.7
8	Ethanol	86.5	0.1	49.4	40.3	9.8
9	Methanol	90.7	0.4	21.7	36.4	41.5
10	Water	86	—	18.5	12.0	69.7
11	Coal (untreated)	—	—	6.3	6.0	87.7

^a Extract yields are normalized to 100%.

^b Weight of product/weight of coal (maf basis).

The molecular size distribution was determined using GPC with a series of four μ Styragel columns (500 Å, 3 × 100 Å). Tetrahydrofuran (THF) was used as the elution solvent at a flow rate of 1 mL/in. The chromatograms shown in Figures 1 and 2 were obtained on the THF-soluble portion of the products using a variable wavelength UV-visible detector set at 254 nm. Calibration curves (Figure 3) were obtained under the same conditions for linear polymers and a series of aromatic hydrocarbons.

The ¹³NMR spectra were obtained on a Bruker WP-60 at 15.08 MHz, with 3-sec delays, no decoupling, and typically 50,000 scans. The samples of chloroform-soluble product were made up to 50% (wt/vol) in deuteriochloroform with carbon disulfide as an internal standard. The f_a was determined from integration of the peaks in the aliphatic and aromatic regions. It was shown that lengthening the delay period did not result in larger f_a .

Results and Discussion

Effect of the Coal Rank. In general, at lower temperature ($\leq 250^\circ\text{C}$) only low-rank coals are solubilized appreciably by alkali hydrolysis (5). This observation appears to be true for the ethylene glycol/KOH reaction on the higher-rank bituminous coals as shown in Table II. However, an important exception must be noted concerning the Wyoming lignite—a large portion of the product was insoluble. Although the H/C ratios of the benzene/methanol and pyridine extracts, 1.14 and 0.97, respectively, were greater than the lignite (0.87), the insoluble residue has a much lower H/C ratio of 0.64. The poor extraction yield may be attributable in part to the occurrence of a large number of polyphenols that tend to have a limited solubility. This would not be surprising since the lignite contains a large percentage of oxygen.

This solubilization procedure appears to work best for high volatile bituminous coals with an intermediate amount of oxygen, such as the

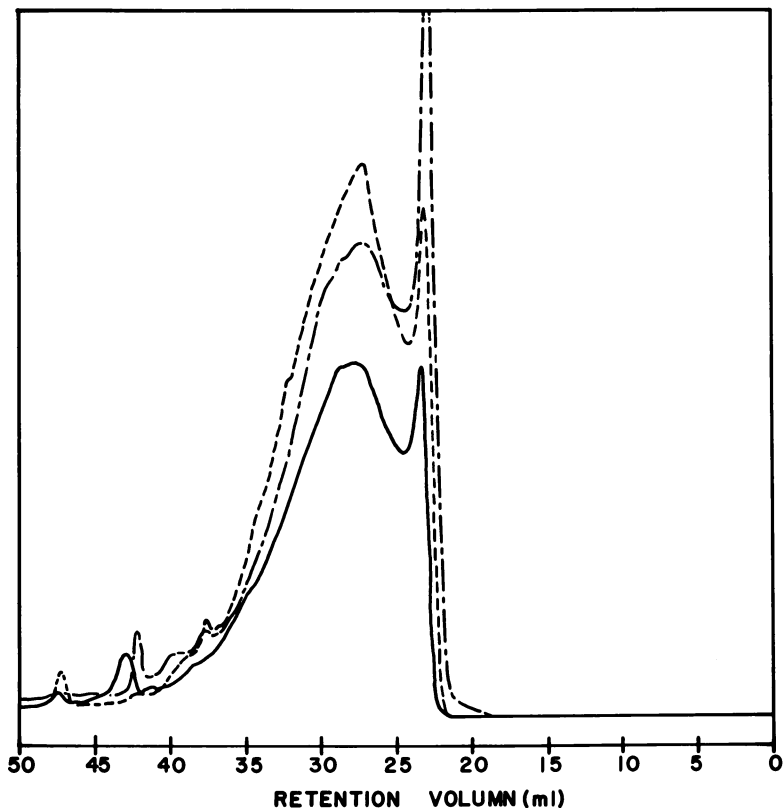


Figure 1. Gel permeation chromatograms of the THF-soluble products from the reaction of KOH and Illinois No. 2 bituminous coal in the following solvents: ethylene glycol (—), ethanol (— - —), and methanol (----), Reactions 2, 8, and 9, respectively

Illinois No. 2. One variable that was not examined in this study on the effects of rank is maceral distribution. Experiments are being planned on the reaction of different macerals to this treatment.

Figure 1 shows the gel permeation chromatograms for the hydrolytic product of two bituminous coals, an Illinois No. 6 and a Pittsburgh No. 8. Also included is a GPC for an SRC produced from the same Pittsburgh No. 8 coal (from the Wilsonville, Alabama pilot plant operated by Catalytic, Inc., *see Ref 14*). The hydrolytic reaction products give a higher molecular weight (size) distribution than the SRC, roughly 500 for the SRC and 800 for the main peak of the Pittsburgh No. 8 hydrolytic product. A higher molecular weight peak appears for both bituminous coals at 3200. Although the Illinois No. 6 has less carbon content and gave a higher yield of soluble products, its molecular weight distribution was larger than that of the Pittsburgh No. 8. The molecular weights

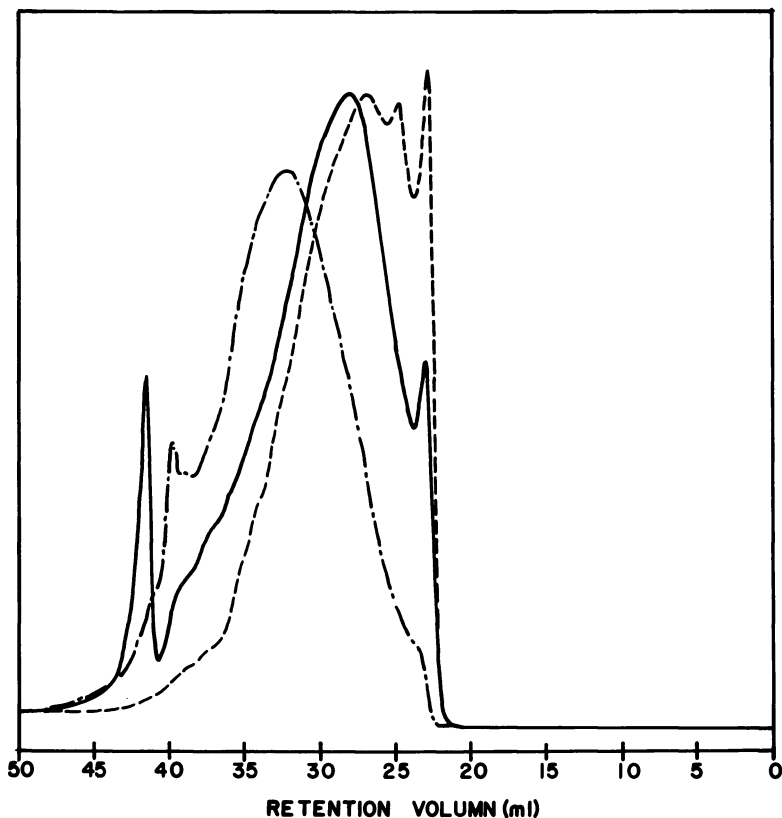


Figure 2. Gel permeation chromatograms of the THF-soluble products from the reaction of KOH in ethylene glycol on a Pittsburgh No. 8 bituminous coal (—), and an Illinois No. 6 bituminous coal (---), and of the THF-soluble portion of an SRC from the Pittsburgh No. 8 (— - —)

were determined from the calibration curve in Figure 3, but should be considered only as approximate weights. Because of the lack of coal molecule-type authentic standards of fairly high molecular weight in the 500 to 10,000 range, this type of data is best evaluated by comparison, as was done in Figure 1. The fact that the coal is not as extensively fragmented in the hydrolytic reaction compared to solvent refining is demonstrated in the comparison of the chromatograms.

Solvent Composition. In Table III the solubilities of Illinois No. 2 after treatment with KOH and various protic solvents are given. Note that both the glycols and ethanol gave similar yields of extraction products; both methanol and water result in large amounts of insoluble products. The superiority of alcohols compared to water for reduction and solubilization of coal also has been noted in acid $ZnCl_2$ melt reductions (15).

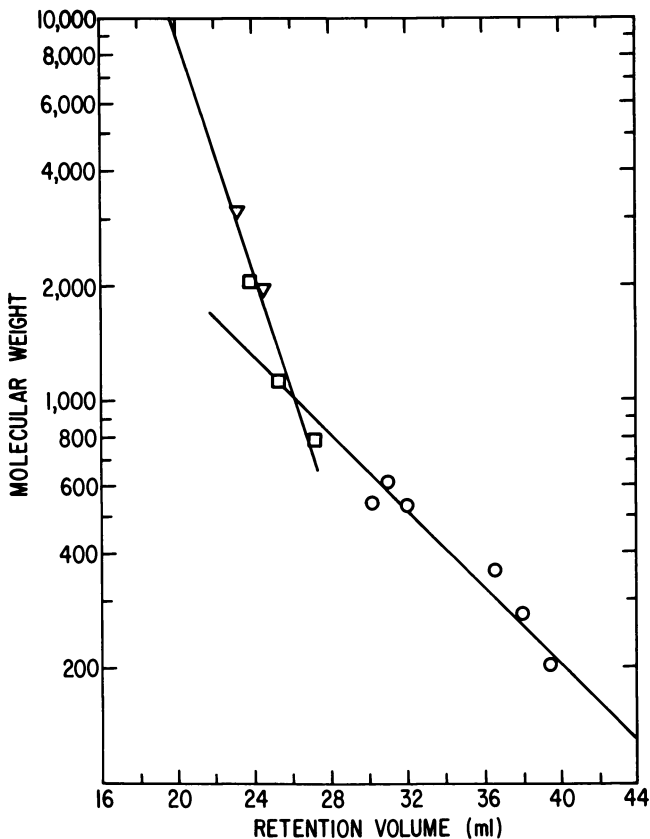


Figure 3. Calibration curves for GPC: (O) aromatics; (□) polyethylene standard; and (Δ) polystyrene standard

Prior treatment of the coal was important in determining final extraction yields. Drying the ground coal in a vacuum oven resulted in a lower solubility than if the coal were ground in reaction solvent and transferred directly as a slurry to the reactor. For the methanol reaction the insoluble fraction decreases from 54 to 42% when the coal is not dried. This is probably attributable to pore collapse during drying, a phenomenon that recently has been reported by Gorbaty (16).

A comparison of the molecular weight distribution for the KOH reactions with Illinois No. 2 in ethylene glycol, methanol, and ethanol is shown in Figure 2. The products from all three solvents show two peaks, one at 3200 and the broader one at 800. However, the distribution differs for all three, with the high molecular weight peak decreasing in relation to the other peak in the order ethanol, ethylene glycol, methanol. A tentative interpretation would be that the ethanol reaction required less splitting of the coal macromolecules to achieve

solubilization. This may be attributable to an increased attachment of the solvent or solvent-derived groups to the coal.

Aromatic Ring Reduction. In the initial experiments with triethylene glycol (TEG) it was noted that the H/C ratio of the product (1.08) was significantly higher than that of the coal (0.84). This would indicate that either reduction or solvent attachment or both were occurring. Also, the yield of solid product was greater than the amount of the original coal. The hexane extract, which was significant in this case (11.9%), was shown by solid-probe MS and GCMS to be mostly glycol degradation products. When ethylene glycol was used there was no increase in weight and the amount of hexane extractable material was reduced. Both Ouchi (5) and Ross (2) observed an H/C increase with the alcohols.

With the increase in H/C ratio one would expect a decrease in f_a . These f_a values were obtained for the chloroform-soluble fractions of the products by ^{13}C NMR and are listed in Table IV. From the ^{13}C NMR spectra (Figure 4) the f_a for product 1 was determined to be 0.50. This same coal has been shown by fluorination to have an f_a of approximately 0.69 (17). The attachment of ethylene glycol groups ($\text{ROCH}_2\text{CH}_2\text{-O-Coal}$) was determined to be 5.1% of carbons from the integration of the peaks in the 55–65-ppm region. We found these peaks to be absent in other coal products such as SRC. However, these data do not exclude the reaction of ethylene ($\text{CH}_2=\text{CH}_2$) with the coal as mentioned by Ouchi (5).

Contrary to what has been reported in the literature (9), we found that the product from the ethanol reaction had a reduced f_a of 0.54 compared to 0.69 for the whole coal. This value was obtained on 50% of the product, which is a significant proportion. These results would be uncertain only if the hydrolysis solubilized the fraction of the coal with a low aromatic content, which does not seem likely. The chloroform extract of the whole coal had an f_a very close to that for the whole coal itself. Since these trapped species are thought to be cleaved from the macromolecules, such a similarity is not surprising (4). This problem is

Table IV. Fraction of Aromatic Carbons (f_a) Determined by ^{13}C NMR

	f_a
Illinois No. 2	0.69 (17)
Hydrolytic product (Illinois No. 2)	0.50
Hydrolytic product (Illinois No. 2 TEG, PhCH_3)	0.63
Hydrolytic product (Illinois No. 2 EtOH)	0.54
SRC (Pittsburgh No. 8 feed coal)	0.82
SRC hydrolytic product	0.67
SRL (North Dakota lignite, M33C, F1)	0.82
SRL hydrolytic product	0.79
CHCl_3 extract of Illinois No. 2	0.66

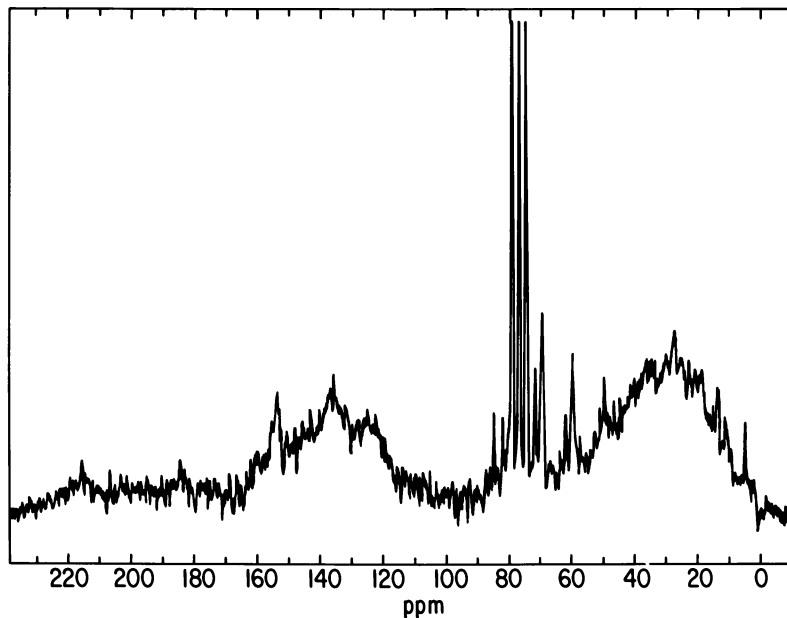
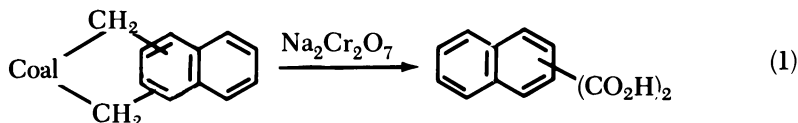


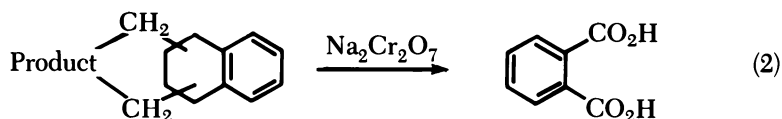
Figure 4. ^{13}C FTNMR spectra of Reaction 6 hydrolytic product in chloroform- d referenced to TMS

being examined further. Also, it was determined that the aromaticity of an SRC could be reduced upon treatment with glycol and KOH. It should be noted that there was not a significant weight increase in the product, which would have resulted from reaction of the solvent with the SRC. However, solvent-refined lignite (from North Dakota, Ref. 18) did not show a decrease in f_a . We cannot explain this, but it indicates one important point. SRC and SRL have been compared analytically and found to be very similar (18). The similarity does not hold for the glycol/KOH reduction, and this difference may hold for other reduction processes.

The best evidence for the occurrence of polycyclic aromatic ring reduction is the comparison of the aqueous $\text{Na}_2\text{Cr}_2\text{O}_7$ oxidation products of the hydrolytic product with those of the original coal. This procedure has been used in this laboratory to identify many of the important aromatic and heteroaromatic units in coals (4). It has been shown to be very selective for these molecules. Equation 1 is an example of the pathway by which polycyclic aromatics are isolated from the raw coal.

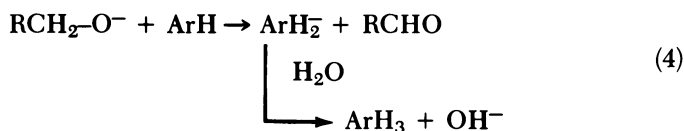
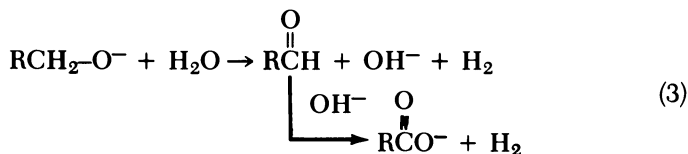


The gas chromatogram for the volatile methyl esters from the original coal oxidation is shown in Figure 5 with identification in Table V. As we have shown before, a significant amount of polycyclic aromatics such as phenanthrene and naphthalene carboxylic acids and heteroaromatics, including dibenzofuran and xanthone carboxylic acids, were isolated (4). Figure 6 is the gas chromatogram for the oxidation products from the hydrolytic product with peak identification in Table V. The major products are benzene, methoxybenzene, and methylbenzene carboxylic acids. The acids from the coal and hydrolytic product are compared in Table VI. It is obvious that the polycyclic aromatics and heteroaromatics have been reduced to hydroaromatics. The degradation of hydroaromatics by dichromate oxidation is shown in Equation 2.



As expected, the furan ring in dibenzofuran was destroyed. Since aqueous alkali treatment has been used as a method for removing sulfur from coal (19), it is not surprising that in Reaction 6 the total sulfur was reduced from 2.4% (1.2% organic) to 0.72%. Most of the loss was attributable to the removal of inorganic sulfur, but a significant amount of organic sulfur including dibenzothiophene was removed. The yield of phenanthrene carboxylic acids and anthracene (isolated as anthraquinone) carboxylic acids has been reduced to a nondetectable level. We and Ross (3) have observed independently that anthracenes are reduced with alcoholic alkali.

Pathway for Reduction. The alkaline oxidation of alcohols and glycols is thought to involve hydride transfer with the intermediate formation of the corresponding aldehydes (12, 20) (Equation 3) where Ar equals naphthalene, phenanthrene, etc.



Therefore, a possible pathway for reduction is by a hydride transfer to an activated aromatic ring (Equation 4). Hydrogenation with H_2 can

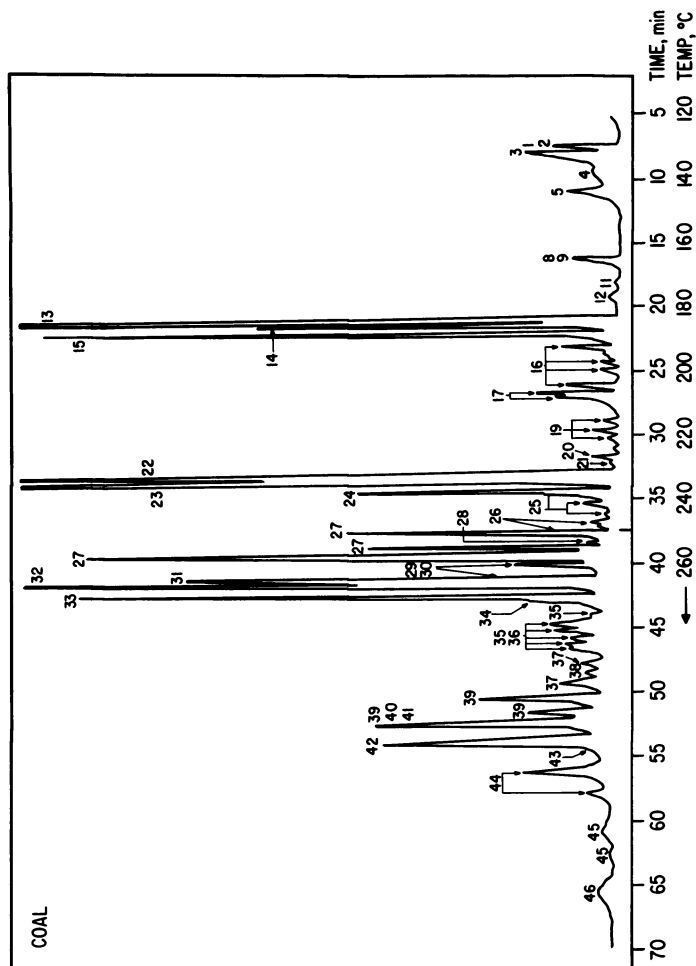


Figure 5. Gas chromatogram of methyl esters from the aqueous $\text{Na}_2\text{Cr}_2\text{O}_7$ oxidation of Illinois No. 2 bituminous coal (separated on an OV-17 support coated open tubular column (SCOT), temperature programmed at $100^\circ\text{--}250^\circ\text{C}$ at $4^\circ/\text{min}$)

**Table V. Methyl Esters of the Oxidation Products from Coal (Figure 5)
and the Hydrolytic Product (Figure 6)**

<i>Peak No.</i>	<i>Compound</i>
1	Methyl succinate
2	Methyl methylsuccinate
3	Methyl benzoate
4	Methyl methylfurancarboxylate
5	Methyl methylbenzoate
9	Methyl methoxybenzoate (+ d_3 -methoxy)
11	Methyl methoxymethylbenzoate
12	Methyl furandicarboxylate
13	Methyl 1,2-benzenedicarboxylate
14	Methyl 1,4-benzenedicarboxylate
15	Methyl 1,3-benzenedicarboxylate
16	Methyl methylbenzenedicarboxylate
17	Methyl naphthalenecarboxylate
18	Methyl pyridinedicarboxylate
19	Methyl methoxybenzenedicarboxylate (+ d_3 -methoxy)
20	Methyl dimethylfurandicarboxylate
21	Methyl biphenylcarboxylate
22	Methyl 1,2,4-benzenetricarboxylate
23	Methyl 1,2,3-benzenetricarboxylate
24	Methyl 1,3,5-benzenetricarboxylate
25	Methyl methylbenzenetricarboxylate
26	Methyl dibenzofurancarboxylate
27	Methyl naphthalenedicarboxylate
28	Methyl pyridinetricarboxylate
29	Methyl methoxybenzenetricarboxylate (+ d_3 -methoxy)
30	Methyl fluorenonecarboxylate
31	Methyl 1,2,4,5-benzenetetracarboxylate
32	Methyl 1,2,3,4-benzenetetracarboxylate
33	Methyl 1,2,3,5-benzenetetracarboxylate
34	Methyl methylbenzenetetracarboxylate
35	Methyl phenanthrenecarboxylate
36	Methyl dibenzothiophenecarboxylate
37	Methyl xanthonecarboxylate
38	Methyl anthraquinonecarboxylate
39	Methyl naphthalenetricarboxylate
40	Methyl methylxanthonecarboxylate
41	Methyl dibenzofurandicarboxylate
42	Methyl benzenepentacarboxylate
43	Methyl benzoquinolinecarboxylate
44	Methyl phenathrenedicarboxylate
45	Methyl carbazolecarboxylate
46	Methyl xanthonecarboxylate

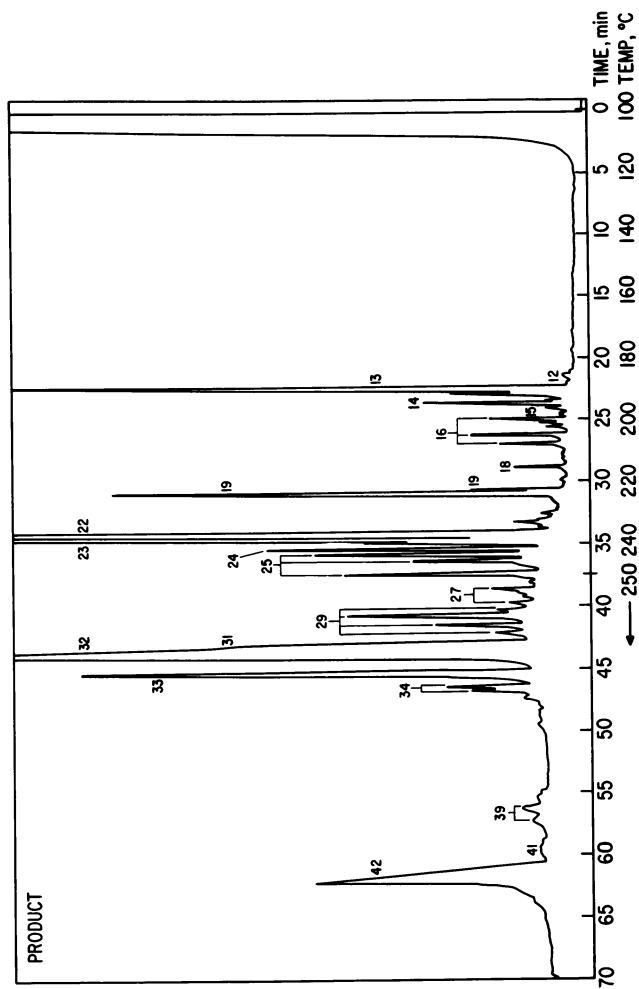


Figure 6. Gas chromatogram of methyl esters from the oxidation of the hydrolytic product from Reaction 6 (same conditions as Figure 5)

Table VI. Relative Mole Abundances Normalized to 100^a

<i>Carboxylic Acids</i>	<i>Illinois No. 2 Bituminous Coal</i>	<i>Hydrolytic Product from Reaction 6 (Table III)</i>
Benzene	100	100
Hydroxybenzene	1.4	10
Methylbenzene	2.3	7
Naphthalene	7.2	1
Phenanthrene	1.1	—
Dibenzofuran	1.5	0.4
Xanthone	1.3	—
Dibenzothiophene	0.5	—
Other heteroaromatics	2.8	<1

^a —not detected.

be ruled out for two reasons. First, there are no active catalysts available. This is especially true for the SRC where the mineral matter has been removed by the process. Secondly, the triethylene glycol reactions were conducted in an open system so that the H₂ could escape, yet the decrease in aromatic carbon was observed. It should be noted that Ross and Blessing observed that adding H₂ did not increase significantly the yield of extractables in the reaction of isopropyl alcohol/isopropyl alkoxide with coal (2).

Ether Linkage Cleavage. While many groups have speculated that the breaking of ether linkages is important in the initial stages of liquefaction (21), others have stated that there are no open-ether linkages in low-rank bituminous coals (22, 23, 24). However, there is evidence that aryl ethers are cleaved, a reaction that is known to occur under hydrolytic conditions (25). This is demonstrated by a seven-fold increase in yield of hydroxybenzene carboxylic acids in the aqueous Na₂Cr₂O₇ oxidation products of the treated coal compared to the oxidation products from raw coal (see Table VI). These additional hydroxylated aryl compounds could only result from the cleaving of aryl ethers.

An experiment was performed that at least partially distinguishes between the two possible mechanisms for solubilization, ether cleavage or aromatic ring reduction. The Illinois No. 2 coal was treated with a 1/1 mole ratio of glycol to KOH in an inert solvent, toluene (Reaction 7). Under these conditions the KOH was soluble because of the chelation of the potassium cation by the glycol yielding a strongly basic system. In this medium ether linkages could be split effectively while the amount of glycol solvent available for reduction was decreased. In this experiment the f_a of the product was reduced only to 0.63, compared to 0.69 for the raw coal and 0.50 for the reaction in a glycol solvent. However, the solubility was very similar to the solubility of the material produced in

pure glycol (*see* Table III). We feel that this is good evidence for ether cleavage playing an important role in the solubilization of bituminous coals.

Conclusions

From the characterization of the hydrolytically solubilized coal, the following observations can be made: (1) the polycyclic aromatic rings are being reduced, and a possible mechanism is hydride transfer from the solvent; (2) oxygen heteroaromatics are destroyed; (3) aryl ethers are being cleaved by this process; (4) the ability of the glycols to chelate the positive alkali metal ions could contribute to the enhanced yields of soluble coal compared to other protic solvents.

This study demonstrated the utility of using a broad analytical and chemical approach to study nonvolatile coal products.

Acknowledgments

This work was supported by the Department of Energy-Fossil Energy, Division of Coal Conversion-Liquefaction. Chemical and instrumental techniques used were developed with support from the Office of Basic Energy Sciences, U.S. Department of Energy.

Literature Cited

1. Pew, J. C.; Withrow, J. R. *Fuel* 1931, 10, 44.
2. Ross, D. S.; Blessing, J. E. *Fuel* 1979, 58, 433.
3. Ross, D. S.; Blessing, J. E. *Fuel* 1979, 58, 438.
4. Hayatsu, R.; Winans, R. E.; Scott, R. G.; Moore, L. P.; Studier, M. H. *Fuel* 1978, 57, 541.
5. Makabe, M.; Hirano, Y.; Ouchi, K. *Fuel* 1978, 57, 289.
6. Makabe, M.; Fuse, S.; Ouchi, K. *Fuel* 1978, 57, 801.
7. Makabe, M.; Ouchi, K. *Fuel Process. Technol.* 1979, 2, 131.
8. Makabe, M.; Ouchi, K. *Fuel* 1979, 58, 43.
9. Ouchi, K.; Iwata, K.; Makabe, M.; Itoh, H. *Am. Chem. Soc., Div. Fuel Chem., Prepr.* (Honolulu, April 1979) 24(1), 185.
10. Augustine, R. L. Ed. "Reduction"; Marcel Dekker: New York, 1968; p. 184.
11. Patai, S., Ed. "The Chemistry of the Ether Linkage"; Interscience: New York, 1967; p. 47.
12. Bently, K. W.; Kirby, G. W., Eds. "Elucidation of Organic Structures by Physical and Chemical Methods"; Wiley-Interscience: New York, 1973; Vol. 4, p. 325.
13. Karr, C., Jr., Ed. "Analytical Methods for Coal and Coal Products"; Academic: New York, 1978; Vol. 2, Chap. 21.
14. Hayatsu, R.; Winans, R. E.; Scott, R. G.; Moore, L. P.; Studier, M. H. In "Organic Chemistry of Coal," *ACS Symp. Ser.* 1978, 71, 108.
15. Shinn, J. H.; Vermeulen, T. *Am. Chem. Soc., Div. Fuel Chem., Prepr.* (Honolulu, Apr., 1979) 24(2), 80.
16. Gorbaty, M. L. *Fuel* 1978, 57, 796.
17. Huston, J. L.; Scott, R. G.; Studier, M. H. *Fuel* 1976, 55, 281.

18. Baltisberger, R. J.; Klabunde, K. L.; Sternberg, V. I.; Woolsey, N. F.; Saito, K.; Sukalski, W. In "Organic Chemistry of Coal", *ACS Symp. Ser.* **1978**, *71*, 294.
19. "Liquefaction and Chemical Refining of Coal," in Battelle Energy Program Report, Battelle Columbus, Columbus, OH, 1974.
20. Dytham, R. A.; Weedon, B. C. L. *Tetrahedron* **1960**, *9*, 246.
21. Szladow, A. J.; Given, P. H. *Am. Chem. Soc., Div. Fuel Chem., Prepr.* (Miami Beach, Sept., 1978) **23**, 161.
22. Wachowska, H.; Pawlak, W. *Fuel* **1977** *56*, 422.
23. Ignasiak, B. S.; Gawlak, M. *Fuel* **1977** *56*, 216.
24. Ignasiak, B.; Carson, C.; Szladow, A. J.; Berkowitz, N. *Am. Chem. Soc., Fuel Chem. Div. Prepr.* (Honolulu, Apr., 1979) **24**, 40.
25. Sharma, J. N.; Wilson, M. J. G. *Fuel* **1961**, *40*, 331.

RECEIVED July 19, 1979.

The Chemistry of Acid-Catalyzed Coal Depolymerization

LASZLO A. HEREDY

Rockwell International, Energy Systems Group,
8900 De Soto Avenue, Canoga Park, CA 91304

Product yields obtained in coal depolymerization experiments are correlated with coal rank and with the product yields obtained from the depolymerization of model compounds containing the same type of bonds that may be present in coal. It is concluded that in low-rank coals (C < 83%), where high depolymerization yields are obtained, the breaking of aliphatic carbon bridges is the primary means of depolymerization. In lignites, the majority of these bridges probably are linked to phenolic rings. In high-volatile bituminous coals, some of the aliphatic bridges may be linked to condensed aromatic structures. It is postulated that in medium to high-rank bituminous coals (C > 83%), where lower depolymerization product yields are obtained, the aliphatic bridges incorporate tetralin-like hydroaromatic structures. The presence of such bridges reduces the effectiveness of the catalyst because several bonds connecting two aromatic groups must be broken to effect depolymerization.

Since its introduction in the early 1960's, acid-catalyzed depolymerization has become a widely used method to convert coal into soluble derivatives for structural investigations. It was first shown by Heredy and Neuworth (1) that coal could be depolymerized by reacting it with phenol-BF₃ complex at temperatures as low as 100°C. The method was based on the assumption that coal contains aromatic structures linked by aliphatic bridges, such as methylene bridges, which are sufficiently reactive to participate in an acid-catalyzed transaryl-alkylation reaction. This general type of structure was proposed by Neuworth and used by Depp, Stevens, and Neuworth (2) to interpret the chemistry of low-temperature

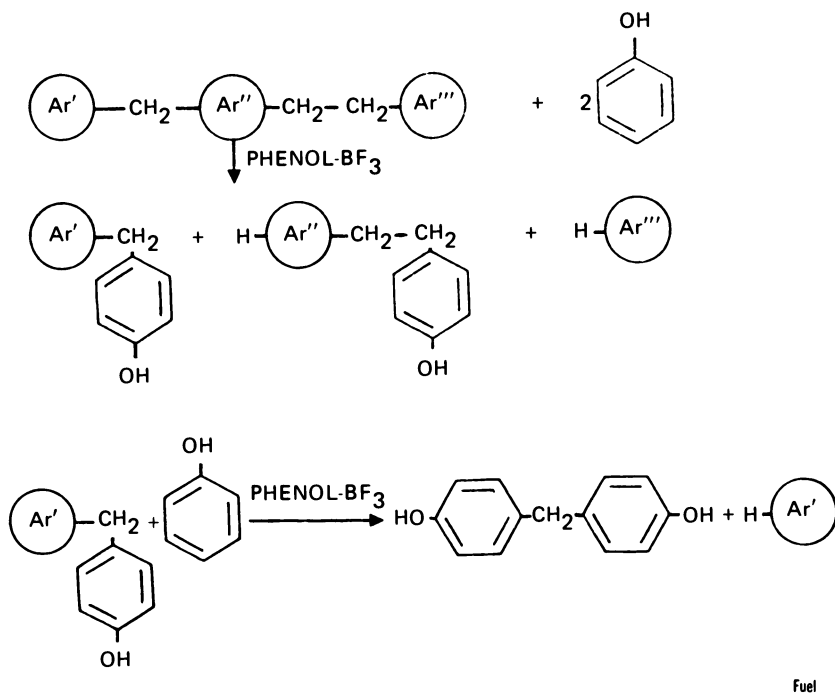


Figure 1. Coal depolymerization via transaralkylation with phenol- BF_3 (1)

pyrolysis of coal. The overall reaction of this proposed structure with phenol- BF_3 is illustrated in Figure 1. One of the final products of the depolymerization is dihydroxydiphenylmethane.

The depolymerization reaction was modified by Ouchi, Imuta, and Yamashita (3), who substituted *p*-toluenesulfonic acid (PTSA) for BF_3 as the catalyst and increased the reaction temperature to 180° to 185°C. A very high degree of depolymerization was achieved under these conditions, with pyridine-soluble product yields over 90%. Darlage and Bailey (4) investigated the effects of reaction temperature, various solvents, and coal preoxidation on depolymerization product yields using a number of acid catalysts. They found that meta-substituted phenols were more effective aromatic substrates for the depolymerization reaction than phenol. The preoxidation of coal, particularly of some sulfur-rich bituminous coals, with dilute aqueous nitric acid considerably increased the yield of depolymerization products (5).

Important information relating to the chemical structure of different coals has been obtained by several investigators by means of the acid-catalyzed depolymerization method. Small quantities of pure compounds, such as methoxyl phenyl derivatives of benzofuran and xanthene as well as unresolved mixtures of derivatives of benzene, naphthalene, diphe-

nylmethane, and phenanthrene, were isolated from the depolymerized products of a brown coal (6). The high-resolution proton and ^{13}C NMR spectra of a number of depolymerized coal products were recorded, and proton and carbon distributions in different structural positions were determined and evaluated (7, 8, 9). The number-average molecular weights of coal depolymerization products obtained under different conditions were compiled and evaluated (10).

The application of acid-catalyzed depolymerization was extended recently to the structural investigation of petroleum asphaltene by Gould (11). Three asphaltene were subjected to depolymerization conditions using phenol and *p*-toluenesulfonic acid, and the products were examined by a variety of analytical methods. The treatment resulted in reduced average molecular weights. The results are consistent with the presence in petroleum asphaltene of condensed-ring, largely aromatic systems linked by aliphatic bridges.

A review of the acid-catalyzed coal depolymerization method has been published by Larsen and Kuemmerle (10). The objective of this chapter is to discuss some specific aspects of the chemistry of coal depolymerization.

The Relative Reactivities of Various Bridge Structures Toward Phenol-BF₃

Although no systematic studies have yet been reported regarding the relative reactivities of aliphatic bridge structures or, more generally, aliphatic-aromatic carbon-carbon bonds (which may be present in various coals), toward phenol-BF₃, some important trends have been established in model compound experiments (1, 12). The results of these experiments are summarized in Tables I and II and in Figure 2.

Table I. BF₃-Catalyzed Isopropyl Group Transfer to Phenol (1- ^{14}C) (12)

Starting Compound ^a	Conversion (%)	Product Distribution (wt %)		
		<i>p</i> -Isopropylphenol (1- ^{14}C)	<i>o</i> -Isopropylphenol (1- ^{14}C)	Residue
Cumene	8.0 ^b	3.5	0.8	3.7
<i>o</i> -Isopropylphenol	100.0	74.5	14.5	11.0
Retene (1-methyl-7-isopropyl-phenanthrene)	100.0 ^c	61.5	10.2	28.3

^aStarting compound to labeled phenol molar ratio: 1 to 20. Reactions performed at 100°C for 4 hr. Mixture saturated with BF₃.

^bBenzene, in an amount equivalent to the isopropylphenols, was also recovered.

^cA methylphenanthrene fraction, in an amount equivalent to isopropylphenols, was also recovered.

Table II. BF_3 -Catalyzed Reaction of *p-n*-Propylphenol with Phenol ($1\text{-}^{14}\text{C}$) (12)

<i>Reaction Conditions</i>	Ratio of <i>p-n</i> -propylphenol to phenol ($1\text{-}^{14}\text{C}$): 1 to 20 Mixture saturated with BF_3 at reaction temperature Temperature: 100°C Reaction period: 4 hr	
<i>Product Distribution (wt %)</i>	<i>p-n</i> -Propylphenol (unreacted)	18.0
	<i>p-n</i> -Propylphenol ($1\text{-}^{14}\text{C}$)	43.0
	<i>o-n</i> -Propylphenol ($1\text{-}^{14}\text{C}$)	14.5
	<i>p</i> -Isopropylphenol ($1\text{-}^{14}\text{C}$)	5.3
	<i>o</i> -Isopropylphenol ($1\text{-}^{14}\text{C}$)	1.2
	Residue	<u>18.0</u>
	Total	100.0

The data on isopropyl group transfer in Table I show that the secondary aliphatic–aromatic carbon–carbon bond is very reactive when the aliphatic group is linked to either a phenolic ring or a phenanthrene ring. The reaction is very slow when the isopropyl group is linked to a nonactivated benzene ring. The relative reactivities of the secondary carbon bond in the first two structures could not be evaluated because the isopropyl group transfer went to completion in the case of *o*-iso-

MODEL COMPOUND	REACTING BOND	RELATIVE REACTIVITY (% REACTED)
A	a'	77
A	b'	2
B	a	70
B	b	41

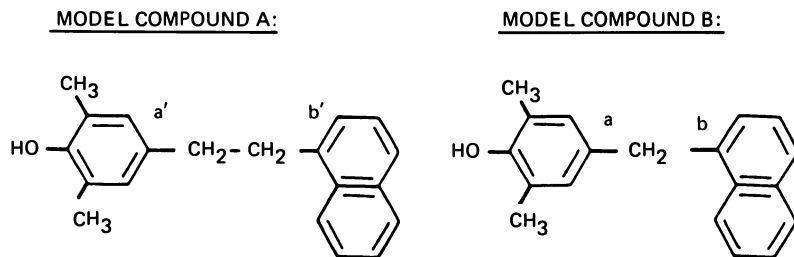


Figure 2. Relative reactivities of model compounds with phenol- BF_3 (1) (reaction conditions: ratio of model compounds to phenol: 1 to 10; mixture saturated with BF_3 at reaction temperature; temperature: 100°C ; reaction period: 4 hr)

propylphenol and that of retene. The data on *n*-propyl group transfer in Table II show, as expected, that a bond between a primary aliphatic carbon and an aromatic carbon is less reactive than a secondary aliphatic-carbon, aromatic-carbon bond under otherwise similar conditions.

Figure 2 shows the comparison of the relative reactivities of four aromatic-aliphatic carbon-carbon linkages. This figure summarizes the results of two experiments in which model compounds A and B, shown in Figure 2, were treated with excess phenol and BF_3 at 100°C for 4 h. A comparison of the reactivities of linkages *a'* and *b'*, both of which involve primary aliphatic carbon atoms, clearly shows enhanced reactivity at bond *a'* attributable to the activating effect of the phenolic hydroxyl group. A comparison of the reactivity of linkage *a'* with that of the corresponding bond in *n*-propylphenol (Table II) indicates that the reactivities of ($-\text{CH}_2-\text{CH}_2-$)-substituted aromatics are similar whether the substitution is in a bridge or in a chain structure. The relative reactivities found with model compound B indicate the $-\text{CH}_2-$ bridges can play a special role in coal depolymerization because in this case bonds on both sides of the bridge structure are activated (compare the reactivities of bonds *b* and *b'*, respectively).

It is probable that cleavage of aliphatic ether bonds contributes to coal depolymerization, particularly in the case of lignites and subbituminous coals. Although the activity of various ethers with phenol- BF_3 has not been investigated, several studies on the BF_3 -catalyzed cleavage of various aliphatic ether linkages have been reported (13, 14). It was shown that the reaction of ethers with benzene gives alkylbenzenes. The relative ease of reaction varied considerably with different ethers. Diisopropyl ether and dibenzyl ether reacted vigorously with benzene upon saturation with BF_3 ; isopropyl, phenyl, and benzyl ethyl ethers reacted violently. On the other hand, ethyl, isoamyl, and *n*-amyl ethers reacted only at higher temperatures and elevated pressures (150°C and 10–20 atm).

Investigation of the Kinetics of BF_3 -Catalyzed Benzyl Group Transfer

Kinetic investigations of BF_3 -catalyzed benzyl group transfer in benzylphenol systems were reported by Heredy (15). These systems were chosen for investigation because of the particular interest in the role that $-\text{CH}_2-$ bridges may play in coal depolymerization.

One of the investigations was made with *p*-benzylphenol. Experiments were made first with the *p*-benzylphenol/phenol($1-^{14}\text{C}$)/ BF_3 system to study the rate of benzyl group transfer from benzylphenol to phenol ($1-^{14}\text{C}$). However, it was found that the rate of benzyl group transfer was much faster to *p*-benzylphenol than to phenol ($1-^{14}\text{C}$); therefore, no meaningful kinetic measurements could be made on the latter system. In another experiment, the kinetics of benzyl group transfer was studied in the *p*-benzylphenol/ BF_3 system. The kinetic measurements were made

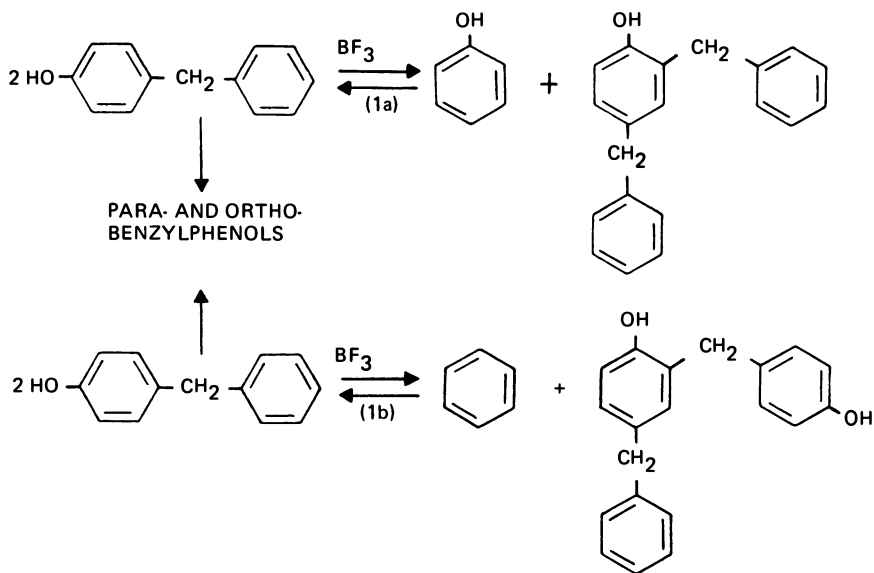


Figure 3. BF_3 -catalyzed benzyl group transfer in benzylphenols (15)

in sealed glass tubes at 100°C using a *p*-benzylphenol/ BF_3 mole ratio of 6.25/1.0. The two principal reactions that take place in this system are shown in Figure 3. In agreement with the reaction scheme shown in Figure 3, the rate of disappearance of the sum of *p*- and *o*-benzylphenols followed a second-order rate equation. The ratio of the initial reaction rates of Reaction 1a to reaction 1b was approximately 4.0. In addition to phenol and benzene, significant amounts of diphenylmethane and some *p*-cresol were formed during the latter part of the reaction. Also, isomerization to *o*-benzylphenol took place as a result of the reverse reactions of 1a and 1b.

A more detailed kinetic study of benzyl group transfer was made using the 4-benzyl-2,6-dimethylphenol/ BF_3 system. This system was selected for investigation for the following reasons:

1. In the benzylphenol/ BF_3 system, two parallel major reactions have taken place, giving dibenzylphenol and phenol in one reaction and hydroxybenzylphenols and benzene in the other. It was expected that the additional activating effect of the two methyl groups on the phenolic ring would sufficiently enhance the reactivity of the methylene-aromatic carbon-carbon bond on the side of the phenolic ring to make the cleavage of that bond the predominant reaction.

Table III. Chemical Shift Values of Methylene and Methyl Protons of Benzyl Derivatives of 2,6-Dimethylphenol (15)

Compound	Chemical Shift (ppm) ^a			
	Methylene		Methyl	
	(3)	(4)	(2)	(6)
2,6-Dimethylphenol	—	—	2.08	2.08
4-Benzyl-2,6-dimethylphenol	—	3.70	2.03	2.03
3,4-Dibenzyl-2,6-dimethylphenol	3.80	3.70	1.95	2.10

^aTetramethylsilane = 0.00 ppm.

2. The chemical shifts of the $-\text{CH}_2-$ protons, of the 2-methyl protons of the starting material, and of the main products were sufficiently different to permit the quantitative analysis of the reaction mixture by proton NMR spectrometry.

The proton chemical shifts of the benzyl $-\text{CH}_2-$ groups, the methyl groups in the starting material, and in the products are shown in Table III. The reaction that was studied is shown in Figure 4.

The kinetic measurements were made in CS_2 solution at 70°C in sealed NMR sample tubes. After completion of the prescribed reaction period, each sample tube was cooled quickly to room temperature and transferred to the NMR spectrometer for recording of the spectra. When a solution of 4-benzyl-2,6-dimethylphenol and BF_3 (mole ratio 4.5/1.0) was used, the absorption under the methylene peak (3) at 3.80 ppm and the methylene peak (2) at 1.95 ppm increased from an initial value of zero, as the reaction advanced, showing the formation of 3,4-dibenzyl-

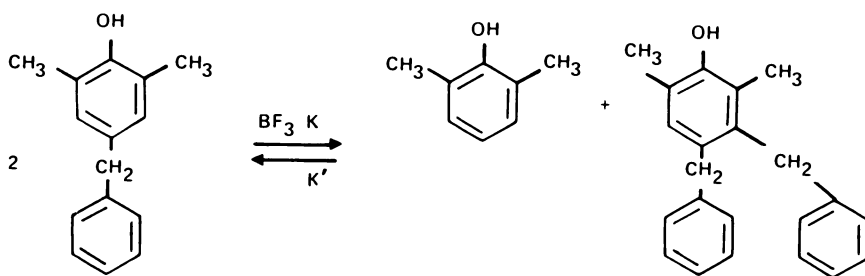


Figure 4. BF_3 -catalyzed benzyl group transfer in 2,6-dimethyl benzylphenols (15)

2,6-dimethylphenol. Independent gas chromatographic analysis showed the formation of an equivalent amount of 2,6-dimethylphenol. Reaction rate constants were determined for both the forward (k) and the reverse (k') reactions for three different BF_3 concentrations. The following correlations were determined:

$$\text{Rate (forward reaction)} = k[\text{BF}_3] [(\text{CH}_3)_2(\text{HO})\text{C}_6\text{H}_2\text{-CH}_2\text{-C}_6\text{H}_5]^2$$

$$\text{Rate (reverse reaction)} = k'[\text{BF}_3] \frac{[(\text{CH}_3)_2(\text{HO})\text{C}_6\text{H}(\text{CH}_2\text{-C}_6\text{H}_5)_2]}{[(\text{CH}_3)_2(\text{HO})\text{C}_6\text{H}_3]}$$

At 70°C and at a concentration of $\text{BF}_3 = 1.0 \text{ mol/L}$, $k = 2.6 \pm 0.3 \times 10^{-4} \text{ min}^{-1} \text{ L mol}^{-1}$ and $k' = 16.0 \pm 1.8 \times 10^{-4} \text{ min}^{-1} \text{ L mol}^{-1}$. The benzyl group transfer in this system is clearly a bimolecular substitution reaction with respect to the phenolic participants where the rate-determining step involves a reaction between a protonated benzyl phenol (benzenium ion) and a phenolic compound or its BF_3 complex. There is no indication of the formation of benzyl cation in this particular system. It should be noted here that the data obtained on the transfer of n -propyl groups (Table II) similarly indicate that the main reaction in that transfer does not involve the formation of the 1-propenium cation. If that were the case, isomerization to the 2-propenium cation would take place with the predominant formation of isopropylphenols. On the other hand, Franz et al. (16) reported the formation of diarylmethenium cations from triarylmethanes under similar conditions, indicating that the attachment of an additional aromatic ring to the benzylic carbon stabilizes the disubstituted methenium cation.

It is worthwhile to review at this point the results of kinetic investigations made with the Friedel-Crafts benzylation of aromatic hydrocarbons because of the close relationship of this reaction with the BF_3 -catalyzed benzyl group transfer. The kinetics of the AlCl_3 -catalyzed benzylation of substituted benzene derivatives with benzyl halides was investigated by Brown and Grayson (17) and by Olah et al. (18, 19, 20). Both groups found that the reaction was first order in the benzyl halide, the benzene derivative, and the aluminum chloride, while the whole reaction followed a third-order rate equation. A similar rate equation was found by Olah et al. (21, 22) for the TiCl_4 -catalyzed benzylation of benzene and toluene. It can be concluded that the BF_3 -catalyzed benzyl group transfer and the Friedel-Crafts benzylation reactions follow the same type of general rate equations.

Comments on the Chemistry of Coal Depolymerization

After reviewing the information on the reactivities of various bridge structures that may be present in coal, it is instructive to summarize

available data on coal depolymerization yields as a function of coal rank. The product yields obtained by depolymerization can then be correlated with important structural features of coals over the coalification range that has been investigated.

Depolymerization yields determined with phenol-BF₃ at 100°C are summarized in Table IV (7), and the yields obtained with phenol-PTSA depolymerization at 185°C are shown in Figure 5 (3). In the case of the phenol-BF₃ catalyst, the phenol-soluble product yield was the highest (75%) for the lignite. It gradually decreased to about 10% for the low-volatile bituminous coal, although the low product yield obtained with subbituminous coal does not fit this correlation. In the case of depolymerization with phenol-PTSA, the pyridine-soluble product yield was over 90% for coals of 70–83% carbon content; for coals with higher carbon content, the yield dropped sharply, reaching about 10% for a coal with 93% carbon. Benzene-ethanol was a more selective solvent than pyridine for fractionating the depolymerization products obtained with PTSA catalyst: a linear relationship between the yield of the soluble extract and the carbon content of the starting coal was observed. For comparison, Figure 5 also shows the depolymerization product yields obtained with phenol-BF₃ at 100°C. It is remarkable that, with the exception of one data point (for the subbituminous coal), the yields of phenol-soluble extract obtained with phenol-BF₃ are very similar to the yields of benzene-ethanol-soluble extract obtained with phenol-PTSA.

The following comments are made with regard to a correlation of the depolymerization product yields with the relative reactivities of aliphatic-aromatic carbon and oxygen-carbon bridge structures in coal:

1. In low-rank coals, particularly in lignites, many of the aliphatic bridges, which participate in depolymerization, may be linked to noncondensed phenolic rings. The reactivity of an aliphatic structure linked to a phenolic ring is suf-

Table IV. Depolymerization of Coals of Different Ranks with Phenol-BF₃ at 100°C (7)

<i>Coal Type</i>	<i>C (% dmmf)</i>	<i>Total Soluble^a Yield (%)</i>	<i>Combined Phenol Content of Soluble Fraction (%)</i>
Lignite	70.6	75.2	41.2
SubB	76.7	23.4	32.8
hvab	82.4	47.4	16.3
hvab	85.1	28.8	12.4
hvab	85.8	25.0	13.0
lvb	90.7	9.8	15.5

^aCoal-derived part of phenol-soluble material.

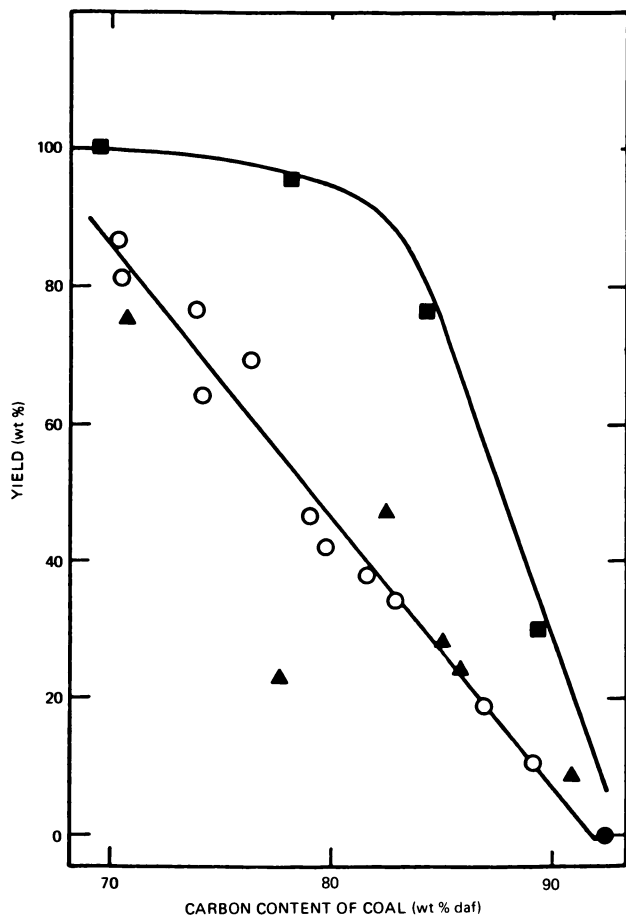


Figure 5. Extract yields from depolymerized coals (3) (PTSA: (■) depolymerized coals, pyridine extracts; (○) depolymerized coals, benzene-ethanol extracts; BF_3 : (△) depolymerized coals, phenol extracts)

ficient to allow for the participation in the depolymerization reaction. On the other hand, spectrometric studies indicate (23) that these coals do not contain significant amounts of sufficiently reactive condensed aromatic structures that could participate in depolymerization. In addition, the cleavage of aliphatic ether or benzyl ether bonds may contribute to the depolymerization. The BF_3 -catalyzed reaction of oxygen-bearing functional groups (including $-\text{COOH}$ groups) with phenol is evidenced by the relatively great chemically combined phenol content in the depolymerized products obtained from these coals (Table IV).

2. In high-volatile bituminous coals ($C = 80\text{--}83\%$), the breaking of aliphatic carbon bridges is seen as the major means of depolymerization. Many of these bridges may be linked to phenolic rings, others to condensed aromatic rings such as phenanthrene.
3. In higher-rank bituminous coals ($C > 83\%$), the depolymerization product yield decreases sharply with increasing rank. It is probable that this decrease is related mainly to the nature of the aliphatic bridge structures. While in lower-rank coals a sufficient number of the bridge structures are short aliphatic chains ($N_c = 1\text{--}4$), it is postulated that in higher-rank coals many bridge structures involve tetralin-like hydroaromatic rings. With structures of this type, several bonds must be broken between two aromatic groups to effect depolymerization. Also, nearly all the ether oxygen in higher-rank bituminous coals is in aromatic ethers, which do not react with BF_3 .
4. Among the aliphatic bridge structures, $-\text{CH}_2-$ bridges may play a particularly important role in coal depolymerization. Even if the number of such bridges is relatively small, the probability of their cleavage is high because, in general, carbon-carbon bonds on both sides of the bridge are activated under the reaction conditions used in coal depolymerization. This view is supported by experimental data obtained in depolymerization studies made with phenol- BF_3 , where the yield of soluble depolymerized products was proportional to the amount of $-\text{CH}_2-$ bridge structures found in the soluble products (7).

Literature Cited

1. Heredy, L. A.; Neuworth, M. B. *Fuel* **1962**, *41*, 221.
2. Depp, E. A.; Stevens, C. M.; Neuworth, M. B. *Fuel* **1956**, *35*, 437.
3. Ouchi, K.; Imuta, K.; Yamashita, Y. *Fuel* **1965**, *44*, 29.
4. Darlage, L. J.; Bailey, M. E. *Fuel* **1976**, *55*, 205.
5. Darlage, L. J.; Weidner, J. P.; Block, S. S. *Fuel* **1974**, *53*, 54.
6. Ouchi, K.; Brooks, J. D. *Fuel* **1967**, *46*, 367.
7. Heredy, L. A.; Kostyo, A. E.; Neuworth, M. B. *Fuel* **1965**, *44*, 125.

8. Heredy, L. A.; Kostyo, A. E.; Neuworth, M. B. In "Coal Science," *Adv. Chem Ser.* **1966**, *55*, 493.
9. Franz, J. A.; Tingey, G. L.; Campbell, J. A.; Morrey, J. R.; Grant, D. M.; Pugmire, R. J. *Amer. Chem. Soc., Fuel Div. Prepr.* (Chicago, August, 1975) **20**(3), 12.
10. Larsen, J. W.; Kuemmerle, E. W. *Fuel* **1976**, *55*, 162.
11. Gould, K. A. *Fuel* **1978**, *57*, 756.
12. Heredy, L. A.; Kostyo, A. E.; Neuworth, M. B. *Fuel* **1963**, *42*, 182.
13. O'Connor, J. J.; Sowa, F. L. *J. Am. Chem. Soc.* **1935**, *60*, 175.
14. Monacelli, W. J.; Hennion, G. F. *J. Am. Chem. Soc.* **1941**, *63*, 1722.
15. Heredy, L. A.; Ph.D. Dissertation, Studies on the Chemistry and Mechanism of Transbenzylation, Carnegie Institute of Technology, Pittsburgh, PA, 1962.
16. Franz, J. A.; Morrey, J. P.; Tingey, G. L.; Skiens, W. E.; Pugmire, R. J.; Grant, D. M. *Fuel* **1977**, *56*, 366.
17. Brown, H. C.; Grayson, M. *J. Am. Chem. Soc.* **1953**, *75*, 6285.
18. Olah, G. A.; Kuhn, S. J.; Flood, S. H. *J. Am. Chem. Soc.* **1961**, *83*, 4571.
19. *Ibid.*, 1962, *84*, 1688.
20. *Ibid.*, 1695.
21. Olah, G. A.; Tashiro, M.; Kobayashi, S. *J. Am. Chem. Soc.* **1970**, *92*, 6369.
22. Olah, G. A.; Kobayashi, S.; Tashiro, M. *J. Am. Chem. soc.* **1972**, *94*, 7448.
23. Retcofsky, H. L. *Appl. Spectros.* **1977**, *31*, 116.

RECEIVED July 19, 1979.

Deduction of the Structure of Brown Coal by Reaction with Phenol

D. G. EVANS¹ and R. J. HOOPER²

Department of Chemical Engineering, University of Melbourne, Parkville 3052, Victoria, Australia

The chemical structure of an Australian brown coal has been deduced by depolymerizing it with phenol to yield a low-molecular-weight product amenable to structural examination. This product was separated by solvents into five fractions with different chemical characteristics, which were then submitted to proton nuclear magnetic resonance (¹H NMR), infrared (IR), and functional group analyses. After allowing for combined phenol and unseparated solvent, the following deductions about the structure of the original coal were made: 55% by mass consisted of aromatic structures with a large number of substituents, consisting of aliphatic side chains (15% by mass, half of which were methylene bridges), functional groups (5% phenol, 5% carboxyl, and 3% carbonyl), and ether and other heteroatom bridges (over 10%). The overall stoichiometry is such that the coal must be highly interlinked by the various bridge groups into a three-dimensional network.

To make any real progress in the ability to predict and control the liquefaction of coal by hydrogenation, we must know what chemical reactions are occurring. Modern preparative and analytical techniques such as elution chromatography, mass spectroscopy, and ¹H NMR have made the task of characterizing the products of liquefaction reactions much easier than hitherto, but the task of characterizing the coal before reaction remains almost as intractable as ever, because these new methods depend on the analysis samples being in the liquid form (or in the case of mass spectroscopy, able to be completely vaporized).

¹ Current address: Centre for Environmental Studies, University of Melbourne, Parkville 3052, Victoria, Australia.

² Current address: Liquid Fuels Trust Board, Box, 17, Wellington, New Zealand.

This is not a new problem, of course. Over the years many solubilization techniques have been suggested as tools for deducing coal structure: e.g., oxidation, hydrogenation, alkaline hydrolysis, pyrolysis, and extraction with powerful solvents (either alone or in conjunction with other methods such as thermal pretreatment, use of ultrasonics, etc.). These techniques suffer from one of two disadvantages: with the relatively mild physical methods, not enough coal is obtained in solution to be useful (less than 20% is typical); with chemical methods, including pyrolysis, the treatment is so harsh that interpretation of the structure of the original coal in terms of that of the products is of dubious validity. In particular, use of elevated temperatures, as in pyrolysis or other thermal treatments, must be avoided, as free radicals formed by cleaving fragments off the main body of the coal molecule may polymerize to form structures that were not present in the original coal.

If it is accepted that coal cannot be solubilized without altering its structure to some extent, we should look for methods in which these changes are not large enough to prohibit the drawing of adequate deductions about the structure of the original coal, while at the same time presenting the reacted coal in a form suitable for structural examination. This criterion would require at least 80% of the coal to be solubilized, with the soluble material low enough in molecular weight to ensure that it in turn is soluble in mild organic solvents, as required for preparative techniques such as solvent fractionation or chromatography.

The methods we considered were Friedel-Crafts reactions of various kinds (alkylation and acylation) and depolymerization of the coal by using it to alkylate phenol, as first proposed by Heredy and co-workers (1) and extensively investigated by them (1-5) and by Ouchi and co-workers (6-11). From the recent review of these methods by Larsen and Kuemmerle (12), it appears that molecular weights of the coal fragments produced are higher for alkylation and acylation methods (typically several thousand, even after allowing for the added acyl or alkyl groups) than for the material depolymerized in phenol (less than a thousand). Phenol depolymerization is less successful than other methods for solubilizing very high rank coals [greater than 90% C, dry, ash-free (DAF) basis], but this disadvantage did not concern us, as we were interested in the structural examination of brown coals of very low rank (less than 70% C, DAF), which Ouchi and Brooks (9) had already shown to be readily depolymerized in this way. The main difficulty to be expected was the possible chemical reaction of the coal with the phenol to form new groups not present in the original coal (13).

In our plan of attack we first depolymerized the coal by using conditions suggested by Imuta and Ouchi (11); then we divided the product into five fractions of progressively increasing polarity, using solvent fractionation. These fractions then were analyzed separately by

elemental and functional group analysis and further characterized by running IR and ^1H NMR spectra on them. After allowing for the effects of combined phenol, we put these data together to build up a composite picture of the structure of the original coal. Heredy et al. (5) have carried out a similar investigation on a series of coals of different ranks. The present work differs from theirs in that it used a more powerful catalyst for the phenolation, a more decisive solvent fractionation scheme, and IR as well as NMR analysis for characterizing the fractions. Also, our coal was lower in rank than any of those they tested.

Experimental

Coal Used. The coal tested was Morwell brown coal from Victoria, Australia. Its composition on a dry basis is shown in Table I. This coal contains over 60% moisture as mined. It was ground wet to 80% less than 25 mesh and used in the wet state (60% moisture).

Phenolation Reaction. For this experiment 179 g of wet ground coal, 75 g of *p*-toluenesulfonic acid catalyst, and 1300 g of laboratory grade phenol were heated under nitrogen, and the water was removed from the coal by boiling at 183° C (the boiling point of phenol is 181.8° C). The remaining mixture was refluxed at 183° C for 4 hr, after which the phenol was removed by steam distillation, leaving a solid, black, tarry material of low melting point, which was separated by

Table I. Yields and Compositions of the Fractions

	Fraction					Composite	Whole Coal
	A	B	C	D	E		
Yield (g/100 g of original coal)	28	66	78	28	2	202	100
Composition (mass %)							
C	76	74	69	71	56	72	63
H	7	6	5	4	6	5	5
O, phenolic	4	4	3	6	ND ^a	[4]	5
O, carboxylic	0	1	3	2	ND	[2]	5
O, carbonyl	ND	ND	ND	ND	ND	ND	3
O, total	17	16	21	18	24	18	25
Ash	ND	ND	2	3	ND	[1]	4
Unaccounted	1	4	3	4	14	4	3

^a ND means not determined. Ash contents were not determined on fractions A, B, and E, which were liquids. Functional group oxygen was not determined on fraction E because of insufficient mass of sample. The figures in brackets for the composition of the composite should be little affected.

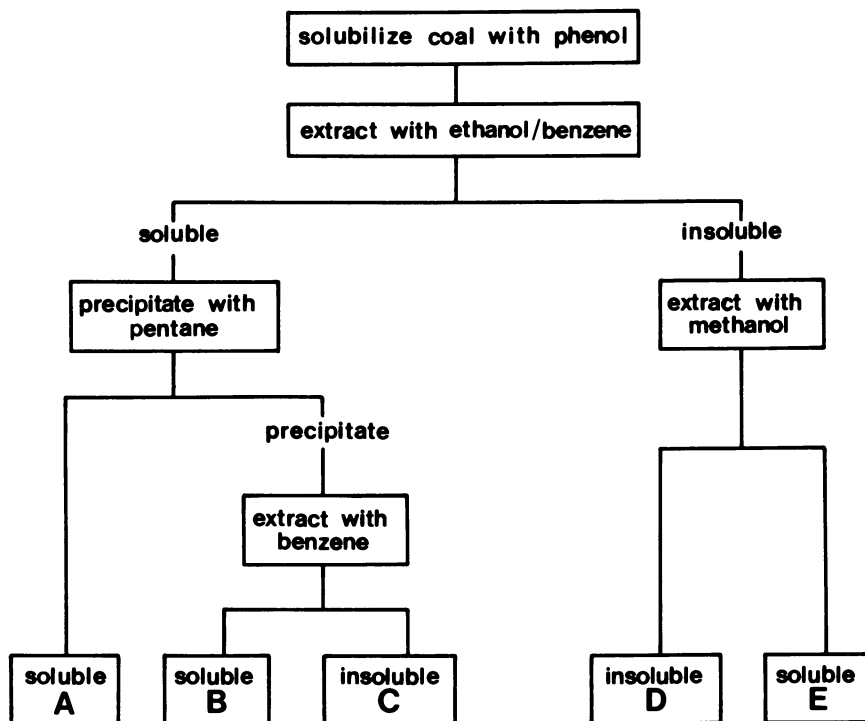


Figure 1. Fractionation scheme used to separate coal into four soluble fractions and an insoluble residue

decantation and extracted by refluxing for 2 hr with 1200 mL of ethanol–benzene azeotrope (65% benzene, 35% ethanol). The insoluble material was filtered off and dried in a vacuum oven for 12 hr at 50°C and 16 kPa of pressure (these conditions were later used to remove excess solvent from all the fractions; see Figure 1).

Solvent Fractionation. To facilitate later structural analysis, we separated the coal into structural types by solvent fractionation. Some other workers using the phenol depolymerization method to solubilize coal have used gas chromatography/mass spectroscopy (GC/MS) techniques to identify individual compounds (11, 13). However, with material containing large amounts of phenol and other polar groups, elaborate preparation and separation schemes have to be used to avoid contamination of the chromatography columns. As the emphasis of the present work was on structural characterization of the whole coal rather than on detailed examination of small parts of it in order to elucidate the chemistry of the phenolation reaction, we used the relatively simple scheme shown in Figure 1.

Analysis. The original coal and the various fractions were analyzed for carbon, hydrogen, and oxygen by the C.S.I.R.O. Microanalytical Service. Ash contents were determined in a standard ashing furnace (14). Phenolic, carboxylic, and carbonyl oxygen contents were determined by the State Electricity Commission of Victoria, using methods developed by them for brown coals (15).

IR spectra of the original coal and the fractions were measured on a Perkin-Elmer 457 grating infrared spectrophotometer. Liquid samples (fractions A and B) were analyzed as a thin film or a smear. Solid samples (C, D, and original coal) were analyzed in KBr disks containing 0.3% by mass of sample. The solid samples were prepared by grinding the KBr mixture for 2 min in a tungsten carbide TEMA grinding barrel, drying for 24 hr in a vacuum desiccator over phosphorus pentoxide, then pressing into disks at 10 tons of force, at room temperature but under vacuum. Because fraction A was dominated by phenol, a sample of it was further separated by elution chromatography in an attempt to separate from it material less dominated by phenol. Elution was carried out in a silica column, using elutants in the following order: hexane, chloroform, methanol.

¹H NMR spectra were recorded on a Varian HA 100 NMR spectrometer at room temperature, with tetramethylsilane (Me₄Si) as internal standard and with a sweep width of 0 to 1000 Hz from Me₄Si. For fraction A a solution of deuterated chloroform was used; fractions B and C were not soluble in CDCl₃, and pyridine-*d*₅ had to be used; fraction D and the whole coal were barely soluble even in pyridine-*d*₅, but enough dissolved to obtain spectra. These will not, of course, be representative of the whole material.

Results

Yields and Compositions. Table I shows the yields of the five fractions per 100 g of original dry coal and their compositions, including a breakdown of the oxygen into carboxylic, phenolic, and other oxygen. Note that part of the ash-forming material has been removed by the solubilizing process (much of the nonorganic material in Morwell coal is ion-exchangeable and would have been replaced by hydrogen ions from the *p*-toluene sulfonic acid; this result was confirmed by ash analysis: e.g., ash from the original coal contained 40% SiO₂ and 10% MgO, whereas fraction D ash contained 80% SiO₂ and only 1% MgO). As the total yield of fractions was 202 g/100 g of original coal, 102 g must have been added. This amount consists of combined phenol and unseparated solvents, as will be discussed later. This dilution results in the fractions having higher carbon contents and lower oxygen contents than the original coal.

IR Spectra. The IR spectra of the fractions and the original coal are shown in Figure 2; those of the eluted subfractions of fraction A are shown in Figure 3.

As already mentioned, fraction A is dominated by phenol; nevertheless, strong aliphatic absorptions can be seen at 2920, 2850, 1460, and 1380 cm⁻¹. The spectra of subfractions A1 (eluted by hexane, a very small part of A) and A2 (eluted by chloroform, about a quarter of A) showed these aliphatic absorptions very strongly. The spectrum for A1 showed little else, and this subfraction is probably virtually pure paraffins. The spectrum for A2 resembled the spectra for phenol ether and

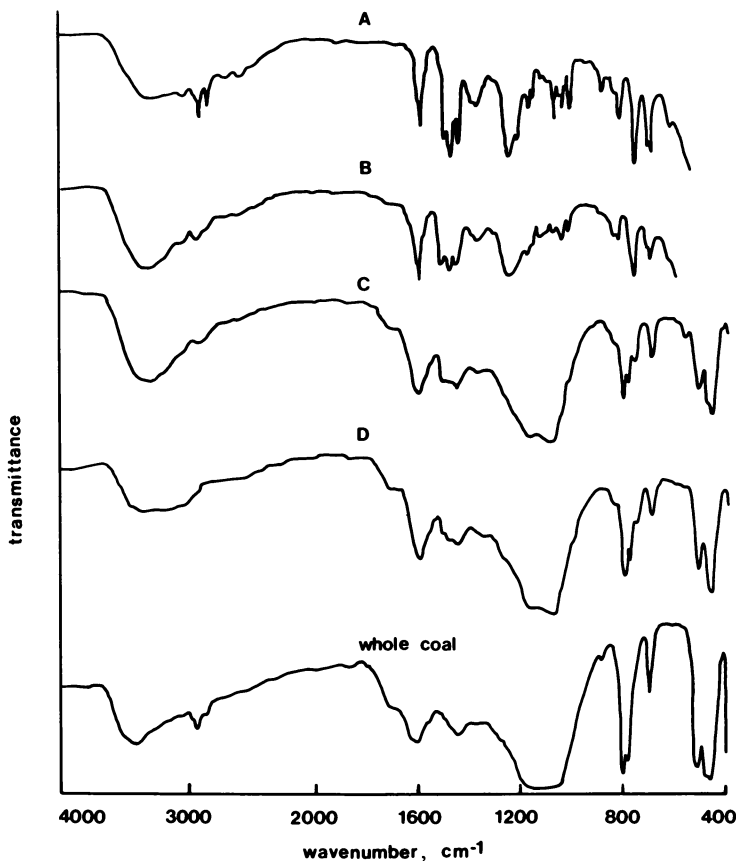


Figure 2. IR spectra for the original coal and the fractions A to D separated by the fractionation scheme shown in Figure 1. Fractions A and B, thin film; fractions C and D and whole coal, KBr disk.

phenetole ($C_6H_5OC_2H_5$). Absorption due to hydrogen-bonded hydrogen is negligible, showing that all the phenol in this subfraction has been converted to ethers. The spectrum for subfraction A3 (which constitutes about three-quarters of A) was dominated by phenol, but some aliphatic absorptions still showed. The absorptions for A, A2, and A3 at 1250 cm^{-1} are probably due to ether oxygen.

Fraction B is in many ways similar to fraction A but with much weaker aliphatic absorption. It has a strong absorption due to hydrogen-

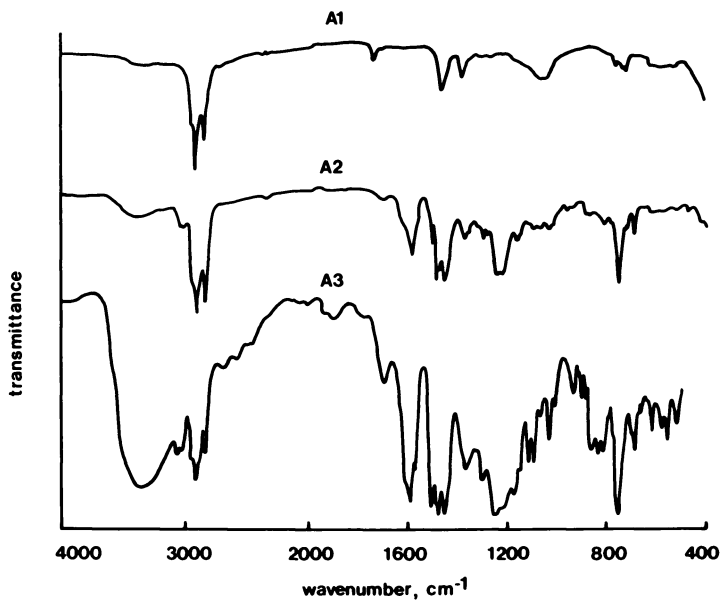


Figure 3. IR spectra for subfractions obtained from fraction A by elution chromatography on nonactivated silica. Subfraction A1 was eluted with *n*-hexane, A2 with chloroform, and A3 with methanol.

bonded hydrogen at 3400 cm^{-1} , a weak aromatic absorption at 3030 cm^{-1} , and many other absorptions characteristic of phenol. It also shows weak aliphatic absorptions at 2920 , 1460 , and 1380 cm^{-1} , and ether oxygen absorption at 1250 cm^{-1} .

Fractions C, D, and E have spectra similar to those of the original coal. Phenol no longer dominates, although the hydrogen-bonded -OH absorption at 3400 cm^{-1} is still strong. Aliphatic absorption is weak in C and E and negligible in D. The shoulder at 1700 cm^{-1} caused by carboxylic oxygen, which was quite strong for the whole coal, is also quite pronounced for fractions C and D. (It was absent from fractions A and B.) This result checks well with the data in Table I obtained by chemical analysis. The broad absorption from $1200\text{--}1000\text{ cm}^{-1}$ present in the whole coal also is present in fractions C and D, although it is absent from A, B, and E. Doubtless oxygen groups contribute to this result, but we believe it is mainly due to silica, which is a major constituent of the ash. It could be removed almost entirely by deashing the coal with strong acids or by float-sink separation.



Figure 4. NMR spectra for fractions A, B, C, and E.

A is dissolved in CDCl_3 : the triplet at $\delta = 1.2$ superimposed on the aliphatic peak at $\delta = 1.3$, and the quartet at $\delta = 3.7$ arise from ethanol from the original solvent. The split resonance pattern of phenol is obvious at $\delta = 6.7\text{--}7.0$ and $7.0\text{--}7.4$. Hydrogen-bonded OH protons appear at $\delta = 8.5$.

B is dissolved in pyridine- d_5 : residual α , β , and γ protons in this solvent appear as peaks at $\delta = 8.6$, 7.1 , and 7.5 , respectively. Hydrogen-bonded OH protons appear at $\delta = 9.5$.

C is dissolved in pyridine- d_5 , which shows peaks at $\delta = 8.6$, 7.1 , and 7.5 arising from residual solvent protons. The broad absorption in the region $\delta = 8.2\text{--}9.2$ disappeared with D_2O exchange and can be attributed to OH protons.

E is dissolved in pyridine- d_5 : again residual solvent protons show at $\delta = 8.6$, 7.1 , and 7.5 . D_2O exchange removed the sharp peak at $\delta = 8.9$, which is attributed to OH protons. However, as it did not affect the peak at $\delta = 4.0$, this peak is unlikely to be due to methanol and is attributed to methylene bridges.

NMR Spectra. Figure 4 shows NMR spectra for fractions A, B, C, and E (as mentioned earlier, fraction D and the whole coal were virtually insoluble in pyridine- d_5 , and spectra from them are not representative). Table II shows the forms the protons are present in, as determined from these spectra. The unrepresentative data for the small soluble parts of fraction D and the whole coal are shown in brackets. This table demonstrates the difficulties the coal chemist faces in trying to use ^1H NMR on physical solutions of coal: e.g., the soluble part of the whole coal shows no hydrogen-bonded protons despite the evidence of Table I; it shows no triaromatic or methylene bridge protons, despite the presence of appreciable amounts of these in the fractions; on the other hand, it shows far more methylene α and methyl β than do the fractions.

The NMR data confirm and amplify the IR data: hydrogen-bonded protons are presented from phenolic and carboxylic groups in the coal and phenol groups added with the chemically combined phenol. The monoaromatic content (of fractions A and B especially) is high, also because of added phenol, but two-ring aromatic material also is present in all fractions (even triaromatic in C), which must have come from the original coal. The aliphatic material observed in the IR spectra of A, B, and C now is seen to consist principally of methylene bridges and short, branched aliphatic chains (α - and β -methyl predominate).

Table II. Distribution of Protons by Type in the Various Fractions as Measured from NMR Spectra

δ (ppm)	Proton Type ^a	Fraction ^b					
		A	B	C	D	E	Whole Coal ^b
> 8.0	Hydrogen-bonded	6	17	19	[0]	27	[0]
8.7-8.0	Triaromatic [5]	0	0	6	[10]	0	[0]
8.0-7.2	Two-ring aromatic [5]	7	10	8	[48]	13	[46]
7.2-6.2	Monoaromatic	72	58	44	[35]	37	
5.8-4.3	Olefinic	1	0	0	[0]	0	[0]
4.3-3.4	Methylene bridge	0	9	17	[trace]	9	[0]
3.4-3.2	Acetylinic	0	0	0	[0]	trace	[0]
3.2-2.4	Methin, methylene α	3	0	0	[0]	0	[11]
2.4-2.0	Methyl α		1	4	[4]	15	
2.0-1.4	Methylene β	3	1	0	[0]	0	[4]
1.4-1.0	Methyl β	8	4	1	[4]	0	[39]
1.0-0.6	Aliphatic γ	0	0	0	[0]	0	[3]

^a α , α , and γ refer to the positions of these protons with respect to aromatic rings.

^bFigures are percentages of the total protons in the particular fraction. Allowance has been made for residual protons in the deuterated solvents (CDCl_3 for A, pyridine- d_5 for others). The figures for fraction D and the whole coal are put in brackets to indicate that these samples were barely soluble and the spectra do not represent the whole material, only the small soluble part. As noted later in the text, there was a small amount of ethanol contaminating fraction A. The proton distribution for this fraction has been calculated on an ethanol-free basis.

Discussion

Correction for Added Material. As already noted, the total yield of fractions was 202 g/100 g of original coal. The 102 g of added material must be due to combined phenol and/or unseparated solvents from the fractionation procedure. As these added materials contribute to the structure shown in Figures 2 and 4 and Table II, appropriate corrections have to be made. To do this we first have to establish what the added material consists of.

In the fractionation scheme shown in Figure 1, fraction A could be contaminated by pentane, benzene, or ethanol; fractions B and C are most likely to be contaminated by benzene; and fractions D and E are most likely to be contaminated by methanol. The NMR spectrum of fraction A showed ethanol contamination amounting to 7% of the sample, but apparently no pentane was present, as none was picked up in the hexane elutriation while preparing subfraction A1. No methanol was detected in the NMR spectra of fractions D and E. All fractions showed monoaromatic hydrogen, which could result from monoaromatic structures in the original coal, from combined phenol, or from contamination by benzene used in the fractionation scheme. Thus apart from the small amount of ethanol in fraction A, the main constituent of the added material was phenol and/or benzene. Fortunately, because of the structural similarities of these two, the final answer obtained for the coal structure will not be very sensitive to assumptions made about the relative quantities of these two present.

The correction was made as follows: First, using the yield and composition data of Table I, we drew up elemental balances, as shown in Table III. The fifth line from the bottom of this table gives the masses of the various constituents of the material added to the coal by the depolymerization and fractionation processes. The fourth line from the bottom represents the added ethanol, and the third line from the bottom gives, by difference, the added phenol and/or benzene. The second line from the bottom is based on the assumption that all the added carbon is from phenol and none from benzene. The last line shows the materials that must have been lost during the reaction, based on this assumption. The loss of ash-forming constituents by ion exchange has already been discussed. The loss of hydrogen and oxygen is consistent with the loss of water during the polymerization reactions. This is certainly expected from Table I, which shows less carboxylic oxygen in the fractions than in the original coal, and far less phenolic oxygen than one would expect from the uptake of oxygen shown in Table III. The formation of other oxygen group from phenolic and carboxylic groups, with the elimination of a water molecule, will be discussed more fully later.

Distribution of Hydrogen on a Phenol- and Solvent-Free Basis. We now can determine the distribution of hydrogen in the origin-

Table III. Elemental Balances^a on Material Added to the Coal by Phenolation

<i>Fraction</i>	<i>C</i>	<i>H</i>	<i>O</i>	<i>Ash</i>	<i>Unaccounted</i>	<i>Total</i>
<i>A</i>	21	2	5	0	0	28
<i>B</i>	49	4	11	0	2	66
<i>C</i>	54	4	16	1	3	78
<i>D</i>	20	1	5	1	1	28
<i>E</i>	1	0	0	0	1	2
<i>Total</i>	145	11	37	2	7	202
<i>Original coal</i>	63	5	25	4	3	100
<i>Added material</i>	82	6	12	-2	4	102
<i>Ethanol in fraction A</i>	1	0	1	0	0	2
<i>Added material less</i>						
<i>ethanol</i>	81	6	11	-2	4	100
<i>Added phenol^b</i>	81	7	18	0	0	106
<i>Deficit</i>	0	1	7	2	-4	6

^a All figures are g/100 g of original dry coal.

^b The added phenol was calculated by assuming all the carbon in the added material (with the exception of 1 g in ethanol present in fraction A) was due to phenol. Based on this assumption, 8 g of the added phenol must have been lost as water (bottom line of table).

al coal, but first we have to estimate the hydrogen distribution in fraction D, which could not be determined by NMR analysis. In another paper presented to the 1979 ACS Congress (16), we reported results of the hydrogenation of fractions A to D in tetralin. Fraction D yielded a low-hydrogen residue, which still could not be analyzed by NMR, and a high-hydrogen liquid product separated by boiling off excess tetralin. From its NMR analysis and the known amount of functional group hydrogen in the original fraction (0.05 g/100 g original coal), we estimated that the aliphatic hydrogen in the original fraction was about 0.3g/100 g, and the remaining 0.8 g of hydrogen/100 g was aromatic hydrogen of various kinds.

In Table IV the results of the NMR analyses (Table II), the estimates of combined phenol and contaminant ethanol (Table III), and the estimates given above of the distribution of hydrogen in fraction D are manipulated to give a composite estimate of hydrogen in various forms in the original coal (the aromatic hydrogen in fraction D is assumed to follow the same pattern as in A, B, and C, and the aliphatic hydrogen also is assumed to be distributed as in A, B, and C). From this composite estimate we can calculate, by difference, the hydrogen present in various forms in the original coal (the second to last line of Table IV).

Distribution of Structural Types. The distribution of hydrogen calculated above together with the distribution of functional group oxygen

Table IV. Hydrogen Present in Various Forms in Fractions, Original Coal, Combined Phenol, and Benzene Contaminant (g/100 g Original Dry Coal)

Fraction	Hydrogen			Aromatic ^a			Methylene			Aliphatic ^a			Total
	Bonded ^a	Tri	Di	Mono	Bridge	α CH ₂	α CH ₃	β CH ₂	β CH ₃	α CH ₃	β CH ₂	β CH ₃	
A ^b	0.10	0.00	0.12	1.22	0.00	[0.02	0.04]	0.06	0.14	0.04]	0.06	0.14	1.70
B	0.67	0.00	0.40	2.30	0.36	0.00	0.04	0.04	0.16	0.04	0.04	0.16	3.97
C	0.74	0.23	0.31	1.72	0.66	0.00	0.16	0.00	0.04	0.00	0.00	0.04	3.86
D	[0.05]	[0.03	0.10	0.65]	[0.16	0.00	0.04	0.02	0.07]	0.04	0.02	0.07]	1.12
E	0.03	0.00	0.02	0.04	0.01	0.00	0.02	0.00	0.00	0.02	0.00	0.00	0.12
Total	1.59	0.26	0.95	5.93	1.19	0.02	0.30	0.12	0.41	0.30	0.12	0.41	10.77
Phenol minus lost water	0.18	—	—	5.33	—	—	—	—	—	—	—	—	5.51
Coal	1.41	0.26	0.95	0.60	1.19	0.02	0.30	0.12	0.41	0.30	0.12	0.41	5.26
Total	1.59	0.26	0.95	5.93	1.19	0.02	0.30	0.12	0.41	0.30	0.12	0.41	10.77

^a Figures in brackets have involved making some assumptions about the distribution; see text.

^b Figures for fraction A are on an ethanol-free basis.

(Table I) define a statistically probable structure for Morwell brown coal. Rather than attempting to draw a structure, we give in Table V estimates of the number of carbon atoms associated with each type of hydrogen atom, which not only predict (approximately) the correct mass of carbon per 100 g of coal but also allow for (approximately) the required number of substituents in the aromatic groups and for the bridges connecting the groups. Of course, there also may be some carbon not associated with hydrogen, such as acyl bridges and tertiary carbons in side chains (see later). We note in passing that the greatest difficulty in meeting the requirements above is in accommodating the oxygen not accounted for in functional groups.

We will conclude with a brief discussion of the forms taken by the three main structural groups: oxygen groups, aromatic groups, and aliphatic groups.

OXYGEN GROUPS. The original coal contained 5 g of phenolic oxygen/100 g of coal (Table I); 18 g of phenolic oxygen was added per 100 g of coal by the reaction (Table III), making 23 g in all. However, the phenolic oxygen measured in the fractions by functional group analysis was only 8 g/100 g of original coal (as calculated from the data of Table I). Thus a large part of the added phenolic oxygen must have been converted to other forms by reaction with active groups in the coal. For example, reaction with phenolic groups in the coal could result in the formation of ethers (the IR spectra for fractions A2 and A3 give evidence of this), and reaction with carboxylic groups could result in the formation of esters (calculations on the data of Table I indicate that about one-fifth

Table V. Calculation of Carbon in Various Structural Forms (g/100 g Dry Coal)

<i>Hydrogen Type</i>	<i>Atomic C/H^a</i>	<i>Mass C/H</i>	<i>H (Table IV) (g/100 g Coal)</i>	<i>C (g/100 g Coal)</i>
<i>Monoaromatic</i>	6/2.5	28.8	0.60	18
<i>Two-ring aromatic</i>	10/4	30	0.95	28
<i>Triaromatic</i>	14/5	33.6	0.26	9
<i>α-Methylene</i>	1/2	6	0.02	0
<i>β-Methylene</i>	1/2	6	0.12	1
<i>Methylene bridge</i>	1/2	6	1.19	7
<i>α-Methyl</i>	1/3	4	0.30	1
<i>β-Methyl</i>	1/3	4	0.40	2
<i>Carboxyl</i>	1/1	12		2
<i>Total</i>				68

^a In the case of the aromatic structures the atomic C/H ratios represent the degree of substitution in the aromatic rings. They have been chosen in such a way as to satisfy simultaneously the overall stoichiometry and the elemental composition of the original coal. Although the figures used are arbitrary, they can be varied very little because of the above constraints

of the carboxylic oxygen has disappeared). Ethers and esters usually are not considered to be formed in the phenolation reaction; presumably they are formed in this case because of the very high reactivity of the phenolic and carboxylic groups in the highly substituted brown coal. Heredy et al. (1) have noted the self-condensation of phenol in this reaction (as already noted, the IR spectrum of subfraction A2 strongly resembled phenol-ether), and Franz et al. (13) have demonstrated the formation of xanthen structures with loss of water from a brown coal, which they note could have come from phenol attack on RCH_2R or HCR_3 structures in the coal, followed by self-condensation.

Because of the reactions above the phenolated fractions tell us no more about the oxygen group structure of the original coal than can be deduced by measurements on the coal itself. As seen from Table I, 25% of the original coal was oxygen, 5% in the form of phenolic groups, 5% carboxylic, and 3% carbonyl. Of the remaining 12%, part is probably ether oxygen, but the presence of ethers in fractions A and B does not prove this; as discussed above they could have come from the phenolation reaction. There was some indication of the presence of benzofuran groups from the IR spectra of residues left after the reaction of fractions C and D with tetralin (16), but, as Franz et al. point out (13), such structures could have been formed in the phenolation reaction. No doubt other heterocyclic oxygen is present also.

AROMATIC GROUPS. The presence of relatively large proportions of higher aromatic structures is noteworthy—and unexpected from previous studies on brown coal (17, 18). From the literature published on the phenolation reaction, it seems unlikely that such structures would have been formed in the reaction itself. The total aromatic content may have been overestimated slightly by the procedure used to estimate the hydrogen distribution of fraction D, but, as seen from Table IV, this procedure could have little effect on the higher aromatics. The assumption regarding material added during the reaction also can affect only the monoaromatics, as the added material must be phenol or benzene. In Table III it was assumed that all the added carbon was due to phenol; if we had taken the opposite view that all the added oxygen was due to phenol and additional carbon was due to benzene, the monoaromatic hydrogen would fall from the value of 0.60 g/100 g of original coal (Table IV) down to 0.47 g/100 g out of a total hydrogen content of about 5%.

The aromaticity of coal is usually quoted as the ratio of aromatic carbon to aromatic plus aliphatic carbon, after making a somewhat arbitrary allowance for the effect of functional groups. In the present work (Table V) we calculated the amounts of aromatic carbon by arbitrarily assigning average substitution indexes to the aromatic rings represented by the mono-, di-, and polyaromatic hydrogen given in Table IV, the only constraints being that the overall stoichiometry and the elemental com-

position of the original coal have to be satisfied simultaneously. Table V then gives a direct estimate of the ratio of aromatic carbon to aromatic plus aliphatic carbon, 81%, which no doubt seems high for a low-rank coal (18, 19). However, no matter how the substitution indexes are manipulated in Table V, within the constraints mentioned above, much the same answer is always obtained, and one is led to the view that the usual method of calculating aromaticity ratios on the basis of aliphatic and aromatic structures alone may not have too much meaning for a coal containing nearly 30% oxygen, which has to be accommodated somewhere in the structure. Certainly the usual assumption that 60% of the oxygen is present as hydroxyl groups is badly in error for our coal, for which the hydroxyl oxygen was only 20% of the total.

ALIPHATICS. The most surprising result of this work is the high methylene bridge content (23% of all hydrogen), which again was not expected from earlier models (17). However, in the study by Heredy et al. (5), which was similar to the present one, 12% of the hydrogen in a lignite was found to be in the form of methylene bridges. It seems unlikely that these bridges were formed by the phenolation reaction (indeed, Heredy's favored mechanism requires the prior presence of such bridges). If the quantities in Table V are calculated in terms of the numbers of structures rather than their masses, we get 0.53 mol of aromatic groups per 100 g of coal and 0.60 mol of methylene bridges per 100 g. These values indicate that there is more than one bridge per aromatic group—i.e., a high degree of cross-linking must be present, probably in a three-dimensional network. Possibly dihydroanthracene structures also may be present.

Another surprising result is the high number of β -methyl and β -methylene groups (0.19 mol/100 g coal) without corresponding α -methylenes (only 0.01 mol/100 g). This result could be explained only by the presence of tertiary butyl groups [note that Swann et al. (20) recovered 2,6-di-*t*-butyl-4-methyl phenol from a similar brown coal by evacuation at 35°C]. The material reported here as β -methyl occurred at $\delta = 1.2$ –1.3 (Figure 4), which Heredy et al. (5) interpret as β -methylene groups in aliphatic chains. However, this interpretation would still require a simultaneous occurrence of α -methylene groups, which is not borne out by our Figure 3. Note also that although paraffins were indicated by the IR spectrum of fraction A1 (material soluble in pentane and eluted by hexane), these could not have contributed significantly to the strong NMR peak for fraction A at $\delta = 1.3$, as fraction A1 was negligible in mass.

Finally, it should be noted that the virtual absence of α -methylene groups is just one aspect of the general low level of aliphatic hydrogen. The broad absorption envelope usually noted in NMR spectra at $\delta = 1.0$ to 3.5 by other workers (5) is absent in our spectra, and only a

few sharp peaks are present. Perhaps one should not be too surprised at this result, remembering again the difficulty of accommodating such a large amount of oxygen in functional groups and heterocyclic structures. Any attempt to write a model structure for a coal with a carbon content less than 70% and an oxygen content approaching 30% will make this quite clear.

Acknowledgments

The work was supported financially by the Australian Research Grants Committee and the New Zealand Department of Scientific and Industrial Research, and chemical analyses were performed by the Chemistry Department of the University of Melbourne and by the State Electricity Commission of Victoria. The assistance of these bodies is gratefully acknowledged. We thank especially H. A. J. Battaerd for his encouragement and advice at many stages of the work.

Literature Cited

1. Heredy, L. A.; Neuworth, M. B. *Fuel* **1962**, *41*, 221.
2. Heredy, L. A.; Kostyo, A. E.; Neuworth, M. B. *Fuel* **1963**, *42*, 182.
3. Heredy, L. A.; Kostyo, A. E.; Neuworth, M. B. *Fuel* **1964**, *43*, 414.
4. Heredy, L. A.; Kostyo, A. E.; Neuworth, M. B. *Fuel* **1965**, *44*, 125.
5. Heredy, L. A.; Kostyo, A. E.; Neuworth, M. B. *Adv. Chem.* **1966**, *55*, 493.
6. Ouchi, K.; Imuta, K.; Yamashita, Y. *Fuel* **1965**, *44*, 29.
7. Ouchi, K.; Imuta, K.; Yamashita, Y. *Fuel*, **1965**, *44*, 205.
8. Ouchi, K. *Fuel* **1967**, *46*, 319.
9. Ouchi, K.; Brooks, J. D. *Fuel* **1967**, *46*, 367.
10. Ouchi, K.; Imuta, K.; Yamashita, Y. *Fuel* **1973**, *52*, 156.
11. Imuta, K.; Ouchi, K. *Fuel* **1973**, *52*, 174.
12. Larsen, J. W.; Kuemmerle, E. W. *Fuel* **1976**, *55*, 162.
13. Franz, J. A.; Morrey, J. R.; Tingey, G. L.; Skiens, W. E.; Pugmire, R. J.; Grant, D. M. *Fuel* **1977**, *56*, 366.
14. BS1076 Part 3 1973.
15. McPhail, I.; Murray J. B. Victorian State Electricity Commission, Sci. Div. Rep. MR-155, 1969.
16. Hooper, R. J.; Evans, D. G. Paper to Coal Liquefaction Fundamentals Symposium, ACS/CSJ Congress, Honolulu, 1979.
17. Anon. *Coal Research in C.S.I.R.O.* No. 6, March 1959, p. 12.
18. van Krevelen, D. W. "Coal"; Elsevier: Amsterdam, 1961.
19. Ouchi, K.; Iwata, K.; Makabe, M.; Itoh, H. Paper to Structure of Coal Symposium, ACS/CSJ Congress, Honolulu, 1979.
20. Swann, P. D.; Harris, J. A.; Siemon, S. R.; Evans, D. G. *Fuel* **1973**, *52*, 154.

RECEIVED July 19, 1979.

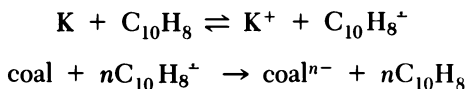
The Alkylation of Coal

LAWRENCE B. ALEMANY, C. INDHIRA HANDY, and LEON M. STOCK

Department of Chemistry, The University of Chicago, Chicago, IL 60637

The reductive alkylation of Illinois No. 6 coal has been examined. Potassium is a more effective reducing agent for this coal than lithium or sodium. Biphenyl is a moderately more effective electron transfer agent than naphthalene or anthracene. Butyl iodide is a more effective alkylating agent than butyl chloride or butyl bromide. Octyl iodide and methyl iodide are as effective as butyl iodide. Under appropriate conditions about 90% of the carbonaceous material in this coal can be converted to compounds that are soluble in tetrahydrofuran. The nuclear magnetic resonance (NMR) spectra of fractions of the soluble product containing butyl-1-¹³C groups are presented. The spectroscopic data indicate that alkylation has occurred on both oxygen and carbon atoms in the coal.

Sternberg and his associates found that the treatment of many coals with alkali metals in the presence of electron transfer agents formed polyanions, which could be alkylated to form compounds that were soluble in common organic solvents including hexane and benzene (1, 2). More recently, we discussed the proton and carbon NMR spectra of typical gel permeation chromatography (GPC) fractions of polybutylated Illinois No. 6 coal (3). This work revealed that there were significant differences in these fractions with variations in the degree of aromaticity, the ratio of C butylation to O butylation, the extent of butylation on aliphatic and aromatic carbon atoms, and the amount of carbonyl and vinyl derivatives. In addition, the low-molecular-weight fractions contained paraffinic hydrocarbons, which presumably were liberated as the coal matrix collapsed. The results obtained in this work are compatible with the essential features of the reaction process proposed by Sternberg and his associates (1, 2). He suggested that naphthalene transfers electrons from the metal to the molecular fragments in the coal.



Under these conditions the aromatic molecules of the coal are reduced, and the basic anions produced react with acidic hydrogen atoms in the coal to yield alkoxides, aryloxides, and stable carbanions. Ether cleavage, elimination reactions, and carbon-carbon bond cleavage reactions take place. Also, carbonyl compounds are reduced to semi-quinones or ketyls. In the presence of sufficient concentrations of soluble electron transfer reagents, an equilibrium mixture of soluble and insoluble polyanions containing carbanions, oxides, mercaptides, ketyls, nitrogenous bases, and so forth is generated. Because few rearrangement reactions occur under basic conditions, the structures of the anionic products are expected to be quite closely related to the structures of the molecular fragments in coal. These anionic compounds are readily alkylated by primary iodides. However, the alkylation reaction is complicated by competitive electron transfer reactions that yield butyl radicals. Thus the coal alkylation reactions occur by the reactions of the nucleophilic anionic compounds with the alkyl iodide and by the reactions of the aromatic hydrocarbon compounds with the butyl radical.

The rich chemistry of the coal polyanion and the presumably close relationship between the structures of the coal polyanion and the initial coal molecules prompted us to study the reaction conditions and the reaction products carefully and then to examine the reaction of the coal polyanion with 90%-enriched butyl-1-¹³C iodide.

Experimental

Materials. Successful alkylations require the use of thoroughly purified reagents in an air- and moisture-free environment. The reagents used in this work were purified carefully by distillation or recrystallization shortly before use. The Illinois No. 6 coal samples [analysis: C, 70.91; H, 5.18; N, 0.62; Cl, 0.14; S (pyritic), 0.82; S (sulfate), 0; S (organic), 2.71; O (by difference), 11.43; ash, 8.19] were dried at 100°C in vacuo for 16 hr. Tetrahydrofuran (THF) was refluxed in a nitrogen atmosphere over lithium aluminum hydride for 4 hr prior to distillation from the hydride. The distillate was stored under argon. Tetrahydrofuran could not be purified as readily by distillation from potassium. We found that the resonances of vinyl, carboxyl, and other unidentified groups were present in the NMR spectra of concentrated samples of the distillate when potassium was used as the purification reagent.

Preliminary Experiments. Initial work centered on the study of the reaction of potassium with tetrahydrofuran and with naphthalene in tetrahydrofuran.

Potassium (20.5 mmol) was added to tetrahydrofuran (55 mL) under argon. Aliquots free of potassium were withdrawn periodically. These aliquots were hydrolyzed and titrated to determine the extent of the reduction of the solvent. This reaction was negligible even after 5 days (Figure 1, Curve A).

In the next experiment potassium (19.9 mmol) was added to a stirred solution of naphthalene (3.16 mmol) in tetrahydrofuran (55 mL) under argon. The characteristic dark green solution of naphthalene radical anion and dianion formed within 4 min. Aliquots free of potassium were withdrawn from the reaction mixture. These aliquots were hydrolyzed and titrated to determine the extent of conversion of naphthalene to the radical anion and dianion. After about 4.5 hr, the titrimetric procedure revealed that the naphthalene was converted to a mixture equal in reducing power to 80% dianions. The reaction was followed for 5 days. The results are shown in Figure 1, Curve B.

In the third experiment of this series potassium (20.1 mmol) and naphthalene (3.10 mmol) in tetrahydrofuran (50 mL) were allowed to react for 4.5 hr. Coal (0.860 g) was then added. The reaction mixture immediately became brown. During the next several days the reaction mixture changed color as the reactions proceeded. Aliquots free of potassium but containing solid coal particles were withdrawn from this mixture and titrated to determine the extent of conversion of the coal to the coal polyanion. In certain instances aliquots free of potassium and solid coal particles were withdrawn from the reaction mixture and titrated to determine the extent of conversion of the solid coal to soluble anionic substances. The reaction was allowed to proceed for 5 days at ambient temperature under argon. An aliquot of the mixture was then withdrawn to establish the extent of the reaction. The results are shown in Figure 1, Curve C.

The results obtained in several experiments revealed that 21 ± 1 negative charges per 100 carbon atoms were introduced into the coal.

Coal Alkylation with Butyl-1-¹³C Iodide. Potassium (26.1 mmol) was added to a stirred solution of naphthalene (3.14 mmol) in tetrahydrofuran (45 mL) under argon. After 45 min, -325 mesh coal (1.00 g) and an additional wash quantity of tetrahydrofuran (10 mL) were added. The mixture was stirred for 5 days. The excess potassium (2.98 mmol) was removed. A small quantity of insoluble coal (0.041 g) was unavoidably lost in the removal of the metal. A solution of 90%-enriched butyl-1-¹³C iodide (6.88 g) in tetrahydrofuran (10 mL) was added to the stirred solution in 15 min. This quantity corresponds to a twofold excess of the amount of reagent needed for the alkylation of a coal polyanion with 21 negative charges per 100 carbon atoms and naphthalene dianion. Potassium iodide began to precipitate from the reaction mixture almost immediately. The alkylation reaction was allowed to proceed for 2 days. Potassium iodide rapidly settled from the reaction mixture when stirring was interrupted.

The reaction mixture then was exposed to the atmosphere, and the coal product was isolated. The mixture was centrifuged, and the very dark brown, tetrahydrofuran-soluble material was removed by pipet. Fresh solvent was added to the residue and the mixture was stirred. The mixture then was centrifuged and the soluble material was removed by pipet. This procedure was repeated several times. The final extracts were clear, pale yellow solutions. The combined extracts were filtered through a 1.40- μ m frit. The filtrate was concentrated in vacuo at 50°C to yield a freely flowing, dark brown material (2.252 g). Residual volatile materials were removed in several stages in vacuo. The amount of material present after 2 hr was 1.956 g; after 16 hr, 1.678 g; after 41 hr, 1.581 g; and after 68 hr, 1.521 g. This product is dark brown and does not flow.

Water was added to dissolve the potassium iodide present in the tetrahydrofuran-insoluble material. The mixture then was stirred and subsequently centrifuged to yield a clear, light yellow, supernatant solution and a small residue. This residue was treated in the same way several times to extract all the water-

soluble materials. The final extracts were colorless and did not yield precipitates when treated with sodium tetraphenylborate. The residue obtained in this way was dried in a stream of dry nitrogen to constant weight (0.686 g).

The water-soluble material was filtered through a 1.4- μm frit. An aliquot of the solution was treated with excess sodium tetraphenylborate. The potassium tetraphenylborate that precipitated was collected and dried. This analysis indicates that 18.7 meq of potassium ion was formed in the reaction.

The tetrahydrofuran-soluble portion of the buytlated, ^{13}C -labeled Illinois No. 6 coal (1.52 g) was chromatographed on silica gel (Baker, 60–200 mesh, 24 g) to remove materials such as the electron transfer agent and the related reduction and alkylation products. These materials were eluted with pure hexane (about 250 mL) and 5:95 tetrahydrofuran:hexane (about 250 mL). The dried eluant weighed 0.997 g. The coal products then were eluted with pure tetrahydrofuran (about 250 mL), followed by 50:50 tetrahydrofuran:methanol (about 250 mL) and pure methanol (about 250 mL). The dried eluant weighed 0.535 g. The recovery was virtually quantitative.

A portion of the coal product (168 mg) was dissolved in pure tetrahydrofuran (2 mL) and chromatographed on Styragel GPC columns (Waters Associates). Columns with a molecular weight exclusion limit of 10,000 (2 \times 61 cm) and 2,000 (2 \times 61 cm) were connected in series. Tetrahydrofuran was used as the mobile phase (0.36 \pm 0.01 mL/min). About 30 fractions (3.7 to 3.8 mL) were collected in each experiment. The tetrahydrofuran was removed in vacuo, and a stream of filtered, dry nitrogen was used to remove the final traces of the solvent. The coal product obtained with labeled butyl iodide was partitioned into 17 fractions (total weight, 178 mg). Samples to be used for NMR spectroscopy were dried thoroughly at 25°C at about 5 torr for 40–45 hr to remove the remaining traces of tetrahydrofuran.

The proton NMR spectra were obtained at 270 MHz with a Bruker HS-270 spectrometer. The carbon NMR spectra were obtained at 22.63 MHz with a Bruker HX90E spectrometer. The T_1 determination was carried out on a degassed sample of the 90%-enriched alkylated material, 68.6 mg, in chloroform-*d*, 2.1 mL.

Other Alkylation Experiments. In other experiments lithium and sodium were used in place of potassium. Biphenyl and anthracene were used in place of naphthalene. 1,2-Dimethoxyethane was used in place of tetrahydrofuran. Butyl chloride, butyl bromide, butyl mesylate, butyl triflate, methyl iodide, and octyl iodide were used in place of butyl iodide. The conditions used in these experiments were very similar to the conditions used in the procedures described in the previous paragraphs. The isolation procedure was modified in those cases where the ionic salt, e.g., sodium iodide, was soluble in tetrahydrofuran. In these instances the tetrahydrofuran-soluble product was washed with water to remove the salt prior to further study.

Repetitive Alkylation Reaction. The tetrahydrofuran-insoluble materials, in certain instances, were subjected to a second alkylation reaction. In these cases there were three notable differences in the experimental results. First, the green color of the naphthalene radical anion and dianion persisted for a significantly longer time following the addition of the coal residue. Second, gas evolution, presumably butene-1, was detectable during the addition of butyl iodide or butyl mesylate but, significantly, not during the addition of methyl iodide. Third, the rate of formation of potassium iodide was much more rapid, such that the rate difference between butyl iodide and methyl iodide was not evident.

The tetrahydrofuran-insoluble residue obtained after two reactions (potassium, naphthalene, butyl iodide) contained only 45.01% carbon and 41.66% ash. The quantity of the sample was insufficient for further analysis.

The reaction products were separated into tetrahydrofuran-soluble and tetrahydrofuran-insoluble fractions as already described. The chromatographic separations and spectroscopic investigations also were performed as described.

Results

The rates of reduction of tetrahydrofuran (Curve A), naphthalene in tetrahydrofuran (Curve B), and a mixture of naphthalene and Illinois No. 6 coal in tetrahydrofuran (Curve C) are shown in Figure 1. These preliminary experiments established that potassium reacted only very slowly with tetrahydrofuran under the experimental conditions used for the formation of the coal polyanion. Naphthalene was rapidly converted to a mixture of anion radicals and dianions under the same conditions. The initial reaction between the electron transfer reagent and the Illinois No. 6 coal was quite rapid. However, the reaction slowed to nearly constant rate after about 12 hr. During the last 4 days of reaction the coal molecules acquired about 0.1 negative charge per 100 carbon atoms per hour.

The titrimetric data indicated that the coal polyanions derived from this coal quite reproducibly had 21 ± 1 negative charges per 100 carbon atoms when potassium was used as the reducing agent.

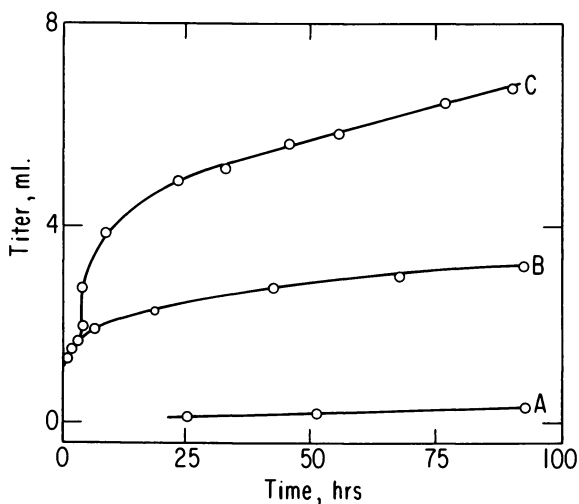


Figure 1. The rates of reduction of tetrahydrofuran (A), naphthalene in tetrahydrofuran (B), and Illinois No. 6 coal and naphthalene in tetrahydrofuran (C) are presented by a comparison of the titer required for aliquots of the reaction mixtures.

Table I. The Reduction and Butylation of Illinois No. 6 Coal with Lithium, Sodium, and Potassium^a

<i>Metal</i>	<i>Product Distribution^b</i>		<i>Butyl Groups/ 100 C Atoms (DAF)</i>
	<i>THF-soluble (g)</i>	<i>THF-insoluble (g)</i>	
Li	0.776	1.058	12.2
Na	1.166	0.768	13.2
K	1.521	0.686	20.1

^a These experiments were carried out with 1.00 g of coal, 26.5 ± 0.4 mmol of metal, 3.22 ± 0.07 mmol of naphthalene, and 55 mL of tetrahydrofuran.

^b THF solubility determined at 1.4 μm .

We first investigated the influence of the metal on the extent of conversion of the Illinois No. 6 coal to a product that was soluble in tetrahydrofuran. The results of a series of experiments conducted under identical conditions are summarized in Table I.

These results establish that potassium is a much more effective reducing agent than either sodium or lithium. This feature is illustrated by the extent of butylation, which is significantly greater for potassium than for the other metals.

We next turned our attention to the influence of the electron transfer reagent on the extent of the reaction. The results are summarized in Table II.

The observations presented in Table II reveal that biphenyl is superior to both naphthalene and anthracene as an electron transfer agent for the reduction reaction.

In the third part of this study we examined the influence of the alkyl group on the formation of soluble products under the same conditions. The results are summarized in Table III.

Table II. The Reduction and Butylation of Illinois No. 6 Coal with Anthracene, Naphthalene, and Biphenyl^a

<i>Electron Transfer Agent</i>	<i>K Consumed (mmol)</i>	<i>Product Distribution^b</i>		<i>Butyl Groups/ 100 C Atoms (DAF)</i>
		<i>THF-Soluble (g)</i>	<i>THF- Insoluble (g)</i>	
Anthracene	13.1	1.586	0.700	8.8
Naphthalene	23.1	1.521	0.686	20.1
Biphenyl	22.9	1.420	0.549	21.3

^a These experiments were carried out with 1.00 g of coal, 26.5 ± 0.4 mmol of metal, 3.22 ± 0.07 mmol of naphthalene, and 55 mL of tetrahydrofuran.

^b THF solubility determined at 1.4 μm .

Table III. The Reduction and Alkylation of Illinois No. 6 Coal with Methyl, Butyl, and Octyl Iodide^a

Alkyl Group	Product Distribution		Alkyl Groups/ 100 C Atoms (DAF)
	THF-Soluble (g)	THF-Insoluble (g)	
Methyl	1.150	0.575	20.9
Butyl	1.521	0.686	20.1
Octyl	— ^b	0.802	18.4

^a Please see the footnotes of Table I. Potassium and naphthalene were used.

^b An accurate weight could not be obtained because the octyl iodide was retained in the sample.

The reaction of the coal polyanion with methyl iodide occurs at least fivefold more rapidly than the reaction with butyl or octyl iodide, as judged by the rate of precipitation of potassium iodide. However, the results shown in the table reveal that there are only very minor differences in the solubility of the reaction products. In addition, we observed that the coal polyanions prepared from the insoluble residues of the first alkylation reaction were considerably more reactive. These polyanions reacted very rapidly with methyl iodide and reacted with butyl iodide to produce butene-1.

The influence of the leaving group was studied by a comparison of the product distributions realized in the butylation reactions of halides and sulfonates. Two equivalents of the butylation reagent were added. The results are presented in Table IV.

The reactions of the potassium-coal polyanion with the butylation reagents differed markedly. Both the percentage of soluble product and

Table IV. The Influence of the Leaving Group on Butylation^a

Reagent	First Reaction		Second Reaction		Total (%)
	Residue ^b (g)	Solubility ^c (%)	Residue ^b (g)	Solubility ^c (%)	
BuCl	1.00	23	—	—	—
BuBr	0.64	51	—	—	—
BuI	0.49	62	0.18	74	79
BuOSO ₂ CH ₃	0.51	64	—	polymer	—
BuOSO ₂ CF ₃	—	polymer	—	—	—

^a Please see the footnotes of Table I for the reagent concentrations used in the reaction between coal and potassium in the presence of naphthalene.

^b The weight of the tetrahydrofuran-insoluble residue. No correction has been applied for either alkylation or mineral matter.

^c The percentage of the original coal that has been converted to soluble product. These values have an uncertainty of about 5% and have been corrected for the extent of the alkylation reaction.

the weight of residue indicate that the reactions of the chloride and the bromide are distinctly less effective than the reactions of the iodide. The butyl sulfonate esters were much more reactive. In one case the addition of freshly distilled butyl triflate to tetrahydrofuran at room temperature caused the slow polymerization of the solvent. When the triflate was added to the potassium-coal polyanion, a rapid exothermic polymerization reaction occurred. On the other hand, the addition of butyl mesylate to the reaction mixture was effective for the production of soluble products. However, when the reaction was repeated with the residue, a slow polymerization reaction ensued, and a gas, 1-butene, was evolved from the reaction mixture.

In another experiment we tested the utility of 1,2-dimethoxyethane as a solvent for the reaction. The results obtained in this experiment revealed that the coal polyanion was formed to the same extent as in tetrahydrofuran. In addition, the alkylation of the polyanion with butyl mesylate gave the same quantity of soluble product in 1,2-dimethoxyethane as it did in tetrahydrofuran. Hence both solvents are equally useful for the alkylation reaction.

When we were satisfied that the alkylation reaction could be accomplished both effectively and reproducibly, we undertook the synthesis of butyl-1-¹³C iodide. Conventional procedures were used to produce the desired compound in 90%-isolated yield.

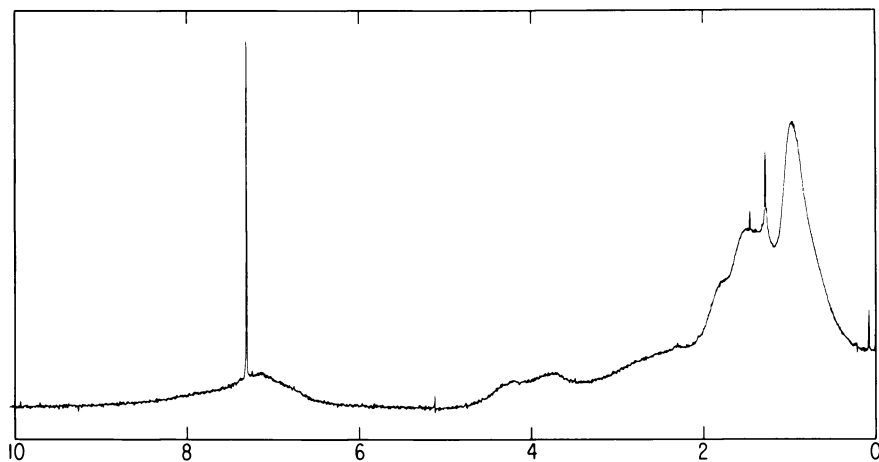
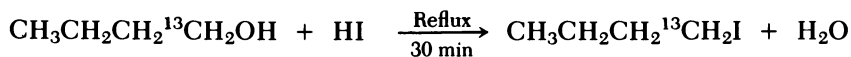


Figure 2. The proton NMR spectrum of a representative fraction of coal butylated with *n*-butyl-1-¹³C iodide. The intense signals at $\delta 7.3$ result from residual chloroform.

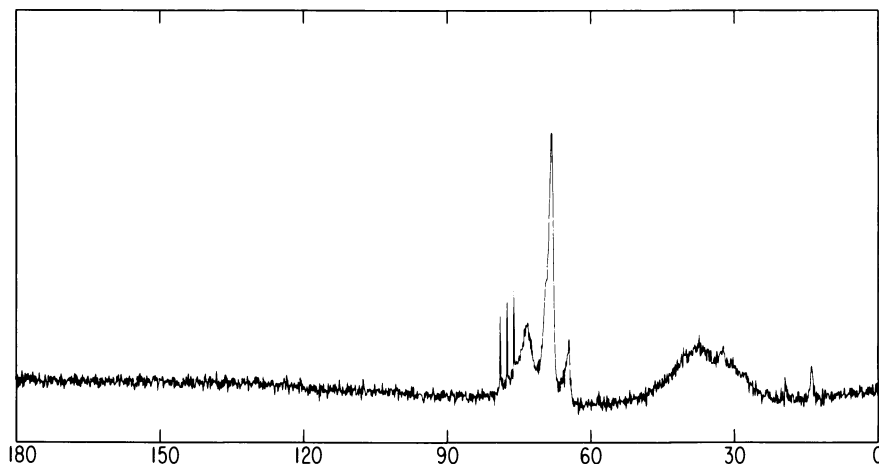


Figure 3. The carbon NMR spectrum of a representative fraction of coal butylated with *n*-butyl-1-¹³C iodide. The three sharp signals at about 77 result from chloroform.

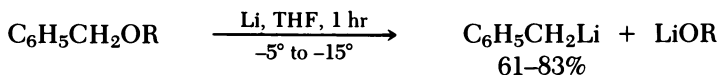
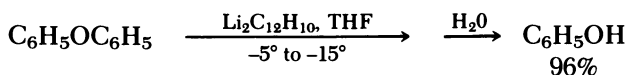
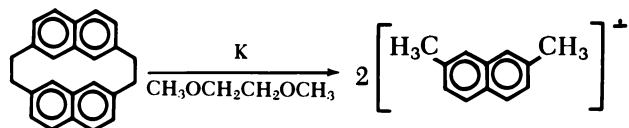
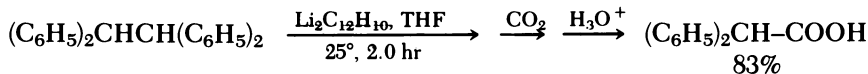
The coal alkylation reaction was carried out by using the enriched compound, and the products were separated by using the procedures described in the Experimental section. The proton and carbon NMR spectra of one fraction [comparable to fraction 9 in the previous report (3)] are presented in Figures 2 and 3.

Discussion

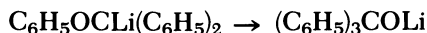
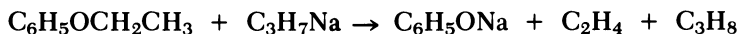
The Alkylation Reaction. Ether solvents and naphthalene often are employed in the Sternberg alkylation reaction. Inasmuch as these substances are reactive in strongly basic solution, concern has been expressed about their polymerization reactions and about their incorporation into the alkylation product. In view of these potential problems we examined the reaction of potassium with carefully purified tetrahydrofuran at 25°C. The results shown in Figure 1, Curve A, indicate that the reaction is insignificant. On the other hand, the results shown in Figure 1, Curve B, indicate that potassium reacts rapidly with naphthalene to form naphthalene anion radical and naphthalene dianion. The reduction to the dianion is about 80% complete after 4.5 hr.

The results presented in Figure 1, Curve C, reveal that Illinois No. 6 coal undergoes an initial, very rapid reduction reaction. There is no initial, rapid reaction when the insoluble alkylation products are treated with potassium and naphthalene in tetrahydrofuran in a second alkylation reaction. The observations suggest that accessible acidic hydrogen atoms and other very readily reduced functional groups, e.g., quinoid

structures, are responsible for the initial, rapid reactions. The results shown in Figure 1, Curve C, also indicate that the initial, very rapid reaction rate slows within a few hours to a constant rate of reduction, 0.1 electron per hour per 100 carbon atoms. The principal degradation reactions, we postulate, occur during this stage of the reaction. Previous work has established that both carbon-carbon and carbon-oxygen bond cleavage reactions are initiated by metals and by hydrocarbon anions (4, 5, 6). Some representative examples are presented.



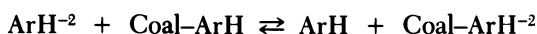
Base-catalyzed elimination reactions and Wittig rearrangement reactions are probably also important under these experimental conditions (7).



The rate of the slow reduction reaction also, we presume, is influenced by the rate of collapse of the coal matrix. Although we have not yet obtained definitive evidence on this point, it is conceivable that the reaction rate is determined by the rate at which the electron transfer reagent interacts with the bulk coal sample. This situation is intriguing, because the electron transfer reactions between the aromatic residues in the coal solid are probably very fast reactions. Moreover, the electron can readily gain access to the fragile bonds rather deep within the solid without a need for the electron transfer agent to pass through the pore structure. In these circumstances the anionic fragments may be produced in the absence of a nearby counterion and, therefore, undergo fragmentation reactions more readily. As the reactions of this type pro-

ceed, the coal matrix will collapse and the anionic fragments will gain access to the cationic counterions and be stabilized by electrostatic interactions.

Coal Conversions. In another phase of the study we examined the factors that influence the conversion of the coal to a soluble product. The results presented in Table I indicate that potassium is a much more effective reducing agent than either sodium or lithium. The results obtained with the Illinois No. 6 coal are very similar to the results obtained by Sternberg and his associates (1). The results presented in Table II indicate that the electron transfer agent influences the course of the reaction. Biphenyl is more effective than naphthalene for the formation of soluble, alkylated product. Anthracene, on the other hand, is less effective than naphthalene. This reactivity pattern accords with the well-known reduction potentials of the aromatic compounds. The finding suggests that the biphenyl anions may be able to cleave certain of the less reactive carbon-carbon and carbon-oxygen bonds in the coal. This suggestion is supported by the related observation that the polyanions produced in the reaction with biphenyl are alkylated more rapidly than the polyanions obtained in the presence of other aromatic compounds. The differences in the reactivity of these aromatic compounds are particularly striking. The qualitative information now available suggests that the electron transfer agents react selectively with the coal molecules in accord with the differences in the reduction potentials.

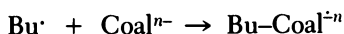


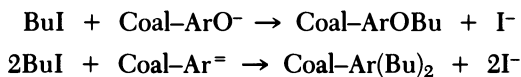
More work with other aromatic compounds will be necessary to verify this conclusion. However, the results for anthracene certainly suggest that the results obtained in the reaction are strongly dependent upon the aromatic substrate. The results obtained thus far also suggest that the reduction and subsequent alkylation of large polycyclic molecules, e.g., compounds such as pyrene, are not the most critical factors for the formation of soluble alkylation products. Studies of the molecular weight distributions and spectroscopic properties of the alkylation products obtained with different metals and different electron transfer agents are underway to resolve this issue.

The alkylation reactions of the coal polyanions also were investigated. The reactions of the polyanion with methyl, butyl, and octyl iodide were compared in tetrahydrofuran. The reaction could be monitored quite readily by the rate at which potassium iodide precipitated from solution. We estimate that methyl iodide is at least fivefold more reactive than butyl or octyl iodide under these conditions. This result, of course, suggests that the S_N2 reactions of the coal polyanion are more

significant than the electron transfer reactions. Although there is a clear distinction in the reaction rate, the extent of the alkylation reaction after 48 hr is the same for methylation, butylation, and octylation with more than 10 alkyl groups added per 100 carbon atoms. The amount of tetrahydrofuran-soluble alkylation product also is similar for these reactions. These experimental observations indicate that butyl iodide is adequately reactive for the alkylation of the polyanion. After two reactions about 90% of the original coal is converted to soluble alkylation products.

The fact that the reactions of butyl chloride and butyl bromide do not give similar results suggests very strongly that S_N2 reactions rather than electron transfer reactions are primarily responsible for the production of soluble materials. This interpretation is based on the fact that the reactivities of nucleophiles with butyl iodide, bromide, and chloride are in the approximate order 150:60:1 and that these substitution reactions are all slow relative to the electron transfer reactions of the butyl halides with anion radicals. To illustrate, the rate constants for the electron transfer reactions of primary alkyl iodides with anion radicals of the kind formed under the conditions of these experiments are about 10^4 to $10^8 \text{ M}^{-1} \text{ sec}^{-1}$ (8). The rate constants for the reactions of primary alkyl iodides with nucleophiles are less, only about $10^4 \text{ M}^{-1} \text{ sec}^{-1}$ in the fastest processes, such as the reaction of hexyl iodide with diphenylmethyl lithium or 9-lithio-9,10-dihydroanthracene in tetrahydrofuran at 20°C (8). We infer that the butyl halides undergo rapid electron transfer reactions to produce butyl radicals only during the initial stages of the alkylation process. We also infer that this process is less important for the formation of soluble products than the alkylation reactions that proceed more slowly. Indeed, the precipitation of potassium iodide from the reaction of butyl iodide with the coal polyanion is complete only after about 24 hr. Thus the much slower reactions of the polyanion with the other halides would not be complete in 48 hr. Our observations indicate that the alkylation reactions of even rather reactive alkyl halides require a considerable time at ambient temperature. The spectroscopic information presented subsequently provides strong support for the view that hindered aryloxides and possibly tertiary alkoxides are present in the polyanions. The O alkylation reactions of these sterically hindered molecules have substantial energy requirements, thereby accounting for the slow reaction rate. The slowness of the alkylation reaction of the polyanion may be responsible for certain discrepancies in the character of the alkylation products obtained in different laboratories because of difference in the time allotted for alkylation.





As already mentioned, several investigators have pointed out that naphthalene or tetrahydrofuran may be incorporated into the coal product (9, 10, 11). In this work we found that chromatographic procedures could be used to separate unbound naphthalene and its reductive alkylation products from the coal alkylation products. The spectroscopic work indicates that the principal resonances of naphthalene and tetrahydrofuran are absent from the butylated coals. Moreover, the mass balance shows that no important quantity of naphthalene or tetrahydrofuran could be incorporated. We supplemented this negative evidence by a comparison of the reaction products obtained from the same coal in a reaction in liquid ammonia. In the most pertinent case the Illinois No. 6 coal was treated with potassium in liquid ammonia. The polyanion was alkylated with butyl iodide. The product distribution obtained by GPC and the spectroscopic properties of these fractions were very closely related to the properties of the reaction products obtained in the reaction with naphthalene in tetrahydrofuran. Recently Larsen and his group found that neither ^{14}C -labeled naphthalene nor tetrahydrofuran was incorporated in chemically significant amounts in the coal products separated from the reaction mixture by chromatography (12).

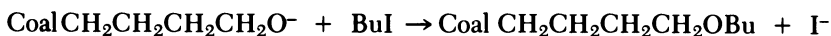
Proton and Carbon NMR Spectra. The alkylated coal products were separated from the reductive alkylation products of naphthalene. The coal products then were separated into several fractions by chromatography on Styragel. The proton and carbon NMR spectra of the individual fractions were recorded.

The proton NMR spectra of the coal products obtained in the butylation reaction with butyl-1- ^{13}C iodide are quite similar to the spectra of the coal products obtained in the reaction with unenriched butyl iodide (3). However, there is one notable difference. A single broad resonance appears near 4 ppm in the spectra of many of the fractions obtained in the butylation reaction with unenriched material. A pair of broad, overlapping resonances appears near 4 ppm in the proton spectra of the products enriched in ^{13}C . The doublet lines appear to be separated by about 125 Hz. These observations support the belief that many of the resonances near 4 ppm arise from butylated aryloxides. Curiously there are no other distinct doublet resonances in the product of the reaction with enriched ^{13}C . In principle, the reductive butylation products of aromatic compounds should yield a doublet resonance near 2 ppm. However, this signal apparently is obscured by the other aliphatic resonances upfield of 2 ppm.

The carbon NMR spectra provide new information about the course of the Sternberg alkylation reaction. There are three groups of ab-

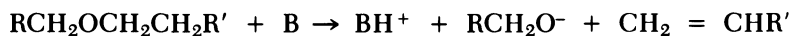
sorptions in the carbon spectra. These are centered near 68, 35, and 15 ppm. Work with many model compounds indicates that the intense, relatively sharp resonances at low field result from butyl ethers and esters and that the intense broad resonances between 25 and 45 ppm arise from carbon butylation products. The weak resonances at δ 23.0, 19.3, and 13.9 result from the γ carbon atoms of butyl groups in the C and O alkylation products, respectively, and from the δ carbon atoms of all the butyl groups.

The resonances in the butyl ether region occur in three distinct bands. Chemical shift data for the α carbon atom resonances in about 20 ethers indicate that the resonances centered about δ 72.9 may result from hindered aryl ethers, for example, butyl 2,6-dimethylphenyl ether, butyl benzyl ethers, or butyl *n*-alkyl ethers, for example, dibutyl ether. The resonances in this region could arise from tetrahydrofuran residues in the coal product. However, the results obtained in this laboratory and in Larsen's laboratory are much more compatible with interpretations that exclude the involvement of tetrahydrofuran and focus on the reactions of the labeled butylation reagent with 2,6-disubstituted phenoxides, benzylic oxides, and primary alkoxides liberated in the formation of the coal polyanion. The most intense resonance centered at δ 67.7 can be assigned with confidence to butyl aryl ethers in which the aryl group does not have 2- and 6-alkyl substituents. The resonance at δ 67.7 also is compatible with the butyl secondary alkyl ethers. It seems certain that the principal contribution, however, results from the aryl ethers, because the doublet resonance due to the coupling of the α -methylene hydrogen atoms of the butyl group with the α -methylene carbon atom is observed at δ 4.0, not δ 3.4, in the proton spectra. As already mentioned, this resonance is uniquely compatible with the resonances of butyl aryl ethers and not butyl secondary alkyl ethers.

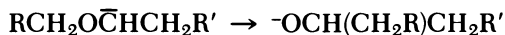
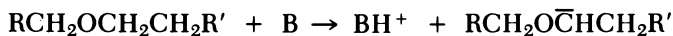


The weak resonance at δ 64.2 is more difficult to assign. This resonance is compatible with the signal expected for butyl esters and the butyl ethers of tertiary alcohols, for example, trityl butyl ether and *t*-butyl *n*-butyl ether. Progress toward a definite assignment can be made by the consideration of other chemical and spectroscopic information.

The matter is significant because the reactions of ethers in the coal may proceed along several paths in the strongly basic solution. On the one hand, simple elimination reactions may occur to yield alkoxides and alkenes.



On the other hand, the acidic hydrogen atom may be abstracted to yield an unstable anion that undergoes the well-known Wittig rearrangement to produce a more branched alkoxide (7).



The broad signal in the high-field region originates from the abundant carbon alkylation products. The broad resonance extends to almost 50 ppm in each spectrum, with a maximum between 37 and 38 ppm. Work with model compounds indicates that these resonances may be attributed to the α carbon atoms of butyl groups bonded to aromatic, benzylic, tertiary sp^3 carbon atoms, and quaternary sp^3 carbon atoms. Derivatives of these kinds exhibit resonances between 32 and 44 ppm. It is not possible to refine the assignment at this time. However, it is pertinent that the signals are very broad. This observation suggests that the resonances have very small T_1 values, even smaller than the T_1 value 0.07 sec determined for the α carbon atom resonances in the butyl ethers (14).

The relative intensities of the C butylation and O butylation signals for the seven most abundant fractions are presented in Table V, and the relative intensities of the three O butylation signals for the same seven fractions are compared in Table VI.

The results presented in Table V indicate that the O butylation reaction has proceeded to a greater degree in the initial, higher-molecular-weight fractions. This same trend was observed in the previous study of the butylation products of the Illinois No. 6 coal (3).

Table V. Relative Intensities of the C Butylation and O Butylation NMR Signals^a

Fraction	Weight Percent	C Butylation/ O Butylation
1	12.5	0.76
2	38.5	0.65
3	21.4	0.75
4	12.1	0.93
5	6.1	0.97
6	3.1	1.4
7	3.4	1.8

^a The area was measured from 25 to 50 ppm for C butylation and from about 62 to 75 ppm for O butylation.

Table VI. Relative Areas of the Absorptions of the Butyl Ethers

Fraction	Weight Percent	Relative Area		
		$\delta 72.9$	$\delta 67.7$	$\delta 64.2$
1	12.5	3.3	6.3	1.0
2	38.5	2.9	4.7	1.0
3	21.4	2.6	4.4	1.0
4	12.1	3.1	5.5	1.0
5	6.1	1.7	4.4	1.0
6	3.1	—	2.2 ^a	1.0
7	3.4	—	3.4 ^a	1.0

^a For these fractions the resonances of $\delta 70 \pm 3$ overlap substantially and have been assigned arbitrarily to the center resonance.

However, the differences in the C butylation/O butylation ratio observed in the present study are much smaller than the differences observed in the previous investigation (3). The results presented in Table VI indicate that the higher-molecular-weight products also have a disproportionately greater quantity of the butyl aryl ethers. These results imply that there is a significant variation in the structural characteristics of the coal molecules.

Conclusion

The results indicate that the Sternberg alkylation reaction can be effectively used for the introduction of labeled reagents into coal and that the alkylation products can be separated and analyzed by NMR methods. The results of the NMR analyses establish that the different molecular weight fractions contain different amounts of C butylation and O butylation products. The distribution of ethereal functional groups also appears to depend upon the molecular weight.

Acknowledgment

This research was supported by the Department of Energy under contract EF-77-S-02-4227.

Literature Cited

1. Sternberg, H. W.; DelleDonne, C. L.; Pantages, P.; Moroni, E. C.; Markby, R. E. *Fuel* 1971, 50, 432.
2. Sternberg, H. W.; DelleDonne, C. L. *Fuel*, 1974, 53, 172.
3. Alemany, L. B.; King, S. R.; Stock, L. M. *Fuel* 1978, 57, 738.
4. Eisch, J. J. *J. Org. Chem.* 1963, 28, 707.
5. Elschenbroich, Ch.; Gerson, F.; Reiss, J. A. *J. Am. Chem. Soc.* 1977, 99, 60.
6. Gilman, H.; McNinch, H. A.; Wittenberg, D. *J. Org. Chem.* 1958, 23, 2044.
7. March, J. "Advanced Organic Chemistry," 2nd ed.; McGraw-Hill: New York, 1977; pp. 925, 1015.

8. Bank, S.; Juckett, D. A. *J. Am. Chem. Soc.* **1976**, *98*, 7742.
9. Franz, J. A.; Skiens, W. E. *Fuel* **1978**, *57*, 502.
10. Ignasiak, B. S.; Gawlak, M. *Fuel* **1977**, *56*, 216.
11. Ignasiak, B. S.; Chakrabartty, S. K.; Berkowitz, N. *Fuel* **1978**, *57*, 507.
12. Larsen, J. J. *Org. Chem.* **1979**, *44*, 3219.
13. Ruberto, R. G.; Cronauer, D. C. In "The Organic Chemistry of Coal," ACS *Symp. Ser.* **1978**, *71*, 50-70.
14. Alemany, L. B.; Stock, L. M., unpublished data.

RECEIVED July 19, 1979.

Complications in the Reductive Alkylation of Coal

L. B. EBERT, D. R. MILLS, and L. MATTY

Corporate Research—Science Laboratories, Exxon Research and Engineering Co., P.O. Box 45, Linden, NJ 07036

R. J. PANCIROV and T. R. ASHE

Analytical and Information Division, Exxon Research and Engineering Co., P.O. Box 121, Linden, NJ 07036

The reductive alkylation of coal, involving reduction by alkali metal naphthalenide followed by alkylation by alkyl halide, involves chemistry that is more complex than that of the reductive alkylation of simple aromatic compounds. With the coal, reduction is not accompanied by formation of significant quantities of radical anions, and alkylation can occur by nonreductive paths. Furthermore, model studies of the reducing system reveal that the solvent tetrahydrofuran decomposes to yield ethylene and that appreciable quantities of hydride are generated.

In 1971 Sternberg et al. reported a new approach to the room temperature solubilization of coal in organic solvents (1). Using a chemistry of reduction followed by alkylation, they found, in the most dramatic case, that the introduction of 8.8 ethyl groups per 100 carbon atoms into Pocahontas low-volatile bituminous coal changes its solubility in benzene from 0.5% to 95%. Since that time a variety of groups have applied the Sternberg procedure of reductive alkylation not only to coal but also to petroleum materials (2-15). Although solubilities are not generally as high as that reported for Pocahontas, there is general agreement that the procedure does enhance solubilities, through as yet not fully determined pathways.

Our goal in this presentation is to evaluate the mechanism of reductive alkylation. The approach is more complicated than previously considered, with disruption of the coal structure occurring through many paths. Before going into the specific details of these complications, we briefly outline the procedure of reductive alkylation.

REDUCTION EMPLOYING NAPHTHALENE AS ELECTRON**TRANSFER AGENT****ALKYLATION OF COAL ANION BY ALKYL HALIDE**

Figure 1. The chemistry of reductive alkylation involves two steps: one of reduction and one of alkylation. Our studies have utilized both sodium and potassium in the reduction step.

Background

The chemistry of reductive alkylation involves two steps, one of reduction and one of alkylation. Initially one generates a solution of naphthalene radical anion in tetrahydrofuran (THF) simply by mixing naphthalene and tetrahydrofuran with excess alkali metal. After 24 hr dried coal is added to this solution and allowed to mix for several days at room temperature. According to Sternberg (1, 2), this reduction step causes a transfer of the unpaired electron of the naphthalene radical anion to aromatic structures in the coal, which causes them to become (radical) anions and dianions. After a consumption of approximately 10 mmol of alkali metal per gram of coal, the excess metal is removed, and the second step, that of alkylation, is executed simply by dropping an alkyl halide, such as ethyl iodide, into the coal anion solution. According to Sternberg, the primary objective of this procedure is the geometrical disruption of stacking of aromatic planes caused by the alkylation, accompanied by reduction, of aromatic carbon atoms in the coal. For reference, this scheme is outlined in Figure 1.

Complications

We have made the following observations, which suggest the chemistry of reductive alkylation to be more complex than previously contemplated:

1. Application of the reductive step to Illinois high-volatile bituminous (Monterey mine) and Wyodak subbituminous coals does not generate significant quantities of radical anions. Furthermore, the spectroscopic *g* value of the new radical set is more suggestive of oxygen than of pi aromatic character.

2. Consumption of alkali metal in the reduction step increases monotonically with time, suggestive of a reagent decomposition reaction. In contrast, the alkali metal consumption in the *n*-butyllithium–hexane–coal reaction reaches a plateau value of about 4 meq/g of coal.
3. In model studies of the naphthalene–sodium–tetrahydrofuran system, tetrahydrofuran was found to decompose to ethylene and the sodium enolate of acetaldehyde, with the ethylene alkylating the naphthalene in both reductive and nonreductive modes. The initial step of this decomposition, proton abstraction from the alpha carbon of tetrahydrofuran, led to formation of a hydride of unknown form.
4. The alkylation step involves measurable formation of alkyl-free radicals, consistent with known behaviour of the interaction of alkyl halides with naphthalenide anion (16, 17, 18). Such radicals, once formed, react not only with the coal but also among themselves through dimerization and disproportionation.

Results

As currently accepted models for coal postulate the predominance of two- and three-ring aromatic compounds in coal (19), one naively might expect, in accordance with the known behavior of two- and three-ring polynuclear aromatic compounds (20, 21), that the reduction step should cause a substantial increase in density of free radicals. Furthermore, the spectroscopic *g* value of these newly created radicals should approach 2.0027, the value of pi aromatic radicals (22); such a value is significantly lower than that of most as-received coals (23).

To determine whether or not the reductive step does indeed cause an increase in the population of free radicals, we studied two coals, Illinois No. 6 from the Monterey mine and a subbituminous coal from the Wyodak mine, both before treatment and after about 3 days of reductive procedure. To obtain an idea of the maximum possible free radical population, we titrated the solution prior to filtration to determine the amount of alkali metal consumed per gram of coal. Thus if every alkali metal atom generated a radical anion in the coal, we should see approximately 5 to 10 mmol of spin per gram of coal.

As seen in Figure 2, the reduction step caused little, if any, change in the free radical population of the coal. Although the presence of spin-paired dianions cannot be excluded, analysis of the spectroscopic *g* value does not suggest formation of large amounts of aromatic radical anions either.

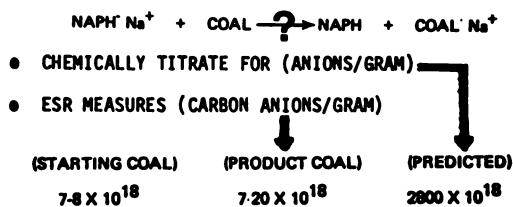


Figure 2. ESR analysis. If one assumed one radical generated for every alkali metal consumed, there is at least a factor of 140 too few radicals. In most cases there is no change in radical density following the reductive step of the Sternberg procedure.

As-received Illinois No. 6 has an electron spin resonance (ESR) spectrum with the vitrinite absorption at $g = 2.0031 \pm 0.0003$. Following the reduction step, the spectrum of the solid product appears as in Figure 3, with a new g value of 2.0040 ± 0.0005 . In previous ESR work large values of g have been associated with increased participation of oxygen in the spin ensemble through the spin-orbit interaction (24, 25).

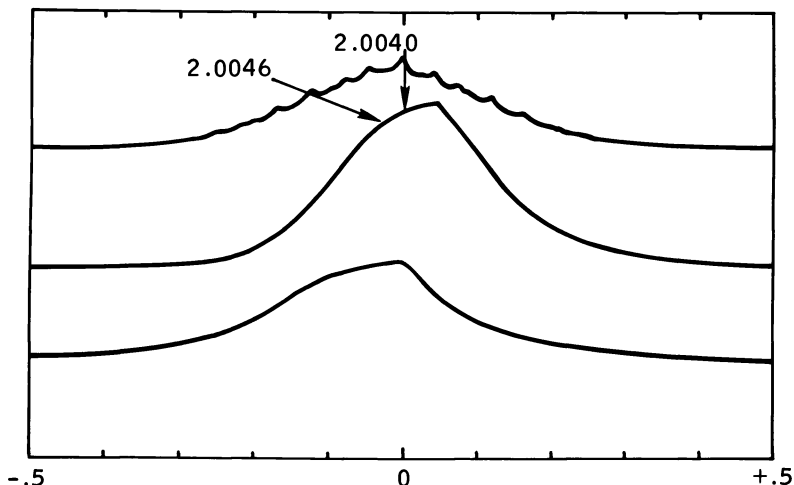


Figure 3. Spectrum of solid product.

The reductive step of the Sternberg procedure actually produces a resonance with a g value higher than that of the starting coal, suggesting possible increased influence of oxygen in the resultant radical ensemble. The top absorption spectrum is of an aliquot removed during reduction and shows the presence of the naphthalene anion. The middle spectrum is of a filtered, reduced Monterey coal (spin density of 7×10^{18} spins/g). The bottom spectrum was obtained following butyl iodide addition. Spectra are 40 G in width but not concentric in g value. (Potassium was used in these examples.)

This failure to find direct evidence for radical anions in coal is consistent with chemical titration studies. Although one would expect a given coal to have a reasonably well-defined fraction of aromatic structures, and thus a well-defined titration equivalent, workers in the field have found the titration equivalent, as meq metal/gram coal, to increase monotonically in time (1). This behavior has been ascribed to tetrahydrofuran decomposition, in the form of carbon-oxygen bond cleavage to $C_4H_8O^-$ fragments (1, 13). Previous attempts to deal with this problem have involved subtraction from the observed titration equivalent of a blank titration equivalent, arising from the reaction of alkali metal-naphthalene with tetrahydrofuran. Even with this correction Sternberg found one anion for every 8.8 carbon atoms in Pocahontas coal, a charge transfer ratio that even the infinite sp^2 hybridized carbons of graphite cannot sustain with alkali metals (26).

Our titration data for Illinois No. 6 coal are given in Figure 4. Although *n*-butyllithium will react with this coal to an extent less than or equal to 4 meq/g of coal, one sees that alkali metal naphthalenide can react easily to an extent greater than 10 meq/g of coal (1 anion for 5.8 carbon atoms). More importantly, although naphthalene has been viewed in the past as an electron transfer agent, one can see from Figure 4 that the total reaction extent is dependent on naphthalene concentration. Such an observation suggests that naphthalene is a reactant in the chemistry, not a catalyst.

To evaluate the possibility of reactive intervention of tetrahydrofuran and naphthalene in the reductive chemistry, we investigated the model system naphthalene-tetrahydrofuran-sodium by combined gas chromatography/mass spectroscopy (GC/MS) techniques. Workup of the system was by reverse quench into D_2O so that stable intermediate anions could be identified.

For the first 24 hr at room temperature the solution remained green, the color of naphthalene radical anions (20). ESR showed the characteristic 25-line pattern with the appropriate radical density, and the quenched product showed a mixture of naphthalene and 1,4-dideutero naphthalene. For periods longer than 48 hr the solution darkened to a red color, and ESR showed less than one radical per naphthalene molecule. The predominant quench product, other than naphthalene itself, was 1-ethyl-4-deutero naphthalene, with minor amounts of ethyl naphthalene also present. All hydrogen on the ethyl group was in the form of protons. Significant amounts of hydrogen gas, mainly in the form of HD, were evolved (about 0.6 mol HD/mol naphthalene). Mass spectroscopic gas analysis indicated HD:(HD + D_2) to be 0.97.

To identify the hydride source, we used per-deutero naphthalene in place of per-protio naphthalene. If the intermediate hydride existed on naphthalene, one might expect a statistical mixture of HD and D_2 . In fact,

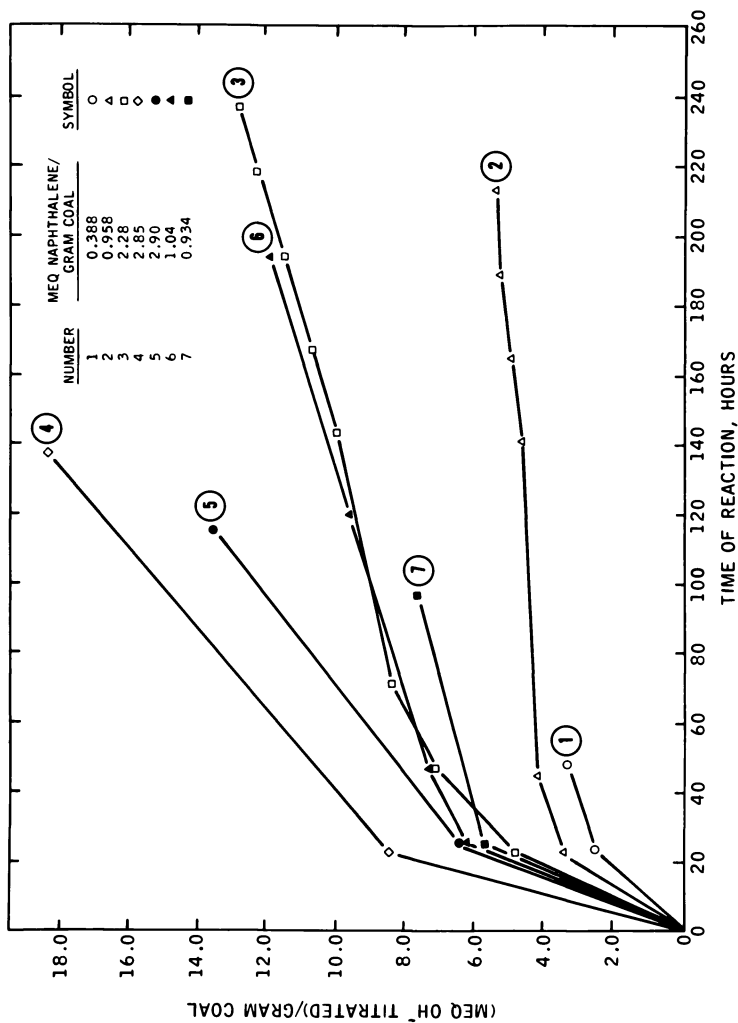
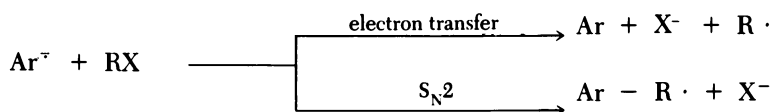


Figure 4. Titration data for Illinois No. 6 coal. The titration equivalent of the reaction not only increases monotonically in time but also depends on the concentration of naphthalene. (All reactions used potassium.)

with other changes as before, the predominant form of hydrogen was again HD, both proving the decomposition of tetrahydrofuran and suggesting the possibility of an inorganic hydride intermediate. Nevertheless, the ratio HD:(HD + D₂) of 0.83 is not outside the range of known primary isotope effects, so no firm conclusions about the nature of the hydride intermediate can be drawn. Proton nuclear magnetic resonance (NMR) of the solution phase product following the D₂O reverse quench did reveal aromatic protons (7.0, 7.3, and 7.7 delta), a conclusion consistent with GC/MS results. As previously, all hydrogen on ethyl groups added to naphthalene was as protons. Replacement of sodium by potassium led to tetrahydrofuran decomposition unaccompanied by hydride formation.

With respect to the alkylation step, we have used spin-trapping techniques (27) to seek intermediate alkyl radicals. Such radicals are well known in the interaction of aromatic anions with alkyl halides (28, 29), and their presence is thus expected in the alkylation step:



As seen in Figure 5, addition of a butyl iodide–phenyl butyl nitron mixture to a coal anion solution of Illinois No. 6 coal does indeed lead to the trapping of butyl radicals. Such radicals, once formed, may alkylate the aromatic substrate, abstract hydrogen from the system, dimerize, or disproportionate (16, 17, 18, 30). In the context of the alkylation step of

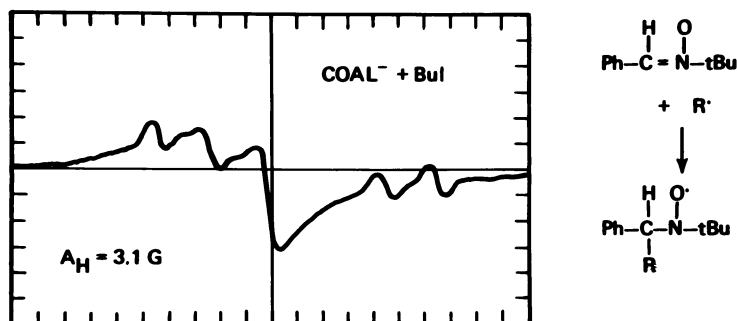


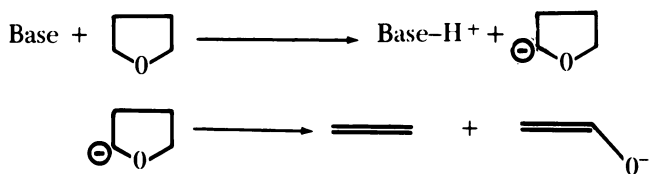
Figure 5. The addition of a solution of phenyl butyl nitron in butyl iodide to coal anion derived from Illinois No. 6 coal demonstrates the presence of butyl radical in the alkylation step ($A_{\text{H}}(\text{Bu} \cdot) = 3.1 \text{ G}$; $A_{\text{H}}(\text{H} \cdot) = 7.1 \text{ G}$; $A_{\text{H}}(\text{Ph} \cdot) = 2.1 \text{ G}$)

Sternberg, the existence of such radicals is a complication, for they may lead to alkylation that is not reductive (17) or to products unattached to the coal (abstraction, dimerization, disproportionation).

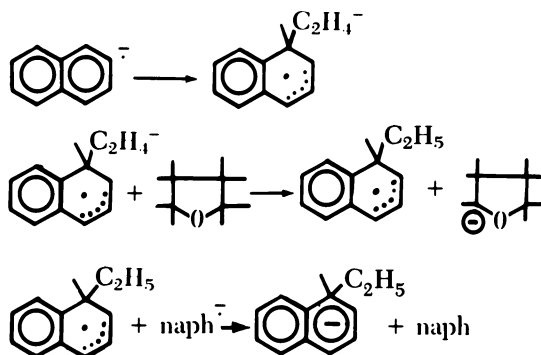
Discussion

Our failure to find significant quantities of aromatic radical anions following the reduction step suggests reduction of nonaromatic functionalities to be important in the reductive alkylation procedure. (Our non-observation of aromatic radical anions is consistent with unpublished work of H. P. Hombach, who failed to observe significant hydrogen pickup in coal following a water quench of reduced coal.) Historically, B. Ignasiak (5, 11), T. Ignasiak (6, 8), and Wachowska (7, 15) have stressed the importance of ether and thioether cleavage in both subsequent solubilization and molecular weight changes. Alkylation of oxygen functionality in the coal was recognized by Sternberg, but ether cleavage, unaccompanied by alkylation, was not considered responsible for gains in solubility (1, 2). Nevertheless, in our study, oxygen anions, whether from cleaved ether, reduced carbonyl, or phenol, logically must constitute a large fraction of the total coal anion extent and cannot be ignored. Another possibility, previously neglected, is the formation of benzylic anions. Alkali metals are known to attack methyl positions on aromatics (31, 32). As coal is considered to possess aromatic clusters containing one, two, or three rings, which are alkylated, chemistry at the benzylic site is possible.

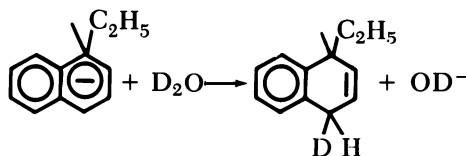
The possible instability of reagents in the reductive step was recognized by Sternberg (1) and has been discussed by other workers (8, 11, 14). Nevertheless, much concern has focused on the tetrahydrofuran-derived C_4H_8O fragment (1, 13), which, although implicated in the lithium naphthalenide studies by Fujita (33), does not seem to be important in the Sternberg procedure. Our model studies on the naphthalene-sodium-tetrahydrofuran system indicate instead that the decomposition pathway suggested by Bates (34) for the tetrahydrofuran-butyllithium interaction is operative:



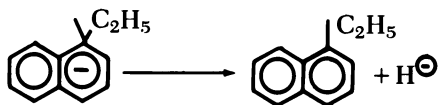
We expect ethylene to attack naphthalene (or dianion) in steps such as the following:



In the reverse quench into D_2O , this anion will form 1-ethyl-1-hydro-4-deutero-4-hydronaphthalene:



The form of the hydride is not clear. As ethyl naphthalene is an observed product, we might expect the following:



Nevertheless, other reaction pathways, as direct interaction of alkali metal with tetrahydrofuran, cannot be precluded.

The ultimate fate of the enolate is obscured by the work-up conditions. Condensation products, rather than acetaldehyde, are observed; there is always a peak in the proton NMR spectrum at 5.7 delta arising from vinylic protons.

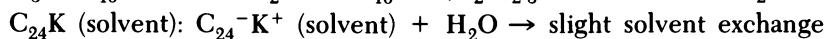
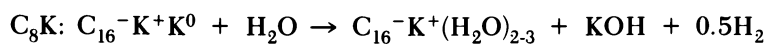
Now we turn from model systems to the reduction of coal. Detailed mass balance considerations suggest the weight of tetrahydrofuran-derived products on coal after the reduction step to be in the range of 4% (48-hr reduction) to 7% (213-hr reduction). These numbers are consistent with results of Larsen and Hombach, who employed ^{14}C -labeled tetrahydrofuran (35). Of direct influence to the application of the Sternberg procedure to coal characterization is Larsen's further observation that 60% of the added tetrahydrofuran is bonded inextricably to the coal (35, 36).

With respect to previous work by B. Ignasiak (14), we are in agreement that alpha proton abstraction from tetrahydrofuran is occurring under Sternberg conditions. The nature of our hydrogen evolution in the model system is different, however, for it comes from a reverse quench into D₂O, not from alkylation conditions. Our results implicate hydride formation during the naphthalene–sodium–tetrahydrofuran reaction.

With respect to previous work by T. Ignasiak (8), we are in agreement that ethylene from decomposed tetrahydrofuran adds to naphthalene forms. Nevertheless, our observation of –C₂H₅ groups on naphthalene, as opposed to –C₂H₄D, argues against the long-term stability of the ethyl carbanion to tetrahydrofuran. The presence of the naphthalene dianion in these reactions is unclear. Although there is a change in color from green to red in model naphthalene–sodium–tetrahydrofuran systems with time, there is no strong literature evidence for the existence of dianion with alkali metals other than lithium (20).

The ability to trap alkyl radicals during the alkylation step is suggestive of a strong balance between electron transfer and substitution reaction. Historically, naphthalene anion, in fact, has been used explicitly to generate alkyl radicals from alkyl halides (16). The presence of alkyl radicals in the alkylation of coal can be expected to complicate interpretation of reaction pathways. The observation of alkylated but unreduced aromatic products led Stock to postulate the presence of alkyl radicals during alkylation (13), although aromatic carbanions could provide similar products through nonradical pathways (1).

Our results on the reductive alkylation of coal offer insights into proposed analogies between coal chemistry and graphite chemistry (37). Graphite, as the largest polynuclear aromatic compound, can be reduced by anions of all other polynuclear aromatic compounds; in fact, this observation has been exploited to synthesize intercalation compounds (38). Although the added electron density of these compounds is predominantly on the carbon planes, these infinite aromatic anions possess chemistry distinct from that of molecular-basis aromatic anions. While naphthalene anion will react with water to form a mixture of 1,4-dihydronaphthalene and naphthalene, the graphite *anion* is inert to water (39–42):



The rigorous analogy between coal chemistry and graphite chemistry fails on two levels: (1) Although graphite undergoes reactions similar to those of polynuclear aromatic compounds, differences do exist. (2) While

analogies between coal and polynuclear aromatics also have some validity, allowance must be made for the chemistry of aliphatic side chains and of heteroatoms. Our failure to find the ESR signature of aromatic radical anions in reductively treated Illinois and Wyodak coals does not suggest the predominance of aromatic chemistry.

Negative results, as we have developed for aromatic radical anions in coal following reduction, nevertheless must always be accepted with caution. Aromatic molecules frequently form dianions, which, although performing the chemistry proposed by Sternberg, are frequently diamagnetic and thus not observable by ESR. However, for the conditions of reductive alkylation, the disproportionation equilibrium between radical anions and dianions for molecules such as anthracene favors the radical anion (21). Furthermore, dianions are easiest to isolate with lithium as a cation (20), yet Sternberg chemistry works best with potassium (1), an observation not suggestive of the dominance of dianions. Although minor amounts of dianion frequently may dominate the chemistry of the less reactive radical anion (43), the absence of increased radical density at $g = 2.0027$ to 2.0028 following reductive treatment (and before alkylation) is inconsistent with the behavior expected for the transfer of an electron from the naphthalene radical anion to more easily reduced aromatic molecules. Coal, divergent from simple aromatic compounds in both chemical and structural aspects, may react with strong reductants in many ways. The work of Hombach (44) and others (45) demonstrates that alkali metal reduction of coal need not be confined to carbon that is aromatic.

Summary

1. Treatment of Illinois No. 6 and Wyodak coals by naphthalene–potassium–tetrahydrofuran at room temperature adds less than 10^{-2} spin per consumed alkali metal atom, a number not suggestive of significant reduction of two- and three-ring aromatic compounds.
2. Alkali metal consumption in this reaction increases monotonically in time, indicating decomposition of reagent materials.
3. Tetrahydrofuran in the naphthalene–sodium–tetrahydrofuran system decomposes to ethylene and the sodium enolate of acetaldehyde. Hydride of unknown structure accompanies this decomposition.
4. Treatment of the coal anion solution by alkyl halides causes the generation of alkyl radicals.
5. Analogies between the chemistry of graphite and the chemistry of coal must be accepted with caution.

Experimental Details

ESR measurements were made by employing a Varian E-Line Century Series console and an E 102 microwave bridge (X band). A Hewlett-Packard 5245 L electronic counter was used to measure frequency. Both radical density and g value measurements were made relative to a sample of diphenylpicrylhydrazyl (DPPH). Runs were made in the single cavity mode, and the g value of DPPH was taken as 2.0037. No detuning of the cavity due to sample conductivity was observed. All data were manipulated in digital form and accumulated through a Nicolet 1180 computer (12-bit, 333-kHz A/D converter; 2048 20-bit words/spectrum; LAB 11 software). Radical density measurements were made by double integration of the derivative spectra.

Mass spectroscopic runs were made on a CEC 21-103C spectrometer. GC/MS runs were made on a DuPont 21-491 system composed of a PE 900 GC and a DuPont 21-491 magnetic scanning mass spectrometer. The samples were run on a 10-ft by 1/8-in. SE 30 column.

Proton NMR was conducted with a Varian EM 360 L spectrometer.

Illinois No. 6 (Monterey mine) and Wyodak coals were dried at 50°–100°C in a vacuum oven (100 μ m) for 24 hr prior to use. The ESR parameters of these coals were found to be as previously reported (23). Detailed microanalysis of the coals will appear in a separate publication.

The Sternberg reductive alkylation procedure was carried out as described in the literature (1, 2), employing up to a 40:1 ratio of alkali metal to naphthalene (molar basis). The model reactions involved mixtures containing 5 g (39 mmol of naphthalene, 2 g (87 mmol) of sodium, and 25 mL of tetrahydrofuran. Tetrahydrofuran was obtained from both Fisher and Aldrich and was either distilled from lithium–aluminum hydride or dried over sodium. No differences in the decomposition behavior was noted for the two drying procedures; furthermore, the presence or absence of the inhibitor butylated hydroxy toluene did not affect the decomposition.

Acknowledgments

The encouragement of R. H. Schlosberg and W. H. Davis, Jr., throughout this work is acknowledged and appreciated. Conversations with J. W. Larsen, L. M. Stock, P. H. Given, and H. P. Hombach contributed to our understanding. Finally, we thank M. K. Landsberg for literature searches and E. Frey for manuscript preparation.

Literature Cited

1. Sternberg, H. W.; Delle Donne, C. L.; Pantages, P.; Moroni, E. C.; Markby, R. E. *Fuel* 1971, 50, 432.
2. Sternberg, H. W.; Delle Donne, C. L. *Fuel* 1974, 53, 172.
3. Larsen, J. W.; Kuemmerle, E. W. *Fuel*, 1976, 55, 162.
4. Itoh, M.; Yoshida, S.; Ando, T.; Miyaura, N. *Chem. Lett.* 1976, 271.
5. Ignasiak, B. S.; Gawlak, M. *Fuel* 1977, 56, 216.
6. Ignasiak, T.; Strausz, O. P.; Montgomery, D. S. *Fuel* 1977, 56, 359.
7. Wachowska, H.; Pawlak, W. *Fuel* 1977, 56, 422.
8. Ignasiak, T.; Kemp-Jones, A. V.; Strausz, O. P. *J. Org. Chem.* 1977, 42, 312.

9. Dogru, R.; Erbatur, G.; Gaines, A. F.; Yurum, Y.; Icli, S.; Wirthlin, T. *Fuel* 1978, 57, 399.
10. Franz, J. A.; Skiens, W. E. *Fuel* 1978, 57, 502.
11. Ignasiak, B. S.; Fryer, J. F.; Jadernik, P. *Fuel* 1978, 57, 578.
12. Lazarov, L.; Rashkov, I.; Angelov, S. *Fuel* 1978, 57, 637.
13. Alemany, L. B.; King, S. R.; Stock, L. M. *Fuel* 1978, 57, 738.
14. Carson, D.; Ignasiak, B. S. *Fuel* 1979, 58, 72.
15. Wachowska, H. *Fuel* 1979, 58, 99.
16. Sargent, G. D.; Cron, J. N.; Bank, S. *J. Am. Chem. Soc.* 1966, 88, 5363.
17. Bilevich, K. A.; Okhlobystin, O. Yu. *Russ Chem. Rev.* (Eng. Transl.) 1968 37, 954.
18. Garst, J. F.; Roberts, R. D.; Abels, B. N. *J. Am Chem. Soc.* 1975, 97, 4925.
19. Given, P. H. *Fuel* 1960, 39, 147.
20. Holy, N. L. *Chem. Rev.* 1974, 74, 243.
21. Jensen, B. S.; Parker, V. D. *J. Am. Chem. Soc.* 1975, 97, 5211.
22. Alger, R. S. "Electron Paramagnetic Resonance: Techniques and Applications"; Wiley: New York, 1968; p. 278.
23. Petrakis, L.; Grandy, D. W. *Anal. Chem.* 1978, 50, 303.
24. Retcofsky, H. L.; Stark, J. M.; Friedel, R. A. *Anal. Chem.* 1968, 40, 1699.
25. Retcofsky, H. L.; Thompson, G. P.; Raymond, R.; Friedel, R. A. *Fuel* 1975, 54, 126.
26. Ebert, L. B. *Annu. Rev. Mater. Sci.* 1976, 6, 181.
27. Janzen, E. F. *Acc. Chem. Res.* 1971, 4, 31.
28. Malissard, M.; Mazaleyrat, J. P.; Welvart, Z. *J. Am. Chem. Soc.* 1977, 99, 6933.
29. Mazaleyrat, J. P.; Welvart, Z. *C. R. Acad. Sci., Ser. C* 1978, 287, 379.
30. Pryor, W. A., Ed. "Organic Free Radicals"; American Chemical Society: Washington, D.C. 1978; p. 343.
31. Hart, H.; Crocker, R. E. *J. Am. Chem. Soc.* 1960, 82, 418.
32. Collignon, N. *J. Organomet. Chem.* 1975, 96, 139.
33. Fujita, Y.; Suga, K.; Watanabe, S. *Synthesis* 1972, 630.
34. Bates, R. B.; Kroposki, L. M.; Potter, D. E. *J. Org. Chem.* 1972, 37, 560.
35. Larsen, J. W., private communication.
36. Hombach, H. P., private communication.
37. Beall, H. *Fuel* 1979, 58, 319.
38. Novikov, Yu. N.; Vol'pin, M. *Russ. Chem. Rev.* (Eng. Transl.) 1971, 40, 733.
39. Bergbreiter, D. E.; Killough, J. M. *J. Am. Chem. Soc.* 1978, 100, 2126.
40. Ebert, L. B. *Bull. Am. Phys. Soc.* 1978, 23, 185.
41. Ebert, L. B.; Scanlon, J. C. *Ind. Eng. Chem. Prod. Res. Dev.* 1980, 19 (2), 103.
42. Ebert, L. B.; Matty, L.; Mills, D. R.; Scanlon, J. C. *Mater. Res. Bull.*, 1980, 15 (2), 251.
43. Rainis, A.; Tung, R.; Szwarc, M. *Proc. R. Soc. London, Ser. A* 1974, 339, 417.
44. Niemann, K., Hombach, H. P. *Fuel* 1979, 58, 853.
45. Schanne, L.; Haenel, M. W. *Tetrahedron Lett.* 1979, 44, 4245.

RECEIVED July 19, 1979.

Data on the Distribution of Organic Sulfur Functional Groups in Coals

AMIR ATTAR¹ and FRANCOIS DUPUIS

Department of Chemical Engineering, University of Houston, Houston, TX 77004

The distribution of the organic sulfur functional groups was determined in five coals and treated coals using thermo-kinetic analysis. The data suggest that 15–30% of the organic sulfur is sulfidic in all coals. About 30–40% of the organic sulfur in lignite is thiolic and the rest is thiophenic. In bituminous coals 40–60% of the organic sulfur is thiophenic. The data suggest that the organic sulfur is trapped in coal as thiolic sulfur, which subsequently condenses to sulfidic and eventually to thiophenic sulfur. Oxidation of coal reduces the accessibility of the organic sulfur to the reducing agent. Extraction of coal with hydrochloric acid dissolves the calcium and magnesium salts. A peak believed to belong to thiolates like $[\phi SCa]^+$ is shifted. The sulfur is determined as ϕSH . An upper bound exists on the maximum portion of the organic sulfur that can be removed without the complete destruction of the coal matrix. Data are available that suggest that only thiolic and portions of the aliphatic sulfides can be removed by mild desulfurization.

Coals contain inorganic sulfur compounds, like iron pyrite and gypsum and organic sulfur, which are bound to the organic matrix. Detailed reviews of sulfur functional groups in coal were published recently by Attar (1) and Attar and Corcoran (2). The chemistry, kinetics, and thermodynamics of the reactions of sulfur were described by Attar (3) and therefore will not be reviewed here in detail.

This work had two objectives: (1) to study the structure of the organic sulfur groups in different coals, and (2) to examine the implications of the structure of the organic sulfur groups on potential desulfurization processes.

¹ Current address: Department of Chemical Engineering, North Carolina State University, Raleigh, NC 27650.

The main results of the test are as follows:

1. The majority of the organic sulfur in high-ranked coals (i.e., LVB) is thiophenic, while in low-ranked coals (i.e., lignites) most of the organic sulfur is thiolic or sulfidic.
2. The aliphatic sulfides constitute 18–25% of the organic sulfur in all coals.
3. Part of the organic thiols are present in the form of thio-lates, probably of calcium.
4. Coals with a large content of organic sulfur can be divided into two groups: coals that can be partially desulfurized and coals that cannot be desulfurized easily. The portion of the organic sulfur that can be desulfurized is that present in the form of thiolic groups and aliphatic sulfides.

Principle of the Method of Analysis

A detailed description of the principle of the method of analysis was published by Attar and Dupuis (4). Therefore, only the main points will be described here.

1. All the organic sulfur functional groups can be reduced to H_2S if a sufficiently strong reducing agent is used.
2. Each sulfur group is reduced at a rate that can be characterized by a unique activation energy and a frequency constant.
3. If a sample that contains many sulfur groups is reduced and the temperature is gradually increased, each sulfur group will release H_2S at a different temperature, given by

$$\frac{A_i RT_{mi}^2}{\alpha E_i} = e^{\frac{E_i}{RT_{mi}}} \quad (1)$$

where T_{mi} is the temperature of the maximum rate of evolution of H_2S , E_i and A_i are the activation energy and the frequency factor for the decomposition, respectively, and α is the linear rate of temperature increase. To a first-order approximation the frequency constant is independent of the group reduced and depends on the reducing agent only. Therefore;

$$A_i \cong A \cong \frac{k'T}{hQ^\ddagger} \quad (2)$$

where k' is Boltzmann's constant, h is Planck's constant, and Q^\ddagger is the partition function of the activated complex of the reducing agent. The rate of evolution of H_2S from the reduction of the i th group can be described by

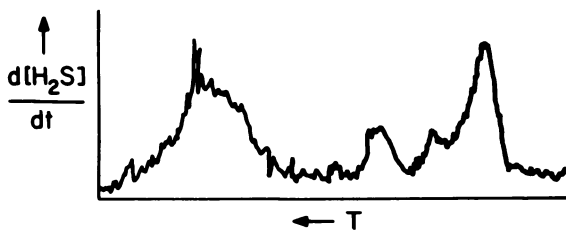


Figure 1. A typical kinetogram

$$\frac{d[\text{H}_2\text{S}]_i}{dt} = \frac{A_i}{\alpha} [\text{H}_2\text{S}]_{i0} \exp \left[-\frac{E_i}{RT} - \frac{A_i RT^2}{\alpha E_i} e^{-\frac{E_i}{RT}} \right] \quad (3)$$

where $[\text{H}_2\text{S}]_{i0}$ is the total amount of H_2S that reduction of this i th group would release. The detailed derivation of the previous equations was done by Jüntgen (5) and by Jüntgen and Van Heek (6).

4. The value of T_{mi} is a characteristic unique to the sulfur group reduced, and the area of each peak is proportional to the quantity of sulfur present in the form of the group reduced.

The implication of these discussions is that the area of the peak having a maximum at T_{mi} is proportional to the concentration of sulfur present in the sample in the form of the i th group. Therefore, quantitative determinations of the i th sulfur group can be accomplished by determining the area of each peak. Figure 1 shows a typical output graph.

Experimental

A detailed description of the experimental system will not be given here since it was recently published by Attar and Dupuis (4). A step-by-step procedure is presented in Ref. 7. The data described in this paper were derived by using an improved version of the same experimental system. The following modifications were made:

1. Stronger reducing conditions were used in order to obtain more complete reductions of the organic sulfur.
2. The sensitivity of the detector was improved.
3. The cell design was changed; it is now possible to obtain detailed analysis on a routine basis.

Results and Discussion

The distributions of sulfur functional groups (DSFG) in four types of solids are described. The four types of solids are sulfur-containing polymers with distinct sulfur functional groups; raw coals; treated coals; and iron pyrite.

The analysis of the DSFG consists of two parts: (1) the qualitative assignment of a peak of a kinetogram to a given thermal structure; and (2) determination of the quantity of each sulfur group in the coal sample.

Qualitative Identification of the Sulfur Groups. Tests of polymers with a known structure were used to identify the temperature at which each sulfur group releases its sulfur. Four polymers were tested:

1. Polyphenylene sulfide (8) as a representative of aromatic sulfides
2. Polythiophene as a representative of thiophenic sulfur
3. A copolymer produced from cyclohexene and 1, 2-ethylene dithiol (8) as a representative of aliphatic and alicyclic sulfides
4. Rubber as a representative of aliphatic sulfides and disulfides

All the polymers contained some thiolic sulfur. The results of the tests are summarized in Table I, which shows the temperature at which the apex corresponding to each functional group appears.

Sulfur-containing polymers can be used to identify the location where each sulfur group is reduced only if two conditions are fulfilled: (1) the rate of the chemical reaction controls the rate of release of H_2S , both when coal samples and when polymer samples are examined; and (2) the rate of the reduction of each sulfur functional group depends only on the hydrocarbon structures in its immediate vicinity. Table I shows the results of tests of the various polymers and the maximum temperature for each group.

Quantitative Analysis of the Concentrations of Sulfur Groups.
RECOVERY OF ORGANIC SULFUR. Quantitative analysis can be accomplished provided that all the sulfur present in the form of each group is reduced to H_2S . It is also assumed that the distribution does not change during the analysis and that all the H_2S released is detected and determined.

Each mole of sulfur, when reduced, produces 1 mol of H_2S . Therefore, the number of moles of H_2S formed during the reduction of each group is proportional to the number of moles of sulfur present in the sample in that form.

Table II shows the results of the quantitation of the kinetogram of six samples of a LVB coal with different particle sizes. The most important conclusions from these tests are the following:

1. The total recovery of organic sulfur was independent of the coal particle size used.
2. The consistency of the data from tests on the small coal particles is much better than that on the total six samples. The dimensionless standard deviation in the case of the -325-mesh particles is consistently smaller than that of the six samples.

Table I. Data on the Kinetograms of Model Sulfur Compounds^a and Polymers

Run No.	Model Compound	Sample (mg)	α ($^{\circ}\text{C}/\text{min}$)	R-SH		R-S-R		$\phi\text{-S-}$		Thiophenes		Condensed Thiophenes		% of Sulfur Accounted for
				T_m ($^{\circ}\text{C}$)	(mg/g)	T_m ($^{\circ}\text{C}$)	(mg/g)	T_m ($^{\circ}\text{C}$)	(mg/g)	T_m ($^{\circ}\text{C}$)	(mg/g)	T_m ($^{\circ}\text{C}$)	(mg/g)	
1	Benzyl sulfide	0.1	16											75
84	Rubber (chunk)	133	4		250	190-270	10.1							92
89	Rubber (ground)	101	4.5		220-280	12.5								
86	Polythiophene	61	4	170	1.29							500	9.98	
87	Polythiophene	58	4.5	185	1.85							570	6.94	
81	Polyphenylene sulfide, cross-linked	12	4.5	170		230					430			
92	Polyphenylene sulfide, low mol wt	4.3	10	160	39			320	19.7	450	221			84
93	Polyphenylene high mol wt	4.2	10	190	50.7			330	9.6	460	118			52
104	Polyethylene dithiol	10.5	9.5	190-230	28.2			290	13.	390	52.1			
105	Thianthrene	12.5	9.5	180	14.			330	4.			420	9.26	32

^a The total sulfur in each model compound was determined by the LECO rapid-combustion method.

Table II. Effect of Particle Size on the Consistency of an Analysis of Illinois No. 6 Coal, Total Organic Sulfur 3.20 wt %

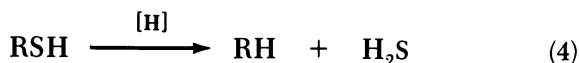
Particle Size Mesh	RSH (mg S/g coal)	ϕ SH (mg S/g coal)	RSR (g S/g coal)	ϕ -S- (mg S/coal)	Organic Sulfur Recovered (%)	Unaccounted Sulfur ^a (mg S/g coal)
-325	2.66	1.08	3.17	12.27	59.94	12.82
-325	3.20	0.99	3.90	11.72	62.16	12.11
-325	2.73	1.12	3.14	7.95	46.69	17.06
A ^b	2.86	1.13	3.43	10.65	56.26	14.00
SD ^c	0.29	0.48	0.48	2.35	8.36	2.68
SD/A	0.10	0.42	0.14	0.22	0.149	0.19
-270 + 325	1.35	0.63	3.84	9.81	48.87	16.36
-270 + 325	1.50	0.88	4.09	11.82	55.12	14.36
-200 + 270	0.69	1.63	3.11	16.78	69.40	9.79
A, All Samples	2.02	1.20	3.55	11.73	57.03	14.42
SD, All Samples	0.98	0.54	0.46	2.96	8.54	3.88
SD/A	0.48	0.45	0.13	0.15	0.15	0.27

^a In order to have all the runs made with the same heating filament in the cell, the temperature was not increased to that required to determine thiophenes. The unaccounted-for sulfur is probably thiophenic.

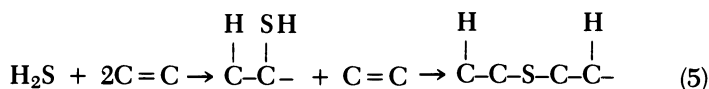
^b Average.

^c Standard deviation.

3. The concentration of aliphatic thiols, RSH, determined in the -325-mesh samples was larger than that found when larger particles were used. Moreover, large concentrations of sulfides were determined in the larger particles. This observation proves that partial transformation of thiolic sulfur to sulfidic sulfur occurs during the analysis; thiolic sulfur releasing H₂S according to



But the H₂S can be trapped in the organic matrix according to



When small particles are analyzed, the H₂S manages to escape and is detected. When large particles are analyzed, a larger portion of the H₂S is trapped according to Reaction (5) and is detected as sulfidic sulfur.

It is conceivable that the interior of large coal particles can condense and form graphitized compounds that are less susceptible to reduction. The strong reducing agent used can penetrate into smaller coal particles and inhibit the rate of condensation. While aliphatic thiols and sulfides are reduced at low temperature, before condensation commences, the reduction of thiophenes occurs simultaneously with the condensation, and, therefore, in large particles thiophenic groups could form condensed thiophenes, which are less amenable to reduction.

The recovery of sulfur from model compounds containing aliphatic thiols, thiophenes, and aryl sulfides was 94–99%.

RECOVERY OF PYRITIC SULFUR. Table III shows that a very small fraction of the pyritic sulfur is recoverable when pure crystalline iron pyrite is tested. In all the cases tested the recovery never exceeded 1–2%. Somewhat larger recovery is obtained when slow heating rates or reducing agents with smaller reducing potential are used. When strong reducing agents are used, a layer of metallic iron is believed to be formed on the surface of the iron sulfide, which prevents diffusion of the reducing species.

Small iron pyrite particles, about 1–10 μm, often are reduced more effectively than larger particles because they are less crystalline and often contain more impurities than larger particles.

Table III. The Effect of Pyrite Particle Size on the Recovery of Sulfur (7)

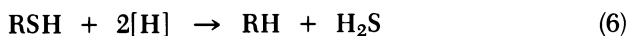
Particle Size		% Recovered ^a
mesh	microns	
-60 + 100	149-250	0.9
-100 + 120	125-149	1.9
-120 + 170	88-125	1.6
-170 + 200	77-88	1.5
-200 + 270	53-74	1.5
-270 + 325	44-53	0.9
-325	<44	2.1

^a The estimated error is $\pm 0.4\%$.

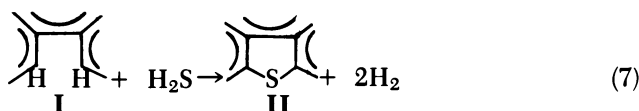
Academic Press

MODELING OF THE TRAPPING OF H₂S IN THE ORGANIC MATRIX. Lack of data on the dependence of various properties of coal on the coal composition, porosity, etc., impedes the feasibility of calculation of the fraction of H₂S that is released from the *i*th group but that is transformed to a more stable group before it is emitted from the particle and detected. However, a simple model can be used to determine which parameters may affect the trapping of sulfur in the coal.

Consider a reduction of a slab of coal in a hydrogen-donor solvent and assume that the temperature is increased linearly. The more easily reducible groups release H₂S at low temperatures. This H₂S may diffuse out of the particle and then be determined, or it may react with the organic matrix and not be detected as part of the sulfur in that group. For example, thiols release H₂S at low temperatures:



The H₂S may react with the organic matrix to form condensed thiophenes:



Let the rate of Reaction 6 be given by

$$-\frac{d[\text{RSH}]}{dt} = k_0' e^{-E_1/RT} [\text{RSH}][\text{H}] \cong k_0 e^{-E_1/RT} [\text{RSH}] \quad (8)$$

and the rate of Reaction 7 be given by

$$-\frac{d[\text{I}]}{dt} = \frac{d[\text{II}]}{dt} = k_0' e^{-E_2/RT} [\text{H}_2\text{S}][\text{I}] \quad (9)$$

It has been assumed that a large excess of reducing agent is present in the system. Material balance on a slab particle with width $2a$ yields the equation

$$\frac{\partial c}{\partial t} = D \left(\frac{\partial^2 c}{\partial r^2} \right) + k_{O_1}[\text{RSH}]e^{-E_1/RT} - k_{O_2}[\text{I}]ce^{-E_2/RT} \quad (10)$$

where c is the local concentration of H_2S .

The boundary conditions are

$$c(t, a) = 0 \quad (11)$$

$$\frac{\partial c}{\partial r}(t, 0) = 0 \quad (12)$$

and initial conditions are

$$c(t = 0, r) = 0 \quad (13)$$

$$T(t = 0, r) = T_0 \quad (14)$$

$$[\text{RSH}](t = 0, r) = [\text{RSH}]_0 \quad (15)$$

$$[\text{I}](t = 0, r) = [\text{I}]_0 \quad (16)$$

and

$$T = T_0 + \alpha t \quad (17)$$

A complete solution can be obtained only numerically. However, an analytical solution can be obtained for the isothermal process provided that the charring effect is negligible and that $[\text{I}]$ does not change much. Under these conditions one obtains

$$\frac{\partial c}{\partial t} = D \left(\frac{\partial^2 c}{\partial r^2} \right) + k_1[\text{RSH}] - k_2c \quad (18)$$

and

$$-\frac{d[\text{RSH}]}{dt} = k_1[\text{RSH}] \quad (19)$$

or

$$[\text{RSH}] = [\text{RSH}]_0 e^{-k_1 t} \quad (20)$$

So

$$\frac{\partial c}{\partial t} = D \left(\frac{\partial^2 c}{\partial x^2} \right) + k_1[\text{RSH}]_0 e^{-k_1 t} - k_2c \quad (21)$$

or, in dimensionless form;

$$\frac{\partial y}{\partial \tau} = \beta^2 \left(\frac{\partial^2 y}{\partial x^2} \right) + e^{-\tau} - \alpha y \quad (22)$$

where

$$y = \frac{c}{[\text{RSH}]_0} \quad (23)$$

$$\tau = k_1 t \quad (24)$$

$$x = \frac{r}{a} \quad (25)$$

$$\beta^2 = \frac{D}{a^2 k_1} \quad (26)$$

$$\alpha = \frac{k_2}{k_1} \quad (27)$$

and

$$y_x(0, \tau) = 0 \quad (28)$$

$$y(1, \tau) = 0 \quad (29)$$

$$y(x, 0) = 0 \quad (30)$$

Equation 22 can be solved with the boundary conditions 28, 29, and 30 by the finite Fourier transform methods by assuming a solution of the form

$$y = \sum_{m=0}^{\infty} a_m \cos \lambda_n x \quad (31)$$

$$\lambda_n = \left(\frac{2m+1}{2} \right) \pi \quad (32)$$

and

$$a_m = a_m(\tau) \quad (33)$$

The solution obtained is

$$a_m = \left(\frac{2}{\pi} \right) \left[\frac{(-1)^m + 1}{\lambda_m (\beta^2 \lambda_m^2 + \alpha - 1)} \right] [e^{-\tau} - e^{-(\beta^2 \lambda^2 + \alpha)\tau}] \quad (34)$$

Equation 34, combined with Equations 27 and 28, gives the distribution of hydrogen sulfide in the slab. The fraction of sulfur that was in the easily removable form, RSH, which is trapped as nonremovable organic sulfur, is F_s :

$$F_s = \frac{\int_0^t \int_0^a k_2 c \, dr \, dt}{a[\text{RSH}]_0} = \alpha \int_0^\tau \int_0^1 y \, dx \, d\tau \quad (35)$$

$$F_s = \sum_{m=0}^{\infty} \left(\frac{2}{\pi}\right) \left[\frac{(-1)^{m+1} \sin \lambda_m}{\lambda_m^2 (\beta^2 \lambda_m^2 + \alpha - 1)} \right] \left[\frac{(\beta^2 \lambda_m^2 + \alpha)(1 - e^{-\tau}) + e^{-(\beta^2 \lambda_m^2 + \alpha)\tau}}{\beta^2 \lambda_m^2 + \alpha} \right] \quad (36)$$

The fraction of sulfur that would have been retained had the reaction been allowed to proceed to completion is $F_{s\infty}$:

$$\begin{aligned} F_{s\infty} &= \left(\frac{2}{\pi}\right) \sum_0^{\infty} \frac{\alpha}{\lambda_m^2 (\beta^2 \lambda_m^2 + \alpha)} \\ &= \left(\frac{2}{\alpha \pi^3}\right) \sum_0^{\infty} \left[\frac{1}{(\lambda_m/\pi)^2} - \frac{1}{(\lambda_m/\pi)^2 + (\sqrt{\alpha}/\pi\beta)^2} \right] \\ F_{s\infty} &= \left[1.22283 - \left(\frac{2.46740\beta}{\alpha}\right) \tanh \left(\frac{\sqrt{\alpha}}{2\beta}\right) \right] \left(\frac{8}{\pi}\right) \\ F_{s\infty} &= 1 - 2 \sqrt{\frac{D}{k_2 a^2}} \tanh \left(\frac{1}{2} \sqrt{\frac{k_2 \alpha^2}{D}} \right) \quad (37) \end{aligned}$$

When $\alpha = 1.34 \times 10^7$ and $B = 1.578 \times 10^4$, then $F_{s\infty} = 4.5 \times 10^{-3}$ ($a = 70 \mu\text{m}$, $D = 10^{-12} \text{ (m}^2/\text{sec)}$, $k_1 = 8.2 \times 10^{-17}$, $k_2 = 1.1 \times 10^{-9}$). Equation (37) shows that the two most important dimensionless groups that determine the retention of organic sulfur are k_1/k_2 and $k_2 a^2/D$. The first relates the rate of production of H_2S to the rate of its trapping; the second relates the rate of trapping of H_2S to the rate of its diffusion out of the particle. Obviously a smaller fraction of organic sulfur will be retained when smaller particles of coal with larger diffusiveness are used.

Resolution. The evolutions of H_2S from aliphatic sulfides and from iron pyrite coincide to the extent that it was almost impossible to resolve the two peaks. However, since only a small fraction of the pyrite is reduced, it was possible to estimate the relative contribution of pyritic sulfur and sulfidic sulfur to the unresolved peaks. Somewhat better resolution was obtainable at slow rates of heating; however, in these cases the overall recovery and the signal-to-noise ratio were reduced. The dependence of the resolution between two peaks on the rate of temperature programming α is given by Equation (38):

$$\frac{dT_m}{d\alpha} = \frac{RT_m^2}{\alpha E [1 + (2RT_m/E)]} \quad (38)$$

Table IV. Sulfur Class Distribution in Five Coals (7)

Coal	Denoted by	Total S (wt %)	Pyritic S (wt %)	Sulfatic S (wt %)	Organic S (wt %)
Illinois No. 6	A	4.5	1.23	0.06	3.2
Kentucky No. 6	B	6.6	5.05	0.135	1.43
Lower Kittanning					
Martinka No. 1	C	2.20	1.48	0.12	0.60
Pittsburgh seam,					
Westland mine	D	2.60	1.05	0.07	1.48
Texas lignite	E	1.20	0.4	—	0.80

Academic Press

Resolution of about 8 min or 56°C can be obtained if the rate of heating is about 7°C/in, $E \approx 12$ kcal/mol, and $T_m \approx 350^\circ\text{C}$.

The Sulfur Distribution in Raw Coals. Table IV shows the distribution of the various classes of sulfur in five coals, and Table V shows the distribution of the organic sulfur groups in the same five coals. The results show that the content of thiols is substantially larger in lignites and HVB coals than in LVB coals. The fraction of aliphatic sulfides is approximately the same in coals with different ranks and varies around 20% of the organic sulfur. If it is accepted that all the unrecovered organic sulfur is due to thiophenes and aromatic sulfides, then the data indicate clearly that a larger fraction of the sulfur is present in the form of thiophenic sulfur in higher-ranked coals than in lower-ranked coals. The accepted theory on the H-C structure of coal is that higher-ranked coals are more condensed than lower-ranked coals. It should not be surprising, therefore, that the sulfur groups are also more condensed, i.e., more thiophenic, in higher-ranked coals than in lower-ranked coals.

The Sulfur Distribution in Treated Coals. Various treatments are known to be selective to specific sulfur groups. Therefore, it was interesting to examine the kinetograms of treated coals. Three treatments are described: oxidation with H_2O_2 , removal of the alkaline minerals with HCl, and methylation of the coal with methyl iodide.

Table V. Distribution of Organic Sulfur Groups in Five Coals (7)

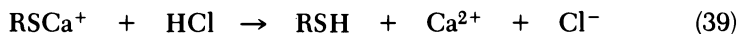
Coal	% Organic S Accounted	Thiolic	Thiophenolic	Aliphatic Sulfide	Aryl Sulfide	Thiophenes ^a
A	44	7	15	18	2	58
B	46.5	18	6	17	4	55
C	81	10	25	25	8.5	21.5
D	97.5	30	30	25.5	—	14.5
E	99.7	6.5	21	17	24	31.5

^a Corrected for unaccounted-for sulfur. C and E are calculated on total sulfur content.

Academic Press

OXIDATION. Mild oxidation of coal with acidic solutions of hydrogen peroxide or nitric acid dissolves the iron pyrite and converts the thiols to sulfuric acid. Some organic functional groups oxidize to the corresponding sulfides, sulfonic acids, and sulfones (9). However, in general, the latter process requires strong oxidizing conditions. From the analytical point of view one might think that it is not important whether the organic sulfur groups are oxidized, since the reducing agent used converts them back very rapidly to the nonoxidized form. Therefore, the results of the analysis will not differentiate between the reduced and the oxidized form of a sulfur group. In other words, oxidation could have been used to remove the interference from pyrite without much effect on the determination of the other sulfur groups. However, oxidation appears to increase the resistance to mass transport and thus to reduce the resolution. Figure 2 shows the kinetograms of two coal samples analyzed for the U.S. Department of Energy. Figure 2(a) shows the original coal; Figure 2(b) shows an oxidized sample. The results show that the oxidation did not remove any organic sulfur, although the pyritic sulfur was removed. The signals, however, are much less resolved in the oxidized sample than in the raw coal.

HCl TREATMENT. Dilute HCl dissolves the organic salts of calcium, magnesium, and iron and their carbonates. Since some H_2S can react with basic calcium and iron salts, it was desired to examine the effect of HCl treatment on the kinetogram. Figure 3 shows the kinetograms of raw coal and HCl-extracted coal. The most important difference between the kinetograms is that the second peak due to thiophenols disappeared and the thiols peak increased. It is plausible that some of the sulfur that is determined as thiophenolic is indeed thiolic. Thiols can bind calcium as calcium thiolates, which may require a larger activation energy for reduction than thiols. HCl treatment replaces the calcium with hydrogen and converts the thiolates into thiols:



TREATMENT WITH METHYL IODIDE. Samples of Illinois No. 6 were treated with methyl iodide, CH_3I , and the products were analyzed by using two methods: the method of Postovski and Harlampovich (10) for thiols and aliphatic sulfides, and our thermokinetic method. The results of the groups analyses are described in Table VI. The results show that only a very small fraction of the organic sulfur is indeed accounted for by the CH_3I method, and therefore the value of this method as an analytical tool is questionable.

The kinetograms of an untreated but demineralized sample and that of a sample treated with CH_3I are shown in Figure 4. The data show that the methyl iodide treatment results in lower recovery of organic sulfur and in a change in its distribution. In particular, some of the

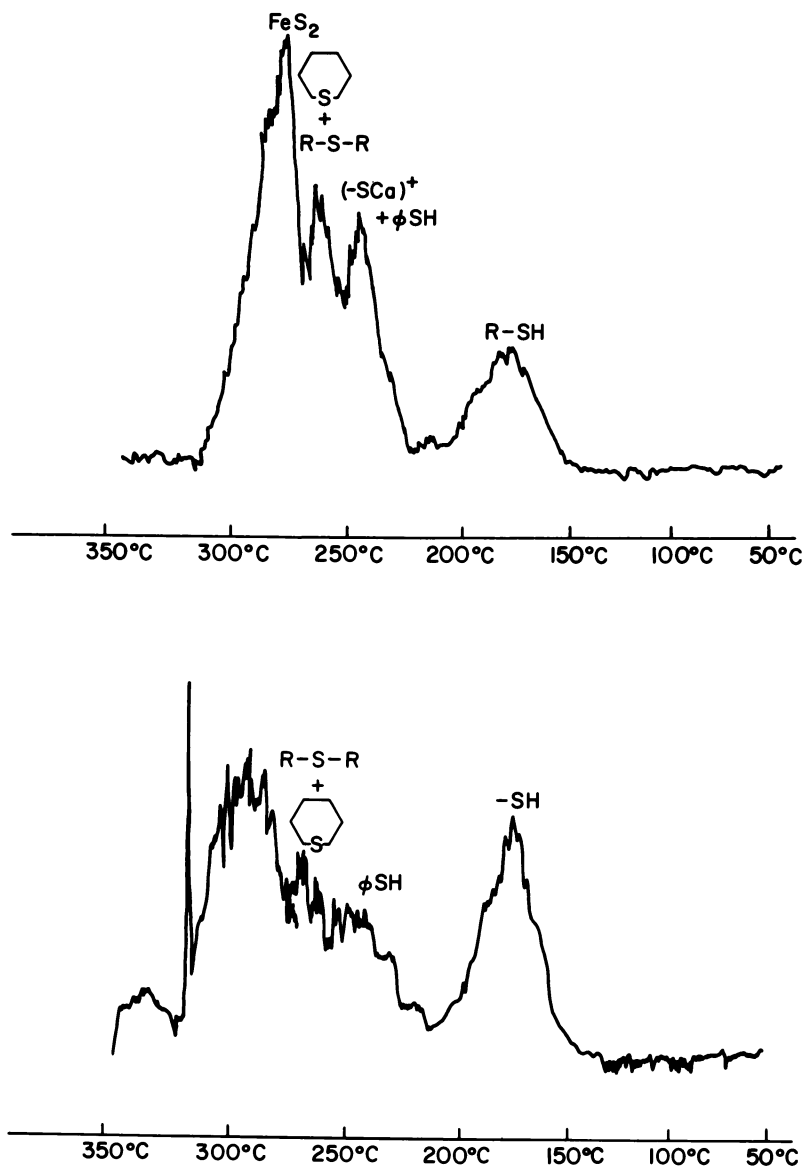


Figure 2. Kinetograms: (top) raw coal; (bottom) oxidized (7)

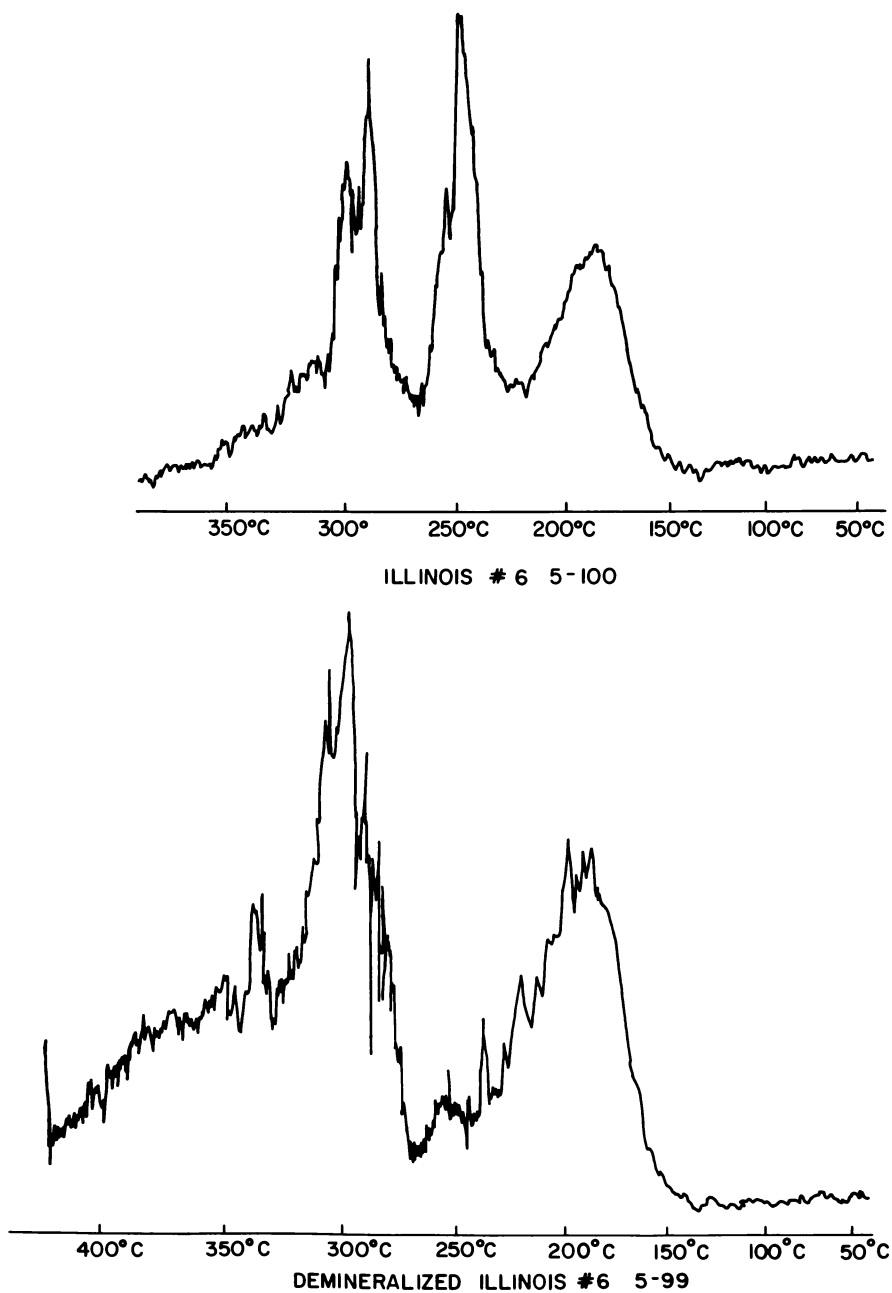


Figure 3. Kinetograms: (top) raw coal; (bottom) HCl-extracted coal

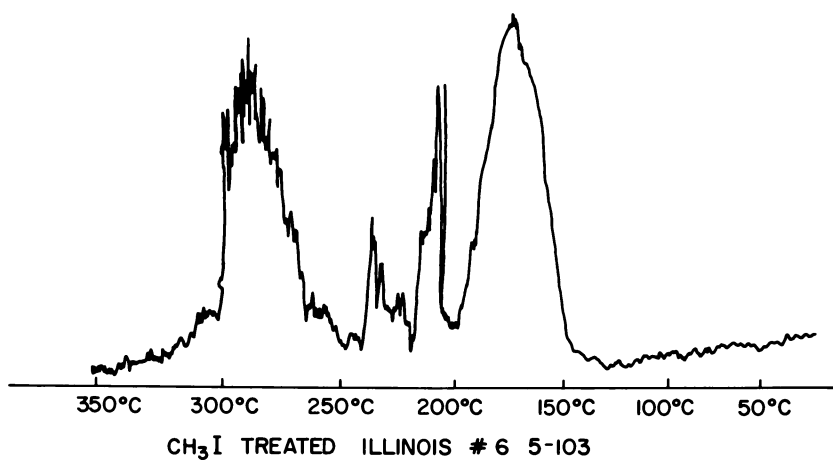
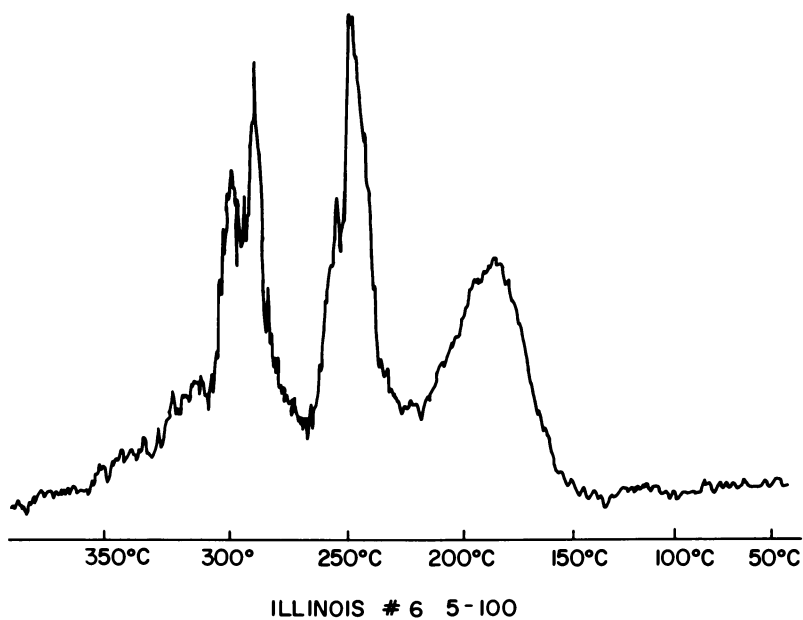


Figure 4. Kinetograms: (top) raw coal; (bottom) CH₃I-treated coal

Table VI. Analysis of Illinois No. 6 Coal by the CH₃I Method by Thermokinetics

	<i>Method of Analysis</i>									
	LECO		ASTM		DSG		CH ₃ I		DSG on CH ₃ I-Treated Coal (No. 10)	
	%	mg/g	%	mg/g	%	mg/g	%	mg/g	%	mg/g
Total sulfur	4.5	45								
Sulfatic sulfur			0.04	0.4						
Pyritic sulfur			1.23	12.3	4.81	0.6				
Organic sulfur										
-SH						6.1	1.36			8.6
φ-SH						8.5				3.45
R-S-R						8.6	0.96			8.0
φ-S-φ						4.3				
Total organic recovered			3.23	32.3	85.1	27.5	7.2	2.32	62.1	20.05

sulfur that is originally detected as aromatic thiols is apparently alkylated and becomes aromatic sulfides. However, the alkylation also must reduce the rate of mass transport, since the thiophenes and aromatic sulfides are not visible in the kinetogram of the treated coal.

Implications to Coal Desulfurization

It is widely recognized today that coal desulfurization efficiency depends on the distribution of sulfur in the original coal to pyritic and organic sulfur. Pyritic sulfur can be desulfurized, but it is more difficult to remove organic sulfur.

However, preliminary data show that part of the organic sulfur can be desulfurized easily. In particular, the thiolic sulfur and part of the sulfidic sulfur can be desulfurized easily. Therefore, the authors suggest that coals with excess organic sulfur be divided into two groups: coals that can be desulfurized easily, in which most of their organic sulfur is thiolic, and coals that cannot be desulfurized easily, in which most sulfur is nonthiolic. Thus thermokinetic tests can be used to screen coals and to determine the process in which they can be utilized.

Acknowledgment

The authors wish to thank Exxon Education Foundation, Dow Chemical Company, Phillips Petroleum, and the U.S. DOE Grant No. DE-FG01-79ET14306 for their support of this work. The helpful comments of S. Taylor, S. Friedman, and A. Dietz particularly are appreciated.

Literature Cited

1. Attar, A. *Chem. Eng. Prog. Tech. Manual*, "Coal Processing Tech.", 1978, 4, 26-34.
2. Attar, A.; Corcoran, W. H. *Ind. Eng. Chem., Prod. Des. Dev.* 1977, 16(2), 168.
3. Attar, A. *Fuel* 1978, 57, 201.
4. Attar, A.; Dupuis, F. *Am. Chem. Soc., Div. Fuel Chem. Prepr.* 1978, 23(2), 44.
5. Jüntgen, H. *Erdoel Kohle* 1964, 17, 180.
6. Jüntgen, H.; Van Heek, K. H. *Fuel* 1968, 47, 103.
7. Attar, A. "Analytical Methods for Coal and Coal Products"; Karr, C., Jr., Ed.; Academic: New York, 1979; Vol. 3, Chapter 56.
8. Phillips Petroleum, personal communication.
9. Attar, A.; Corcoran, W. H. *Ind. Eng. Chem., Prod. Des. Dev.* 1978, 17(2) 102.
10. Postovski, J. J.; Harlampovich, A. B. *Fuel* 1936, 15, 229.

RECEIVED July 19, 1979.

Chemical Structure of Heavy Oils Derived from Coal Hydrogenation Determined by Mass Spectroscopy

S. YOKOYAMA, N. TSUZUKI, T. KATOH, and Y. SANADA
Coal Research Institute, Faculty of Engineering, Hokkaido University,
Sapporo, 060, Japan

D. M. BODILY and W. H. WISER
Department of Mining and Fuels Engineering, University of Utah, Salt Lake
City, UT 84112

The heavy oil from coal hydrogenation was separated by gradient elution chromatography and gel permeation chromatography (GPC) and analyzed by low-ionization-potential mass spectroscopy to determine compound types and molecular weights. The mass spectroscopy results confirm the effectiveness of the chromatographic separations. One-ring aromatic compounds contain from zero to 3 naphthenic rings and up to 35 alkyl carbons. Two-ring aromatic compounds contain from zero to 2 naphthenic rings and up to 15 alkyl carbons. Three- and four-ring aromatic compounds contain mostly zero or one naphthenic ring and up to 12 aliphatic carbons. These results agree with the structures previously determined by ^1H and ^{13}C nuclear magnetic resonance (NMR) measurements. The samples analyzed represent 30% of the heavy oil from coal hydrogenation or 10% by weight of the original coal. Polar fractions were not analyzed. The relation between GPC and molecular weight and the ionization efficiencies in mass spectroscopy are different for each hydrocarbon type. Analysis of whole-oil samples is complicated by these differences in response from different hydrocarbon types.

Hheavy oil derived from coal hydrogenation consists of many complicated hydrocarbon and nonhydrocarbon compounds. Consequently, the elucidation of the chemical structure is extremely difficult and time-

consuming but is of importance in understanding liquefaction mechanisms, in elucidating coal structure, and in selecting processes for upgrading coal liquids. The chemical structure of coal liquids has been investigated mainly by means of ^1H and ^{13}C NMR techniques, or a combination thereof, to determine statistically average structures. The technique of mass spectrometry for structural analyses of coal liquids is advantageous in gaining information on the individual compounds, the distribution of molecular weights, and the carbon numbers of homologous compound types (1–4). A combination of adsorption liquid chromatography (LC) and GPC developed by the U.S. Bureau of Mines (USBM) API Project 60 (5) for the separation of heavy oils into compound types and by molecular size is an appropriate sample preparation procedure for mass analyses. Molecular ionization efficiencies are assumed to be approximately the same for components of respective LC–GPC subfractions, inasmuch as they contain similar compound types with narrow molecular weight distributions.

Heavy oils derived from petroleum were separated by using the method developed by the USBM–API (5) Project 60 and analyzed by means of mass spectroscopy. The procedure used for separation and characterization of petroleum heavy oil was adopted to study heavy oil from coal liquids derived from Char-Oil-Energy-Development (COED) Syncrude from Utah coal (6) and western Kentucky coal (7) and Synthoil from West Virginia coal (1, 8).

In this study the USBM–API separation procedure was modified slightly. Monoaromatic and diaromatic compound types were eluted with specific solvents from an adsorption column. A three- to four-ring aromatic fraction was also desorbed with a stronger eluant. These fractions were separated on the basis of the carbon number of alkyl substituents by GPC. The subfractions obtained from LC and GPC separations were analyzed by mass spectroscopy. This technique provides a method of determining the chemical structure of coal liquids, which is complementary to NMR techniques (9).

Experimental

Heavy Oil Preparation and Separation. Hydrogenation of Hiawatha, Utah, coal [C: 72.0; H: 5.6; N: 1.7; S: 0.90; O: 19.8; dry, ash-free (DAF) %] was performed at a reaction temperature of 510°C and 12.4-MPa hydrogen pressure with ZnCl_2 impregnated on the coal as catalyst in an entrained-flow, tubular coil reactor (10). The reaction products were trapped in three reservoirs connected to the reactor in series and were separated according to their condensability. Heavy-oil products collected in the first reservoir, nearest to the reactor, were used in this study.

Separation procedures are shown in Figure 1. The yield of heavy oil was 31.3% by weight of the coal. The entire heavy-oil product was extracted with benzene to separate benzene-insoluble residue and benzene-soluble portions. In the next step the benzene-soluble portion was washed with 10% NaOH and 15%

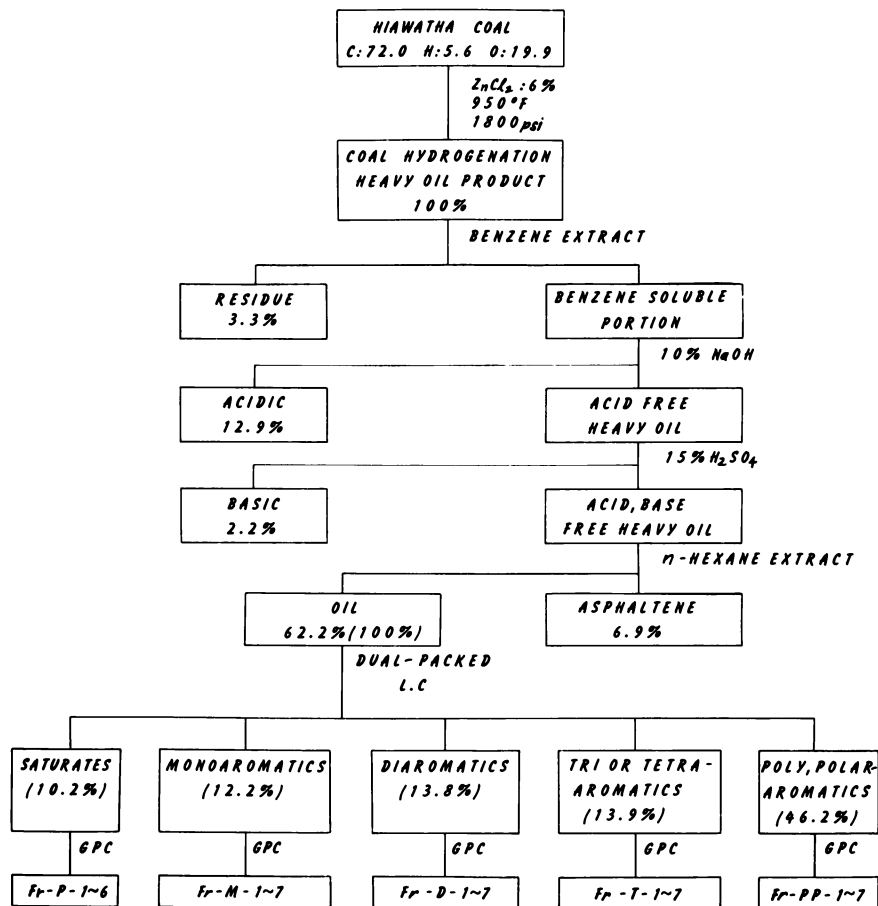


Figure 1. Separation scheme

aqueous H_2SO_4 solutions for the removal of the acidic and basic components. A neutral oil was obtained. The neutral heavy oil was separated into oil and asphaltene by Soxhlet extraction with *n*-hexane. The oil portion was separated through dual-packed, silica-alumina adsorption columns developed by the USBM-API Project 60 (5), modified partly to elute with 30% cyclohexane and 70% benzene for the separation of three- and four-aromatic-ring compounds as a separate fraction. The neutral heavy oil thus was separated into saturated hydrocarbons (Fr-P), monoaromatic (Fr-M), diaromatic (Fr-D), three- and four-aromatic rings (Fr-T), and polyaromatic-polar compounds (Fr-PP). Elution conditions are shown in Figure 2. The fractions M, D, and T were separated further according to molecular size into seven fractions by GPC columns packed with Bio-beads S-X4 and S-X8 and benzene as a solvent.

Measurement by Mass Spectroscopy. Mass spectra of the GPC subfractions, Fr-M, D, and T, were obtained by a low-resolution and low-ionization voltage (10 eV) method using gas chromatography-mass spectroscopy (GCMS) techniques for Fr-M-3 to 7 and Fr-D-3 to 7 and by a direct insert technique for high-

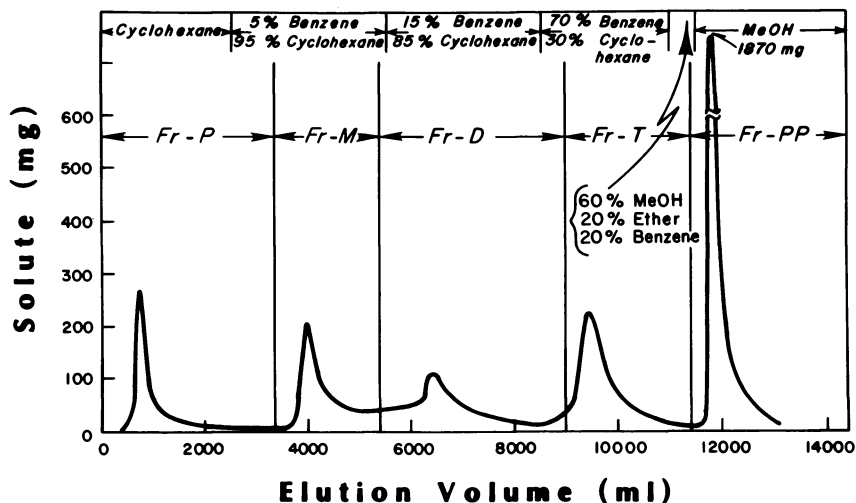


Figure 2. Elution curve from LC

molecular-weight fractions Fr-M-1 and 2, Fr-D-1 and 2, and Fr-T-1 to 7. Mass spectra were obtained with a Hitachi M-52 GCMS spectrometer. The GC column conditions were temperature programming at $2^{\circ}\text{C}/\text{min}$, starting at 100°C and holding at 200°C . A glass capillary column, 15 m in length, coated with OV-101 was used. The mass spectrometer scanned repeatedly at 6- or 10-sec intervals of time during the appearance of the ions while checking the total ion monitor. From 50 to 800 multiple mass spectra of the respective LC-GPC subfractions were measured to obtain the gross mass spectral data for complicated mixtures. The mass spectra were treated by computer (Hitachi, HITAC 10 II) to calculate integrated mass spectra. The samples were expected to be eluted completely from the GC column and vaporized in the source of the mass spectrometer, although this was not confirmed experimentally.

Results and Discussion

Chromatographic Separation. The LC elution curve is shown in Figure 2, and the elution range of individual fractions designated Fr-P, M, D, T, and PP are indicated. Elution curves from GPC and the range of elution volume for GPC subfractions are shown in Figure 3.

Each series of LC-GPC subfractions was investigated previously by ^1H and ^{13}C NMR methods and was found to have approximately mono-, di-, and tri- and/or tetraaromatic derivatives for Fr-M, D, and T, respectively, as the average structural units (9). It was confirmed also that values of aromaticity increase gradually with the increasing GPC fraction number from 1 to 7 within each subfraction; the value is largest for the T series and smallest for the M series at equivalent elution volumes. From the results described above, the separations by LC and GPC according to

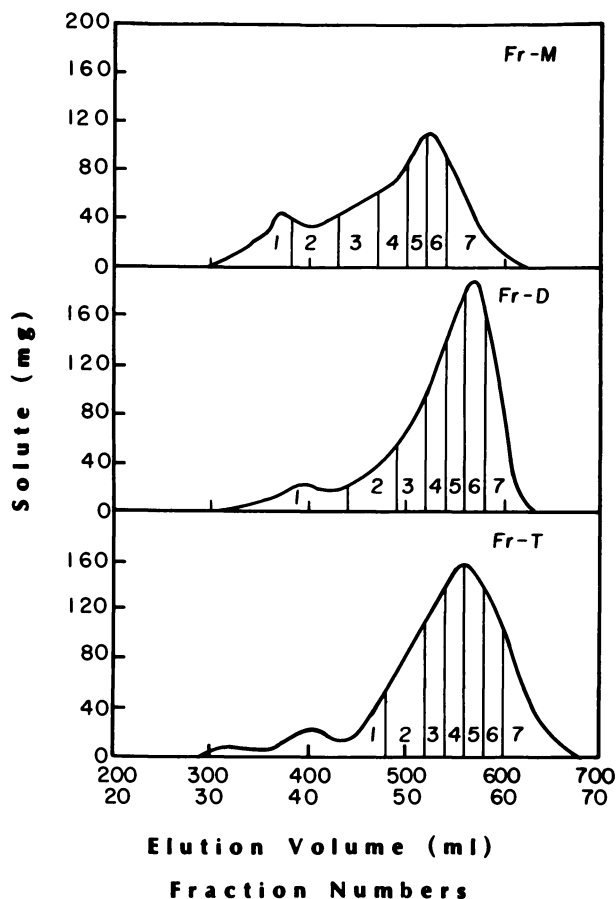


Figure 3. Elution curves from GPC

compound types and molecular size were assumed to be satisfactory. The LC-GPC subfractions are found to be suitable as samples for mass analyses since the difference in the molecular ionization efficiencies is not large among individual compounds of the same subfraction because of the resemblance of the homologous aromatic ring classes and their narrow molecular weight distributions.

Integral Mass Spectra of LC-GPC Subfractions. The heavy oil from coal liquids consists of numerous components with wide differences in boiling point. The size of molecular ions changes progressively with the GC retention time or with the residence of the sample in the ion source for the direct injection method. Mass spectra were measured repeatedly at short interval times. The sum of these spectra represents the whole

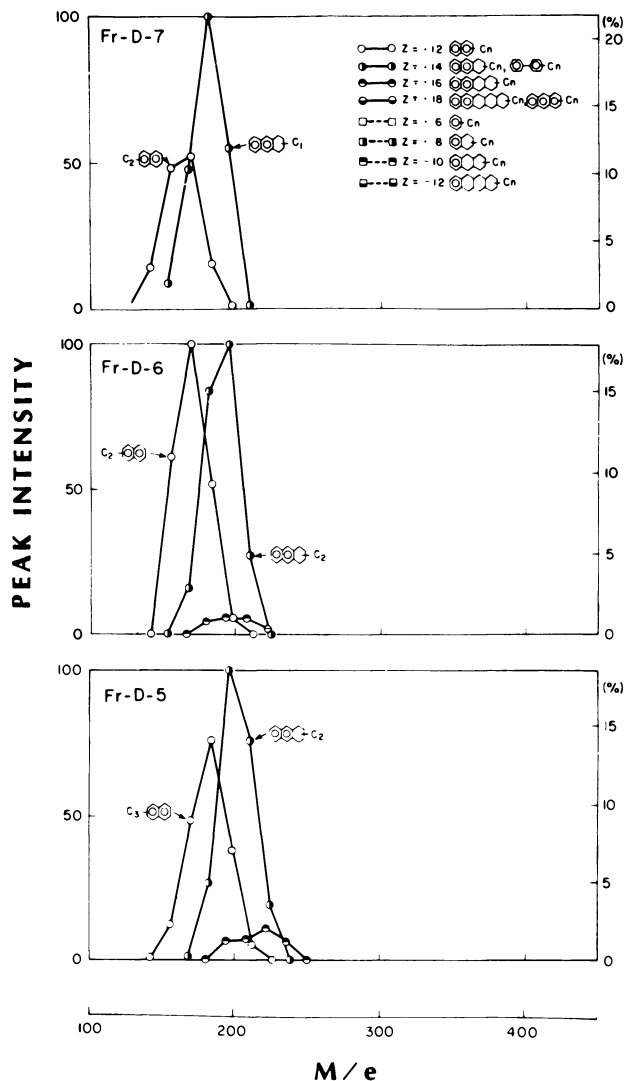


Figure 4. Distribution of peak intensities for diaromatic compounds of different Z number

sample. Integral mass spectra were obtained by summation of the peak intensities at the various mass-to-charge ratios, m/e . Integral mass spectra for the D series are shown in Figure 4. The distribution of compound types is shown as a function of mass-to-charge ratio for each LC-GPC subfraction.

In the low-energy ionization method employed, major ion peaks observed were mostly parent ion and isotopic ion ($P + 1$) peaks, while minor peaks corresponded to fragments such as $P - 1$, indicating that cleavage of the molecules was minor. Subfractions D-1 and T-1 have

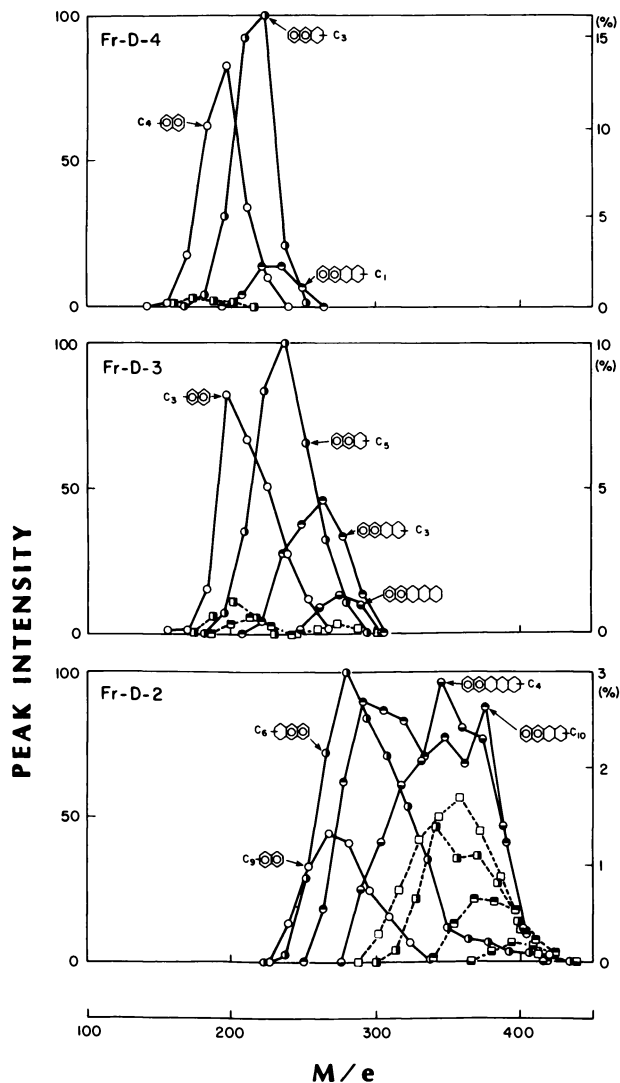


Figure 4. Continued

high molecular weight due to large aliphatic substitution. Their spectra show predominant fragment peaks at odd mass numbers in the lower mass range. Therefore, the data from these fractions were not included in this report.

The mass distribution from integrated mass spectra for subfractions of series D moves gradually from low molecular weight for Fr-D-7 to higher molecular weight for Fr-D-2. The subfractions of the other series also were observed to follow this relationship between the mass range and the elution volume.

Number average molecular weights were calculated from the m/e values and peak intensities of parent peaks for each of the compound types. In Figure 5 average molecular weights measured by vapor pressure osmometry (VPO) are compared with those calculated from mass analyses. The correlation is good except for one point that deviates from the line at the higher molecular weights. However, the slope of the line is greater than one. This is an indication of underestimation of the molecular weight from mass analyses due to low volatilization of parts of the higher-molecular-weight fractions or high VPO molecular weights due to association in solution. With increasing subfraction numbers for Fr-M, D, and T, the average molecular weight diminishes progressively from about 400 or 500 to 200, indicating a satisfactory fractionation by GPC.

The molecular ionization efficiency is different for each series of compound types (mono-, di-, triaromatic, etc.). The ionization efficiency

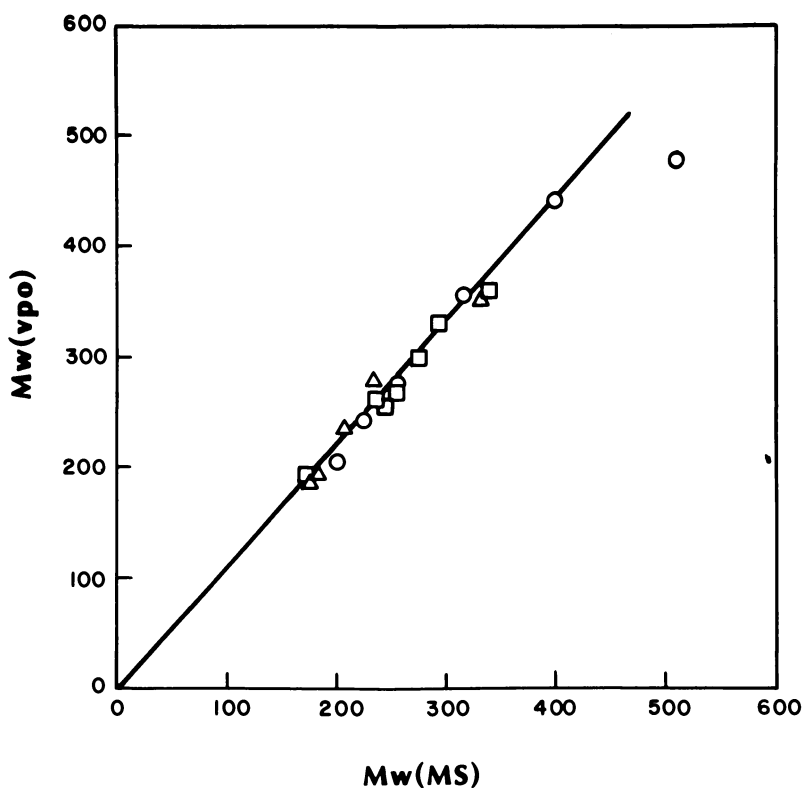


Figure 5. Comparison of molecular weights from VPO and MS (○) Fr-M; (△) Fr-D; (□) Fr-T

increases with increasing number of aromatic rings and decreases with molecular weight (11). As described previously, the preparation of these samples provides a narrow distribution of saturated carbons attached to aromatic ring systems. The results of molecular weight measurements by VPO and mass analysis support this conclusion. It may be presumed that the molecular ionization efficiency is not very different for the individual compounds constituting one LC-GPC subfraction. On the other hand, the molecular ionization efficiency for the different LC-GPC subfractions may be assumed to be quite different because of the difference in compound type and molecular weight. The problem of different efficiency for LC-GPC subfractions in quantitative analyses of the whole fraction can be resolved by calculating the weight percent yield for each LC-GPC subfraction and the molecular weight derived by mass analyses for each respective subfraction.

Compound Type Analyses of LC-GPC Subfractions. Deficiency of hydrogen number (Z values) in the formula $C_N H_{2N+Z}$ for parent peaks can be used to predict the type of compound. By assuming that the molecular ionization efficiency is approximately the same for compounds constituting the same LC-GPC subfraction, the total content of aromatic compound types in fractions M, D, and T was estimated semiquantitatively by summing the content of each GPC subfraction. The distribution of various compound types is shown in Figure 6. The distribution is calcu-

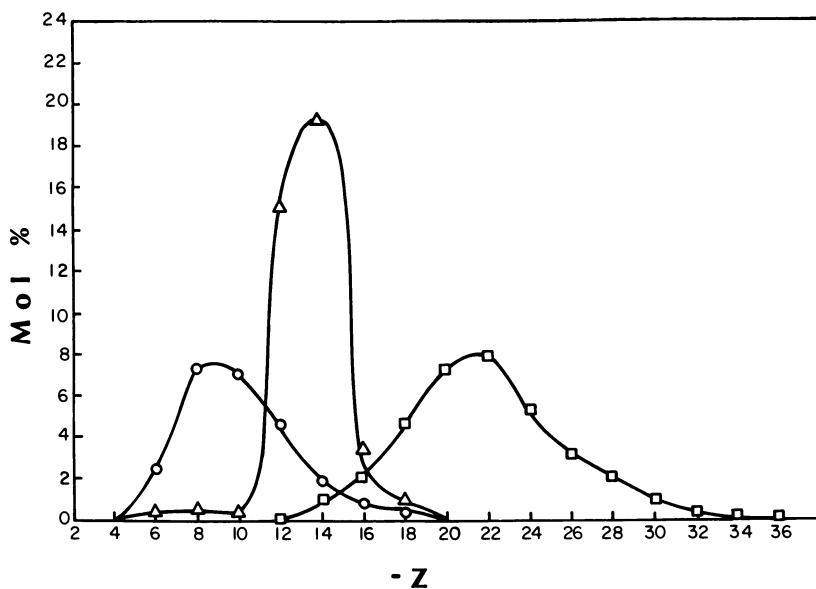


Figure 6. Distribution of hydrocarbon types for LC fractions (O) Fr-M; (Δ) Fr-D; (\square) Fr-T

lated by using the peak intensities to calculate the mole fraction of hydrocarbon types corresponding to each Z number for each subfraction. The mole fraction of hydrocarbon type and the weight fraction of the subfraction are used to calculate the mole fraction of each hydrocarbon type in the whole fraction. Hydrocarbon types for the M series are assigned mainly to alkylbenzenes ($Z = -6$), alkylmononaphthenobenzenes ($Z = -8$), and alkylindanaphthenobenzenes ($Z = -10$). The types of the D series are assigned to alkylnaphthalenes ($Z = -12$), alkylmononaphthenonaphthalenes ($Z = -14$), and alkylindanaphthenonaphthalenes ($Z = -16$). Those of the T series are assigned to alkylphenanthrene or alkylanthracene ($Z = -18$), alkylpyrene ($Z = -22$), alkylchrysene, ($Z = -24$) and naphthenologues ($Z = -20-26$). It can be concluded from the results of mass analyses for hydrocarbon type distributions that separation according to aromatic ring number by means of the modified USBM-API procedure is satisfactory.

The number of naphthenic rings in aromatic compounds is determined by the assignment of Z values, where every naphthenic ring indicates a deficiency of two hydrogens. The distribution of compound types indicates that monoaromatic compounds consist largely of mono-

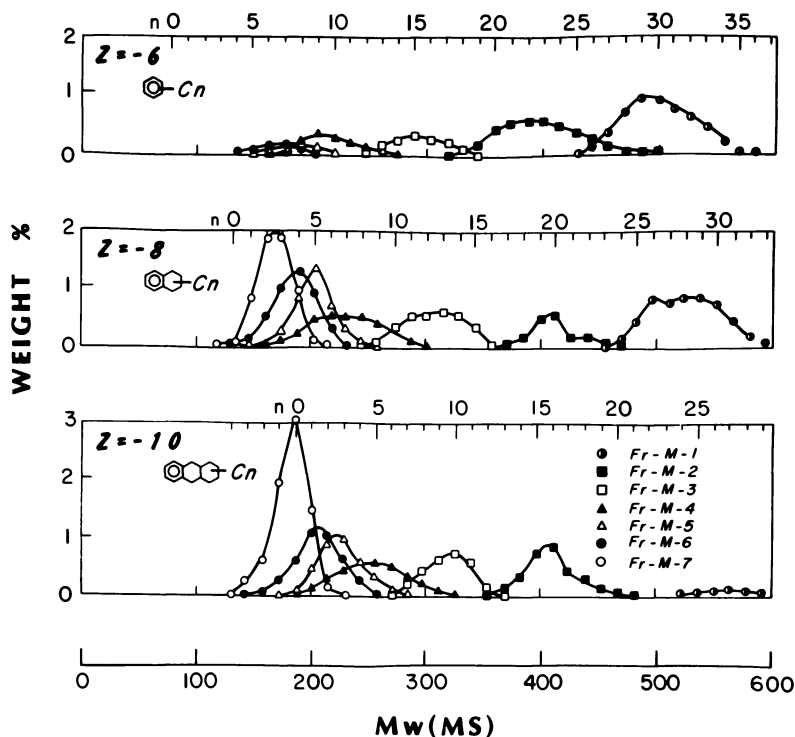


Figure 7. Distribution of hydrocarbon types for monoaromatic subfractions

di-, and trinaphtheno structures, that diaromatic compounds have an intermediate degree of naphthenic structures, and that tri- and tetra-aromatic compounds have a lesser degree of naphthenic structures. The number of naphthenic rings decreases with increasing aromatic ring number.

Alkyl Carbon Distribution in Compound Types. The Z values of parent peaks in the integrated mass spectra for individual LC-GPC subfractions were used to obtain the distribution of alkyl carbon in respective hydrocarbon types. In Figures 7, 8, and 9 the distribution of molecular weights or alkyl carbon numbers for the same Z values are plotted for the M, D, and T series. The range of alkyl carbon numbers increases progressively for GPC fractions 7 to 1 for the respective hydrocarbon types. Therefore, the GPC separations of various hydrocarbon types were confirmed by mass analyses to have been according to molecular size. It can be seen that Fr-M consists of compounds with large alkyl group substitution, which reaches 35 carbons for the $Z = -6$ series; this result indicates a lower aromaticity for series M. Increasing the naphthenic ring structure shifts the distribution of alkyl carbon numbers

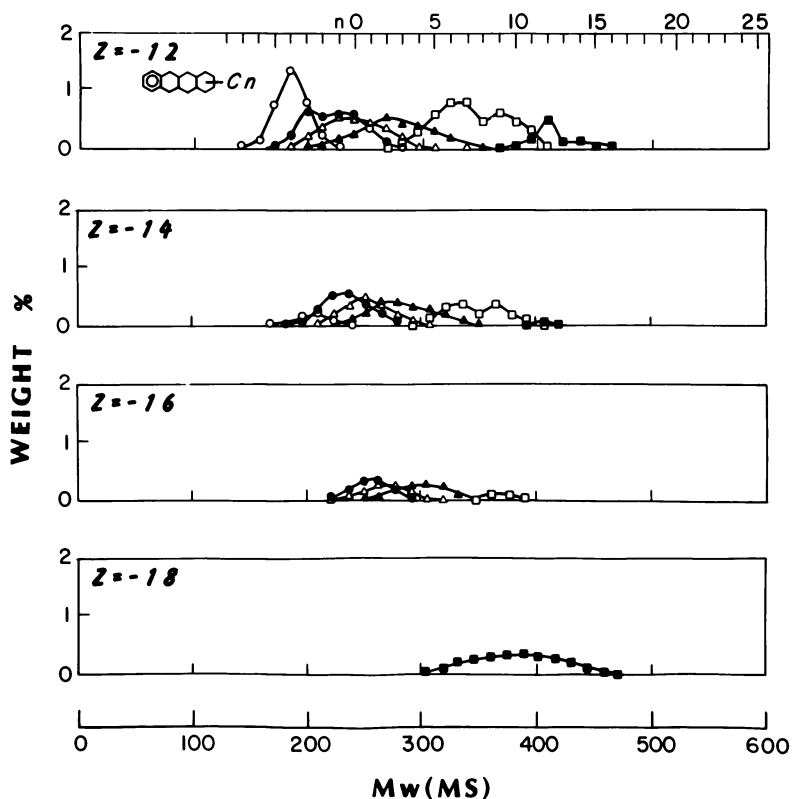


Figure 7. Continued

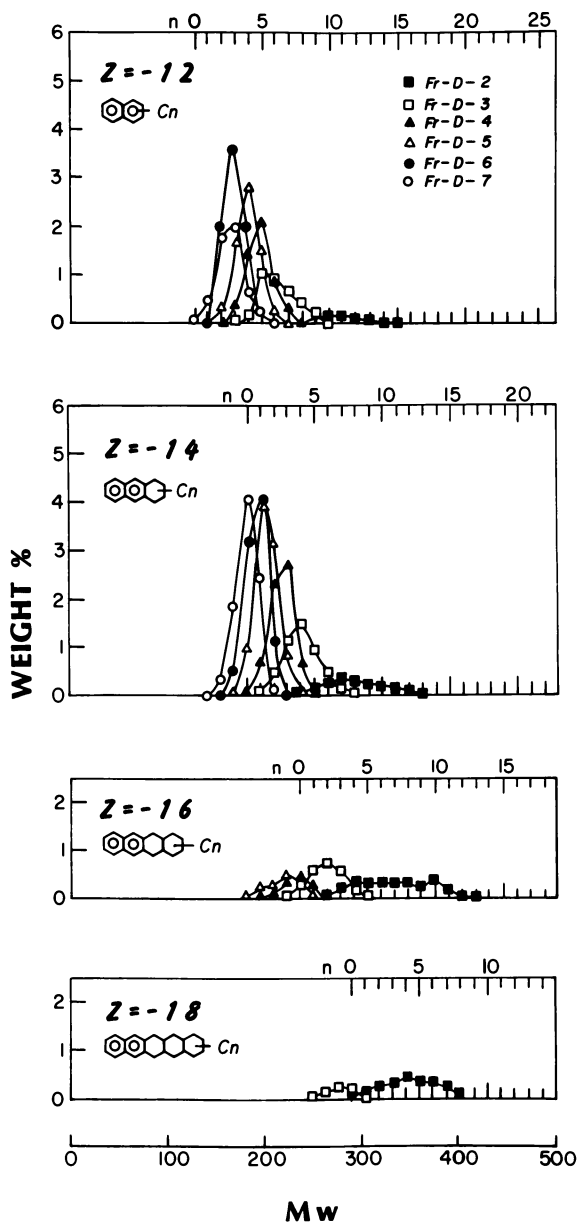


Figure 8. Distribution of hydrocarbon types for diaromatic subfractions

to lower values. The distribution of alkyl carbon numbers of series T has a range from zero to approximately 12, indicating a higher aromaticity. This result is in agreement with the results derived from ^1H NMR structural analyses (9). In the case of series D this distribution of alkyl carbon numbers is from zero to about 15, indicating an intermediate value of aromaticity in comparison with series M and T.

Molecular Weight Distributions. Information on the molecular weight distribution of coal-derived oils is important in evaluating the characteristics of chemical structure, since degradation of the macromolecular coal structure results in complicated molecular species. The GPC technique for elucidation of the molecular weight distribution of polymer compounds is applied widely. The application of GPC to the heavy oil derived from coal and petroleum is performed for sample preparation and chemical characterization. Actual distributions cannot be derived from the GPC elution data because each hydrocarbon type has a different elution behavior.

The molecular weight distributions for whole fractions M, D, and T were constructed by summation of the peak intensities of the parent peak for all GPC subfractions shown in Figures 7, 8, and 9. These are shown with the solid lines in Figure 10. The GPC elution curves corresponding to molecular weight distribution for series M, D, and T are shown in the same figures for comparison. The results derived from mass analyses for series D and T do not include the data of Fr-D-1 and Fr-T-1 because of the uncertainty of the results of mass analyses for these subfractions, as explained previously. A slight discrepancy is recognized in the high-molecular-weight range. The agreement between both distribution curves obtained by different methods is quite satisfactory. However, the relationship between molecular weight and GPC elution volume must be adjusted for the different correlation factors for different compound types due to differences in molecular volume-weight relationships. Molecular weight-elution volume correlations for the M, D, and T series were obtained by comparison of molecular weights derived from mass analyses and the elution volume for each GPC subfraction. The results are shown in Figure 11. The correlations are different for each series.

GPC Elution Behavior for Aromatic Compound Types. To predict molecular weight and the chemical structure of fractions separated by GPC, we must understand the elution behavior for characteristic compound types. However, it was very difficult to gain information on these relations because of the limited studies on coal products. Dooley and co-workers (12, 13) extensively studied GPC mass correlations for petroleum heavy oil.

If coal liquids can be used as the reference compounds for calibration, useful GPC correlations for various compound types are obtained. Molecular weight at the maxima in the distributions of compound types with

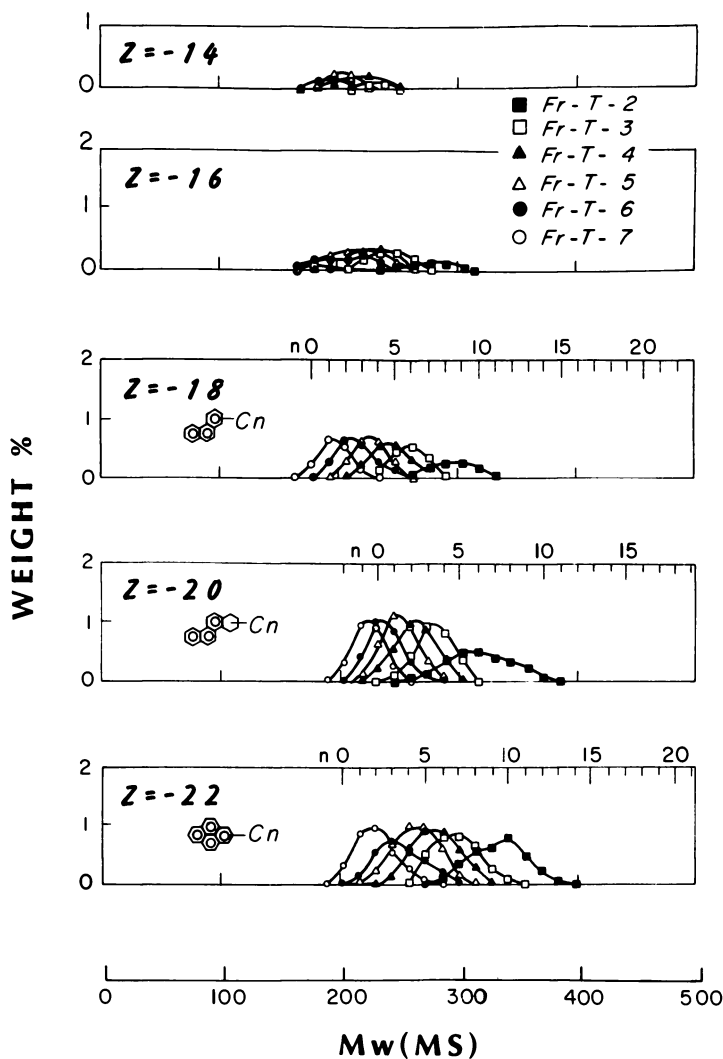
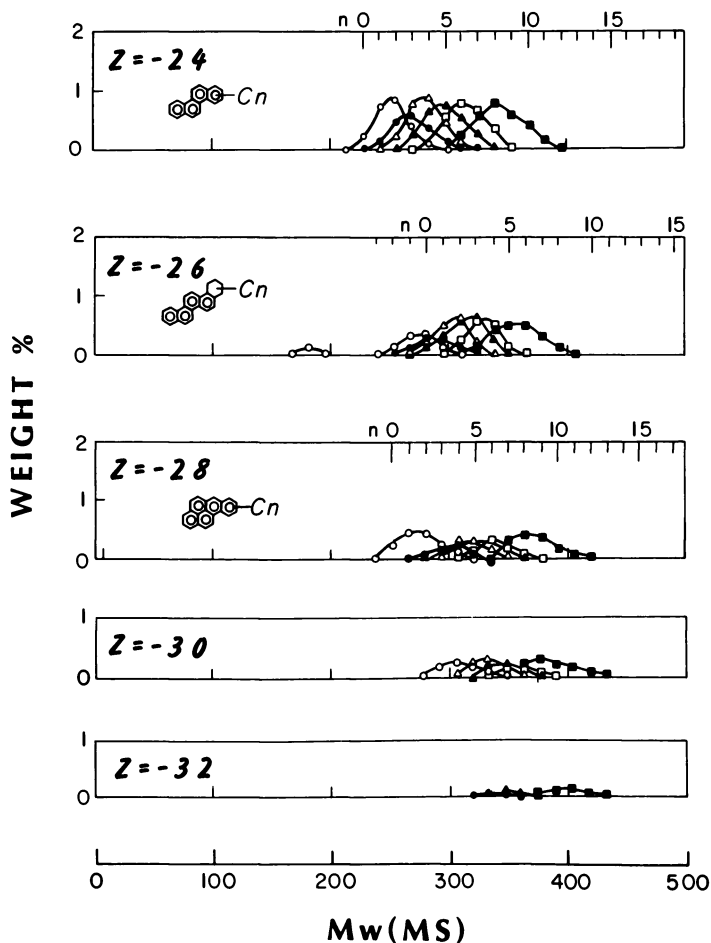


Figure 9. Distribution of hydrocarbon types for tri- and tetraaromatic subfractions

different alkyl carbon numbers, shown in Figures 7, 8, and 9, was compared with the elution volume for corresponding GPC subfractions. The correlations between the two are shown in Figure 12. These GPC mass correlations may be useful in relating GPC data to molecular weights.

Conclusions

Low-ionization-potential mass spectroscopy is an effective technique for analyzing the hydrocarbon content of coal-derived liquids. Approx-

Figure 9. *Continued*

imately 30% of the heavy liquid (10% by weight of the coal) was analyzed by this method. The acidic, basic, polyaromatic-polar, and asphaltene fractions are more difficult to analyze because of the higher heteroatom content and higher molecular weights.

The average molecular weights calculated from mass spectra correlate with those determined by VPO. The slight differences in absolute values indicate either an underestimation of mass spectral molecular weights arising from limited vaporization of the higher-molecular-weight molecules or an overestimation of VPO molecular weights caused by association in solution. GPC is effective in separating subfractions of specific compound types by molecular weight. Correlation factors relating GPC elution volume and molecular weight can be estimated by the use of mass spectral molecular weights.

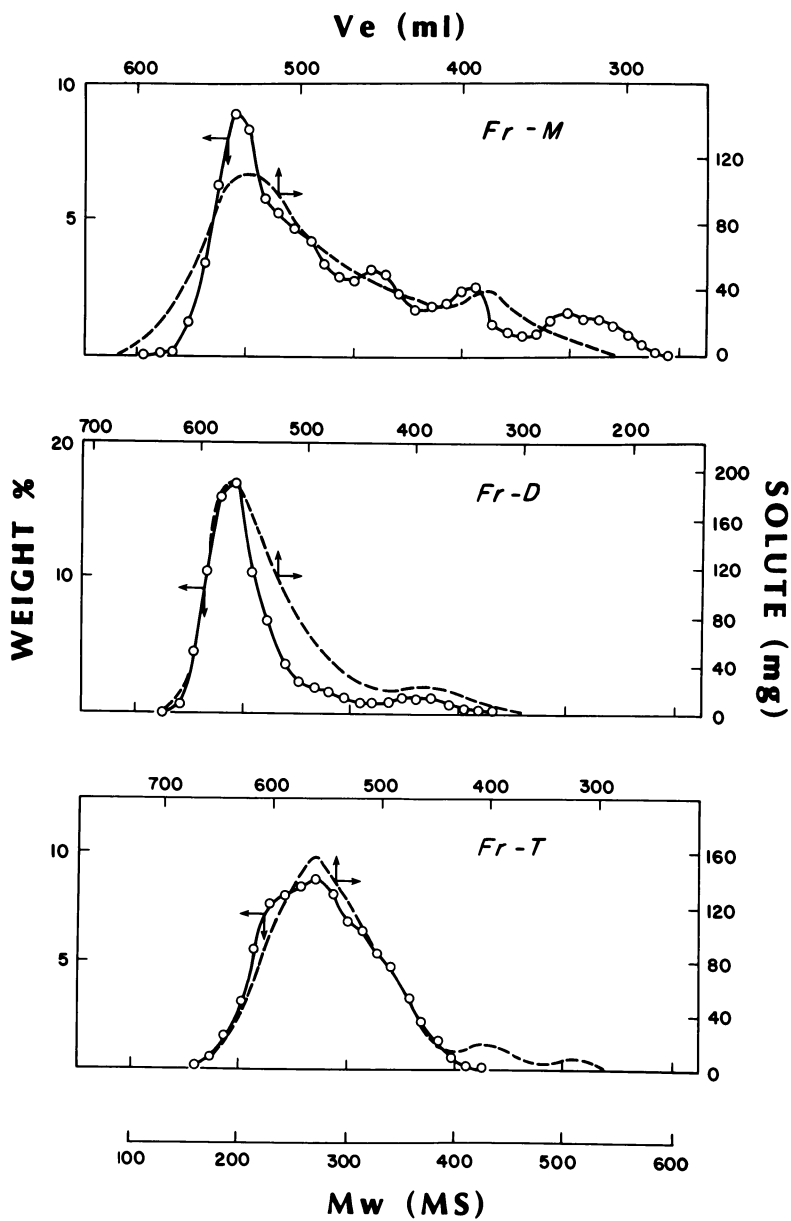


Figure 10. Comparison of molecular weights from MS with GPC elution curves

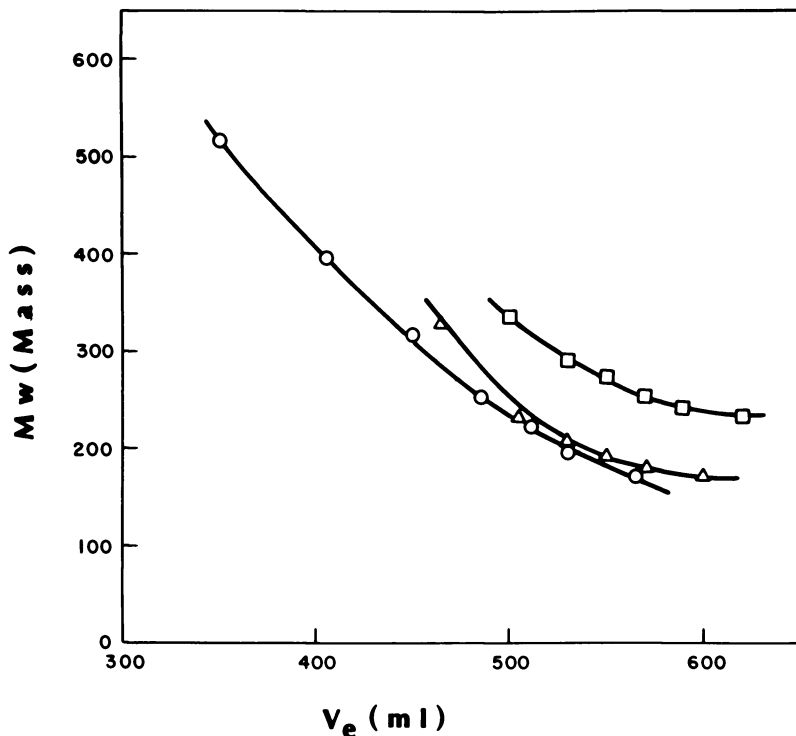


Figure 11. Relationship between molecular weight from MS and GPC elution volume ((O) Fr-M; (Δ) Fr-D; (□) Fr-T)

One-ring aromatic compounds are shown to be highly substituted with alkyl groups and/or naphthenic rings. The total alkyl carbons substituted on the aromatic ring range from about 5 to 35. The range of naphthenic rings is zero to 3. Two-ring aromatic compounds have from zero to 2 naphthenic rings and up to 15 total alkyl carbons. Three-ring and four-ring aromatic compounds rarely have more than one naphthenic ring. They may have up to 12 carbons in substituted alkyl groups. These results are in agreement with results previously obtained by ^1H and ^{13}C NMR results.

Low-ionization-potential mass spectral studies provide information on coal-derived liquids, which is useful in following reactions and in elucidating the effect of process variables. Structural studies are helpful in determining procedures for upgrading the liquids. A major limitation of the technique is that it is difficult to apply to the entire heavy-oil

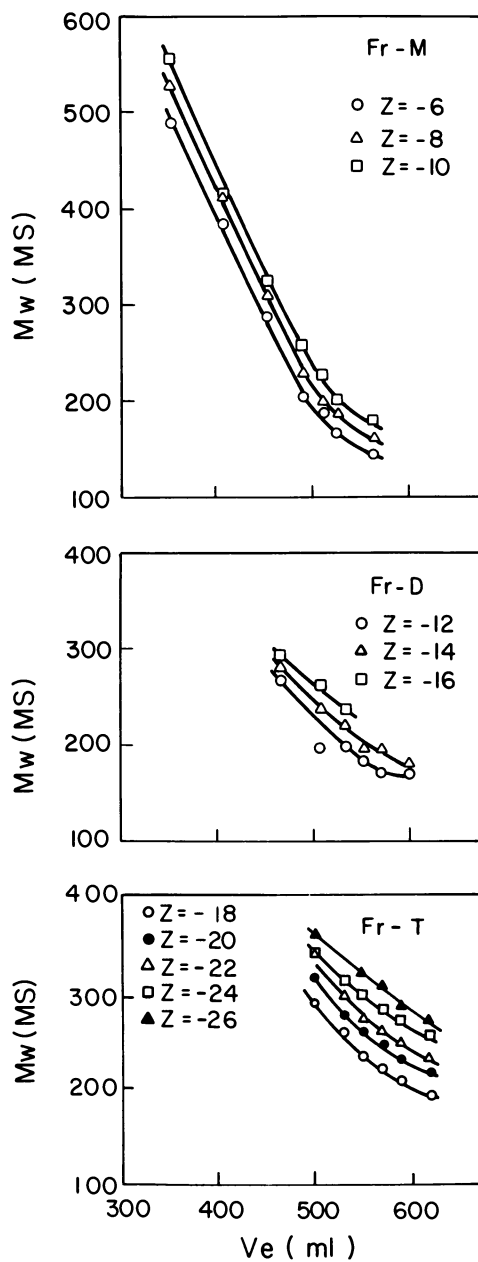


Figure 12. Relationship between molecular weight from MS and GPC elution volume for hydrocarbon types

fraction. The polar fractions that contain heteroatoms are difficult to analyze but are often more important in explaining mechanisms and selecting upgrading processes.

Literature Cited

1. Sharkey, A. G., Jr.; Shultz, J. L.; Kessler, T.; Friedel, R. A., "Spectrometry of Fuels"; Plenum: New York, 1970; p. 1.
2. Dooley, J. E.; Thompson, C. J. "Liquid Fuels from Coal"; Academic: New York, 1977; p. 221.
3. Dooley, J. E.; Thompson, C. J.; Scheppele, S. E. "Analytical Methods for Coal and Coal Products"; Academic: New York, 1978; Vol. 1, p. 467.
4. Aczel, T.; Williams, R. B.; Brown, R. A.; Pancirov, R. J. "Analytical Methods for Coal and Coal Products"; Academic: New York, 1978; Vol. 1, p. 499.
5. Hirsch, D. F.; Hopkins, R. L.; Coleman, H. J.; Cotton, F. O.; Thompson, C. J. *Anal. Chem.* **1972**, *44*, 915.
6. Dooley, J. E.; Sturm, G. P., Jr.; Woodward, P. W.; Vogh, J. W.; Thompson, C. J. ERDA-BERC Rept. of Invest. 75/7, August 1975.
7. Sturm, G. P., Jr.; Woodward, P. W.; Vogh, J. W.; Holmes, S. A.; Dooley, J. E. ERDA-BERC Rept. of Invest. 75/12, November 1975.
8. Woodward, P. W.; Sturm, G. P.; Vogh, J. W.; Holmes, S. A.; Dooley, J. E. ERDA-BERC Rept. of Invest. 76/2, January 1976.
9. Yokoyama, S.; Bodily, D. M.; Wisner, W. H. Quarterly Progress Report, FE-2006-5; July-September 1976, DOE Contract E (49-18)-2006, p. 72. To be published.
10. Wood, R. E.; Wisner, W. H. *Ind. Eng. Chem. Process Des. Dev.* **1976**, *15*, 144.
11. Lumpkin, H. E. *Anal. Chem.* **1958**, *30*, 321.
12. Hirsch, D. E.; Dooley, J. E.; Coleman, J. H. U.S. Bureau of Mines, R.I. 7875, 1974.
13. Coleman, J. J.; Dooley, J. E.; Hirsch, D. E.; Thompson, C. J. *Anal. Chem.* **1973**, *45*, 1724.

RECEIVED JULY 19, 1979.

The Effect of Reagent Access on the Reactivity of Coals

JOHN W. LARSEN, THOMAS K. GREEN, P. CHOUDHURY,
and E. W. KUEMMERLE

Department of Chemistry, University of Tennessee, Knoxville, TN 37916

It is argued that diffusion of reagents through solid coal, as distinct from diffusion through pores in the solid coal, may be the rate-limiting step in many reactions of coals. Brief consideration is given to diffusion in polymeric systems. Examples of reactions that may be limited by reagent accessibility considerations are given. These include several methods of determining OH groups, depolymerization, and Friedel—Crafts acylation. Heat has rapid access to the interior of solid coal, and this is one of the reasons for the popularity of pyrolysis-based processes. Research into methods of increasing the rate and extent of diffusion of reagents into coal is an important and neglected area.

This article is an abecedarian inquiry into the relationship between accessibility of reactive sites in coals to reagents and the rate and extent of reaction at those sites. As will become clear, so little attention has been given to this area [except by Peters and Fuentgen (1)] that definitive answers to the questions raised are not yet possible. Still, the questions are important and must be considered. It seems likely that accessibility to reagents is an important limiting factor in many coal reactions. By writing this article we hope to convince coal chemists that the accessibility problem is one that should be considered when designing experiments and interpreting results.

Consider a reactive group located within solid coal, not at any surface; neither an external surface nor an internal pore surface. If the coal is treated with reagents incapable of penetrating the solid coal, that group will not react unless it is brought to the surface. One way this can be done is by removing solid coal. When the reaction has proceeded far enough to uncover the group in question, it will react. However, if the

reagents are soluble in the solid coal, they then can diffuse through the solid until they reach the group and react. This diffusion may be a very slow process and may be the rate-controlling step in the reaction. If a reactive group is located in a variety of environments of differing accessibilities, the kinetics of its reaction will be exceedingly complex. However, if diffusion into coal is quite rapid, then the normal activation energy for the reaction in question may be the rate-limiting factor. Thus it is clear that both the location of a reactive group in the coal and the rate of transport of the reagents into the coal may have significant effects on the reactivity of a group.

This situation is caused by the coal's insolubility. Most coals are nearly insoluble in nearly everything. Although selective solvents may dissolve as much as 20–25% of some coals without reaction, the bulk of the material remains insoluble. Thus the reagent must penetrate the coal to reach the reactive group. The fact that coals are highly porous certainly helps. We will return to this point later. Now our concern is with reagent transport into the solid material as distinguished from transport in the pore system. The character of the solid material will control that diffusion rate.

A strong argument for the macromolecular character of coal has been made by Van Krevelen (2) and need not be repeated here. The nature of the macromolecular structure is important. Since it does not dissolve in solvents that can swell it to more than twice its original volume (*see* Table I), it must be a three-dimensionally cross-linked gel or consist of large molecules that are so entangled with each other that they cannot be separated. Coals are viscoelastic (3). When stretched, they snap back. They do flow but with high viscosities, approaching that of bakelite. A very careful study of this behavior led Macrae and Mitchell and others to conclude that coals were highly cross-linked materials (3, 4). It seems improbable that a significant part of such cross-linking could be due to entanglements. X-ray data and most structural models show coals to be sheetlike molecules. This idea is supported by the asymmetry of the mechanical properties (5), indicating more cross-linking parallel to the

Table I. Swelling of Four Pyridine-Extracted Coals with a Series of Organic Solvents; Ratio of Weight of Swollen Coal at Equilibrium to Weight of Dry Coal

<i>Coal</i>	<i>Toluene</i>	<i>Ethanol</i>	<i>Acetone</i>	<i>1,4-Di-oxane</i>	<i>Pyridine</i>
N.D. Lignite	1.20	1.35	1.44	1.49	1.82
Wyodak	1.33	1.43	1.54	1.71	2.16
Illinois No. 6	1.44	1.41	1.54	1.83	2.18
Bruceton	1.43	1.39	1.46	1.78	2.03

bedding plane than perpendicular to it. It is difficult to visualize large numbers of entanglements between sheetlike molecules. The view that the association of macromolecules in coals is due to forces other than covalent bonds has been forcefully expressed (6). We prefer a three-dimensionally cross-linked structure, but it is clear that the definitive answer is not yet available.

Since coals are highly porous materials, diffusion will occur both through the pores and within the bulk solid. It is not easy to distinguish between them. Clearly, when two atoms that are part of the coal are in contact and must be separated by a diffusing molecule, this process is diffusion in a solid. Just as clearly, when the diffusing molecule can move through an open space without altering the position of any atoms in the coal, then that is diffusion through a pore. However, there will be cases in which the coal atoms are not touching, there is empty space between them, yet the diffusion of a molecule into this space increases their separation. This situation obviously will occur when the separation distance is smaller than the diffusing molecule.

The pore structure of coals and the diffusion of small molecules within the pore systems of coals have been thoroughly studied (7-12). Certainly diffusion of larger molecules through this pore system may be slow and rate limiting. Our concern here is much more with diffusion of reagents into the solid coal. This diffusion process requires displacement of atoms in the coal and will usually be a slow process at room temperature. There seems to be a general consensus that diffusion through the solid material itself, not an open pore, may be necessary and may be the limiting factor in chemical reactions.

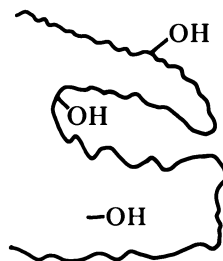
Diffusion in nonporous polymers has been extensively studied (13). Unfortunately for our present concerns, most attention has been given to permanent gases and light hydrocarbons. Nonetheless, the effects of many properties of polymeric systems on diffusion rates are known. It is worth describing them in a brief and qualitative manner.

1. Size of the diffusing molecule: the diffusion coefficient decreases as molecular size increases. Linear molecules diffuse more rapidly than branched molecules of the same size.
2. Nature of the polymer: the greater the flexibility of the polymer chains, the greater will be the diffusivity. An increase in the cohesive energy of the polymer reduces diffusivity.
3. Effect of the glass transition: this effect is small to nonexistent for the diffusivity of small molecules.
4. Effect of cross-linking: increasing the degree of cross-linking increases both the activation energy and the pre-expon-

ential factor for diffusion. The diffusion coefficient drops. This effect increases with increasing size of the diffusing molecule.

5. Effect of plasticizers: a plasticizer decreases the cohesive forces between polymer units and so increases diffusivity.
6. Effect of fillers: the presence of particles distributed in the polymer has complex and conflicting effects. In general, diffusion is hindered. However, if the filler is not thoroughly wet by the polymer, gaps can result, which are filled by the diffusing molecules, and the diffusion rate increases.
7. Presence of crystallites: diffusing molecules normally are not soluble in crystallites, and they act as fillers, inhibiting diffusion.

All of the comments above apply to diffusion through solid coal, not through coal's pore structure. Diffusion through the pore network has been studied thoroughly and seems to be understood (8-12). The considerations above are relevant to a reagent penetrating the solid coal to reach a functional group that is not located at a surface.



Consider a functional group, say, a phenolic OH group in coal. It may be found in three different regions. An -OH group at the external surface of coal will obviously react quickly, at a rate similar to an -OH group on a molecule in solution. An -OH group located at the surface of a pore will react more slowly, or perhaps not at all. To react, the reagents must penetrate into the pore. If they are large and the pore is small, this process will be an activated process. In fact, the reagent may not be capable of entering the pore, in which case the -OH group will not react unless the coal structure is altered to permit access. Reagent accessibility to the -OH group located within the solid coal may be very slow. Only two routes are possible. Some coal can be removed so that the group is uncovered and is at the surface. In this case reaction rate will be affected strongly by the coal surface area that is accessible to the reagents. The other possibility is that the reagent diffuses through the solid coal to reach the site. This process may be very slow. Swelling

coal in solvent vapors (Table I) required 2–3 days to approach equilibrium (5). Reagents with less affinity for coal than the swelling solvents would diffuse even slower, as would molecules of larger size. This situation sets a lower limit on the rate of reaction of a buried group with reagents whose diffusion rates are similar to those of these solvents.

It is apparent from these considerations that mass transport may severely limit reactions of coals. We next proceed to a brief discussion of some examples of mass transport limitations on reactions.

A variety of techniques for analyzing –OH groups in coal have been developed, and a good selection is listed in Van Krevelen's book (2). From his table (12) we have abstracted the reactions used to determine –OH groups in coals and the recommended reaction times. In Table II these are compared with the reaction times recommended for these reactions in solution.

Reaction times for coals are invariably much longer than those required for the same reaction between molecules in solution. Often reactions with coals are several thousand times slower. This reduction in rate occurs for a variety of reactions of varying charge character and type, suggesting that it is not a normal medium effect. It is most readily ascribed to rate limitations due to the inaccessibility of reactive sites to reagents.

Table II. Reactions Used to Determine –OH Groups in Coals

<i>Reaction</i>	<i>Time Required with Coals</i>	<i>Time Required for Solution Reaction</i>
Esterification with acetic anhydride in pyridine at 90°C	24 hr	45 min (15)
Etherification with trimethylsilylchloride and hexamethyldisilazane in pyridine at 115°C	1–4 days	5 min at room temperature (16)
Exchange with D ₂ O (20% in pyridine) at 80°C	a few days	minutes
Etherification with CH ₂ N ₂ in Et ₂ O at 0°C	1 week	minutes (17)
Reaction with dinitrofluorobenzene in DMF/H ₂ O at 20°C	a few days	5 min (18)
Acetylation with ketene at room temperature	a few days to a week	minutes (19)
Esterification with phthalic anhydride in pyridine at 90°C	a few days	1 hr (5)

Another facet of this problem is revealed by the work of Maher. Using potentiometric titration with base in ethylenediamine solvent (20), Maher and O'Shea measured the phenolic -OH content of Greta seam coal (21) [82.4% C, 6.2% H, 1.7% N, 1.0% S, dry, ash-free basis (DAF)]. The coal was extracted with a variety of solvents, and then the phenolic -OH content was measured in both the residue and the material extracted from it. The results are shown in Table III. It is clear that the solvents used to extract the coal have an effect on the total number of OH groups found. Clearly this result must be due to the effect of the solvents on reagent access to the -OH groups, since the total number of -OH groups in the coal is fixed. Thus the various solvents differ in their abilities to expose OH groups to the reagents, as pointed out by Maher and O'Shea (21). Interestingly, there is no relationship between the ability of a solvent to extract material from the coal and its ability to uncover -OH groups.

As shown by Hodek and Kolling (22), bituminous coals can be readily acylated. In connection with our studies of some Friedel-Crafts reactions of coals, we carried out several acylations using Bruceton coal and octanoyl chloride under Hodek's conditions. Sufficient octanoyl groups were added to increase the weight of the coal by 40%. The ^1H nuclear magnetic resonance (NMR) spectra of the extractable fraction (Figure 1) contained no absorption due to hydrogens on aromatic nuclei. Only the sharp singlet due to residual ^1H in DCCl_3 appears near the aromatic region. Hodek reported that the solubility of the acylated coal depended on the chain length of the acyl group, increasing as the chain length increased. This observation was the key to an explanation of the phenomenon.

It was postulated that reaction occurred primarily at the coal surface. The large octanoyl chloride molecules could not readily penetrate the coal but rather reacted at available *surface* sites. This reaction produced very tiny particles of coal, their surfaces covered with covalently bonded acyl chains. It is suggested that these units are suspended in a solvent by the favorable interactions between the octanoyl chains and the solvent. The situation is analogous to that of a reversed micelle. In this situation the aliphatic chains are in a liquid environment and will show nearly normal ^1H NMR absorption. However, most of the aromatic hydrogens in the coal remain in a solid environment and will have absorptions characteristic of that state. The line widths for hydrogens in a solid are very broad and are not detected by a high-resolution NMR instrument designed for work with solutions. Thus the aromatic hydrogens in their solid environment are invisible to our NMR instrument, and only the aliphatic hydrogens appear.

Two further observations supported this interpretation. The first was the ^{13}C NMR spectrum of octanoylated Bruceton coal shown in Figure 2. The peaks in the octanoyl group were assigned by analogy

Table III. Sum of Phenolic Groups in Extracts and Residues Basis: 100 g of DAF Coal; 160 meq of -OH (21)

Solvent	Extract			Residue			
	Weight (g)	Total acidity (meq/g)	Product (meq)	Weight (g)	Total acidity (meq/g) Mean	Product (meq)	Total meq
Iso-amyl alcohol	2.2	ND ^a	ND	97.8	1.99	195	> 195
Dimethyl formamide	22	3.21	71	78	1.35	105	176
Diethylamine	4.1	1.73 ^b	7	95.9	1.86	178	185
Pyridine	16	2.51	40	84	1.75	147	187
Aniline	15	2.82	42	85	1.53	130	172
Ethylenediamine	23	2.88	66	77	1.24	95	161
Chloroform	4.7	0.92	4	95.3	3.03	289	293
Dichloromethane	2.0	0.30	1	98	2.32	227	228

^a ND = Not determined.^b Approximate figure only, obtained from stirred extractor experiment where yield was 3.5%.

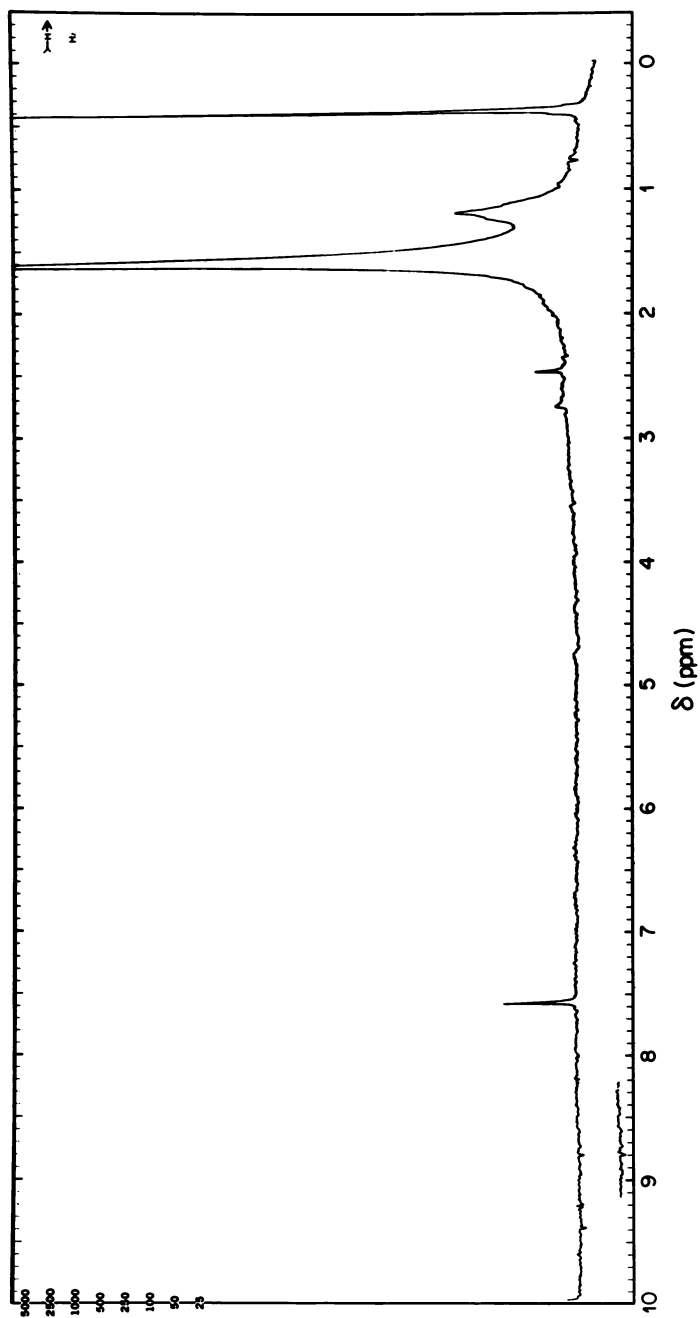
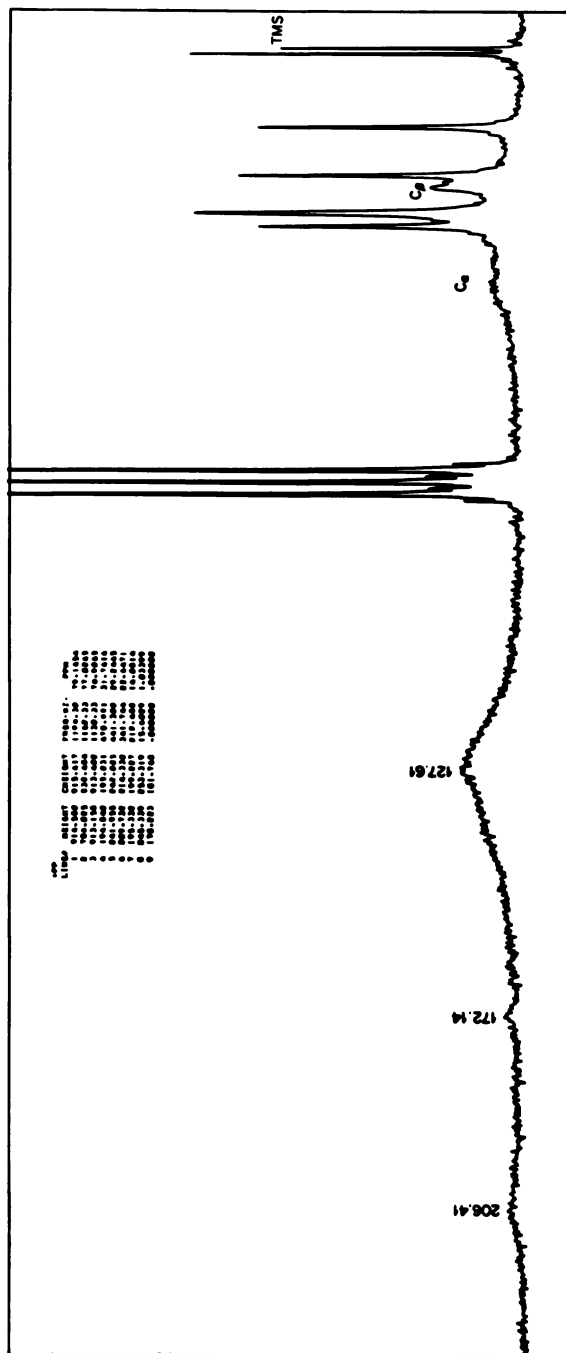


Figure 1. ^1H NMR spectrum of octanoylated Bruceton coal in CDCl_3

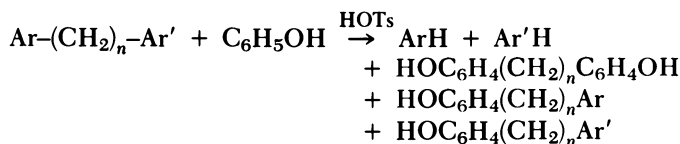


with octanoylphenone. Note that the two absorptions labeled C_α and C_β are broadened, while the other methylene groups in the chain have narrow, normal line widths. The absorptions labeled C_α and C_β were assigned to the methylene groups α and β to the carbonyl, respectively. The line broadening is typical of that expected from hindered rotation. If extensive surface octanoylation of the coal had occurred, the chains near the surface would be crowded together, and the crowding would decrease as the distance from the surface increases. The rotation of the methylene groups near the surface, therefore, might be hindered because of this crowding, while the groups at the far end would be able to rotate freely. This situation is exactly what is observed. The methylenes near the far end of the chain and the methyl group seem to have normal line widths, while those caused by the methylenes close to the surface are broadened by hindered rotation.

The second piece of evidence supporting the occurrence of a surface reaction is the molecular weight distribution of the products. In his original paper Hodek reported number average molecular weights for the acylated coals. For the octanoylated coals these were between 2300 and 3900, depending on coal and solvent. More recent work has revealed that the weight-average molecular weight is much higher and that much of the acylated coals have molecular weights greater than 10^5 (23).

The NMR data can be explained without recourse to surface reactions if the ^1H NMR is of poor quality and the broadening in the α and β methylene peaks in the ^{13}C NMR is due to chemical shift differences arising from different groups in the coal having been octanolyated. However, considering the very high molecular weights of the products (above 10^5), the peculiar dependence of solubility on chain length, and the large numbers of octanoyl groups added that would be crowded at the surface, it seems quite likely that the acylation of Bruceton coal was dominated by a surface reaction, which still resulted in the production of extractable products. The obvious explanation for the dominance of the surface reaction is limited accessibility of the reagents to the interior of the solid coal.

We have undertaken a thorough study of the Heredy-Neuworth procedure for solubilizing (depolymerizing) coals (24, 25, 26). The reaction is an acid-catalyzed transalkylation, which, when carried out on coals, renders them soluble.



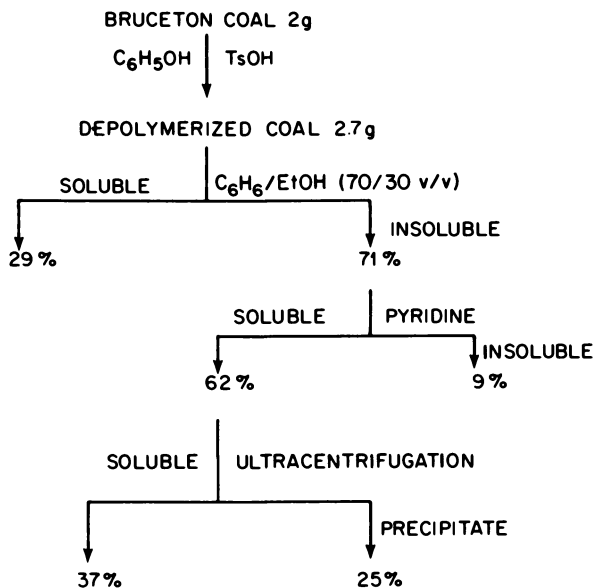
The reaction is second order, first order in phenol and first order in the methylene-bridged aromatic (27). Presumably the mechanism involves ipso protonation of the aromatic followed by attack of phenol on the cationic intermediate (27). When applied to coals, it renders them almost completely extractable into pyridine, and the number average molecular weights of the extractable material generally range between 300 and 750 (24).

For the reaction to occur both phenol and a solvated proton must diffuse into the coal to reach an aromatic methylene bond. Phenol is a better solvent for bituminous coals than is pyridine (28) and is expected to interact strongly with coal and probably swell it. The penetration of coal by phenol at its boiling point should be rapid and extensive. However, the proton has little affinity for a hydrocarbon environment, and its diffusion into the hydrophobic coal is not expected to be facile. The way in which the solvation of the proton will affect its diffusion in coals is unknown. As a result of limitations on proton transport, this reaction may be subject to accessibility limitations.

Bruceton coal was depolymerized in refluxing phenol using *p*-toluenesulfonic acid (HOTs) catalyst (29). The products were 91% extractable into pyridine and had a number average molecular weight of 400 in pyridine, measured by vapor pressure osmometry. Yet most of the materials in this solution have molecular weights above 2500.

The fractionation scheme shown in Figure 3 was applied to the reaction products. The benzene-ethanol soluble fraction consisted primarily of a dozen individual compounds of low molecular weight, which probably come from condensation reactions of phenol. It is the large number, but small mass, of these low-molecular-weight materials that dominates the number average molecular weight \overline{M}_n . Most of the mass of the product is contained in smaller numbers of very large molecules. The molecular weight distribution of the pyridine solubles, after the very high molecular weight and colloidal material was removed by centrifugation, is shown in Figure 4.

Of the material extractable into pyridine, about 8% will not pass a 7.5- μm filter. After this material is removed, the solution still plugs a 0.5- μm Millipore filter. Clearly much colloidal material is present. Centrifugation at $360,000 \times g$ gives a precipitate. Before centrifugation, evaporation of the pyridine gives a solid that will not redissolve. Once the pyridine solution has been centrifuged and the precipitate recovered, the pyridine can be removed from the remaining solubles, and they will redissolve. Clearly the principal coal-derived products from this reaction at the end of 24 hr are high-molecular-weight materials. Reaction for much longer periods of time does result in the very slow depolymerization of the precipitable material. It is reactive, but the reactions are quite slow.



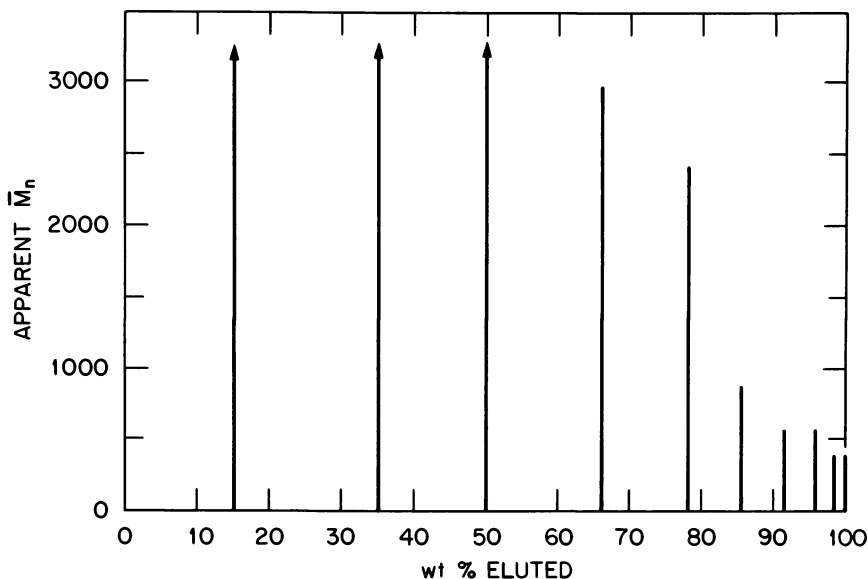
The Journal of Organic Chemistry

Figure 3. Fractionation of depolymerized Bruceton coal (29)

One explanation for the persistence of colloidal material is limited reagent accessibility. Coals are known to contain aromatic-methylene carbon-carbon bonds. These bonds are known to be cleaved by the Heredy-Neuworth reaction, yet large particles persist during the reaction. If there are regions of the coal that the reagents cannot penetrate, then these bonds will not be cleaved and the regions will persist, will not react. Continued investigation of this reaction will show whether this explanation is correct.

There are numerous other cases in the literature that could be used as examples of reagent access limitations. This review is not exhaustive, and those cases cited here serve to establish the point that the limited accessibility of reagents is an important factor in coal chemistry. Clearly it is worthwhile to attempt to improve the accessibility of coals to reagents. Perhaps in this way significant increases in coal reactivity can be obtained.

It may be possible to increase accessibility by modifying either the coal or the reagent. First let us consider the coal modifications. Physical changes can be made. Extracting coals increases their surface area (30) and their reactivity (31). We know of no attempts to explore thoroughly or to maximize this effect. Any treatment that expands pores or increases surface area will help. Such a treatment can be as simple as grinding. It has been shown that going from 100-mesh to 325-mesh coal



The Journal of Organic Chemistry

Figure 4. Apparent \bar{M}_n for true pyridine solubles from depolymerized Bruceton coal (29)

increases the percentage of OH found by acetylation (32). Swelling the coals with solvents should increase diffusion rates of reactants soluble in the swelling liquid and may increase reactivity.

The reagents also can be modified. Desirable are erinaceous reagents, ones that can burrow into and readily penetrate the coal. Again we know of no work that intentionally has modified reagents to give them an affinity for coal. Clearly reagents that are hydrophobic should be more effective than those that are hydrophilic, other things being equal. One interesting report of a rapid (2-hr) reaction of OH groups in an unswollen coal has recently appeared (33). Research to discover those factors that influence reagent diffusion in coals and to learn to design reagents or to modify coals to permit rapid diffusion and reaction could have enormous impact on coal chemistry. Unless such work is done, low-temperature reactions of coals may remain too slow to be useful commercially, particularly for fuel production. The development of means for gaining rapid access to buried groups in coals would have an enormous favorable impact on coal chemistry and is a research goal of great value.

The access-limited reactivity of coals has profound implications for any industrial processing of coal. Rapid rates are desirable, since smaller reactors and associated equipment usually mean smaller costs. If rapid access of reagents to all the coal cannot be gained, reagents that chew their way in from the surface will have to be used. This technique may be

acceptable for chemical production, but for fuel production it probably will be too slow. The massive amounts of material to be handled demand rapid reactions. There is one reagent that has very rapid access to the interior of a coal particle: heat. The interior of a coal particle can be heated rapidly, and once pyrolysis starts, the network structure will break down and reagents may penetrate easily and rapidly. Thus pyrolysis may be a necessary first step in all coal conversion processes, necessary because it may be the only quick way to carry out reactions within a coal particle. Consequently, reactions at lower temperatures (i.e., less than 400°C) may not be feasible commercially unless techniques are developed that permit very rapid reagent penetration of all the coal.

Acknowledgement

Various parts of the work described here were supported by the Electric Power Research Institute (EPRI) and the Department of Energy, to whom we are grateful.

Literature Cited

1. Peters, I. W.; Fuentgen, H. *Brennstoff-Chem.* 1965, 46, 56, 175.
2. Van Krevelen, D. W. "Coal"; Elsevier: New York, 1961; Chap. 23.
3. Macrae, J. C.; Mitchell, A. R. *Fuel* 1957, 36, 423.
4. Larsen, J. W.; Kovac J. In "The Organic Chemistry of Coal"; ACS Symp. Ser. 1978, 71, and references cited therein.
5. Lowry, H. H., Ed. "Chemistry of Coal Utilization", Suppl. Vol.; Wiley: New York, 1963.
6. Hombach, H. P.; Krolling, G. *Erdrol Kohle, Erdgas, Petrochem. Brennst.-Chem.* 1972, 25, 644.
7. Mahajan, O. P.; Walker P. L., Jr. In "Analytical Methods for Coal and Coal Products"; Karr, C., Jr., Ed.; Academic: New York, 1978; Chap. 4.
8. Karn, F. S.; Friedel, R. A.; Thames, B. M.; Sharkey, A. G., Jr. *Fuel* 1970, 49, 249.
9. Nandi, S. P.; Walker, P. L., Jr. *Fuel* 1970, 49, 309.
10. Hanbaby, P.; Juentgen, H.; Peters, W. *Ber. Bunsenges. Phys. Chem.* 1960, 72, 554.
11. Thimons, E. D.; Kissell, F. N. *Fuel* 1973, 52, 274.
12. Walker, P. L., Jr.; Mahajan, O. P. In "Analytical Methods for Coal and Coal Products"; Karr, C., Jr., Ed.; Academic: New York, 1978; Chap. 5.
13. Crank, J.; Park, G. S., Eds. "Diffusion in Polymers"; Academic: New York, 1968.
14. Macrae, J. C.; Mitchell, A. R. *Fuel* 1957, 36, 162.
15. Siggia, S. "Quantitative Organic Analysis"; Wiley: New York, 1966.
16. Sweeley, C. C.; Bentley, R.; Makita, M.; Wells, J. *J. Am. Chem. Soc.* 1963, 85, 2497.
17. Vogel, A. I. "Practical Organic Chemistry," 3rd ed.; Wiley: New York, 1957; p. 972.
18. Reinheimer, J. D.; Douglass, J. P.; Leister, H.; Yoelkel, M. B. *J. Org. Chem.* 1957, 22, 1743.
19. Siggia, S. "Quantitative Organic Analysis"; Wiley: New York, 1966; p. 372.
20. Brooks, J. D.; Maher, T. P. *Fuel* 1957, 36, 51.
21. Maher, T. P.; O'Shea, J. M. *Fuel* 1967, 46, 283.

22. Hodek, W.; Kolling, G. *Fuel* **1975**, *52*, 220.
23. Hombach, H. P. *Erdröl und Kohle, Erdgas, Petrochemie, Compendium* **1975**, *74/275*, 750.
24. Larsen, J. W.; Kuemmerle, E. W. *Fuel* **1976**, *55*, 162.
25. Moore, R. H.; Martin, E. C.; Cox, J. L.; Elliott, D. C. In "Industrial Laboratory Alkylations", *ACS Symp. Ser.* **1977**, *55*.
26. Darlage, L. J.; Bailey, M. E. *Fuel* **1976**, *55*, 205.
27. Heredy, L., personal communication.
28. Kiebler, M. *Gas J.* **1940**, 433.
29. Larsen, J. W.; Choudhury, P. *J. Org. Chem.* **1979**, *44*, 2856.
30. Jenkins, R. G.; Mitchell, S. **1978**, *57*, 394.
31. Huntington, J. G.; Mayo, F. R.; Kirshen, N. A. *Fuel* **1979**, *58*, 24.
32. Ruberto, R. G.; Cronauer, D. C. In "The Organic Chemistry of Coal," *ACS Symp. Ser.* **1978**, *71*.
33. Liotta, R. *Fuel* **1979**, *58*, 724.

RECEIVED July 19, 1979.

Physical and Chemical Structure of Coals: Sorption Studies

E. L. FULLER, JR.

Chemistry Division, Oak Ridge National Laboratory, Oak Ridge, TN 37830

The chemical and physical structure of coal has been shown to control the sorption of vapors in a bituminous coal. Microgravimetric sorption studies with nitrogen, carbon dioxide, and water have shown markedly different sorption processes. The magnitude and energetics of sorption vary systematically with respect to the molecular properties of the sorbate (polarizability and dipole moment) and the consequential energetic and structural changes induced in the substrate coal. In light of these studies we must question the existence of a fixed, definable pore structure and/or internal surface area of coal. "Accessibility" is probably a better term to use to define these extensive properties related to reactivity of coals.

Current and proposed efficient uses of coal involve the interaction of fluid phases with coal and coal chars. This study deals with a detailed analysis of the thermodynamics and mechanisms of sorption of various gases with coal under relatively mild, nondestructive conditions. The results are beneficial in terms of defining the accessibility of the reactive sites in the coal structure to various reagents. The current status is best described in an excellent review of the situation: "Coal is an amorphous substance and it is difficult to define its structure. . . . The fundamental chemistry of coal liquefaction will probably remain poorly understood until coal structure is better defined" (1).

Currently there is considerable effort being expended in several institutions to continue sorption analyses to evaluate the porosity and internal surface area of coal. These studies involve studies of vapor (2, 3, 4) and liquid (5) sorption analyses. We have employed proven microgravimetric sorption equipment and techniques (6) for a detailed examination of the thermodynamics and mechanisms of sorption of various vapors on well-characterized coals. Specifically, the coals used for this study are classified as C-bituminous, Illinois No. 6, from the Sahara

Table I. Chemical Analysis of Coal Sample

<i>Ultimate Analysis</i>	<i>%MAF</i>
Carbon	77.7
Hydrogen	5.83
Oxygen	10.60
Nitrogen	1.43
Sulfur	4.50
<i>Proximate Analysis</i>	<i>% Dry Wt.</i>
Ash	12.20
Volatiles	38.80
Fixed Carbon	49.10
<i>Moisture</i>	<i>% As Received</i>
	5.50

mine. Coal samples were obtained from a freshly opened mine face and placed in an argon atmosphere in opaque containers for transport and storage. Thus the bed moisture was retained and no weathering was allowed. In this manner we expect to be able to characterize the coal in its natural state and subsequently determine changes wrought in transport and storage. An aliquot was removed for this study and ground under argon to pass a 200-mesh screen in toto. Analyses of the material are given in Table I. The sample was placed in the microgravimetric sorption apparatus and exposed to vacuum (10^{-6} torr) overnight prior to the reported analyses. The outgassing was essentially complete in about 6 hr, as witnessed in continuous record of the sample mass. There was no detectable mass loss in the following 10 hr within the instrumental precision ($\pm 0.1 \mu\text{g}$). Mass spectrometric analyses of the vapors showed that the evolved vapors were H_2O (99.9%) and CO_2 (about 0.1%). No methane or other hydrocarbons were detected for this room temperature ($25 \pm 2^\circ\text{C}$) experiment, in contrast to higher-temperature (pyrolysis?) studies.

Results

Nitrogen Sorption. The outgassed sample was cooled to 77 K by a stirred liquid nitrogen bath maintained at a constant level (6, 7). Nitrogen vapor was introduced and controlled at a constant pressure until the steady state conditions shown in Figure 1 prevailed. Maintaining fixed temperature and pressure on selected intermediate pressures for both adsorption and desorption assured us that there were no slow processes in play detectable in the 2–3-day periods used. The disparity between desorption and adsorption isotherms can be attributed confi-

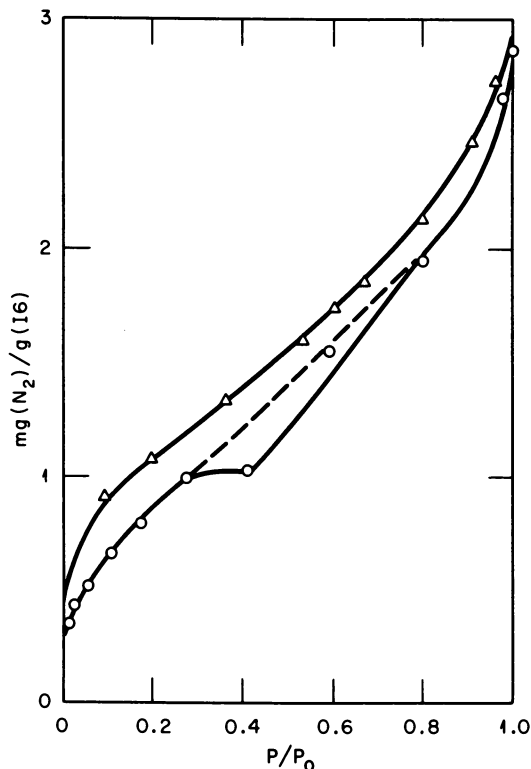


Figure 1. Nitrogen sorption at 77 K: steady state values showing hysteresis. (Sorption value at $0.41 P_0$ may be suspect. The trend was not noted on subsequent resorption. The hysteresis closes on desorption to about $10^{-3} P_0$.)
 ((O) adsorption; (Δ) desorption)

dently to true hysteresis phenomena and not to an inadequate equilibration to allow some slow process to occur. This hysteretic retention is removed completely in vacuum ($10^{-10} P_0$), albeit quite slowly (over 24 hr). This phenomenon cannot be attributed to sorption of an impurity (i.e., H_2O) from the nitrogen. We have used 99.9995% N_2 and have not noted such retention on rigid inert substrates (6, 7). Furthermore, such impurities would not be removed in vacuum at 77 K.

The sigmoidal shape of the nitrogen isotherm of Figure 1 is quite amenable to analyses by the Brunauer–Emmett–Teller (BET) multilayer theory (8). The BET surface area calculated is $2.8 \text{ m}^2/\text{g}$. This value is quite consistent with the predominant 1-to-10- μm size distribution observed on this sample with an optical microscope. Assuming cubic habits and density of about $2.3 \text{ g}/\text{cm}^3$, we find the range of specific surface area to be 0.26 to $2.6 \text{ m}^2/\text{g}$. Apparently the sorbed N_2 does penetrate into the internal portion of the particles only to a limited extent.

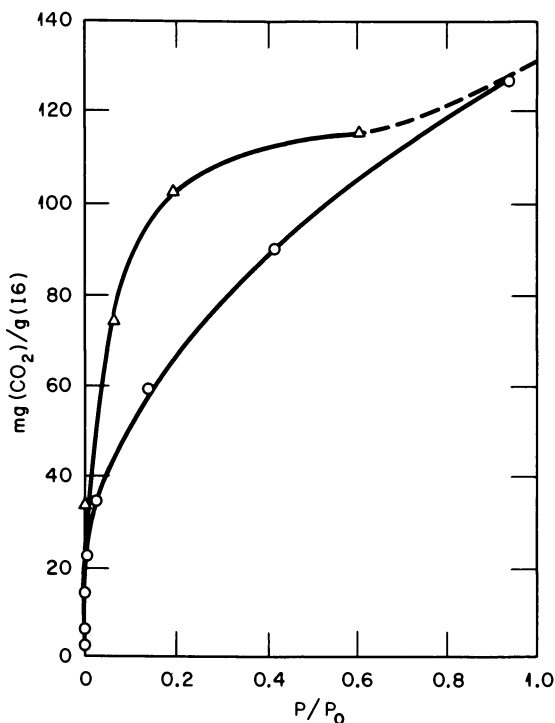


Figure 2. Carbon dioxide sorption at 195 K: marked hysteresis on desorption is noted to a closure at vacuum ($10^{-10} P_0$) on desorption (O) adsorption; (Δ) desorption)

Carbon Dioxide Sorption. Our results for carbon dioxide sorption at 195 K are given in Figure 2. The results are given with respect to the measured (vapor pressure thermometer) saturation pressure, P_0 . The marked difference in both the magnitude and shape, compared to nitrogen isotherms, is quite common for coal. This has led to the advocacy (2) of employing carbon dioxide to measure the internal area of coals. The BET (apparent) specific surface area is calculated to be $128 \text{ m}^2/\text{g}$ based on the carbon dioxide adsorption data. The desorption hysteresis was confirmed to be a steady state property of the sample based on kinetic continuity and accountability as described for nitrogen. BET analysis of the desorption data yields an apparent area of $373 \text{ m}^2/\text{g}$. Here again the hysteresis loop closes (the original vacuum weight is achieved on desorption).

Water Sorption. The water vapor sorption isotherm (293 K) is given in Figure 3. The general sigmoidal shape is evident, and the hysteretic phenomenon is quite pronounced, even when desorption is instigated from intermediate pressures (about $0.6 P_0$), and vacuum closure

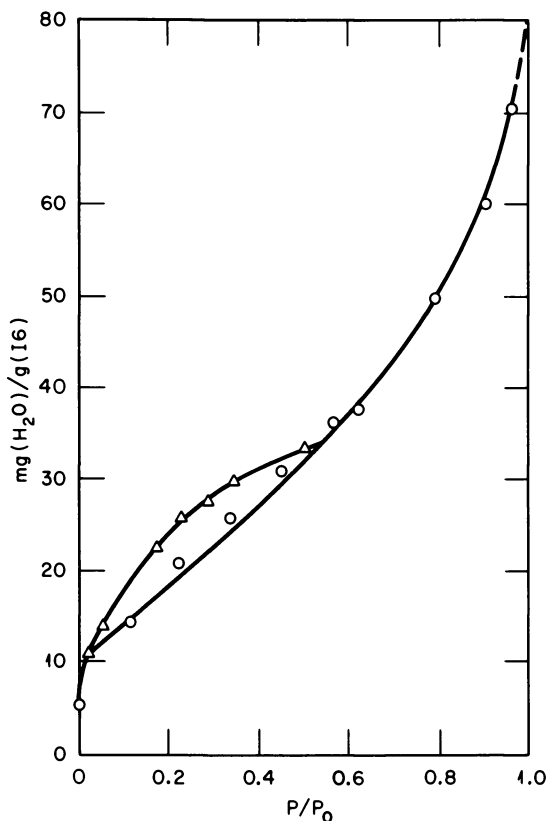


Figure 3. Water sorption at 293 K: hysteresis is evident even when desorption is effected from intermediate pressures ($0.6 P_0$) and closure is noted in desorption vacuum ($10^{-10} P_0$) ((\circ) adsorption; (Δ) desorption)

is noted also for this sample after the moderate (298 K) degassing. The BET areas are 41.1 and 68.2 m²/g, based on the adsorption and desorption data, respectively.

Discussion

Throughout the preceding section we have tabulated the measure of sorption expressed in terms of that obtained by the application of the BET theory. In general, the theory and data are compatible over the classical range limited to about $0.05 P_0$ to $0.35 P_0$. Such a correlation should not be construed to serve as proof of the BET mechanism or even to measure a true specific surface area. The BET theory is, by its very nature and derivation, a theory for multilayer formation. Such a process is probably in play for nitrogen sorption but is questionable for water and

carbon dioxide. The sorbed water and carbon dioxide must reside within the structure of the coal, where there is not space to form multilayers in the context of the BET theory (heat of adsorption only slightly greater than the condensation heat).

We have continued to report BET sorption capacities (expressed as specific surface areas) in light of current practices. Such practice allows us to compare our results to those reported by others where no other measure of sorption capacity is given. This is really a tribute to the landmark work of Brunauer, Emmett, and Teller (8), for providing a comprehensive and useful tool for studying surface phenomena. The fault lies in the application of the theory beyond its realm of applicability. Even the concept of "internal surface area" derived in this manner is misleading. Actually, the BET sorption capacity is only a measure of the sorption capacity in the region of the "knee" and probably should be reported in concentration terms (mmol/g, mg/g, cm³ (STP)/g, etc.) to avoid providing an erroneous concept to the novice.

The merits of isotherm analyses by the BET method and other theories are probably best outlined by Adamson (9). We have analyzed our results in terms of several sorption theories (9) and have concluded that those based on the sorption potential are most informative. Polanyi first proposed that the sorption process is dictated by the sorption potential ϵ , where

$$\frac{\epsilon}{RT} = -\ln P/P_0 \quad (1)$$

and that the isotherm is really the distribution function or variation of sorbate concentration with respect to this sorption potential. In other words, the amount sorbed will equilibrate to the free energy state of the vapor in the head space. Equation 1 is the free energy of the gas phase (assuming ideal gas behavior) with respect to P_0 . Normal calculations refer to 1 atm or some other reference pressure. The form of Equation 1 is viewed very conveniently as the free energy of any sorbed species, in equilibrium with the vapor at P , with respect to the bulk stable form of the sorbate, where at P_0 the free energy of transfer from bulk to vapor is zero by definition ($\ln P/P_0 = 0$). Thus any sorbed entity can be defined in terms of its free energy relative to the bulk sorbate.

Such an analysis is inherent in the Dubinin-Radushkevich (DR) theory (9) often used in isotherm analysis:

$$V = V_0 \exp(-b\epsilon^2) \quad (2)$$

where b is a constant. Such an analysis assumes a filling of a fixed internal volume and the results should be interpreted as such. Often the DR theory is used to measure the sorption capacity, and subsequently

a DR surface area is calculated (9). This ostensibly is an application of BET concepts to the DR results, and the previously given analysis is applicable.

We can examine current available knowledge of coal chemical (10, 11) and physical (12) structures to gain some insight into the sorption mechanisms and the applicable sorption theories. Coal is regarded generally as polynuclear aromatic units with methylenic cross-linking with varying amounts of polar functional groups (hydroxyl, carbonyl, amine, etc.) dispersed in the statistically representative segments. The size of the segments and the degree of aromaticity generally increase for higher ranks, and the relative amount of heteroatom functional groups decreases as coalification processes proceed. These chemical changes give rise to the greater degree of ordering for higher-rank coals. There is enhanced structural order in both the interplanar and intraplanar context.

This coal of intermediate rank has rather extensive polynuclear formation and polar functional groups. Thus we would expect dispersion, polarizability, and dipolar interactions between the substrate entities and the sorbate molecules. The polar portion of the substrate as well as the highly conjugated pi-bonded electrons most assuredly are involved in the sorption process. Such a concept is quite suggestive and compatible with the polarization theory for sorption processes (9, 13, 14), where the energetics are predicted to follow the relationship

$$\frac{\epsilon}{RT} = \frac{\epsilon_0}{RT} \exp(-a\Gamma) \quad (3)$$

where Γ is the concentration of sorbate. Indeed, this relationship describes the sorptive process very well for all three vapors studied here when we conveniently use the analytic form

$$\ln \frac{\epsilon}{RT} = \ln \left(\frac{\epsilon_0}{RT} \right) - a\Gamma \quad (4)$$

Our results for water are given (Figure 4) for sorbed concentration Γ , linearized in the form of Equation 3. Least-squares analyses of our isotherms in this form show an excellent linearity; typical coefficients of determination are 0.937 (N_2), 0.973 (CO_2), and 0.997 (H_2O). Such a relationship allows us to reproduce the adsorption branch of the isotherms with respect to various coordinates (i.e. Figures 1, 2, 3) well within the experimental accuracy over the entire range of the experiment (0.001 P_0 to 1.0 P_0). This result is a boon in several respects: (1) interpolation to intermediate concentrations is accurate and straightforward; (2) interlaboratory comparisons can be obtained easily at virtually any pressure; and (3) further insight into the sorption process is available.

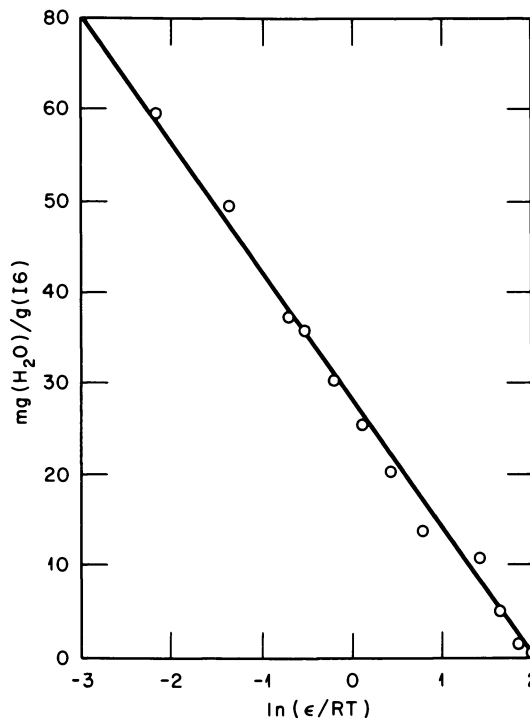


Figure 4. Linear presentation of water sorption data at 293 K: evaluation in terms of Equations 3 and 4

We can hardly view the coal as an inert substrate, as is often done. Most assuredly there are energetic (electronic) changes in the substrate similar to the image forces induced in the mobile electrons when sorption occurs on metals (15). The magnitude of the energetic perturbation of the substrate will be proportional to the energy involved as two identical sorbate molecules interact in the gas phase (i.e., N_2-N_2 , CO_2-CO_2 , and H_2O-H_2O). This gas phase interaction is known to be controlled by an attractive energetic term $\bar{\Phi}$, of the form (16)

$$\bar{\Phi} + \bar{\Phi}(\text{es}) + \bar{\Phi}(\text{dis}) + \bar{\Phi}(\text{ind}) \quad (5)$$

as a sum of the electrostatic, dispersion, and induction terms, respectively. Each of these components can be evaluated in terms of the properties of the sorbate gas molecules, as shown in Table II. An evaluation of ϵ_0 for each of these sorbates by coal should be an accurate measure of the sorbate-sorbent interaction energy at essentially zero uptake. In this state we are measuring the energetics of the coal system alone without the presence of sorbed entities and the

Table II. Contributions to the Interactions Between Like Molecules (14)

Sorbate	Electrostatic $\bar{\phi} (es) r^6$ $2/3 \mu^4/kT \times 10^{60}$ (10^{-60} erg-cm ⁶)	Dispersion $\bar{\phi} (disp) r^6$ $3/4 \alpha^2 h\nu_0 \times 10^{60}$ (10^{-60} erg-cm ⁶)	Induction $\bar{\phi} (ind) r^6$ $2 \mu^2 \times 10^{60}$ (10^{-60} erg-cm ⁶)	Total $\bar{\phi}$ $\bar{\phi} (es) + \bar{\phi} (disp) + \bar{\phi} (ind)$ (10^{-60} erg-cm ⁶)
N ₂	0	66.8	0	66.8
CO ₂	0	180	0	180
H ₂ O	190	47	10	247

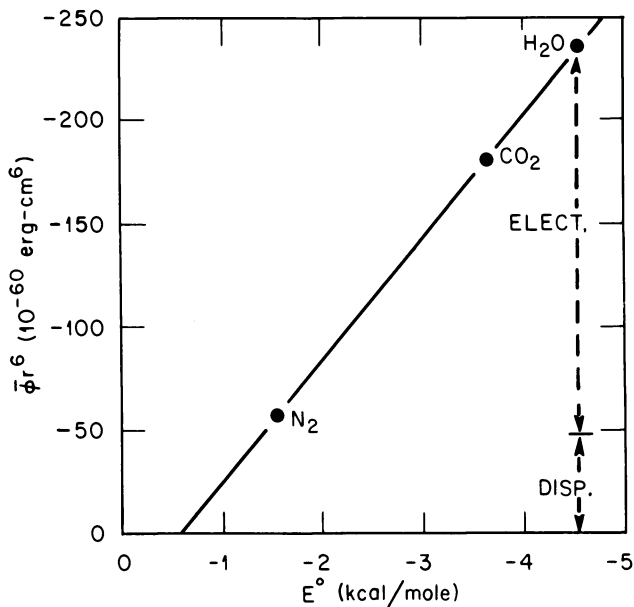


Figure 5. Energetic correlation: theoretical (ordinate) vs. experimental (abscissa)

resultant system energy change and/or sorbate-sorbate interactions. The correlation of these parameters, ϵ_0 , and $\bar{\phi}$ is given in Figure 5. The anticipated proportionality is quite apparent. These results can be contrasted readily to the results predicted for a rigid ("hard") electrostatic field (15). For a refractory, ionic, silicate substrate, the ϵ_0 values vary linearly with the first power (17) of the polarizability (α) and the second power of the dipole moment (μ). These results lead us to conclude that the coal structure yields, at least electronically and quite possibly physically, to accept sorbate molecules to an extent dictated by the nature of the sorbate itself.

Essentially this is an alternative explanation for the large difference in uptake for the various gases where processes seem to be "dominated by dipolar and London forces," as noted in related studies (5). This phenomenon has been attributed to activation energy barriers for diffusion of sorbate into the coal matrix (18). We have satisfied ourselves that there are no very slow processes in play and if this activation energy barrier exists, it must be essentially infinite in magnitude. We have analyzed the kinetics of the sorption processes in terms of diffusional mechanisms (19) with very little success. Alternatively, we have gone back to analyze our data in terms of mass action kinetics (20). All our data were acquired at constant (controlled) pressure conditions (21). If, indeed, the sorption

process involves the interaction of sorbed entities with discrete sites (pi-bonded hexagons, polar functional groups, etc.), we would anticipate a rate relationship of the type

$$\frac{dm}{dt} = k_n (m - m_x)^n \quad (6)$$

where n is the order of the reaction (20). Previous analyses of this type have been quite fruitful (21). In the current study we have found excellent adherence to second-order kinetics for water sorption and desorption:

$$\frac{dm}{dt} = k_2 (m - m_x)^2 \quad (7)$$

for a wide range of pressures ($0.01 P_0$ – $0.999 P_0$), as shown in Figure 6 for an incremental pressure change imposed on the system during the construction of the water isotherm. The results for CO_2 were more complex and are either a composite of two second-order processes or a combination of diffusion and mass action processes (22). Further experiments and analyses are required to describe the CO_2 sorption mechanism.

Additional structural information relevant to these studies is inherent in the scanning electron micrographic analyses of this ground coal sample, as shown in Figure 7. The laminar structure of the coal is quite evident, and it appears that the laminae have been opened somewhat in the grinding process. Apparently the sorption processes occur within these laminae, giving rise to the asymmetric swelling of the coal particle (23). One additional piece of evidence for the structural yielding of the sorbent is apparent in Figure 8. This photograph was taken after the aforementioned sorption studies. The pan was originally level and full to the top. The swelling–shrinking during sorption–desorption restructured the bed to this expanded configuration with considerably more interparticulate void space.

Finally, we can analyze the sorption hysteresis in terms of the “change in ‘structural’ arrangement in the molecular network” (24) noted for similar systems where swelling–shrinking occur on sorption–desorption. The concept of a yielding coal structure is quite valid in view of the comprehensive work to show that swelling and shrinking are appreciable (even for CO_2 and CH_4 sorption) (23, 25, 26).

Conclusions

We have analyzed our results in an objective manner, questioning assumptions made in past studies where the sorption processes are assumed to involve an inert, nonreactive substrate. Even pore size anal-

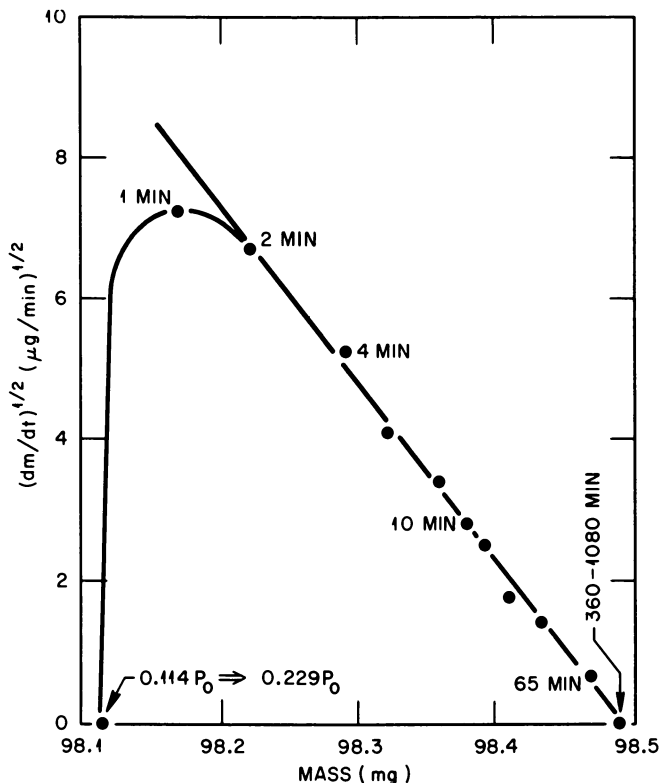


Figure 6. Kinetics of water sorption: mass action kinetics in terms of Equation 7 water rate analysis

yses should be subjected to scrutiny. How much of the porosity is inherent in the coal and how much is induced by the sorption process itself? How much of the surface area is inherent and how much is accessed by yielding of the coal? Our analyses seem to indicate that coal is a flexible structure with the rigidity determined by the degree of coalification (increasing with rank). The energetics and the amount of sorption depend upon the molecular properties of the sorbate and its ability to interact with the chemical entities of the coal. Thus determinations of specific surface area, porosity, pore size distributions, etc. are questionable. The existence of a rigid structure is assumed in most theories used for evaluation. One would expect that these results might range from the marked sorption swelling of cellulosic materials to the interlaminar penetration noted for graphite (24). At this juncture we have adopted the term "accessibility," in lieu of specific surface area, porosity, etc., until the basic tenets, assumed or implied, are scrutinized in the context of calculating the latter from the former.

Acknowledgments

This work is the result of the diligent and conscientious efforts of the members of the Massachusetts Institute of Technology School of Chemical Engineering Practice, M. M. Alger, O. K. Chow, M. Z. Khan, and S. M. Senkan (director). Many valuable discussions with R. A. Strehlow, L. H. Harris, and J. W. Larson were involved in the evaluation and interpretation of the results. Research sponsored by the Office of Basic Energy Sciences, Division of Material Sciences, U.S. Department of Energy, under contract W-7405-eng-26 with the Union Carbide Corp.

Addendum

The author is extremely grateful to the anonymous reviewer of this paper for his astute analyses of the concepts utilized in our data interpretation.

One must be cautious in interpreting the physical significance of these relationships (Equation 3), for "it has been emphasized repeatedly that the fact that an isotherm equation fits the data is an insufficient test of its validity (although not of its practical usefulness)" (9). However, the concepts and correlations noted below will bolster the model (13, 14). The original derivation of Equation 3 involved the polarization of the sorbate (13) by the electrostatic forces emanating from a free surface. Thus this concept often is regarded as "a still different approach to multilayer adsorption" (9) and subject to the restraints. Strictly speaking, this theory is not a multilayer theory and is applicable over a wide range of sorbate concentrations even for systems where classical multilayer formation is hindered (13). In essence we have utilized the general approach of establishing credibility of the model in terms of the linearization shown by Figure 4 and further substantiated the credibility by virtue of the highly plausible correlation of Figure 5. Thus this alternative treatment of the sorption results seems to be productive, with a minimum of postulates, assumptions, and adjustable parameters.

There is a basic enigma associated with the evaluation of ϵ_0 , as shown in the text, for many theories postulate Henry's law,

$$\lim \Gamma = cP \text{ for } \Gamma \rightarrow 0 \quad (8)$$

as a linear proportionality between sorbed concentration and pressure. From Equation 3 we indeed can note that

$$\Gamma = c' (P - P^*) \text{ for } \Gamma \rightarrow 0 \quad (9)$$

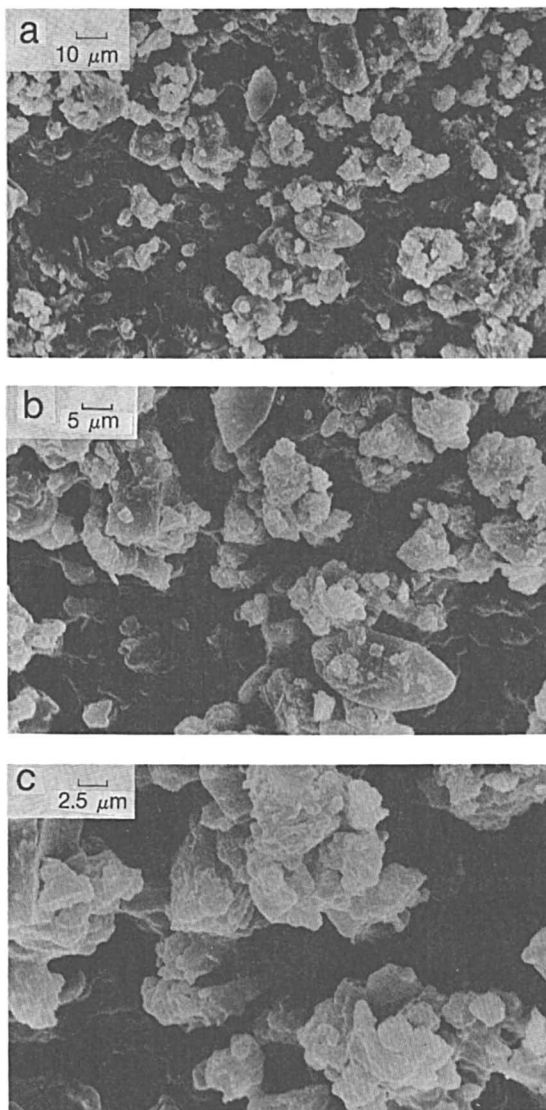


Figure 7. Scanning electron micrograph of Illinois No. 6 coal used in this study.

(a) The heterogeneous character is quite apparent as a mixture of framboidal, conchoidal, and angular fragments; (b) enlargement of a portion of part (a): the polyglot nature is quite evident as a broad range of size, texture, and morphology; (c) enlargement of a portion of part (b): adhesion of fine particles to larger particles is quite visible, and the contrast between the framboidal and angular fractions is quite striking; (d) enlargement of a portion of part (c): the texture of the framboidal fraction is seen to be a rather open structure comprised of smaller entities; (e) enlargement of a portion of part (d): the framboidal structure is resolved to reveal the platelet structure with step fracture faces quite visible. This is probably the site where much of the slow sorption-desorption occurs, with access achieved between these laminar entities.

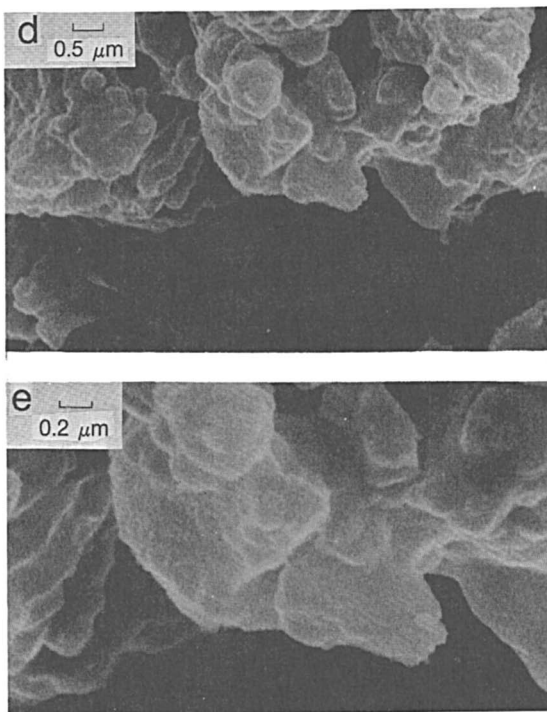


Figure 7. Continued

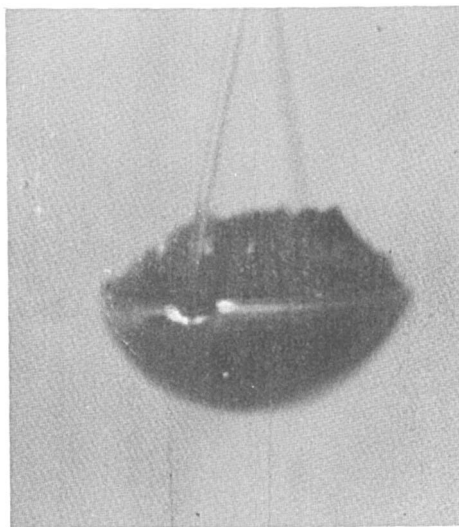


Figure 8. Expanded sample bed: original sample expanded about 40% as a result of the intraparticle swelling occurring during the course of sorption-desorption experiments

where P^* is the pressure corresponding to ϵ_0 , the sorption potential associated with the first increment of sorption. Generally, experimental data are acquired under conditions such that $P \gg P^*$, where Equation 9 is described accurately by Equation 8. It is not unrealistic to conceive of the situation at such low pressure ($P < P^*$) that the sorbate molecules remain in the gas phase. In other words, the probability of a gas molecule being in the rarified atmosphere is much greater than the probability of it residing in the sorbent in this stringent condition.

In evaluating the mechanistic models for sorption by coals, one is well advised to consider the contrast of the two general classes of sorbents: "physical adsorption (sometimes called physisorption) will likely alter the surface structure of a molecular solid adsorbent (such as ice, paraffin, and polymers), but not that of high surface energy, refractory solids (such as the usual metals and metal oxides, and carbon black)" (9). Adamson (27) has proposed

$$\epsilon = g/x^3 + \epsilon_0 \exp(-ax) - \beta \exp(-\alpha x) \quad (10)$$

as a comprehensive means of data analysis and isotherm evaluation. In this work we have not found it necessary to utilize more than the one term as defined by Equation 3. Such a simplification is in accord with the molecular nature of coal and the resultant structural modification induced in the sorption-desorption processes.

Very recently other investigators have found that one cannot assume the coal to be a truly inert sorbent (28, 29). This report is not to be construed as a definitive description of the structure of coal. However, the concepts and data described above should aid in more efficient use of this abundant but not unlimited resource.

Glossary of Symbols

- a* Adjustable parameter in polarization theory
- b* Adjustable parameter in pore-filling theory
- c* Adjustable parameter in Henry's law
- h* Planck's constant
- k_n Mass action rate constant
- m* Mass of sample
- n* Order of reaction rate
- P* Pressure
- P^* Pressure associated with initial sorption
- P_0 Vapor pressure of condensed sorbate at T
- r* Intermolecular distance
- R* Gas constant

- t Time
- T Temperature
- V Pore volume of sorbent filled at P and T
- V_0 Total pore volume of sorbent
- α Polarizability
- Γ Sorbate concentration
- ϵ Sorption potential
- ϵ_0 Initial sorption potential
- μ Dipole moment
- ϕ Intermolecular potential
- ν_0 Characteristic vibrational frequency

Literature Cited

1. Wiser, W. H.; Anderson, L. L. *Annu. Rev. Phys. Chem.* **1975**, *26*, 339.
2. Medik, J. *Fuel* **1977**, *56*, 131.
3. Tomkow, K. *Fuel* **1977**, *56*, 101.
4. Spitzer, Z. *Fuel* **1977**, *56*, 313.
5. Larson, J. W. *Fuel* **1978**, *57*, 309.
6. Fuller, E. L., Jr. *Prog. Vac. Microbalance Tech.* **1974**, *3*, 71.
7. *Ibid.*, **1972**, *1*, 265.
8. Brunauer, S.; Emmett, P. H.; Teller, E. *J. Am. Chem. Soc.* **1938**, *60*, 309.
9. Adamson, A. W. "Physical Chemistry of Surface"; Wiley: New York, 1976; p. 575.
10. Hall, G. R.; Lyon, L. B. *Ind. Eng. Chem.* **1962**, *56*, 36.
11. Wiser, W. H.; Anderson, L. L. *Annu. Rev. Phys. Chem.* **1975**, *26*, 339.
12. Hirsch, P. B. *Proc. R. Soc. London, Ser. A* **1975**, *226*, 143.
13. deBoer, J. H.; Zwikker, C. Z. *Phys. Chem. B* **1929**, *3*, 407.
14. Bradley, R. S. *J. Chem. Soc.* **1936**, 1799.
15. Steele, W. A. "The Interactions of Gases with Solid Surface"; Pergamon: Elmsford, 1974; Chap. 2.
16. Hirschfelder, J. O. "Molecular Theory of Gases and Liquids"; Wiley: New York, 1954; Chap. 13.
17. Fuller, E. L., Jr.; Agron, P. A. March 1976, ORNL Report 5129.
18. Nandi, S. P.; Walker, P. L. *Fuel* **1964**, *43*, 385.
19. Crank, J. "The Mathematics of Diffusion"; Oxford Univ. Press: New York, 1956.
20. Benson, S. W. "The Foundations of Chemical Kinetics"; McGraw-Hill: New York, 1960.
21. Fuller, E. L., Jr. "Microgravimetric Studies of Catalysts in Microweighing in Vacuum and Controlled Environments"; Czanderna, A. W., Ed.; in press.
22. Debelak, K. A. Ph.D. Thesis, University of Kentucky, Lexington, 1977.
23. Briggs, H.; Sinha, R. P. *Proc. R. Soc. Edinburgh* **1933**, *53*, 48.
24. Sereda, P. J.; Feldman, R. F. In "The Solid-Gas Interface"; Flood, E. A., Ed.; Marcel Dekker: New York, 1967; Vol. II, Chap. 24.
25. Czaplinski, A. *Arch. Gorn.* **1971**, *16*, 227.
26. Flood, E. A.; Heyding, R. H. *Can. J. Chem.* **1954**, *32*, 660.
27. Adamson, A. W. *J. Colloid Interface Sci.* **1973**, *44*, 273.
28. Debalek, K. A. *J. Colloid Interface Sci.* **1979**, *70*, 67.
29. Rouques, M.; Bastik, M. *Fuel* **1979**, *58*, 561.

RECEIVED July 19, 1979.

The Nature and Possible Significance of Particulate Structure in Alkali-Treated Brown Coal

R. J. CAMIER¹, S. R. SIEMON, H. A. J. BATTARD, and B. R. STANMORE

Department of Chemical Engineering, University of Melbourne, Parkville, Victoria 3052, Australia

An investigation has been made into the fine structure of Victorian brown coal by means of a particle size analysis of alkali-treated coal at pH 13. Examination of the $-40\ \mu\text{m} + 1\ \mu\text{m}$ fraction revealed periodic maxima in Stokesian diameter, which corresponded to repetitive mass units, and it was found that microscopic rod shapes $1\ \mu\text{m}$ in diameter and $6-8\ \mu\text{m}$ long were present in large quantities. These aggregated into clusters to give the particle size increments. In the smaller-sized fraction $-1\ \mu\text{m}$, no particles were detected until around the 2-nm mark, revealing a huge particle size gap. The sizes found indicate molecules of mass less than 10,000, i.e., humic acids. The mass of detritus and rods, etc., is surrounded by a matrix of humic acid gel. Three possible explanations for the presence of rodlike particles have been considered. The first suggests that the rods could be remnants of microbial protoplasm. The second considers the rods to be the heavily lignified remains of plant cell wall material. The third postulates a modification of the theory of coal genesis and assumes that lignin has been digested to humic acid types of molecules, which repolymerize by condensation. As the carbon content of the polymers rises, phase separation occurs and cylindrical domains form in a way similar to those found in copolymers of petrochemical origin.

¹ Present address: State Electricity Commission of Victoria, Herman Research Laboratory, Howard Street, Richmond, Victoria 3121, Australia.

The behavior of coal during processing is determined by its physicochemical composition and structure. The examination of the coal molecule has been hampered by the inability to find techniques that measure any meaningful properties of such large complex structures. Most attacks on the problem have been by means of breaking down the structure into smaller, more tractable pieces, examining these, and inferring the original structure. With bituminous coals the severity of the treatment needed to rupture the molecules raises doubts as to the validity of the method. There is uncertainty even with brown coals that are geologically younger and bear more resemblance to the molecules of classical organic chemistry. This uncertainty is reflected, for instance, in the diversity of models proposed for basic molecular arrangement (1-5).

Brown coals have the advantage that they can be broken down by the comparatively gentle treatment of alkali digestion (6) into fragments in the micron and submicron range. This breakdown results in a soluble fraction of humic acids and an insoluble residue, humins. With Victorian coals maximum digestion occurs at pH 13, to give humic acid yields ranging from 15% to 40% of the dry coal mass (7).

This paper reports on a study of digested coal fractions that were subjected to particle size analysis using sedimentation techniques. For the humins fractions a gravitational sedimentation technique was adopted, while the more finely divided humic acids required an ultracentrifuge to generate a sufficiently large force field. The nature of the fragments generated by this technique has resulted in a modified hypothesis of coal genesis.

Experimental

The coal examined was a sample of about 10 kg of medium light, earthy coal from the Yallourn mine in the Latrobe Valley, Victoria. Its ultimate analysis on a dry, mineral matter- and inorganic-free (DMIF) basis is given in Table I. A stock sample was prepared by wet ball milling followed by further size reduction in a domestic food pulper and was then stored under water in a closed vessel.

Table I. Particle Size Fractions

Fraction	Yield (%)	Carbon (%)	Hydrogen (%)	Oxygen (%)	Nitrogen (%)	Sulfur (%)
Original coal	—	65.6	5.18	27.9	0.75	0.4
+43- μ m fraction	20.3	62.7	4.88	31.6	0.63	0.3
Rod concentrate (-43, + 1.2 μ m)	46.4	65.8	5.94	27.2	0.78	0.3
Humic acids (-1.2 μ m)	31.0	59.7	3.90	35.3	0.70	0.3
Fulvic acids	2.2	23.1	8.48	68.5	—	—

For each test a 15-mL quantity of slurry was mixed with a 500-mL quantity of 0.1M NaOH solution to maintain pH at 13. After digesting overnight, the slurry was wet screened on a B.S. 350-mesh screen to remove +43- μm oversize particles. The underflow then was passed through a micropore filter of nominal pore size of 1.2 μm . The coal thus was fractionated into three particle size ranges.

Some of each of the fractions was acid-washed to remove sodium and reprecipitate the humic acids. A yellow supernatant liquid remained after precipitation of the humic acids, caused by small quantities of fulvic acid. An elemental analysis then was carried out on the dried solids of each fraction.

Other samples of alkaline slurry were subjected to particle size analysis by sedimentation. With the -43 μm + 1.2 μm fraction this analysis was done in a 50-mm-diameter settling column of dilute slurry with a tared pan at the base to record continuously the mass of sedimented solid. The data were analyzed by the method of Oden (8), and the particle size distribution (Stokesian diameter), expressed on a mass percent basis, was calculated.

The humic acid fraction (-1.2 μm), which was a dark brown suspension containing 4.7 mg/L of coal, did not settle even after standing for 6 months. This slurry was spun in a Beckman ultracentrifuge with special long tubes to generate high g values. Alkali-resistant polyallomer tubes were used so that the solids collected in the base could be removed in a special guillotine, then dried and weighed. The heights of suspension charged varied from 10 to 80 mm, and rotational speeds up to 40,000 rpm were used. The data were analyzed again by Oden's method, modified according to Brown (9).

Results

Results of the fractionation experiments are summarized in Table I.

A typical output from the sedimentation balance for -43 μm + 1.2 μm material is shown in Figure 1. The occurrence of distinct peaks indicates that groups of closely sized particles are present, the smallest being about 6 μm in effective (Stokesian) diameter. The frequent occur-

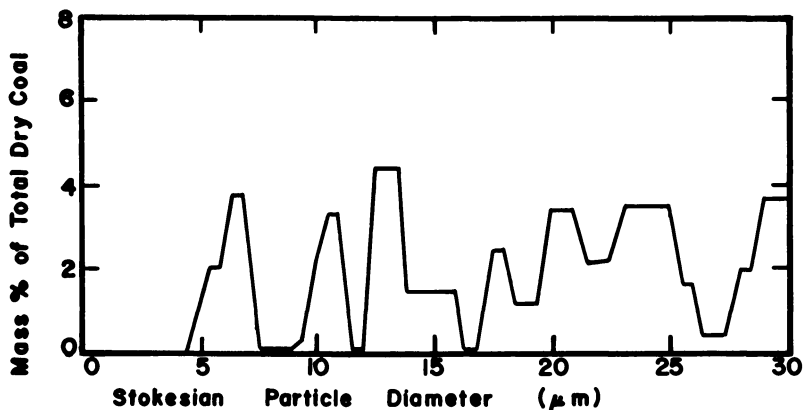


Figure 1. Particle size distribution (-43 + 1.2 μm size fraction)

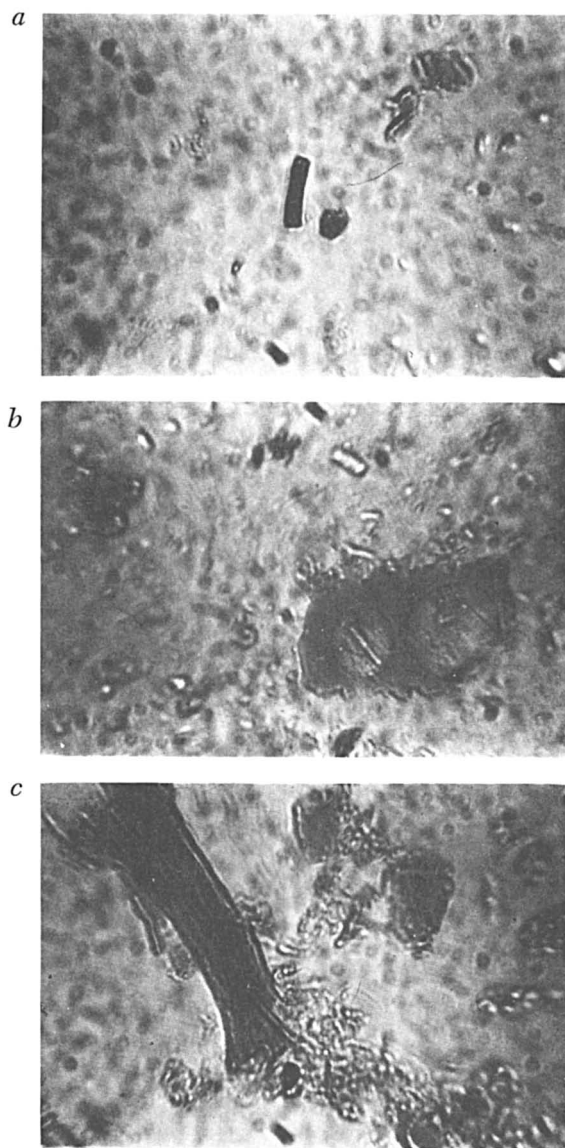


Figure 2. Photomicrographs of brown coal in pH 13 solution: (a) pair of typical rods; (b) cross section of cell remains; (c) rod peeling from xylitic fragment (14).

rence of similar-sized groups in tests with pH values ranging from 7 to 14, and with similar tests on five other Latrobe Valley coals (10), suggested that some fundamental unit was present. A microscopic examination of the material revealed that cylindrical rods about $0.9 \mu\text{m}$ in diameter and

6–8 μm long were common (Figure 2). When the drag coefficient for such particles was calculated from Lamb's formula for cylinders at low Reynold's number [*see* Prandtl (11)], the terminal setting velocity was the same as for a spherical particle of about 6- μm diameter.

The larger particle sizes thus could be accretions of these basic units, and several such agglomerations were noted. The rods were arranged side by side, closely packed in bundles. Apparently the alkali peels these rods from the coal mass, and they subsequently agglomerate in solution, similar to tactoid formation (12), according to a crystal growth type of clustering theory (13, 14.)

Elemental analyses of the fractions showed that the rod fraction ($-43 \mu\text{m} + 1.2 \mu\text{m}$) is rich in both hydrogen and carbon when compared with the original coal, Figure 3, although the effect is obscured partly by the slight oxidation that takes place in alkaline solution (10). The higher carbon and hydrogen contents of the rod-concentrate fraction are attributable mainly to the liptinite material (pollen, spores, waxes, etc.) that predominates in this size range.

The particle size distribution for the humic acid fraction is depicted in Figure 4. No material sedimented out until the most extreme conditions were applied (40,000 rpm for 24 hr), when some lightening of color at the top of the solution was observed. The sedimented particles had a Stokesian diameter of around 2 nm, which means that a particle size gap of three orders of magnitude exists between these and the next largest particles detected (5 μm). From the experimentally determined coal particle density of 1.43 g/cm³, it was calculated that a solid sphere of diameter 2 nm would have a molecular mass of 4000. If the molecules were rod-shaped, even smaller molecular masses would be predicted. Literature values of the molecular mass of regenerated humic acids range between 800 and 20,000, with the values clustering around 1,000 and 10,000 (15, 16, 17).

Since the humic acid fraction constitutes 30% of the dry coal mass, about one-third of the coal is in the form of small macromolecules that are bound to the coal structure with bonds weak enough to be disrupted by dilute alkali.

It is of interest to note that the particle size gap supplies a rational basis to the traditional German classification scheme of defining humic acid and humins on the basis of a particle size separation (filtration).

Discussion

The presence of geometrically uniform rods and the absence of particles over such a wide particle size range have implications for our understanding of coal chemistry and genesis. The following discussion attempts to harmonize these observations.

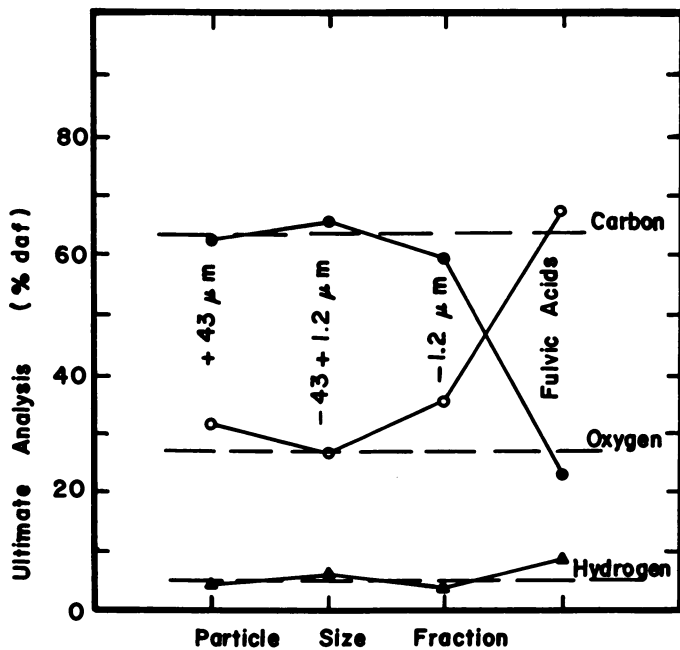


Figure 3. Ultimate analysis of fractions (--) original coal; (○) carbon; (●) oxygen; (▲) hydrogen

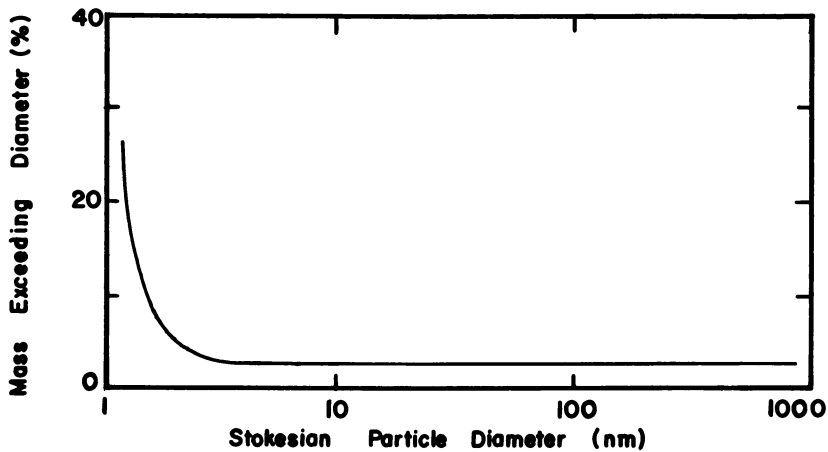


Figure 4. Particle size distribution (-1.2 μm size fraction)

Three hypotheses have been considered to explain the origin of the rods found during this work: (1) bacterial remains; (2) plant cell remains; (3) artifacts formed during phase separation in the coalification process.

Since bacteria, including rodlike bacilli, are active during the biological digestion stage of coalification, remnants of their protoplasm may have been incorporated into the coal matrix. If this were so, their protein content (about 15% nitrogen) should result in a high nitrogen content. Table I shows, however, that although the nitrogen content of the rod fraction is higher than the others, it can only be significant if the rods constitute a very small portion of the total mass of the $-43 \mu\text{m} + 1.2 \mu\text{m}$ fraction. Since their concentration appears to be much greater than this, the hypothesis is unattractive.

The abundance of identifiable cell fragments observed under the microscope lends weight to the second hypothesis. The microfibril structure of the walls of the coniferous wood cells [from which brown coal is largely derived (10)] suggests that these walls may be composed of several layers of rodlike particles. This idea is supported by the fact that these cell walls are known to consist principally of lignin, and that during the coalification process the lignin is less affected than the other major component cellulose (18). Hence it would be expected that the cell walls would be only partly decomposed. Furthermore, the composition of the wood fraction is close to that of lignin, and the rods have been microscopically observed peeling off larger wood fragments under the influence of alkali (14).

The third hypothesis is more speculative and far-reaching in its implications. It is generally accepted (19) that the first steps in the genesis of coal are the destruction of cellulose and the degradation of lignin to monomer, which either is a humic acid or polymerizes to give humic acids. The polymerization of these acids takes place by condensation, as indicated by the decrease in acidity with increase in molecular mass. As the concentration of monomer decreases, a gel point is reached and a giant network is formed, swollen by the solvent water. As the polymerization proceeds further, the network will become cross-linked, resulting in shrinkage and water exclusion.

Considering macromolecules in surface energy terms, the solubility parameter has been defined as

$$\delta = \left[\frac{E}{V} \right]^{1/2} \quad (1)$$

where E is the molar cohesive energy and V is the molar volume. For two polymers A and B, the materials are compatible if (15)

$$(\delta_A - \delta_B)^2 < 4.2 \text{ kJ/L} \quad (2)$$

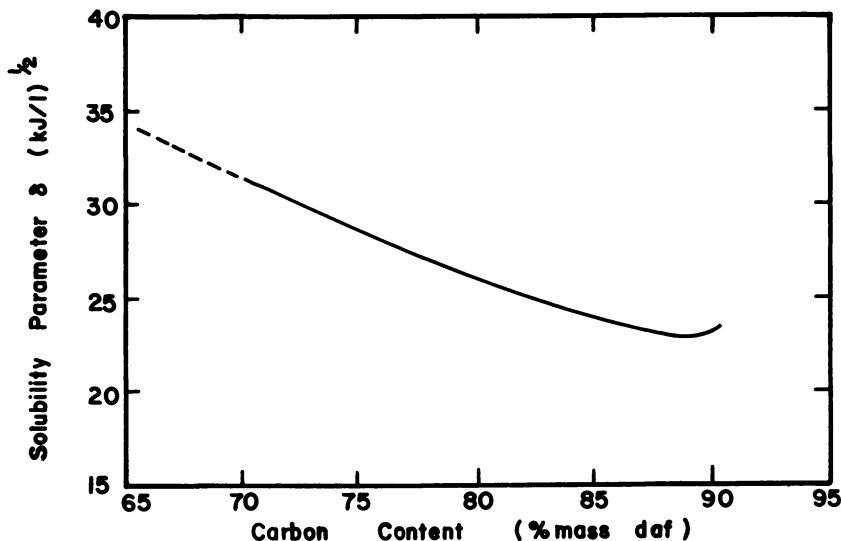


Figure 5. Solubility parameter vs. % carbon

If this inequality does not hold, phase separation of polymers will occur. The solubility parameter of coal over a wide range of coal ranks has been measured (20–23) and is plotted in Figure 5. The value of δ falls nearly linearly from 32 to 23 as the carbon content rises from 70% to 89% and rises slowly thereafter. At 89% carbon, polar groups are largely absent and aromatization has commenced. By extrapolation back to the 65–70% carbon range occupied by brown coals, the line is steep enough that only a small change in carbon content is sufficient to create incompatibility between coal molecules, resulting in phase separation.

A large polymer molecule is able to exist with different parts of the chain in different phases, and an increase in the concentration of the species will concentrate solvated parts together as well as concentrating the precipitated parts. With two different polymers, e.g., polystyrene and polybutadiene, blocks of one will form within a continuous phase of the other, with domain sizes between 10 and 100 nm usual. This segregation into phases will be enhanced by the swelling effect of the remaining polymer.

In the case of coal formation, woody residues could intermingle with condensation polymers that are swollen by the water-soluble products from the degradation of cellulose and lignin. The local changes in carbon content brought about by condensation polymerization may be sufficiently large for phase separation to occur, and the rods may be formed from local high-carbon regions (compare Figure 3). Rod-shaped inclusions are known to form in materials like polyethylene oxide–polypropylene oxide copolymers within certain concentration limits as listed below:

- High concentration of A: spheres of B dispersed in A
rods of B dispersed in A
alternate layers of A and B
rods of A dispersed in B
- Low concentration of A: spheres of A dispersed in B

In this view rods are precipitates formed from the humic acid groundmass and represent a further step in the coalification chain.

The revised model of coal structure that emerges from this study envisages a gel of humic acid molecules swollen by water and incorporating particulates. These include rods and detrital matter like pollen, cell remains, exinite material, etc., which are held together by the humic acid glue. The bonds linking this mass together must be of a homopolar, nonregenerable type, as rheological studies of Victorian coals have shown that the bonds are broken by shear action during mechanical working and do not remake on standing (24). This excludes the hydrogen bonds, which are known to remake after rupture. Ester bonds, which are known to hydrolyze in the presence of alkali, and van der Waals types of bonds could be responsible for holding the structure together. On rupture, the water that is liberated by shearing would be able to attach at the vacant sites and thus prevent the remaking of the original, stronger bonds.

Conclusions

1. Particle size analysis of alkali-digested brown coal provides a useful insight into coal structure.
2. Victorian coals contain significant quantities of cylindrical rod-shaped particles, 1 μm in diameter and 6–8 μm long, which are high in carbon and hydrogen.
3. No particles exist in alkali-digested coal solutions between 6 μm and 2 nm Stokesian diameter.
4. Brown coal can be regarded as a gel of humic acids that incorporates larger particles bound by nonregenerable bonds.

Acknowledgments

The authors thank the Victorian Brown Coal Research and Development Committee, The National Coal Research Advisory Committee, and the Australian Research Grants Committee whose financial assistance enabled the work to be carried out. The responsibility for the views expressed rests entirely with the authors.

Literature Cited

1. Agroskin, A. A. "Chemistry and Technology of Coal" (English translation from Russian); Israel Program for Scientific Translations: Jerusalem, 1966.
2. Fuchs, W. "Die chemie der Kohle"; Springer: Berlin, 1931.

3. Durie, R. In "Chemistry of Brown Coals", *Coal Research in CSIRO* 1959, 6, 12.
4. Breger, I. A. "Chemical and Structural Relationship of Lignin to Humic Substances," *Fuel* 1951, 9, 204.
5. Dragunov, S. S. In "Soil Organic Matter"; Konova, M. M., Ed.; Pergamon: London, 1961; p. 65.
6. Mukherjee, P. N.; Bhowmik, J. N.; Lahiri, A. *Fuel*, 1957, 36, 417.
7. Camier, R. J.; Siemon, S. R. *Fuel* 1978, 57, 85.
8. Oden, S. *Soil Sci.* 1925, 19, 1.
9. Brown, C. "Particle Size Distribution by Centrifugal Sedimentation," *J. Phys. Chem.* 1944, 48, 246.
10. Camier, R. J., Ph.D. thesis, University of Melbourne, 1977.
11. Prandtl, L. "The Essentials of Fluid Dynamics"; Blackie: London, 1960; p. 190.
12. Jurgensons, B.; Straumanis, M. E. "A Short Textbook of Colloid Chemistry"; Pergamon: London, 1954.
13. Herrera, R., Ph.D. thesis, University of Melbourne, 1973.
14. Camier, R. J.; Siemon, S. R. *Fuel* 1978, 57, 693.
15. Brooks, J. D. "Advances in Coal Chemistry 1950-1970", *Coal Research in CSIRO* 1971, 45, 20.
16. Samec, M.; Pirkmaier, B. *Kolloid-Z* 1930, 51, 96.
17. Fuchs, W. *Brennstoff-Chem* 1928, 9, 178.
18. Spackman, W.; Barghoorn, E. S. *Adv. Chem. Ser.* 1966, 55, 274.
19. Flaig, W. "The Use of Isotopes in Soil Organic Matter Studies"; Pergamon: New York, 1966.
20. Brandrup, J.; Immergut, E. H. "Polymer Handbook"; Wiley: New York, 1966.
21. Van Krevelen, D. W. *Fuel* 1965, 44, 229.
22. Kirov, N. Y.; O'Shea, J. M.; Sergeant, G. D. *Fuel* 1967, 46, 415.
23. Sanada, Y; Honda, H. *Fuel* 1966; 45, 451.
24. Covey, G. H. Stanmore, B. R. *Fuel* 1980, 59, 123.

RECEIVED July 19, 1979.

The Ultrafine Structure of Coal Determined by Electron Microscopy

L. A. HARRIS and C. S. YUST

Oak Ridge National Laboratory, Oak Ridge, TN 37830

The size and distribution of pores and the size, distribution, and identity of minerals in coal specimens from an eastern Kentucky splint coal and the Illinois No. 6 coal seam were determined by means of transmission electron microscopy (TEM) and analytical electron microscopy (AEM). The observed porosity varies with the macerals such that the finest pores (<2–5 nm) are located in vitrinite, with a broad range of coarser porosity (40–500 nm) associated with the macerals exinite and inertinite. Elemental analyses, for elements of atomic number 11 or greater, in conjunction with selected area diffraction (SAD) experiments served to identify the source of the titanium observed in the granular material as the mineral rutile. Only sulfur could be detected in the other coal macerals. Dark-field microscopy is introduced as a means for determining the domain size of the coal macerals. This method should prove useful in the determination of the molecular structure of coal.

The technological utilization of coal is dependent upon its physical characteristics as well as its chemistry. The size and spatial distribution of pores and the size, distribution, and identity of the submicron-size minerals are physical attributes of particular interest because of their influence in coal conversion processes such as liquefaction and gasification.

The advantages to be gained by the use of the electron microscope in performing detailed studies of coal were recognized by McCartney (1) as early as 1949 and subsequently employed by McCartney and his co-workers (2–6) at the U.S. Bureau of Mines. Additional significant contributions were made by Alpern and Pregermain (7) and Pregermain and Guillemot (8) at the Center for Coal Study and Research in France. Both of these research groups developed methods for coal specimen preparation and performed studies of coal macerals. However, these studies were

limited in scope by the available microscopes and sample preparation techniques. Recent advances in electron microscopy, especially in analytical electron microscopy, have resulted in a resurgence of interest in the study of coal by these methods.

The present paper is one of a series in which advantage has been taken of these more advanced electron microscope methods and instruments to examine bituminous coals (9, 10). These techniques have the advantage of revealing the microstructures of coal at magnifications greater than those available with light microscopy and at substantially increased microscope voltages than had been attainable previously. In addition, AEM for the detection of ions of mass greater than 11 on areas as small as 10 nm in diameter is now possible. Consequently, a more detailed direct observation of the pores and submicron-size minerals within the coal may be obtained as well as limited elemental analyses of minerals and macerals.

Experimental

Sample Selection and Preparation. Samples were selected from two high-volatile bituminous coals, namely, Illinois No. 6 bright coal and an eastern Kentucky splint coal from Perry County. The choice of these coals was based on the desire to contrast the fine structure of coals of equal rank but of different lithotypes. For both coals the samples were obtained from limited regions of their respective coal seams. Detailed coal petrography was performed on these samples, and TEM specimens were subsequently selected from representative polished blocks.

Specimens were prepared from the samples above by slicing sections normal to the bedding and subsequently grinding them into optically thin sections 10–12 nm thick. The optical sections were removed from the slide by acetone and thinned to electron transparency by ion bombardment (ion milled). The ion-milling process was performed on fragments 3 mm on edge, using argon gas and a liquid nitrogen cold stage in order to ensure a sample free from thermal damage. The relative resistance of the minerals to ion milling in comparison to the macerals results in specimens that are differentially thinned such that some of the larger mineral fragments stand out in relief. The finished ion-milled samples were fixed to electron microscope grids by using silver conductive paints.

Analytical Methods. Both a high-voltage TEM (1 MeV) and a scanning transmission electron microscope (STEM) (120 kV) were used in this study. The STEM was fitted with an energy dispersion system utilizing a Si(Li) solid state detector. Microchemical analyses of particles as small as 20 nm for elements of atomic number 11 or greater could be attained by use of the STEM and the energy dispersive X-ray (EDX) unit. In addition to utilizing a much smaller probe diameter, STEM eliminates the large scatter volume involved in microprobe analyses of bulk samples and reduces X-ray absorption and fluorescence errors. Therefore, a more accurate analysis of the sample volume being irradiated is achieved.

Results and Discussion

Observations of Microstructures and Porosity. Figures 1 and 2 are TEM micrographs of specimens from the splint and bright coals, respec-

tively. The micrographs illustrate the differences in microstructures between these coals of the same rank. In general, the splint coal contains fragments of exinite, inertinite, and vitrinite closely compacted together, with the former two macerals making up over 70 vol % of the material. In contrast, the Illinois No. 6 coal contains large bands of vitrinite interbedded with inertinite and exinite; the latter two macerals combined comprise between 10 and 20 vol % of the total macerals.

Examination of the microstructure in Figure 1 reveals that the exinitic material (E_1) is predominantly featureless in electron transmission. This material, however, occasionally contains relatively large and irregularly shaped pores (P). Immediately adjacent to the exinite is a region of vitrinite (V), containing a nearly uniform distribution of fine porosity. The boundary between the exinite and the vitrinite contains opaque fragments of mineral-bearing inertinite as well as more finely divided inertinitic matter. The coarse porosity associated with the granular inertinite at the boundary is seen by detailed study to be continuous with the finer porosity that is observed in the vitrinite. This gradation of

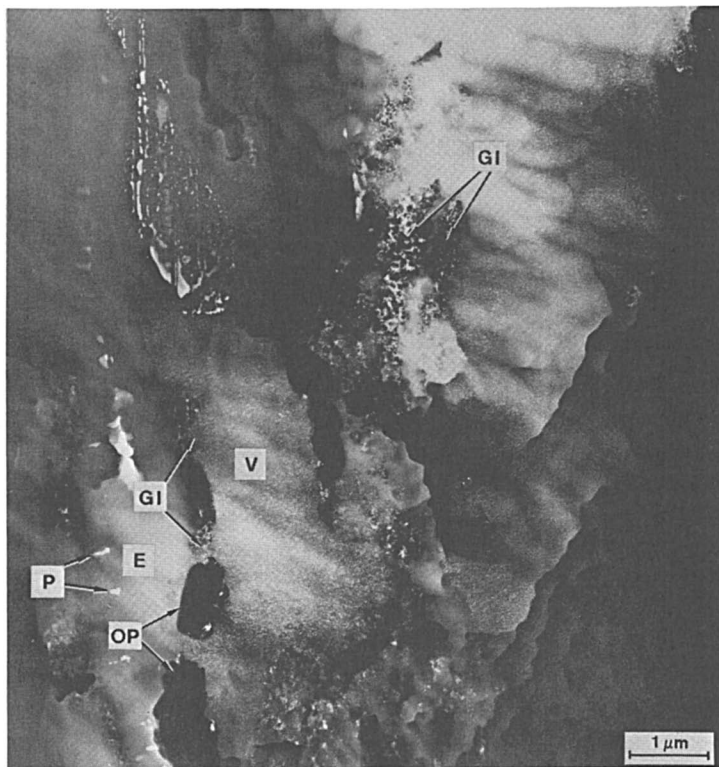


Figure 1. TEM of splint coal (E) exinite, (V) vitrinite, (GI) granular inertinite, (OP) opaque particles, and (P) pores in exinites)

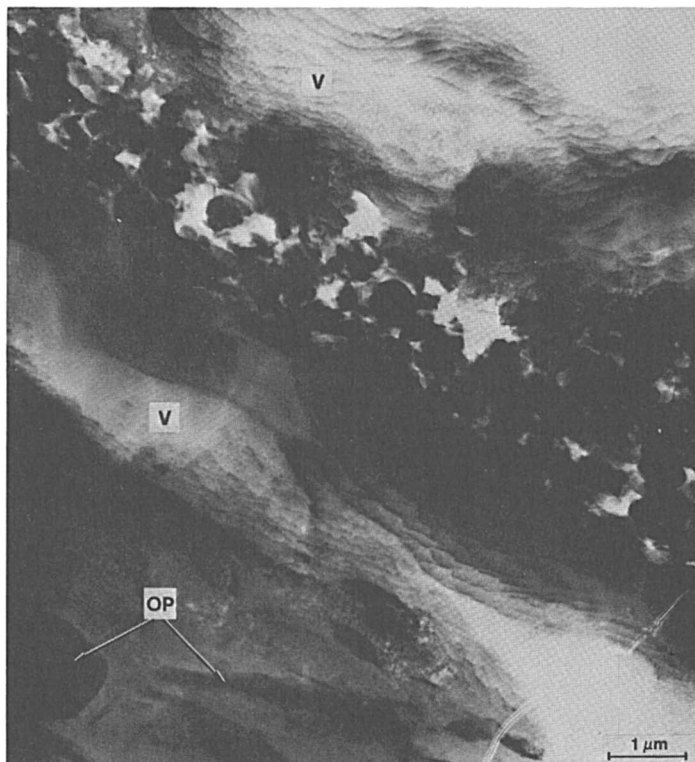


Figure 2. TEM of Illinois No. 6 coal ((V) vitrinite and (OP) opaque particles)

porosity from the inertinite to the vitrinite may be indicative of a transitional zone between the two macerals (perhaps semifusinites.) The vitrinite bands observed in this field are relatively porous and, as might be expected in a low-density body, the porosity is highly interconnected.

On the other hand, in Figure 2 the granular constituent shown in the Illinois No. 6 microstructure contains a broad range of interconnecting pores (about 40–500 nm in diameter), which may be classified as predominantly macropores (<50 nm). The exact identity of the granular constituent is not clear; however, it is thought to be a mixture of inertinite and exinite. Large vitrinite bands dominate the microstructure of the Illinois No. 6 coal. Areas of interconnected fine porosity can be observed in both the vitrinite bands. Also noteworthy in this microstructure are the opaque (OP) fragments similar to those observed in the splint coal that have been found to contain minerals. The opacity of these regions (OP) is probably caused by the greater resistance to ion

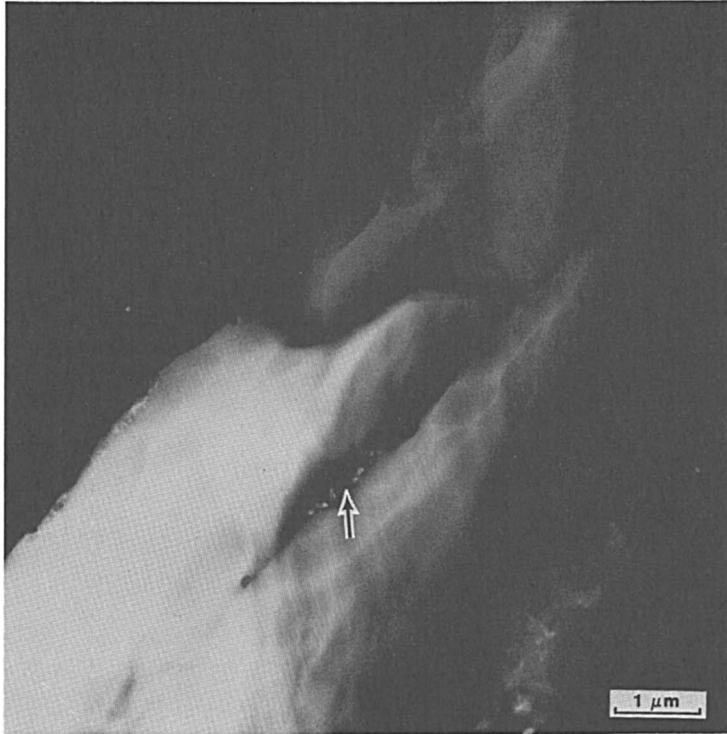


Figure 3. TEM micrograph of microspore showing fracture surfaces and granular inertinite fill in the compressed spore cavity (see arrow)

milling of the included mineral matter that is intimately mixed with the organic constituents.

The spore exines (exinite) in these low-rank bituminous coals exhibit highly fractured surfaces (Figure 3) as a result of ion milling. The appearance of this surface is suggestive of a hard, brittle material, which may be contrasted with the usual view of spore exines in coals of this rank as being very tough (11), typically standing out in relief upon being polished. Also of interest in this micrograph is the presence of the highly porous granular inertinite inside the compressed spore cavity (see arrow).

The porosity associated with the exinitic maceral of the splint coal can be seen more clearly in Figure 4. The large, irregularly shaped pores often form distinct tubular channels, which extend from the apparent center of the spore exine to the boundary between the spore and the surrounding inertinite. Commonly the channels contain spherical particles, whose identity as the mineral aragonite (CaCO_3) was based on

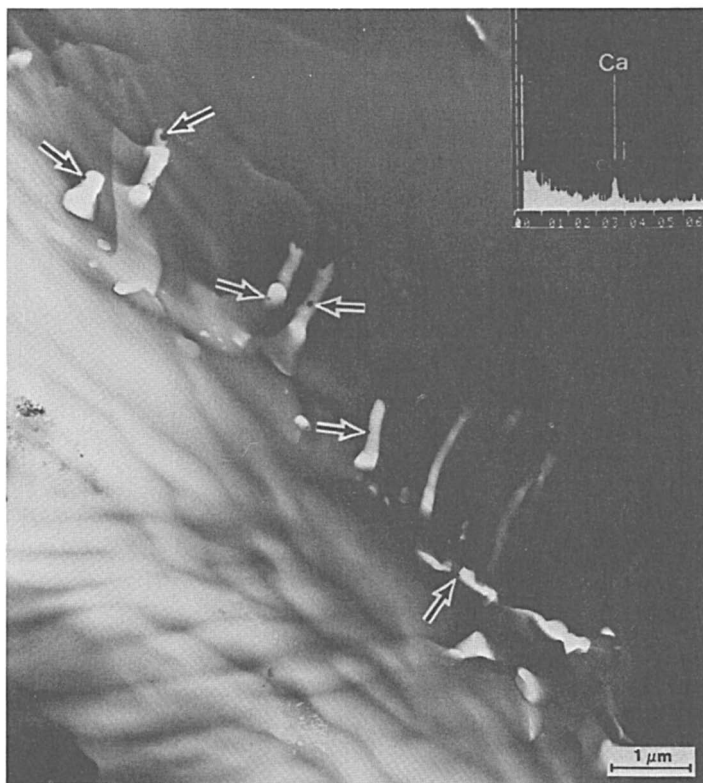


Figure 4. TEM of tubular and irregular pores in exinite showing the location (see arrows) and X-ray spectrum (see insets) of spherical particles

EDX analyses (see inset in Figure 4) and SAD data. These latter data were based on limited diffraction information from three separate particles and were combined to form a table of interplanar spacings, which were found to be in good agreement with similar aragonite data from JCPDS card No. 22-25A (Table 1).

A previous study (12) on the interaction of fine metal particles on graphite surfaces demonstrated that particles can catalyze surface reactions and lead to the generation of elongated pores of the type shown in Figure 4. The similarities of the pore geometry and the presence of mineral particulates led to the speculation that the pores observed in the exinite were the consequence of a reaction catalyzed by the mineral particles. The source of the particles is believed to be the mineral-rich granular inertinite that typically surrounds the spore exine. However, further studies revealed that all particles analyzed to date contain only calcium as the heavy atom, which leads one to question the absence of

Table I. Comparison of Composite Electron Diffraction Data with X-Ray Diffraction Data of Aragonite (JCPDS Card No. 22-25A)

<i>d</i> (Å) Composite SAD Data	<i>d</i> (Å) Aragonite
3.37	3.39
2.18	2.189
2.11	2.106
1.84	1.877
	1.827
1.75	1.759
	1.742
1.68	1.697
1.44	1.466
	1.412
1.12	1.125
	1.107
1.09	1.095
	1.089

other minerals in the exinitic pores. Two possible causes for the exclusive presence of aragonite are that (1) aragonite formed in situ within the spore exine in a manner similar to that reported for dolomite [$\text{MgCa}(\text{CO}_3)_2$] crystals grown from organic materials in situ (13) and (2) other minerals do not act as catalysts for the formation of pores. The latter cause appears to be contrary to available data on catalysts in that no calcium carbonate mineral is reported to act as a catalyst, thus lending strength to the in-situ growth concept.

Previous porosity studies of coal by gas absorption methods (14) reveal a direct relationship between the fine porosity and the vitrinite content of a coal. These observations are confirmed by this study for both the splint coal and the Illinois No. 6 coal inasmuch as all the vitrinite observed by TEM was found to contain large regions of fine porosity. In Figure 5, a TEM micrograph of a vitrinite fragment in the splint coal, the range of pore diameters extends from 2 nm to > 50 nm. The smallest pores, some of which may even be < 2 nm, appear to be related to connecting channels or irregularly shaped pores that cannot be described as spherical. Stereo pairs of these vitrinite fragments indicate a connecting network of pores suggesting high permeability.

Figure 6 is a TEM micrograph of a region of vitrinite in the Illinois No. 6 coal obtained at high magnification (50 K) in order to perform a more detailed analysis of the porosity associated with this maceral. Pore dimensions range from 1 to 10 nm, which classifies them as a mixture of micropores (<2 nm) and mesopores (2–50 nm). The observation of porosity in the two-dimensional image becomes more difficult as the specimen thick-

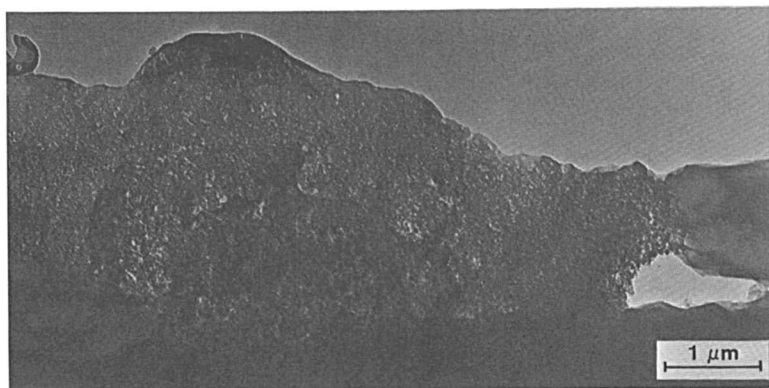
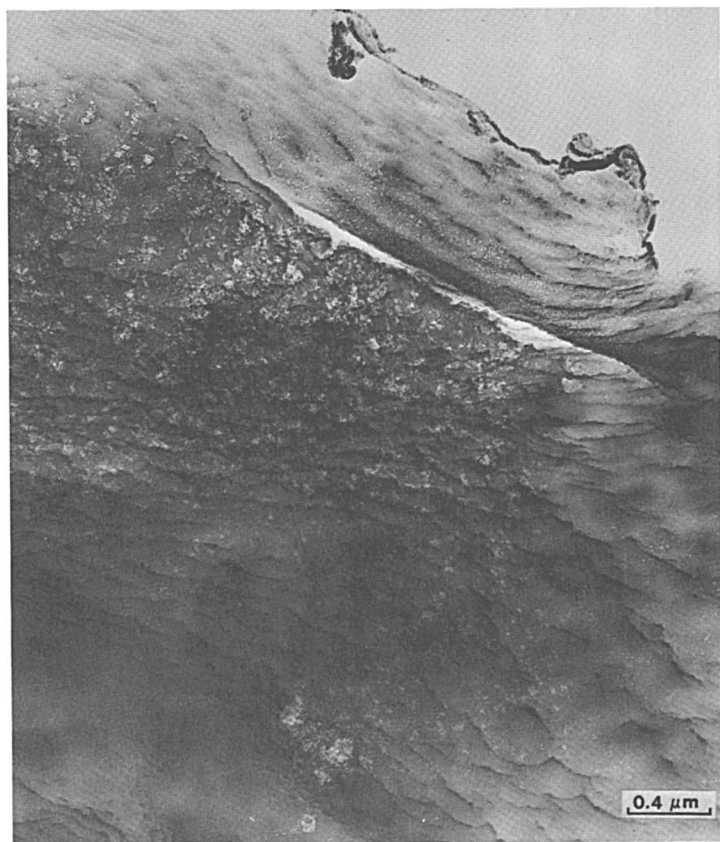


Figure 5. Fine porosity observed in vitrinite fragment in splint coal by TEM

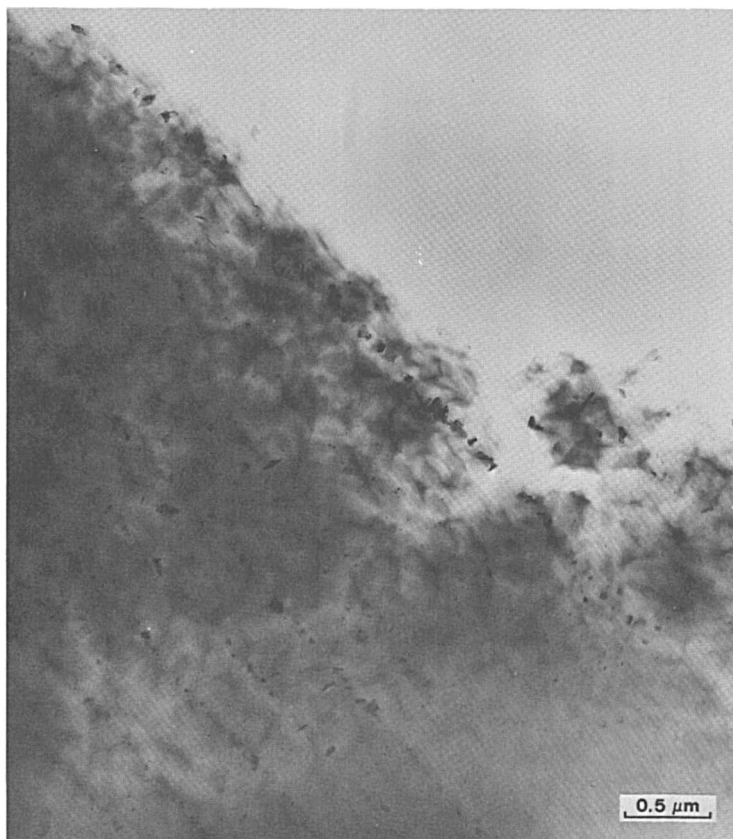


Journal of Applied Crystallography

Figure 6. Fine porosity observed in vitrinite fragment of Illinois No. 6 coal by TEM (16)

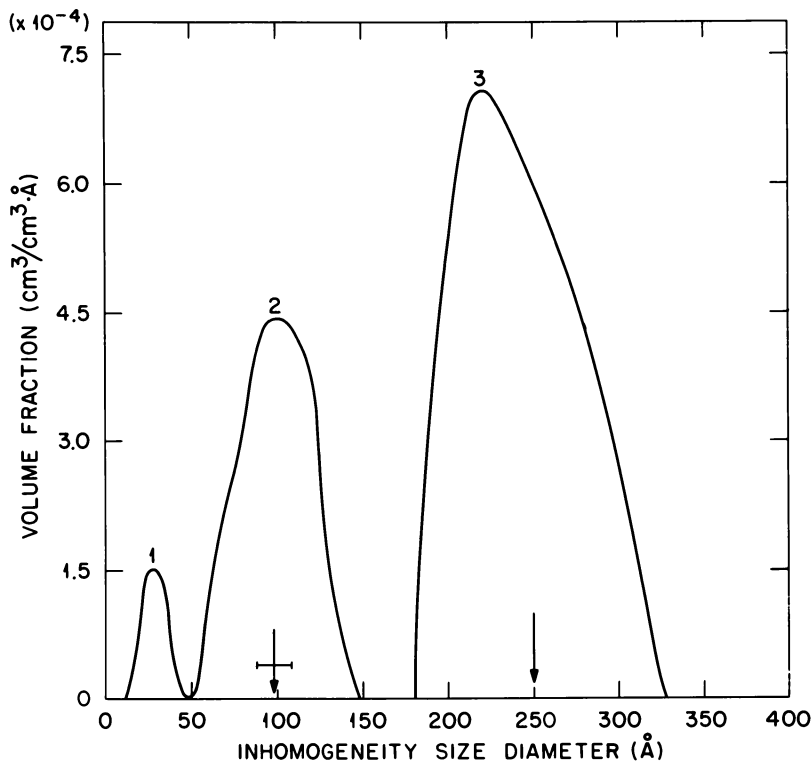
ens. However, when viewed in three dimensions via a stereo pair, the porosity in the thicker regions remains clear. Three-dimensional viewing also reveals that the porosity is irregularly shaped and is often present as volumes of highly interconnecting pores. In regions of locally high porosity, as is observed in the center of Figure 6, the degree of interconnectivity is relatively great, whereas in the surrounding region the pore volumes are largely isolated.

Several vitrinite fragments were found to contain bands of minerals, aligned parallel to the bedding plane of the coal (Figure 7). Many of the minerals exhibit well-developed growth habits. A size analysis of the minerals (15) by direct measurement from the TEM micrographs reveals that the majority of minerals were under 30 nm in diameter, with the average diameter being 10 nm. Larger mineral fragments up to 300 nm on an edge were recorded but comprised only a small fraction of the total



Journal of Applied Crystallography

Figure 7. TEM of vitrinite of Illinois No. 6 coal showing bands of minerals (16)



Journal of Applied Crystallography

Figure 8. The size distribution of pores and minerals from vitrinite (Illinois No. 6) obtained by SAXS (16)

observable mineral matter. A subsequent analysis of a similar sample of Illinois No. 6 coal by small-angle X-ray scattering (SAXS) (16) showed a multimodal size distribution (Figure 8), which essentially confirmed the TEM observations. For example, the peak at 3 nm relates to the fine pores observed in the vitrinite component, whereas the peak at 10 nm fits the average mineral diameter, and, finally, the peak at 25 nm accounts for the larger mineral fragment plus the larger pores observed in the granular constituent.

AEM. EDX analyses by means of a STEM were performed on numerous microareas of the specimens under investigation. Typically the analyses obtained from the opaque fragments and the coarse granular inertinite yielded X-ray spectra for such elements as Al, Si, Fe, S, Ca, and K. These elements could generally be assigned to such minerals as clays, pyrite, gypsum, calcite, and quartz. However, several analyses of the granular constituent either filling the compressed spore cavities or surrounding the spores revealed less common elements, e.g., titanium (see Figure 9). In a detailed scan of the granular material the source of

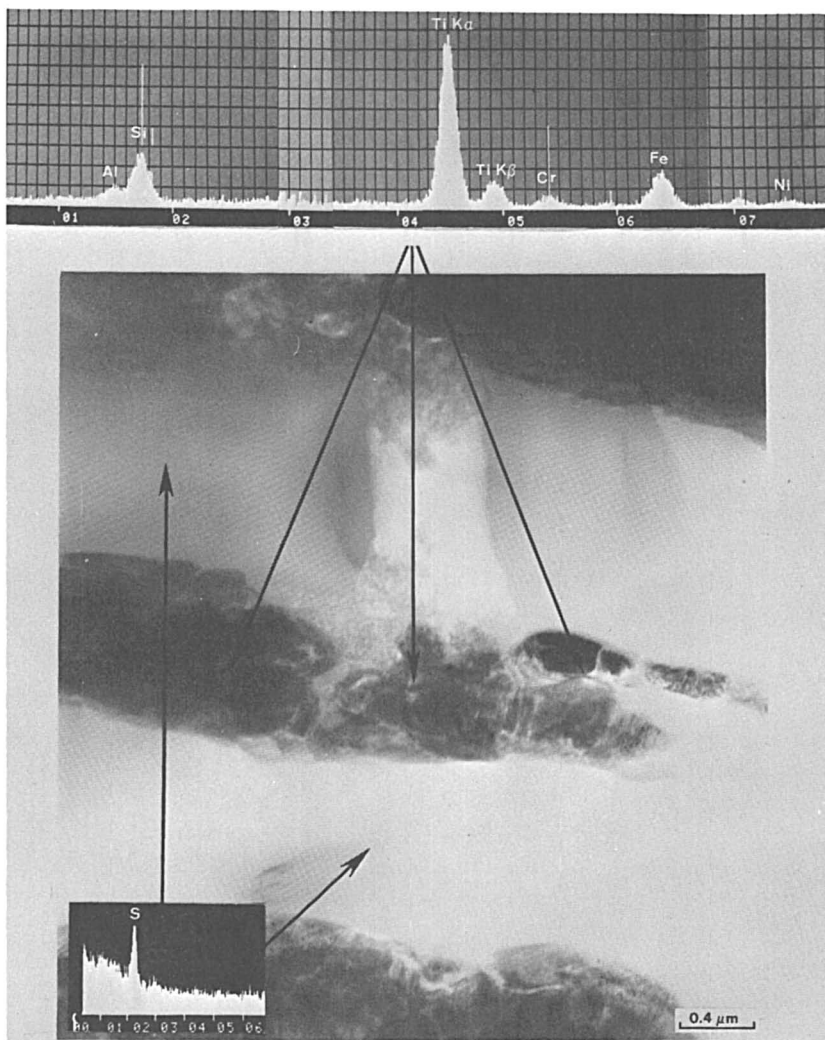


Figure 9. TEM micrograph of sporinite with associated granular constituent showing typical EDX analyses of these constituents at the top and lower left-hand corner, respectively

the titanium X-ray spectrum was isolated and led to the identification of a particular mineral fragment. The thickness of the fragment precluded obtaining a good diffraction pattern; nevertheless, at least five individual reflections could be measured and were found to be in good agreement with interplanar spacings (d values) listed for rutile (TiO_2).

In contrast to the EDX analyses of the granular constituent, the analyses of the exinite performed under identical conditions yielded only the X-ray spectrum of sulfur (see insert at bottom of Figure 9). It is

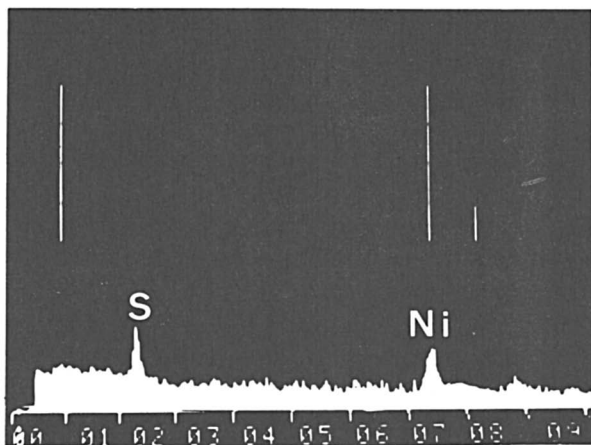


Figure 10. X-ray spectrum of nickel sulfide mineral located in granular opaque constituent

interesting to note that in all EDX analyses of coal macerals in these samples, which were relatively transparent and featureless (except for porosity), the only detectable element is sulfur.

Other less common elements recorded in these analyses are tin, chromium, and nickel. The tin is found among some of the opaque constituents (minerals) and is thought to be present as the mineral cassiterite (SnO_2), which is reportedly (17) associated with sulfide mineralization. Less is known about the location of the chromium, which may be a minor element in more than one mineral, e.g., pyrite and calcite. Nickel, on the other hand, is associated with sulfur, as can be shown in the X-ray spectra (Figure 10) obtained from a diamond-shaped mineral fragment. The analysis was obtained in the reflection (SEM) mode on the STEM, which excluded the recording of an electron diffraction pattern. The mineral tentatively is identified as millerite, a nickel sulfide (NiS) with no iron and a 1:1 ratio of nickel to sulfur. However, these conclusions must be considered as tentative until positive identification of the nickel sulfide is possible.

In addition to those minerals associated with the granular constituent, there are numerous submicron-sized minerals that are intimately mixed with other coal macerals. A typical example can be seen in Figure 11, which is a TEM micrograph of vitrinite, where the circular aperture identifies the region from which the electron diffraction pattern, shown in the inset, was obtained. The mineral, which was identified as kaolinite, appears to have been deposited as plates parallel with the coal bedding, based upon an analysis of the diffraction pattern. Also present in these coals is the clay mineral illite, which can be distinguished from kaolinite by both EDX and SAD analyses. Illites contain potassium (K)



Figure 11. TEM micrograph of splint coal showing SAD pattern of kaolinite interbedded with vitrinite

in the interlayer position along with some iron substituting for aluminum in the alumina-silicate network. The ion exchange capacity of illite is much greater than that of kaolinite and thus may play a more significant role in coal chemical reactions. Furthermore, the effect of these clay minerals, which comprise a large irregular surface area in intimate contact with a highly porous body (vitrinite), on coal utilization is not clear, but certainly their size precludes their removal from the organic matrix.

Many of the fine minerals shown previously in Figure 7 can be seen to be randomly oriented; in fact, some of the platy minerals are found to be perpendicular to the layering. SAD experiments on some of the larger mineral plates typical of those shown in Figure 12 resulted in diffraction patterns of the type shown in the inset. The pattern was indexed as the $(hk0)$ plane of kaolinite, indicating that the electron beam is parallel to the c -axis of the crystal.

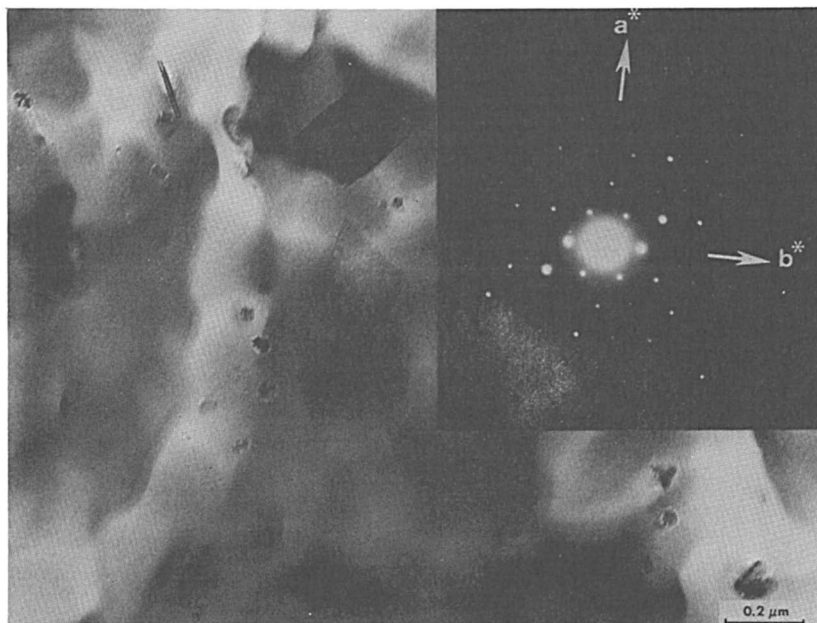


Figure 12. Indexed SAD pattern (see inset) shows orientation of large platy kaolinite crystals of the type shown in the TEM micrograph

The broad, inner diffraction ring observed in the diffraction pattern above was attributed to the organic constituent vitrinite. It is believed to be the low-angle diffraction maximum observed in X-ray diffraction studies of vitrinite and discussed in detail by Nelson (18). An average interplanar spacing of 0.365 nm was computed for this ring. An effort to determine the size of the domains contributing to the maximum was performed using dark-field techniques (19). The results were inconclusive. However, a second experiment with a higher-rank coal (low-volatile bituminous) did produce a mottled pattern (Figure 13) with bright spots about 3 nm in diameter. Although these results are limited, the technique of dark-field microscopy may be applicable to coal studies and could yield data on the building blocks of the coal macerals.

Conclusions

The shape and size of pores in two high-volatile bituminous coals of differing lithotypes have been directly observed by means of TEM. The distributions of the porosity with respect to their maceral associations were ascertained, as were the sizes and distributions of the microminerals. The use of stereo pairs revealed the interconnectivity of the pores in microvolumes of the macerals, indicating a high degree of permeability within those regions.



Figure 13. Dark-field, 0.36-nm ring image showing domains (bright spots)

The finest porosity was observed in vitrinite fragments of both coals and ranged in size from 2 nm to 20 nm in diameter, with the majority in the smaller end of the size range. On the other hand, inertinite appears to be the most porous maceral, typically containing a broad range of pores from 5 through 50 nm. Much of the inertinite is granular material, varying from fine- to coarse-grained particles, with the former corresponding to micrinite.

The least porous maceral is exinite, which generally appears as a featureless material except for the presence of irregular and tabular pores thought to be initiated by the catalytic action of minerals. The intimate relationship between exinite and inertinite such as exists in splints, where the inertinite contains large amounts of fine mineral matter, therefore may promote the generation of porosity in exinites. However, a second new hypothesis has been offered to take into account the presence of only aragonite in the exinitic pores, i.e., that aragonite has been grown in situ within the exinite. Support for this thesis is derived from previous studies dealing with carbonate minerals grown from organic mixtures.

Finally, the minerals rutile (TiO_2) and millerite (NiS) tentatively have been identified as the mineral species in which at least some fraction of the titanium and nickel resides. Additional elemental analyses revealed that the granular inertinite hosts numerous minerals, typically clays, calcite, gypsum, pyrite, and quartz. Of special significance in these analyses has been the experiment performed on the featureless regions of the exinite and vitrinite, which consistently showed only sulfur as a detectable element (note only elements of atomic number 11, Na, or greater are detectable). However, it should be remembered that microchemical techniques analyze only small volumes of the total specimen.

Acknowledgments

Research sponsored by the Division of Basic Energy Science, U.S. Department of Energy, under contract W-7405-eng-26, with the Union Carbide Corp.

Literature Cited

1. McCartney, J. T. *Econ. Geol.* **1949**, *44*, 617.
2. McCartney, J. T.; Walline, R. E.; Ergun, S. *U.S. Rep. Invest. Bur. Mines* **1961**, 5885.
3. McCartney, J. T.; O'Donnell, H. J.; Ergun, S. "Coal Science," *Adv. Chem. Ser.* **1966**, *55*, 261.
4. McCartney, J. T.; Ergun, S. *Nature* **1965**, *205*, 962.
5. McCartney, J. T. *Fuel* **1970**, *49*, 409.
6. McCartney, J. T. *Fuel* **1971**, *50*, 457.
7. Alpern, B.; Pregermain, S. *Bull. Microsc. Appl.* **1956**, *6*, 16.
8. Pregermain, S.; Guillemot, C. *Int. Kong. Electronenmikroskopie, Verh. 4th* **1960**, *1*, 384.
9. Harris, L. A.; Yust, C. S. *Fuel* **1976**, *55*, 233.
10. Harris, L. A.; Yust, C. S. *Microstruct. Sci.* **1977**, *5*, 351.
11. Stach, E. "Coal and Coal-Bearing Strata"; Oliver and Boyd: Edinburgh and London, 1968, 3.
12. Hennig, G. R. *J. Inorg. Nucl. Chem.* **1962**, *24*, 1129.
13. Spotts, J. H.; Silverman, S. R. *Am. Mineral.* **1966**, *51*, 1144.
14. Gan, H.; Nandi, S. P.; Walker, P. L. *Fuel* **1972**, *51*, 272.
15. Strehlow, R. A.; Harris, L. A.; Yust, C. S. *Fuel* **1978**, *57*, 185.
16. Lin, J. S.; Hendricks, R. W.; Harris, L. A.; Yust, C. S. *J. Appl. Crystallogr.* **1978**, *11*, 621.
17. O'Gorman, J. V.; Walker, P. L. *Fuel* **1971**, *50*, 135.
18. Nelson, J. B. *Fuel* **1954**, *32*, 153.
19. Rudee, M. L. *Carbon* **1967**, *5*, 155.

RECEIVED July 19, 1979.

Characterization of Iron-Bearing Minerals in Coal

PEDRO A. MONTANO

Department of Physics, West Virginia University, Morgantown, WV 26506

A systematic classification of the major iron-bearing minerals in coal has been carried out by using Mössbauer spectroscopy. In order to accomplish this, we measured the isomer shift, the quadrupole splitting, and the magnetic hyperfine splittings for those minerals at various temperatures, including low-temperature measurements in the presence of an external magnetic field. The purpose of these measurements was to give a set of standard Mössbauer parameters that can be used for identification of the iron-bearing minerals in coal. We have applied this technique to the study of West Virginia coals and have identified the major iron-bearing minerals present. They are, in order of importance, pyrite, marcasite, clays (mainly illite), sulfates, and carbonates. Other minerals appear in quantities less than 0.1% by total weight. Mössbauer spectroscopy was used to identify the iron sulfides in liquefaction residues. This technique is extremely valuable for determining the $Fe_{1-x}S$ composition and the average number of vacancies in the compound. There are indications of a strong relationship between $Fe_{1-x}S$ composition and liquefaction yields.

Because of the importance of coal as a major source of energy and the environmental hazards involved in its use, considerable research has become necessary in order to understand fully the different compounds appearing in the coal and their transformation during processing and to know how those compounds contribute to the pollution of the environment, i.e., acidity of water streams near the coal mines and pollution by power plants. Some positive properties can be associated with the mineral matter in coal. For example, recently several researchers have shown that the mineral matter in the coal may play an important role in the liquefaction process (1). Of all the minerals in the coal, the iron-bearing minerals seem

to be the most important. In most coal utilization techniques the coal is used as raw material, and as a result both organic and inorganic components may be critical in the acceptance or rejection of a coal for a particular process. Owing to the great importance of iron as a major constituent of the mineral matter in many coals, the Mössbauer effect becomes a powerful tool in the characterization of the iron-bearing minerals and their transformations during coal processing.

The most common use of the Mössbauer effect in mineralogy and geology has been the determination of the oxidation states of iron in various minerals (2). The study of the Mössbauer spectral area also gives valuable information on the concentration of the different minerals in rocks (2). Recently the Mössbauer effect was applied to the study of iron-bearing minerals in coal to determine the amount of pyritic sulfur (3, 4, 5).

In this paper the application of Mössbauer spectroscopy (^{57}Fe) to determine the iron-bearing minerals will be described, and a critical view of the advantages and disadvantages of the technique will be presented. In this study more than 200 coal samples were investigated and more than 2000 Mössbauer runs were carried out on those samples. Before going into the experimental results, a brief description of the Mössbauer parameters that give the necessary information to determine the compounds seems appropriate.

The Mössbauer Effect

Consider a γ source in gas form, with atoms moving at a thermal velocity v ; the momentum of the source is given by Mv , where M is the mass of the atom. So the total energy before the emission is given by $E_b = E_e + \frac{1}{2}Mv^2$, where E_e is the excited state energy. The total momentum is conserved during the γ ray emission. The atom after the emission has the momentum $\vec{P}_a = \vec{P} - \vec{P}_\gamma$. The total energy of the atom after the emission process is $E_a = E_g + P_a^2 / 2M$, and the energy difference is taken by the γ quantum $E_\gamma = E_b - E_a = E_0 + (\vec{P} \cdot \vec{P}_\gamma / M) - (P_\gamma^2 / 2Mc^2)$. Consequently, the emission line is centered at $E_0 - (P_\gamma^2 / 2M)$ ($P_\gamma^2 / 2M = E_0^2 / 2Mc^2$, recoil energy), with Doppler shift given by $\vec{P}_\gamma \cdot \vec{v}$. The thermal velocity \vec{v} , where averaged over all possible directions, has the effect of producing a broadening of the γ ray line. For an absorbing nucleus in gas form the energy is partitioned between the internal energy of the nucleus and its recoil $E_\gamma = E_0 + (E_0^2 / 2Mc^2)$. For observation of resonance absorption the emitting and absorbing lines would have to overlap; this effect is negligible for nuclear transitions. In solid sources or absorbers it is possible to emit or absorb a γ quantum without phonon excitations (zero phonons) with an energy equal to that of the nuclear transition. This effect was observed by R. L. Mössbauer in 1958 (6) and is called the Mössbauer effect. Its usefulness is related to the fact that the line width exhibited is of the order of the natural line width of the excited nuclear states.

The probability of finding the lattice in the same state after emission is given by (7)

$$| \langle L | \exp(-i\vec{k}\vec{x}) | L \rangle |^2 \quad (1)$$

where $| L \rangle$ is the wave function of the lattice, \vec{k} is the wave vector of the gamma ray, and \vec{x} is the position of the emitting atom. If the initial states are occupied with probability g_L in thermal equilibrium, then the fraction of recoilless emission is

$$f(T) = \sum_L g_L | \langle L | \exp(-i\vec{k}\vec{x}) | L \rangle |^2 \quad (2)$$

For a harmonic solid the probability of recoilless emission or absorption is given by $\exp(-k^2 \langle x^2 \rangle_T)$, where k is the wave vector of the gamma ray and $\langle x^2 \rangle_T$ is the mean square displacement, $\langle \rangle_T$ denoting thermal average. If the Debye model is used to describe the solid, then

$$k^2 \langle x^2 \rangle_T = \left(\frac{6E_R}{k_B \theta_D} \right) \left[\frac{1}{4} + \left(\frac{T}{\theta_D} \right)^2 \int_0^{\theta_D/T} \frac{x dx}{e^x - 1} \right] \quad (3)$$

where θ_D is the Debye temperature. Thus if the nuclear transition is of low energy and if the Debye temperature of the crystal is high, then the probability for recoilless emission or absorption is high; this probability is also dependent on particle size.

The theoretical interpretation of the effect was done by R. L. Mössbauer himself, using the theory of W. E. Lamb, Jr. (8), for neutron capture by atoms in a crystal. According to this theory the resonance-absorption cross section is given by

$$\sigma_r(E) = \beta f_a \sigma_0 \left[\frac{\Gamma^2/2}{(E-E_0)^2 + (\Gamma/2)^2} \right] \quad (4)$$

$$\sigma_0 = \left(\frac{2\pi}{k^2} \right) \left(\frac{1}{1 + \alpha} \right) \left(\frac{2I^* + 1}{2I + 1} \right) \quad (5)$$

where β is the natural abundance of the Mössbauer isotope, f_a is the probability of recoilless absorption, I^* and I are the spins of the nucleus in the excited and ground state, respectively, α is the internal conversion coefficient, Γ is the natural line width, and k is the wave vector of the gamma ray.

In a standard Mössbauer transmission experiment the absorber is placed between the source and the detector. In order to observe the effect,

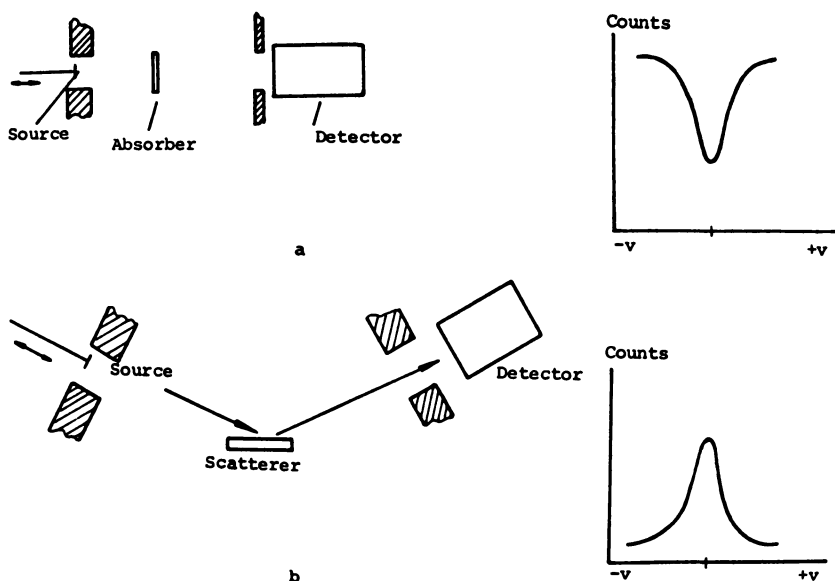


Figure 1. Typical geometries for Mössbauer spectroscopy experiments: (a) transmission; (b) scattering

one usually imparts a velocity to the source, and through a Doppler shift of the energy a velocity spectrum, as seen in Figure 1(a), can be recorded. The count rate in the detector is then given by (7)

$$N(v) = (1 - f_s) \exp(-d\mu_a) + \int \frac{f_s (\Gamma/2\pi)}{\{E - E_0 [1 + v/c]^2\} + (\Gamma/2)^2} \exp[-d(\mu_a + \mu_r)] dE \quad (6)$$

where f_s is the Mössbauer fraction of the source, μ_a is the mass attenuation coefficient of the absorber, $\mu_r = n\sigma_r$ is the resonance coefficient, n is the number of atoms per cubic centimeter, d is the absorber thickness, and $(1 - f_s)$ is the nonresonant fraction of γ rays emitted by the source. The count rate off resonance is given by $N(\infty) = \exp(-d\mu_a)$. If $dn\sigma_r \ll 1$, an analytical expression can be obtained for the count rate in the detector (9):

$$\frac{N(\infty) - N(v)}{N(\infty)} = \frac{\beta f_s f_a n \sigma_0 d}{2} \frac{\Gamma}{(E_0 \frac{v}{c})^2 + \Gamma^2} \quad (7)$$

The Mössbauer spectral area is given for a single line source and absorber by (10)

$$\text{area} = P^{-1} f_s \Gamma \left(\frac{\pi}{2} \right) \sum_{n=1}^{\infty} \left[\frac{(-1)^{n+1}}{n!} \right] \left[\frac{(2n-3)!!}{(2n-2)!!} \right] t^n \quad (8)$$

$$P = 1 - \frac{B}{N(\infty)} \quad t = nd\beta\sigma_a f_a$$

where B is the background (non-Mössbauer radiation). The formula above has to be corrected for lines split by hyperfine interactions (11). When the Mössbauer effect is used as a quantitative analytical tool, care must be taken that B , f_s , and f_a are known. When the thickness of the absorber does not permit transmission of the γ rays, the scattering experiment becomes more appropriate [Figure 1(b)]. In the scattering experiment either the reemitted γ ray or the X-rays for the internal conversion are detected.

Mössbauer Parameters

Isomer Shift (IS). The shift observed in the Mössbauer lines with respect to zero velocity is produced by the electrostatic interaction of the nuclear and electron charge distributions inside the nuclear region. One assumes the nucleus is a uniformly charged sphere of radius R , and the electronic charge density is taken to be uniformly distributed over the nucleus. Then the difference between the electrostatic interaction of a point nucleus and a nucleus with radius R is given by

$$\delta E = (2\pi / 5) (Ze^2 R^2) |\Psi(0)|^2 \quad (9)$$

where Ze = nuclear charge and the electron density at the nucleus is given by $-e |\Psi(0)|^2$. For a transition from the excited state to the ground state,

$$\begin{aligned} \delta E_{\text{ex}} - \delta E_{\text{g}} &= (2\pi / 5) (Ze^2) (R_{\text{ex}}^2 - R_{\text{g}}^2) |\Psi(0)|^2 \\ &\approx (4\pi / 5) (Ze^2 R^2) (\delta R / R) |\Psi(0)|^2 \end{aligned} \quad (10)$$

$$\delta R = R_{\text{ex}} - R_{\text{g}} \quad R_{\text{ex}} + R_{\text{g}} = 2R$$

The shift observed in the Mössbauer effect is given by the difference between the shift in the source and the shift in the absorber. Kistner and Sunyar (12) were the first to observe the isomer shift (IS) of the Mössbauer spectral lines:

$$\text{IS} = (4\pi / 5) (Ze^2 R^2) (\delta R / R) [|\Psi_a(0)|^2 - |\Psi_s(0)|^2] \quad (11)$$

The sign and magnitude of $\delta R/R$ are known for most of the Mössbauer nuclides. In general, IS values must always be given with respect to a reference material (for ^{57}Fe , metallic iron and $\text{Na}_2[\text{Fe}(\text{CN})_5\text{NO}] \cdot 2\text{H}_2\text{O}$ are

standard references). The IS can give unique information on the valence states of iron, in particular for high-spin Fe^{2+} and Fe^{3+} . Low-spin Fe^{2+} and Fe^{3+} iron compounds exhibit IS's similar to one another; consequently, one needs to measure other Mössbauer parameters in order to distinguish between the two cases.

Besides the IS there exists a shift of the Mössbauer lines due to the second-order Doppler effect (13, 14). This shift is given by

$$\delta E_{\text{SODS}} = (-E_0 / 2) \langle v^2 \rangle_T / c^2 \quad (12)$$

where $\langle v^2 \rangle_T$ is the thermal average of the square of the velocity of the Mössbauer atom in the solid. It is a parameter that strongly depends on the lattice dynamical properties of the solid.

Electric Quadrupole Interaction (Quadrupole Splitting). This interaction exists when the electrons and/or the neighboring atoms produce an inhomogeneous electric field at the nucleus and when the nucleus possesses a quadrupole moment. The interaction between the nuclear electric quadrupole moment Q and the electric field gradient (EFG) is given by (15)

$$\mathcal{H} = [e^2 Q q / 4I(2I - 1)] [3I_z^2 - I(I + 1) + (\eta / 2)(I_+^2 + I_-^2)] \quad (13)$$

where I_+ and I_- are the raising and lowering operators of the spin; the electric field is equal to minus gradient V , $eq = V_{zz} = \partial^2 V / \partial z^2$ (x, y, z are the principal axes of the field gradient tensor); and $\eta = (V_{xx} - V_{yy}) / V_{zz}$ is called the asymmetry parameter.

For the excited level of ^{57}Fe ,

$$\Delta E_q = (1/2) (e^2 q Q) (1 + \eta^2/3)^{1/2} \quad (14)$$

The ground state $I = 1/2$ has a zero quadrupole moment and remains degenerate in the presence of an EFG. The excited state $I = 3/2$ possesses a quadrupole moment, and in the presence of an EFG the degeneracy $(2I + 1)$ is partially removed.

Common iron compounds are either ferrous $3d^6$ or ferric $3d^5$, having a different electron configuration. This strongly affects the EFG observed in iron compounds. The degeneracy of the five $3d$ electron orbitals of an iron ion is removed in a crystalline field. In a cubic field the five orbitals split into two sets, a triplet t_{2g} and a doublet e_g (16). The spin degeneracy remains. If the splitting between the t_{2g} and e_g is small, the electrons favor a configuration with a maximum number of unpaired spins, the high-spin configuration. When the splitting between the t_{2g} and e_g levels is large compared with the Coulomb interaction between the electrons, a low-spin configuration is attained. In a high-spin ferric iron, Fe^{3+} , the EFG is caused by the external charges and not the ions' own electrons,

because Fe^{3+} is an S state ion, ${}^6\text{S}$, having a spherically symmetric electronic distribution. By contrast, the high-spin ferrous ion, Fe^{2+} has an additional d electron and an Fe^{3+} core. The EFG arises here from this electron and the external charges. In this case the temperature dependence of the quadrupole splitting is very pronounced. The absolute value of the quadrupole splitting depends on the degree of covalency of the compound. The EFG in low-spin compounds is more complicated and depends very strongly on the nature of the bonding to the ligands.

In general, the crystal field affects the electrons of the atom, even those that possess spherical symmetry. These electrons are distorted and produce an electric field gradient at the nucleus that is frequently larger than the electric field gradient due to the crystal field. The electrons that do not possess spherical symmetry also produce a distortion of the closed electronic shells and an additional field gradient. The effective field gradient in an axial symmetric field is given by

$$V_{zz}^{\text{effect}} = (1 - R) V_{zz}^{\text{electrons}} + (1 - \gamma) V_{zz}^{\text{crystal}} \quad (15)$$

The term $(1 - R)$ is the Sternheimer factor that corrects for the polarization of the ferric core by the EFG of the odd d electron, and $(1 - \gamma)$ is the Sternheimer factor that takes into consideration the polarization of the ion's core electron by the external crystalline EFG (17, 18).

Magnetic Hyperfine Interaction (MHI). This interaction arises from the interaction of the nuclear dipole moment with a magnetic field due to the atom's own electrons. The nuclear Zeeman effect may be described by the Hamiltonian (15)

$$\mathcal{H} = -g_n \mu_n \vec{I} \cdot \vec{B} \quad (16)$$

where g_n is the nuclear gyromagnetic factor, μ_n is the nuclear magneton, \vec{I} is the nuclear spin, and \vec{B} is the effective magnetic field at the nucleus. The MHI splits the nuclear state with spin I into $2I + 1$ equally spaced sublevels. In a standard Mössbauer experiment with single line source and a magnetically ordered absorber, one would observe six lines. The magnetic hyperfine splitting enables one to determine the effective magnetic field acting on the nucleus. From the value of the magnetic field, information about the electronic structure and magnetic moment of the iron ion can be obtained. Typical fields for Fe^{3+} high spin are between -400 to -550 kOe.

If an EFG and an effective magnetic field \vec{B} are present at the nucleus, then the positions of the sublevels of the hyperfine split lines depend on the ratio of magnetic to electric interaction energy, on the symmetry of the EFG, and on the angle θ between the z principal axis of the electric field gradient tensor and the effective magnetic field at the nucleus. It is possible to write the Hamiltonian for this general case, but there is no general solution (the Hamiltonian has to be solved numerically for each particular

case). There exists an approximation for the case where the electric quadrupole interaction is smaller than the MHI, as in $\alpha\text{-Fe}_2\text{O}_3$; a discussion of the solution can be found in Wertheim (19).

In many iron compound magnetic hyperfine splitting can appear at low temperatures, even in the absence of long-range order; this effect is caused by slow spin relaxation or superparamagnetism (20). One can induce magnetic hyperfine splitting at low temperatures by applying a large external magnetic field. This technique is particularly useful for the study of the electronic ground state of iron ions in minerals (21, 22, 23).

Experimental

The coal samples used in this work were collected by strictly following ASTM procedure D2013-72. The samples were mounted in lucite containers that were hermetically sealed. Pressed pellets of the ground coal were used also as samples. The average surface densities of the samples used were between 150 and 300 mg/cm^2 . Several samples from the same seam were analyzed in order to check for consistency of the results. Some runs were carried out on raw coals (not ground) as well, for testing purposes. The bulk of the samples used in this study were from West Virginia coals. The Mössbauer spectrometer used in this work was a conventional constant-acceleration spectrometer. A 50mC $^{57}\text{Co}:\text{Pd}$ source was used. The Mössbauer spectra were analyzed by using a nonlinear, least-squares fit program and assuming Lorentzian line shapes. The measurements covered a wide temperature range. Many runs were carried out at low temperatures (4.2 K) and in the presence of an external magnetic field (40 kOe). The velocity calibration is given with respect to $\alpha\text{-Fe}$ at room temperature (RT). The minimum amount of ^{57}Fe detectable in the coal was about 5 $\mu\text{g}/\text{cm}^2$; with thicker samples (500 mg/cm^2 of coal or more) the detection limit can go as low as 1 $\mu\text{g}/\text{cm}^2$ of ^{57}Fe .

Experimental Results and Discussion

The different iron-bearing minerals detected in coal by using Mössbauer spectroscopy are classified below according to their major groups, i.e., sulfides, clays, carbonates, and sulfates.

Sulfides. Iron disulfide (pyrite) is the most important of the iron-bearing minerals in coal. In pyrite the iron ion is the low-spin configuration, Fe (II). The six d electrons are occupying the T_{2g} ground state, and no magnetic moment is present at the iron site (21). In pyrite each cation has a distorted octahedral coordination of six nearest-neighbor sulfur, the octahedron being slightly compressed along one of the axes. Consequently, the crystalline field at the iron site is lower than cubic, and an electric field gradient exists at the ^{57}Fe nucleus, producing a characteristic QS in the Mössbauer spectrum.

There is a metastable phase of FeS_2 , marcasite, which is the orthorhombic dimorph of pyrite and appears also in several coals. Marcasite has slightly different IS and QS (Table I). When the amount of marcasite in coal is more than 20% of the total iron disulfide content, its detection using Mössbauer spectroscopy is possible. In general, petrographical techniques

Table I. Iron Sulfides

Name	IS (mm/sec)	QS (mm/sec)	MHF (kOe)	Ref.
Pyrite (FeS ₂)	0.32(2)	0.63(2)	0	^a
Marcasite (FeS ₂)	0.25(2)	0.56(2)	0 (4.2K)	^a
Greigite (Fe ₃ S ₄)	0.70	0.30	322	
	0.40 (T = 4.2 K)	0	486 (4.2K)	(32)
	0.45	0.4	465	
Fe ₂ S ₃ (amorphous)	0.35(6)	0.82(6)		(33, 34)
	0.51(12)	0.88(12)	253(4.2K)	
Sphalerite (ZnFe)S (FeS) synthetic	0.66	0.80	—	(35)
	0.81	-0.32	315(RT) ^b	(32)
Troilite (FeS) natural	0.86	-0.28	310 (RT)	(36)
Pyrrhotites:				
Fe ₇ S ₈	0.69(8)	0.18(15)	307(8)	
	0.64(10)	0.31(15)	255(10) (RT)	(36)
	0.64(10)	0.30(15)	255(10)	
Fe ₇ S ₈ (77 K)	0.81(1)	-0.36(8)	344	
	0.79(5)	0.60(8)	311	
	0.79(3)	0.12(12)	267	(32)
	0.77(2)	0.32(2)	229	
	0.39(2)	0.25(2)	0	
Fe _{0.881} S		0.31(3)	305(3)	
		0.31(4)	253(4) (RT)	(30)
		0.43(4)	224(3)	
Fe _{0.909} S		0.23(10)	302(10)	
		0.00(10)	274(10) (RT)	(30)
		0.30(10)	256(10)	

^aThis work.^bRT = room temperature.

seem to be more appropriate for identification of marcasite (at least for qualitative measurements). In Table I a list of the different iron sulfides and their respective Mössbauer parameters is given.

A typical spectrum of a coal is given in Figure 2. The sample has been treated with HCl (following ASTM standard D-2492) to get rid of the nonpyrite iron (sulfates). The spectrum is typical of pyrite. All the approximately 2000 spectra run in this work show the presence of pyrite (contents ranging from 7 to 0.1%). While studying several coal macerals, we observed a new Mössbauer spectrum associated with pyrite in three different samples (22, 23) rich in framboidal pyrite. The extra Mössbauer doublet showed the same magnetic behavior as pyrite (low spin). However, its Mössbauer parameters are different, and the IS suggests a smaller electron density at the nucleus than exists for FeS₂. The low-temperature measurements indicate that the spectrum cannot be associated with any of the other minerals. It is possible that this phase is highly disordered (or amorphous) FeS₂. The spectrum may be produced also by small particles

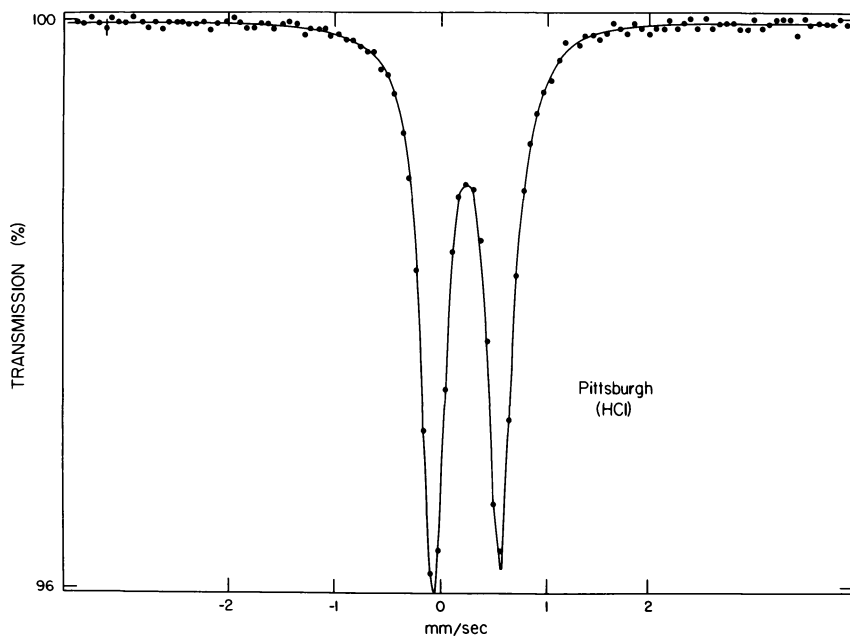


Figure 2. Pittsburgh coal treated with HCl. Continuous line is the least-squares fit (RT).

of Fe_3S_4 . Note that the spectra observed for these macerals were an exception, and no similar spectra were detected in any other sample. Consequently, it is suspected that this iron compound is rare in coal.

In this study no other sulfide-containing minerals, except the ones mentioned above, were detected in fresh coals by using Mössbauer spectroscopy. Pyrrhotite was detected in some heavy, weathered coal (Figure 3). The presence of Fe_{1-x}S was determined by temperature-dependent measurements and the analysis of low-temperature ashes, both by X-ray diffraction and Mössbauer spectroscopy. Other minerals, like sphalerite, chalcopyrite, and arsenopyrite, were not detectable in these experiments. Some of the latter minerals have been identified by using scanning electron microscopy, but their presence in the coal was too small to make their contribution to the Mössbauer spectrum significant.

Other iron sulfides are produced during coal processing. Pyrrhotites are common constituents of coke and of coal liquefaction mineral residues. For compositions varying between FeS (troilite) and Fe_7S_8 (monoclinic pyrrhotite), the compounds are referred to generally as pyrrhotites (24). There have been several studies of the pyrrhotites, both synthetic and natural, and three major reviews have been written on the iron sulfur system (24, 25, 26). The nomenclature used in the recent literature for these compounds is based on their superstructures, which may be integral or nonintegral values

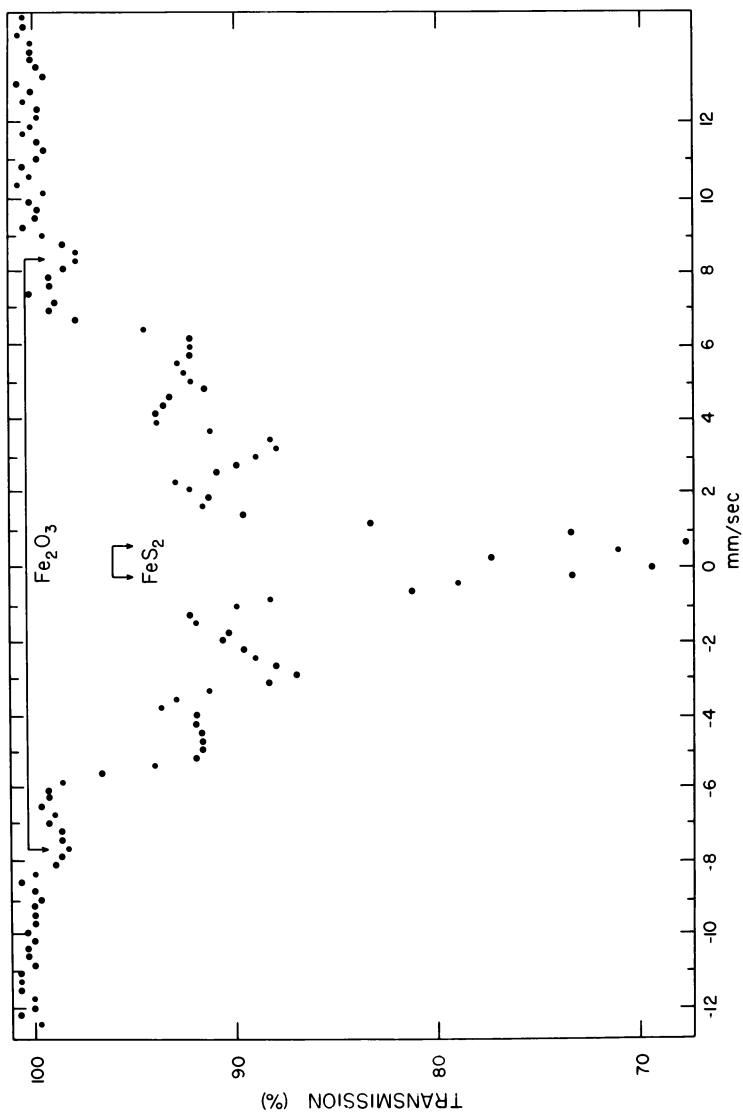


Figure 3. Mössbauer spectrum of a heavy, weathered Pittsburgh coal. Pyrrhotite, hematite, and pyrite are identifiable (RT).

of the cell edges of the hexagonal NiAs structure. At about 140°C there is a transition in troilite, and the 1C structure of NiAs is adopted (α transition) (24, 27).

Above 308°C and below its maximum point of 1190°C, pyrrhotite exhibits a rather wide homogeneity range as a single solid solution extending from the stoichiometric value FeS to Fe_{0.81}S. The NiAs structure is the basic cell of this high-temperature pyrrhotite. The iron deficiency in the high-temperature pyrrhotites is due to iron vacancies in the lattice (24, 25, 26). Monoclinic pyrrhotite is referred to usually as Fe₇S₈, and it is now generally agreed that it has a narrow composition range at room temperature. Monoclinic pyrrhotite is ferrimagnetic. Fe₇S₈ is not a stable phase at 300°C, and exsolution of FeS₂ produces a phase of Fe₉S₁₀ composition. This observation has been confirmed by optical observations on polished samples, electron microprobe, X-ray, and Mössbauer studies (25).

Both troilite and pyrrhotites show a change in their Mössbauer spectrum at high pressure, with the six-peak magnetic hyperfine spectrum produced by the magnetic ordering of the high-spin Fe²⁺ collapsing to a single peak with a different isomer shift (28, 29). This change is reversible. It has been interpreted as a result of spin pairing in Fe²⁺. It is certainly an interesting phenomenon and of considerable importance for understanding the behavior of pyrrhotite in a liquefaction process. In the reactor the coal and catalyst are under high pressure at high temperature, and the electron structure of iron in the sulfides is expected to be considerably different from the one at atmospheric pressure. It has been observed that synthetic samples of pyrrhotite may differ considerably from the natural ones. Many high-temperature phases are nonquenchable, and, as a result, metastable phases appear during rapid cooling (24).

There is a strong relation between the vacancy distribution and magnetic hyperfine splittings in the pyrrhotites. The magnetic hyperfine field (MHF) differs considerably between the different iron sites in the pyrrhotites, depending on the number of vacancies in their immediate vicinity. Ovanesyan et al. (30) have identified three types of iron sites in Fe_{0.881}S with different amounts of vacancies around it. They measured an MHF of 305 kOe for 0 vacancy, 253 kOe for two vacancies, and 224 kOe for four vacancies nearest-neighbor (nn). A similar analysis was carried out in the range of Fe_{0.909}S to Fe_{0.881}S. The high sensitivity of the Mössbauer effect to detect small changes in the local environment of the iron atoms makes it an ideal tool to study liquefaction residues. In Figure 4 a liquefaction residue of a Ky 9/14 coal (2000 psig H₂) is shown. The spectrum shows the presence of two iron sites, one with zero vacancy nn (MHF = 306 kOe) and the other with two vacancies nn (MHF = 258 kOe). The relative area of the two sites can be used to determine the relative stoichiometry as well as to detect changes in the different sites as a function of temperature and pressure. If the H₂ pressure is increased, the site with two vacancies decreases. There are some traces of clay in the sample (coal illite). All the pyrite was converted

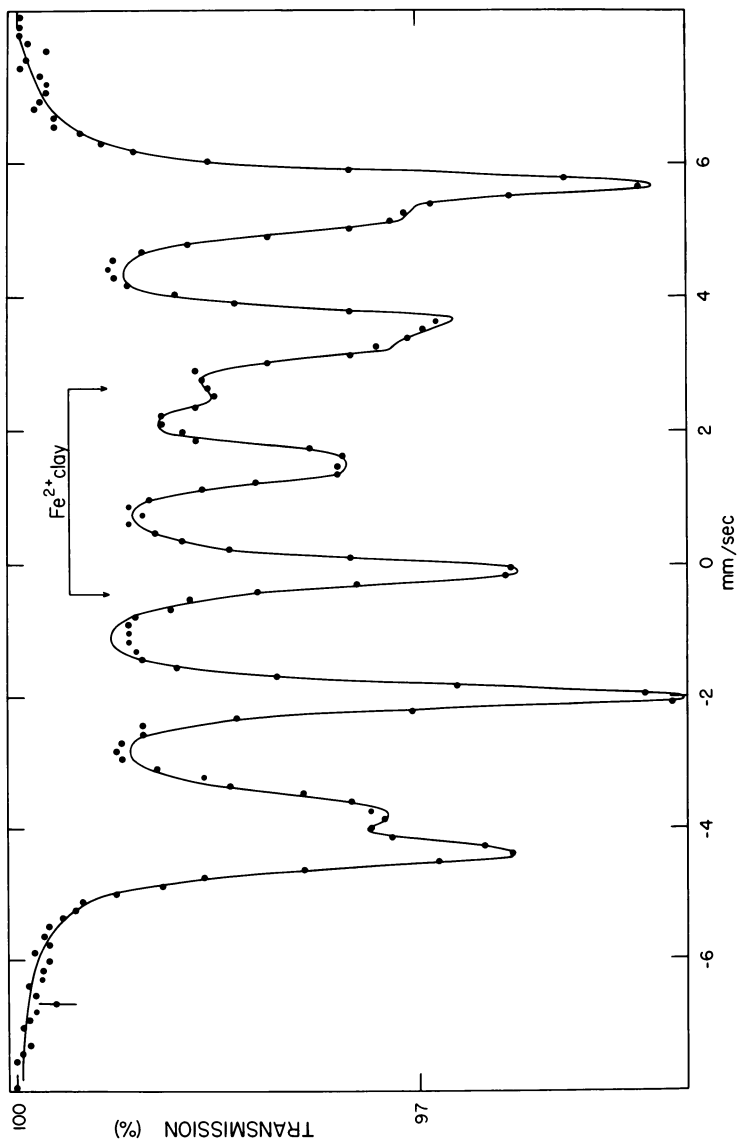


Figure 4. Mössbauer spectrum of a Ky 9/14 liquefaction residue (RT)

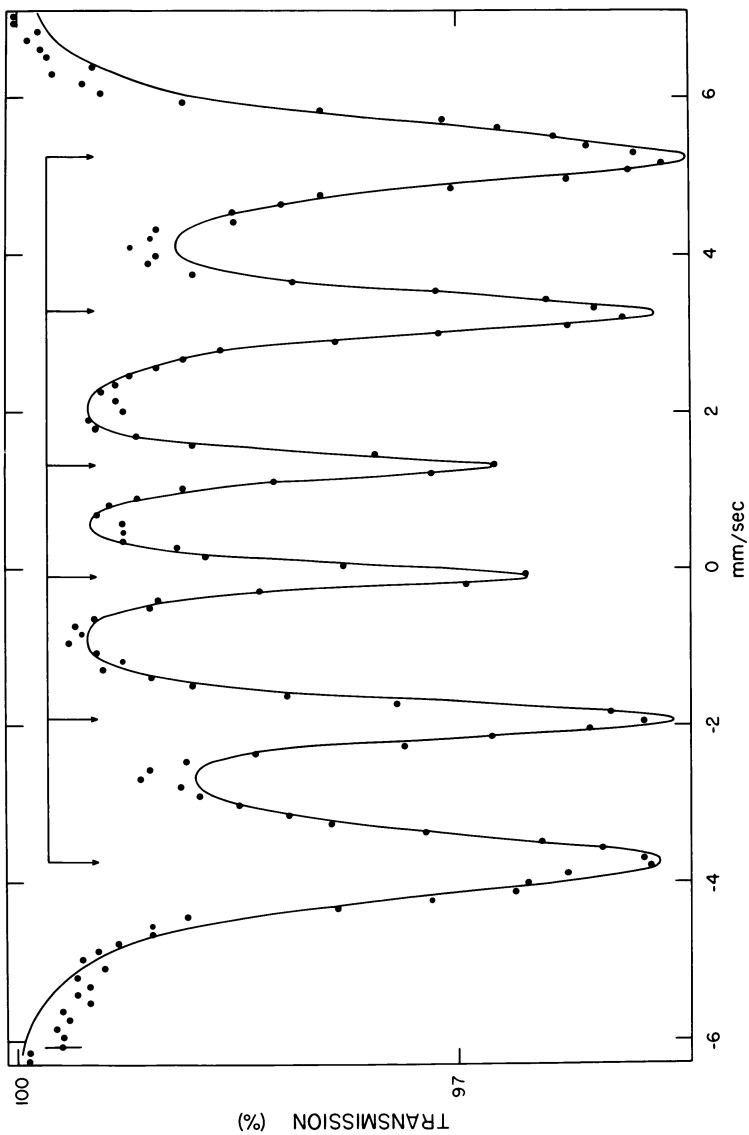


Figure 5. Mössbauer spectrum of FeS₂ residue (RT)

to pyrrhotite. By contrast, if only FeS_2 is run (no coal present), the spectrum is characteristic of a highly disordered compound ($\text{MHF} = 268$) (the vacancies are not ordered). Figure 5 shows the residue of a simple pyrite run. In a study carried out by the author in collaboration with B. Granoff, remarkable differences were detected among the residues from WV (Blacksville, Pittsburgh coal), Ky 9/14, and Illinois No. 6 coal runs under identical liquefaction conditions (31). It is probable that Mössbauer spectroscopy will be used more and more as an analytical tool in coal conversion studies.

A summary of the Mössbauer parameters for the different iron sulfides is given in Table I (32–36).

Clay Minerals. Clay minerals represent a large percentage of the inorganic mineral content in coal. Illite, kaolinite and mixed clays are the major clay minerals present in coal. The crystal structures of the clay minerals are basically derived from two types of sheets: a sheet typically made of tetrahedral SiO_4 units and a sheet typically made of octahedral $\text{Al}(\text{O},\text{OH})_6$ units (37). The ideal formula, i.e., for kaolinite, is $\text{Al}_2^{3+}\text{Si}_2^{4+}\text{O}_5^{2-}(\text{OH}^-)_4$, but as in all clay minerals, a certain amount of cation substitution is possible. In mica and its derived clay minerals, illites, the octahedral sheet contains only Al^{3+} , but in the tetrahedral sites one-quarter of the Si^{4+} is replaced by Al^{3+} . The net negative charge of the layer is balanced by interlayer alkali cations, which also bond the layers together. The interlayer in montmorillonite or vermiculite is occupied by H_2O and/or cations, whereas in chlorite there is a complete sheet of aluminum (magnesium) hydroxide, the brucite sheet. Continuous ranges of chemical composition are often possible between the different clays, and there is a variety of mixed layer structures. Iron can be substituted in the octahedral layer in its high-spin ferrous and ferric forms and occasionally in the tetrahedral layer. A typical illite spectrum is shown in Figure 6; the Mössbauer parameters are given in Table II. Three different iron sites are detectable in this clay. The iron concentration in illite and kaolinite is relatively small (a few percentage points by weight); thus, although these clays are the most abundant in coal (38), their identification becomes difficult with standard Mössbauer spectroscopy. In general, the clays appearing in coal show slightly different Mössbauer parameters from those in pure clays. A striking result is the small amount of trivalent iron observed in the clays in coal. In general, with very few exceptions (heavy, weathered coals), divalent iron is the dominant valence state in coal. This result suggests that at the time of the formation of the mineral matter in the coal, the environment was strongly reducing.

The usual method utilized to identify the clay minerals in coal is X-ray diffraction of the low-temperature ash (LTA), but because of the poor crystallinity of the clays in the coal, the technique cannot be used for quantitative measurements. The Mössbauer effect does not provide much improvement owing to the small iron content of the clays. A coal rich in clays is shown in Figure 7 (about 10% mineral matter). The two peaks at higher

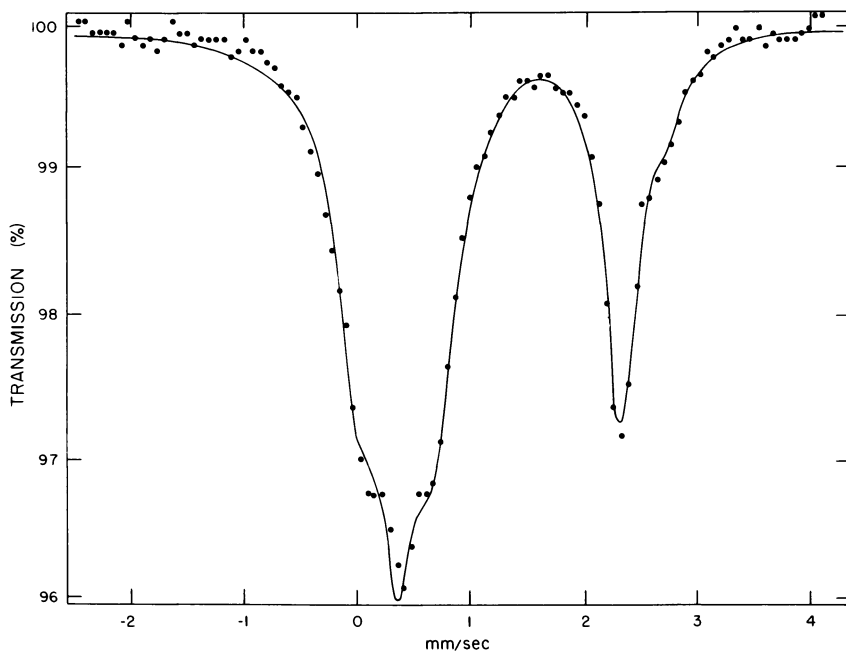


Figure 6. Mössbauer spectrum of illite No. 36 (Morris, Illinois) (RT). Parameters are given in Table II.

velocity are caused by the higher velocity components of two quadrupole split doublets, one from szomolnokite and one from a clay. When the sample was treated with HCl, the sulfate was washed away and the clay (possibly illite) could be clearly seen (Figure 8). Treating the coal with HNO₃ dissolves the pyritic iron, and the spectrum of clays can be detected more clearly (chlorite is altered by treatment with HNO₃). Figure 9 shows the Pittsburgh coal (230 mesh), which was shown in Figure 2, after treatment with HNO₃. The spectrum (notice the smaller Mössbauer effect) is identified as that of kaolinite. (This result was confirmed also by X-ray diffraction. The spectral line in Figure 9 is very broad, suggesting the presence of a QS.)

In general, to study the clays in coal, one should treat the samples as described above or run the experiments at low temperatures in order to resolve the overlapping lines (sometimes measurements in an external magnetic field become necessary (21, 22, 23). Mössbauer parameters for the principal clay minerals, pure and as they appear in coal, are given in Table II (39–43).

Sulfates. The iron sulfates were detected in more than 90% of the coal samples studied. The sulfates are considered to be produced by weathering of the coal. The amounts detected in this study ranged from 0.2 to 0.005% of total weight.

Table II. Clay Minerals

Name	IS (mm/sec)	QS (mm/sec)	MHF (kOe)	Ref.
Kaolinite	0.36	0.52	492 (4.2K)	(39)
Chamosite	0.38(4)	0.78(8)		(40)
	1.14(2)	2.57(8)		
Antigorite	1.16(2)	2.74(4)		(41)
Muskovite	0.37(5)	0.75(8)	500	^a
	1.17(3)	3.08(7)	40 (4.2K)	
Glauconite	0.36(5)	0.52(12)		
	0.38(3)	1.21(5)		(40)
	1.14(6)	2.30(6)		
Nontronite	0.36(2)	0.30(6)		
	0.36(2)	0.62(6)		(42)
Montmorillonite	0.38(8)	0.50(13)		(40)
	1.15(6)	2.81(6)		
Fayalite	1.17(6)	2.85(8)		
	0.99(7)	1.72(10)		^a
Illite	0.33(2)	0.65(5)		
	0.38(4)	1.21(8)		(42)
	1.14(1)	2.75		
Illite No. 36 (Morris)	0.34(3)	0.43(4)	0	
	1.24(5)	2.60(6)	(4.2K)	^a
	1.27(3)	1.92(4)	20–30	
Illite No. 35 (Fithian)	0.28(6)	0.60(8)	0	
	1.14(7)	2.77(7)	(4.2K)	^a
	1.25(8)	2.54(8)	20–30	
Illite No. 35 (Fithian) after treatment with HNO ₃	0.25(4)	0.58(6)		^a
	1.05(4)	2.73(6)		
	1.20(5)	2.51(6)		
Illite (coal)	1.1–1.2	2.6–2.8	15 (4.2K)	^a
Biotite, Annite	0.47(8)	0.52(18)		
	0.47(6)	0.96(20)		
	1.11(5)	2.62(8)		(42)
	1.09(5)	2.18(10)		
Phlogopite	0.52(8)	1.05(12)		
	0.19(2)	0.47(3)		(43)
	1.20(10)	2.70(20)		
	1.10(8)	2.40(20)		
Talc	1.13(3)	2.63(3)		(42)
Chlorite	0.17(6)	0.78(8)	505	
	1.13(1)	2.67(6)	20 (4.2K)	^a
Vermiculite	0.45(5)	0.48(5)		
	1.07(7)	2.58(7)		^a

^aThis work.

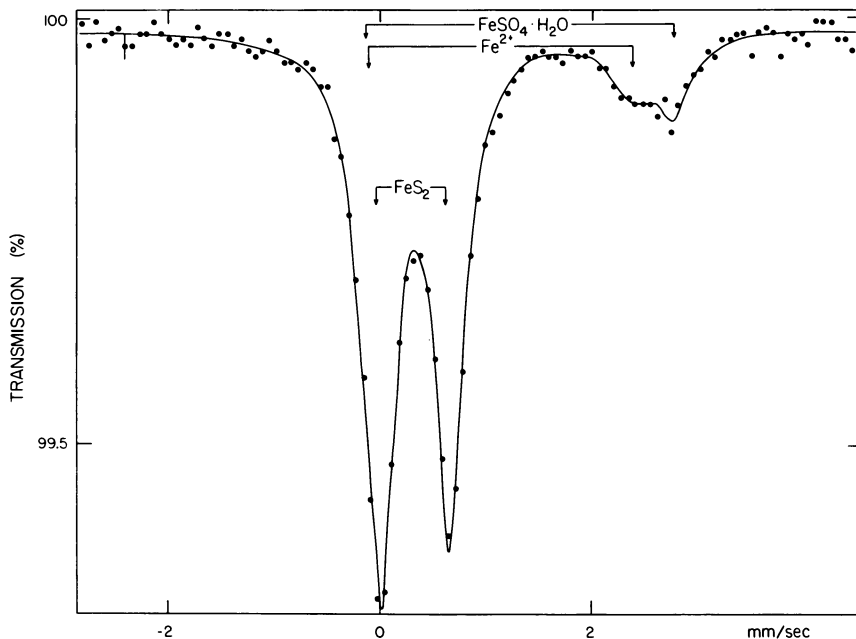


Figure 7. Mössbauer spectrum of a Waynesburg coal (RT). Szomolnokite, ilite, and pyrite are identifiable.

The standard technique used for detection of sulfates is X-ray diffraction of the LTA. Nevertheless, we have observed that in some cases sulfates are present in the coal, but the X-ray does not show any line attributable to them (44). The most abundant divalent iron sulfate observed in the coals studied is $\text{FeSO}_4 \cdot \text{H}_2\text{O}$ (szomolnokite), a monoclinic crystal with a tetramolecular unit cell (45). This compound orders antiferromagnetically around 10 K with an effective internal field of 359 kOe (22, 23). Other sulfate minerals found less frequently are $\text{FeSO}_4 \cdot 4\text{H}_2\text{O}$ (rozenite) and $\text{FeSO}_4 \cdot 7\text{H}_2\text{O}$ (melanterite); anhydrous ferrous sulfate was detected when the coal was stored under vacuum. The ferric sulfates commonly observed in several coals are coquimbite and jarosites (16).

A word of caution concerning the presence of trivalent sulfates in the coal is appropriate here. These sulfates have, in general, lines that overlap with the Mössbauer pyrite lines. The result is the detection of a slightly asymmetric pyrite spectrum. If one treats the samples with HCl, it will appear as if some of the pyrite had dissolved in HCl, but this observation, of course, is not true; the observation results from the presence of the iron sulfates. The ferric sulfates are easily distinguishable from pyrite. When Mössbauer measurements are carried out at 4.2 K in the presence of a large external field, the characteristic hyperfine field of Fe^{3+} is detected (about 500 kOe). It was observed also that many of the ferric sulfates are formed during LTA experiments (3).

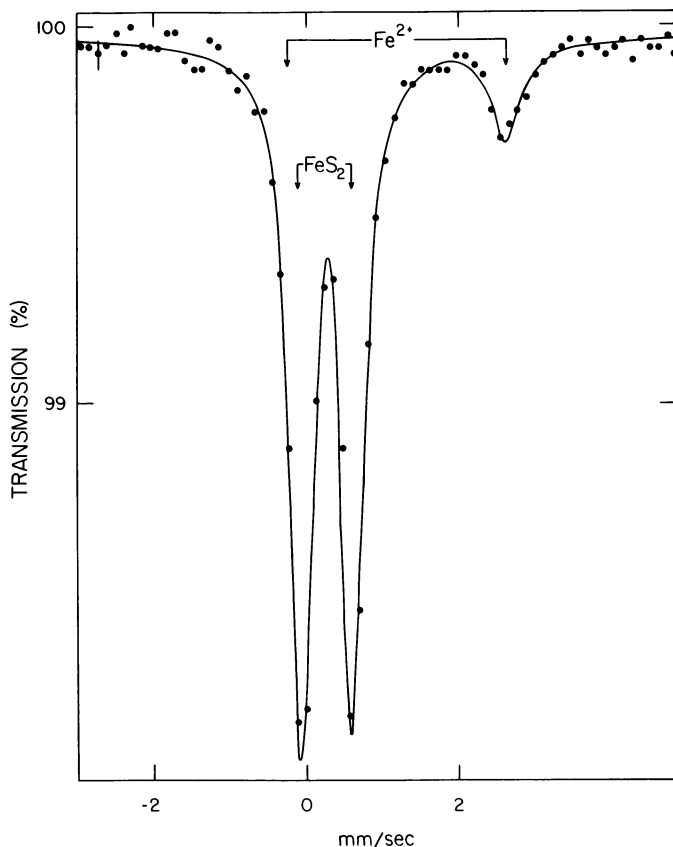


Figure 8. Waynesburg coal after treatment with HCl (RT)

In Figure 10 a Mössbauer spectrum for a mixture of szomolnokite (A) and rozenite (B) is shown. The sample was characterized by X-ray diffraction as well as Mössbauer spectroscopy. After the LTA was obtained, the Mössbauer spectrum shows the presence of szomolnokite (no rozenite) and ferric sulfate (Figure 11). This conversion was observed for all the coal samples studied that contained sulfates. In Table III a list of the iron sulfates and their respective Mössbauer parameters is given.

Carbonates. The Mössbauer spectra of some of the coal samples show the presence of FeCO_3 (siderite). Siderite has a rhombohedral structure with an octahedron of oxygens around the iron with a small trigonal distortion along the c axis. Siderite is magnetically ordered at low temperatures ($T_N = 38$ K), with a very distinctive Mössbauer spectrum (49). During this study it was observed on several occasions that a Mössbauer spectrum appeared to be that of FeCO_3 ; however, by carrying out low-temperature measurements, we could infer the presence of either clay or ankerite. Ankerite, $\text{Ca}(\text{FeMg})(\text{CO}_3)_2$, is another carbonate that appears in

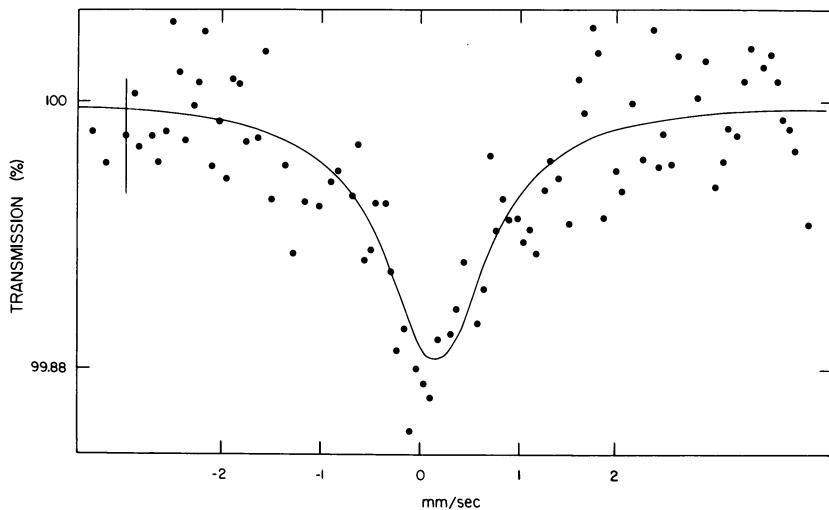


Figure 9. Pittsburgh coal after treatment with HNO_3 (RT). All the pyrite was removed.

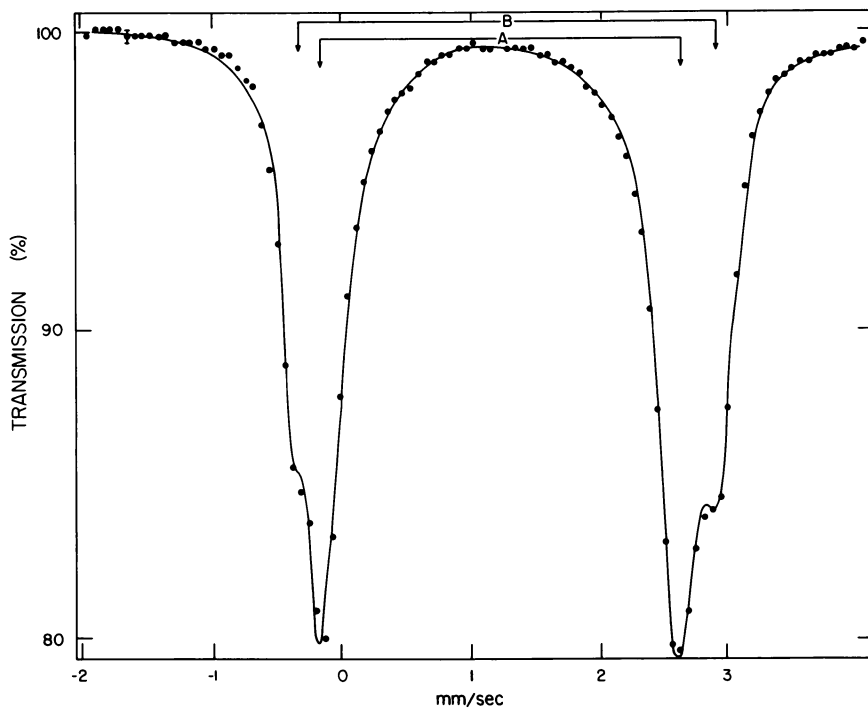


Figure 10. Mössbauer spectrum of rozenite (B) and szomolnokite (A) (RT)

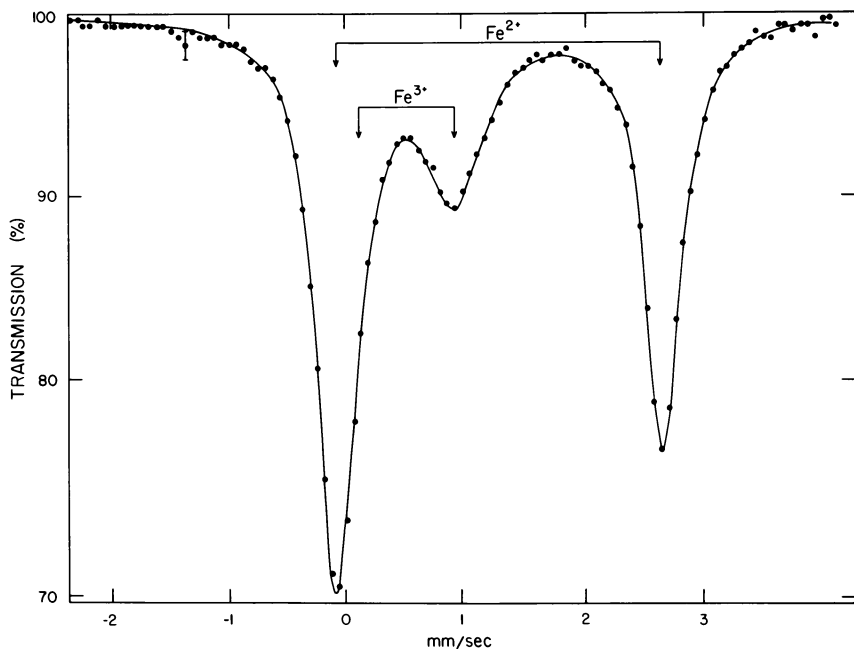


Figure 11. Mössbauer spectrum of szomolnokite and rozenite after LTA obtained (90°C). All the rozenite has disappeared (RT).

some coals. It is nearly impossible to distinguish ankerite from siderite when using Mössbauer spectroscopy at room temperature. One has to make low-temperature measurements. In Table III the relevant Mössbauer parameters are given for the iron carbonates observed in coal. In all the measurements no more than 0.1% siderite by weight was detected.

Table III. Iron Sulfates and Carbonates

Name	IS (mm/sec)	QS (mm/sec)	MHF (kOe)	Ref.
FeSO ₄	1.28(2)	2.90(2)	185 (4.2K)	^a
Szomolnokite (FeSO ₄ ·H ₂ O)	1.18(2)	2.69(2)	359 (4.2K)	^a (22, 23)
Rozenite (FeSO ₄ ·4H ₂ O)	1.32(4)	3.17		^a (46)
Melanterite (FeSO ₄ ·7H ₂ O)	1.31	3.20		(46)
Coquimbite	0.39(3)	0.60(5)	550 (4.2K)	^a (47)
Jarosit	0.43(2)	1.1–1.2	470–480(4.2K)	^a (48)
Siderite (FeCO ₃)	1.24(2)	1.87(5)	184 (4.2K)	(48)

^aThis work.

Table IV. Iron Oxides and Oxyhydroxides

Name	IS (mm/sec)	QS (mm/sec)	MHF (kOe)	Ref.
Hematite α -Fe ₂ O ₃	0.37	-0.10	515 (RT) ^a	(47)
γ -Fe ₂ O ₃	0.27		488	(47)
	0.41		499	(47)
Magnetite Fe ₃ O ₄	0.31		498	(RT) (50)
	0.67		463	(RT) (50)
Wustite (FeO)	1.08	0.55		(47)
Goethite α -FeOOH	0.37	0.25	390	(51)
Lepidocrocite γ -FeOOH	0.39	0.55		(47)
Fe(OH) ₂	1.16	3.00	200 (4.2K)	(47)
Fe(OH) ₃	0.33	0.72	458 (4.2K)	(47)

^aRT = room temperature.

Other Minerals. In this work only the minerals mentioned above were detected using Mössbauer spectroscopy. However, in heavily weathered coals and coal refuse the presence of iron oxides (hematite and, to a lesser extent, magnetite) was observed. The Mössbauer parameters for the major iron oxides are given in Table IV.

Mössbauer Spectroscopy as a Tool for Quantitative Determination of Pyritic Sulfur. The use of Mössbauer spectroscopy to determine the amount of iron in a sample presents several serious problems to the experimenter. One has to know the Debye-Waller factor (DWF) of pyrite and the background radiation accurately. The DWF of FeS₂ can be determined from the temperature dependence of the spectral area for pure crystals of known thicknesses. However, in many coals pyrite is highly dispersed and forms very small particles that have low crystallinity; consequently, the DWF might differ considerably from that of large FeS₂ crystals. The homogeneity of the sample should be tested with respect to distribution of pyrite. Also, a very important source of error is the determination of the nonresonant radiation background. In all the runs made in this study it was observed that variations of 10 to 30% occur in background counting rates for samples of coals with the same weight per unit area. The differences are caused by the heterogeneity of the mineral composition of the coals. The background radiation arises from the nonresonant scattering (Raleigh, Compton, and the photoelectric effects) from the 14.4-keV and high-energy X-rays. All these factors indicate that a full analysis of the γ ray spectrum for each sample is necessary. Any use of standards to determine the amount of pyritic sulfur will have to take into consideration the problems mentioned above (5). The use of Mössbauer spectroscopy for quantitative analysis has to go hand in hand with the standard chemical procedures (ASTM D2492-68), as a complementary technique and not as a substitute. In general, the most accurate Mössbauer quantitative measurement will give an error of about 10%.

Conclusions

The Mössbauer effect has been used as an analytical tool to characterize the different iron-bearing minerals in coal. It has been pointed out that by the use of low-temperature measurements (in the presence of a large external magnetic field) and treatment of the coal samples, all the iron-bearing minerals can be identified correctly. The use of Mössbauer spectroscopy as a quantitative analytical tool presents several experimental difficulties. It is recommended that this spectroscopy be used as a complement to and not as a substitute for the standard techniques.

Acknowledgments

The author thanks A. H. Stiller and J. J. Renton of the West Virginia Geological Survey for their invaluable help in carrying out this investigation. The technical assistance of William Dyson and P. Russell in some of the measurements is gratefully acknowledged. This work was supported by the Energy Research Center of West Virginia University.

Glossary of Symbols

\vec{P}	Linear momentum
E_0	Recoilless γ -ray energy
$E_0^2/2Mc^2$	Recoil energy
f	Debye–Waller factor
k_B	Boltzmann constant
θ_D	Debye–temperature
\vec{k}	Wave vector
\vec{x}	Position of the emitting atom
σ_r	Resonance–absorption cross section
μ_a, μ_s	Mass attenuation coefficients
Γ	Line width
β	Isotope abundance
n	Number of atoms per cubic centimeter
d	Absorber thickness
B	Background radiation
IS	Isomer shift
$-e \Psi(0) ^2$	Electron density at the nucleus
R_{ex}	Radius of the excited state
R_g	Radius of the ground state
c	Velocity of light
I^*, I	Nuclear spin
Q	Quadrupole moment of the nucleus
$eq = V_{zz}$	Electric field gradient
η	Asymmetry parameter

g_n	Nuclear gyromagnetic factor
μ_n	Nuclear magneton
B	Effective magnetic field at the nucleus

Literature Cited

1. Thomas, M. G.; Granoff, B.; Baca, P.M.; Noles, G.T. *Am. Chem. Soc., Div. of Fuel Chem.* 1978, 23(1), 23.
2. Bancroft, G. M. "Mössbauer Spectroscopy: An Introduction for Inorganic Chemists and Geochemists"; John Wiley & Sons: New York, 1973.
3. Montano, P. A. *Fuel* 1977, 56, 397.
4. Levison, L. M.; Jacobs, I. S. *Fuel* 1977, 56, 453.
5. Huffman, G. P.; Higgins, F. E., submitted for publication in *Fuel*.
6. Mossbauer, R. L. *Z. Phys.* 1958, 151, 124.
7. Lipkin, H. *Ann. Phys.* 1960, 2, 332.
8. Lamb, W. E., Jr. *Phys. Rev.* 1939, 55, 190.
9. Margulies, S.; Ehrman, J. R. *Nucl. Instrum. Methods* 1961, 12, 131.
10. Lang, G. *Nucl. Instrum. Methods* 1961, 24, 425.
11. Housley, R. M.; Grant, R. W.; Gonser, U. *Phys. Rev.* 1969, 178, 514.
12. Kistner, O. C.; Sunyar, A. W. *Phys. Rev. Lett.* 1960, 4, 412.
13. Pound, R. V.; Rebka, G.A., Jr. *Phys. Rev. Lett.* 1960, 4, 274.
14. Josephson, B. D. *Phys. Rev. Lett.* 1960, 4, 342.
15. Abragam, A. "L'Effect Mössbauer et ses applications a l'Etude des Champs Internes"; Gordon and Breach: Paris, 1964.
16. Griffith, J. S. "The Theory of Transition-Metal Ions"; Cambridge Univ. Press: Cambridge, 1964.
17. Sternheimer, R. L. *Phys. Rev.* 1950, 80, 102.
18. *Ibid.* 1951, 84, 244.
19. Wertheim, G. K. "Mössbauer Effect, Principles and Applications"; Academic: New York, 1964.
20. Wickman, H. H. In "Mössbauer Effect Methodology"; Gruverman, I. J., Ed.; Plenum: New York, 1966; Vol. 2.
21. Montano, P. A.; Seehra, M. S. *Solid State Commun.* 1976, 20, 897.
22. Russell, P.; Montano, P.A. *J. Appl. Phys.* 1978, 49(3), 1573.
23. *Ibid.* 49(8), 4615.
24. Power, L. F.; Fine, H. A. *Miner. Sci. Eng.* 1976, 8, 106.
25. Ward, J. C. *Rev. Pure Appl. Chem.* 1970, 20, 175.
26. Vaughan, David J.; Craig, James R. "Mineral Chemistry of Metal Sulfides"; Cambridge Univ. Press: Cambridge, 1978.
27. Thiel, R. C.; van den Berg, C. B. *Phys. Status Solidi* 1968 29, 837.
28. Kasper, H.; Drickhamer, H. G. *Proc. Natl. Acad. Sci. USA* 1968, 60, 773.
29. Vaughan, P. J.; Tossell, J. A. *Science* 1973, 179, 375.
30. Ovanesyan, N. S.; Trukhtanov, V. A.; Odinets, G. Yu; Novikov, G. V. *Sov. Phys. JETP Engl. Transl.* 1971, 33, 1193.
31. Montano, P. A.; Granoff, B., unpublished data.
32. Vaughan, D. J.; Ridout, M. S. *J. Inorg. Nucl. Chem.* 1971, 33, 741.
33. Schrader, R.; Pietzch, C. *Krist. Tech.* 1969, 4, 385.
34. Stiller, A. H.; McCormick, B.; Jack, Russell P.; Montano, P. A. *J. Am. Chem. Soc.* 1978, 100, 2553.
35. Marfunin, A. S.; Mkrtychyan, A. R. *Geochem Int.* 1967, 4, 980.
36. Hafner, S. S.; Kalvius, M. Z. *Kristallogr.* 1966, 123, 443.
37. Millot, G. "Geologie der Argiles"; Masson: Paris, 1970.
38. Rao, C. Prasada; Gluskoter, J. Harold. *Illinois State Geological Survey, Circ.* 1973, No. 476.
39. Jefferson, D. A.; Tricker, M. J.; Winterbottom, A. P. *Clays Clay Miner.* 1975, 23, 355.

40. Coey, J. M. D. *Int. Conf. on Mössbauer Spectroscopy 333, Cracow, 1975.*
41. Malysheva, T. V. "Effekt Mossbauer v Geokimii i Kosmokitii"; Navk: Moscow, 1975.
42. Coey, J. M. D. "Clay Minerals and Their Transformations Studied with Nuclear Techniques: The Contribution of Mössbauer Spectroscopy"; in press.
43. Hogarth, D. D.; Brown, F. F.; Pritchard, A. M. *Can. Mineral* **1970**, *10*, 710.
44. Stiller, A. H.; Renton, J. J.; Montano, P. A.; Russell, P. E. *Fuel* **1978**, *57*, 477.
45. Pistorius, C. W. F. T. *Bull. Soc. Chim. Belg.* **1960**, *69*, 570.
46. Vertes, A.; Zsoldos, B. *Acta Chim. Acad. Sci. Hung.* **1970**, *65*, 261.
47. Greenwood, N. N.; Gibb, T. C. "Mössbauer Spectroscopy"; Chapman and Hall: London, 1971.
48. Hryniewicz, A. Z.; Kubisz, J.; Kulgawczuk, D. S. *J. Inorg. Nucl. Chem.* **1965**, *27*, 2513.
49. Ono, K.; Ito, A. *J. Phys. Soc. Jpn.* **1964**, *19*, 889.
50. Daniels, J. M.; Rosencwaig, A. *J. Phys. Chem. Solids* **1969**, *30*, 1561.
51. Govaert, A.; Dauve, C.; Plinke, P.; De Grove, E.; Desitter, J. *J. Phys.* (colloq. c-6) **1976**, *37*, 825.

RECEIVED July 19, 1979.

INDEX

A

Acid(s)
 in black coal, *n*-alkanoic 127
 carboxylic 171
 and coal structure 113-129
 naphthalene 171
 phenanthrene 171
 -catalyzed coal depolymerization, chemistry of 179-189
 cinnamic 147
 in coals
 branched-chain 128
 diunsaturated 129
 unsaturated 128
p-coumaric 147
 fatty (*see* Fatty acids)
 ferulic 147
 fulvic 145
 humic 145
 hydroxynaphthalenecarboxylic 145
 identified as *d*₃-methyl esters,
 organic 144t
 isomers of hydroxybenzene-dicarboxylic 145
 phenolic polycarboxylic 145
 as products of oxidation of
 coals, aromatic 138
 trihydroxybenzoic 145
 Acylation reactions, Friedel-Crafts 192
 Acylations using Bruceton coal
 and octanoyl chloride 282
 Alcohols 167
 Aldehydes and ketones as oxidation
 products of lignin,
 aromatic 138
 Alkali-digested brown coal, particle
 size analysis of 311-319
 Alkali-treated brown coal, particulate
 structure in 311-319
 Alkaline cupric oxide (CuO)
 oxidation method 134
 Alkaline oxidation of alcohols
 and glycols 171
n-Alkanes in coals 113
n-Alkanoic acids in black coal ... 127
n-Alkanoic acids in coals, distributions
 of 122
 Alkyl
 carbon distributions 267
 group on conversion of Illinois
 No. 6 coal, influence of ... 212
 halides, alkylation reactions of .. 218
 radicals 231
 Alkylated coal products, proton
 and carbon NMR spectra of . 219
 Alkylation
 coal 207-222
 with butyl-1-C iodide 209-210

Alkylation (*continued*)
 coal (*continued*)
 complications in the reductive
 225-236
 of oxygen functionality in ... 232
 reaction 215
 chemistry of reductive 226
 reactions of alkyl halides 218
 reactions, Friedel-Crafts 192
 Aliphatic(s)
 -aromatic carbon bridge structures
 in coal, correlation of
 depolymerization product
 yields with reactivities
 of 187, 189
 -aromatic carbon-carbon bonds
 in coals, reactivity of ... 181-183
 chains containing oxygen or sulfur
 functional groups,
 oxidation of 135
 coal(s)
 bridges in low-rank 187, 189
 in brown 205
 ether bonds, cleavage of 183
 long-chain 104
 part in coal, structure of 159
 side chain of aromatics, oxidation
 of ether linkages in ... 135
 Anion(s)
 benzylic 232
 graphite 234
 naphthalene 234
 radical 226
 aromatic 232
 in coal 229
 Ankerite (Ca(FeMg)(CO₃)₂) ... 355
 Anthracene 212, 217
 Anthracene coals
 coalification from lignite to
 bituminous and 148
 meta- 40
 solvent-extractable material of . 145
 Aromatic
 acids as products of oxidation
 of coals 138
 aldehydes and ketones as oxidation
 products of lignin 138
 in coal(s)
 carbon bridge structures,
 correlation of depolymerization
 product yields with
 reactivities of ali-
 phatic- 187, 189
 carbon-carbon bonds, reactivity
 of aliphatic- ... 181-183
 and heteroaromatic units 170
 compounds, GPC elution
 behavior for 269

- Aromatic (*continued*)
 compounds, naphthenic rings in 266
 groups in brown coal 204-205
 hydrocarbons 145
 Friedel-Crafts benzylation of 186
 radical anions 232
 ring reduction in coal solubili-
 zation 169
 Aromatics from coal, isolation of
 polycyclic 170
 Aromatics, oxidation of ether link-
 ages in aliphatic side chain of 135
 Aromaticity of coal 204
 solvent-refined (SRC) 170
 Arrhenius equation 67
 Aryl ethers, cleaving of 175
 Ash, ESR spectra of a coal and
 its low-temperature 42, 43f
 Asphaltenes 54, 78
 coal-derived 44, 51-53
 ESR *g* values and spectral line
 widths for selected 53t
 evolution of molecular weight of 80
 and oils, conversion of coal to
 preasphaltenes 75
 petroleum 44, 53
 structural investigation of ... 181
 ASTM classification of coals
 according to rank 7
 Australian brown coal lithotypes,
 monocarboxylic fatty acid
 content of 114
 Australian Morwell brown coal .. 193
- B**
- Bacteria 317
 Benzene-ethanol solvent 187
 Benzenium ion 186
 Benzyl derivatives of 2,6-dimethyl-
 phenol, chemical shift values
 of methylene and methyl
 protons of 185t
 4-Benzyl-2,6-dimethylphenol/BF₃ . 184
 Benzylation of aromatic hydrocar-
 bons, Friedel-Crafts 186
 Benzylic anions 232
 Benzylphenols, BF₃-catalyzed
 group transfer in 184f
 2,6-dimethyl 185f
p-Benzylphenol 183
 BET (*see* Brunauer-Emmett-
 Teller)
 Biological digestion stage of
 coalification 317
 Biphenyl 212, 217
 Bituminous coal(s) 155
 and anthracite coals, coalifica-
 tion from lignite to 148
 bridge structures in higher-rank
 high-volatile 49, 322
 kinetic constants for lignite and . 96t
 organic acids 145
- Bituminous coal(s) (*continued*)
 photomicrograph of a polished
 surface of 2f
 Pocahontas low-volatile 225
 solvent 287
 -extractable material 145
 after treatment with KOH in
 various solvents, solubilities
 of Illinois No. 2 165t, 167
 BF₃-catalyzed
 benzyl group transfer
 in benzylphenols 184f
 2,6-dimethyl 185f
 kinetics of 183-186
 isopropyl to phenol (1-¹⁴C) ... 181t
 reaction of *p*-*n*-propylphenol
 with phenol (1-¹⁴C) 182t
- Bonds
 aromatic-methylene carbon-
 carbon 288
 cleavage of aliphatic ether 183
 cleavage, carbon-oxygen 229
 in coal, carbon-carbon 152
 in coal, chemical 152
- Bridges in coal(s)
 low-rank aliphatic 187, 189
 methylene 199
 brown 205
 structures
 aliphatic 189
 correlation of depolymeriza-
 tion product yields with
 reactivities of aliphatic-
 aromatic carbon 187, 189
 higher-rank bituminous 189
 toward phenol-BF₃, reac-
 tivities of 181-183
- Brown coal, particulate structure
 in alkali-treated 311-319
- Bruceton coal
¹³C NMR spectrum of octa-
 noylated 285
 fractionation of depolymerized . 288f
¹H NMR spectrum of octa-
 noylated 284f
 and octanoyl chloride, acyla-
 tions using 282
- Brunauer-Emmett-Teller (BET)
 method, isotherm analyses by 298
 Brunauer-Emmett-Teller (BET)
 multilayer theory 295
- Bureau of mines (USBM) API
 project 60, U.S. 258
- 1-Butene 214
- Butyl
 -1-C iodide, coal alkylation
 with 209-210
 -1-¹³C iodide, synthesis of ... 214
 ethers 220
 halides 218
 mesylate 214
 reactions of coal polyanions
 with 212, 213t, 217
- Butylation reactions of halides
 and sulfonates 213

Butylation reagents, reactions of
the potassium-coal polyanion
with 213

C

^{13}C and ^1H in solid coals, aromatic
in Pocahontas No. 4 vitrain,
high-resolution NMR spectra
of16, 17*f*
in Star vitrain, high-resolution
NMR spectra of16, 17*f*

C_6D_6 , quadrupole coupling
constants for 29

C_6D_6 uptake in coal 25

$\text{C}_5\text{D}_5\text{N}$, quadrupole coupling
constants for 29

$\text{C}_5\text{D}_5\text{N}$ uptake in coal 25

CH_2 bridges in coal depolymeri-
zation, role of183, 189

$\text{Ca}(\text{FeMg})(\text{CO}_3)_2$ (ankerite) ... 355

CuO oxidation for lignin,
mechanism of 138

CuO-NaOH oxidation products of
coal 139*t*

Calcium 251

Carbon 187

bridge structures in coal, corre-
lation of depolymerization
product yields with reac-
tivities of aliphatic-aro-
matic187, 189

-carbon bond(s)

aromatic-methylene 288

cleavage 216

in coal(s) 152

reactivity of aliphatic-aro-
matic181-183

dioxide sorption in coal 296

distributions, alkyl 267

in the oxidation products of
coals, distribution of 140*t*

-oxygen bond cleavage216, 229

preference index (CPI) for

fatty acids in coal127, 128*t*

skeleton of coal 153

in Pocahontas No. 4 vitrain,
fraction of aliphatic and

aromatic15-21

in Star vitrain, fraction of ali-
phatic and aromatic15-21

Carbonates 357*t*

in coal, iron355-357

Carbonization

chances of hydrogen aromaticity
of coal during 60

chances of hydrogen aromaticity
of pitch during 60

coal 59

Carboxylic acid(s) 171

and coal structure113-129

Carboxylic groups in coal, hydro-
gen-bonded protons from
phenolic and 199

Cellulose 317

Char(s) 105

hydrogen in105, 108*f*

distribution105, 107*f*

spectra of105, 106*f*

infrared 96

Charge-transfer interactions 44

Chloride, acylations using Bruceton

coal and octanoyl 282

Chromium 332

Cinnamic acids 147

Classification of coals according

to rank, ASTM 7

Clay minerals332, 353*t*

in coal351-352

Coal(s)

according to rank, ASTM

classification of 7

acids in

branched-chain 128

diunsaturated 129

unsaturated 128

aliphatic bridges in187, 189

n-alkanes in 113

alkylation of207-222, 232

complications in the reduc-

tive225-236

aromatic and heteroaromatic

units in 170

aromaticity of 204

bituminous 155

bridge structures in higher-

rank 189

high-volatile49, 322

kinetic constants for lignite

and 96*t*

photomicrograph of a

polished surface of 2*f*

black 114

n-alkanoic acids in122, 127

fatty acid distribution in ... 127

solvent extraction of 119

brown

aliphatics in 205

Australian Morwell 193

cylindrical rods in 314

distribution of hydrogen in 201, 202*t*

groups in

aromatic204-205

β -methyl and β -methylene 205

oxygen203-204

methylene bridges in 205

monocarboxylic fatty acid

content of Australian ... 114

particle size analysis of

alkali-digested311-319

particulate structure in

alkali-treated311-319

photomicrographs of 314*f*

by reaction with phenol, de-

duction of the structure

of191-206

solvent extraction of 119

Bruceton

fractionation of depolymerized 288*f*

Coal(s) (*continued*)
 Bruneton (*continued*)
¹H NMR spectrum of
 octanoylated 284*f*
 and octanoyl chloride,
 acylations using 282
 carbon-carbon bonds in 152
 carbon skeleton of 153
 carbonization 59, 60
 characterization of hydro-
 lytically solubilized 161-176
 classification methods of 2-3
 concentrations of unpaired
 electrons in 41
 conversions 212, 217
 cylindrical rod-shaped particles
 in Victorian 319
 depolymerization 192
 chemistry of acid-catalyzed 179-189
 phenol, method to solubilize . 194
 role of CH₂ bridges in ... 183, 189
 via transaryl-alkylation with
 phenol-BF₃ 179, 180*f*
 yields as a function of coal
 rank 187, 188*f*
 -derived
 asphaltenes 44, 51-53
 humic acids, reductive degra-
 dations of 133
 liquids, hydrocarbon content
 of 257-275
 oils 53-54
 molecular weight distribu-
 tion of 269
 products, ¹³C chemical shifts
 in 83
 desulfurization 255
 of different rank
 differences in the fatty acid
 distributions of 128
 with phenol-BF₃, depolymeri-
 zation of 187*t*
 properties of vitrinites in ... 6*t*
 diffusion of reagents through
 solid 279
 distribution of organic sulfur
 functional groups in ... 239-255
 dry mineral-matter-free
 (DMMF) 99
 effect of reagent access on the
 reactivity of 277-290
 elemental composition of 152
 elemental and hydroxyl group
 analyses of Kaiparowitz ... 77*t*
 from the Eocene epoch or the
 Permian period 129
 ESR *g* values for West Virginia
 (Ireland Mine) hvAb ... 49, 50*f*
¹⁹F wide-line NMR studies of .. 27
 fatty acids in 113, 126*f*
 carbon preference index
 (CPI) for 127, 128*t*
 extraction of free and bound . 116
 2-fluorophenol in 32
 formation 317, 318

Coal(s) (*continued*)
 fragmentation 155
 fragments, structural formulas of 157
 free radicals in 37-57, 227
 aromatic 46
 EST and ENDOR spectrome-
 tries characterizing 56
 pyrolyzed 37-57
 fusinite-rich 3
 general features of EST and
 ENDOR spectra of 39-42
 glycol-solubilized 162
 grade, orthogonal influences of
 coal rank and type on ... 11*f*
 HCl treatment of 251
 heteroatoms in 47, 153
 hydrogen distribution in 104*t*
 with hydrogen peroxide, oxida-
 tion of 251
 hydrogenation, chemical struc-
 ture of heavy oils from . 257-275
 hydrolytic product of Pittsburgh
 No. 8 166
 hyperfine coupling constants
 for 46*t*, 48
 Illinois No. 6 (*see* Illinois
 No. 6 coal)
 Ireland Mine 38
 iron
 carbonates in 355-357
 sulfates in 352-355
 sulfides in 344-351
 processing 346
 isolation of polycyclic aro-
 matics from 170
 kinetic analysis of hydrogen
 aromaticity changes in ... 67-69
 kinetogram(s) of
 CH₂I-treated 254*f*
 HCl-extracted 253*f*
 oxidized 252*f*
 raw 252*f*, 254*f*
 lignin-like polymers in 133-148
 liquefaction 59
 changes in the quantity and
 nature of free radicals
 during 54
 mechanisms of 49
 PDU, Pittsburgh Energy Tech-
 nology Center's 38
 products, free radicals in ... 37-57
 short-time reaction prod-
 ucts of 151-159
 liquids, chemical structure of .. 258
 lithotype classification of
 air-dried 115*t*
 and its low temperature ash,
 ESR spectra of 42, 43*f*
 meta-anthracite 40
 metamorphism 46
 methyl iodide (CH₃I) treatment
 of 251
 methylene bridges in 199
 minerals in
 clay 351-352

Coal(s) (*continued*)
 minerals in (*continued*)
 macerals 332
 by Mössbauer spectroscopy,
 characterization of
 iron-bearing 337-360
 molecules in
 ESR studies of 23-35
 fluorinated 34
 magnetic resonance study of
 labeled guest 23-35
 NMR studies of 23-35
 Monterey 152
 nitrogen in 152
 nonhydrocarbon functions in .. 152
 oxidation products 145
 aromatic acids as 138
 CuO-NaOH 139*t*
 lignin 134
 low-rank, *p*-hydroxybenzoic
 acids in 138
 Na₂Cr₂O₂ 170
 oxygen in 152
 particle size distribution for
 humic acid fraction of .315, 316*f*
 phenolic OH group in 280
 polyanion(s) 208, 211
 with butyl 212, 213*t*, 217
 with butylation reagents, re-
 actions of the potassium- 213
 with iodide 212, 213, 217
 with methyl 212, 213*t*, 217
 with octyl 212, 213*t*, 217
 pore structure of 279
 porosity
 of exinitic maceral of splint 325, 326*f*
 and internal surface area of .. 293
 studies of 321-336
 to preasphaltenes, asphaltenes,
 and oils, conversion of 75
 products of thermal decompo-
 sition of 108*f*, 109*f*
 properties 117*t*
 pyrolyzed 49-51
 radical anions in 229
 rank 41
 coal depolymerization yields
 as a function of 187, 188*f*
 relationship between the *g*
 values of coals and 47
 relationship between ESR
 intensities and 46
 on solubilization of coal,
 effect of 165-167
 and type on coal grade,
 orthogonal influences of . 11*f*
 and type on metallurgical coke
 strength, influence of ... 12*f*
 reactions of
 with ethanolic NaOH 162
 ethers in 220
 Friedel-Crafts 282
 reactivity of aliphatic-aro-
 matic carbon-carbon bonds
 in 181-183

Coal(s) (*continued*)
 reflectance distribution of
 macerals in 5, 6*f*
 seam 114
 separation scheme of heavy oil
 from 258, 259*f*
 solubility parameter of 318
 solubilization ether linkage
 cleavage in 175
 solubilization techniques 192
 solubilizing (depolymerizing) .. 286
 solvent fractionation scheme
 to separate 194*f*
 solvent-refined (SCR) 51
 aromaticity of 170
 ESR *g* values and spectral
 line widths for 51*t*
 free radicals in 37-57
 sorption (in)
 carbon dioxide 296
 studies of 293-309
 water 296
 spectra of West Virginia
 (Ireland Mine) hvAb 40*f*
 structure
 of the aliphatic part in 159
 carboxylic acids and 113-129
 model of 319
 and science 1-13
 and thermal decomposition
 products, relation
 between 95-111
 ultrafine 321-336
 subbituminous 49
 products from the thermal
 dissolution of Kaiparo-
 witz 75-92
 in tetralin, application of NMR
 and GPC to the study of
 structural evolution
 of 75-92
 sulfur in 152
 distribution
 class 250*t*
 raw 250
 treated 250
 Taiheiyo 62
 ¹H NMR spectra of 63*f*
 tar pitch 62
 tars 96
 TEM micrograph of vitrinite
 in splint 327, 328*f*, 332
 TEM of splint 323*f*
 temperature dependence of ¹H
 NMR absorption in 59-74
 U.S. 7
 Wyodak 24, 227
 deuterated guests in 25
 distribution of chemical classes
 in the solubilized prod-
 ucts from 155*t*
 TEMPOL ESR spin label
 studies in 30*f*
 Yubarishinko 62
 ¹H NMR spectra of 63*f*

Coalification	47
biological digestion stage of ...	317
from lignite to bituminous and anthracite coals	148
Combined rotation and multiple-pulsed NMR spectroscopy (CRAMPS)	16
<i>p</i> -Coumaric acids	147
Crystallites	280
Cupric oxide (CuO) oxidation method, alkaline	134
Curie's Law	44

D

² D nuclei as probes for use in transient NMR studies	34
² D wide-line NMR studies of coals	28
Debye-Waller factor of pyrite ...	358
Decomposition, thermal of coal, products of	108f, 109f
model	96
products, relation between coal structure and	95-111
Depolymerization method to solubilize coal, phenol	194
Deuterium	87
scrambling	90-91
Dianions	235
Dichromate oxidation, degradation of hydroaromatics by	171
1,1-Dideuterotetraline, reactions of coal and tetralin or	76
Diffusion in nonporous polymers ..	279
Diffusion of reagents through solid coal	279
Dihydroxy-diphenylmethane	180
3,4-Dihydroxybenzoic acids in the oxidation products of low-rank coals	138
1,2-Dimethoxyethane	214
2,6-Dimethoxyphenol	135-138
2,6-Dimethyl benzylphenols, BF ₃ -catalyzed benzyl group transfer in	185f
2,6-Dimethylbenzoic acid, high-resolution NMR protons in ..	16, 18f
2,6-Dimethylphenol, chemical shift values of methylene and methyl protons of benzyl derivatives of	185t
Diphenylpicrylhydrazyl (DPPH) ..	52
Doppler effect	342
Dubinin-Radushkevith (DR) theory	298

E

Electron(s)	
in coals, concentrations of unpaired	41
microscopy, transmission (TEM) ..	322
scanning (STEM)	322

Electron(s) (*continued*)

nuclear	
double resonance (ENDOR) spectrometry(ies)	38
characterizing the free radicals in coals	37-57
double resonance (ENDOR) spectrum(a)	
of coals, general features of ESR and	39-42
of organic free radicals ...	43
of vitrain-rich Pittsburgh coal	41, 42f
hyperfine constants for coals as determined by ENDOR spectrometry	46
spin resonance (ESR)	23
and ENDOR spectra of coals, general features of	39-42
<i>g</i> value (spectroscopic splitting factor)	40-41
and coal heat treatment, relationship between ..	50
intensities and coal rank, relationship between	46
spectra of coal(s)	44
and its low-temperature ash	42, 43f
spectrometry(ies)	38
characterizing the free radicals in coals ...	37-57
spin studies in Wyodak coal, TEMPOL	30f
studies of molecules in coal ..	23-35
transfer	
agents	207
reactions	218
reagent on conversion of Illinois No. 6 coal, influence of	212
Elimination reactions, base-catalyzed	216
Elution behavior for aromatic compounds, GPC	269
Elution volume, relationship between molecular weight and GPC	257-275
ENDOR (<i>see</i> Electron nuclear double resonance)	
ESR (<i>see</i> Electron spin resonance)	
Esters	
from lithotypes, monocarboxylic organic acids identified as <i>d</i> ₃ -methyl	144t
of the oxidation products from coal, methyl	173t
Ethanollic NaOH, reactions of coals with	162
Ether(s)	
bonds, cleavage of aliphatic ...	183
butyl	220
cleavage of phenyl methyl ...	138
cleaving of aryl	175
in coal, reactions of	220

- Ether(s) (*continued*)
 linkage cleavage in coal solubilization 175
 linkages in the aliphatic side chain of aromatics, oxidation of 135
 phenol 195
 Ethylene
 attack on naphthalene 232-233
 glycol, solubilities of coals after treatment with KOH in 164*t*, 165
 tar pitch 62
¹H NMR spectra 66*f*, 70, 71*f*
 Exines in coals, spore 325
 Exinite 323
 Exinitic maceral of splint coal, porosity of 325, 326*f*

F

- ¹⁹F nuclei as probes for use in transient NMR studies 34
 FeCO₃ (siderite) 355
 FeS (troilite) 346
 Fe₇S₈ (monoclinic pyrrhotite) ... 346
 FeSO₄ · H₂O (szomolnokite) ... 354
 FeSO₄ · 4H₂O (rozenite) 354
 FeSO₄ · 7H₂O (melanterite) ... 354
 Fatty acid(s) 145
 bound 114
 in coal(s) 113
 carbon preference index (CPI) for 127, 128*t*
 extraction of free and bound . 116
 concentration vs. lithotype ... 123*f*
 content of Australian brown coal lithotypes, monocarboxylic . 114
 distribution(s)
 of coal(s) 126*f*
 of different rank, differences in 128
 in black coal 127
 lithotype 124*f*, 125*f*
 free (solvent-extractable) 114
 in lithotypes, ratio of high to low molecular-weight .. 123, 126*t*, 127
 n-Fatty acid distributions due to lithotype, changes in 129
 Ferric sulfates 354
 Ferulic acid 147
 Fillers 280
 2-Fluorophenol
 in coal 32
 uptake 25
 molecules in coal, spin lattice relaxation measurements for 32, 33*f*
 molecules in neat liquids, spin lattice relaxation measurements for 32, 33*f*
 2-Fluoropyridine, Illinois No. 6 coal containing 28
 2-Fluoropyridine uptake in coal .. 25

- Fossil walnut stones 129
 Fourier transform infrared spectrometry (FTIR) 96
 Friedel-Crafts benzylation of aromatic hydrocarbons 186
 Friedel-Crafts reactions
 acylation 192
 alkylation 192
 of coals 282
 FTIR (Fourier transform infrared spectrometry) 96
 Fulvic acid 145
 Fusain 39
 Fusinite-rich coal 3

G

- g*-value(s) (spectroscopic splitting factor)
 and coal heat treatment, relationship between ESR 50
 of coals and coal rank, relationship between 47
 ESR 40-41
 Gieseler plastometer method 72
 Glycol(s) 162
 alkaline oxidation of alcohols and solubilities of coals after treatment with KOH in
 ethylene 164*t*, 165
 -solubilized coal 162
 GPC
 elution behavior for aromatic compounds 269
 elution volume, relationship between molecular weight and 257-275
 separations, subfractions from 258-275 to the study of structural evolution of subbituminous coal in tetralin, application of NMR and 75-92
 Graphite anion 234
 Graphite surfaces, interaction of metal particles on 326

H

- ¹H in solid coals, aromatic ¹³C and HCl treatment of coal 251
 Halides
 alkylation reactions of alkyl ... 218
 butyl 218
 and sulfonates, butylation reactions of 213
 Heteroaromatic units in coals, aromatic and 170
 Humic acid(s) 145, 312
 fraction of coal, particle size distribution for 315, 316*f*
 oxidation products of 135
 Humins 312
 Humocollinite 119*t*

Humodetrinite	119t
Humotelinite	119t
Hydride transfer	171
Hydroaromatics by dichromate oxidation, degradation of	171
Hydrocarbon(s)	
aromatic	145
content of coal-derived liquids	257-275
Friedel-Crafts benzylation of aromatic	186
ring size in Pocahontas No. 4 vitrain, average polyaromatic	20
ring size in Star vitrain, average polyaromatic	20
Hydrogen	
aromaticity	
changes in coal, kinetic analysis of	67-69
of coal during carbonization, chances of	60
of pitch during carbonization, chances of	60
bonding temperature, variation of	102f
in char	105, 108f
distribution	105, 107f
distribution in coals	104t
peroxide, oxidation of coal with.	251
sulfide	240
from aliphatic sulfides, evolu- tions of	249
from iron pyrite, evolutions of	249
<p>-Hydroxy-benzoic acids in the oxidation products of low-rank coals</p>	138
Hydroxybenzenedicarboxylic acids, isomers of	145
Hydroxynaphthalenecarboxylic acids	145
Hyperfine coupling contents for coals	46t, 48

I

Illinois No. 6 coal	24, 227
with anthracene, naphthalene, and biphenyl, reduction and butylation of	212t
bituminous after treatment with KOH in various solvents, solubilities of	165t, 167
containing 2-fluoropyridine	28
deuterated guests in	25
hydrolytic product of	166
influence of, on conversion of alkyl group	212
electron transfer reagent	212
metals	212
with lithium, sodium, and potas- sium, reduction and butyla- tion of	212t
with methyl butyl and octyl iodide, reduction and alkylation of	213t

Illinois No. 6 coal (<i>continued</i>)	
scanning electron micrograph of	303, 306f, 307f
TEM	324f
micrograph of vitrinite in	327, 328f, 329f
titration data for	230f
wide-line NMR spectra from ...	28f
Illite	332, 351
Inertinite	2f, 3, 119t, 323
Iodide	
coal alkylation with butyl-1-C	209-210
reactions of coal polyanions with	212, 213t, 217
synthesis of butyl-1- ¹³ C	214
treatment of coal, methyl (CH ₃ I)	251
Ionization efficiency, molecular ...	264
Iowa vitrain, average polynuclear aromatic ring size in	15-21
Ireland Mine coal	38
hvAb, ESR <i>g</i> values for	49, 50f
hvAb, spectra of West Virginia.	40f
Iron	
-bearing minerals in coal by Mössbauer spectroscopy, characterization of	337-360
carbonates in coal	355-357
disulfide (pyrite)	344-360
oxides	358t
pyrite	245
evolutions of H ₂ S from	249
sulfates	357t
in coal	352-355
sulfides	345t
in coal	344-351
produced during coal process- ing	346
Isomer shift in Mössbauer spectroscopy	341
Isopropyl group transfer to phenol(1- ¹⁴ C), BF ₃ -catalyzed	181t

K

Kaiparowitz coal, elemental and hydroxyl group analyses of ..	77t
Kaiparowitz coal, products from the thermal dissolution of subbituminous	75-92
Kaolinite (Al ₂ ³⁺ Si ₂ ⁴⁺ O ₅ ²⁻ (OH ⁻) ₄) 332-334, 351	
Kerogen	114
Ketones as oxidation products of lignin, aromatic aldehydes and	138
KOH (<i>see</i> Potassium hydroxide)	
Kureha pitch, ¹ H NMR spectrum of	69, 70f

L

LC separations, subfractions from	258-275
Lignin(s)	317
during coalification, roles of ...	133

- Lignin(s) (*continued*)
 -like polymers in coals133-148
 oxidation
 mechanism of CuO 138
 products 145
 from coals 134
- Lignite
 to bituminous and anthracite
 coals, coalification from ... 148
 and bituminous coals, kinetic
 constants 96*t*
 coal organic acids 145
 solvent-refined (SRL) 170
- Liptinite 2*f*, 3, 119*t*
 in lithotypes 120
- Liquefaction, coal 59
 mechanisms of 49, 50*f*
 Pittsburgh Energy Technology
 Center's PDU 38
 products 51
 short-time reaction products
 of 151-159
- Liquefaction process, behavior of
 pyrrhotite in 348
- Liquids, hydrocarbon content of
 coal-derived 257-275
- Lithotype(s)
 changes in the *n*-fatty acid dis-
 tributions due to 129
 classification of air-dried coal .. 115*t*
 definition of 114
 fatty acid concentration vs. 123*f*
 fatty acid distributions ... 124*f*, 125*f*
 liptinite in 120
 monocarboxylic esters from ... 121
 monocarboxylic fatty acid con-
 tent of Australian brown
 coal 114
 ratio of high to low molecu-
 lar-weight fatty acids
 in 123, 126*t*, 127
- Lorentzian lines 16
- M**
- Maceral(s) 1, 323
 analyses 120*t*
 in coal(s)
 major classes of 2*f*, 3
 minerals 332
 reflectance distribution of ... 5, 6*f*
 groups, definitions of 119*t*
 principal features of the major
 classes of 3, 4*f*
 of splint coal, porosity of
 exinitic 325, 326*f*
 vitrinitic 5
- Magnetic
 hyperfine interaction in Möss-
 bauer spectroscopy 343
 resonance methods to study mo-
 lecular motion in coal ... 23-35
- Marcasite 344
- Marine sediments, oxidation prod-
 ucts of land-derived 135
- Mass spectroscopy, low-ioniza-
 tion-potential 257-275
- Mass spectroscopy, molecular
 weight from 261-264
- Melanterite (FeSO₄ · 7H₂O) 354
- Mesophas
 fibrous-domain 72
 formation 60
 microstructure of 62
- Metal particles on graphite sur-
 faces, interaction of 326
- Metals on conversion of Illinois
 No. 6 coal, influence of 212
- Methyl
 esters of the oxidation products
 from coal 173*t*
 iodide (CH₃I) treatment of coal 251
 protons of benzyl derivatives of
 2,6-dimethylphenol, chemi-
 cal shift values of methyl-
 ene and 185*t*
 reactions of coal polyanions
 with 212, 213*t*, 217
- β-Methyl and β-methylene groups
 in brown coal 205
- d*₃-Methyl esters, organic acids
 identified as 144*t*
- Methylene bridges in coal 199
- Methylene and methyl protons of
 benzyl derivatives of 2,6-di-
 methylphenol, chemical shift
 values of 185*t*
- β-Methylene groups in brown coal,
 β-methyl and 205
- Microlithotypes 3
 classification of 5*t*
- Millerite 332
- Minerals 1
 clay 332, 353*t*
 in coal
 clay 351-352
 macerals 332
 by Mössbauer spectroscopy,
 characterization of iron-
 bearing 337-360
- Molecular
 ionization efficiency 264
 motion and magnetic resonance 26-27
 weight from mass spectros-
 copy 261-264
 weights measured by vapor
 pressure osmometry (VPO) 264
- Monocarboxylic esters from
 lithotypes 121
- Monocarboxylic fatty acid content
 of Australian brown coal
 lithotypes 114
- Monterey coal 152
- Morwell brown coal, Australian .. 193
- Mössbauer
 effect 338-341
 parameters 341-344
 spectroscopy
 characterization of iron-bearing
 minerals in coal by ... 337-360

- Mössbauer (*continued*)
 spectroscopy (*continued*)
 isomer shift in 341
 magnetic hyperfine interaction
 in 343
 quadrupole splitting in ... 342-343

N

- $\text{Na}_2\text{Cr}_2\text{O}_7$ oxidation products of
 coal 170
 NaOH, reactions of coals with
 ethanolic 162
 Naphthalene 212, 217, 226, 229
 anion 234
 carboxylic acids 171
 ethylene attack on 232-233
 in tetrahydrofuran
 rate of reduction of 211f
 and Illinois No. 6 coal 211f
 reaction of potassium with 208-209
 Naphthenic rings in aromatic
 compounds 266
 Nickel sulfide 332
 Nitrogen in coal 152
 sorption 294-295
 Nuclear magnetic resonance
 (NMR) 15, 23
 and ESR spectra, narrowing of
 wide-line 26, 27f
 and GPC to the study of struc-
 tural evolution of subbitu-
 minous coal in Tetralin,
 application 75-92
 spectra from Illinois No. 6 coal,
 wide-line 28f
 studies
 of coals, ^2D wide-line 28
 of coals, ^{19}F wide-line 27
 ^2D nuclei as probes for use
 in transient 34
 ^{19}F nuclei as probes for use
 in transient 34
 of molecules in coal 23-35
 spin labels for 23-35

O

- 4-OH-1,2-di-COOH 145
 4-OH-1,3-di-COOH 145
 OH group in coal, phenolic 280
 -OH groups in coals, reactions
 to determine 281
 Octanoyl chloride, acylations using
 Bruceton coal and 282
 Octyl, reactions of coal polyanions
 with 212, 213t, 217
 Oil(s)
 coal-derived 53-54
 molecular weight distribution
 of 269
 conversion of coal to preasphal-
 tenes, asphaltenes and 75

Oil(s) (*continued*)

- heavy
 from coal hydrogenation,
 chemical structure of .257-275
 from coal, separation scheme
 of 258, 259f
 from petroleum 258
 Organic
 acids
 bituminous coal 145
 identified as d_3 -methyl esters. 144t
 lignite coal 145
 part of coal, ratio of atoms in .. 152
 sulfur functional groups in coals,
 distribution of 239-255
 Osmometry, molecular weights
 measured by vapor pressure
 (VPO) 264
 Oxidation
 of alcohols and glycols, alkaline 171
 of aliphatic chains containing
 oxygen or sulfur functional
 groups 135
 of coals, aromatic acids as
 products of 138
 degradation of hydroaromatics
 by dichromate 171
 of ether linkages in aliphatic
 side chain of aromatics 135
 for lignin, mechanisms of CuO . 138
 method, alkaline CuO 134
 of mono- and dihydric phenols . 138
 products
 of coal(s) 145
 CuO-NaOH 139t
 distribution of carbon in .. 140t
 methyl esters of 173t
 $\text{Na}_2\text{Cr}_2\text{O}_7$ 170
 of humic acids 135
 of lignin(s) 145
 aromatic aldehydes and
 ketones as 138
 of land-derived marine
 sediments 135
 of low-rank coals, 3,4-dihy-
 droxybenzoic acids in ... 138
 of low-rank coals, *p*-hydroxy-
 benzoic acids in 138
 Oxides, iron 358t
 Oxygen
 in coal 152
 functional groups 83
 functionality in coal, alkylation. 232
 groups in brown coal 203-204
 or sulfur functional groups, oxi-
 dation of aliphatic chains
 containing 135
 Oxyhydroxides 358t

P

- Particle size
 analysis of alkali-digested
 brown coal 311-319

- Particle size (*continued*)
 analysis using sedimentation techniques 312
 distribution for humic acid fraction of coal 315, 316f
- Particles in Victorian coals, cylindrical rod-shaped 319
- PDU (*see* Process development unit)
- Peat 1
 swamp 3
- Pentane-insoluble products of reaction of subbituminous coal in tetralin, THF-soluble 83
- Pentane-soluble products of reaction of subbituminous coal in tetralin 85-87
- Petroleum asphaltenes 44, 51
 structural investigation of 181
- Petroleum, heavy oils from 258
- Phenanthrene carboxylic acid 171
- Phenetole (C₆H₅OC₂H₅) 196
- Phenol(s) 200, 287
 -BF₃
 coal depolymerization via transarylation with 179, 180f
 depolymerization of coals of different ranks with 187t
 reactivities of bridge structures toward 181-183
 deduction of the structure of brown coal by reaction with 191-206
 depolymerization 192
 method to solubilize coal 194
 ether 195
 oxidation of mono- and dihydric plant 147
- Phenol(1-¹⁴C), BF₃-catalyzed reaction of *p-n*-propyl phenol with 182t
- Phenol(1-¹⁴C), BF₃-catalyzed isopropyl group transfer to 181t
- Phenolation reaction 193
- Phenolic
 and carboxylic groups in coal, hydrogen-bonded protons from 199
 compounds 133
 OH group in coal 280
 polycarboxylic acids 145
- Phenyl(s) 134
 methyl ether, cleavage of 138
- Phenylpropane compounds 147
- Pitch
 during carbonization, chances of hydrogen aromaticity of. 60
 ethylene tar 62
¹H NMR spectra of .. 66t, 70, 71f
¹H NMR spectrum of Kureha .69, 70f
 temperature dependence of ¹H NMR absorption in 59-74
- Pittsburgh
 coal, ENDOR spectrum of vitrain-rich 41, 42f
- Pittsburgh (*continued*)
 Energy Technology Center's coal liquefaction process development unit 38
 No. 8 coal, hydrolytic product of 166
- Plant(s)
 material, decay and decomposition of 114
 phenols 147
 structural tissues (wood) of ... 4
- Plasticizers 280
- Plastometer method, Gieseler 72
- Pocahontas low-volatile bituminous coal 225
- Pocahontas No. 4 vitrain
 average polyaromatic hydrocarbon ring size in 20
 elemental analyses of 17t, 18
 fraction of aliphatic and aromatic carbon in 15-21
 high-resolution NMR spectra of ¹³C in 16, 17f
 high-resolution NMR spectra of protons in 16, 19f
- Polarization theory for sorption processes 299
- Polyanion(s), coal 208, 211
 with butylation reagents, reactions of the potassium- 213
 with reactions of
 butyl 212, 213t, 217
 iodide 212, 213t, 217
 methyl 212, 213t, 217
 octyl 212, 213t, 217
- Polycarboxylic acids, phenolic 145
- Polymers in coals, lignin-like .. 133-148
- Polymers, diffusion in nonporous . 279
- Polyphenylene sulfide 242
- Polythiophene 242
- Pore structure of coals 279
- Porosity studies of coal 321-336
- Potassium 212, 217
 hydroxide 162
 in ethylene glycol, solubilities of coals after treatment with 164t, 165
 in various solvents, solubilities of Illinois No. 2 bituminous coal after treatment with 165t, 167
 reactions of
 -coal polyanion with butylation reagents 213
 with naphthalene in tetrahydrofuran 208-209
 with tetrahydrofuran 208-209
- Preasphaltenes 54, 78
 asphaltenes and oils, conversion of coals to 75
 evolution of molecular weight of 80
- Process development unit (PDU). 38
- Pittsburgh Energy Technology Center's coal liquefaction . 38
- Propenium cation 186

<i>p-n</i> -Propylphenol with phenol- (1- ¹⁴ C), BF ₃ -catalyzed reac- tion of	182 <i>t</i>
Protic solvents	167
to solubilize coal, use of alkali in	162
Protons	
in 2,6-dimethylbenzoic acid, high-resolution NMR of ..16, 18 <i>f</i>	
from phenolic and carboxylic groups in coal, hydrogen- bonded	199
in Pocahontas No. 4 vitrain, high-resolution spectra of ..16, 19 <i>f</i>	
in Star vitrain, high-resolution NMR spectra of	16, 19 <i>f</i>
Pyridine	287
solvent	187
Pyrite (iron disulfide)	344-360
Debye-Waller factor of	358
evolutions of H ₂ S from iron ...	249
iron	245
Pyritic sulfur	245, 358
Pyrrhotite(s)	346
in liquefaction process, behavior of	348
monoclinic (Fe ₇ S ₈)	346

Q

Quadrupole coupling constants ...	29
for C ₆ D ₆	29
for C ₅ D ₅ N	29
Quadrupole splitting in Mössbauer spectroscopy	342-343

R

Radical(s)	
alkyl	231
anions, aromatic	232
anions in coal	229
free	
in coal(s)	37-57, 227
aromatic	46
ESR and ENDOR spec- tometries to charac- terize	37-57
hetroatomic	47
liquefaction products	37-57
pyrolyzed	37-57
solvent-refined	37-57
during coal liquefaction, changes in the quantity and nature of	54
ENDOR spectra of organic ..	43
Reducing agents	212
Reflectance distribution of macerals in coals	5, 6 <i>f</i>
Ring size, average polynuclear aromatic	
in coals	15-21
in Iowa vitrain	15-21
in Virginia vitrain	15-21

Rozenite (FeSO ₄ · H ₂ O)	354
Mössbauer spectrum of 355, 356 <i>f</i> , 357 <i>f</i>	
Rubber	242

S

S _N 2 reactions	217
Scanning transmission electron microscopy (STEM)	322
Sedimentation techniques, particle size analysis using	312
Sediments	128
Siderite (FeCO ₃)	355
Size distribution for humic acid fraction of coal, particle ..	315, 316 <i>f</i>
Soil acids	145
Soil, reductive degradations of ...	133
Solubilization techniques, coal ...	192
Solvent(s)	
benzene-ethanol	187
coal(s)	
for bituminous	287
extraction of black	119
extraction of brown	119
fractionation scheme to separate	194 <i>f</i>
-refined (SRC)	51
aromaticity of	170
ESR <i>g</i> values and spectral line widths for	51 <i>t</i>
protic	167
to solubilize coal, use of alkali in	162
pyridine	187
-refined lignite (SRL)	170
solubilities of Illinois No. 2 bitu- minous coal after treatment with KOH in various ..	165 <i>t</i> , 167
Sorption	
in coal	296
carbon dioxide	296
nitrogen	294-295
water	296
kinetics of water	303, 304 <i>f</i>
processes, polarization theory for	299
studies of coals	293-309
Spectrometry(ies), ENDOR	38
characterizing free radicals in coals	37-57
Spectrometry(ies), ESR	38
characterizing free radicals in coals	37-57
Spectroscopic splitting factor, ESR <i>g</i> value	40-41
Spectroscopy, low-ionization-poten- tial mass	257-275
Spectroscopy, molecular weight from mass	261-264
Spin labels for NMR studies	23-35
Spin lattice relaxation time	27
Spore exines in coals	325
Sporinite, TEM micrograph of ...	331 <i>f</i>
SRC (solvent-refined coal)	170
SRL (solvent-refined lignite)	170

- Star vitrain
 average polyaromatic hydrocarbon ring size in 20
 elemental analysis of17*t*, 18
 fraction of aliphatic and aromatic carbon in15-21
 high-resolution NMR spectra of ¹³C in 17*f*
 high-resolution NMR spectra of protons in16, 19*f*
- STEM (scanning transmission electron microscopy)
- Subbituminous coal(s) 49
 in tetralin, application of NMR and GPC to the study of structural evolution of75-92
 in tetralin, pentane-soluble products of reaction of85-87
 THF-soluble pentane-insoluble products of reaction of ... 83
 uptake of hydrogen and product formation in the conversion of78-80
- Sulfates, iron354, 357*t*
 in coal352-355
- Sulfide(s)
 aliphatic 240
 and alicyclic 242
 evolutions of H₂S from 249
 aromatic 242
 iron 345*t*
 in coal344-351
 produced during coal processing 346
 nickel 332
 polyphenylene 242
- Sulfidic sulfur, transformation of thiolic sulfur to 245
- Sulfonates, butylation reactions of halides and 213
- Sulfur 331
 (in) coal(s) 152
 distribution
 class 250*t*
 raw 250
 treated 250
 organic
 groups, distribution of 250*t*
 functional239-255
 in high-ranked 240
 in low-ranked 240
 compounds and polymers, data on kinetograms of 243*t*
 groups
 functional, oxidation of aliphatic chains containing oxygen or 135
 qualitative identification of .. 242
 quantitative analysis of 242
 pyritic245, 358
 to sulfidic sulfur, transformation of thiolic 245
 thiophenic 242
 transformation of thiolic sulfur to sulfidic 245
- SYNTHOIL 51
 Syringaldehyde 138
 Szomolnokite (FeSO₄ · H₂O) . . .352, 354
 Mössbauer spectrum of 355, 356*f*, 357*f*
- T**
- Taiheiyō coal 62
¹H NMR spectra of 63*f*
- Tar(s)
 coal 96
 pitch 62
 infrared spectra of 96
 pitch, ethylene 62
 pitch, ¹H NMR spectra of 66*f*, 70, 71*f*
- TEG (triethylene glycol) 169
- TEM (*see* Transmission electron microscopy)
- TEMPOL (*see* 2,2,6,6-Tetramethyl-4-piperidinol-1-oxyl)
- Tetrahydrofuran (THF) 226
 decomposition 229
 rate of reduction of 211*f*
 reaction of potassium with ... 208
 -soluble, pentane-insoluble products of reaction of subbituminous coal in tetralin 83
- Tetralin or 1,1-dideuterotetralin, reactions of coal and 76
- 2,2,6,6-Tetramethyl-4-piperidinol-1-oxyl (TEMPOL)29-31
 ESR spin label studies in Wyodak coal 30*f*
- Thermal decomposition
 of coal, products of108*f*, 109*f*
 model 96
 products, relation between coal structure and95-111
- Thermal intramolecular reactions
 in coal 162
- THF (*see* Tetrahydrofuran)
- Thiolates 240
- Thiolic sulfur to sulfidic sulfur, transformation of 245
- Thiols240, 251
- Thiophenes 245
- Thiophenic sulfur 242
- Thiophenols 251
- Tin 332
- p*-Toluenesulfonic acid (PTSA) .. 180
- Transaryl-alkylation with phenol-BF₃, coal depolymerization via179, 180*f*
- Transmission electron microscopy (TEM) 322
 of splint coal 323*f*
- Triethylene glycol (TEG) 169
- Trihydroxybenzenes 135
- Trihydroxybenzoic acids 145
- Troilite (FeS) 346
- U**
- U.S. Bureau of Mines (USBM)
 API project 60 258
- U.S. coals 7

V	W
Vapor pressure osmometry (VPO), molecular weights measured by	Walnut stones, fossil
264	129
Victorian coals, cylindrical rod- shaped particles in	Water sorption in coal
319	296
Virginia vitrain, average poly- nuclear aromatic ring size in	Water sorption, kinetics of
15-21	303, 304f
Vitrain, Pocahontas No. 4	West Virginia (Ireland Mine)
average polyaromatic hydro- carbon ring size in	hvAb coal, ESR <i>g</i> values
20	of
elemental analysis of	49, 50f
17t, 18	West Virginia (Ireland Mine)
high-resolution NMR spectra	hvAb coal, spectra of
of protons in	40f
16, 19f	Wittig rearrangement
Vitrain, Star	221
average polyaromatic hydrocar- bon ring size in	reactions
20	216
elemental analyses of	Wood cells, coniferous
17t, 18	317
high-resolution NMR spectra of protons in	Wyodak coal(s)
16, 19f	deuterated guests in
Vitrinite(s)	24, 227
in coals of different ranks, prop- erties of	distribution of chemical classes
6t	in the solubilized products
in Illinois No. 6 coal, TEM	from
micrograph of	155t
in splint coal, TEM micrograph	TEMPOL ESR spin label
of	studies in
327, 328f, 332	30f
Vitrinitic macerals	
5	

Y

Yubarishinko coal	62
¹ H NMR spectra of	63f

*Jacket design by Joe Phillips.
Editing by Carol Beal.
Production by Susan Moses.*

*The textual material was composed by Carolina
Academic Press, Durham, NC. The front matter and
index were composed by Service Composition, Balti-
more, MD. The book was printed and bound by
The Maple Press Co., York, PA.*